

280
5-8-78

Ar. 54

ALO/2744-13(Vol.3)(Pt.1)

CONCEPTUAL DESIGN AND SYSTEMS ANALYSIS OF PHOTOVOLTAIC
POWER SYSTEMS. FINAL REPORT

Volume 3(1). Technology

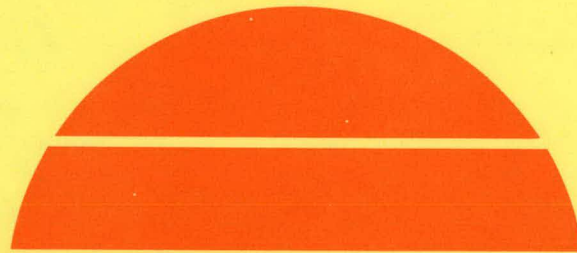
By
P. F. Pittman

May 1977

Work Performed Under Contract No. EY-76-C-04-2744

MASTER

Westinghouse Electric Corporation
Research and Development Center
Pittsburgh, Pennsylvania



U.S. Department of Energy



Solar Energy

DISTRIBUTION OF THIS DOCUMENT IS UNLIMITED

DISCLAIMER

This report was prepared as an account of work sponsored by an agency of the United States Government. Neither the United States Government nor any agency Thereof, nor any of their employees, makes any warranty, express or implied, or assumes any legal liability or responsibility for the accuracy, completeness, or usefulness of any information, apparatus, product, or process disclosed, or represents that its use would not infringe privately owned rights. Reference herein to any specific commercial product, process, or service by trade name, trademark, manufacturer, or otherwise does not necessarily constitute or imply its endorsement, recommendation, or favoring by the United States Government or any agency thereof. The views and opinions of authors expressed herein do not necessarily state or reflect those of the United States Government or any agency thereof.

DISCLAIMER

Portions of this document may be illegible in electronic image products. Images are produced from the best available original document.

NOTICE

This report was prepared as an account of work sponsored by the United States Government. Neither the United States nor the United States Department of Energy, nor any of their employees, nor any of their contractors, subcontractors, or their employees, makes any warranty, express or implied, or assumes any legal liability or responsibility for the accuracy, completeness or usefulness of any information, apparatus, product or process disclosed, or represents that its use would not infringe privately owned rights.

This report has been reproduced directly from the best available copy.

Available from the National Technical Information Service, U. S. Department of Commerce, Springfield, Virginia 22161.

Price: Paper Copy \$16.25
Microfiche \$3.00

FINAL REPORT
CONCEPTUAL DESIGN AND SYSTEMS ANALYSIS OF
PHOTOVOLTAIC POWER SYSTEMS
VOLUME III(1) - TECHNOLOGY

by

P. F. Pittman

Westinghouse Electric Corporation
Research and Development Center
Pittsburgh, PA 15235

Prepared for
Energy Research and Development Administration
May 1977

ERDA-ALBUQUERQUE OPERATIONS OFFICE

Contract E(11-1)2744
Dr. Donald G. Schueler
Sandia Laboratories

NOTICE
This report was prepared as an account of work sponsored by the United States Government. Neither the United States nor the United States Department of Energy, nor any of their employees, nor any of their contractors, subcontractors, or their employees, makes any warranty, express or implied, or assumes any legal liability or responsibility for the accuracy, completeness or usefulness of any information, apparatus, product or process disclosed, or represents that its use would not infringe privately owned rights.

FOREWORD

The work described in this report was done by Westinghouse and its subcontractors under ERDA Contract E(11-1)2744. This program is part of the National Photovoltaic Program managed by ERDA through the Division of Solar Energy, Dr. Morton B. Prince, Acting Assistant Director, Photovoltaic, and The Silicon Technology Branch, Dr. Leonard M. Magid, Acting Chief.

Responsibility for the management of the Systems Definition Project of the National Photovoltaic Program, under which this contract fell, was delegated by ERDA to the Sandia Laboratories. The Program Manager at Sandia with responsibility for this contract was Dr. Donald Schueler, who was assisted by Dr. Billy W. Marshall who was the Task Leader for the Systems Definition and Analysis Task.

PREFACE

This volume contains the first part of a description of the in-depth studies of the technologies which underlie the system designs performed on the contract entitled, "Conceptual Design and System Analysis of Solar Photovoltaic Power Systems", sponsored by the Energy Research and Development Administration.

This is the first part of Volume III of the final report which contains five volumes in all. The other volumes are as follows:

Volume I - Executive Summary

Volume II - Systems

Volume IV - Nontechnical Issues

Volume V - Additional Studies

ACKNOWLEDGEMENTS

The work described in this report was performed under ERDA Contract E(11-1)2744 by more than thirty contributors from Westinghouse and its subcontractors. A listing of contributors together with their areas of specialization is contained in the following paragraphs.

The program was organized with a coordinator responsible for the design and analysis of each of the three types of systems included in the study. The coordinator for the Residential Power System was Edward F. Federmann, and the coordinator for both the Intermediate and Central Power Systems was Dr. Robert R. Ferber. During the program, Dr. Ferber became ill and the responsibility for coordination of the later two systems was assumed by Carl R. Chowaniec. Mr. Federmann is a staff member of the Research and Development Center, while Dr. Ferber and Mr. Chowaniec are members of the Advanced Systems Technology Division.

A number of specialists in different areas of technology were called upon to contribute to the design and analysis of each of the systems. Members of the staff of the Research and Development Center who contributed in this way are as follows:

<u>Technical Area</u>	<u>Contributor</u>
Batteries	Edward S. Buzzelli
Costing	Henry B. Kellogg James A. Richard Ronald E. Vaill
Heat Transfer	Ralph E. Grimble
Optics	Dr. Johanna Schruben
Power Conditioning	Peter Wood
Solar Cells - CdS - Silicon	Fred A. Shirland J. Ransford Davis
Structures	Kenneth Gerkey Walter R. Wallace

System Analysis	William J. McAllister
Thermal Systems	Joseph M. Cardito Dr. Herbert S. Kirschbaum

Three subcontractors contributed to the program. A listing of the firms and principal contributors in each area is as follows:

<u>Firm</u>	<u>Contributor</u>
Burt, Hill & Assoc.	P. Richard Rittelmann Steven Nearhoof
Ford, Bacon, & Davis	George Conover Gad Williams
Univ. of Pennsylvania	Martin Wolf Thomas Wolf

In addition to the contributors listed, many other people within the Westinghouse Research and Development Center contributed to the design and analysis tasks as well as report preparation. Included were typing, drafting and duplicating services. In particular, Denise Horvath spent many hours preparing the drafts and final copy of this report.

TABLE OF CONTENTS

	<u>Page</u>
SUMMARY	1
INTRODUCTION	3
1. SUBSYSTEM TECHNOLOGY	7
1.1 Insolation	7
1.2 Concentration	9
1.2.1 Solar Concentrator Fortran Subroutines for Photovoltaic Systems	9
1.2.1.1 Introduction	9
1.2.1.2 The Concentrators	10
1.2.1.3 Calling Sequence for the Concentrator Subroutines: FRENEL, TRUSS, VTRGH, WINSTN	16
1.2.1.4 Sample Program	17
1.2.1.5 Conclusion	20
References	28
1.2.2 Collector/Reflector (Solar Truss) Tilt Optimization	29
1.2.2.1 Introduction	29
1.2.2.2 Description of Analysis	29
1.2.2.3 Description of Results	31
1.3 Silicon Solar Cell Modules	83
1.3.1 Cell Characteristics	83
1.3.2 Module Analysis	89
1.3.2.1 Basic Photovoltaic Modularity	89
1.3.2.1.1 General Considerations	89
1.3.2.1.2 Width Tolerance	99
1.3.2.1.3 Height Tolerance	101
1.3.2.1.4 Joint Tolerance	102
1.3.2.1.5 System Dimension	103
1.3.2.1.6 Residential Module	106
1.3.2.2 Module Voltage and Shadowing Analyses	108
1.3.2.2.1 Description of Program	108
1.3.2.2.2 Presentation of Results	115
1.3.3 Heat Transfer	125
1.3.3.1 Forced Cooling	125
1.3.3.2 Passive Cooling	136

TABLE OF CONTENTS (CONT.)

	<u>Page</u>
1.3.4 Module Design	138
1.3.4.1 RPS Module	138
1.3.4.1.1 Background	138
1.3.4.1.2 Flat Plate System	138
1.3.4.1.3 RPS Air Cooled Photovoltaic Array Module	143
1.3.4.2 IPS and CPS Modules	145
1.3.5 Cost Estimates	163
1.3.5.1 RPS	163
1.3.5.2 IPS	165
1.3.5.3 CPS	165
1.4 CdS Solar Cell Module	175
1.4.1 Cell Characteristics	175
1.4.2 Module Analysis	182
1.4.3 Heat Transfer	182
1.4.4 Module Design and Application	184
1.4.4.1 Module Design	184
1.4.4.2 Module Application Considerations	188
1.4.5 Cost Estimates	190
1.5 Array Structure	193
1.5.1 RPS Array Structure	193
1.5.1.1 Silicon Water Cooled Array Structure	193
1.5.1.2 Air Cooled Array	198
1.5.1.2.1 Silicon Air Cooled Array	198
1.5.1.2.2 Cadmium Sulfide (CdS) Array Structure	202
1.5.2 IPS Array Structure	204
1.5.2.1 Silicon Array Options	204
1.5.2.1.1 Total Roof System - Interconnected Triangular Truss (Modified Truss)	204
1.5.2.1.2 Molded Polyurethane Cylindrical Concentrator	208
1.5.2.1.3 Non-Waterproof Non-Thermal IPS Photovoltaic Array	212
1.5.2.1.4 Fresnel Type Lens	212
1.5.2.2 Cadmium Sulfide Array Options	215
1.5.2.2.1 Flexible - Non-Thermal - IPS Photovoltaic Array	215
1.5.3 CPS Array Structure	217
1.5.3.1 Task Definition	217
1.5.3.2 Analysis Philosophy and Assumptions	217
1.5.3.3 Array Evaluation Techniques	221
1.5.3.4 Description of Arrays Analyzed	222

TABLE OF CONTENTS (CONT.)

	<u>Page</u>
1.5.3.5 Discussion of Results	242
1.5.3.6 Conclusions	247
1.6 Battery Energy Storage	251
1.6.1 Battery Storage Technology	251
1.6.2 Battery Storage for the Residential Power System	269
1.6.3 Battery Storage for the Intermediate Power System	279
1.7 Power Conditioning	301
1.7.1 Residential Power System	301
1.7.1.1 Power Conditioning Subsystem Requirements	301
1.7.1.2 Subsystem Cost/Performance Analysis	306
References	336
1.7.2 Intermediate Power System	337
1.7.2.1 General Considerations	337
1.7.2.2 Sample Designs for a 1 MW Installation	349
1.7.3 Central Power System	364
1.7.3.1 Inverter Tradeoffs	364
1.7.3.2 Design Considerations	371
1.7.3.3 dc Buswork Considerations	378
References	385
1.8 RPS Architectural Designs	387
1.8.1 General Architectural Considerations	387
1.8.1.1 Climatic Considerations	387
1.8.1.2 Building Configuration in Relation to Array Tilt	389
1.8.1.3 General System Placement	398
1.8.2 General System Descriptions	407
1.8.2.1 Direct Solar Heating Systems	409
1.8.2.1.1 Hybrid Silicon Water-Cooled and Air-Cooled Array with a Fossil Fuel Backup	409
1.8.2.1.2 Hybrid Silicon Water-Cooled Array and Roof Membrane Cadmium Sulfide Array	416
1.8.2.1.3 Total Silicon Water-Cooled Array	416
1.8.2.1.4 Mode Descriptions of the Direct Solar Heating Systems	418

TABLE OF CONTENTS (CONT.)

	<u>Page</u>
1.8.2.1.5 Modes of the Non-Heat Pump Hybrid Silicon and Cadmium Sulfide Array Systems	424
1.8.2.1.6 Modes of Silicon Water-Cooled Non-Heat-Pump System	424
1.8.2.2 Water Cooled Photovoltaic Array Used in Conjunction with a Solar-Assisted Heat Pump	424
1.8.2.2.1 General Description	424
1.8.2.2.2 Water-Cooled Photovoltaic Array Used in Conjunction with the Solar Heat Pump Mode Definition	433
1.8.3 Madison Residential Schematic	437
1.8.3.1 Form in Relation to Climate	437
1.8.3.2 RPS - Madison System Integration	442
1.8.4 Phoenix Residential Schematic	450
1.8.4.1 Form in Relation to Climate	450
1.8.4.2 RPS System Integration - Phoenix	454
1.8.5 Santa Maria Residential Schematic	458
1.8.5.1 Form in Relation to Climate	458
1.8.5.2 Santa Maria System Integration	460
1.8.6 Atlanta Residential Schematic	464
1.8.6.1 Form in Relation to Climate	464
1.8.6.2 Atlanta System Integration	467
1.8.7 Garage Retro-Fit System	469
1.8.7.1 General System Description	469
1.8.7.2 Garage Options	471
1.8.7.3 Garage Mechanical System	475
1.8.8 RPS Equipment Lists and Cost Summaries	477
1.9 IPS Structural Design	493
1.10 CPS Site Survey	495
1.11 CPS Facilities	531

ABSTRACT

Conceptual designs were made and analyses were performed on three types of solar photovoltaic power systems. Included were Residential (1 - 10 kW), Intermediate (0.1 - 10 MW), and Central (50 - 1000 MW) Power Systems to be installed in the 1985 to 2000 time period. In the residence, a total energy system where the waste heat from the array is used to heat the dwelling appears optimum. If a suitable government incentive is forthcoming, Residential Systems begin to become economically viable in selected areas in the 1985 to 1990 period, while Intermediate and Central Power Systems begin to become viable in the 1990 to 2000 period.

SUMMARY

This volume contains a number of independent discussions of separate areas of technology all of which are needed for the conceptual design and systems analysis of the solar photovoltaic power systems considered in this program. Each major section is separate and self-contained, and describes an in-depth investigation of the technological area as it relates to solar photovoltaic power system design and analysis.

Included are discussions of all subsystem technologies needed for solar photovoltaic power system construction. The results of these investigations show that all of the basic technology needed to construct the types of subsystems required exists, but much design and development is yet to be done. No technology voids were uncovered which would preclude the successful construction of the solar photovoltaic power systems studied.

THIS PAGE
WAS INTENTIONALLY
LEFT BLANK

INTRODUCTION

During the 1960's solar photovoltaic electric power systems were of interest primarily for use in space vehicles where the variability of weather need not be considered. Spacecraft systems started at power levels less than 100W in the early 1960's and increased in size to levels of several kilowatts in the early 1970's.

Until the advent of the oil embargo several years ago, terrestrial applications were limited to small, special purpose installations where the advantages of a totally isolated power supply made it possible to justify the high cost of the solar photovoltaic power system. Since the embargo, however, a great deal of thought and effort has been devoted to the use of solar power in general and solar photovoltaic power in particular as an alternative source of energy for terrestrial applications.

The National Photovoltaic Conversion Program, managed by ERDA, is oriented toward developing photovoltaic conversion of solar energy as an economically viable energy source. The effort of this contract is oriented toward the conceptual design and system analysis subtask of the Systems Definition Project which is one of the many facets of the National Photovoltaic Conversion Program. The principal objective of this contract is to provide conceptual designs and system analyses of three types of solar photovoltaic electric power systems. Included are:

- Residential Power System (1 - 10 kW).
- Intermediate Power System (0.1 - 10 MW).
- Central Station Power System (50 - 1000 MW).

The Residential Power System (RPS) considered provides a substantial fraction of the electrical and thermal needs of a residence. Two options were considered as means to obtain the supplemental energy needed. One assumed that the energy required would be supplied by a utility. For this case, the billing rate used by the utility for the small amount of energy used becomes a critical parameter. The other option assumes that the residence can be autonomous and require no utility connection at all. In this case, the supplemental electrical energy is furnished by a small engine/generator, and the thermal energy either from the same engine/generator or from a fossil fueled heater. For the systems utilizing utility energy to supplement the RPS output, the return of excess solar generated electrical energy to the utility grid was not considered.

In the Intermediate Power System (IPS), power may flow either from the solar array or from the battery into the utility system. The battery may be charged from the solar array or from the utility line, depending upon the strategy used, and would be used primarily for load leveling. The IPS would most likely be located at an industrial or commercial substation.

The Central Power System (CPS) is assumed to be tied into a large utility grid which would contain pumped hydro or other storage. Energy storage within the CPS itself was not included. Energy from the CPS would be dispatched directly into the utility grid whenever available. The operation of storage would be a separate utility system consideration.

The analysis of the performance of the RPS was accomplished with the aid of a mathematical model of the system analyzed by means of a computer program. Inputs to the computer model included weather and load data for the location selected. An additional input was operating strategy relating to power flow and timing within the system. The output was a description of system performance over a one year period to be used to verify the suitability of the parametric values chosen.

The performances of the Intermediate and Central Power Systems were determined using a computer program which contained an analytical model of the solar cell. The annual energy and peak power outputs of the cell were then determined on a per unit area basis for arrays operated in various tracking and non-tracking modes using hourly weather data.

After the performance of each system was determined, an appropriate economic analysis was made to determine the economic viability of each system installed during the 1985 to 2000 time period.

The final report on this program is divided into five volumes. This is the first part of Volume III entitled, "Technology", which contains in-depth descriptions of the investigations into the required subsystem technologies. Volume I entitled, "Executive Summary", contains a brief description of the entire program. Volume II entitled, "Systems", contains a detailed description of the conceptual designs and analyses of all three systems as well as a summary of the nontechnical issues task. The in-depth studies of the nontechnical issues are reported in Volume IV entitled, "Nontechnical Issues." The results of the follow-on efforts are not included in Volumes II, III or IV but are reported in Volume V entitled, "Additional Studies."

During discussions regarding subsystem analysis, a continuing problem was encountered with varying definitions of the terms "array", "module", and "field" used in relation to the solar cell arrays. The following definitions are used throughout this report.

Module - A module consists of solar cells and backplates, as well as concentrators, cover plate, and heat transfer means if used.

Array - An array consists of one or more modules mounted in a rigid supporting structure which may move as a unit if tracking is provided. The modules comprising the array are replaceable.

Field - A field comprises one or more arrays providing power for a solar photovoltaic power system.

Throughout this report, values of electrical power quoted are always peak and not average or rated. In addition, all economic analyses performed used constant dollars with the year 1975 as the base.

1. SUBSYSTEM TECHNOLOGY

1.1 Insolation

Insolation data was obtained for at least one year for the following seven sites:

Atlanta, Ga.

Cleveland, Ohio

Madison, Wisc.

Mobile, Ala.

Phoenix, Ariz.

Santa Maria, Calif.

Wilmington, Del.

Summaries of the insolation data obtained and discussions of its origins are contained in Section 2.1 entitled, "RPS Computer Simulation", of Volume III (2) of this report.

THIS PAGE
WAS INTENTIONALLY
LEFT BLANK

1.2 Concentration

1.2.1 Solar Concentrator Fortran Subroutines for Photovoltaic Systems

1.2.1.1 Introduction

For photovoltaic systems, the purpose of concentration is to reduce the amount of photovoltaic material required for energy collection. Photovoltaic cells can be replaced by reflectors, lenses, and/or tracking mechanisms. Trade-offs arise due to the relative costs of these items. With the projected decrease of solar cell cost to \$500/kW by 1985, low concentration systems would appear to be the most desirable. Such systems have the advantages of having less expensive optics and cooling systems, and requiring less accurate tracking mechanisms. Also, solar cell irradiance is more likely to be more uniform than for higher concentration systems. In addition, solar cells are more efficient under uniform illumination.

Many concentrating systems have been invented for solar energy.¹ Some of the most promising for relatively low cost photovoltaic material are the Fresnel lens, the solar truss, the v-trough, and the compound parabolic collector (CPC).

Computer subroutines, contained in Appendix A of this report, evaluate the concentrations of these selected concentrators for arbitrary solar incidence angles. These subroutines were designed as inputs to a computer program which determines the photovoltaic efficiency for the various configurations under different tracking and insolation conditions.

Certain simplifications are assumed in the calculation of concentration. For one, only average irradiances are evaluated; non-uniformities and selective absorption for different angles of incidence on the solar

cells have not been considered. Also, the trough-type concentrators are assumed to be sufficiently long that their end-effects may be neglected.

Reflectivities of the reflecting concentrators are taken as 81% as in Ref. 2. Future improvements in reflective materials and coatings could increase this value and together with it the concentration ratios.

1.2.1.2 The Concentrators

Fresnel lenses

We considered three different Fresnel concentrators, each with two different geometric concentrations. See Fig. 1.2.1. The linear lenses of geometric concentration of 3 and 10 were designed to be essentially similar to those discussed in Ref. 3. The cross-sections of the circular lenses are identical to the linear ones. To obtain a higher acceptance angle, a movable absorber is analyzed for the linear lenses. The absorber is rotated on a radial path on a fixed arm to a position of highest irradiance for each given solar angle of incidence.

Loss of efficiency of these lenses occurs because of blockage of light by the facet edges, and by Fresnel reflection losses⁴ at surface interfaces (the index of refraction is assumed to be that of acrylic, 1.49). These losses are higher at higher angles of incidence. No anti-reflection coatings have been assumed. It is difficult to maintain such a coating on the outer surface, but a coating could be designed for the inner faceted surface which would improve the light collection efficiency.

Because of the higher concentration ratios, the circular lenses have smaller acceptance angles. These lenses are assumed to be tracked normally to the sun.

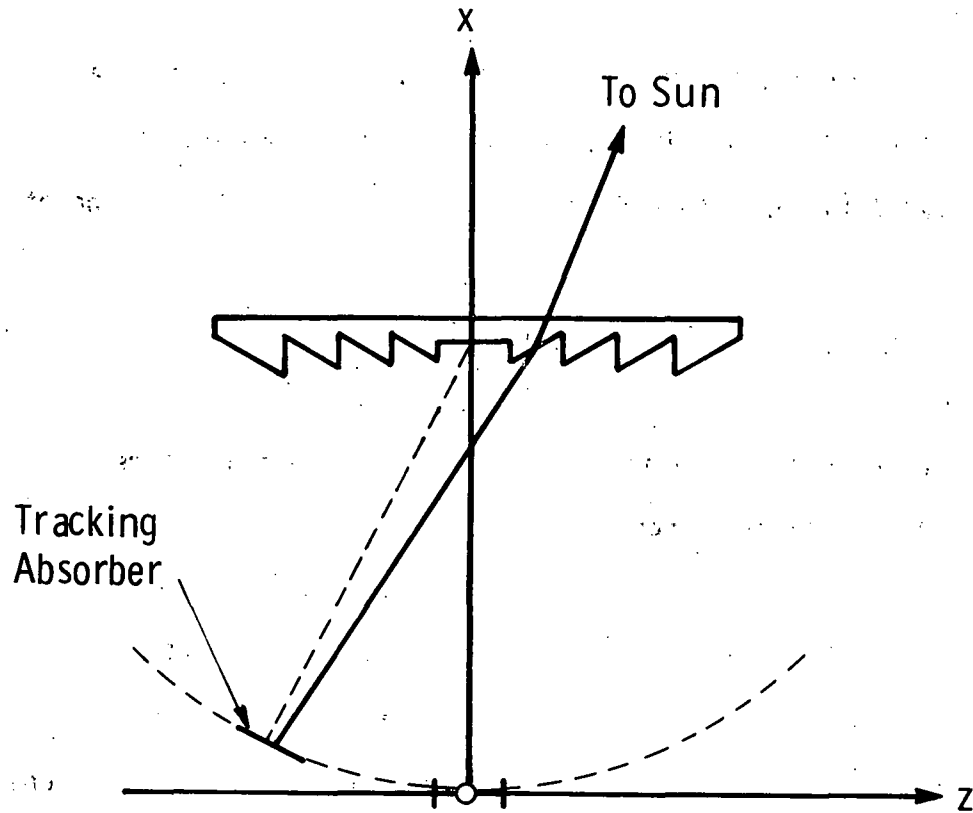


Fig. 1.2.1 — Cross-sectional schema of the Fresnel lenses. The concentration 3 Fresnel has a relative aperture of 1.12 with a focal length of 3.0 and an aperture of width 3.0. The concentration 10 Fresnel has a relative aperture of 0.94 with a focal length of 8.0 and an aperture of width 10.0. All numbers are relative to unit solar cell width.

Solar Truss

Better collection can be achieved from flat panels by tilting them toward the south. The placement of reflectors on the back side of the support structure for the panels further increases the solar absorption. See Fig. 1.2.2.

The angles of tilt of absorber and reflector were optimized to obtain maximum yearly collection at Phoenix using the ASHRAE "Sun" solar insolation computer program.⁵ This optimization, presented in Section 1.2.2, showed that there should be no separation on the ground between the mirror and the solar panel.

V-Trough

The maximum possible concentration from a V-trough is 3. Such a unit would have infinite sides. To obtain a compact collector, a geometric concentration of 2 was chosen. The reflector sides have the same width as the absorber (Fig. 1.2.3). If the angle ψ^* between the normal to the collector and the projection of the sun's rays in the cross-sectional plane of the collector is between 30° and 60° , only direct light is accepted. The absorber receives both direct and reflected light if ψ is less than 30° . No direct light reaches the absorber if ψ is greater than 60° .

Compound Parabolic Collector (CPC)

The CPC was invented by Winston⁷ as a concentrator requiring minimal tracking. See Fig. 1.2.4. It collects all the radiation with ψ 's (defined above) falling within its acceptance angle. Of course, some of the light is absorbed due to the non-unity reflectivity of the

*The angle ψ is essentially similar to the East-West Viewing angle defined by Tabor.⁶

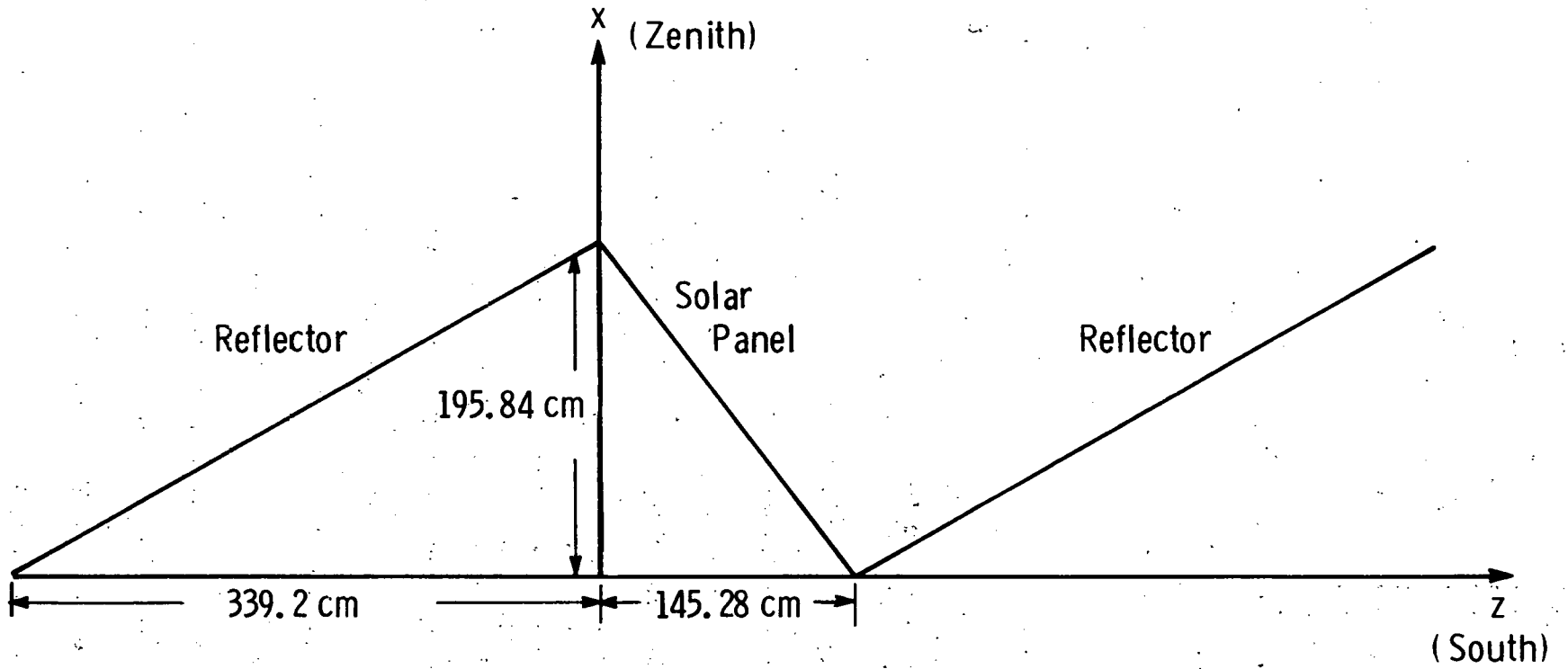


Fig. 1.2.2—Solar truss

Dwg.6382A10

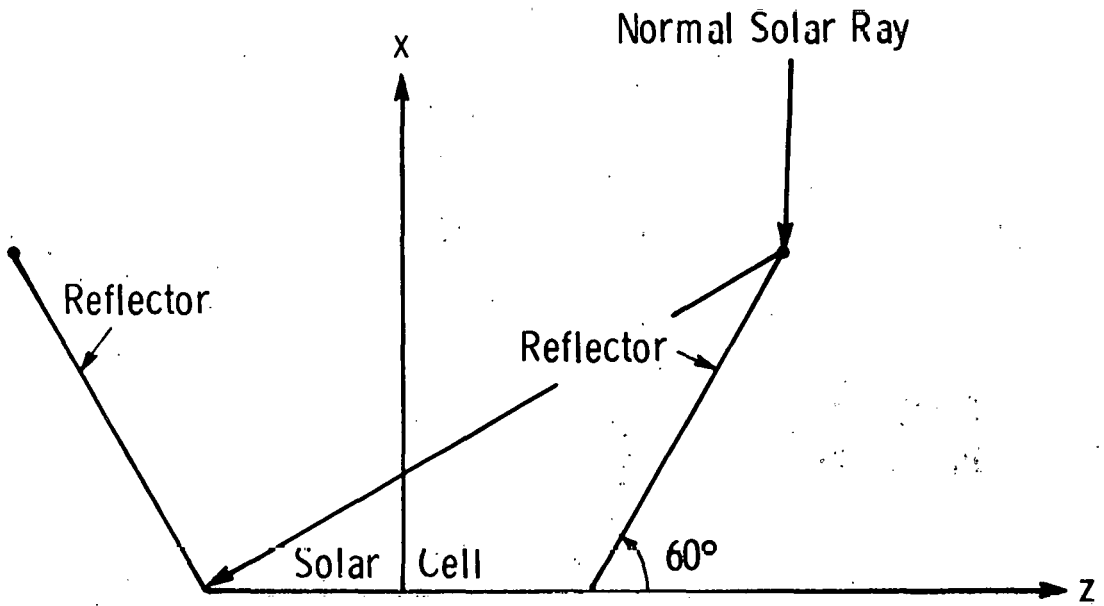


Fig. 1. 2. 3 - V - Trough

Dwg.6382A14

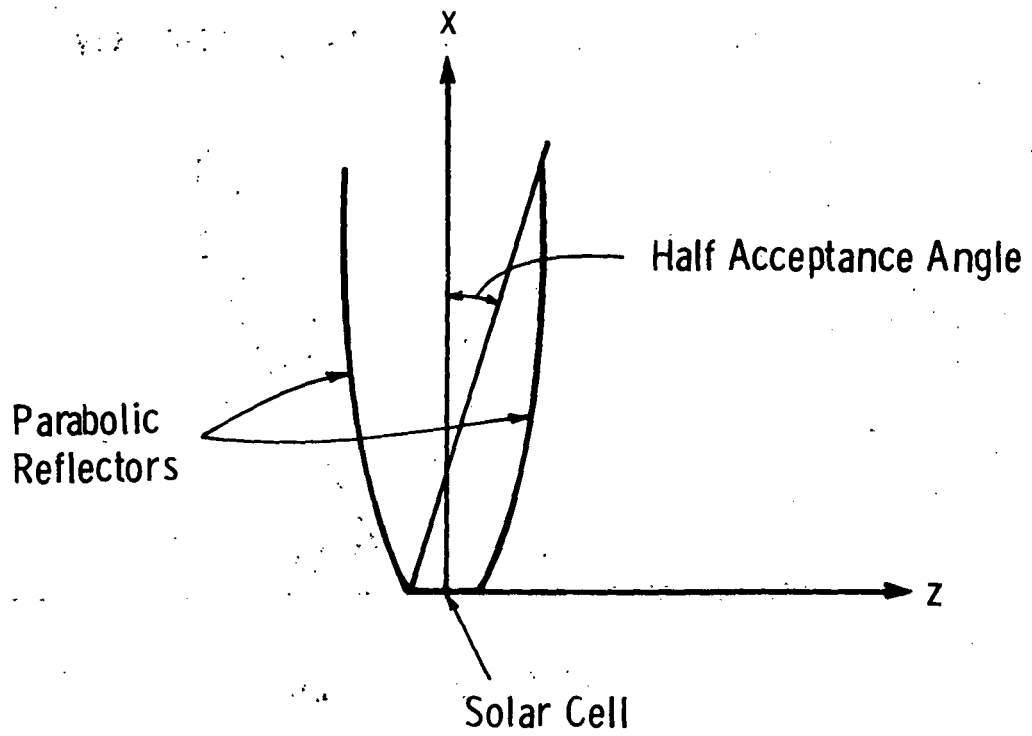


Fig. 1.2.4-Compound parabolic collector

mirrors. The geometric concentration ratio is the reciprocal of the sine of the acceptance angle. And we see that the lower the concentration, the less tracking is required.

Geometric concentrations of 3 and 10 were chosen. The CPC of concentration 10 was truncated to reduce its height in half from 55 times the absorber width. Multiple reflection losses and direct light shading were evaluated to give effective concentration ratios. The actual photovoltaic efficiency will be reduced from that expected from these values because of the strong non-linearity of irradiance on the cells, especially at angles of incidence near the acceptance angle.

1.2.1.3 Calling Sequence for the Concentrator Subroutines: FRENEL, TRUSS, VTRGH, WINSTN

The user of the concentrator subroutines must pass ten variables to the subroutines via COMMON. These variables are described below.

ALPHA, BETA, GAMMA have similar meanings in each of the subroutines. They are the direction cosines of the sun's rays relative to the collector being evaluated. ALPHA is the cosine of the angle between the sun and the upward normal to the collector. BETA is the cosine of the angle between the sun and the lengthwise axis of the collector. GAMMA is the cosine of the angle between the sun and the crosswise axis of the collector. These angles are pictured in Fig. 1.2.5 with the x-axis as the upward normal, the y-axis as the lengthwise axis and z-axis as the crosswise axis to the collector. DNR is the input that scales the resulting flux on the absorber to the desired units and represents the normal radiation of the sun in units of flux per unit area.

W is the width of the absorber in arbitrary but consistent units. It is input to all the subroutines except "TRUSS". In "TRUSS" the solar panel has a fixed width of 243.84 cm.

EL is the length of the absorber. It is input to all the subroutines.

CON, which refers to geometric concentration, is used by "FRENEL" and "WINSTN" and can be set to either 3.0 or 10.0. In "FRENEL", it determines the ratio of the width of the lens to the width of the absorber, and also in "WINSTN" for $CON = 3.0$. Setting $CON = 10.0$ in "WINSTN" gives a geometric concentration of 9.08 since this CPC collector is truncated in half.

LIN is an integer variable used only in "FRENEL".

LIN = 0 evaluates a linear Fresnel lens.

LIN = 1 evaluates a circular Fresnel lens with a circular absorber of diameter W .

LIN = -1 evaluates a linear Fresnel lens with an absorber tracking on a fixed radius.

TDF is the output of each subroutine. It is the total direct (as distinguished from diffuse) flux on the absorber as a result of the collector's concentration.

E is output from "TRUSS". It is the irradiance on the solar panel in flux per unit area.

1.2.1.4 Sample Program

Appendix A contains a sample program designed for the purpose of comparing the effective concentration ratios of the various collectors for different angles of incidence. The angle ψ varies in steps of 5° . The angle ω between the collector's normal and projection of the sun's rays in the lengthwise plane varies in steps of 15° . The angles ψ and ω are illustrated in Fig. 1.2.5.

The effective concentration is defined as the ratio of irradiance on the absorber to irradiance on the aperture of the collector. For the "TRUSS" subroutine, the irradiance on the absorber is given directly by the variable "E". For the other subroutines, this irradiance is obtained from "TDF", by setting $W = EL = 1.0$. Exceptions are the circular Fresnel lenses. Their absorbers would have an area of $\pi/4$ and this is divided from TDF to obtain the irradiance.

From the geometry of Fig. 1.2.5, it can be seen that

$$\tan \omega = \text{BETA}/\text{ALPHA}$$

$$\tan \psi = \text{GAMMA}/\text{ALPHA} .$$

Since ALPHA, BETA, and GAMMA are direction cosines, the above equations imply that

$$\text{ALPHA} = (1 + \tan^2 \omega + \tan^2 \psi)^{-1/2}$$

$$\text{BETA} = \tan \omega \times \text{ALPHA}$$

$$\text{GAMMA} = \tan \psi \times \text{ALPHA} .$$

Since ALPHA is the cosine of the incidence angle, the direct irradiance on the aperture is $\text{DNR} \times \text{ALPHA}$. Since concentration is the ratio of the two irradiances and DNR is simply a scaling factor, the concentration may be found directly from "TDF" or "E" by setting $\text{DNR} = 1.0/\text{ALPHA}$.

If the collectors are not tilted with respect to the horizon, the direction cosines can be converted to solar altitude and azimuth. See Fig. 1.2.5. If the azimuth is measured from the z-axis (pointing across the collector), the relationships may be expressed as

$$\text{ALT} = \text{altitude} = \arcsin (\text{ALPHA})$$

$$\text{AZI} = \text{azimuth} = \arctan (\text{BETA}/\text{GAMMA})$$

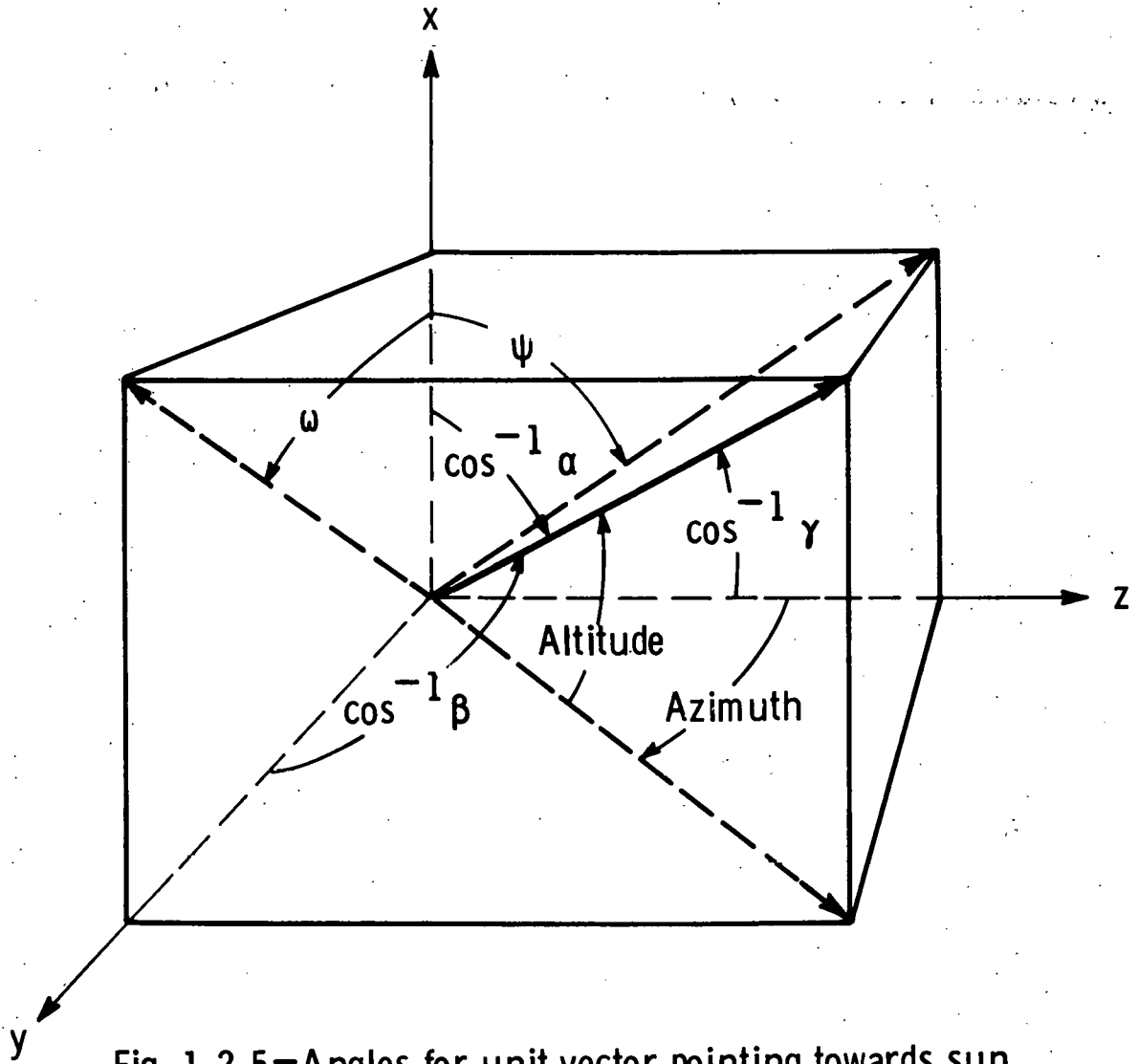


Fig. 1.2.5—Angles for unit vector pointing towards sun

The direction cosines, altitudes, azimuths, and concentrations are printed out for each collector. A sample of this output is shown. The remaining data is plotted in graphical form (Figs. 1.2.6-1.2.11).

1.2.1.5 Conclusion

The effective concentrations of the reflective collectors are plotted in Figs. 1.2.6 and 1.2.7 as functions of angle ψ . Indeed, the computer output shows that these concentrations are independent of the angle ω . Therefore, although two-axis tracking would improve light collection, one-axis tracking is sufficient for maintaining optimum concentrations.

The CPC's have nearly constant concentrations within their acceptance angles (except for some multiple reflection loss at normal incidence), but these drop sharply to zero for larger ψ . Consequently, if a CPC is fixed in a north-south orientation, direct energy would reach the absorber only for a short time each day. If it is fixed in a east-west position, no direct energy would be absorbed for some days in the year since the solar noon altitude varies nearly 50° from summer to winter, whereas the acceptance angles are 39° for the concentration 3 CPC and $11\frac{1}{2}^\circ$ for the concentration 10 CPC. Some tracking would be desirable for these CPC's.

The V-trough experiences linear variations of its concentration from 1.8 to 0 as ψ varies from 0 to $\pm 60^\circ$. The V-trough could be fixed either in a north-south position or an east-west position. In the former position, there would be fall-off of energy collection in the spring and autumn when the sun has wide variations in the east-west direction. In the latter position, the collector should be tilted toward the south in order to collect any light in the winter since the sun does not rise

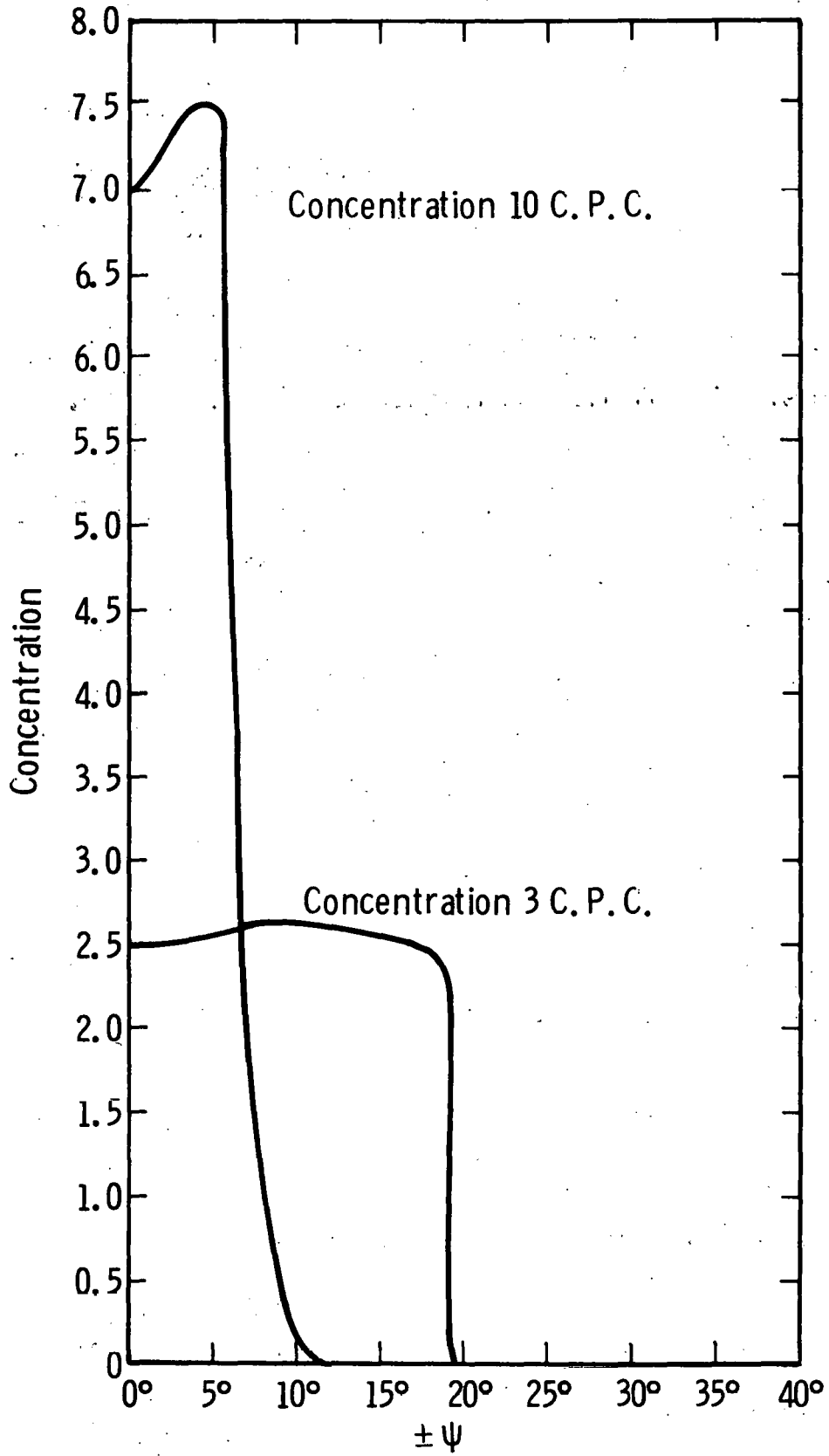


Fig. 1.2.6 - Performances of concentration 3 and 10 CPC concentrators as functions of solar incidence angle

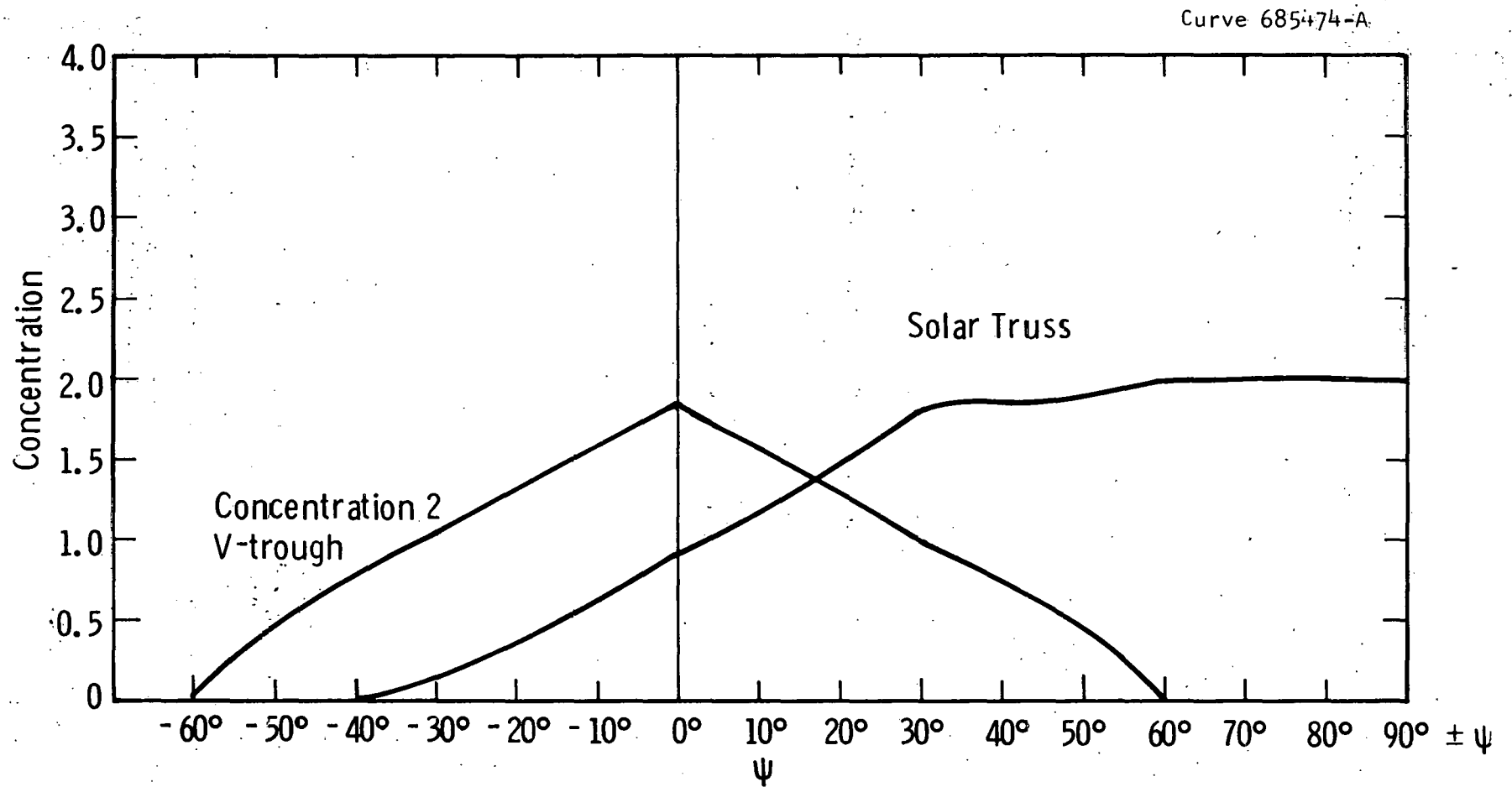


Fig. 1.2.7 — Performances of concentration 2 V-trough and solar truss collectors as functions of solar incidence angle

much above 30° altitude. With such a tilt, light collection in the summer would be lessened since the sun stays in the northern half of the sky for a good part of the morning and afternoon.

The solar truss is designed to be fixed horizontally in an east-west position. Its best concentration can be expected in the winter when the sun is in the southern half of the sky. Since insolation is higher in the summer, energy collection should be fairly uniform throughout the year.

The concentrations of the linear Fresnel lenses are shown graphically in Figs. 1.2.8-1.2.11. The periodic wiggles in the graphs are due to the relatively large sized facets of these designs. Their concentrations fall-off not only with increasing ψ but also with increasing ω . Nelson, Evans, and Bansal³ found that the concentration 3 Fresnel lens lost its effectiveness beyond two hours either side of solar noon for a one-axis tracked east-west oriented lens. The concentration 10 Fresnel lens loses its concentration even more quickly.

If the absorber is tracked on a fixed radius arm instead of the lens itself, the same effect occurs. For large values of ψ , however, the concentration remains nearly constant in ω .

Since the concentrations of the movable absorber Fresnel lens, do not decrease monotonically in ψ and ω , it is evidence that this tracking scheme is not optimum. Fixed arm tracking was chosen purely for convenience and cannot track the best line of focus. A redesign of the Fresnel lens itself and/or the tracking mechanism would produce a more efficient concentrator for one-axis tracking.

Curve 589532-A

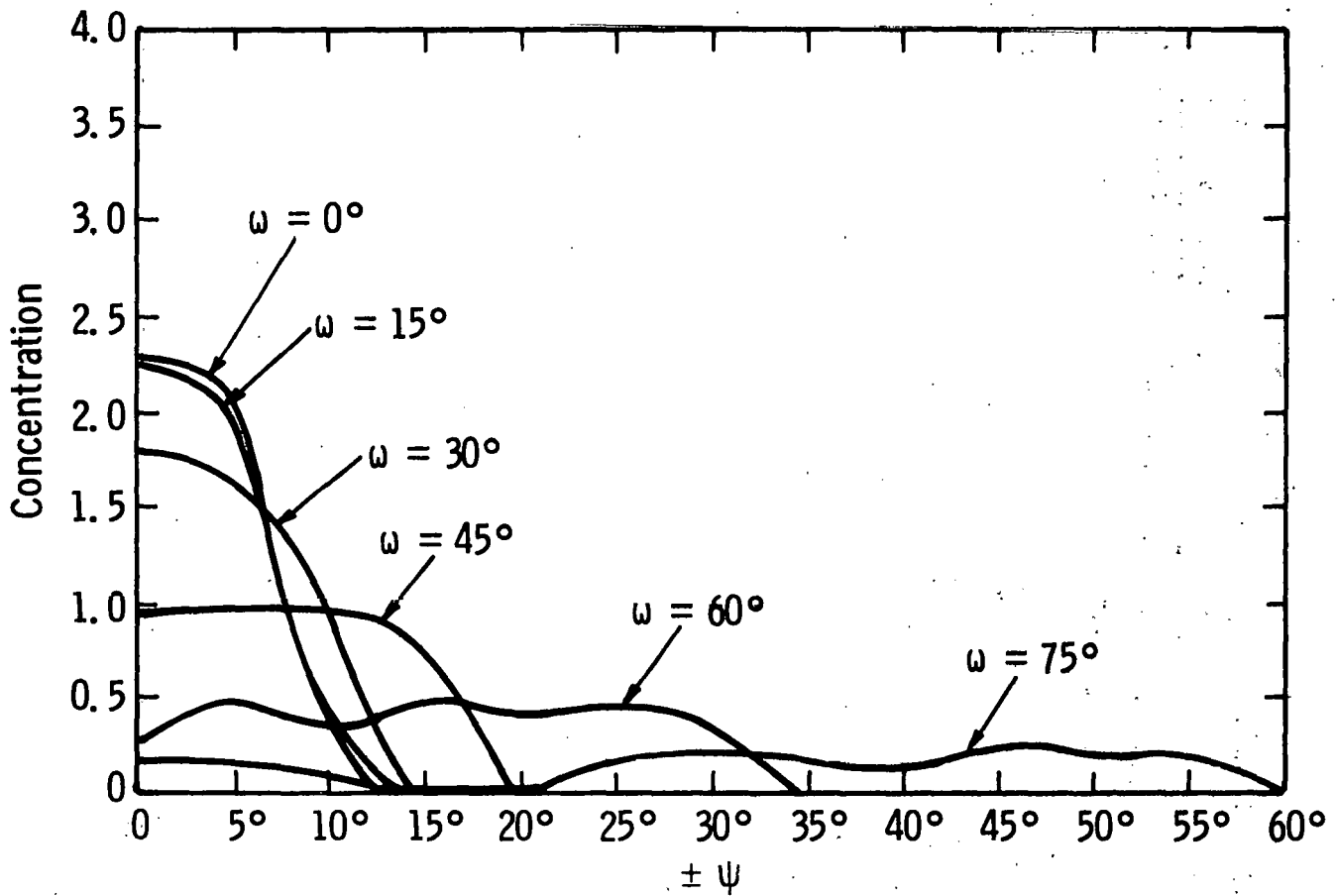


Fig. 1.2.8 — Performance of concentration 3 linear Fresnel lens as a function of solar incidence angle

Curve 689531-A

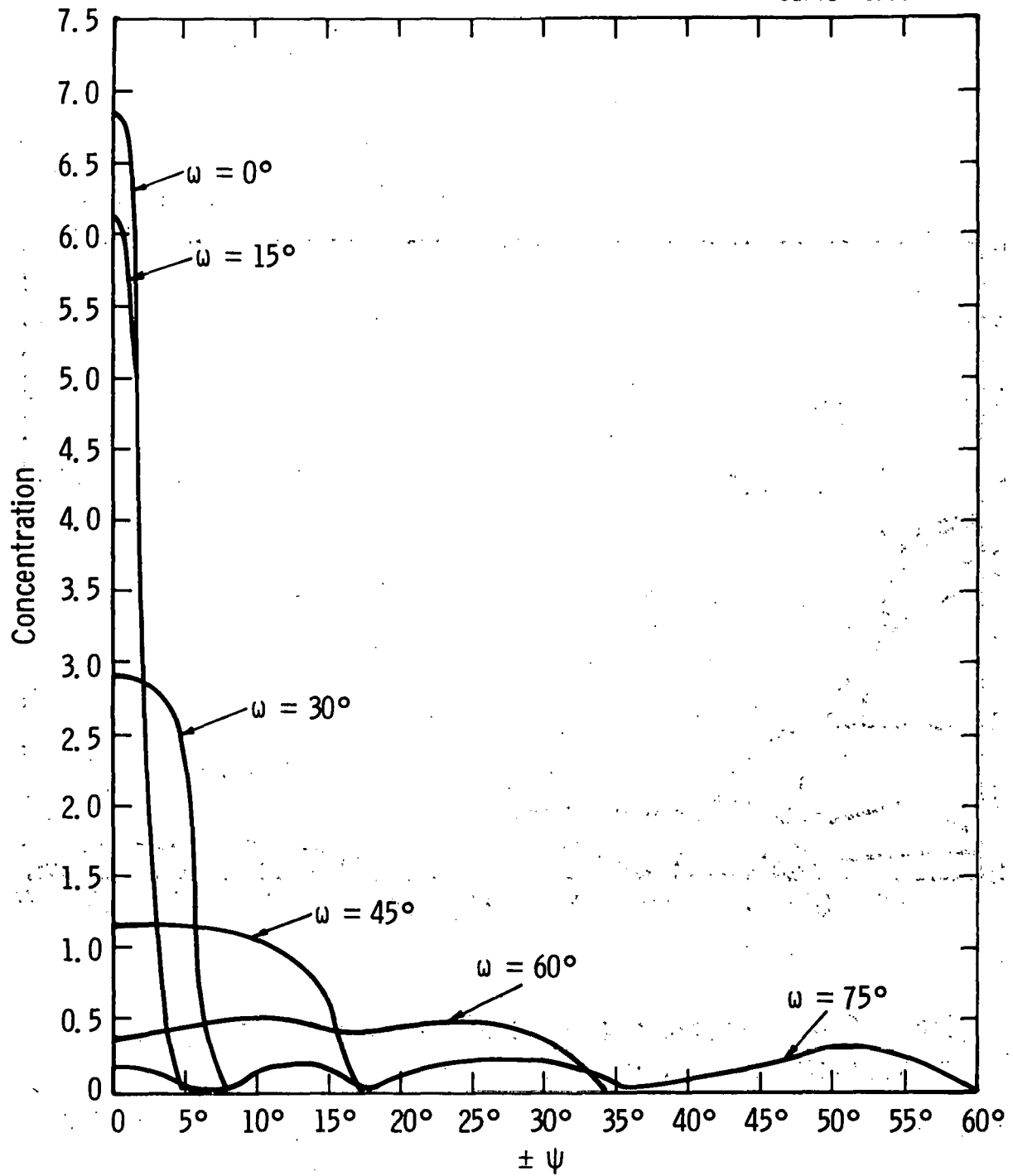


Fig. 1.2.9 — Performance of concentration 10 linear Fresnel lens as a function of solar incidence angle

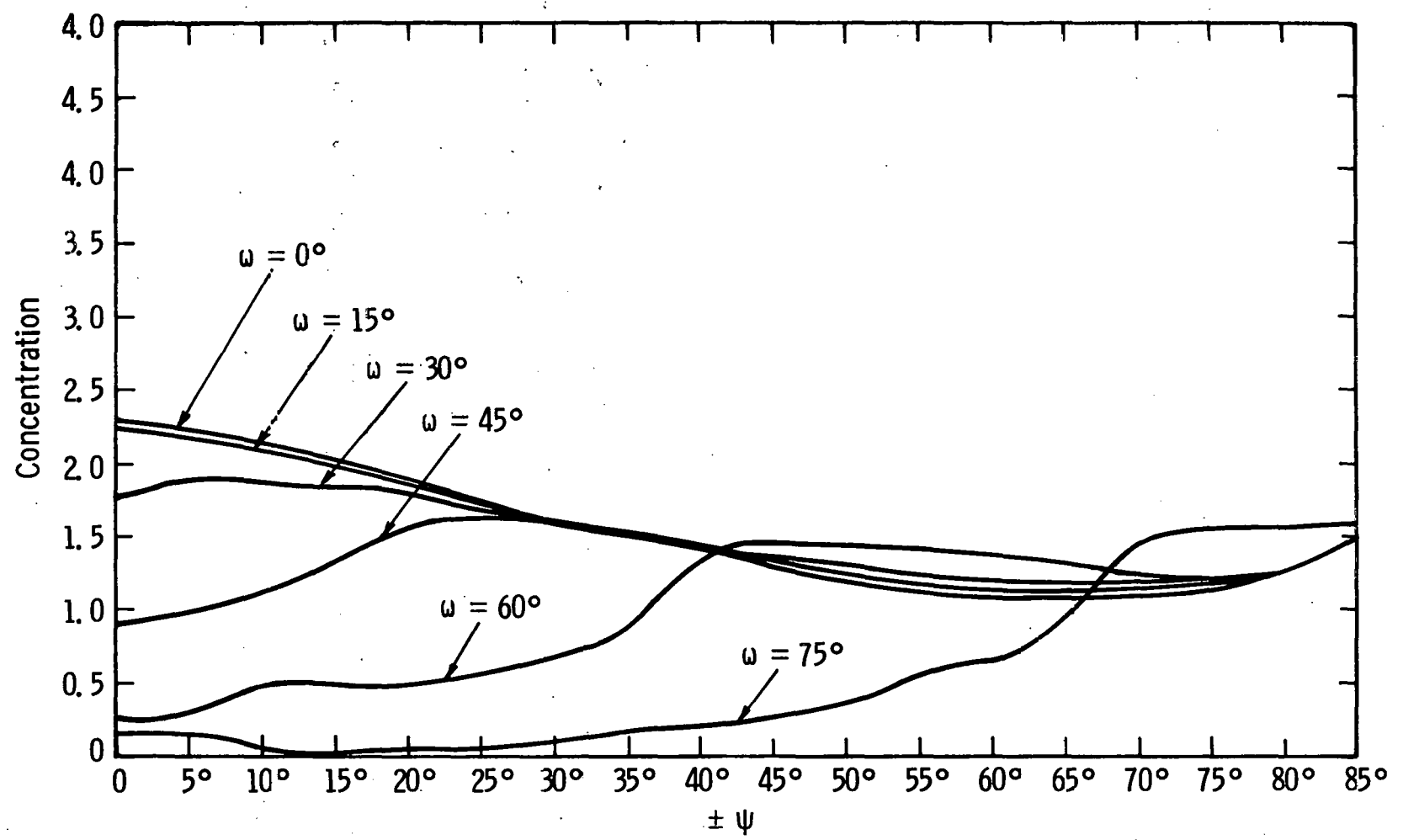


Fig. 1.2.10 - Performance of concentration 3 moveable focus linear Fresnel lens as a function of solar incidence angle

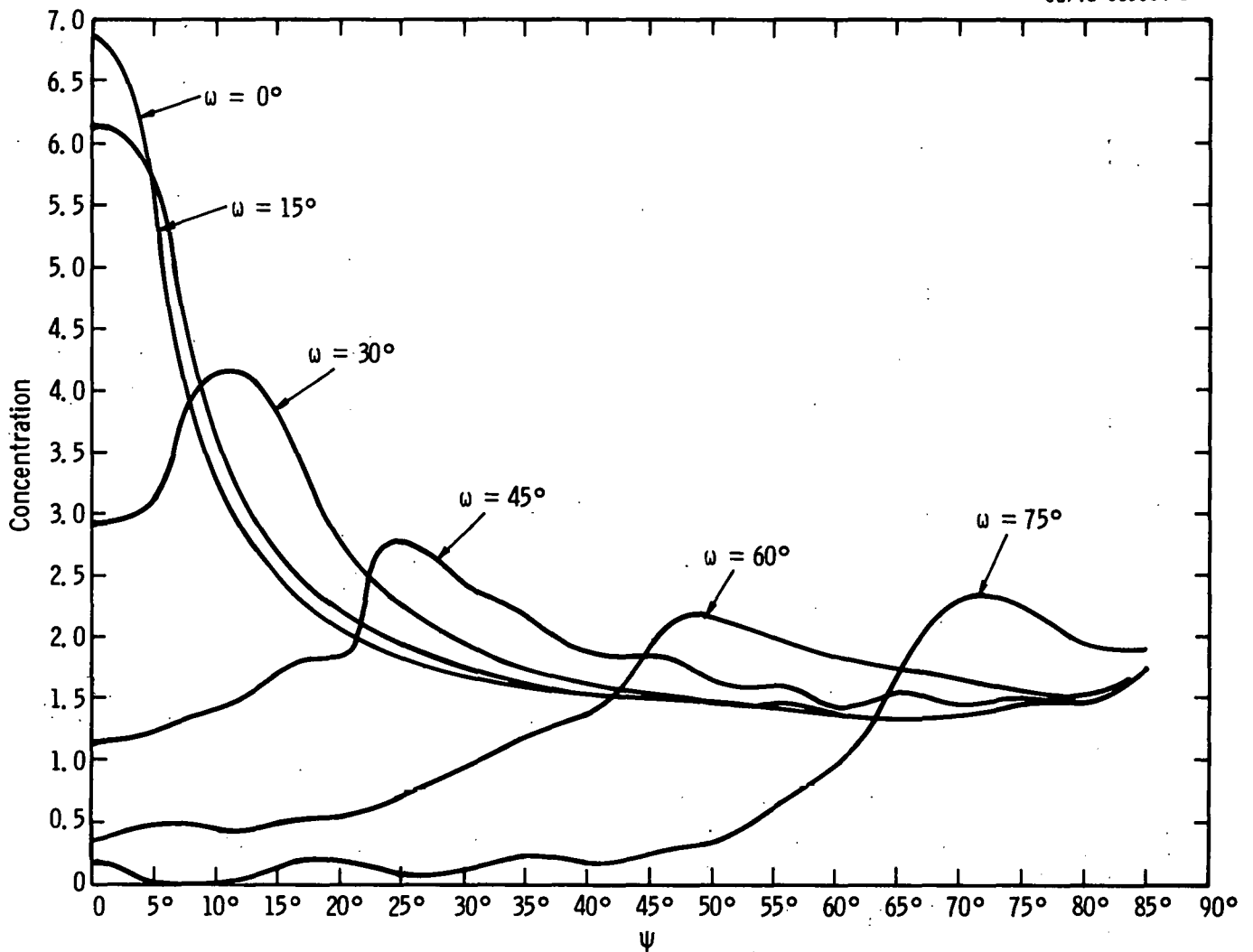


Fig. 1.2.11 - Performance of concentration 10 moveable focus linear Fresnel lens as a function of solar incidence angle

References

1. "Terrestrial Photovoltaic Power Systems with Sunlight Concentration," Progress Reports 1974-1975, prepared for the National Science Foundation (GI-41894) by Arizona State University and Spectrolab, Inc.
2. "Research Applied to Solar-Thermal Power Systems", Report No. 4 prepared for the National Science Foundation (GI-34871) by University of Minnesota and Honeywell.
3. D. T. Nelson, D. L. Evans, and R. K. Bansal, "Linear Fresnel Lens Concentrators", submitted to International Solar Energy Society Journal and 1975 Conference.
4. Max Born and Emil Wolf, "Principles of Optics", Chapter 1, Pergamon Press, 1959.
5. "Procedures for Determining Heating and Cooling Loads for Computerized Energy Calculations--Algorithms for Building Heat Transfer Subroutines", by ASHRAE Task Group on Energy Requirements for Heating and Cooling, edited by M. Takmanhekim, 1971.
6. H. Tabor, "Stationary Mirror Systems for Solar Collectors," Solar Energy, Vol. 2, Nos. 3-4, 1958, pp. 27-33.
7. Roland Winston, "Light Collection within the Framework of Geometrical Optics," J. Opt. Soc. Am., Vol. 60, No. 2, February, 1970, pp. 245-247.
8. O. E. Miller, J. H. McLeod, and W. T. Sherwood, "Thin Sheet Plastic Fresnel Lenses of High Aperture", J. Opt. Soc. Am., Vol. 41, No. 11, 1951, pp. 849-857.

1.2.2 Collector/Reflector (Solar Truss) Tilt Optimization

1.2.2.1 Introduction

The use of a reflective surface in the "dead space" between adjacent rows of fixed-orientation collectors has been proposed for photovoltaic applications. This approach has been used with success in several solar heating applications, most notable among them being the George A. Towns Elementary School in Atlanta, Georgia.

The performance characteristics of the collector/reflector combination are very sensitive to the particular design used. Changes in the inclination angles of the active and reflective surfaces affect not only the annual energy incident on the collector, but also the seasonal variations in daily energy collection as well. To investigate these effects more fully, a series of computer simulations were made in which the inclination of both the collector and reflector were varied parametrically.

The analysis employed a combination of the ASHRAE "Sun" routine and the "TRUSS" subroutine described previously to model the performance of the collector/reflector arrangement for any given set of angles.

1.2.2.2 Description of Analysis

Figure 1.2.12 shows a sketch of the configuration used and identifies the parameters. The length of the collector surface was specified to be 2.44 m (96") in order to be consistent with the reference module design which was established. Having specified the angles of both sides of the collector/reflector grouping, the remainder

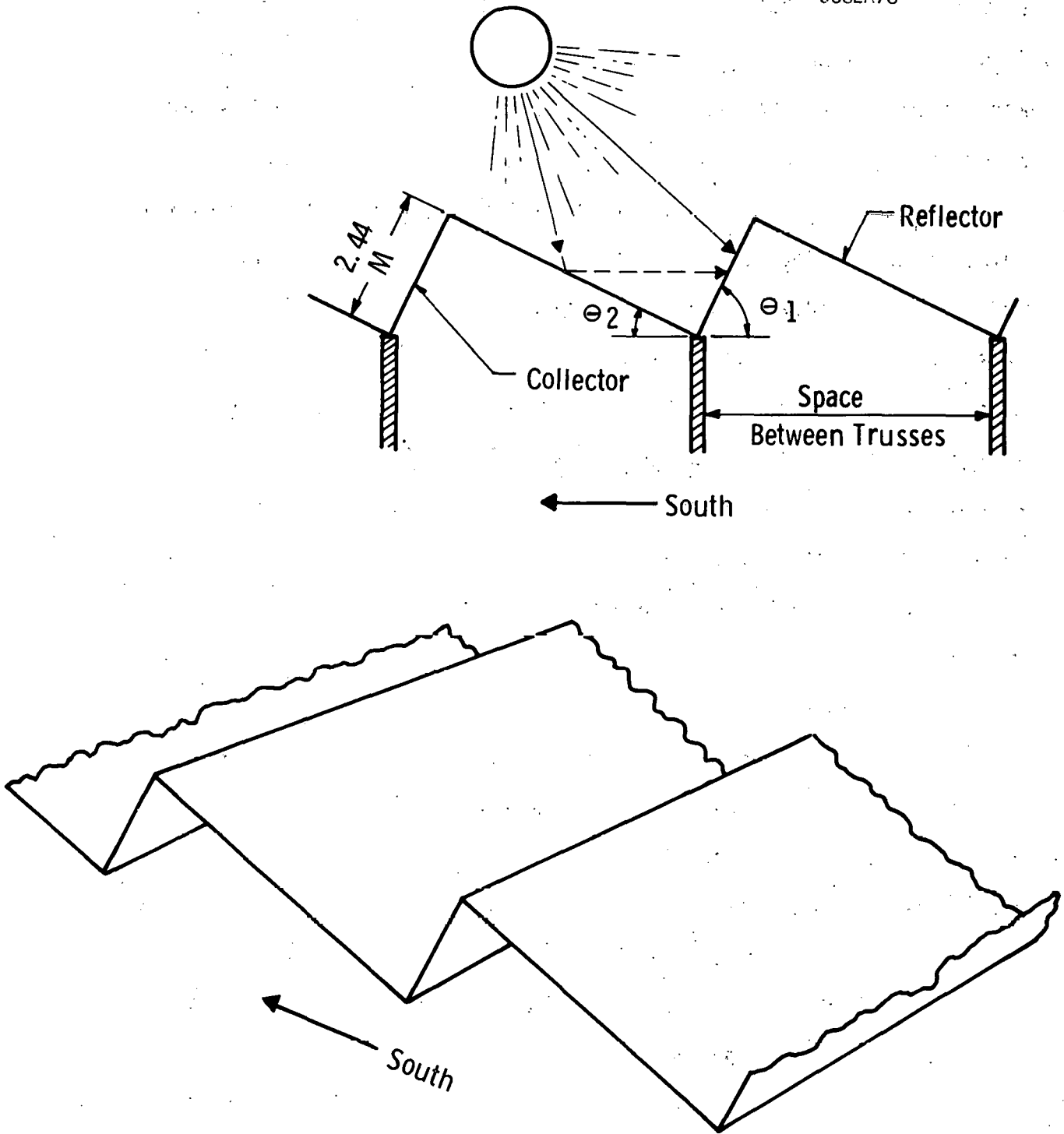


Fig. 1.2.12 - Geometry of a collector/reflector grouping

of the design is established. It should be noted that the results reported here will not be changed if a different collector length is used. The geometries would be the same (i.e., similar triangles) and, unless noted otherwise, values are specified in units per square meter of collector area.

The direct, diffuse, and reflected components of the sunlight which irradiates the absorber panel were determined individually and the total solar flux was arrived at by adding these three together. This was done for hourly increments of the twenty-first day of each month, and the hourly insolation values were then summed to obtain the energy incident on the absorber for each of the 12 days considered. A summation of the energy received on each of the 12 days yields a value representative of the annual energy collected. For the purposes of this investigation, which compares alternatives, the use of only 12 days was deemed adequate. This facilitated the analysis by minimizing the amount of data handled.

1.2.2.3 Description of Results

The study involved varying the angle of inclination of the reflector (θ_2) from 10° to 50° in 10° degree steps for collector panel orientations (θ_1) ranging from 23.43° to 73.43° (also in 10° increments). The results of the computer simulations for total and reflected energy are plotted parametrically in Figure 1.2.13, and the output summary sheets are included in Appendix B.

If total energy were the only criterion used for selection of the two angles, then a THETA 1/THETA 2 (collector angle/reflector angle)

Curve 68.836-A

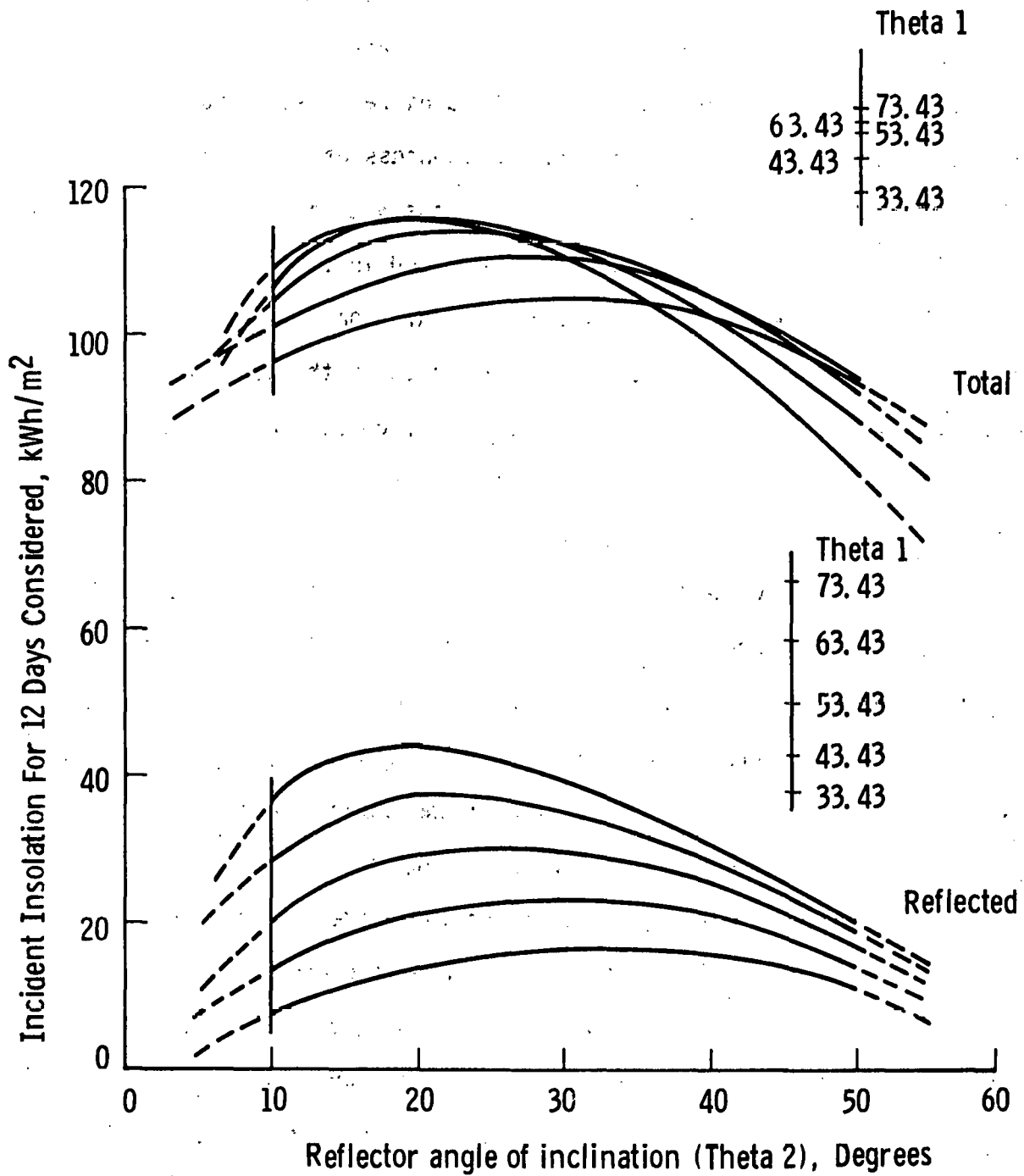


Fig. 1.2.13 - Variation of incident energy with reflector angle for various collector angles. (Phoenix location)

combination of 63/20 or 73/20 would be optimal for a Phoenix latitude site. However, a number of other considerations enter into the problem and force a more subjective selection of design variables. Among the items which should be considered are the area required, annual energy collection, peak insolation, and the evenness of the isolation profile. Factors related to these considerations and pertinent to the selection of an "optimum" design are listed in Table 1.2.1

The base area required for a particular geometry may or may not be important, depending on the relative values of the collector and the mounting areas. Where roof mounting is required the available area may limit the ultimate size of the system, and effective area utilization may be of primary concern.

A high peak value of solar flux is desirable to reduce the specific cost (in dollars per kilowatt) of the system. However, the ratio of the total incident energy to the peak flux, a measure somewhat analogous to the capacity factor, decreases as this peak level is increased; indicating a lower utilization of the other components of the system if they are sized for the peak output.

The seasonal derating factor gives the range (in per cent of peak) within which the daily peaks will vary over the course of the year. Perhaps even more significant is the ability to select the reflector angle to augment either the summer or winter performance or varying proportions of each. This is best illustrated by the parametric plots of Figure 1.2.14, which show the way in which variations in the reflector tilt angle affect the reflected component, and thus the total

TABLE 1.2.1

Summary of Performance Characteristics for a
Collector/Reflector System

<u>Collector/ Reflector Angle</u>	<u>Base Area Per m² Collector</u>	<u>Total^{1,2} Incident Energy (kWh/m²)</u>	<u>Peak¹ Solar Flux (kW/m²)</u>	<u>Minimum Daily Peak Flux (kW/m²)</u>	<u>Total Energy Peak Flux (Hrs.)</u>	<u>Seasonal De-Rating (<u>Min. Peak</u> <u>Max. Peak</u>)</u>
33/20	2.35	102.9	1.50	1.00	68.6	0.67
33/30	1.79	104.4	1.54	1.03	67.8	0.67
33/40	1.49	102.2	1.42	0.88	72.0	0.67
43/20	2.62	108.8	1.66	0.96	65.5	0.58
43/30	1.92	109.7	1.63	1.10	67.3	0.67
43/40	1.55	104.9	1.45	0.92	72.3	0.63
53/20	2.80	113.6	1.76	0.99	64.5	0.56
53/30	1.99	112.4	1.68	1.15	66.9	0.68
53/40	1.55	104.9	1.44	0.93	72.8	0.65
63/20	2.90	115.9	1.82	1.00	63.7	0.55
63/30	2.00	112.2	1.68	1.16	66.8	0.69
63/40	1.51	102.3	1.40	0.92	73.1	0.65
73/20	2.92	115.5	1.82	0.98	63.5	0.54
73/30	1.95	109.1	1.64	1.14	66.5	0.70

¹Per m² of Collector.

²Based on 12 days/year

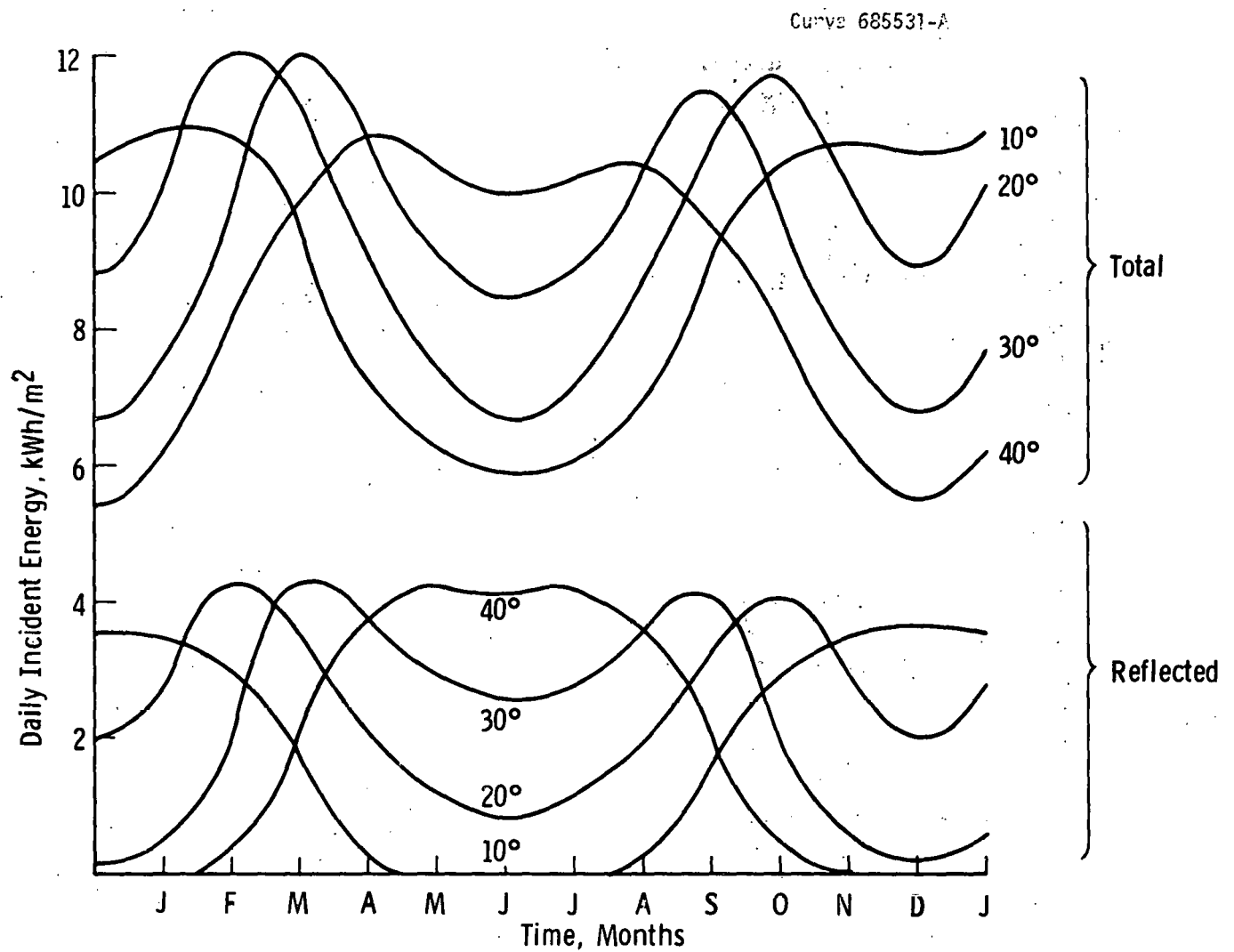


Fig. 1, 2, 14 - Daily incident energy profile for collector tilted at 53.43° (Phoenix location)

energy of the absorber panel. Shallow angles serve to augment the winter collection whereas a steeper angle will enhance the summer performance. A steeper angle also requires less mounting area, but collects slightly less energy and has a lower peak value of insolation. For a summer-peaking utility owner, the ability to generate at higher levels in the summer would offset the lower annual collection. Therefore, the actual design used will be determined by specific application.

Plots of the daily energy collection for four collector/reflector combinations which had a high value of total incident energy are shown in Figure 1.2.15. The 63/20 and 73/20 arrangements exhibit slightly higher energy collection capabilities than the 53/30 and 63/30 cases, but the daily values vary over a wider range with the minimum occurring in June. The 63/20 and 73/20 cases also require about 50% more area. Because the Phoenix area utilities are summer peaking and the land utilization is better with the 53/30 and 63/30 cases, these were preferred. Although there is a minor reduction in the energy collection for the cases selected (about 3%), it is expected that the higher summertime production (30% greater) will more than offset this. The 53/30 system has a slight edge relative to 63/30 in regard to most of the performance indices listed in Table 1.2.1, and therefore it was chosen as the collector/reflector system to be used in the system analyses of this program.

The incident insolation profile has the same basically sinusoidal shape from day to day throughout the year, as shown in Figure 1.2.16. Only the magnitude (and some time of operation) varies between the best

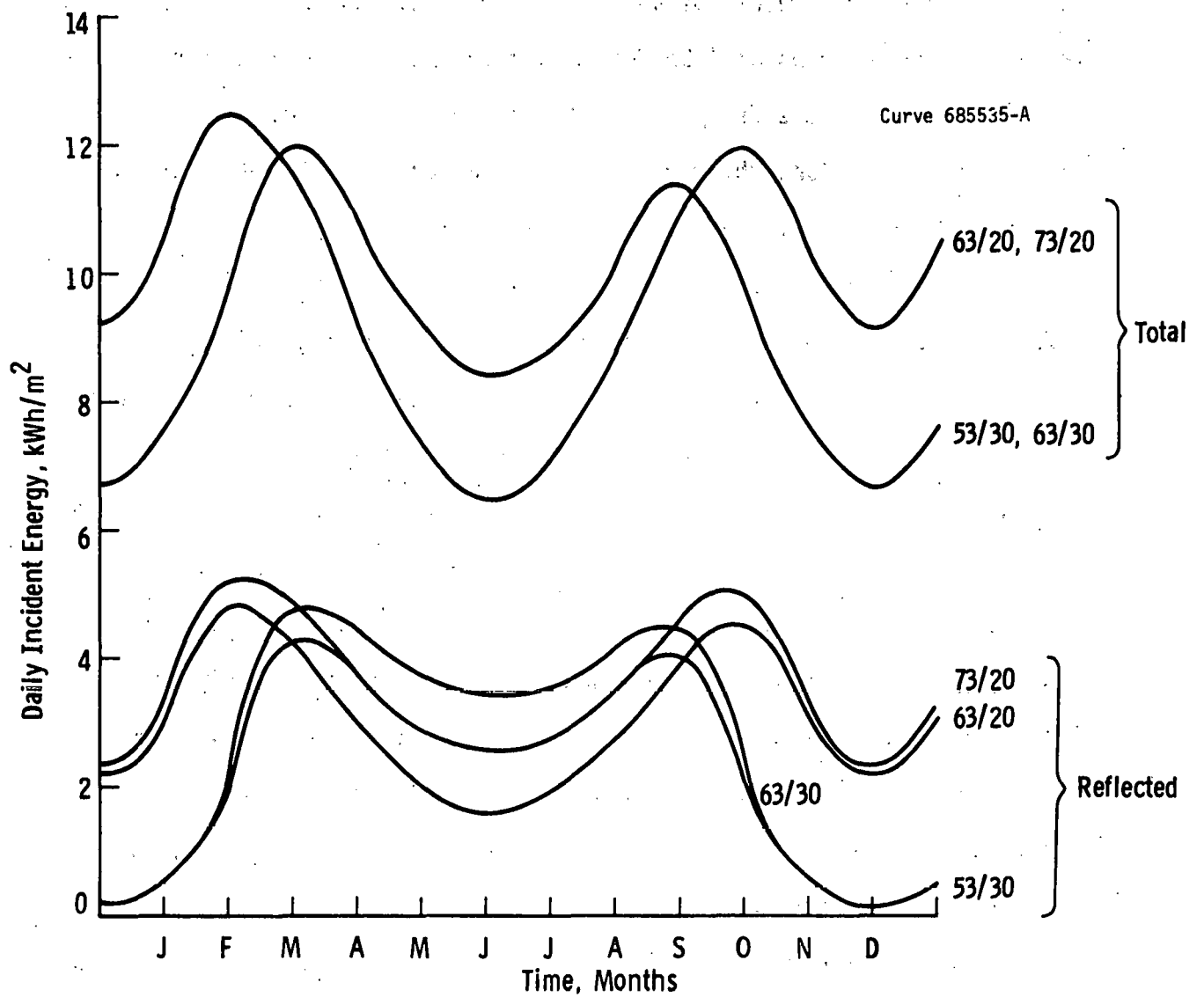


Figure 1,2, 15 – Variation of daily incident energy over a year for various collector and reflector angles. (Phoenix location)

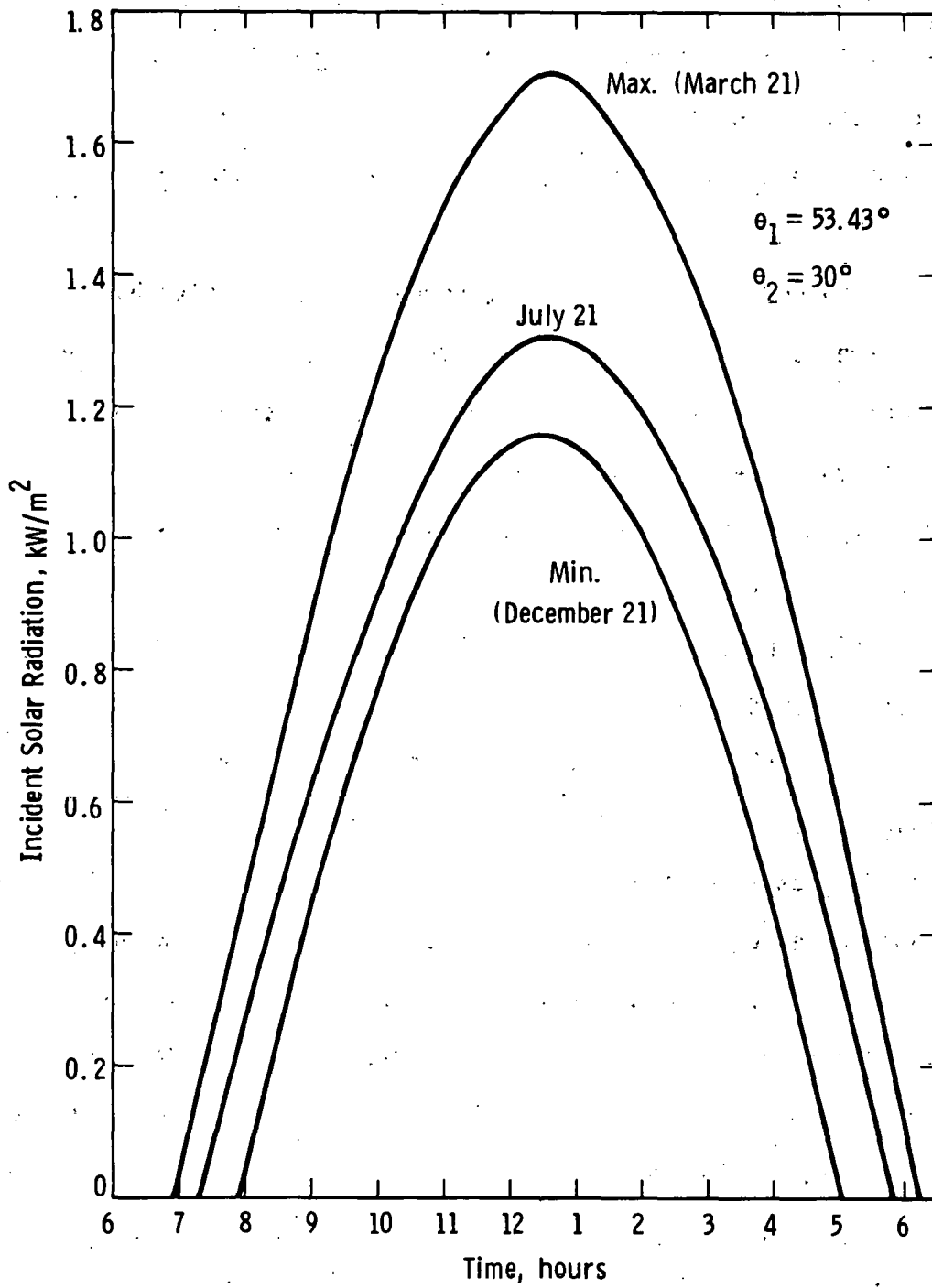


Fig. 1, 2, 16 – Seasonal variation of incident radiation profile (Phoenix)

and worst case. A duration curve, which shows the amount of time the solar irradiation of the collector plate is above a given level, is plotted in Figure 1.2.17. For a constant conversion efficiency, a 53/30 system delivers in excess of 50% of its peak capacity for 5 hours in December and 8 hours in March. As is the case with the hourly profile, the shape of the duration curve does not change appreciably. The energy collected by the absorber is represented by the area within the duration curve, so the effects of seasonal variation on energy collection can be seen as the area between two curves. The impact of system requirements which allow operation only to some level below peak capacity can also be quickly assessed with these curves. An "annual" duration curve has also been plotted (Figure 1.2.18) to show the way in which the varying levels of incident radiation affect performance. In contrast to the daily duration curve, which has a gradual roll-off from the peak, the annual curve shows a pronounced peak which only begins to taper off at about 80% of peak. The amount of this peak is indicative of the amount of system capacity needed to handle only a small percentage of the total energy, but requiring an equal expenditure in power conditioning equipment. It is particularly interesting to compare this curve with that for two-axis tracking. The comparison serves to highlight the highly variable nature of the output which can be expected from a collector/reflector system when used for photovoltaic applications.

Curve 685534-A

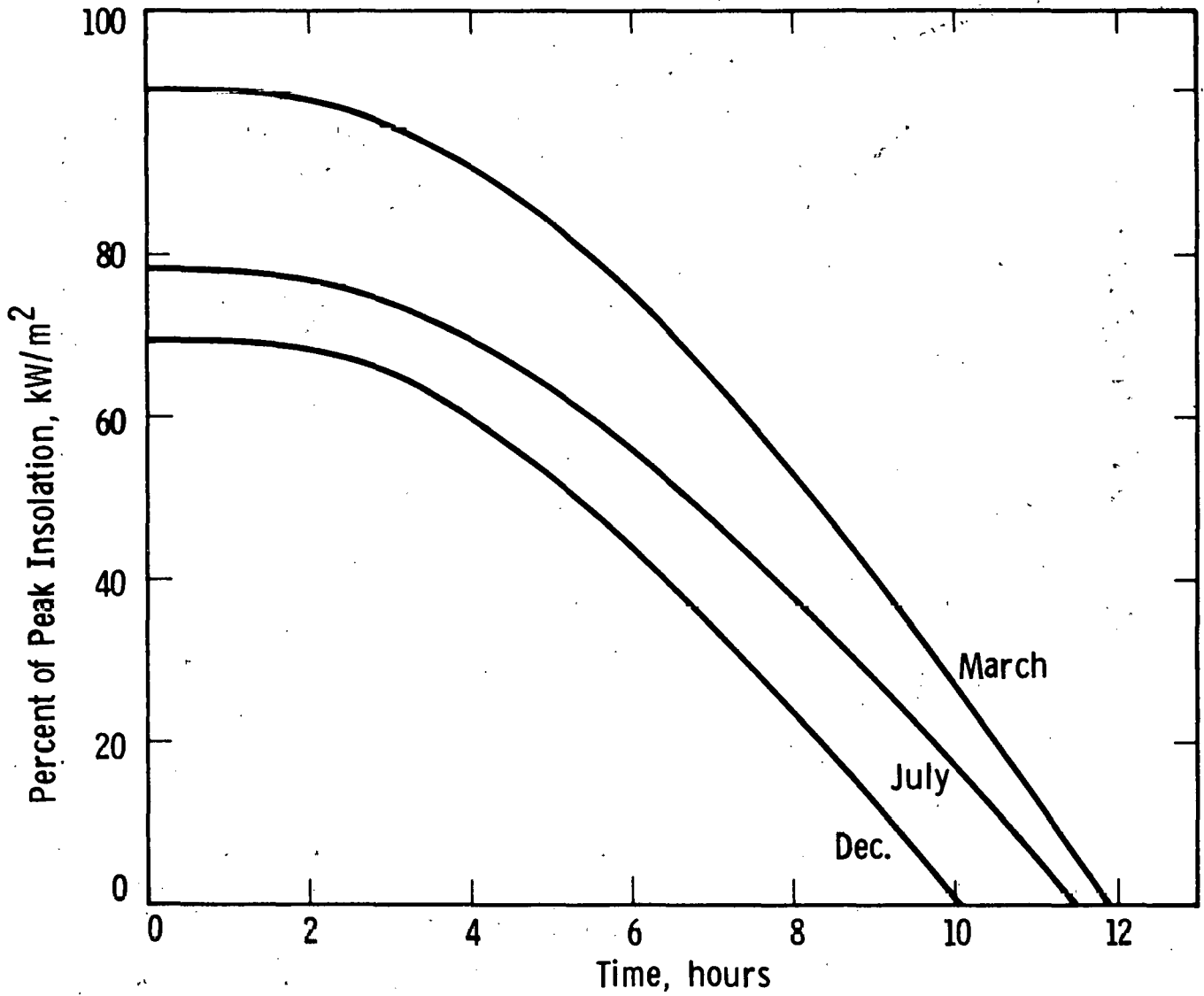


Fig. 1, 2, 17 — Daily duration curve of incident insolation for 53/30 collector/reflector (Phoenix location)

Curve 685533-A

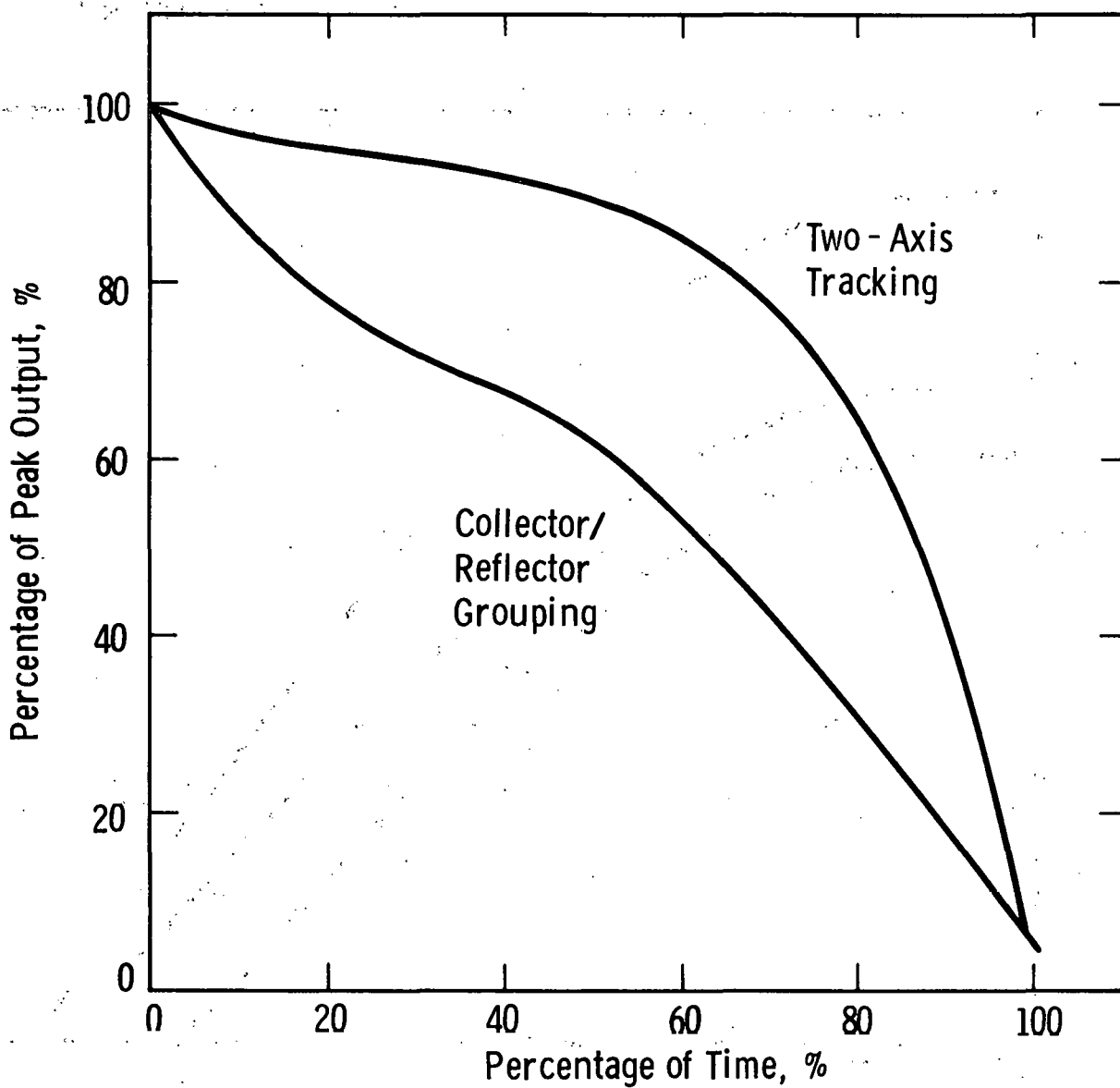


Fig. 1,2, 18 - Annual output power duration curves
(Phoenix location)

APPENDIX A

OPTICAL ANALYSIS COMPUTER PROGRAM LISTING

SOLAR CONCENTRATORS

DATE 111676

PAGE 3

```

00141 28* TDF = TDF*4.*PI*
00142 29* #WRITE(KOUT,1002) TDF
00143 30* 1002 FORMAT(1A,22H10CON CIRCULAR FRFSNEL,18X,1F5.2)
00144 31* ALT = 90.
00145 32* AZI = 0.
00150 33* DO 100 I = 1,6
00153 34* DO 50 J = 1,18
00156 35* IF (I.EQ.1.AND.J.EQ.1) GO TO 10
00160 36* ALT = ASIN(ALPHA)/PI
00161 37* AZI = ATAN2(META,GAMMA)/PI
00162 38* 10 WRITE(KOUT,1003) A,PHA,META,GAMMA,ALT,AZI
00171 39* 1003 FORMAT(1H0,6HALPHA=.1F5.3,1X,5HBETA=.1F5.3,1X,6HGAMMA=.1F5.3,
00171 40* 1X,9HAZI TDF=.1F8.3,1X,RHAZIMUTH=.1F8.3//)
00172 41* DNR = 1./ALPHA
00173 42* LINE = 1
00174 43* CON = 3.
00175 44* CALL FRENEL
00176 45* WRITE(KOUT,1004) TDF
00201 46* 1004 FORMAT(1X,34H3CON 40VEARLF FOCUS LINEAR FRESNEL,6A,1F5.2)
00202 47* CON = 10.
00203 48* CALL FRENEL
00204 49* WRITE(KOUT,1005) TDF
00207 50* 1005 FORMAT(1X,35H10CON MOVEABLE FOCUS LINEAR FRESNEL,5X,1F5.2)
00210 51* LINE = 0
00211 52* CON = 3.
00212 53* CALL FRENEL
00213 54* WRITE(KOUT,1006) TDF
00216 55* 1006 FORMAT(1X,19H3CON LINEAR FRESNEL,21X,1F5.2)
00217 56* CON = 10.
00220 57* CALL FRENEL
00221 58* WRITE(KOUT,1007) TDF
00224 59* 1007 FORMAT(1X,20H10CON LINEAR FRFSNEL,20X,1F5.2)
00225 60* CALL TRUSS
00226 61* WRITE(KOUT,1008) TDF
00231 62* 1008 FORMAT(1X,11HSOLAR TRUSS,24X,1F5.2)
00232 63* CALL TROUGH
00233 64* WRITE(KOUT,1009) TDF
00236 65* 1009 FORMAT(1X,13H2CON #TROUGH,27X,1F5.2)
00237 66* CON = 3.
00240 67* CALL #INSTN
00241 68* WRITE(KOUT,1010) TDF
00244 69* 1010 FORMAT(1X,12H3CON #INSTON,28X,1F5.2)
00245 70* CON = 10.
00246 71* CALL #INSTN
00247 72* WRITE(KOUT,1011) TDF
00252 73* 1011 FORMAT(1X,13H10CON #INSTON,27X,1F5.2)
00253 74* TA = TAN(DA*J)
00254 75* ALPHA2 = 1./(1.+TR2+TA**2)
00255 76* ALPHA = SQRT(ALPHA2)
00256 77* BETA = TB*ALPHA
00257 78* GAMMA = TA*ALPHA
00260 79* 50 CONTINUE
00262 80* TB = TAN(DB*1)
00263 81* TB2 = TB**2
00264 82* ALPHA2 = 1./(1.+TR2)
00265 83* ALPHA = SQRT(ALPHA2)
00266 84* BETA = TB*ALPHA
00267 85* GAMMA = 0.
00270 86* 100 CONTINUE
00272 87* END

```

END OF COMPILATION: NO DIAGNOSTICS.

#FOR,15 FRENEL
 FOR DT-3-11/16/76-18:53:35 (10)

SUBROUTINE FRENEL ENTRY POINT 001431

STORAGE USED: (CDF(1)) 001944; DATA(0) 180652; BLANK COMMON(2) 000012

EXTERNAL REFERENCES (HLOCK, NAME)

SOLAR CONCENTRATORS

DATE 111674

PAGE 6

```

00125 430 DO 2 I= 1,N
00130 440 X(I)= X(I,1)**2
00131 450 2 Z(I)= Z(I,1)**2
00133 460 GO TO 5
00134 470 3 X1= 8.*#
00135 480 N= 20
00136 490 ZMAX= 5.*#
00137 500 DO 4 I= 1,N
00142 510 X(I)= X(I,2)**2
00143 520 4 Z(I)= Z(I,2)**2
00145 530 5 CONTINUE
00146 540 OTHET= ATAN(W2/XT)
00147 550 AU= 1.
00150 560 CU= 0.
00151 570 XU= 0.
00152 580 ZO= -W2
00153 590 ZA= 0.
00154 600 XK= XT
00155 610 EN= 1.49
00156 620 ENR= 1./EN
00157 630 EN2= EN**2
00160 640 ALPHA1= SQRT(EN2+ALPHA**2-1.) *ENN
00161 650 BETA1= BETA*ENN
00162 660 GAMMA1= GAMMA*ENN
00163 670 TPER1= 4.*EN*ALPHA*ALPHA1
00164 680 TPAR1= TPER1/(EN*ALPHA+ALPHA1)**2
00165 690 TPER1= TPER1/(ALPHA+EN*ALPHA1)**2
00166 700 XKU= XK
00167 710 ANG= 0.
00170 720 TR= 0.
00171 730 DO 500 K= 1,N
00172 740 ZK1= Z(K)
00175 750 AK2= X(K)
00176 760 AKZ= ZK1-ZK
00177 770 CK= 2.*(XK-XT)
00200 780 DEN= 1./SQRT(AK**2+EK**2)
00201 790 AK= AK*DEN
00202 800 CK= CK*DEN
00203 810 XK1= 2.*AT-XK
00204 820 DO 400 I= 1,2
00207 830 TRANS= 0.
00210 840 T= GAMMA1*AK-CK*ALPHA1
00211 850 BETA12= BETA1**2
00212 860 BETA2= 1.-EN2*(BETA 2-T**2)
00213 870 AC= ALPHA1*AK+GAMMA1*CK
00214 880 IF (BETA2 .LE. 0. *#R. AC .LF.0.) GO TO 399
00216 890 BETA2= SQRT(BETA2)
00217 900 ALPHA2= BETA2*AK-CK*T*EN
00220 910 GAMMA2= BETA2*CK+AK*T*EN
00221 920 BETA2= EN*BETA1
00222 930 AC2= ALPHA2*AK+GAMMA2*CK
00223 940 IF (ALPHA2 .LE. 0. .OR. AC2 .LE. 0.) GO TO 399
00225 950 TPER2= 4.*EN*AC*AC2
00226 960 TPAR2= TPER2/(AC+EN*AC2)**2
00227 970 TPER2= TPER2/(EN*AC+AC2)**2
00230 980 CT2= BETA12*CK**2
00231 990 IF (BETA12 .NE. 0.)
00231 1000 ICT2= CT2/(CT2+(GAMMA1*T+AK*BETA12)**2)
00233 1010 TRANS= .5*(CT2*(TPAR1+TPER2+TPAR2+TPER1)**2+ICT2)
00233 1020 1 (TPAR1+TPAR2+TPER1+TPER2)
00234 1030 IF (LIN .LE. 0) GO TO 11
00236 1040 TDF= TDF+(ZK1**2-ZK**2)*TRANS
00237 1050 GO TO 401
00240 1060 11 DEN= GAMMA2*CU+ALPHA2*AD
00241 1070 XK12= XK-AKU
00242 1080 X2= XK
00243 1090 Z2= ZK
00244 1100 IF (XK12 .GT. 0. .AND. GAMMA2 .GT. 0.) X2= AKU
00246 1110 IF (XK12 .GE. 0. .OR. GAMMA1 .GE. 0.) GO TO 20
00250 1120 X2= (GAMMA1*CK+XKU*ALPHA1+AK*XK1)/AC
00251 1130 Z2= ZK +GAMMA1*AK*XK12/AC
00252 1140 20 TD= (GAMMA2*(X0-X2)*ALPHA2+(Z2-Z0))/DEN
00253 1150 XK12= XK1-XK2
00254 1160 IF (XK12 .LT. 0. .AND. GAMMA1 .GT. 0.) GO TO 30
00254 1170 X2= XK1
00257 1180 Z2= ZK1

```

```

000032
000032
000034
000040
000042
000044
000046
000055
000055
000057
000064
000064
000071
000073
000074
000075
000077
000100
000102
000104
000106
000110
000121
000124
000127
000135
000143
000152
000153
000154
000206
000214
000216
000220
000222
000224
000237
000241
000244
000262
000300
000301
000305
000307
000314
000320
000332
000335
000343
000352
000354
000360
000373
000377
000405
000414
000417
000417
000433
000433
000454
000456
000461
000463
000470
000472
000474
000474
000476
000514
000530
000536
000545
000555
000557
000577
000574

```

SOLAR CONCENTRATORS

DATE 111676

PAGE 6

```

00260 .119. IF (GAMMA2 .LT. 0. .AND. AK12 .GT. 0.) X2= XK2
00262 .120. GO TO 40
00263 .121. 30 X2= (GAMMA1*CK*XK2+ALPHA1*AK*XK1)/AC
00264 .122. Z2= ZK1+GAMMA1*AK*XK12/AC
00265 .123. 40 T1= (GAMMA2*(10-X2)+ALPHA2*(Z2-Z0))/DEN
00266 .124. ZUT1= Z0+T1
00267 .125. ZUT0= Z0+T0
00270 .126. IF (I .EQ. 1) GO TO 50
00272 .127. T= TU
00273 .128. TU= -T1
00274 .129. T1= -T
00275 .130. GAMMA2= -GAMMA2
00276 .131. ZUT0= -Z0+T0
00277 .132. ZUT1= -Z0+T1
00300 .133. 50 CONTINUE
00301 .134. ZET0(K,1)= T0
00302 .135. ZET1(K,1)= T1
00303 .136. IF (L1N .GE. 0 .ON. T1 .LE. T0) GO TO 80
00305 .137. PSI= ATAN(GAMMA2/ALPHA2)
00306 .138. AG= SQRT(ALPHA2**2+GAMMA2**2)
00307 .139. SPT= (GAMMA2+ALPHA2*(ZUT1)/XT)/AG
00310 .140. SPT2= SPT**2
00311 .141. IF (SPT2 .LT. 1.) GO TO 60
00313 .142. THET0= SIGN(P1*.5.SPT)
00314 .143. GO TO 65
00315 .144. 60 PT= ATAN(SPT/SQRT(1.-SPT2))
00316 .145. THET0= PT-PSI
00317 .146. THET1= SIGN(P1.PT)-PT-PSI
00320 .147. IF (COS(THET1) .GT. COS(THET0)) THFT0= THET1
00322 .148. 65 SPT= (GAMMA2+ALPHA2*(ZUT1)/XT)/AG
00323 .149. SPT2= SPT**2
00324 .150. IF (SPT2 .LT. 1.) GO TO 70
00326 .151. THET1= SIGN(P1*.5.SPT)
00327 .152. GO TO 75
00330 .153. 70 PT= ATAN(SPT/SQRT(1.-SPT2))
00331 .154. THET1= PT-PSI
00332 .155. THET1= SIGN(P1.PT)-PT-PSI
00333 .156. IF (COS(THET1) .GT. COS(THET0)) THET1=THET1
00335 .157. 75 THETA= (THET0+THET1)*.5
00336 .158. THMIN= AMIN(THET0,THMIN)
00337 .159. THMAX= AMAX(THET1,THMAX)
00340 .160. ANG= THETA+TRANS+ANG
00341 .161. TR= TRANS+ TR
00342 .162. 80 IF ( T1 .LE. T0 .ON. T0 .GT. W .ON. T1 .LE. 0.) GO TO 399
00344 .163. TU= AMAX(0.,TU)
00345 .164. T1= AMIN(W,T1)
00346 .165. TDF= TDF+(T1-T0)*DEN*TRANS
00347 .166. 399 IF (L1N .GT. 0) GO TO 401
00351 .167. GAMMA1= -GAMMA1
00352 .168. ZU= -Z0
00353 .169. CU= -CU
00354 .170. F(K,1)= DEN*TRANS
00355 .171. GAMM(K,1)= GAMMA2
00356 .172. AL(K,1)= ALPHA2
00357 .173. 400 CONTINUE
00361 .174. 401 CONTINUE
00362 .175. XK= XK2
00363 .176. XK0= XK1
00364 .177. ZK= ZK1
00365 .178. 500 CONTINUE
00367 .179. IF (L1N) 600,700,800
00372 .180. 600 ANG= ANG/TR
00373 .181. IF (ANG-THMIN .LT. DTHFT .AND. THMAX-ANG .GT. DTHET)
00373 .182. IANG= THMIN+DTHET
00375 .183. IF (THMAX-ANG .LT. DTHET .AND. ANG-THMIN .GT. DTHET)
00375 .184. IANG= THMAX-DTHET
00377 .185. AU= COS(ANG)
00400 .186. CU= -SIN(ANG)
00401 .187. XU= XT*(1.-AU)*(C0**2)
00402 .188. ZU= -XT*CU-AD**2
00403 .189. X2= 0.
00404 .190. TDF= 0.
00405 .191. DU 65U I=1,2
00410 .192. DU 63U K=1,0
00413 .193. Z2= -W2*ZET0(K,1)
00414 .194. GAMMA2= GAMM(K,1)

```

000576
000614
000616
000623
000632
000642
000644
000647
000652
000654
000656
000657
000661
000663
000666
000666
000667
000671
000705
000713
000724
000732
000734
000737
000743
000745
000757
000761
000767
001002
001007
001011
001014
001020
001022
001034
001036
001044
001057
001062
001070
001074
001101
001105
001130
001134
001144
001152
001154
001156
001160
001162
001165
001167
001174
001174
001174
001175
001177
001203
001203
001206
001211
001211
001234
001234
001257
001262
001265
001273
001301
001307
001311
001311
001311

SOLAR CONCENTRATORS

DATE 111676 PAGE 8

00133 34* RETURN
00134 35* END

000126
000143

END OF COMPIATION: NO DIAGNOSTICS.

QFOR IS VTRGM
FOR DT-3-11/16/76- 8:54:19 (L0)

SUBROUTINE VTRGM ENTRY POINT 000057

STORAGE USED: CODE(1) 000062; DATA(0) 000012; BLANK COMMON(2) 000012

EXTERNAL REFERENCES (BLOCK, NAME)

0003 SQRT

STORAGE ASSIGNMENT (BLOCK, TYPE, RELATIVE LOCATION, NAME)

0003	000021	UL	0001	000041	ZOL	0001	000054	ZOL	0002	K	000000	ALPHA	0002	000001	BETA			
0002	000006	CUN	0002	K	000003	DNR	0000	000003	DYN	0002	000011	E	0002	K	000005	EL		
0002	K	000002	GAMMA	0002	000007	LIN	0000	K	000001	REFL	0000	K	000000	SQ3	0000	K	000002	TAE#V
0002	K	000010	TDF	0002	K	000004	*											

00101	1*				SUBROUTINE VTRGM								000000	
00101	2*	C	(ALPHA,BETA,GAMMA)	ARE	THE	DIRECTION	COSINES	OF	THE	SUN	RELATIVE	TO	THE	000000
00101	3*	C	COLLECTOR	IN	A	RIGHT	HANDED	COORDINATE	SYSTEM;	X-AXIS	POINTING	UPWARDS	AND	000000
00101	4*	C	NORMAL	TO	THE	ABSORBER,	Y-AXIS	ALONG	THE	AXIS	OF	THE	TROUGH,	000000
00101	5*	C	Z-AXIS	CROSS	THE	TROUGH.							000000	
00101	6*	C	DNR	IS	DIRECT	NORMAL	RADIATION	IN	FLUX	PER	UNIT	AREA.	000000	
00101	7*	C	W	IS	WIDTH	OF	ABSORBER.						000000	
00101	8*	C	EL	IS	LENGTH	OF	ABSORBER.						000000	
00101	9*	C	TDF	IS	TOTAL	DIRECT	FLUX	ON	ABSORBER.				000000	
00101	10*	C	END	EFFECTS	ARE	NEGLECTED.							000000	
00103	11*		COMMON	ALPHA	RTA	GAMMA	DNR	W	EL	CON	LIN	TDF	E	000000
00104	12*		SQ3	=	SQRT(3.)								000000	
00105	13*		REFL	=	.81								000002	
00106	14*		TAE#V	=	ABS(GAMMA/ALPHA)								000004	
00107	15*		TDF	=	0.								000010	
00110	16*		IF	(ALPHA	.LE.	0.1	GO	TO	30				000011	
00112	17*		IF	(TAE#V	.LT.	SQ3)	GO	TO	10				000014	
00114	18*		GO	TO	30								000017	
00115	19*	10	IF	(TAE#V	.LT.	(.1/SQ3)	GO	TO	20				000021	
00117	20*		TDF	=	DNR*	ALPHA	*(3.-SQ3*TAE#V)	*.5**EL					000025	
00120	21*		GO	TO	30								000037	
00121	22*	20	TDF	=	DNR*	ALPHA	*(1.-REFL*(1.-SQ3*TAE#V))**EL						000041	
00122	23*	30	CONTINUE										000061	
00123	24*		END										000061	

END OF COMPIATION: NO DIAGNOSTICS.

QFOR IS #INSTN
FOR DT-3-11/16/76- 8:54:33 (L0)

SUBROUTINE #INSTN ENTRY POINT 000701

STORAGE USED: CODE(1) 000712; DATA(0) 000111; BLANK COMMON(2) 000012

EXTERNAL REFERENCES (BLOCK, NAME)

0003 SQRT

SOLAR CONCENTRATORS

DATE 111676

PAGE 10

```

00170 58* IF (X2 .LE. W *CD) GO TO 40
00172 59* RF= REFL
00173 60* IFLAG= 1
00174 61* GAMM = ALPH
00175 62* DELTA= RET
00176 63* 10 GC= GAMM *CD+DELTA*SD
00177 64* GS= GAMM *SD-DELTA*CD
00200 65* RN= 1./SQRT(GC**2+GS**2)
00201 66* GC= GC*RN
00202 67* GS= GS*RN
00203 68* DEN= 1./((X2*GC-Y2*GS)
00204 69* YP= Y2*P2
00205 70* RHO= GAMM*DEN*YP**2
00206 71* IF (RHO .GE. 0.) GO TO 20
00210 72* IF (IFLAG1 .GT. 0 ) TRF=TRF*RF1*((RHO*X11-RHO1*X1)/(RHO-RHO1)-X10)
00212 73* X11=X1
00213 74* RHO1= RHO
00214 75* IFLAG1= -1
00215 76* GO TO 50
00216 77* 20 IF (IFLAG1 .EQ. -1) X10=(RHO*X11-RHO1*X1)/(RHO-RHO1)
00220 78* IF (IFLAG .EQ. 1) RHO2= RHO
00222 79* IF (RHO .LE. W) GO TO 30
00224 80* IFLAG= IFLAG+1
00225 81* IF (IFLAG .EQ. 10) GO TO 40
00227 82* IF (IFLAG .LE. IFLAG1) GO TO 25
00231 83* X11= (X1*(W-RHO1)+X11*(RHO-W))/(RHO-RHO1)
00232 84* TRF= TRF * (X11-X10)*RF1
00233 85* X10= X11
00234 86* 25 RF= RF*REFL
00235 87* RHO2= RHO
00236 88* GT= GAMM
00237 89* GAMM = (DELTA*X2-GT*Y2)/YP
00240 90* DELTA= (GT*X2-DF1*TA*Y2)/YP
00241 91* RN= 1./SQRT(GAMM**2+DELTA**2)
00242 92* GAMM= GAMM*RN
00243 93* DELTA= DELTA*RN
00244 94* X2= P4*DELTA/GAMM -X2
00245 95* Y2= X2**2/P4-P
00246 96* GO TO 10
00247 97* 30 IF (IFLAG .GE. IFLAG1) GO TO 40
00251 98* X11= (X1*(W-RHO3)+X11*(RHO-W))/(RHO-RHO3)
00252 99* IF (IFLAG .NE. 10) TRF= TRF*(X11-X10)*RF1
00254 100* X10= X11
00255 101* 40 RF1= RF
00256 102* X11= X1
00257 103* RHO1= RHO
00260 104* RHO3= RHO2
00261 105* IFLAG1= IFLAG
00262 106* IF (L .EQ. 101) TRF= TRF*(X14-X10)*RF
00264 107* 50 X1= X14*(FLOAT(L)*.01-.1.E-6)
00266 108* 60 CONTINUE
00270 109* 70 TR= DNR*TRF*EL *F
00271 110* TRF= TR+DNR*F*EL*AMINI(AMAXI(0.,8*X10-ABS(A)*Y2),6.*W)
00272 111* END
000301
000306
000310
000312
000314
000317
000324
000332
000343
000345
000350
000356
000361
000365
000367
000406
000410
000412
000414
000416
000431
000436
000442
000445
000447
000453
000466
000472
000475
000477
000501
000503
000511
000520
000531
000533
000536
000542
000546
000550
000553
000566
000576
000601
000602
000604
000606
000610
000612
000623
000636
000636
000642
000711

```

END OF COMPILATION: NO DIAGNOSTICS.

QMAP.SIX
MAP28RI RL71-3 11/16/76 18:54:44
1. LIR MONITOR/FUR.

ADDRESS LIMITS 001000 005715 2510 IRANK WORDS DECIMAL
040000 046174 3197 DRANK WORDS DECIMAL
STARTING ADDRESS 005423

SEGMENT SNAINS 001000 005715 040000 046174

N TABS/WRL \$ (2) 040000 040035
N RECAS/FOM-TJ \$ (2) 040036 040150
N ERCOMS/FUR-TE3 \$ (1) 001000 001057 \$ (2) 040151 040164

CONCENTRATIONS

3CON CIRCULAR FRESNEL 8.11
 10CON CIRCULAR FRESNEL 47.12

ALPHA=1.000 BETA= .000 GAMMA= .000
 ALTITUDE= 90.000 AZIMUTH= .000

3CON MOVEABLE FOCUS LINEAR FRESNEL 2.28
 10CON MOVEABLE FOCUS LINEAR FRESNEL 6.86
 3CON LINEAR FRESNEL 2.28
 10CON LINEAR FRESNEL 6.86
 SOLAR TRUSS .92
 2CON V-THROUGH 1.81
 3CON WINSTON 2.50
 10CON WINSTON 6.99

ALPHA= .996 BETA= .000 GAMMA= .087
 ALTITUDE= 85.000 AZIMUTH= .000

3CON MOVEABLE FOCUS LINEAR FRESNEL 2.23
 10CON MOVEABLE FOCUS LINEAR FRESNEL 5.56
 3CON LINEAR FRESNEL 2.07
 10CON LINEAR FRESNEL .00
 SOLAR TRUSS 1.05
 2CON V-THROUGH 1.49
 3CON WINSTON 2.57
 10CON WINSTON 7.50

ALPHA= .985 BETA= .000 GAMMA= .174
 ALTITUDE= 80.000 AZIMUTH= .000

3CON MOVEABLE FOCUS LINEAR FRESNEL 2.12
 10CON MOVEABLE FOCUS LINEAR FRESNEL 3.27
 3CON LINEAR FRESNEL .37
 10CON LINEAR FRESNEL .00
 SOLAR TRUSS 1.19
 2CON V-THROUGH 1.56
 3CON WINSTON 2.62
 10CON WINSTON .19

ALPHA= .966 BETA= .000 GAMMA= .259
 ALTITUDE= 75.000 AZIMUTH= .000

3CON MOVEABLE FOCUS LINEAR FRESNEL 1.99
 10CON MOVEABLE FOCUS LINEAR FRESNEL 2.51
 3CON LINEAR FRESNEL .00
 10CON LINEAR FRESNEL .00
 SOLAR TRUSS 1.33
 2CON V-THROUGH 1.43
 3CON WINSTON 2.52
 10CON WINSTON .00

ALPHA= .940 BETA= .000 GAMMA= .342
 ALTITUDE= 70.000 AZIMUTH= .000

3CON MOVEABLE FOCUS LINEAR FRESNEL 1.83
 10CON MOVEABLE FOCUS LINEAR FRESNEL 4.07
 3CON LINEAR FRESNEL .00
 10CON LINEAR FRESNEL .00
 SOLAR TRUSS 1.48
 2CON V-THROUGH 1.30
 3CON WINSTON .00
 10CON WINSTON .00

ALPHA= .906 BETA= .000 GAMMA= .423
 ALTITUDE= 65.000 AZIMUTH= .000

APPENDIX B

Collector/Reflector Tilt Computer Optimization

THIS IS CASE 1 OF 30 FOR 12 DAYS
 SOUTH FACING ARRAY AT FIXED TILT
 TRUSS WITH BACK REFLECTING SURFACE
 CELL SURFACE TILT = 23.43 REFLECTOR TILT = 10.00 SPACE BETWEEN TRUSSES = 773.61

DAILY INSOLATION IN KWH/M2 AND PEAK TOTAL INSOLATION FOR 12 DAYS

DAY	DIRECT	DIFFUSE	TOTAL	PEAK	REFLECTED
21.	5.584656	.464365	7.031143	1.046206	.982123
51.	6.531001	.561180	7.292074	1.047057	.199894
81.	7.136983	.756530	7.893513	1.103244	0.000000
112.	7.167707	1.012529	8.180296	1.099071	0.000000
142.	6.930665	1.228851	8.159517	1.070114	0.000000
173.	6.743018	1.354803	8.097821	1.047396	0.000000
203.	6.726736	1.336121	8.062857	1.056607	0.000000
234.	6.797034	1.169648	7.966682	1.073229	0.000000
265.	6.704014	.897210	7.601224	1.072561	0.000000
295.	6.250546	.646728	7.063893	1.025396	.166620
326.	5.483121	.491635	6.924081	1.033662	.949325
356.	5.067448	.437441	6.716371	1.032397	1.211481

TOTAL INSOLATION IN KWH/M2 AND PEAK IN KW/M2 FOR THE 12 DAYS CONSIDERED

DIRECT	DIFFUSE	TOTAL	PEAK	REFLECTED
77.122989	10.357042	90.989473	1.103244	3.509442

THIS IS CASE 2 OF 30 FOR 12 DAYS
 SOUTH FACING ARRAY AT FIXED TILT
 TRUSS WITH BACK REFLECTING SURFACE
 CELL SURFACE TILT = 23.45 REFLECTOR TILT = 20.00 SPACE BETWEEN TRUSSES = 490.12

DAILY INSOLATION IN KWH/M2 AND PEAK TOTAL INSOLATION FOR 12 DAYS

DAY	DIRECT	DIFFUSE	TOTAL	PEAK	REFLECTED
21.	5.540585	.464365	7.376452	1.214462	1.371502
51.	6.528748	.561180	8.981957	1.309003	1.892029
81.	7.136983	.756530	8.542136	1.196779	.648622
112.	7.167767	1.012529	8.180296	1.099071	0.000000
142.	6.930665	1.228851	8.159517	1.070114	0.000000
173.	6.743018	1.354803	8.097821	1.047396	0.000000
203.	6.726736	1.336121	8.062857	1.056607	0.000000
234.	6.797034	1.169648	7.966682	1.073229	0.000000
265.	6.704014	.897210	8.222650	1.162646	.621426
295.	6.246678	.646728	8.678684	1.272724	1.785278
326.	5.460786	.491635	7.335237	1.211680	1.382816
356.	5.033117	.437441	6.442922	1.099196	.972363

TOTAL INSOLATION IN KWH/M2 AND PEAK IN KW/M2 FOR THE 12 DAYS CONSIDERED

DIRECT	DIFFUSE	TOTAL	PEAK	REFLECTED
77.016133	10.357042	96.047210	1.309003	8.674036

THIS IS CASE 3 OF 30 FOR 12 DAYS
 SOUTH FACING ARRAY AT FIXED TILT
 TRUSS WITH BACK REFLECTING SURFACE
 CELL SURFACE TILT = 23.43 REFLECTOR TILT = 30.00 SPACE BETWEEN TRUSSES = 391.67

DAILY INSOLATION IN KWH/M2 AND PEAK TOTAL INSOLATION FOR 12 DAYS

DAY	DIRECT	DIFFUSE	TOTAL	PEAK	REFLECTED
21.	5.441742	.464365	6.180671	1.017553	.274565
51.	6.516136	.561180	8.065815	1.224426	.988499
81.	7.136983	.756530	10.015187	1.401346	2.121673
112.	7.167767	1.012529	9.325068	1.303556	1.144772
142.	6.930665	1.228851	8.510373	1.158944	.350856
173.	6.743018	1.354803	8.219385	1.088445	.121564
203.	6.726736	1.336121	8.364724	1.136080	.301867
234.	6.797034	1.169648	9.048636	1.266892	1.081954
265.	6.704014	.897210	9.586412	1.354994	1.985187
295.	6.232825	.646728	7.857626	1.200059	.978074
326.	5.368627	.491635	6.151438	1.015872	.291175
356.	4.860317	.437441	5.395836	.923050	.098077

TOTAL INSOLATION IN KWH/M2 AND PEAK IN KW/M2 FOR THE 12 DAYS CONSIDERED

DIRECT	DIFFUSE	TOTAL	PEAK	REFLECTED
76.625865	10.357042	96.721170	1.401346	9.738263

THIS IS CASE 4 OF 30 FOR 12 DAYS
 SOUTH FACING ARRAY AT FIXED TILT
 TRUSS WITH BACK REFLECTING SURFACE
 CELL SURFACE TILT = 23.43 REFLECTOR TILT = 40.00 SPACE BETWEEN TRUSSES = 339.28

DAILY INSOLATION IN KWH/M2 AND PEAK TOTAL INSOLATION FOR 12 DAYS

DAY	DIRECT	DIFFUSE	TOTAL	PEAK	REFLECTED
21.	5.007539	.464365	5.471904	.905213	0.000000
51.	6.450422	.561180	7.215174	1.095562	.203573
81.	7.136983	.756530	8.958208	1.252369	1.064695
112.	7.167767	1.012529	9.978369	1.332367	1.798073
142.	6.930665	1.228851	10.008803	1.352352	1.849286
173.	6.743018	1.354803	9.750747	1.340113	1.652925
203.	6.726736	1.336121	9.845679	1.334801	1.782822
234.	6.797034	1.169648	9.676787	1.296270	1.710105
265.	6.704014	.897210	8.594595	1.213562	.993371
295.	6.180550	.646728	7.041627	1.075232	.214349
326.	4.461968	.491635	5.453603	.905080	0.000000
356.	4.315137	.437441	4.752578	.815360	0.000000

TOTAL INSOLATION IN KWH/M2 AND PEAK IN KW/M2 FOR THE 12 DAYS CONSIDERED

DIRECT	DIFFUSE	TOTAL	PEAK	REFLECTED
75.121834	10.357042	96.748074	1.352352	11.269198

THIS IS CASE 5 OF 30 FOR 12 DAYS
 SOUTH FACING ARRAY AT FIXED TILT
 TRUSS WITH BACK REFLECTING SURFACE
 CELL SURFACE TILT = 23.43 REFLECTOR TILT = 50.00 SPACE BETWEEN TRUSSES = 305.09

DAILY INSOLATION IN KWH/M2 AND PEAK TOTAL INSOLATION FOR 12 DAYS

DAY	DIRECT	DIFFUSE	TOTAL	PEAK	REFLECTED
21.	4.502888	.464365	4.967252	.820787	0.000000
51.	6.026355	.561180	6.587535	1.003101	0.000000
81.	7.136983	.756530	8.268314	1.155131	.374801
112.	7.167767	1.012529	9.319631	1.229136	1.139335
142.	6.930665	1.228851	9.719092	1.248253	1.559576
173.	6.743018	1.354803	9.758613	1.242104	1.660792
203.	6.726736	1.336121	9.604833	1.233253	1.541975
234.	6.797034	1.169648	9.049359	1.197817	1.082677
265.	6.704014	.897210	7.947233	1.121248	.346008
295.	5.795644	.646728	6.442371	.986335	0.000000
326.	4.461909	.491635	4.953544	.821125	0.000000
356.	3.880264	.437441	4.317705	.739835	0.000000

TOTAL INSOLATION IN KWH/M2 AND PEAK IN KW/M2 FOR THE 12 DAYS CONSIDERED

DIRECT	DIFFUSE	TOTAL	PEAK	REFLECTED
72.873277	10.357042	90.935483	1.248253	7.705164

THIS IS CASE 6 OF 30 FOR 12 DAYS

SOUTH FACING ARRAY AT FIXED TILT

TRUSS WITH BACK REFLECTING SURFACE

CELL SURFACE TILT = 33.43 REFLECTOR TILT = 10.00 SPACE BETWEEN TRUSSES = 965.36

DAILY INSOLATION IN KWH/M2 AND PEAK TOTAL INSOLATION FOR 12 DAYS

DAY	DIRECT	DIFFUSE	TOTAL	PEAK	REFLECTED
21.	6.165933	.525048	8.566906	1.271190	1.875925
51.	6.945361	.625835	8.695302	1.226047	1.124107
81.	7.235805	.818839	8.054644	1.126320	0.000000
112.	6.910551	1.058073	7.968624	1.084992	0.000000
142.	6.430295	1.251334	7.681629	1.030679	0.000000
173.	6.151644	1.363337	7.514980	.997950	0.000000
203.	6.226757	1.351974	7.578731	1.016095	0.000000
234.	6.552998	1.210034	7.763032	1.059246	0.000000
265.	6.799450	.959050	7.758500	1.095204	0.000000
295.	6.637314	.713421	8.377338	1.192285	1.026603
326.	6.039558	.553552	8.427844	1.254663	1.834734
356.	5.666653	.495844	8.206271	1.258088	2.043773

TOTAL INSOLATION IN KWH/M2 AND PEAK IN KW/M2 FOR THE 12 DAYS CONSIDERED

DIRECT	DIFFUSE	TOTAL	PEAK	REFLECTED
77.762317	10.926341	96.593800	1.271190	7.905142

THIS IS CASE 7 OF 30 FOR 12 DAYS

SOUTH FACING ARRAY AT FIXED TILT

TRUSS WITH BACK REFLECTING SURFACE

CELL SURFACE TILT = 33.43 REFLECTOR TILT = 20.00 SPACE BETWEEN TRUSSES = 572.58

DAILY INSOLATION IN KWH/M2 AND PEAK TOTAL INSOLATION FOR 12 DAYS

DAY	DIRECT	DIFFUSE	TOTAL	PEAK	REFLECTED
21.	6.104873	.525048	8.530150	1.403106	1.900229
51.	6.942240	.625835	10.333214	1.504456	2.765139
81.	7.235805	.818839	9.704952	1.361190	1.650309
112.	6.910551	1.058073	8.254143	1.153599	.285519
142.	6.430295	1.251334	7.681629	1.030679	0.000000
173.	6.151644	1.363337	7.514980	.997950	0.000000
203.	6.226757	1.351974	7.578731	1.016095	0.000000
234.	6.552998	1.210034	8.028941	1.123369	.265909
265.	6.799450	.959050	9.320775	1.319560	1.562276
295.	6.631955	.713421	9.970218	1.460861	2.624842
326.	6.008612	.553552	8.478069	1.399197	1.915904
356.	5.619087	.495844	7.462150	1.271629	1.347218

TOTAL INSOLATION IN KWH/M2 AND PEAK IN KW/M2 FOR THE 12 DAYS CONSIDERED

DIRECT	DIFFUSE	TOTAL	PEAK	REFLECTED
77.614266	10.926341	102.857951	1.504456	14.317344

THIS IS CASE 8 OF 30 FOR 12 DAYS
 SOUTH FACING ARRAY AT FIXED TILT
 TRUSS WITH BACK REFLECTING SURFACE
 CELL SURFACE TILT = 33.43 REFLECTOR TILT = 30.00 SPACE BETWEEN TRUSSES = 436.18

DAILY INSOLATION IN KWH/M2 AND PEAK TOTAL INSOLATION FOR 12 DAYS

DAY	DIRECT	DIFFUSE	TOTAL	PEAK	REFLECTED
21.	5.967924	.525048	6.873384	1.130287	.580412
51.	6.924766	.625835	8.920175	1.353031	1.369574
81.	7.235805	.818839	10.994241	1.539343	2.939598
112.	6.910551	1.058073	10.048460	1.419140	2.079835
142.	6.430295	1.251334	8.839359	1.249700	1.157730
173.	6.151644	1.363337	8.323629	1.167407	.808649
203.	6.226757	1.351974	8.656176	1.222535	1.077445
234.	6.552998	1.210034	9.732058	1.376565	1.969026
265.	6.799450	.959050	10.508995	1.486518	2.750495
295.	6.612761	.713421	8.681312	1.324999	1.355130
326.	5.880926	.553552	6.837904	1.127903	.403426
356.	5.379671	.495844	6.011402	1.027577	.135887

TOTAL INSOLATION IN KWH/M2 AND PEAK IN KW/M2 FOR THE 12 DAYS CONSIDERED

DIRECT	DIFFUSE	TOTAL	PEAK	REFLECTED
77.073547	10.926341	104.427097	1.539343	16.427208

THIS IS CASE 9 OF 30 FOR 12 DAYS

SOUTH FACING ARRAY AT FIXED TILT

TRUSS WITH BACK REFLECTING SURFACE

CELL SURFACE TILT = 33.43 REFLECTOR TILT = 40.00 SPACE BETWEEN TRUSSES = 365.59

DAILY INSOLATION IN KWH/M2 AND PEAK TOTAL INSOLATION FOR 12 DAYS

DAY	DIRECT	DIFFUSE	TOTAL	PEAK	REFLECTED
21.	5.366333	.525048	5.891381	.974639	0.000000
51.	6.833718	.625835	7.459553	1.174489	.282052
81.	7.235805	.818839	8.054644	1.332934	1.475144
112.	6.910551	1.054073	7.964624	1.408225	2.516072
142.	6.430295	1.251334	7.681629	1.421723	2.721773
173.	6.151644	1.363337	7.514981	1.405033	2.540670
203.	6.226757	1.351974	7.578731	1.401537	2.639768
234.	6.552998	1.210034	7.763032	1.368271	2.390103
265.	6.799450	.959050	7.758500	1.290562	1.376324
295.	6.540334	.713421	7.253755	1.152050	.296982
326.	5.317496	.553552	5.871048	.974400	0.000000
356.	4.624319	.495844	5.120163	.878371	0.000000

TOTAL INSOLATION IN KWH/M2 AND PEAK IN KW/M2 FOR THE 12 DAYS CONSIDERED

DIRECT	DIFFUSE	TOTAL	PEAK	REFLECTED
74.989698	10.926341	102.154927	1.421723	16.238889

THIS IS CASE 10 OF 30 FOR 12 DAYS
 SOUTH FACING ARRAY AT FIXED TILT
 TRUSS WITH BACK REFLECTING SURFACE
 CELL SURFACE TILT = 33.43 REFLECTOR TILT = 50.00 SPACE BETWEEN TRUSSES = 316.22

DAILY INSOLATION IN KWH/M2 AND PEAK TOTAL INSOLATION FOR 12 DAYS

DAY	DIRECT	DIFFUSE	TOTAL	PEAK	REFLECTED
21.	4.667133	.525048	5.192181	.857665	0.000000
51.	6.246169	.625835	6.872004	1.046383	0.000000
81.	7.235805	.818839	8.054644	1.198210	.519290
112.	6.910551	1.058073	7.968624	1.265198	1.601011
142.	6.430295	1.251334	7.681629	1.277493	2.205435
173.	6.151644	1.363337	7.514981	1.267720	2.352449
203.	6.226757	1.351974	7.578731	1.260841	2.177849
234.	6.552998	1.210034	7.763032	1.231864	1.520657
265.	6.799450	.959050	7.758500	1.162661	.479398
295.	6.007043	.713421	6.720464	1.028883	0.000000
326.	4.624659	.553552	5.178211	.858079	0.000000
356.	4.021799	.495844	4.517643	.773731	0.000000

TOTAL INSOLATION IN KWH/M2 AND PEAK IN KW/M2 FOR THE 12 DAYS CONSIDERED

DIRECT	DIFFUSE	TOTAL	PEAK	REFLECTED
71.874302	10.926341	93.656731	1.277493	10.856088

THIS IS CASE 11 OF 30 FOR 12 DAYS
 SOUTH FACING ARRAY AT FIXED TILT
 TRUSS WITH BACK REFLECTING SURFACE
 CELL SURFACE TILT = 43.43 REFLECTOR TILT = 10.00 SPACE BETWEEN TRUSSES = 1127.77

DAILY INSOLATION IN KWH/M2 AND PEAK TOTAL INSOLATION FOR 12 DAYS

DAY	DIRECT	DIFFUSE	TOTAL	PEAK	REFLECTED
21.	6.559861	.587734	9.860324	1.460118	2.712729
51.	7.148689	.693456	9.937172	1.398721	2.095026
81.	7.114770	.884294	8.647686	1.212036	.648622
112.	6.443361	1.106715	7.550076	1.041739	0.000000
142.	5.734542	1.277886	7.012429	.964169	0.000000
173.	5.373354	1.376830	6.750184	.922673	0.000000
203.	5.537581	1.370510	6.908091	.949046	0.000000
234.	6.109853	1.250106	7.359959	1.016934	0.000000
265.	6.688288	1.020439	8.330152	1.178011	.621426
295.	6.822411	.781029	9.557345	1.357974	1.953906
326.	6.412486	.616845	9.693726	1.440142	2.664395
356.	6.093680	.555638	9.463284	1.447997	2.813966

TOTAL INSOLATION IN KWH/M2 AND PEAK IN KW/M2 FOR THE 12 DAYS CONSIDERED

DIRECT	DIFFUSE	TOTAL	PEAK	REFLECTED
76.038876	11.521482	101.070428	1.460118	13.510070

THIS IS CASE 12 OF 30 FOR 12 DAYS
 SOUTH FACING ARRAY AT FIXED TILT
 TRUSS WITH BACK REFLECTING SURFACE
 CELL SURFACE TILT = 43.43 REFLECTOR TILT = 20.00 SPACE BETWEEN TRUSSES = 637.65

DAILY INSOLATION IN KWH/M2 AND PEAK TOTAL INSOLATION FOR 12 DAYS

DAY	DIRECT	DIFFUSE	TOTAL	PEAK	REFLECTED
21.	6.483667	.587734	9.442618	1.551686	2.371218
51.	7.144796	.693456	11.392483	1.657104	3.554231
81.	7.114770	.884294	10.600916	1.487570	2.601852
112.	6.443361	1.106715	8.694848	1.246224	1.144772
142.	5.734542	1.277886	7.363285	1.052999	.350856
173.	5.373354	1.376830	6.871748	.963721	.121564
203.	5.537581	1.370510	7.209958	1.028520	.301867
234.	6.109853	1.250106	8.441913	1.210596	1.081954
265.	6.688288	1.020439	10.164383	1.439734	2.455657
295.	6.815723	.781029	10.981403	1.607553	3.384651
326.	6.373871	.616845	9.381494	1.546800	2.390779
356.	6.034325	.555638	8.271101	1.407868	1.681139

TOTAL INSOLATION IN KWH/M2 AND PEAK IN KW/M2 FOR THE 12 DAYS CONSIDERED

DIRECT	DIFFUSE	TOTAL	PEAK	REFLECTED
75.854129	11.521482	108.816150	1.657104	21.440539

THIS IS CASE 13 OF 30 FOR 12 DAYS

SOUTH FACING ARRAY AT FIXED TILT

TRUSS WITH BACK REFLECTING SURFACE

CELL SURFACE TILT = 43.43 REFLECTOR TILT = 30.00 SPACE BETWEEN TRUSSES = 467.43

DAILY INSOLATION IN KWH/M2 AND PEAK TOTAL INSOLATION FOR 12 DAYS

DAY	DIRECT	DIFFUSE	TOTAL	PEAK	REFLECTED
21.	6.312774	.587734	7.375208	1.211246	.474701
51.	7.122990	.693456	9.525483	1.443431	1.709036
81.	7.114770	.884294	11.667268	1.633896	3.668204
112.	6.443361	1.106715	10.518639	1.495398	2.968563
142.	5.734542	1.277886	9.043566	1.305725	2.031137
173.	5.373354	1.376830	8.403110	1.215390	1.652925
203.	5.537581	1.370510	8.830210	1.276178	1.922120
234.	6.109853	1.250106	10.173536	1.448266	2.813577
265.	6.688288	1.020439	11.140957	1.576230	3.432231
295.	6.791772	.781029	9.263813	1.412624	1.691012
326.	6.214536	.616845	7.334800	1.208263	.503419
356.	5.735567	.555638	6.460773	1.103326	.169568

TOTAL INSOLATION IN KWH/M2 AND PEAK IN KW/M2 FOR THE 12 DAYS CONSIDERED

DIRECT	DIFFUSE	TOTAL	PEAK	REFLECTED
75.179388	11.521482	109.737362	1.633896	23.036492

THIS IS CASE 14 OF 30 FOR 12 DAYS
 SOUTH FACING ARRAY AT FIXED TILT
 TRUSS WITH BACK REFLECTING SURFACE

CELL SURFACE TILT = 43.43 REFLECTOR TILT = 40.00 SPACE BETWEEN TRUSSES = 376.86

DAILY INSOLATION IN KWH/M2 AND PEAK TOTAL INSOLATION FOR 12 DAYS

DAY	DIRECT	DIFFUSE	TOTAL	PEAK	REFLECTED
21.	5.562072	.587734	6.149806	1.017019	0.000000
51.	7.009375	.693456	8.054792	1.220636	.351961
81.	7.114770	.884294	9.839836	1.376327	1.840773
112.	6.443361	1.106715	10.733224	1.445089	3.183148
142.	5.734542	1.277886	10.523989	1.452137	3.511560
173.	5.373354	1.376830	10.122272	1.431752	3.372088
203.	5.537581	1.370510	10.324597	1.430023	3.416506
234.	6.109853	1.250106	10.385347	1.402552	3.025388
265.	6.588288	1.020439	9.426185	1.331704	1.717459
295.	6.701393	.781029	7.853015	1.196808	.370592
326.	5.511454	.616845	6.128299	1.016712	0.000000
356.	4.792993	.555638	5.348631	.917138	0.000000

TOTAL INSOLATION IN KWH/M2 AND PEAK IN KW/M2 FOR THE 12 DAYS CONSIDERED

DIRECT	DIFFUSE	TOTAL	PEAK	REFLECTED
72.579037	11.521482	104.889993	1.452137	20.789474

THIS IS CASE 15 OF 30 FOR 12 DAYS
 SOUTH FACING ARRAY AT FIXED TILT
 TRUSS WITH BACK REFLECTING SURFACE
 CELL SURFACE TILT = 43.43 REFLECTOR TILT = 50.00 SPACE BETWEEN TRUSSES = 317.74

DAILY INSOLATION IN KWH/M2 AND PEAK TOTAL INSOLATION FOR 12 DAYS

DAY	DIRECT	DIFFUSE	TOTAL	PEAK	REFLECTED
21.	4.689570	.587734	5.277303	.871052	0.000000
51.	6.276197	.693456	6.969653	1.060777	0.000000
81.	7.114770	.884294	8.647065	1.208210	.648001
112.	6.443361	1.106715	9.564118	1.266611	2.014041
142.	5.734542	1.277886	9.817065	1.272157	2.804636
173.	5.373354	1.376830	9.768311	1.259308	3.018127
203.	5.537581	1.370510	9.678888	1.254455	2.770798
234.	6.109853	1.250106	9.272391	1.232336	1.912432
265.	6.688288	1.020439	8.306947	1.172101	.598221
295.	6.035921	.781029	6.816950	1.043112	0.000000
326.	4.646892	.616845	5.263736	.871561	0.000000
356.	4.041133	.555638	4.596771	.786562	0.000000

TOTAL INSOLATION IN KWH/M2 AND PEAK IN KW/M2 FOR THE 12 DAYS CONSIDERED

DIRECT	DIFFUSE	TOTAL	PEAK	REFLECTED
68.691461	11.521482	93.979200	1.272157	13.766256

THIS IS CASE 16 OF 30 FOR 12 DAYS
 SOUTH FACING ARRAY AT FIXED TILT
 TRUSS WITH BACK REFLECTING SURFACE
 CELL SURFACE TILT = 53.43 REFLECTOR TILT = 10.00 SPACE BETWEEN TRUSSES = 1255.92

DAILY INSOLATION IN KWH/M2 AND PEAK TOTAL INSOLATION FOR 12 DAYS

DAY	DIRECT	DIFFUSE	TOTAL	PEAK	REFLECTED
21.	6.754471	.649615	10.871194	1.607118	3.467108
51.	7.134809	.761524	10.898622	1.531743	3.002289
81.	6.777556	.951275	9.379140	1.314957	1.650309
112.	5.780393	1.158589	7.224500	1.039474	.285519
142.	4.877106	1.310469	6.187575	.872999	0.000000
173.	4.460653	1.397578	5.858231	.824324	0.000000
203.	4.691718	1.393692	6.085410	.857936	0.000000
234.	5.481063	1.290546	7.037517	1.011980	.265909
265.	6.373905	1.079951	9.016132	1.275377	1.562276
295.	6.800212	.846982	10.469034	1.485278	2.821840
326.	6.590575	.678652	10.682327	1.584325	3.413100
356.	6.335553	.613972	10.448184	1.596196	3.498658

TOTAL INSOLATION IN KWH/M2 AND PEAK IN KW/M2 FOR THE 12 DAYS CONSIDERED

DIRECT	DIFFUSE	TOTAL	PEAK	REFLECTED
72.058014	12.132846	104.157867	1.607118	19.967007

THIS IS CASE 17 OF 30 FOR 12 DAYS
 SOUTH FACING ARRAY AT FIXED TILT
 TRUSS WITH BACK REFLECTING SURFACE
 CELL SURFACE TILT = 53.43 REFLECTOR TILT = 20.00 SPACE BETWEEN TRUSSES = 683.33

DAILY INSOLATION IN KWH/M2 AND PEAK TOTAL INSOLATION FOR 12 DAYS

DAY	DIRECT	DIFFUSE	TOTAL	PEAK	REFLECTED
21.	6.665458	.649615	10.085231	1.655554	2.770159
51.	7.130260	.761524	12.127115	1.762247	4.235330
81.	6.777556	.951275	11.203170	1.572191	3.474339
112.	5.780393	1.158589	9.018817	1.305015	2.079835
142.	4.877106	1.310469	7.345306	1.092020	1.157730
173.	4.460653	1.397578	6.666880	.993781	.808649
203.	4.691718	1.393692	7.162855	1.064375	1.077445
234.	5.481063	1.290546	8.740635	1.265176	1.969026
265.	6.373905	1.079951	10.728280	1.519593	3.274424
295.	6.792399	.846982	11.681002	1.708278	4.041620
326.	6.545462	.678652	10.017125	1.649866	2.793011
356.	6.266212	.613972	8.844163	1.503617	1.463979

TOTAL INSOLATION IN KWH/M2 AND PEAK IN KW/M2 FOR THE 12 DAYS CONSIDERED

DIRECT	DIFFUSE	TOTAL	PEAK	REFLECTED
71.842185	12.132846	113.620577	1.762247	29.645547

THIS IS CASE 18 OF 30 FOR 12 DAYS

SOUTH FACING ARRAY AT FIXED TILT

TRUSS WITH BACK REFLECTING SURFACE

CELL SURFACE TILT = 53.43 REFLECTOR TILT = 30.00 SPACE BETWEEN TRUSSES = 484.48

DAILY INSOLATION IN KWH/M2 AND PEAK TOTAL INSOLATION FOR 12 DAYS

DAY	DIRECT	DIFFUSE	TOTAL	PEAK	REFLECTED
21.	6.465813	.649615	7.669994	1.257838	.554566
51.	7.104786	.761524	9.862880	1.492820	1.996569
81.	6.777556	.951275	12.014185	1.682194	4.285354
112.	5.780393	1.158589	10.709409	1.530253	3.770428
142.	4.877106	1.310469	9.104229	1.328683	2.916654
173.	4.460653	1.397578	8.398901	1.231406	2.540670
203.	4.691718	1.393692	8.674457	1.295821	2.789046
234.	5.481063	1.290546	10.344248	1.480099	3.572639
265.	6.373905	1.079951	11.463536	1.621479	4.009680
295.	6.764419	.846982	9.586914	1.460204	1.975513
326.	6.359320	.678652	7.626088	1.254373	.568116
356.	5.917190	.613972	6.729259	1.147837	.198096

TOTAL INSOLATION IN KWH/M2 AND PEAK IN KW/M2 FOR THE 12 DAYS CONSIDERED

DIRECT	DIFFUSE	TOTAL	PEAK	REFLECTED
71.053923	12.132846	112.384101	1.682194	29.197332

THIS IS CASE 19 OF 30 FOR 12 DAYS
 SOUTH FACING ARRAY AT FIXED TILT
 TRUSS WITH BACK REFLECTING SURFACE
 CELL SURFACE TILT = 53.43 REFLECTOR TILT = 40.00 SPACE BETWEEN TRUSSES = 378.67

DAILY INSOLATION IN KWH/M2 AND PEAK TOTAL INSOLATION FOR 12 DAYS

DAY	DIRECT	DIFFUSE	TOTAL	PEAK	REFLECTED
21.	5.588811	.649615	6.238427	1.030934	0.000000
51.	6.972056	.761524	8.144756	1.232541	.411176
81.	6.777556	.951275	9.879301	1.381290	2.150470
112.	5.780393	1.158589	10.699527	1.442077	3.760545
142.	4.877106	1.310469	10.413153	1.443064	4.225578
173.	4.460653	1.397578	9.961211	1.419932	4.102950
203.	4.691718	1.393692	10.201693	1.419834	4.116282
234.	5.481063	1.290546	10.344652	1.398354	3.573044
265.	6.373905	1.079951	9.460265	1.335814	2.006409
295.	6.658834	.846982	7.938758	1.208078	.432942
326.	5.537950	.678652	6.216602	1.030595	0.000000
356.	4.816035	.613972	5.430007	.930324	0.000000

TOTAL INSOLATION IN KWH/M2 AND PEAK IN KW/M2 FOR THE 12 DAYS CONSIDERED

DIRECT	DIFFUSE	TOTAL	PEAK	REFLECTED
68.016081	12.132846	104.928353	1.443064	24.779426

THIS IS CASE 20 OF 30 FOR 12 DAYS
 SOUTH FACING ARRAY AT FIXED TILT
 TRUSS WITH BACK REFLECTING SURFACE
 CELL SURFACE TILT = 53.43 REFLECTOR TILT = 50.00 SPACE BETWEEN TRUSSES = 309.61

DAILY INSOLATION IN KWH/M2 AND PEAK TOTAL INSOLATION FOR 12 DAYS

DAY	DIRECT	DIFFUSE	TOTAL	PEAK	REFLECTED
21.	4.569516	.649615	5.219131	.860409	0.000000
51.	6.115526	.761524	6.877050	1.045787	0.000000
81.	6.777556	.951275	8.485854	1.184889	.757023
112.	5.780393	1.158589	9.304858	1.233572	2.365876
142.	4.877106	1.310469	9.496023	1.232804	3.308448
173.	4.460653	1.397578	9.426960	1.217595	3.568728
203.	4.691718	1.393692	9.355596	1.214727	3.270186
234.	5.481063	1.290546	9.017708	1.199500	2.246099
265.	6.373905	1.079951	8.152723	1.149359	.698867
295.	5.881401	.846982	6.728383	1.028524	0.000000
326.	4.527931	.678652	5.206583	.861023	0.000000
356.	3.937680	.613972	4.551652	.777780	0.000000

TOTAL INSOLATION IN KWH/M2 AND PEAK IN KW/M2 FOR THE 12 DAYS CONSIDERED

DIRECT	DIFFUSE	TOTAL	PEAK	REFLECTED
63.474448	12.132846	91.822522	1.233572	16.215229

THIS IS CASE 21 OF 30 FOR 12 DAYS
 SOUTH FACING ARRAY AT FIXED TILT
 TRUSS WITH BACK REFLECTING SURFACE
 CELL SURFACE TILT = 63.43 REFLECTOR TILT = 10.00 SPACE BETWEEN TRUSSES = 1345.90

DAILY INSOLATION IN KWH/M2 AND PEAK TOTAL INSOLATION FOR 12 DAYS

DAY	DIRECT	DIFFUSE	TOTAL	PEAK	REFLECTED
21.	6.743850	.708372	11.568362	1.707676	4.116141
51.	6.904141	.828055	11.550524	1.621106	3.818328
81.	6.234410	1.018746	9.855008	1.381486	2.601852
112.	4.944063	1.214304	7.303138	1.079357	1.144772
142.	3.922996	1.351941	5.625792	.849252	.350856
173.	3.470735	1.430246	5.022545	.747487	.121564
203.	3.759208	1.425561	5.486636	.825538	.501867
234.	4.685733	1.332696	7.100382	1.648187	1.081954
265.	5.865855	1.136985	9.458497	1.337630	2.455657
295.	6.571392	.909404	11.084831	1.570376	3.604034
326.	6.568412	.736655	11.363167	1.682785	4.058100
356.	6.384924	.668471	11.130441	1.698105	4.077045

TOTAL INSOLATION IN KWH/M2 AND PEAK IN KW/M2 FOR THE 12 DAYS CONSIDERED

DIRECT	DIFFUSE	TOTAL	PEAK	REFLECTED
66.055717	12.761435	106.549322	1.707676	27.732170

THIS IS CASE 22 OF 30 FOR 12 DAYS
 SOUTH FACING ARRAY AT FIXED TILT
 TRUSS WITH BACK REFLECTING SURFACE
 CELL SURFACE TILT = 63.43 REFLECTOR TILT = 20.00 SPACE BETWEEN TRUSSES = 708.26

DAILY INSOLATION IN KWH/M2 AND PEAK TOTAL INSOLATION FOR 12 DAYS

DAY	DIRECT	DIFFUSE	TOTAL	PEAK	REFLECTED
21.	6.644722	.708372	10.438023	1.711510	3.084930
51.	6.899075	.828055	12.514871	1.816729	4.787741
81.	6.234410	1.018746	11.494416	1.612505	4.241260
112.	4.944063	1.214304	9.126929	1.328532	2.968563
142.	3.922996	1.351941	7.306073	1.102978	2.031137
173.	3.470735	1.430246	6.553906	.999155	1.652925
203.	3.759208	1.425561	7.106888	1.073196	1.922120
234.	4.685733	1.332696	8.832006	1.285857	2.813577
265.	5.869855	1.136985	10.996539	1.556920	3.993699
295.	6.562692	.909404	12.047882	1.760021	4.575786
326.	6.518173	.736655	10.365206	1.705217	3.110378
356.	6.307703	.668471	9.163319	1.555889	2.187144

TOTAL INSOLATION IN KWH/M2 AND PEAK IN KW/M2 FOR THE 12 DAYS CONSIDERED

DIRECT	DIFFUSE	TOTAL	PEAK	REFLECTED
65.815364	12.761435	115.946059	1.816729	37.369260

THIS IS CASE 23 OF 30 FOR 12 DAYS
 SOUTH FACING ARRAY AT FIXED TILT
 TRUSS WITH BACK REFLECTING SURFACE
 CELL SURFACE TILT = 63.43 REFLECTOR TILT = 30.00 SPACE BETWEEN TRUSSES = 486.81

DAILY INSOLATION IN KWH/M2 AND PEAK TOTAL INSOLATION FOR 12 DAYS

DAY	DIRECT	DIFFUSE	TOTAL	PEAK	REFLECTED
21.	6.422392	.708372	7.748345	1.268601	.617581
51.	6.870707	.828555	9.922200	1.499733	2.223438
81.	6.234410	1.018746	12.025452	1.682940	4.772296
112.	4.944063	1.214304	10.639783	1.522989	4.481416
142.	3.922996	1.351941	8.988485	1.315387	3.713549
173.	3.470735	1.430246	8.273068	1.215518	3.372088
203.	3.759208	1.425561	8.755998	1.231398	3.571230
234.	4.685733	1.332596	10.269487	1.471502	4.251058
265.	5.865855	1.136985	11.468137	1.621101	4.465297
295.	6.531532	.909404	9.640925	1.456340	2.199989
326.	6.310880	.736655	7.702478	1.254785	.654943
356.	5.919023	.668471	6.808100	1.159682	.220606

TOTAL INSOLATION IN KWH/M2 AND PEAK IN KW/M2 FOR THE 12 DAYS CONSIDERED

DIRECT	DIFFUSE	TOTAL	PEAK	REFLECTED
64.937533	12.761435	112.242457	1.682940	34.543490

THIS IS CASE 24 OF 30 FOR 12 DAYS

SOUTH FACING ARRAY AT FIXED TILT

TRUSS WITH BACK REFLECTING SURFACE

CELL SURFACE TILT = 63.43 REFLECTOR TILT = 40.00 SPACE BETWEEN TRUSSES = 368.97

DAILY INSOLATION IN KWH/M2 AND PEAK TOTAL INSOLATION FOR 12 DAYS

DAY	DIRECT	DIFFUSE	TOTAL	PEAK	REFLECTED
21.	5.445737	.708372	6.154109	1.015914	0.000000
51.	6.722895	.828055	8.008847	1.209879	.457897
81.	6.234410	1.018746	9.647952	1.347845	2.394826
112.	4.944063	1.214304	10.380206	1.399626	4.221839
142.	3.922996	1.351941	10.064036	1.395263	4.789100
173.	3.470735	1.430246	9.608261	1.370478	4.707281
203.	3.759208	1.425561	9.853719	1.371810	4.668951
234.	4.685733	1.332696	10.030563	1.356210	4.012135
265.	5.865855	1.136985	9.237236	1.302975	2.234396
295.	6.413950	.909404	7.805491	1.185565	.482137
326.	5.396178	.736655	6.132833	1.015579	0.000000
356.	4.692744	.668471	5.361215	.917453	0.000000

TOTAL INSOLATION IN KWH/M2 AND PEAK IN KW/M2 FOR THE 12 DAYS CONSIDERED.

DIRECT	DIFFUSE	TOTAL	PEAK	REFLECTED
61.554503	12.761435	102.284500	1.399626	27.968562

THIS IS CASE 25 OF 30 FOR 12 DAYS
 SOUTH FACING ARRAY AT FIXED TILT
 TRUSS WITH BACK REFLECTING SURFACE
 CELL SURFACE TILT = 63.43 REFLECTOR TILT = 50.00 SPACE BETWEEN TRUSSES = 292.06

DAILY INSOLATION IN KWH/M2 AND PEAK TOTAL INSOLATION FOR 12 DAYS

DAY	DIRECT	DIFFUSE	TOTAL	PEAK	REFLECTED
21.	4.310620	.708372	5.018992	.826012	0.000000
51.	5.769038	.828055	6.597093	1.001904	0.000000
81.	6.234410	1.018746	8.096199	1.129127	.843043
112.	4.944063	1.214304	8.802350	1.167429	2.643984
142.	3.922996	1.351941	8.944945	1.161112	3.670009
173.	3.470735	1.430246	8.864639	1.144397	3.963658
203.	3.759208	1.425561	8.809695	1.143398	3.624926
234.	4.685733	1.332696	8.529949	1.134760	2.511520
265.	5.865855	1.136985	7.781119	1.095334	.778279
295.	5.548177	.909404	6.457581	.985609	0.000000
326.	4.271391	.736655	5.008046	.826739	0.000000
356.	3.714582	.668471	4.383053	.747575	0.000000

TOTAL INSOLATION IN KWH/M2 AND PEAK IN KW/M2 FOR THE 12 DAYS CONSIDERED

DIRECT	DIFFUSE	TOTAL	PEAK	REFLECTED
56.496807	12.761435	87.293661	1.167429	18.035419

THIS IS CASE 26 OF 30 FOR 12 DAYS

SOUTH FACING ARRAY AT FIXED TILT

TRUSS WITH BACK REFLECTING SURFACE

CELL SURFACE TILT = 73.43 REFLECTOR TILT = 10.00 SPACE BETWEEN TRUSSES = 1395.00

DAILY INSOLATION IN KWH/M2 AND PEAK TOTAL INSOLATION FOR 12 DAYS

DAY	DIRECT	DIFFUSE	TOTAL	PEAK	REFLECTED
21.	6.528320	.762293	11.930719	1.758780	4.640106
51.	6.463694	.891653	11.873697	1.664224	4.518350
81.	5.501834	1.086167	10.062340	1.409860	3.474339
112.	3.987928	1.274664	7.342427	1.091233	2.079835
142.	2.560680	1.403368	5.421778	.849391	1.157730
173.	2.375360	1.475656	4.659665	.742611	.808649
203.	2.718408	1.467529	5.263382	.823832	1.077445
234.	3.780589	1.378207	7.127822	1.057572	1.969026
265.	5.179573	1.191639	9.645636	1.363199	3.274424
295.	6.142904	.967152	11.386778	1.610839	4.276722
326.	6.346671	.789196	11.715663	1.732580	4.579797
356.	6.240292	.717380	11.489225	1.750642	4.531553

TOTAL INSOLATION IN KWH/M2 AND PEAK IN KW/M2 FOR THE 12 DAYS CONSIDERED

DIRECT	DIFFUSE	TOTAL	PEAK	REFLECTED
58.126252	13.404905	107.919133	1.758780	36.387976

THIS IS CASE 27 OF 30 FOR 12 DAYS
 SOUTH FACING ARRAY AT FIXED TILT
 TRUSS WITH BACK REFLECTING SURFACE
 CELL SURFACE TILT = 73.43 REFLECTOR TILT = 20.00 SPACE BETWEEN TRUSSES = 711.66

DAILY INSOLATION IN KWH/M2 AND PEAK TOTAL INSOLATION FOR 12 DAYS

DAY	DIRECT	DIFFUSE	TOTAL	PEAK	REFLECTED
21.	6.422090	.762293	10.490350	1.717894	3.305967
51.	6.458265	.891653	12.544597	1.819021	5.194678
81.	5.501834	1.086167	11.467314	1.607595	4.879312
112.	3.987928	1.274664	9.029683	1.316471	3.767092
142.	2.860680	1.403368	7.180701	1.086054	2.916654
173.	2.375360	1.475656	6.391687	.980236	2.540670
203.	2.718408	1.467529	6.974983	1.055278	2.789046
234.	3.780589	1.378207	8.731435	1.272494	3.572639
265.	5.179573	1.191639	10.962840	1.550899	4.591628
295.	6.133580	.967152	12.071652	1.761366	4.970919
326.	6.292832	.789196	10.415267	1.711223	3.333239
356.	6.157538	.717380	9.218772	1.563109	2.343854

TOTAL INSOLATION IN KWH/M2 AND PEAK IN KW/M2 FOR THE 12 DAYS CONSIDERED

DIRECT	DIFFUSE	TOTAL	PEAK	REFLECTED
57.868677	13.404905	115.479281	1.819021	44.205699

THIS IS CASE 28 OF 30 FOR 12 DAYS
 SOUTH FACING ARRAY AT FIXED TILT
 TRUSS WITH BACK REFLECTING SURFACE
 CELL SURFACE TILT = 73.43 REFLECTOR TILT = 30.00 SPACE BETWEEN TRUSSES = 474.34

DAILY INSOLATION IN KWH/M2 AND PEAK TOTAL INSOLATION FOR 12 DAYS

DAY	DIRECT	DIFFUSE	TOTAL	PEAK	REFLECTED
21.	6.183830	.762293	7.607954	1.243251	.661851
51.	6.427864	.891653	9.702266	1.464089	2.382749
81.	5.501834	1.086167	11.702235	1.636373	5.114234
112.	3.987928	1.274664	10.301232	1.474238	5.038640
142.	2.860680	1.403368	8.661658	1.267755	4.397610
173.	2.375360	1.475656	7.952062	1.168762	4.101046
203.	2.718408	1.467529	8.430839	1.233908	4.244903
234.	3.780589	1.378207	9.937030	1.423220	4.778234
265.	5.179573	1.191639	11.156450	1.575424	4.745238
295.	6.100188	.967152	9.424959	1.431001	2.357619
326.	6.070687	.789196	7.561753	1.239232	.701870
356.	5.741009	.717380	6.694801	1.138514	.236412

TOTAL INSOLATION IN KWH/M2 AND PEAK IN KW/M2 FOR THE 12 DAYS CONSIDERED

DIRECT	DIFFUSE	TOTAL	PEAK	REFLECTED
56.927949	13.404905	109.133240	1.636373	38.800386

THIS PAGE
WAS INTENTIONALLY
LEFT BLANK

1.3 Silicon Solar Cell Modules

1.3.1 Cell Characteristics

Solar cell performance was determined for each site by Professor Martin Wolf and his associates at the University of Pennsylvania using a proprietary computer program. His analyses and results are described in detail in Volume III(2) under Section 2.4 entitled, "Array Comparative Performance". The analytical model of the silicon solar cell used in his work is described in the following paragraphs.

The silicon solar cell is represented by the commonly used model for the pn-junction device:

$$j = j_0 \left[\exp\left(\frac{q(V - jR_s)}{AkT}\right) - 1 \right] - j_L \frac{A_L}{A_j} \quad [\text{A/cm}^{-2}] \quad (1.3.1)$$

where

j = terminal current density

V = terminal voltage

j_0 = diode saturation current density

j_L = light generated current density

A = empirical adjustment factor ($A = 1$ for 1985 and 2000 silicon solar cells)

R_s = effective lumped series resistance based on unit junction area

A_L = light exposed area

A_j = junction area

T = cell temperature

q, k = physical constants (electronic charge, Boltzman constant)

Terminal voltage, maximum power point, open circuit voltage, power under given load conditions, etc. are all derived from this relationship. The quantities j_L and j_0 are the determining quantities in this relationship, and they are computed in the program from first principles, using the detailed charge balance and the small signal approximations. The latter can easily be shown to be applicable up to optical concentration ratios near 1000. Both quantities are computed using similar algorithms based on charge carrier transport by both diffusion and drift. They permit modeling of both the base and the diffused regions of the cell by up to 3 sublayers of differing material properties. This sublayer approach has been taken to obtain closed form solutions for the collection efficiency and the saturation current. These closed form solutions require constant coefficients. That means that the material parameters are assumed to be constant within each layer of the device, and that the collection efficiency results are assumed valid for a particular value of absorption coefficient, that is, a particular wavelength interval. Thus, the spectral collection efficiency, a form of spectral response, is obtained which is multiplied, in wavelength intervals, by the spectral photon distribution of the incident light to obtain the light generated current. Where the assumptions of the small signal theory hold, that is, the parameters are light intensity independent, the approach has full validity.

A detailed description of the algorithm used for the collection efficiency is contained in the published literature, while the algorithm for the saturation current is fully analogous, omitting only

the generation term, which means solving the homogeneous differential equation rather than the inhomogeneous one. All relevant material and dimensional parameters, including the thickness of each layer and the recombination velocities at all surfaces, are used as variables to permit highly accurate simulation.

One of the tasks of the project was to model a silicon solar cell which would be in low-cost mass production in the year 1985, and another which could be available from such production lines in the year 2000. The performance/characteristic and design/material parameters of the silicon solar cell to be in production in 1985 were assumed to be equal to those of the Comsat Non-Reflective Cell, which is a cell that has been fabricated on a laboratory pilot line in significant quantities and with verified performance of over 15% airmass zero conversion efficiency, or near 17% idealized airmass 1 efficiency. Since the collection efficiency related parameters of this cell are, for practical purposes, fully optimized, the predicted improvements of the "year 2000" cell consist of an increase in the voltages of the cell, such as an open circuit voltage increase from 0.60 V to 0.68 V. The design/material parameters for the two cells are listed in Table 1.3.1. The current-voltage characteristic is of the single exponential type, corresponding to equation 1.3.1, and is shown plotted in Figure 1.3.1. While most of the current production solar cells exhibit the "double exponential type" of characteristic, which causes a 5 to 10% loss of output power, the Cosmat "violet" and "nonreflective" cells have the saturation current

Table 1.3.1

Projected Silicon Solar Cell Parameters

<u>Parameter</u>	<u>1985</u>	<u>2000</u>	<u>Units</u>
Thickness	300	300	μm
Junction Depth	0.2	0.2	μm
Mobility			
Base (e1/hole)	1180/420	760/260	$\text{cm}^2\text{V}^{-1}\text{s}^{-1}$
Diff. Region	40	40	$\text{cm}^2\text{V}^{-1}\text{s}^{-1}$
Carrier Conc.			
Base (p-type)	$4 \cdot 10^{15}$	$7 \cdot 10^{16}$	cm^{-3}
Diff. Region	10^{19}	10^{19}	cm^{-3}
Surface Recomb.			
Base (Back Surface Field)	1	1	cm s^{-1}
Diff. Region	100	100	cm s^{-1}
Minority Carrier Lifetime			
Base	25	25	μs
Diff. Region	3	3	ns
Light Exposed Area	0.92	0.92	cm^2
Junction Area	1.0	1.0	cm^2
Series Resistance	0.34	0.34	Ωcm^2
Reflectance	0.03	0.03	-

Curve 686813-A

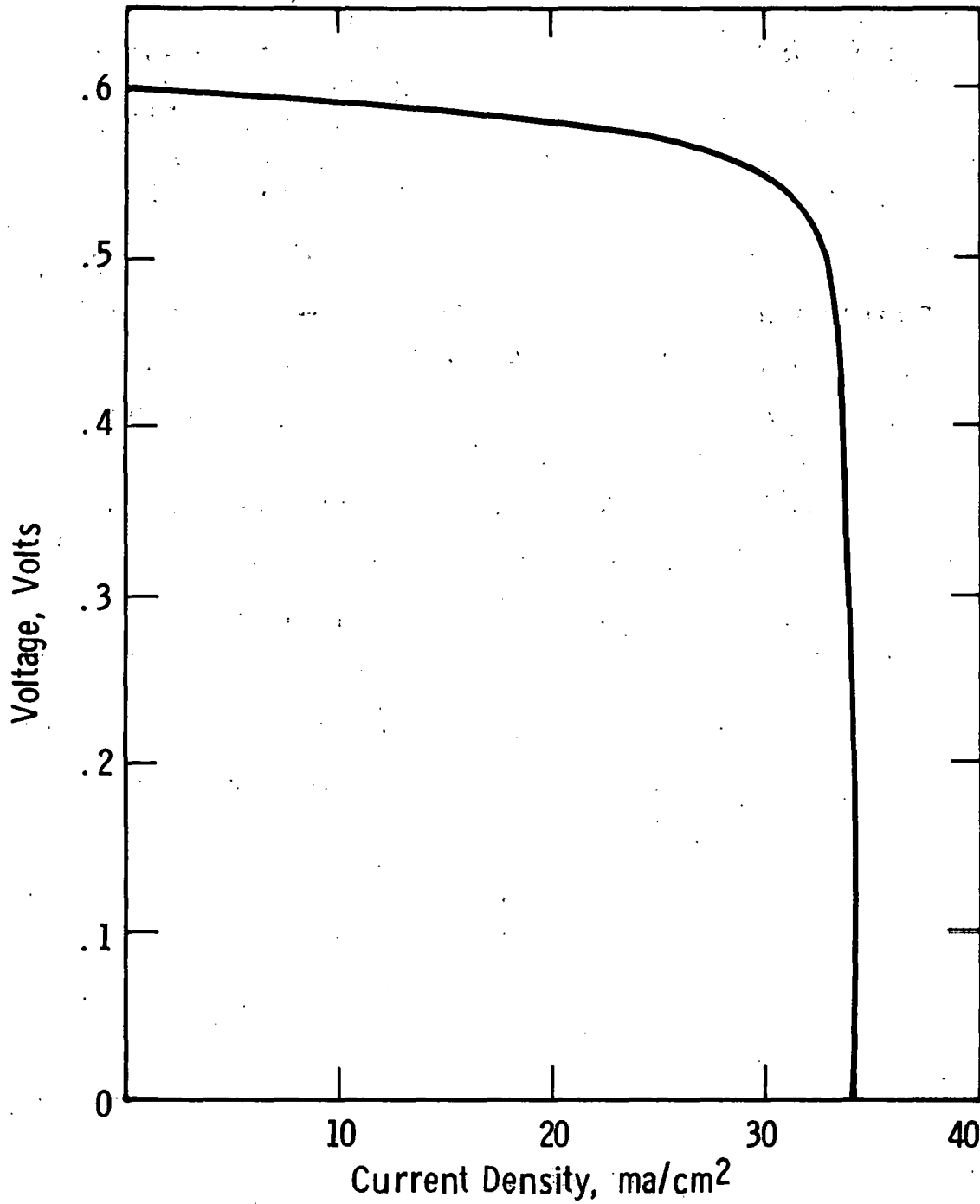


Fig. 1.3.1—Projected 1985 silicon solar cell characteristics
AM1, 25°C - Efficiency \cong 16%

of the second exponential term sufficiently reduced to have a current-voltage characteristic of essentially the single exponential type.

The temperature dependences of the performance parameters are partially contained in the algebraic relationships partially introduced through the temperature dependence of the material parameters. Accordingly, the absorption coefficients, dependent on wavelength, are determined by interpolation and extrapolation from empirically determined, published data for a few fixed temperatures. The energy gap, E_g , which dominantly determines the saturation current j_0 based on carrier diffusion is assumed to be:

$$E_g = 1.12 - (T - 300) \cdot 2.8 \cdot 10^{-4} \text{ [eV]} \quad (1.3.2)$$

Since the temperature dependences of the mobilities and minority carrier lifetimes are of lesser importance in the temperature range of interest, these quantities have been kept constant.

1.3.2 Module Analysis

1.3.2.1 Basic Photovoltaic Modularity

1.3.2.1.1 General Considerations

The flat plate IPS Photovoltaic System was investigated to determine the most appropriate reference or standard module and accompanying sub-modules which might be manufactured to give the total array system increased flexibility and closer compatibility with existing building practices. The material module considerations of photovoltaic cells are flexible enough to allow primary consideration of sizes and tolerances to be determined by current glazing system requirements. The most often practiced dimensions for glazing systems usually do not reflect aesthetics, but economic considerations. Therefore, a close adherence to current glazing module sizes should in fact give the photovoltaic system the most widespread application as well as the best economic profile. In addition to these reasons, consideration was given to the fact that watertight glazing systems are already manufactured that adhere to current glazing module sizes. Labor unions and contractors already have the skills required to install these systems and building designers are experienced in incorporating these module systems into their building design.

On large building projects, the horizontal wall module is most often 2.5' with the vertical module relating floor to ceiling spacing at 8' intervals. Consider the 2.5' x 8' dimension to be the standard module. If flexibility is desired to allow for maximum utilization of

existing roof areas, a series of panels could be designed to generate a modular array system which could be assembled in one foot increments.

"Architectural Planning often demands the flexibility to vary spaces by a module of one foot. If it is not possible to achieve 1' flexibility by combining components of dissimilar sizes, it would be necessary to manufacture components of every modular size. It is clear that components of almost an infinite number of sizes exist on the present market. The problem exists when the dimensioning does not relate to the standard module which we suggest is the most suitable".

"Because the smallest number of components make generally for the least expensive and fastest method of construction, certain critical dimensions become most obvious and prevalent in design, especially if one is attempting to create plan and building type flexibility with good architectural design".

"It does not make much sense to have the simplistic notion of one module with incremental growth of 1' and 1' and 1'. It is infinitely more logical to work an increase based on something like the famed Fibonnaci series of 1' + 2' + 3' + 5' + 8' + 13'."

"Choosing particular numerically related sizes, as for example 3' and 5', works. Using two widths of 3' only gives the designer 3' flexibility. Usually, a manufacturer will double and triple his basic sizes as in panels -- a width of 3' will have a second size of 6' offered. This is common practice for manufacturers, but we lost flexibility because two 3' panels will give 6' already and 12' with four threes, etc. A common factor between two sizes is self-defeating and not worthwhile as a module system".

"To avoid this 'factor effect' one can choose 5' as a second size. Two widths of 3' and 5' will fill every modular space from 8'. That is to say that, with only two components in addition to the standard module, we have 1' flexibility from 8' onwards."¹

Therefore, if both compatibility with existing building systems and flexibility are required, three modules -- 2.5' x 8', 2.5' x 5', 2.5' x 3' -- would satisfy these requirements. These basic dimensions would be center line related. Actual dimensions of components would be slightly smaller. Therefore, the dimensions defining a module would include a shared support and watertight glazing gasket with adjoining collector panels.

Once basic dimensions are set, the physical characteristics of the system are investigated to determine whether the size chosen cannot be met with existing materials or is not cost effective. The primary limiter in this system is the actual glazing, which can initially be specified as 1/8" double strength PPG Pennvernon Sheet Glass. However, when checking the ability of the glass to meet the dimension required (see Figure 1.3.2), we find that the maximum standard size available is only 60" x 80". Therefore, single strength 3/16" glass sheet was chosen. The cost difference between 1/8" and 3/16" was only \$.02/sq. ft., or \$.40 per standard collector module. This is not excessive and perfectly acceptable.

¹Cutler, L, and Cutler, S, Handbook of Housing System for Designers and Developers, Van Nostrand Reinhold Company, 450 West 33rd Street, New York, New York, 10001, p. 128

AVAILABILITY TABLE

PRODUCT	THICKNESS		WEIGHT Approx. lb./sq.ft.	MAXIMUM SIZE ¹ Standard Inches	QUALITY ²
	Nominal Inches	Tolerance Inches			
PENNVERNON Clear					
Photo	1/16	0.058 to 0.068	0.81	36 x 50	A,B(q5, q6) A,B(q5, q6) Greenhouse(q9)
Picture	5/64	0.070 to 0.080	1.01	36 x 50	
Single Strength ³	3/32	0.085 to 0.101	1.22	40 x 50	
Double Strength ^{3, 4}	1/8	0.115 to 0.134	1.65	60 x 80	
3/16 Sheet ^{3, 4}	3/16	0.182 to 0.200	2.45	120 x 84	
7/32 Sheet ⁴	7/32	0.212 to 0.230	2.88	120 x 84	
1/4 Sheet ⁴	1/4	0.240 to 0.260	3.24	120 x 84	
3/8 Sheet	3/8	0.357 to 0.384	4.86	60 x 84	
7/16 Sheet	7/16	0.400 to 0.430	5.67	60 x 84	
Greenhouse ⁵	1/8	0.115 to 0.134	1.65	20 x 20	
PENNVERNON GRAYLITE Tinted					
GRAYLITE 55 ^{3, 4}	1/8	0.115 to 0.134	1.65	60 x 84	B(q6)
GRAYLITE 45 ^{3, 4}	3/16	0.182 to 0.200	2.45	120 x 84	B(q6)
GRAYLITE 31 ^{3, 6}	1/8	0.115 to 0.134	1.65	60 x 84	B(q6)
GRAYLITE 14 ^{3, 6}	7/32	0.212 to 0.230	2.88	100 x 84	B(q6)

FIGURE 1.3.2.

PPG FLOAT GLASS To Meet Wind Load Requirements

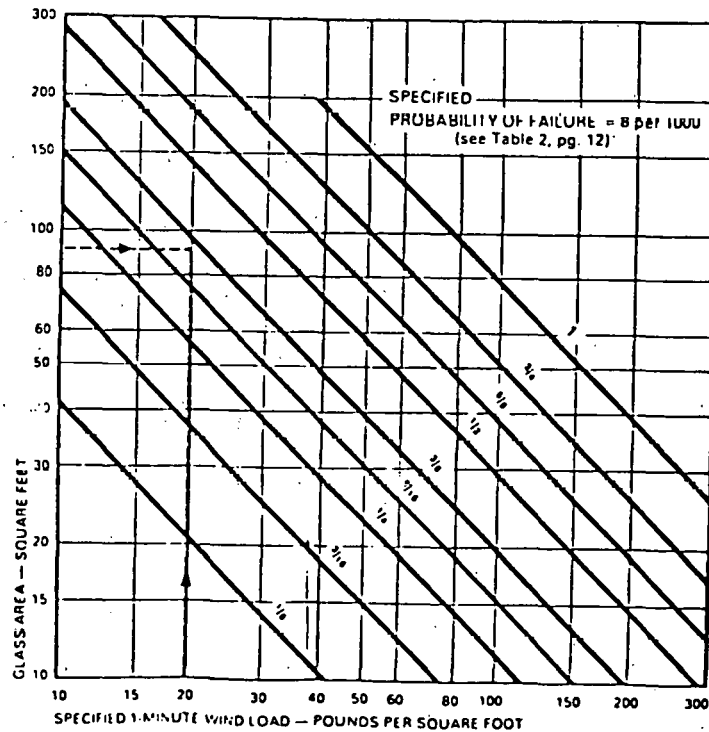


Figure 1.3.3

We can also see by Figure 1.3.3, a 3/16" single strength glass will resist approximately 38 lb/ft² of wind load which exceeds all national building code requirements.

Another item which now must be considered due to the change in glass thickness is the reduction in solar energy transmittance. Using ordinary clear lime glass (float) as a replacement (see Figure 1.3.4) shows a reduction in solar transmission from 87% to 85%. This is not a severe penalty to pay. However, by using water white crystal glass which has the same physical properties as ordinary clear lime glass (float) as shown by Figures 1.3.5 through 1.3.8, an increase in solar transmittance occurs. Therefore, it can be a direct replacement.

The collector absorber plate shall be copper Roll Bond which has 22" as its largest currently available horizontal dimension. Larger sizes can be fabricated by combining two pieces. If by the projected project date of 1985, a significant market can be generated for the chosen standard module, machinery could possibly be made to fabricate a single piece of Roll-Bond plate to fit the standard module.

Tolerance - Until recently, tolerance presented no great problem to the building industry, except in certain specialized fields such as mechanical and structural engineering. For the past 40 years, an increasing number of components have been prefabricated away from the building site, but hitherto these have been built into dimensionally adjustable work on-site and problems of fit have been solved automatically. For example, when factory-made windows are set in masonry wall construction, inaccuracies in the size, shape, or position of the windows

PERTINENT PHYSICAL PROPERTIES OF TRANSPARENT GLAZING MEDIA				
GLAZING MEDIA	REFRACTIVE INDEX	**SOLAR ENERGY TRANSMISSION (PER SHEET)	**SOLAR ENERGY LOSSES PER SHEET (2 SURFACE REFLECTION PLUS ABSORPTION)	***MAXIMUM OPERATING TEMP.
ORDINARY CLEAR LIME GLASS (FLOAT) (IRON OXIDE CONTENT 0.10% TO 0.13%)	1.52	1/8" (3.2 mm) - 85% 3/16" (4.8 mm) - 81% 1/4" (6.0 mm) - 78%	15% (8.2%R + 6.8%A) 19% (8.0%R + 11.0%A) 22% (7.9%R + 14.1%A)	400° F (204°C)
SHEET LIME GLASS (LOW IRON OXIDE CONTENT 0.05% TO 0.06%)	1.51	DS (3.2 mm) - 87% 3/16" (4.8 mm) - 85%	13% (8.1%R + 4.9%A) 15% (8.0%R + 7.0%A)	400° F (204°C)
WATER-WHITE CRYSTAL GLASS #76 (0.01% IRON OXIDE)	1.50	5/32" (4.0 mm) - 91% 3/16" (4.7 mm) - 90.5% 7/32" (5.5 mm) - 90%	9% (8.0%R + 1.0%A) 9.5% (8.0%R + 1.5%A) 10% (8.0%R + 2.0%A)	400° F (204°C)
*METHYL METHACRYLATE (100% ACRYLIC COLORLESS CAST SHEET)	1.49	1/8" (3.2 mm) - 89% 3/16" (4.7 mm) - 87% 1/4" (6.2 mm) - 85%	11% (7.6%R + 3.4%A) 13% (7.5%R + 5.5%A) 15% (7.42R + 7.6%A)	180° TO 190° F (82° TO 93°C)
*POLYCARBONATE CLEAR SHEET (LIGHT STABLE TYPE)	1.586	1/8" (3.2 mm) - 81% 3/16" (4.7 mm) - 78% 1/4" (6.2 mm) - 74%	19% (9.8%R + 9.2%A) 22% (9.6%R + 12.4%A) 26% (9.4%R + 16.6%A)	250° TO 270° F (121°C TO 132°C)

*Data obtained from manufacturers' Literature and/or Photometric Testing.

**Solar Radiation Calculations based on "Standard Solar Radiation Curve for Engineering Calculations", by Parry Moon, Journal of Franklin Institute, 1947.

***Maximum Operating Temperature for Continuous Operation. For Annealed Glass Thermal Expansion Coefficient is 9.0 x 10⁻⁶ per degree Fahrenheit.

Figure 1.3.4

PERTINENT PHYSICAL PROPERTIES OF TRANSPARENT GLAZING MEDIA				
GLAZING MEDIA	NOMINAL THICKNESS	NOMINAL MAXIMUM SIZES RECOMMENDED	WEIGHT (LBS./SQ.FT.)	EXPANSION COEFFICIENT
ORDINARY CLEAR LIME GLASS (FLOAT) (IRON OXIDE CONTENT 0.10% TO 0.13%)	1/8"	34" x 76"	1.63	48 x 10 ⁻⁷ PER ° F
	3/16"	36" x 96"	2.51	
	1/4"	48" x 120"	3.02	
SHEET LIME GLASS (LOW IRON OXIDE CONTENT 0.05% TO 0.06%)	DS (1/8")	34" x 76"	1.63	50 x 10 ⁻⁷ PER ° F
	3/16"	36" x 96"	2.51	
WATER-WHITE CRYSTAL GLASS #76 (0.01% IRON OXIDE)	5/32"	34" x 76"	2.03	47 x 10 ⁻⁷ PER ° F
	3/16"	36" x 96"	2.41	
	7/32"	48" x 96"	2.80	
*METHYL METHACRYLATE (100% ACRYLIC COLORLESS CAST SHEET)	1/8"	**24" Short Dimen.	0.75	410 x 10 ⁻⁷ PER ° F
	3/16"	**36" Short Dimen.	1.10	
	1/4"	**48" Short Dimen.	1.50	
*POLYCARBONATE CLEAR SHEET (LIGHT STABLE TYPE)	1/8"	**24" Short Dimen.	0.78	375 x 10 ⁻⁷ PER ° F
	3/16"	**36" Short Dimen.	1.17	
	1/4"	**48" Short Dimen.	1.56	

*Data obtained from manufacturers' literature and/or photometric testing.

**A General Guideline for Flat Sheets under Moderate Windload and Deadload.

Special Designs should be submitted to the Plastic Manufacturer for deflection and thermal analysis. Thermoforming to flanged dish shape may be necessary to provide required rigidity and mechanical stability.

Figure 1.3.5

PERTINENT PHYSICAL PROPERTIES OF TRANSPARENT GLAZING MEDIA

GLAZING MEDIA	NOMINAL THICKNESS	NOMINAL MAXIMUM SIZES RECOMMENDED	WEIGHT (LBS./SQ.FT.)	EXPANSION COEFFICIENT
ORDINARY CLEAR LIME GLASS (FLOAT) (IRON OXIDE CONTENT 0.10% TO 0.13%)	3.2 mm	86.4 cm x 193 cm	7.96	87 x 10 ⁻⁷ PER °C
	4.8 mm	91.4 cm x 244 cm	12.25	
	6.0 mm	122 cm x 305 cm	14.74	
SHEET LIME GLASS (LOW IRON OXIDE CONTENT 0.05% TO 0.06%)	3.2 mm	86.4 cm x 193 cm	7.96	90 x 10 ⁻⁷ PER °C
	4.8 mm	91.4 cm x 244 cm	12.25	
WATER-WHITE CRYSTAL GLASS #76 (0.01% IRON OXIDE)	4.0 mm	86.4 cm x 193 cm	9.91	85 x 10 ⁻⁷ PER °C
	4.7 mm	91.4 cm x 244 cm	11.77	
	5.5 mm	122 cm x 244 cm	13.67	
*METHYL METHACRYLATE (100% ACRYLIC COLORLESS CAST SHEET)	3.2 mm	61.0 cm Short Dimen	3.66	738 x 10 ⁻⁷ PER °C
	4.7 mm	91.4 cm Short Dimen	5.37	
	6.2 mm	122 cm Short Dimen	7.32	
*POLYCARBONATE CLEAR SHEET (LIGHT STABLE TYPE)	3.2 mm	61.0 cm Short Dimen	3.81	675 x 10 ⁻⁷ PER °C
	4.7 mm	91.4 cm Short Dimen	5.71	
	6.2 mm	122 cm Short Dimen	7.62	

*Data obtained from manufacturers' Literature and/or Photometric Testing.

**A General Guideline for Flat Sheets under Moderate Windload and Deadload.

Specific Designs should be submitted to the Plastic Manufacturer for Deflection and thermal analysis.

Thermoforming to flanged dish shape may be necessary to provide required rigidity and mechanical stability.

Figure 1.3.6

PERTINENT PHYSICAL PROPERTIES OF TRANSPARENT GLAZING MEDIA

GLAZING MEDIA	ELASTIC MODULUS	DESIGN TENSILE STRENGTH	HEAT DEFLECTION TEMPERATURE	IMPACT RESISTANCE
ORDINARY CLEAR LIME GLASS (FLOAT) (IRON OXIDE CONTENT 0.10% TO 0.13%)	10.5×10^6 psi	**Annealed: 1600 psi **Tempered: 6400 psi	In Excess of 1100° F.	Steel ball impact per ANSI Z26.1-1966 requires testing 12" x 12" samples. Fully tempered glass must withstand 10' drop of 1/2 lb. steel ball (5 ft.lbs. impact). Also, it must withstand soft body impact of 11 lb. shot bag dropped 8'. (88 ft.lbs. impact). 1/8" Fully Tempered glass and thicker will withstand these tests, temperature level having little effect on this performance.
SHEET LIME GLASS (LOW IRON OXIDE CONTENT 0.05% TO 0.06%)	10.5×10^6 psi	**Annealed: 1600 psi **Tempered: 6400 psi	In Excess of 1100° F.	Fully Tempered glass and thicker will withstand these tests, temperature level having little effect on this performance.
WATER-WHITE CRYSTAL GLASS #76 (0.01% IRON OXIDE)	10.5×10^6 psi	**Annealed: 1600 psi **Tempered: 6400 psi	In Excess of 1100° F.	
*METHYL METHACRYLATE (100% ACRYLIC COLORLESS CAST SHEET)	0.45×10^6 psi	10,500 psi average ultimate tensile strength	215° F at 264 psi	Per ANSI Z26.1-1966 passes impact from steel ball: 1/8" - 3 ft.lbs. 3/16" - 5.25 ft.lbs. 1/4" - 9 ft. lbs.
*POLYCARBONATE CLEAR SHEET (LIGHT STABLE TYPE)	0.345×10^6 psi	9,500 psi average ultimate tensile strength	270° F at 264 psi	Polycarbonate data per Z26.1 basis not available but withstands much higher impact than acrylic and over greater temperature range.

*Data obtained from manufacturers' Literature and/or Photometric Testing.

**Design Tensile values for glasses are for a safety factor of 2.5 and probability of 0.8% failure under one-minute windloading.

Figure 1.3.7

PERTINENT PHYSICAL PROPERTIES OF TRANSPARENT GLAZING MEDIA				
GLAZING MEDIA	ELASTIC MODULUS	DESIGN TENSILE STRENGTH	HEAT DEFLECTION TEMPERATURE	IMPACT RESISTANCE
ORDINARY CLEAR LIME GLASS (FLOAT) (IRON OXIDE CONTENT 0.10% TO 0.13%)	0.738×10^6 kgs/sq. cm.	**Annealed: 112.5 kgs/sq.cm. **Tempered: 450 kgs/sq.cm.	In Excess of 600° C	Steel ball impact per ANSI Z26.1-1966 requires testing 30.5cm x 30.5cm samples. Fully Tempered glass must withstand 3.05 m drop of 0.227 kg steel ball (0.69 kg-m impact). Also it must withstand soft body impact of 4.99 kg shot bag dropped 2.44m (12.2 kg-m impact). 3.2 mm Fully Tempered glass and thicker will withstand these tests, temperature level having little effect on this performance
SHEET LIME GLASS (LOW IRON OXIDE CONTENT 0.05% TO 0.06%)	0.738×10^6 kgs/sq. cm.	**Annealed: 112.5 kgs/sq.cm. **Tempered: 450 kgs/sq.cm.	In Excess of 600° C	Per ANSI Z26 1-1966 passes impact from steel ball: 3.2 mm - 1.36 kg-m 4.7 mm - 2.38 kg-m 6.2 mm - 4.08 kg-m
WATER-WHITE CRYSTAL GLASS #76 (0.01% IRON OXIDE)	0.738×10^6 kgs/sq. cm.	**Annealed: 112.5 kgs/sq.cm. **Tempered: 450 kgs/sq.cm.	In Excess of 600° C	Polycarbonate data per Z26.1 basis not available but withstands much higher impact than acrylic and over greater temperature range.
*METHYL METHACRYLATE (100% ACRYLIC COLORLESS CAST SHEET)	0.032×10^6 kgs/sq. cm.	738 kgs/sq.cm. average ultimate tensile strength	119° C at 18.6 kgs/sq.cm.	
*POLYCARBONATE CLEAR SHEET (LIGHT STABLE TYPE)	0.024×10^6 kgs/sq. cm.	668 kgs/sq.cm. average ultimate tensile strength	130° C at 18.6 kgs/sq.cm.	

*Data obtained from manufacturers' Literature and/or Photometric Testing.

**Design Tensile values for glasses are for a safety factor of 2.5 and probability of 0.8% failure under one-minute windloading.

Figure 1.3.8

are taken up by the masonry and only inaccuracies in the masonry units themselves are adjusted by the mortar joints.

"When, however, a complete functional element, such as a photovoltaic collector, neoprene gasket lattice, is to be composed of factory-made or prefabricated components, the question of tolerance, that is to say the degree of inaccuracy that can be tolerated, becomes acute, if the functional element is to be satisfactorily assembled".

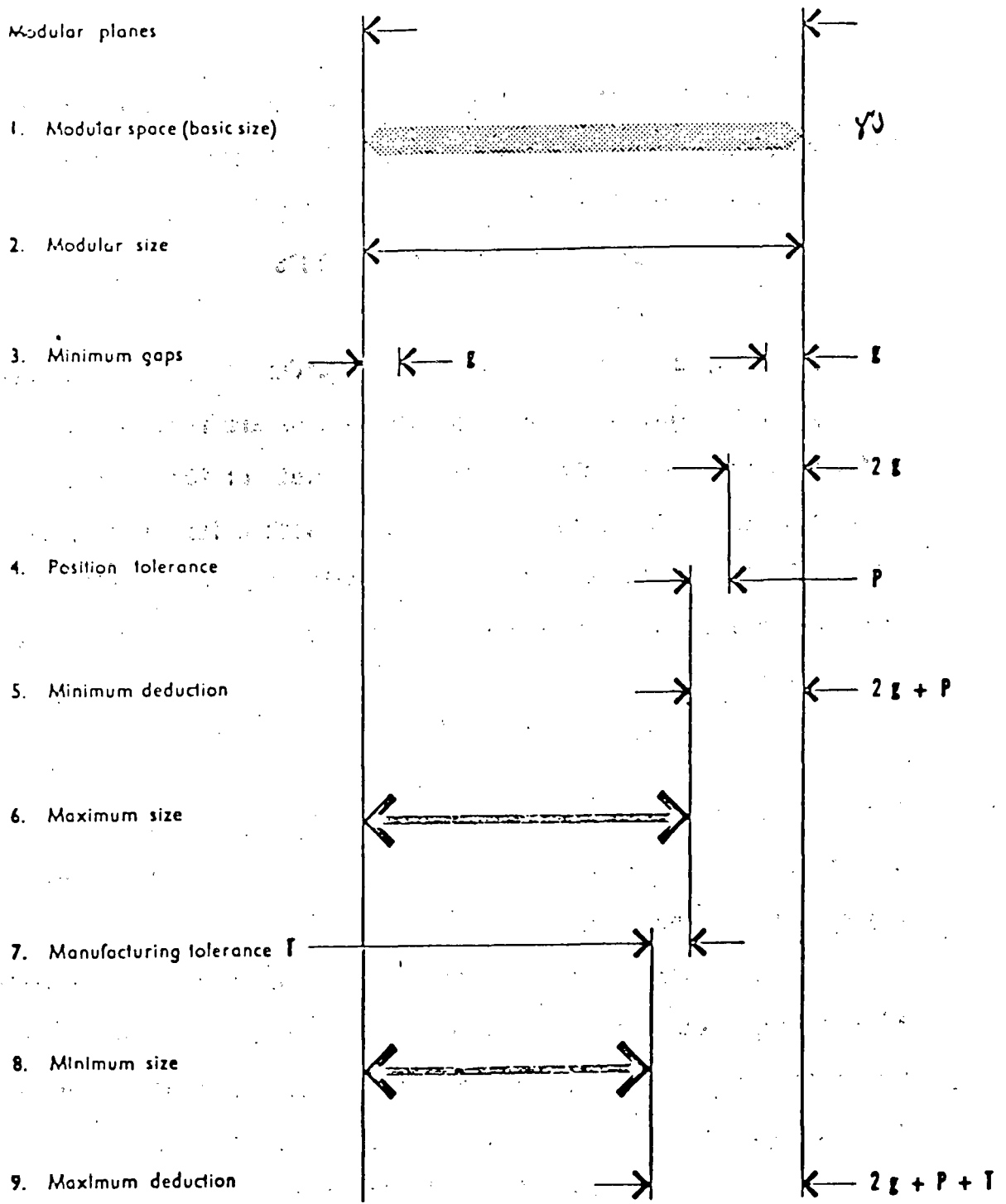
1.3.2.1.2 Width Tolerance

The first tolerance to be determined will be the width variances in the glazing itself. This glass module is established and the amounts are specified for each aspect of the tolerance shown below. The square root of the sum of the squares gives the overall tolerance for the width of the panel. Tolerance limits which were used for glazing with neoprene gaskets can be found in Figure 1.3.9.

tpw = total overall tolerance of the width of the panel	
tsi = size tolerance	= $\pm .09375"$
tsq = square tolerance	= $\pm .09375"$
tpl = plumbness tolerance	= $.09375"$
tpo = position tolerance	= $.328125"$

For the total overall tolerance (tpw), squareness and plumbness are, because of the interaction that occurs between them within the array, arbitrarily reduced to .75 of the amounts shown in Figure 1.3.10.

APPLICATION OF THE SYSTEM OF TOLERANCES TO A MODULAR COMPONENT



Source: OEEC, Modular Co-ordination: Second Report of EPA Project 174, op. cit., p. 175.

Figure 1.3.9

Therefore, the total overall tolerance of the width of the panel according to "Modular Coordination of Low Cost Housing" is:

$$\begin{aligned} \text{tpw} &= (\text{tsi})^2 + (.75 + \text{sq})^2 + (.75 + \text{pl})^2 = (\text{tpo})^2 \\ &= .035" + .0197" + .0049" + .1076" \\ &= .1672" \end{aligned}$$

A typical case is shown when 3 standard modules are placed side by side to form an array. In doing so, we are requiring the modules to keep within their total modular width of 90" but not insisting that each component should remain within its own modular space. Based on this assumption, their tolerances may be combined to give the overall tolerance in width when they are placed next to each other:

$$\begin{aligned} \text{tpwd} &= 3(.1672")^2 &= .2895" \\ & & \pm .145" \end{aligned}$$

Finally, this means that the work size for the width of the glass is the specified glazing size less a deduction for minimum joint less .1672" for tolerance.

"The work size of components should be as large as possible, after making a statistical analysis as indicated here. There is no virtue in making a large minimum deduction from the modular size to cover all possible errors. This can result in over-large joints."²

1.3.2.1.3 Height Tolerance

The height tolerance considerations are exactly the same as the width tolerances in this case because all interfaces are between identical modules. Therefore, the total overall tolerance of the height of the panel is:

²ibid, p. 134, 135, 136

$$\begin{aligned}
tph &= (tsi)^2 + (.75 + sq)^2 + (.75 + pl)^2 + (tpo)^2 \\
&= .35" + .0197" + .0049" + .1076" \\
&= .1672"
\end{aligned}$$

The overall 3 module height tolerance is:

$$\begin{aligned}
tphd &= 3(.1672")^2 &= .2895" \\
& &+ .145"
\end{aligned}$$

1.3.2.1.4 Joint Tolerance

Practical tolerances must be considered in order to insure performance of the system. Both H-type and spline-type neoprene glazing gaskets are designed to accept metal banded glass. They provide an adequate bite on the glass in the normal manufacturing tolerance range, which is $+1/8"$, $-1/16"$ under 48", and $+3/16"$, $-1/16"$ over 48". However, the frame tolerances must be held to $\pm 1/8"$. Since the glass is factory-cut and fabricated, sizes are generally uniform, whereas field variations may occur in the frame. It is therefore essential that the frame openings be within the specified tolerances because they are the basis from which the gaskets and glass are made to fit the frame properly. For example: if the frames are on the minus side and the glass on the plus side, difficulty with installing the glass and gasket will occur.

Far more serious problems will occur if sufficient clearance is not provided for edge movement, since stresses may occur which will cause fracturing of the glazing units. The resilient structural gasket will accommodate limited thermal movement, shock, and misalignment, thus reducing the possibility of glass breakage.

1.3.2.1.5 System Dimension

The system dimensions can be determined by the process referred to in Figure 1.3.9. The modular size in this case is the given standard module or 2.5' x 8'. The minimum gap or joint is half the center web of the glazing gasket (see Figure 1.3.10) plus the allowable joint tolerance. The web is .1719" thick, half of that is .0859". The allowable joint tolerance for the entire width or length is $\pm .125"$ or .25" total. Therefore, the maximum size as shown in Figure 1.3.9 is equivalent to the glazing size or the modular size (2 x the gap).

$$\begin{aligned}\text{Maximum width} &= 30" - 2(.0859" + .125") \\ &= 29.5782" \\ \text{Maximum length} &= 96" - 2(.0859" + .125") \\ &= 95.5782"\end{aligned}$$

These maximum dimensions are further reduced by subtracting the manufacturing tolerance which is .1672" in both the width and length directions. This would then correspond to the minimum glazing size.

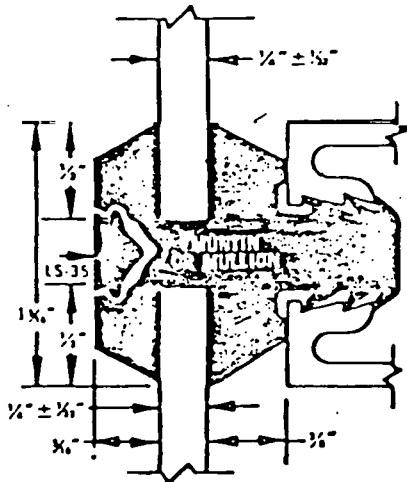
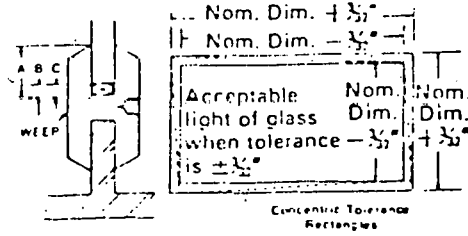
$$\begin{aligned}\text{Minimum width} &= 29.4062" - .1672" = 29.411" \\ \text{Minimum length} &= 95.4062" - .1672" = 95.411"\end{aligned}$$

See Figure 1.3.9 which combines these relationships.

Further justification of the standard module size beyond its relation to current building dimensions and array size options can be seen in a comparison with a 4' x 4' panel. Although the single glazing system proposed (see Figure 1.3.11) will be as cost effective as the 4' x 4' module, it will exhibit all of the following benefits:

FLOAT GLASS (CLEAR AND TINTED)

1/4"	140	229	$\pm 1/16$	$\pm 1/32$	1/4"	11/16"	1/32" x 1/4"
1/4"	207	229	$\pm 1/32$	$\pm 1/32$	7/8"	1/4"	1/8" x 7/8"
3/16"	140	229	$\pm 1/16$	$\pm 1/32$	1/4"	11/16"	1/32" x 1/4"
3/16"	207	229	$\pm 1/32$	$\pm 1/32$	7/8"	1/4"	1/8" x 7/8"
1/2"	207	229	$\pm 1/32$	$\pm 1/32$	1/2"	11/16"	1/32" x 1/4"
1/2"	258	286	$\pm 1/32$	$\pm 1/8$	7/8"	1/4"	1/8" x 7/8"
1/2"	258	286	$\pm 1/8$	$\pm 1/32$ (D)	7/8"	1/4"	1/8" x 7/8"
1/2"	258	286	$\pm 1/8$	$\pm 1/32$	11/16"	9/32"	1/8" x 9/32"
1/2"	258	286	$\pm 1/8$	$\pm 1/32$ (D)	7/8"	1/4"	1/8" x 7/8"
1/2"	258	286	$\pm 1/8$	$\pm 1/32$	11/16"	9/32"	1/8" x 9/32"

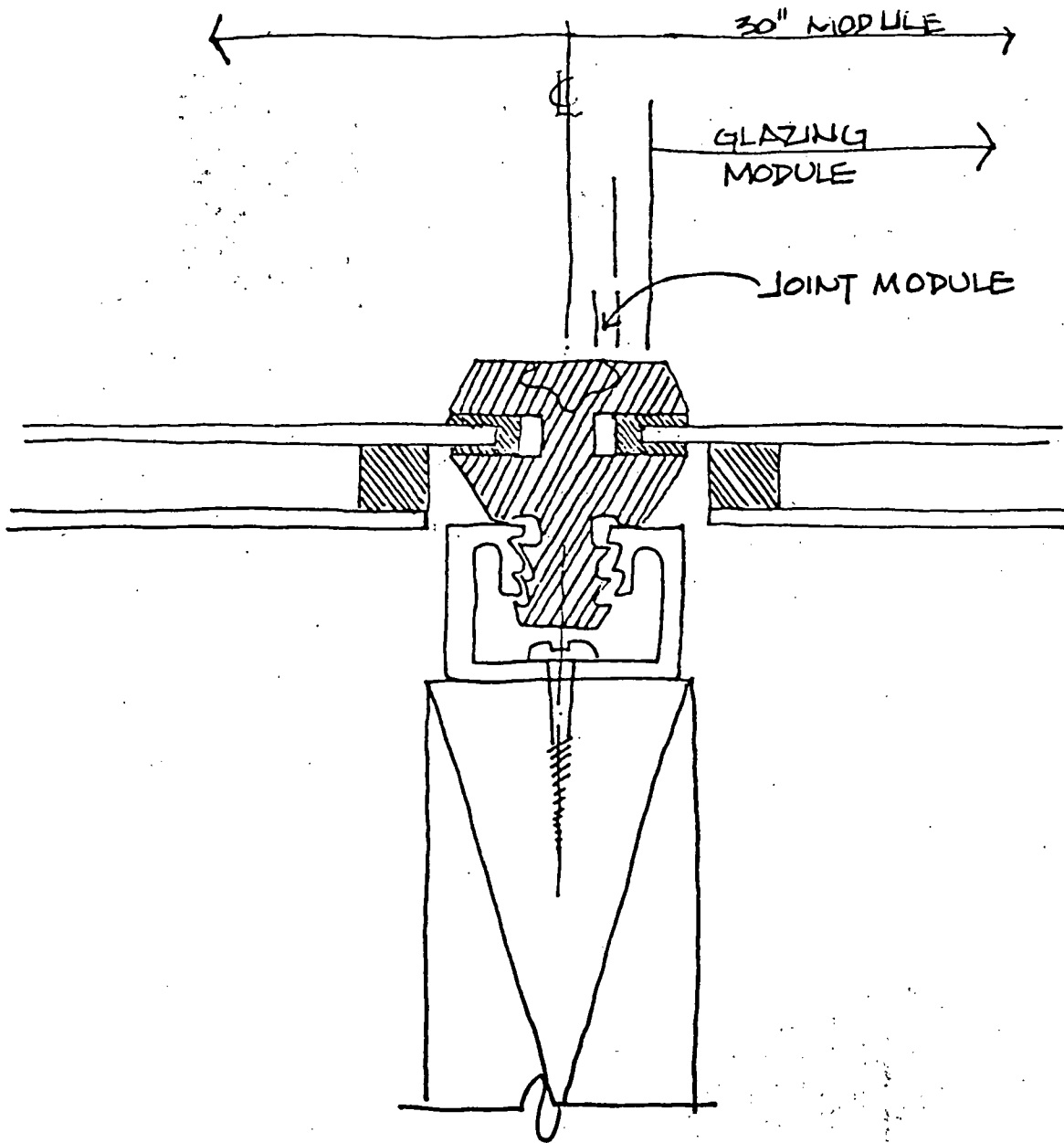


SL-1616-M4

DETAIL OF GASKET SECTION FOR SUPPORTED LADDER-TYPE SYSTEMS

Muntin (or Mullion) Section SL-1616-M4 is designed to fit into a matching aluminum ratchet-faced, splined extrusion. Use of this Section provides improved resistance to blowout and deflection as compared with unsupported ladder or grid systems.

FIGURE 1.3.10



PROPOSED COLLECTOR FRAMING
MODULAR DIMENSION

FIGURE 1.3.11

Standard Module

4 x 4 Module

$\frac{20 \text{ sq. ft. of glass}}{21 \text{ lineal ft. of gasket}}$ vs $\frac{16 \text{ sq. ft. of glass}}{16 \text{ lineal ft. of glazing}}$

- packing and shading of the photovoltaic cells is reduced
- less labor required on site
- less edge joining over the entire array, therefore fewer breaks can occur in the weather seal
- better material usage - glass is utilized to its structural limit
- fewer horizontal joints - these are the hardest to seal
- fewer electrical and fluid connections between collectors

The larger standard module exhibits some problems however:

- cracking during shipping and handling
- expansion difficulties in the absorber plate because of its non-rectilinear shape
- less array size flexibility unless the 2.5' x 5' and the 2.5' x 3' modules are also produced
- assumes Roll-Bond plates could be made large enough to satisfy standard module condition

1.3.2.1.6 Residential Module

All of the tolerance specifications established in the 2.5' x 8' standard module will also apply here. However, because of existing residential building systems, a module 32" wide by 96" long on centerline dimensions is preferred. This allows for the following additional benefits:

- o if trusses are 32" on center, the collector could be nested between them, allowing for easier detailing.

- plywood sheathing of the 4' x 8' variety could still be used on roof area not covered by the collector system
- minimum additional structural costs would be incurred due to the increase of truss spacing from 24" to 32"
- collector waterproof joints would be minimized
- glazing would be non-tempered 3/16" white water crystal which has a significant cost benefit over tempered glazing
- installation of the system could be handled by 2 men
- maximizes square footage installed in relation to labor steps involved
- all benefits relating to the 2.5' x 8' standard module also apply here

1.3.2.2 Module Voltage and Shadowing Analyses

1.3.2.2.1 Description of Program

The design of photovoltaic modules will most likely proceed from specifications of sizes and shapes compatible with existing construction modules, and they will be chosen to provide reasonable ease of handling, array assembly, and maintenance. Furthermore, the same considerations are equally likely to be starting points for concentrator systems, although the precise nature of the optical systems impose some added constraints on the cell and module designs.

Once size and the concentration ratio are chosen, the power output of the module depends only on the cell and module efficiencies. For example, a module 32 by 96 inches, appropriate for residential construction, would supply about 300 watts peak assuming a 15% overall efficiency. At this point, the power conditioning system requirements must be considered. Efficient, low cost inverters must operate at relatively high voltages. Since the cell provides only about 0.5V, achieving, for example, a 1000V module output would require about 2000 series connected cells assuming a single string. For the residential 32 by 96 inch module, this would require cells 10 cm^2 in area if 100% module area utilization is assumed.

There are obvious trade-offs between module voltage and assembly costs. The approach to module design optimization is based on creating a computer model with which the relationships between module voltage, cost and performance can be examined. The input parameters consist of projected cell performance functions, module

dimensions and voltage rating, interconnect and bus resistances, protection diode factors, and assembly area margins. Also required are estimated assembly costs per cell including attachment, interconnect bonding, handling and testing. There may also be an overhead cost associated with fabricating cells for high voltage strings since single large area cells will probably be simpler to produce than a multiplicity of small cells or a larger integrated high voltage device.

The performance analysis combines the projected cell characteristics with the module interconnect parameters and determines the module voltage/current behavior as a function of light intensity and temperature. In addition, provisions are included to examine the effects of non-uniform temperature and illumination distributions.

The computer model developed permits the examination of the inter-relationships between module design, costs, and performance. Given module dimensions, nominal operation temperature, light intensity, and required voltage, the program designs a module, determines its cost, and calculates its characteristics. The cell dimensions and characteristics are determined by the nominal operation conditions, temperature and light intensity, and a design voltage. Additional required input specifications include the cell width, module dimensions, assembly clearances, and the interconnect and protective diode arrangements.

The cells are assumed to be rectangular, sheet, ribbon, or thin-film, with energy conversion behavior shown in this single exponential expression:

$$I = I_L - I_0 \exp ([V + IR]/kT) \quad (1.3.3)$$

where I = output current in amperes

V = output voltage

$$I_L = K_5 A_1 (K_1 + K_2 T) U$$

$$I_0 = A_1 K_3 T^3 \exp (-E_g/kT)$$

$$E_g = K_6 + (T - 300) K_7$$

$$R = K_4/A_1$$

A_1 = cell junction area (cm^2)

U = light intensity (watts/cm^2)

T = temperature ($^{\circ}\text{K}$)

k = Boltzman constant ($\text{ev}/^{\circ}\text{K}$).

The form of the analytical model used to represent the silicon solar cell in this analysis is not quite the same as that used by Professor Martin Wolf for his calculation of array performance. They are sufficiently similar, however, that their results are compatible. As explained in Section 1.3.1, Professor Wolf's double exponential model reduces to one using only a single exponential for the higher efficiency cells projected for the 1985 to 2000 era. For the purposes of these calculations, then, the minor differences between these models can be assumed to be negligible.

The remaining parameters, K_i , depend on the type of cell and its projected characteristics. The values used in the present analyses are given in Table 1.3.2.

Table 1.3.2

Projected Solar Cell Parameters

<u>Year</u>	<u>Silicon Cells</u>		<u>Units</u>
	<u>1985</u>	<u>2000</u>	
			<u>Electrical Parameters</u>
K ₁	.0347371	.0344318	Amp/watt cm ²
K ₂	7.1972 x 10 ⁻⁶	7.4348 x 10 ⁻⁶	Amp/watt °K cm ²
K ₃	.652	.0308	Amp/°K cm ²
K ₄	.34	.34	.34 ohm cm ²
K ₅	.92	.92	Contact area coverage factor
K ₆	1.12	1.12	eV
K ₇	2.8 x 10 ⁻⁴	.0001	eV/°K
			<u>Cost Parameters</u>
C ₀	.002	-	Cell cost (\$/cm ²)
C ₁	.0002	-	Covering (\$/cm ²)
C ₂	.001	-	Substrate (\$/cm ²)
C ₃	.01	-	Protection Diode (\$/diode)
C ₄	.00875	-	Assembly/attachment (\$/cell)
C ₅	.005	-	Interconnects (\$/interconnect)
C ₆	.0005	-	Bonding (\$/bond)

The formulations of the module voltage-current equations and maximum-power calculations are constructed to permit the division of the module arbitrarily into two regions with differing temperatures and illumination intensities. To accomplish this, it is necessary to include the behavior of the protective diodes and their arrangement. For example; in a series-string provided with diodes bridging each twenty cells, a shadow covering from one to twenty cells of a diode-substring, causes the voltage contribution of that substring to be replaced by negative voltage equal to the protective diode forward drop.

This two-region capability permits the examination of important design relationships involving the thermal design of heat-exchange systems, the effects of component failure and the design trade-offs influencing illumination uniformity in concentration systems.

An analysis for four- and six-region modules has been carried out which permits series-parallel module designs. However these formulations are not presently implemented in the computer model, principally because the series-parallel designs imply undesirably small cells for modules of reasonable size and voltage.

This program includes a highly simplified cost analysis which provides the capability of an examination of the relative influence of various design choices on module cost. A sufficiently broad set of factors was chosen in order to cover all anticipated methods of module fabrication. The list of module cost parameters and their values is shown also in Table 1.3.2. The values chosen for the cost parameters used in the analysis represent one approach to a \$50/m²

module. The breakdown assumed is shown in Table 1.3.3. Shown also in the table are the per kW costs of the parameters if module efficiency were 10%. The derivation of the \$10/m² aluminum substrate figure assumption is presented in the following paragraphs.

Table 1.3.3

Assumed Module Cost Breakdown

<u>Parameter</u>	<u>\$/m²</u>	<u>\$/kW @ 10%</u>
Cell	20	200
Cover	2	20
Substrate (Alum.)	10	100
Prot. Diode (\$.01/diode)	4	40
Handling and Assy.	6	60
Interconnects	4	40
Bonds	4	40
	<u>50/m²</u>	<u>500/kW</u>

A roll formed aluminum structure was designed to withstand a wind loading of 146 Kg/m² (30 lb/ft² with a 25% safety margin). Module size was assumed to be .813 x 2.44 meters (32 in. x 96 in.). The limiting structure cost can be found by determining the cost of raw material used. Assuming that aluminum costs \$0.86/pound, the module substrate costs \$9.70/m² in 1975 dollars. If the solar cell efficiency is assumed to be 14% at the operating temperature, then array electrical losses and less than 100% cell packing factor would reduce overall array solar conversion efficiency to approximately 10%. At 10% array efficiency and 100 mW/cm² insolation, the required module

area is $10 \text{ m}^2/\text{kW}_e$. For this case, the total module cost must be $\$50/\text{m}^2$. Since the aluminum substrate costs $\$9.70/\text{m}^2$, there is $\$40.30$ left for cells, insulation, interconnects, fabrication, and cell and interconnect protection. The $\$500/\text{kW}$ cost goal is based on module output at $100 \text{ mW}/\text{cm}^2$ insolation with the cells operating at 60°C . If a desert site in the Phoenix area which reaches a noontime temperature of 45°C is assumed giving an aluminum fin backed panel a ΔT above ambient of about 15°C (this assumes a wind of approximately $3\text{m}/\text{sec}$.), then the cell temperature would be approximately 60°C . If we assumed, however, that the panel is mounted to a wood backing such as a roof, the rear side cooling is minimal and the panel temperature can exceed 100°C . For our studies we will assume the reference $\$500/\text{kW}$ module has cooling on both the front and back module faces. We must make such an assumption since cell efficiency is strongly affected by cell temperature and the required cell area per rated kW is inversely proportional to cell efficiency.

It is emphasized that, while these calculations were intended to provide reasonably plausible projected costs, a detailed economic model was not warranted and the numbers should be interpreted with this in mind.

This program, in addition to various tabular outputs, includes a simple terminal plotting routine to provide quick graphical presentations showing parameter relationships.

A listing of the program is included as Appendix A.

1.3.2.2.2 Presentation of Results

The module size chosen for use in the analysis was 32" x 96". Rectangular solar cells were assumed, and each edge of each cell was assumed to be spaced from that of its adjacent neighbor by a specified cell margin. In addition, a distance specified as the module (or panel)* margin must exist between the edge of the module and the edge of the nearest cell. Parametric data were obtained for modules with nominal voltages of 200, 400, 600 and 800V.

Effect of Solar Cell Size

The first module analysis included a determination of cell sizes for the given module dimension and the various values of nominal module voltage assumed. Copies of cell and module output data for the four nominal input voltage cases chosen are shown in Table 1.3.4. For the data shown in the table, cell width was held constant at 5 cm while cell length was allowed to vary as necessary to make possible incorporation of the proper number of cells to obtain the required nominal module voltage.

The results of this study are summarized in Table 1.3.5. Note that as nominal module voltage increases, individual cell size decreases while module cost per kilowatt of output increases. The increased cost per kilowatt of the module will have to be traded off against the decreased cost per kilowatt of power conditioning equipment as voltage increases. In addition, the series connection

*The word panel is used interchangeably with module in this analysis.

CELL DATA, YEAR 1985 SILICON CELLS
TEMP=325DEG-K ILLUMINATION= .100W/CM2
AREA= 38.34CM2 WIDTH= 5.08CM LENGTH= 7.55CM
VOC=.5412VOLTS ISC = 1.3078AMPS
VP= .4511VOLTS IP = 1.2292AMPS POWER= .5545WATTS
EFFICIENCY=14.46% FILL=.7834 RS= .0089OHMS

PANEL DATA, YEAR 1985 SILICON CELLS
LENGTH=243.84CM WIDTH= 81.28CM AREA= 1.98M2
DESIGN VOLTAGE= 200VOLTS NO. OF STRINGS= 1
MARGINS: PANEL= 1.00CM CELL= .010CM
CELLS/STRING= 480 CELLS/PANEL= 480 CELLS/DIODE= 5
15 ACROSS BY 32 DOWN PACKING FACTOR=.929
R/CELL=.0089OHMS R/INTERCONNECT=.0089 R TOTAL= 8.51OHMS
REGION 1 T=325DEG K INTENSITY= .100WATTS/CM2 NO.OF CELLS= 480
REGION 2 T=325DEG K INTENSITY= .000WATTS/CM2 NO.OF CELLS= 0
VOC= 259.76VOLTS ISC= 1.308AMPS
VP = 205.56VOLTS IP = 1.226AMPS POWER= 251.94WATTS
EFFICIENCY=12.71% FILL=.7416
PANEL COST= \$80.16 \$318.18/KW

CELL DATA, YEAR 1985 SILICON CELLS
TEMP=325DEG-K ILLUMINATION= .100W/CM2
AREA= 19.45CM2 WIDTH= 5.08CM LENGTH= 3.83CM
VOC=.5412VOLTS ISC = .6634AMPS
VP= .4511VOLTS IP = .6235AMPS POWER= .2813WATTS
EFFICIENCY=14.46% FILL=.7834 RS= .0175OHMS

PANEL DATA, YEAR 1985 SILICON CELLS
LENGTH=243.84CM WIDTH= 81.28CM AREA= 1.98M2
DESIGN VOLTAGE= 400VOLTS NO. OF STRINGS= 1
MARGINS: PANEL= 1.00CM CELL= .010CM
CELLS/STRING= 945 CELLS/PANEL= 945 CELLS/DIODE= 5
15 ACROSS BY 63 DOWN PACKING FACTOR=.927
R/CELL=.0175OHMS R/INTERCONNECT=.0175 R TOTAL=33.04OHMS
REGION 1 T=325DEG K INTENSITY= .100WATTS/CM2 NO.OF CELLS= 945
REGION 2 T=325DEG K INTENSITY= .000WATTS/CM2 NO.OF CELLS= 0
VOC= 511.40VOLTS ISC= .663AMPS
VP = 404.70VOLTS IP = .622AMPS POWER= 251.61WATTS
EFFICIENCY=12.70% FILL=.7416
PANEL COST= \$89.61 \$356.15/KW

Table 1.3.4(a)

Computations for 200 and 400V Modules

CELL DATA, YEAR 1985 SILICON CELLS
 TEMP=325DEG-K ILLUMINATION= .100W/CM2
 AREA= 12.88CM2 WIDTH= 5.08CM LENGTH= 2.54CM
 VOC=.5412VOLTS ISC = .4394AMPS
 VP= .4511VOLTS IP = .4130AMPS POWER= .1863WATTS
 EFFICIENCY=14.46% FILL=.7834 RS= .0264OHMS

PANEL DATA, YEAR 1985 SILICON CELLS
 LENGTH=243.84CM WIDTH= 81.28CM AREA= 1.98M2
 DESIGN VOLTAGE= 600VOLTS NO. OF STRINGS= 1
 MARGINS: PANEL= 1.00CM CELL= .010CM
 CELLS/STRING=1425 CELLS/PANEL=1425 CELLS/DIODE= 5
 15 ACROSS BY 95 DOWN PACKING FACTOR=.926
 R/CELL=.0264OHMS R/INTERCONNECT=.0264 R TOTAL=75.23OHMS
 REGION 1 T=325DEG K INTENSITY= .100WATTS/CM2 NO.OF CELLS=1425
 REGION 2 T=325DEG K INTENSITY= .000WATTS/CM2 NO.OF CELLS= 0
 VOC= 771.16VOLTS ISC= .439AMPS
 VP = 610.27VOLTS IP = .412AMPS POWER= 251.28WATTS
 EFFICIENCY=12.68% FILL=.7416
 PANEL COST= \$97.20 \$386.82/KW

CELL DATA, YEAR 1985 SILICON CELLS
 TEMP=325DEG-K ILLUMINATION= .100W/CM2
 AREA= 9.70CM2 WIDTH= 5.08CM LENGTH= 1.91CM
 VOC=.5412VOLTS ISC = .3309AMPS
 VP= .4511VOLTS IP = .3110AMPS POWER= .1403WATTS
 EFFICIENCY=14.46% FILL=.7834 RS= .0351OHMS

PANEL DATA, YEAR 1985 SILICON CELLS
 LENGTH=243.84CM WIDTH= 81.28CM AREA= 1.98M2
 DESIGN VOLTAGE= 800VOLTS NO. OF STRINGS= 1
 MARGINS: PANEL= 1.00CM CELL= .010CM
 CELLS/STRING=1890 CELLS/PANEL=1890 CELLS/DIODE= 5
 15 ACROSS BY 126 DOWN PACKING FACTOR=.925
 R/CELL=.0351OHMS R/INTERCONNECT=.0351 R TOTAL=*****OHMS
 REGION 1 T=325DEG K INTENSITY= .100WATTS/CM2 NO.OF CELLS=1890
 REGION 2 T=325DEG K INTENSITY= .000WATTS/CM2 NO.OF CELLS= 0
 VOC=1022.80VOLTS ISC= .331AMPS
 VP = 809.41VOLTS IP = .310AMPS POWER= 250.96WATTS
 EFFICIENCY=12.66% FILL=.7416
 PANEL COST= \$109.13 \$434.84/KW

Table 1.3.4(b)

Computations for 600 and 800V Modules

of lower voltage modules to obtain a higher voltage for the power conditioning system appears to offer a cost performance advantage. A lower limit to series connected modules would be associated with system reliability in the event of an open circuit in a single series string of cells and modules.

Table 1.3.5

Summary of Cell Size Analyses

<u>Parameter</u>	<u>Units</u>	<u>Nominal Voltage</u>			
		<u>200V</u>	<u>400V</u>	<u>600V</u>	<u>800V</u>
Cell Width	cm	5.0	5.0	5.0	5.0
Cell Length	cm	7.5	3.8	2.5	1.9
Cell Area	cm ²	38.4	19.4	12.9	9.7
Cell Efficiency	%	————— 14.4 —————			
Panel Size	in	————— 32 x 96 —————			
Panel Power	W	————— 252 —————			
Panel Efficiency	%	————— 12.7 —————			
Panel Cost (CM = .01 cm)	\$/kW	318	356	387	435
Panel Cost (CM = 0.1 cm)	\$/kW	313	350	381	430

Shown also in Table 1.3.5 are costs for modules with cell margins of 0.01 cm, used for all other calculations, and 0.1 cm. The difference in cost per kilowatt is negligible indicating that either value is satisfactory.

The performance of the modules simulated as cell temperature was varied is shown in Figure 1.3.12. Shown in the figure are the

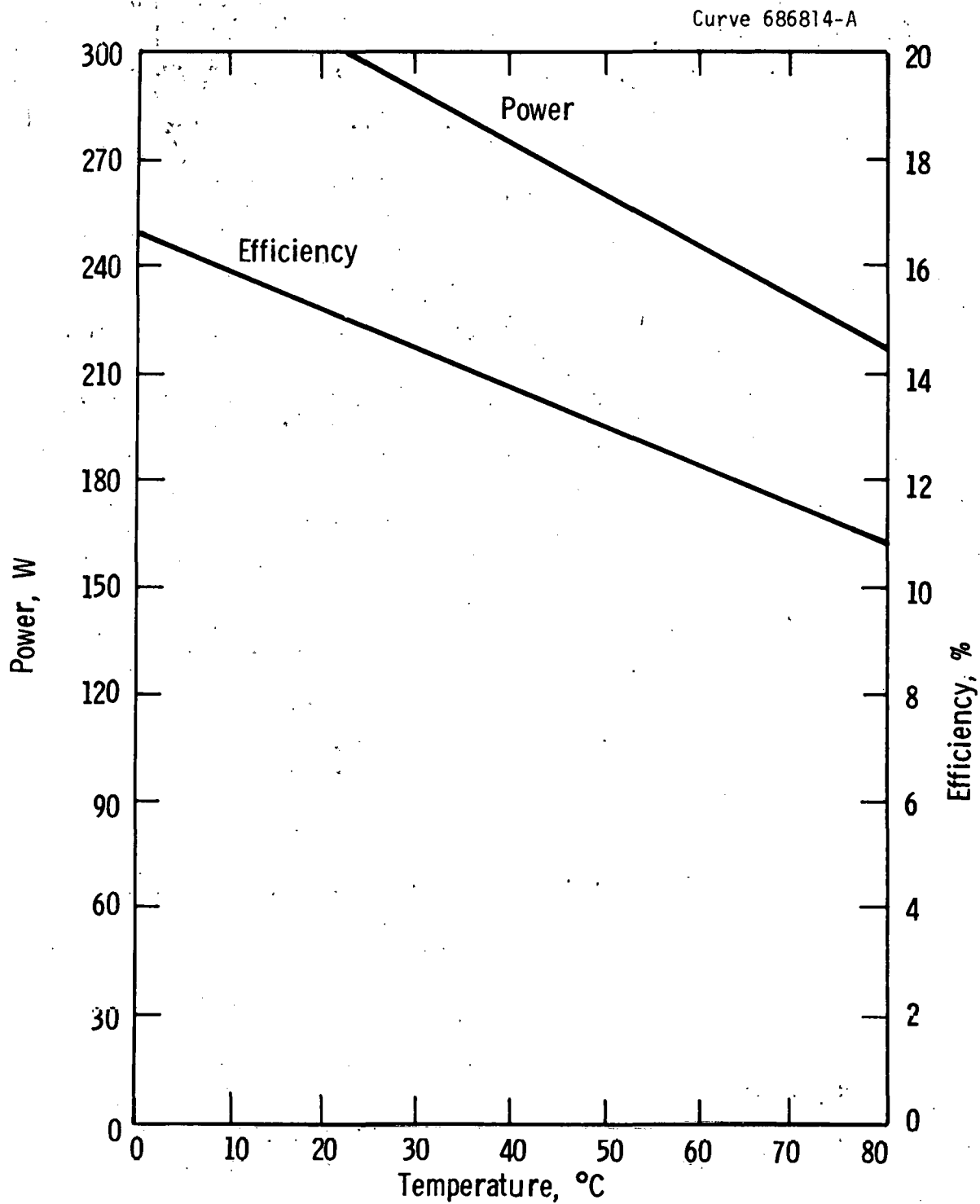


Fig. 1.3.12 - Temperature performance of modules described in Table 1.3.4.

variations of the module power and efficiency with temperature. The performance is the same for all four cases analyzed.

An additional investigation was made to determine the effect of varying cell width about the value of 5 cm used for the previous analysis. A series of calculations was made for an intermediate voltage module of 500V using cells with widths ranging from 2 to 10 cm. Cell length was then calculated to make possible the proper number of cells to obtain the require module voltage.

The results of this analysis are summarized in Table 1.3.6. The effects are not dramatic, but the data does show a tendancy toward increased cost as cell widths approach 8 cm.

Table 1.3.6

Effect on Module Cost of Varying Cell Width

<u>Parameter</u>	<u>Units</u>	<u>Cell Width (cm)</u>				
		<u>2</u>	<u>4</u>	<u>6</u>	<u>8</u>	<u>10</u>
Panel Voltage	V	500				
Panel Power	W	252				
Panel Cost	\$/kW	375	375	375	385	395

Effect of Different Temperatures

For this calculation, the cells of a module were divided into two groups of equal size, and while the temperature of one group was held at approximately 50°C, that of the other group was varied from 50°C by a ΔT . The resulting effect on module power and efficiency of a variation in ΔT is shown in Figure 1.3.13. The data can be used

Curve 686815-A

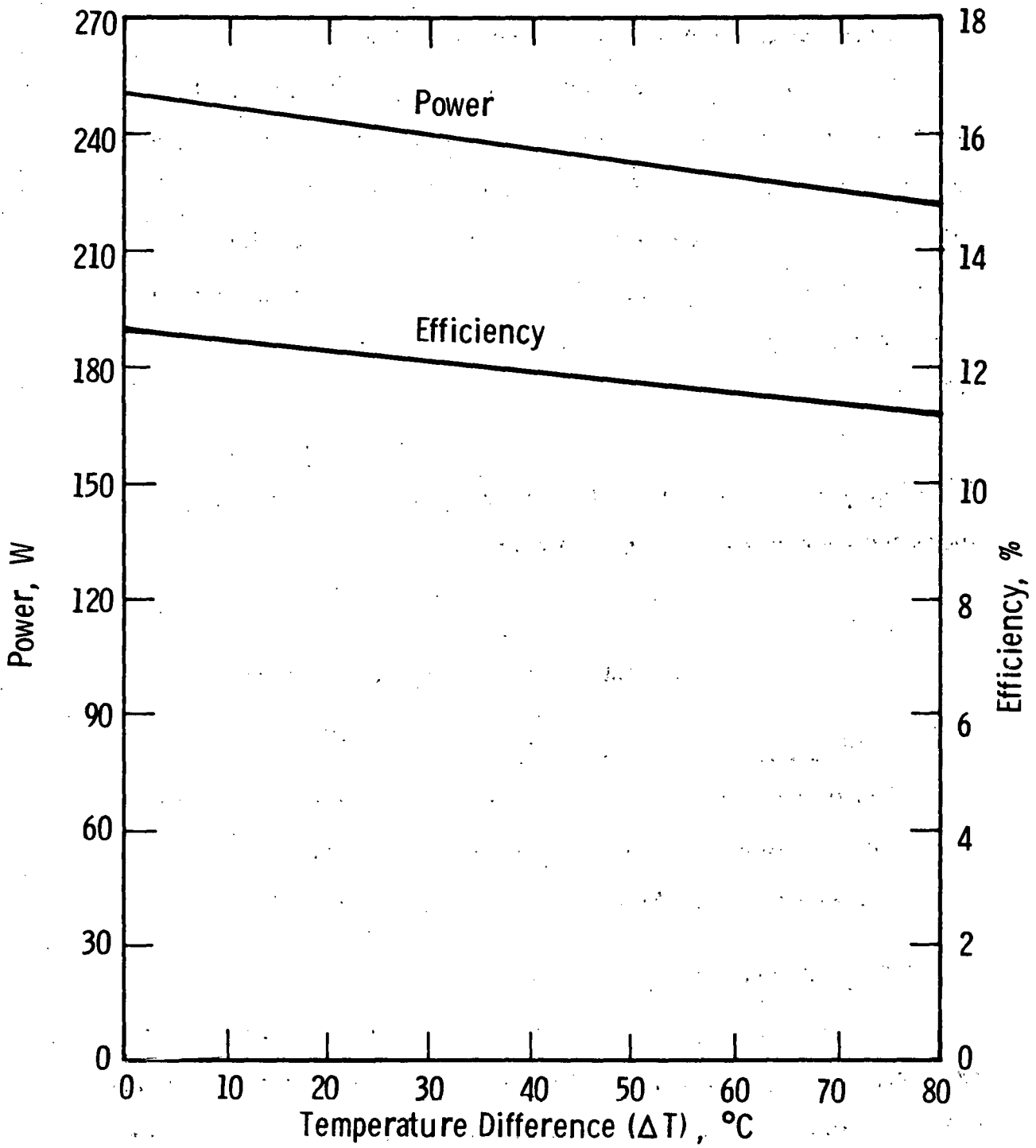


Fig. 1.3.13 - Variation of module power and efficiency with ΔT
Nominal cell temperature 50°C - cells divided into 2 groups of equal size.

to determine the degree of non-uniformity that can be tolerated in a module heat transfer system.

A similar calculation was made where one group of cells was increased above 50°C by ΔT while the other was dropped below 50°C by ΔT also. The net result was that neither module power or efficiency changed. The effects were compensating.

Effect of Shadowing

Calculations were made of the effect on module power of percentage of illumination (1-percentage of shadowing) for various values of numbers of cells per shunting diode. The results of the calculations are shown plotted in Figure 1.3.14. For small numbers of cells/diode, the variations in the curves were too small to be picked up by the plotting routine used. However, for 100 cells/diode, the steps are obviously large enough to be seen.

The results of the cost calculations for the same arrays are presented in Table 1.3.7. From the standpoint of cost, the number of cells/diode should be large, but if it becomes too large, the power variation becomes excessive. There is clearly room here for further cost/performance analysis.

Table 1.3.7

Summary of Module Shadowing Results

<u>Solar Cells Per Diode</u>	<u>Panel Cost (\$/kW)</u>
2	367
5	356
25	350
50	349
100	349
300	349

Total number of cells/panel - 945

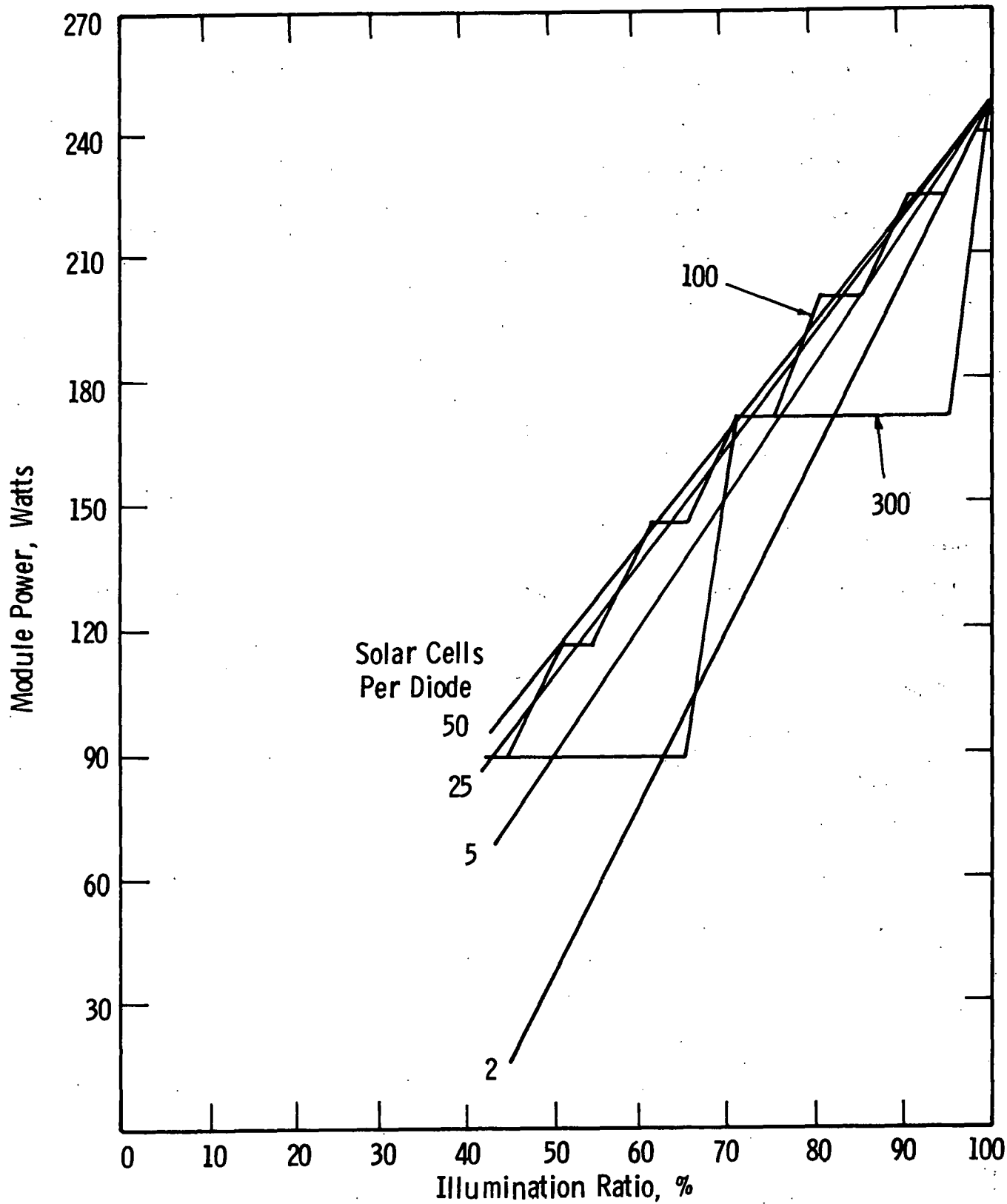


Fig. 1.3.14 - Effect on module power of shading

The effects of uneven illumination or shadowing are quite sensitive to the geometric relationship between the shadowed area and the physical arrangement of individual substrings defined by the bridging diodes.

For the calculated data shown in Fig. 1.3.14, it was assumed that the shadow progresses across the panel from string to string, covering each string before advancing to the next. In a more realistic case where the shadow region advances into several substrings at the source, the power degradation effect changes more rapidly with illumination ratio. In the worst case shadowing one cell in each substring reduces the panel output to zero.

1.3.3 Heat Transfer

1.3.3.1 Forced Cooling

One of the major considerations that must govern the cooling system design is the fact that the quantity of thermal energy to be dissipated is approximately one order of magnitude greater than the electrical energy produced. Thus an improperly designed cooling system could easily consume more energy than could be credited to it by reduced cell temperatures.

We have attempted to examine forced cooling in as general a manner as possible - recognizing the necessity of being able to choose size and shape parameters to optimize structural properties, cost, and manufacturing ease as well as cooling.

The actual geometry analyzed is that formed by continuous fins attached to the back sides of a solar panel in such a way as to form rectangular cooling passages. (See Figure 1.3.15) By varying the values of friction factor and heat transfer coefficient, the same analysis may be made by proper interpretation, to apply to other geometries including short fins aligned with the coolant flow direction.

Referring to this geometry, the cell temperature at any point, Z, along the channel is

$$T = T_a + \frac{\phi_a X'Z}{\rho VAC_p} + \frac{\phi_a X'}{hbe} \quad (1.3.4)$$

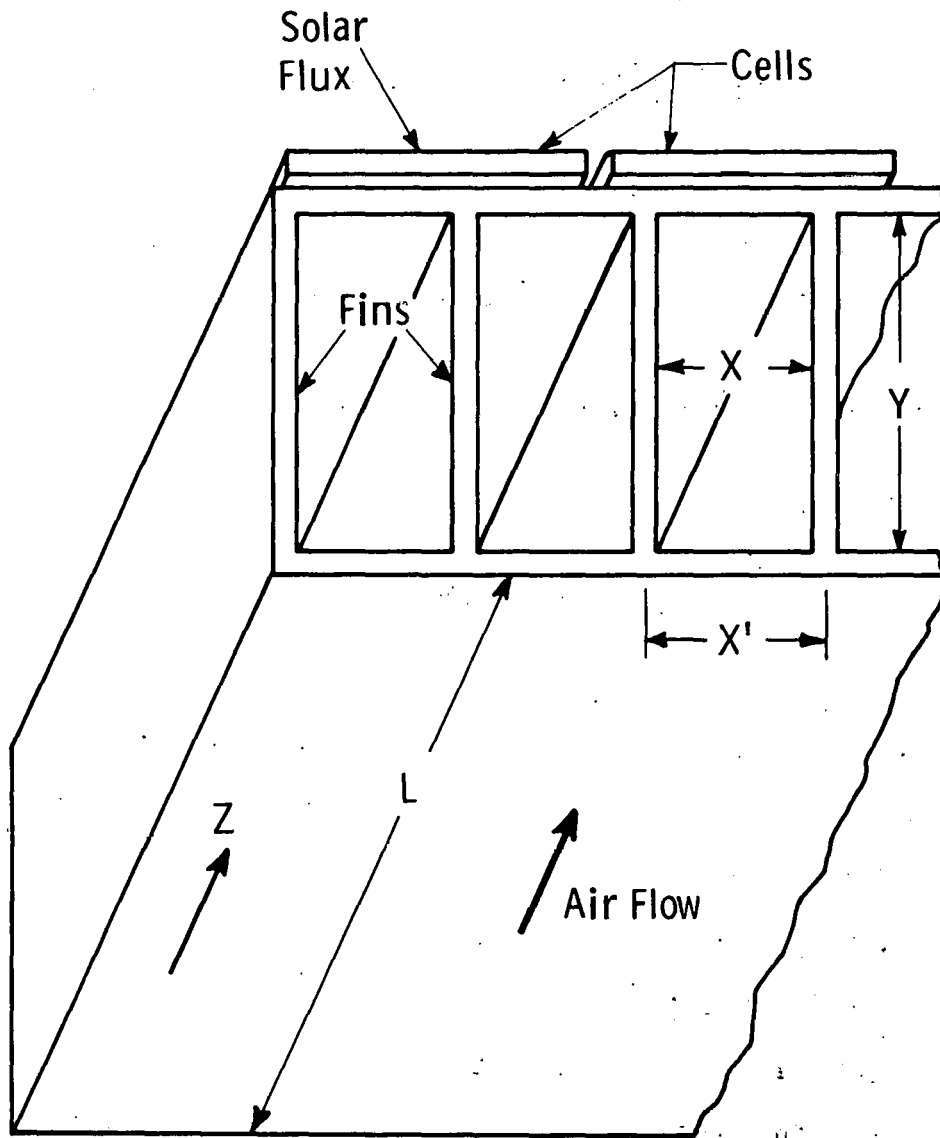


Fig. 1.3.15—Forced cooling structure

The electrical power output per unit panel surface area is

$$P_e = \phi_s n_0 [1 - \beta (T - T_0)]$$

$$P_e = \phi_s n_0 \left[1 - \beta (T_a - T_0) - \beta \left(\frac{\phi_a X' Z}{AV C_p} + \frac{\phi_a X'}{h b e} \right) \right] \quad (1.3.5)$$

The cooling system will consume power at the rate

$$P_p = \frac{f L (\rho V^2) (AV)}{2g D \eta_p (X'L)}$$

The channel dimensions X' , X , y and L , and the axial coordinate Z are defined in Figure 1.3.15. In addition we define

A = channel flow area

b = channel "wetted" perimeter

C_p = fluid specific heat

D_e = channel equivalent diameter where $D_e = \frac{4A}{b}$

e = fin effectiveness applied to the channel perimeter

f = Darch-Weisbach friction factor

g = gravitational acceleration

h = heat transfer coefficient

K = fluid thermal conductivity

P_e = cell electrical power output per unit area

P_p = coolant pumping power per unit cell area

$$P_{net} = P_e - P_p$$

T_0 = reference temperature on which cell characteristics are based

T_a = coolant inlet temperature

T = cell temperature

V = fluid velocity

R_e = Reynold's number

$$R_e = \frac{PVDe}{\mu}$$

P_r = Prandtl number

$$P_r = \frac{C_p \mu}{K}$$

β = cell temperature coefficient

η_0 = cell conversion efficiency at reference temperature

η = cell efficiency at temperature T , it is assumed that

$$\eta = \eta_0 [1 - \beta (T - T_0)]$$

ρ = coolant density

μ = coolant viscosity

ϕ_s = incident solar energy flux per unit cell area

ϕ_a = heat flux to be dissipated per unit cell area

We will also make the following approximations applicable to rectangular channel of high aspect ratio

$$b = 2y$$

$$D_e = 2X,$$

and assume that $X \approx X'$.

The net power delivered to the inverter by the solar panel and cooling system is

$$P_{\text{net}} = \phi_s \eta_0 [1 - \beta (T_a - T_0) - \beta \left(\frac{\phi_a X' L}{\rho A V C_p} + \frac{\phi_a X'}{h b e} \right)] - \frac{f L A \rho V^3}{2 \eta_p D g} \quad (1.3.6)$$

where the cell temperature has been averaged over the panel surface.

We wish to choose the geometric and flow parameters that maximize P_{net} within certain practical restraints. It was found that forced air cooling generally leads to an optimization point in the turbulent flow regime while liquid cooling will be in the laminar range. Thus both forms of Equation 1.3.6 must be examined.

For low Reynolds number turbulent flow, the friction factor may be correlated by

$$f = F(R)^{-0.2}$$

and the heat transfer coefficient by

$$\frac{hD}{K} = H(R)^{-0.8} (Pr)^{1/3}$$

Hence F and H are dimensionless empirically derived constants. We have taken $F = .22$ and $H = .023$ as base case values. However, in the course of parametric analysis, F and H were varied together while holding their ratio constant. This kind of variation, based on the heat transfer-friction factor analogy would be expected with short thin fins aligned in the flow direction - that is where most of the pressure drop is caused by skin losses as opposed to form losses.

If we define

$$A_t = \frac{\beta \eta_0 \phi_a}{2 \rho C_p}$$

$$B_t = \frac{\beta \eta_0 \mu^{.8} \phi_a}{eHK(2\rho)^{.8} (Pr)^{1/3}}$$

$$C_t = \frac{\rho^{.8} F \mu^{.2}}{2 \cdot 24 g \eta_p \phi_s}$$

$$W_t = \left[\frac{P_{net}}{\phi_s} - \eta_0 [1 - \beta (T_a - T_0)] \right] \frac{1}{\eta_0}$$

$$\tau_t = yV$$

$$x_t = X^{1.2}$$

then

$$W_t = \left[\frac{A_t L}{\tau_t} + \frac{B_t x_t}{y \cdot 2 \tau_t^{.8}} + \frac{e_t \tau_t^{2.8}}{y \cdot 1.8 x_t} \right] \frac{1}{\eta_0} \quad (1.3.7)$$

where W_t is the relative loss in power per unit area with reference to the idealized case with no temperature coefficient. The subscript t merely indicates applicability to turbulent flow.

We wish to minimize W_t . It is seen that no minimum exists with respect to L and y , but that W_t will be greater the smaller L , and the larger y .

By letting

$$\frac{\partial \alpha_t}{\partial x_t} = 0$$

and

$$\frac{\partial \alpha_t}{\partial \tau_t} = 0$$

the minima with respect to τ and x are given by

$$\tau_t = \left[\frac{A_t L y}{2} \right]^{1/2} [B_t C_t]^{-1/4}, \text{ and} \quad (1.3.8)$$

$$x_t = \left[\frac{C_t}{B_t} \right]^{1/2} \left[\frac{A_t L y}{2 \sqrt{B_t C_t}} \right]^{.9} \frac{1}{y^{.8}} \quad (1.3.9)$$

Substituting the values of τ_t and x_t from Equations (1.3.8) and (1.3.9) into Equation (1.3.7), then

$$W_t = \frac{2}{n_0} \sqrt{\frac{2AL}{y}} [BC]^{1/4}$$

$$W_t = \left[\frac{L}{ye^2} \right] \left[\frac{\mu^{1/6}}{C_p^{7/12} \rho^{1/2} K^{1/6}} \right] \left[\frac{\phi_a}{\phi_s} \frac{\rho}{(n_0)^{1/3}} \right]^{3/4} [\phi_s]^{1/2} \left[\frac{F}{g(2)^7 H} \right]^{1/4} \quad (1.3.10)$$

In Equation (1.3.10), the parameters have been grouped into the (1) fin geometry characteristics, (2) the fluid properties, (3) the solar cell properties, (4) the solar flux level, and (5) the flow characteristics respectively. The values of β and n_0 have been varied from the base case above to show their effect on power degradation as plotted in Figure 1.3.16.

Curve 684254-A

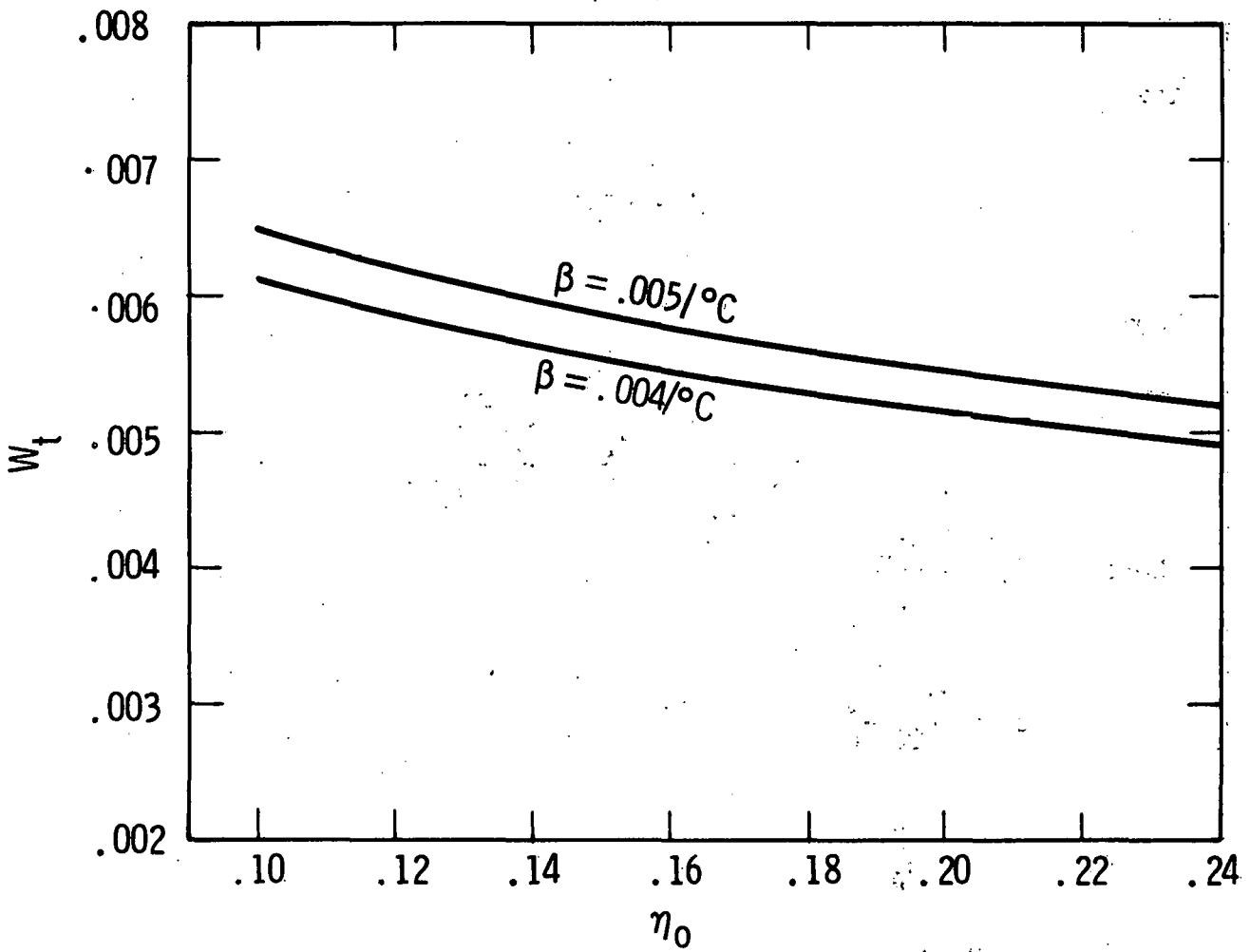


Fig. I. 3. 16 - Variation of W_t with efficiency

For laminar flow in a rectangular channel with constant surface heat flux

$$h = \frac{140}{17} \frac{K}{X}$$

and

$$\Delta P = \frac{12\mu L}{X^2}$$

Then

$$W_{\ell} = \left[\frac{A_{\ell} L}{\tau} + \frac{B_{\ell} X}{y} + \frac{C_{\ell} \tau^2}{yX} \right] \frac{1}{\eta_0}$$

where

$$A_{\ell} = \frac{\beta \eta_0 \phi_a}{2\rho C_p}$$

$$B_{\ell} = \frac{17\beta \eta_0 \phi_a}{280 Ke}$$

$$C_{\ell} = \frac{12\mu}{\phi_s \eta_p}$$

$$\tau_{\ell} = \nu y$$

$$X_{\ell} = X^2$$

The optimization point is at

$$\tau_{\ell} = \left[\frac{A_{\ell} L y}{2} \right]^{1/2} \left[\frac{C_{\ell}}{B_{\ell}^3} \right]^{-1/4}$$

A computer program was written, with both a turbulent and a laminar flow version, to calculate optimum fin spacing and fluid flow velocity with the other parameters specified. Parametric studies were then performed for various channel lengths, fin widths, and incident solar fluxes. These were done with both air and water properties and under the assumptions of both laminar and turbulent flow. The results of these studies are summarized in Table 1.3.8. It should be kept in mind that the laminar flow results are valid only for Reynolds numbers below about 2,200 while the turbulent flow results apply only for Reynolds numbers larger than that number.

It should be understood that these results are for preliminary design evaluations only. Exact channel shapes should be evaluated in detail design calculations.

These results make quantitative the following more or less obvious points:

- 1) While the incident solar energy may be concentrated onto a smaller cell area, the heat transfer area for dissipating most of that energy cannot be reduced without a penalty in efficiency.
- 2) Short parallel channels are superior in terms of cooling the one long or series connected coolant channels.
- 3) Water is much superior to air as a coolant but this advantage may be offset by the need for purchasing heat transfer equipment to cool the water.

Table 1.3.8

Equivalent Temperature Excess ($T - T_a$)

Thermal Flux = 0.1 W/cm²

<u>Fin Width</u>	<u>Channel Length</u>	<u>(Laminar Flow) Temperature</u>	<u>(Turbulent Flow) Temperature</u>
<u>Forced Air Cooling</u>			
1.0 in.	2.75 ft.	12.6 °C	14.7 °C
2.0	2.75	8.9	10.3
3.0	2.75	7.2	8.5
1.0	8.0	21.1	25.1
2.0	8.0	15.2	17.8
3.0	8.0	12.4	14.5
<u>Water Cooling</u>			
1.0 in.	2.75 ft.	0.22 °C	
2.0	2.75	0.15	
3.0	2.75	0.12	
1.0	8.0	0.32	0.38 °C
2.0	8.0	0.26	0.27
3.0	8.0	0.21	0.22

1.3.3.2 Passive Cooling

Passive cooling is feasible for modest concentration ratios and can lead to lower equipment and maintenance costs. Passive cooling relies on radiation heat transfer, natural convection to the atmosphere and/or the wind. Using standard heat transfer correlations, cell temperature has been calculated versus surface heat flux for several cases as plotted in Figure 1.3.17.

Curve I assumes both sides of the panel exposed for heat transfer to calm air by radiation and natural convection. Curve IV represents the front surface only exposed. Curve II assumes the addition of 1/2 in. wide fins one inch apart on the back surface while Curve III superposes the effect of a 5 kt. wind on the front surface only.

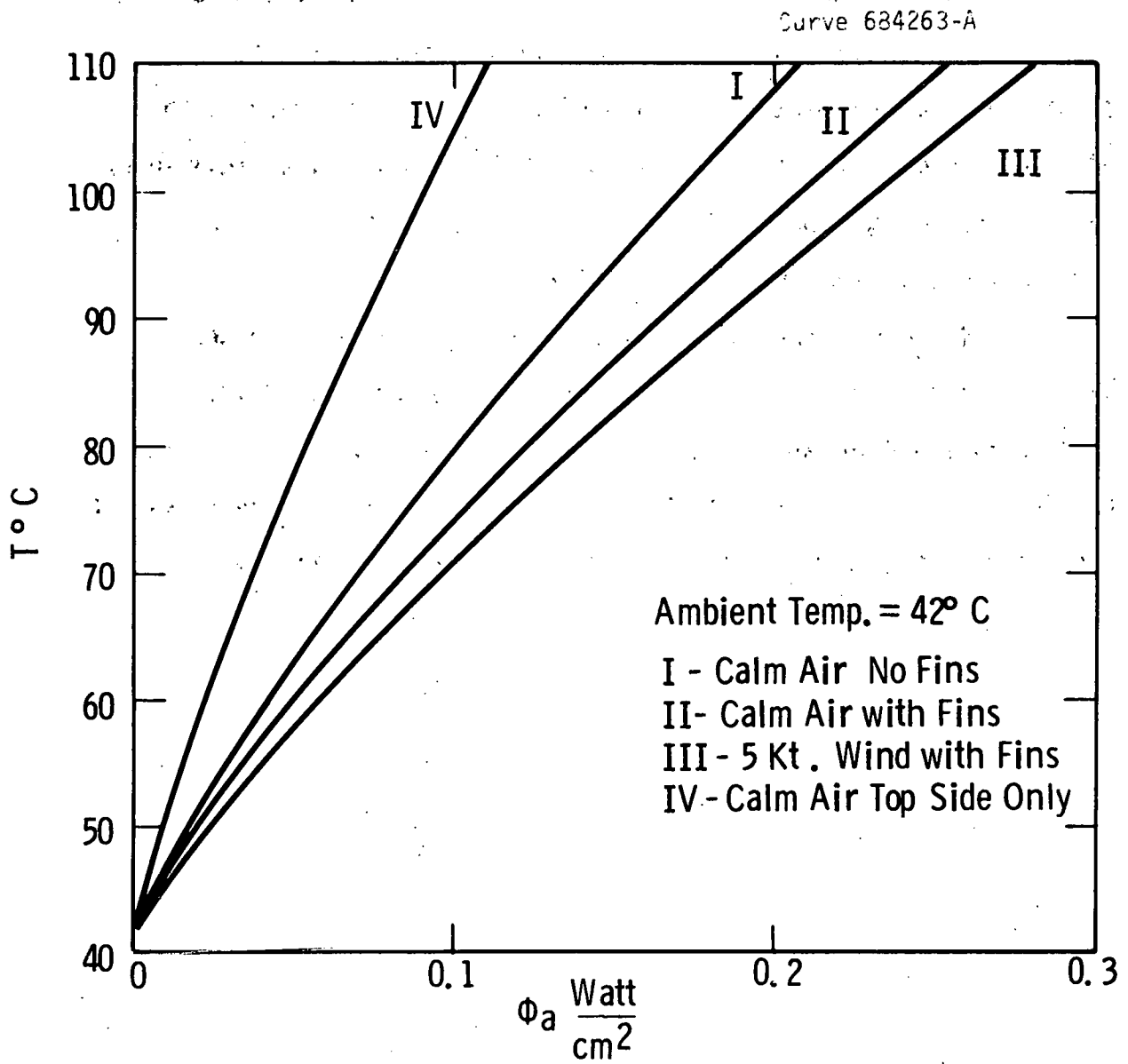


Fig. 1. 3. 17 -Variation of solar cell temperature with heat flux

1.3.4 Module Design

1.3.4.1 RPS Module

The design of the RPS module follows the dimensioning procedures set forth in Section 1.3.2.1 - Basic Photovoltaic Modularity. For ease of discussion, the module dimensions referred to will always be center-line dimensions -- 32" x 96" -- rather than the actual physical dimension of the module.

1.3.4.1.1 Background

Design studies for the RPS module centered primarily on structurally and visually integrating the module into the residential roof structure (see Figure 1.3.18). Structural integration allowed for the module to replace conventional building materials such as plywood and roofing membranes, and therefore, could give a cost credit to the rooftop portion of the photovoltaic system of about \$1 per square foot of roof surface replaced.

1.3.4.1.2 Flat Plate System

The design of the RPS flat plate module, that part of the rooftop unit which includes the glass, the desiccant spacer, the photovoltaic cells and the thermal absorber plate, follows the dimensioning procedures set forth in Section 1.3.2 - Module Analysis. For ease in discussion, the module dimensions referred to will always be center-line dimension (32" x 96") rather than the actual physical dimensions of the module. Because a total system design was set forth with a life-cycle cost or pay-back period of 30 years, the system that was to be designed would have to be reasonably inexpensive to build under

volume conditions as well as inexpensive to maintain. Therefore, a closed integral glass and absorber plate system was used (see Figures 1.3.18 and 1.3.19).

The glazing or cover plate, a single piece of glass, is 3/16" water-white crystal as mentioned in Section 1.3.2 - Module Analysis. Double glazing was avoided because the transmission loss through both pieces of glass would decrease the electrical productivity of the module by approximately 15 percent. Although double glazing acting as an insulating space would increase the thermal production of the module especially in areas of the country where daytime winter temperatures are significantly lower than the collector body, we are in this case optimizing for electrical production (see Figure 1.3.20).

The spacer between the glass and the absorber plate is a metal channel with an encased desiccant to absorb moisture which might leak into the sealed air space and condense on the cover glass or the photovoltaic cells, thus causing reduced electrical production or damage to the module.

The absorber is a "Roll-bond"^R type copper panel which has a flat top surface to receive the photovoltaic cells. The cells are in turn bonded to the absorber panel with a thin layer of silicone sealant which will accommodate thermal expansion. This panel would then be bonded, along with the desiccant spacer and the glazing into an integral airtight unit which would be received on the rooftop by a neoprene lattice glazing system.

^R Roll-Bond is an Olin-Brass Corporation Trademark

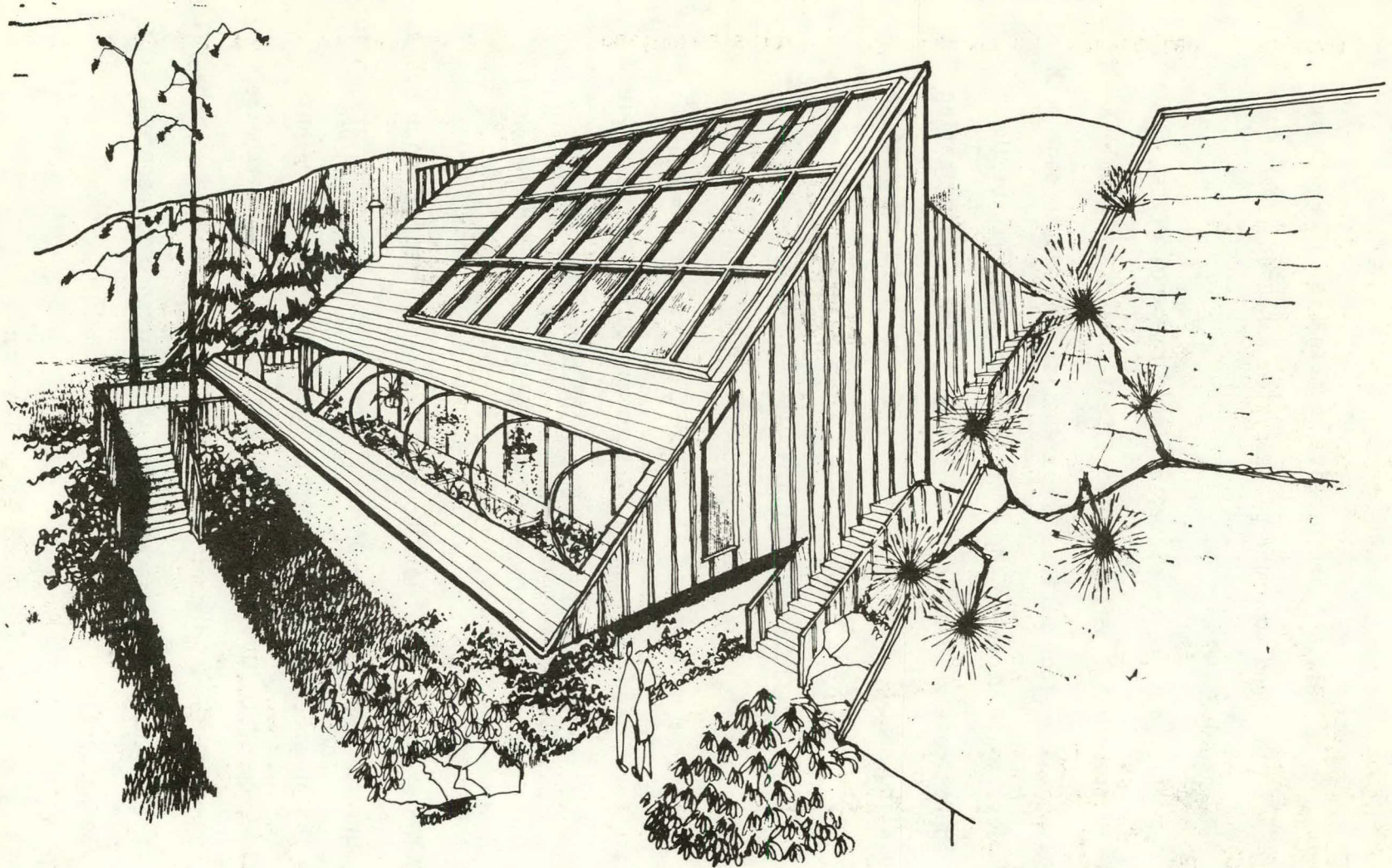


Figure 1.3.18 - Artists sketch of a residence suitable for the region represented by Cleveland, Madison and Wilmington

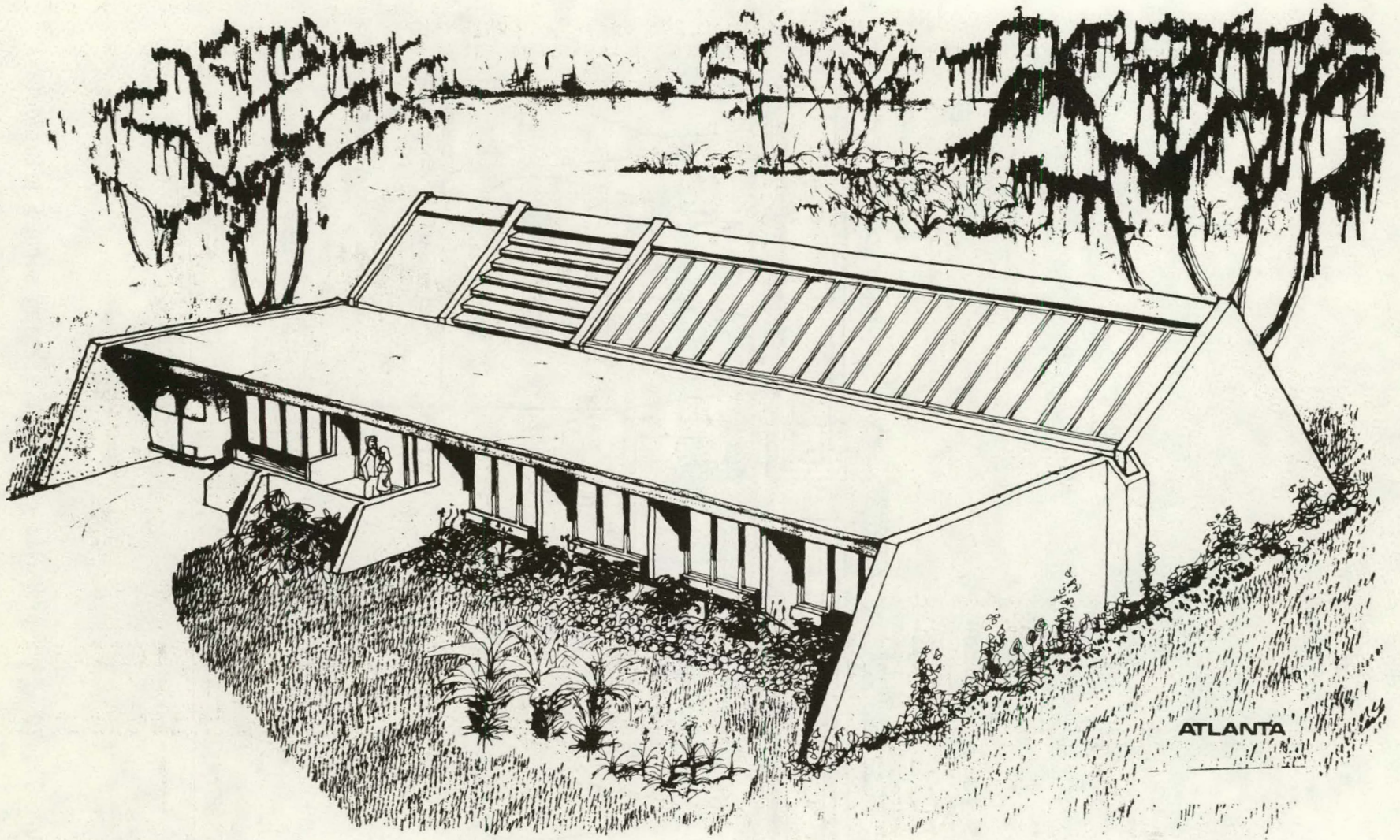


Figure 1.3.19 - Artist's sketch of a residence suitable for the region represented by Atlanta

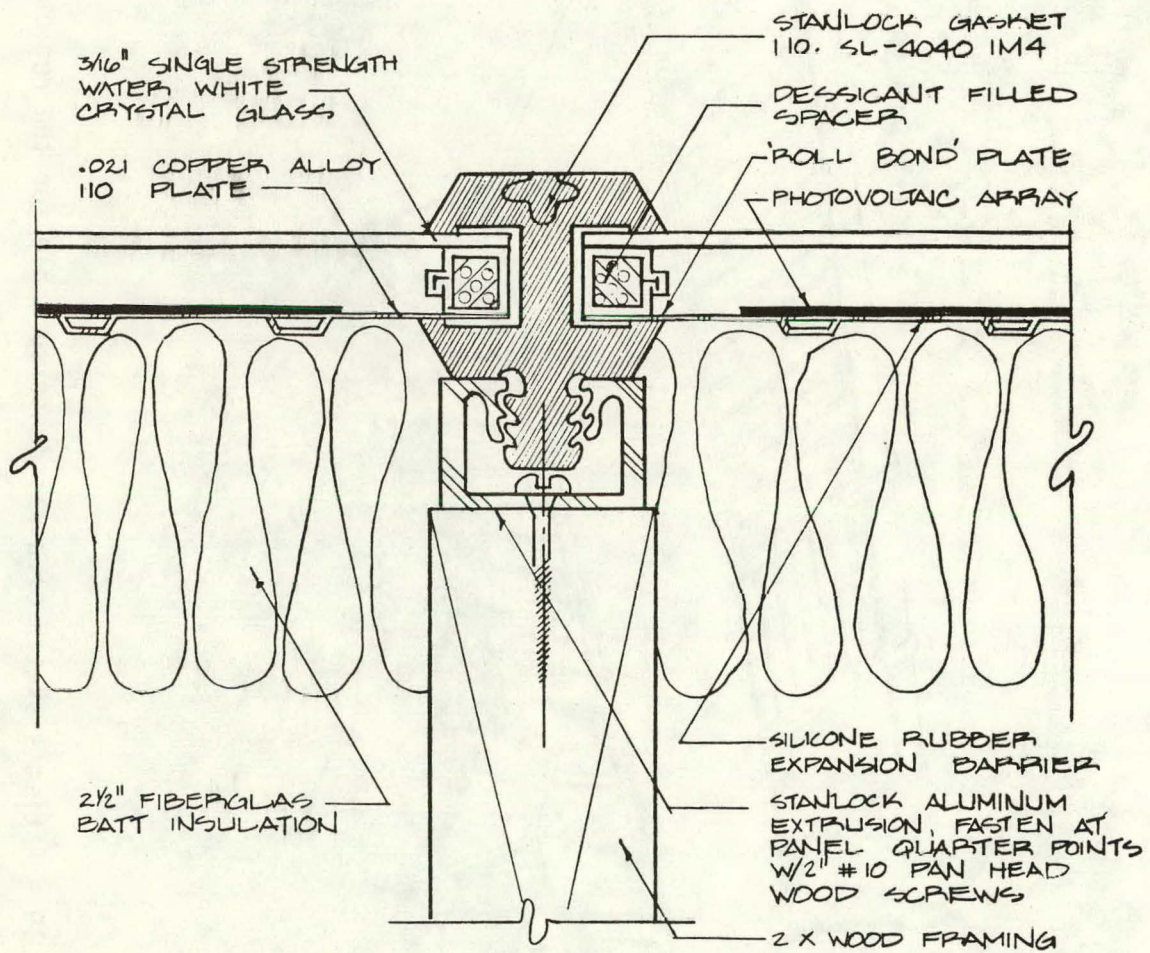


Figure 1.3.20 - RPS proposed collector framing sloped joint detail

The photovoltaic array is kept within its optimum thermal operating range by circulating water through channels in the absorber panel (see Figure 1.3.21). A more detailed discussion will be given to the piping and module interconnection problems in Section 1.5.1 - RPS Array Structure.

1.3.4.1.3 RPS Air Cooled Photovoltaic Array Module

The residential silicon SC module is in this case identical to the module design developed for the CPS systems (see Section 1.3.4.2).

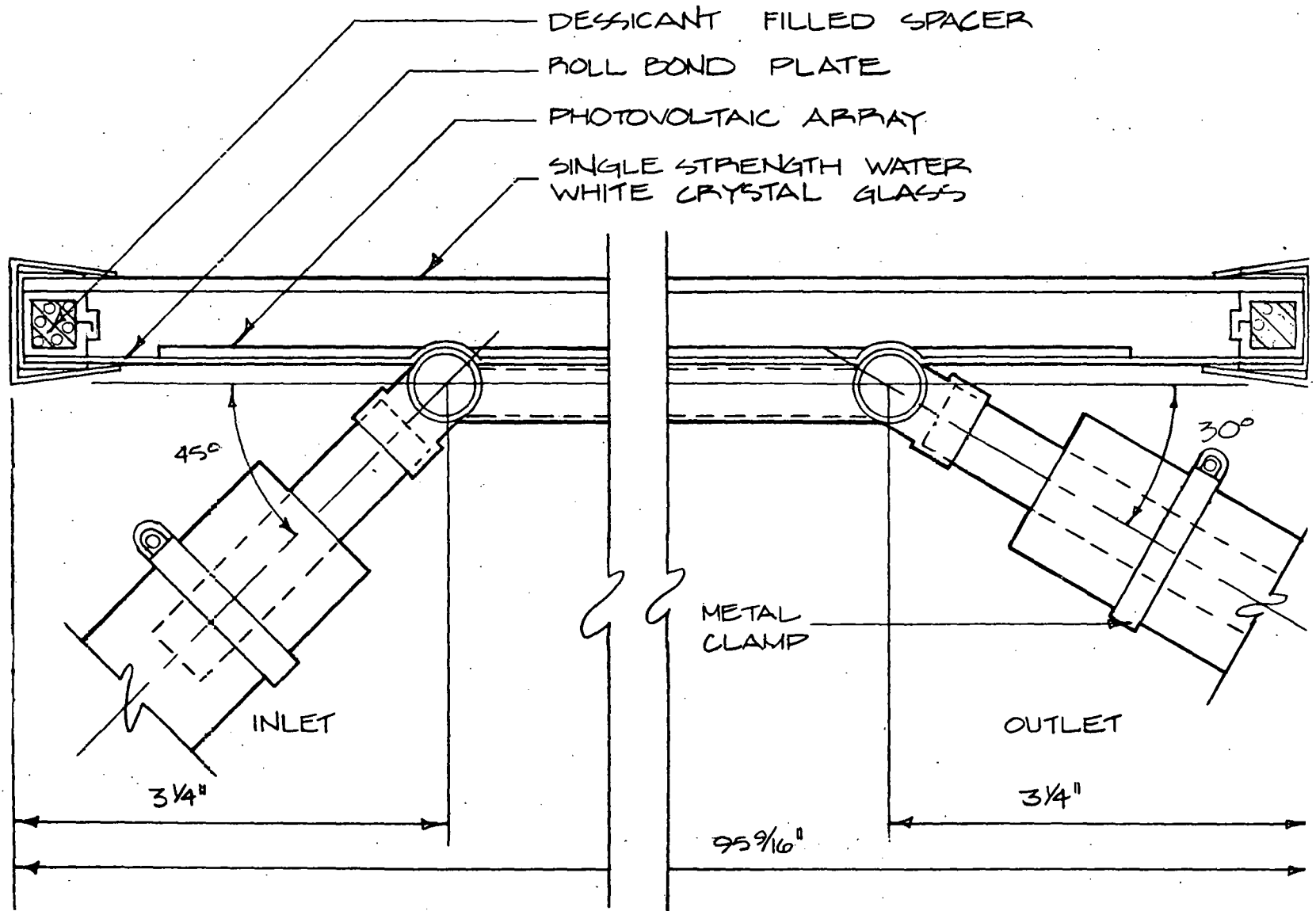


Figure 1.3.21. Photovoltaic water cooled module piping connections

1.3.4.2 IPS and CPS Modules

A large number of module designs were made for the CPS owing to the great flexibility available there for use of tracking and concentrating arrays. Selected results from these designs were then used for the IPS.

Following development of five types of CPS Modules, a structural analysis was performed on each design. The purpose of the analysis was to insure that all modules were designed to the same operational parameters as the CPS Arrays, and that all modules were designed to one set of criteria allowing direct cross-comparison. The factors of module weight and concentration ratio are the most significant features which must be considered in the choice of the most efficient module design to be used.

Parametric variations of size and wind loading were not performed for the modules as they were for the CPS Arrays. But, several dimensional parameters (e.g., width, sheet thickness, fin depth and fin quantity) were varied to arrive at the optimum structural design of the Flat Plate and the Vee-Trough Modules.

In performing the structural analysis of each of the modules, it was assumed that current fabrication technology and materials would be employed in their construction because little change in these areas is expected in the next ten years. The types of fabrication used were roll formed panels, welded construction using structural extrusions and epoxy bonded roll formed components.

The structural materials chosen for construction were Type 1100 Aluminum for all major load bearing components and polycarbonate plastic

or soda-lime-silica glass for glazing of the module in two of the designs developed. These materials were chosen for their low cost, resistance to environmental deterioration and availability.

For those applications where the module is exposed to strong winds, the substrate must be adequate to withstand the same wind loadings as those experienced by the array without suffering damage. This is particularly important where large-area cells are being used. If the module is not properly designed, the deflection of the substrate under wind loading can be enough to shatter the cells. Also, the heat transfer element adds depth to the module, whether by fins or channel walls, which adds to the structural rigidity.

In order to properly account for the structural limitations on module design, criteria have been established for the development of the cross-sectional properties of all of the modules. These are:

1. The maximum bending stress in the module must be less than or equal to 75% of the yield stress when the module is subjected to a uniform 146 kg/m^2 (30 lb/ft^2) loads.
2. The minimum radius of curvature allowable for the silicon cell must be 61 cm (24 in) to preclude cell fracture under the 146 kg/m^2 (30 lb/ft^2) load. The deflection of the module must be small enough to accommodate this requirement.
3. The module will be loaded to no more than 75% of the critical buckling load that will cause elastic instability in the module cross-section.

Consider a 81 cm x 244 cm (32 in x 96 in) module. The wind load, uniformly distributed on the module, is

$$W = 146 \text{ kG/m}^2 \times \left(\frac{81 \times 244}{10^4} \right) \\ = 288 \text{ kG (640 lb)}$$

The maximum moment for a simply supported beam (supported at each end) with a span of length L carrying the distributed load W, is

$$M = 1/8 W L$$

The minimum section modulus (ratio of moment of inertia and distance from section neutral axis to outermost edge) required to meet the stress criteria is related to the maximum moment by

$$Z_S = \frac{M}{0.75 S_y}$$

where Z_S is the section modulus and S_y is the yield stress of the material used.

The radius of curvature of the elastic curve line (maximum limit for elastic deformation) for a deflected simple beam is defined as

$$\rho = \frac{E I_r}{M}$$

so that

$$I_r = \frac{\rho M}{E}$$

where ρ = radius of curvature

E = elastic modulus

I_r = minimum moment of inertia required to meet the curvature criterion

The critical buckling load is

$$W_{\text{critical}} = \frac{9\pi\sqrt{CE I_B}}{L^2}$$

where C = torsional rigidity (ratio of angle of twist to twisting torque)

I_B = minimum moment of inertia required to meet the buckling criterion

Based on the design specification that the wind load will be no more than 75% of the critical load

$$W_{\text{critical}} = \frac{W}{0.75}$$

Solving for I_B ,

$$I_B = \frac{W^2 L^4}{450 CE}$$

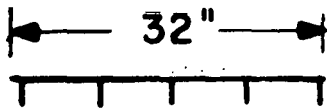
For the cases considered, I_B has been larger than I_r , and it represents the constraining moment of inertia. Therefore, to be consistent with the design criteria which have been adopted, a module design must have a moment of inertia greater than I_B .

The first step in the evaluation of the Flat Plate and Vee-Trough Modules was to develop a catalogue of section properties based on various cross-sectional parameters. In the case of the Fresnel and Compound Parabolic Collector Modules, a particular design configuration for each one was picked to suit the optical performance criteria. Those configurations were then used to develop the section properties of each design.

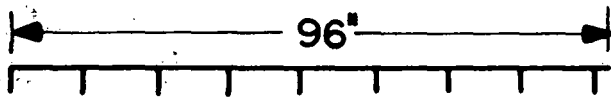
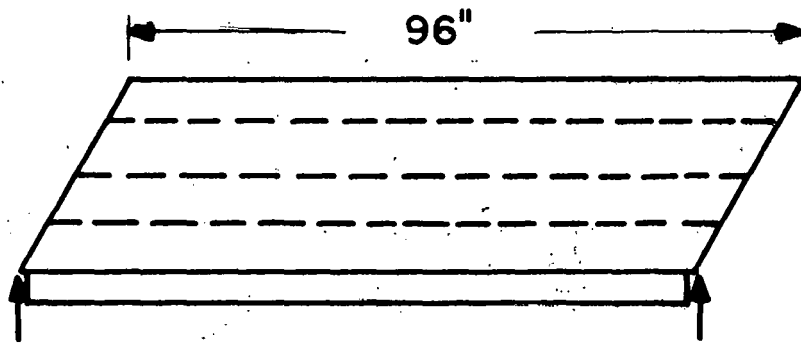
The next step in the analysis is to calculate the limiting values of the section properties as explained in the previous section, i.e., Z_S , I_r and I_B . These values assure that the module designs will meet the design criteria developed earlier.

The values of Z_S , I_r and I_B are all dependent on the way the module is supported. Two cases have been considered. In Case I, shown in Figure 1.3.22, the module is supported along its lateral edges with fins parallel to the longitudinal axis, while in Case II, the module is supported along the longitudinal edges with the fins parallel to the lateral axis. The span in Case I is three times greater than that in Case II, therefore the section modulus and moment of inertia will have to be greater for the Case I module. This requirement for added rigidity implies the use of thicker material, so the Case I module will be heavier than that of Case II.

Dwg. 6389A13



CASE I



CASE II

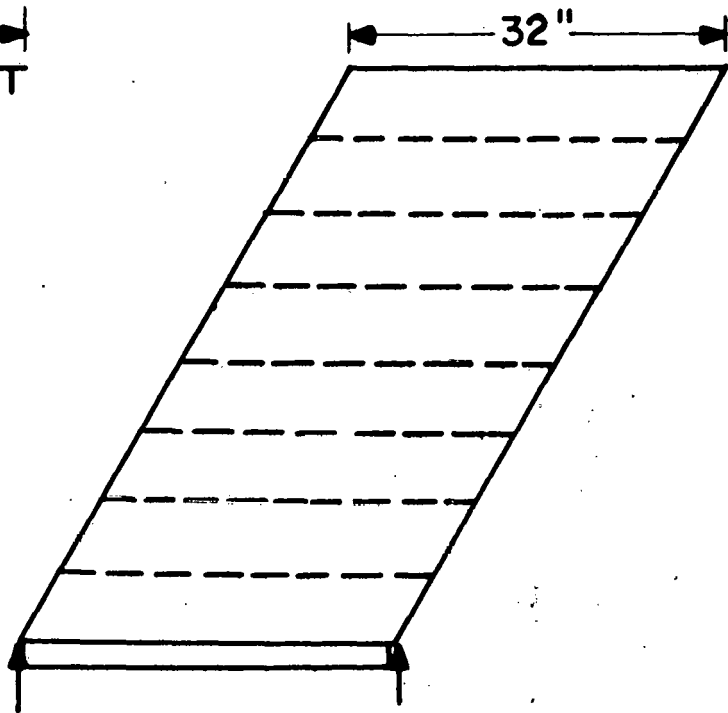


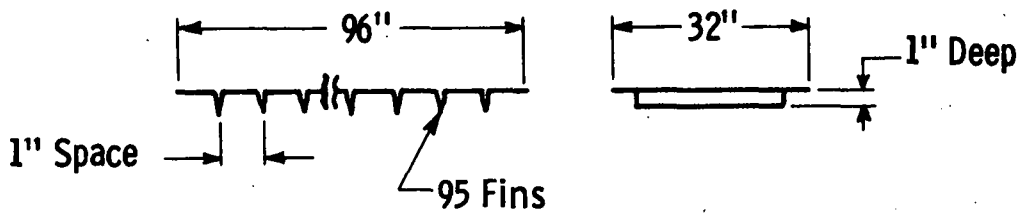
Fig. 1.3.22 — Finned heat sink substrate designs

The final step in the analysis is to compare the limiting values of Z_S , I_r and I_B to the values of Z and I calculated for the module sections. The most economical module design from the standpoint of structural integrity, was then picked from the available configurations. It corresponded to the lightest weight section whose values of Z and I exceeded the limiting values of Z_S , I_r and I_B .

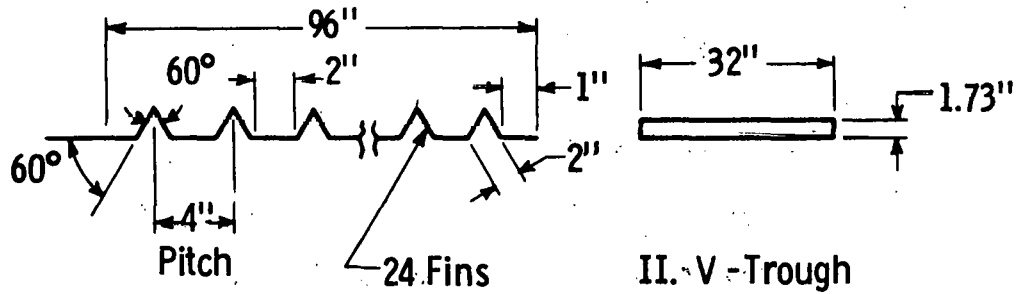
An area recommended for further analysis is the structural design of the modules which would be water cooled. The calculations performed for this analysis consider only wind loading and neglect the weight of the module and any cooling water that might be associated with it.

A total of twenty two module designs were developed during this program; one of each of five design configurations was carried through all phases of the project. These designs are the Flat Plate, the Vee-Trough, the Fresnel, and two types (3X and 10X concentration) of Compound Parabolic Collector modules, as shown in Figure 1.3.23. A brief description of each module design appears in Tables 1.3.9 through 1.3.13.

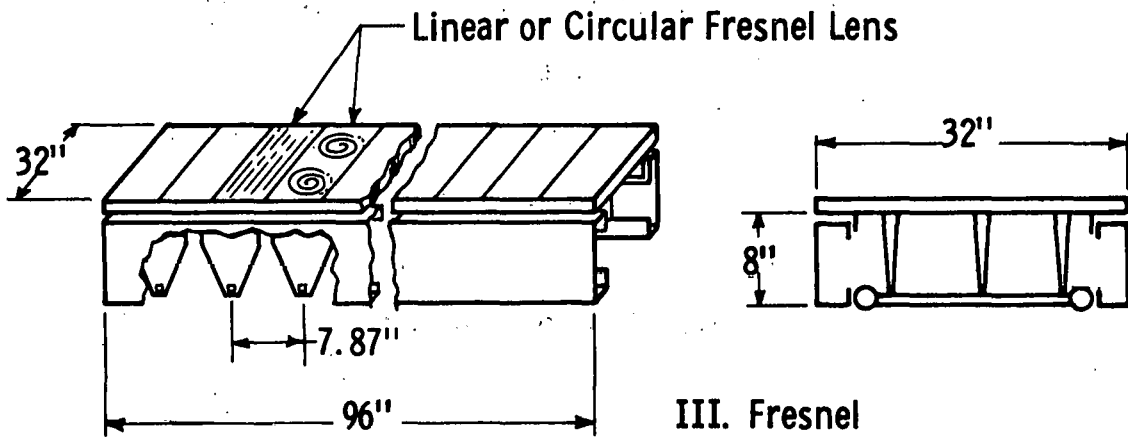
Two methods of incorporating the fin geometry into the substrate for the passive cooling of the solar cells have been investigated. The first method involves roll forming, a process in which an aluminum sheet is essentially folded into the desired shape. The two sides of a fin are then held together by tabs periodically notched in the fin and folded back, or by an occasional spot weld.



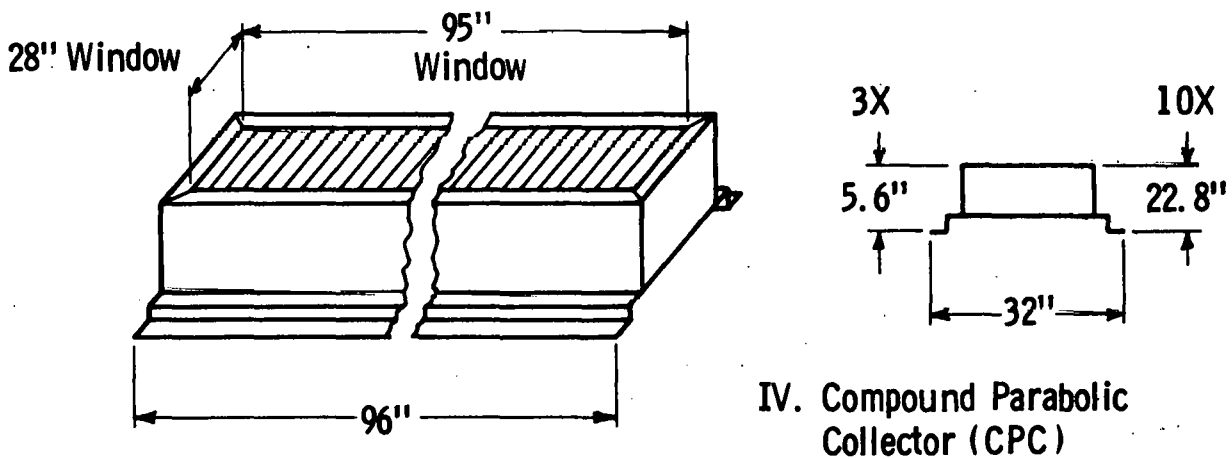
I. Flat Plate



II. V-Trough



III. Fresnel



IV. Compound Parabolic Collector (CPC)

Fig. 1.3.23 - Solar cell module concepts analyzed

TABLE 1.3.9

Flat Plate Module

(Figure 1.3.23)

- 1X concentration ratio.
- 32" wide x 96" long.
- 95 cooling fins; 0.012" thick x 1 in. deep x 30" long.
- 1100-0 Aluminum x 0.006 in. thick roll formed construction.
- 5.09 lbs. total weight.
- 21.33 ft² projected module front surface area.
- 21.33 ft² cell area.
- 0.24 lb/ft² weight/unit area

TABLE 1.3.10
Vee-Trough Module
(Figure 1.3.23)

- 2X concentration ratio.
- 32" wide x 96" long
- 24 cooling/reflector troughs; 2 in.
on a side all angles 60° x 32" long.
- 1100-0 Aluminum x 0.008 in. thick
roll formed construction.
- 4.55 lbs. total weight
- 0.21 lb/ft² weight/unit area
- 21.33 ft² projected module front surface area.
- 9.58 ft² cell area.

TABLE 1.3.11
Fresnel Module
(Figure 1.3.23)

- 10X concentration ratio.
- 32 in. wide x 96 in. long.
- 11 linear or circular fresnel lenses 7.87 in. wide x 32 in. long.
- 1100-0 and 1100-18 Aluminum, welded extrusions and roll formed construction.
- 120.2 lbs. total weight
- 5.64 lb/ft² weight/unit area
- 21.33 ft² projected module front surface area.
- 1.80 ft² cell area.
- Glass or plastic fresnel lens.

TABLE 1.3.12

3X CPC Module

(Figure 1.3.23)

- 3X concentration ratio.
- 32 in. wide x 96 in. long.
- 40 Compound Parabolic Collector lenses, 2.37 in. wide x 4.45 in. deep x 30 in. long.
- 1100-0 and 1100-18 Aluminum roll formed and epoxy bonded construction.
- 57.27 lbs. total weight
- 2.68 lb/ft² weight/unit area
- 21.33 ft² projected module front surface area.
- 6.12 ft² cell area.
- Glass or plastic cover glazing.

TABLE 1.3.13

10X CPC Module

(Figure 1.3.23)

- 10X concentration ratio.
- 32 in. wide x 96 in. long.
- 13 Compound Parabolic Collector lenses, 7.16 in. wide x 21.65 in. deep x 30 in. long.
- 1100-0 and 1100-18 Aluminum roll formed and epoxy bonded construction.
- 76.30 lbs. total weight
- 3.58 lb/ft² weight/unit area
- 21.33 ft² projected module front surface area.
- 1.99 ft² cell area
- Glass or plastic cover glazing.

The other process considered is extrusion. Based on present technology, the minimum section thickness for an extrusion is 0.1 cm (0.04 in), and the ratio of overall section width to the thickness of the thinnest element should not exceed 70:1. These constraints are both violated for the thicknesses of 0.015 cm to 0.08 cm (.006 in to .032 in) and overall dimensions 81 cm x 244 cm (32 in x 96 in) being considered for the optimized module. An attempt to conform to these limitations would result in a module which is much heavier and more costly than the same module made by the roll-forming process.

From this discussion, it appears that a module can be manufactured, using roll formed construction, with sufficient rigidity to withstand 146 kg/m^2 (30 lb/ft^2) loading without consequent damage to the cells. The unit can be very light, as low as 2.2 kG (5 lb), and because it is made from aluminum, it has the added advantage of good heat transfer to the ambient. In addition, ways to integrate either forced air or liquid cooling channels into the substrate have been conceived. These should afford the greatest advantage in both heat transfer and structural support.

Figure 1.3.24 shows a plot of the module weight factor (module weight/unit surface area) versus cell area. It was made from the data contained in Table 1.3.14, Module Weight and Area Parameters. From it the relationship between the factors influencing the cost of the modules can be visualized. Since the weight/unit area of the module and the cell area contained in the module are both directly proportional

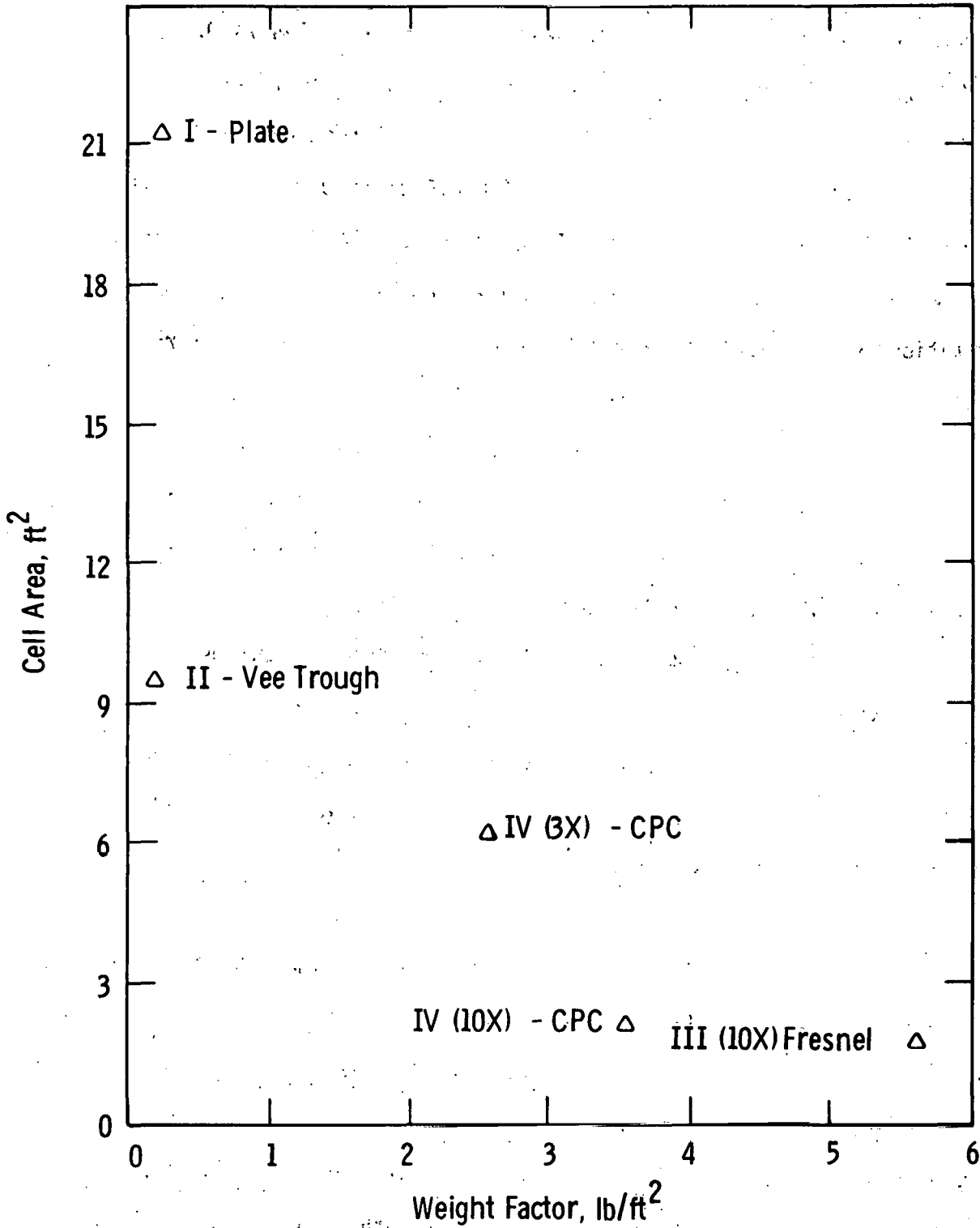


Fig. 1. 3. 24- Cell area vs. weight factor (module weight per unit surface area)

TABLE 1.3.14

Module Weight and Area Parameters

<u>Module No. (Concentration Ratio)</u>	<u>Module Wgt. (lb)</u>	<u>Cell Area (ft²)</u>	<u>Module Surface Area (Projected) (ft²)</u>	<u>Module Weight Per Unit Surface/Area (lb/ft²)</u>
I (1X)	5.09	21.3	21.3	0.24
II (2X)	4.55	9.58	21.3	0.21
III (10X)	120.2	1.80	21.3	5.64
IV (3X)	57.3	6.12	21.3	2.68
IV (10X)	76.3	1.99	21.3	3.58

to the cost of these components, the relative proportions of cell cost to structural material cost can be obtained from Figure 1.3.24.

Selection of a single preferred Module design, as in the case of array structures, will not be as straightforward as picking the lightest weight design. The two major factors involved in the choice of the most economical overall design are cell cost and structural material cost. Depending on the magnitudes of each of these costs the most economical module design will vary with time.

As the long term cost of silicon cells is reduced, the module with the largest cell area and least structural material will be most cost effective. This can be seen in Figure 1.3.24 where the Flat Plate and the Vee-Trough modules are shown having the highest cell area and a very low structural material content.

However, in the short run, with the cost of silicon cells being very high in relation to the cost of the structural materials, the Fresnel and the CPC modules with 10X concentration ratios will be the most cost effective.

Finally, incorporation of any of the module designs into a Central Power Station system will introduce many other general economic factors and trade-offs which have an indirect but none-the-less strong influence on the choice of the final design to be chosen.

Areas for further analysis include: detailed design of the modules to reduce the material content and construction complexity

to minimize the cost of the structural components; analysis of the modules to provide structural integrity for water cooled versions; development of operating and maintenance costs for all modules; and construction of 1:4 scale operational prototypes of the most cost effective design in today's economy.

1.3.5 Cost Estimates

1.3.5.1 RPS

Cost estimates for the RPS modules are difficult to present in simplified form because seven different sites throughout the country were considered, and the costs of material and labor vary with each site. Complete lists of material and labor required for installation are provided for each site in Section 1.5.1 of this volume, which will not be repeated here. However, array costs averaged over all seven sites are presented in the following table.

Two types of silicon modules were used for the RPS designs. One included removal of array excess thermal energy using water as a heat transfer mechanism to make possible the use of the thermal energy to satisfy a portion of the heating load of the residence. The second type of module made no use of the array excess thermal energy, and dissipated it using air cooling fins.

Average costs for both water and air-cooled silicon arrays are presented in Table 1.3.15. The solar cell costs per unit area are the same for both types of modules, but the more costly thermal portion of the water cooled array reflects the necessity to form water channels in the substrate material as opposed to simple fins needed for air cooling.

Table 1.3.15

Average RPS Module Costs

<u>Item</u>	<u>Units</u>	<u>1985</u>	<u>1990</u>	<u>2000</u>
<u>Water Cooled Si</u>				
Thermal	\$/m ²	85	65	45
Solar Cell	\$/m ²	<u>50</u>	<u>40</u>	<u>20</u>
TOTAL	\$/m ²	135	105	65
<u>Air Cooled Si</u>				
Thermal	\$/m ²	25	20	20
Solar Cell	\$/m ²	<u>50</u>	<u>40</u>	<u>20</u>
TOTAL	\$/m ²	75	60	40

1.3.5.2 IPS

The modules considered for use in IPS designs are the same as those considered for the CPS. The cost estimates for these modules are included in the next section.

1.3.5.3 CPS

Cost estimates for the five types of modules considered for the design of CPS systems are shown in Table 1.3.16. These are based on detailed designs which were used to obtain estimates of material and labor for high volume manufacture of each one. Material cost estimates are based on weight.

Table 1.3.16

Cost Estimates for 32" x 96" Modules

<u>Module Type</u>	<u>Geometric Concentration Ratio</u>	<u>Module Weight [KG]</u>	<u>Cost (Less Cells) (1975 \$)</u>	<u>Packing Factor</u>
Flat Plate	1X	2.3	2.30	1.0
V-Trough	2X	2.1	2.04	0.9
Fresnel Lens	10X	54.6	51.06	0.84
Compound Parabolic	3X	26.0	13.40	0.86
Compound Parabolic	10X	34.6	27.66	0.93

APPENDIX A

Module Voltage and Shadowing Analysis
Computer Program Listing

LIS-P
PANEL

```
20 FILES PLOT1,DUMMY
40 DIM A$(198),B$(198)
60 PRINT #2,1;0
80 READ #2,1;V0
100 LET V0=V0+200
120 PRINT #2,1;V0
140 IF V0>1000 THEN 1440
160 LET A$="PANEL POWER(P),VOLTAGE(V) AND EFFICIENCY(E) VERSUS TEMPERA
180 PRINT #1,1;A$
200 LET A$="DIFFERENTIAL(D)DESIGN VOLTAGE, V0="
220 LET A$(LEN(A$)+1)=CONV(V0)
240 LET A$(LEN(A$)+1)="T1=T0+DELTA T, T2=T0"
260 PRINT #1;A$
280 LET A$="DPVE"
300 PRINT #1;A$
320 REM 10=1985 DATA
340 DATA "YEAR 1985 SILICON CELLS"
360 DATA 3.47371E-02,7.1972E-06,.652,.34,.92,1.12,.0001
380 DATA .002,.0002,.001,.01,.00875,.005,.0005
400 DATA "YEAR 2000 SILICON CELLS"
440 DATA 3.44318E-02,7.4348E-06,.0308,.34,.92,1.12,.0001
460 DATA "YEAR 1985 CADMIUM-SULPHIDE CELLS"
480 DATA .0275,0,.0015,1,.95,.9,0
500 DATA .001,0,0,.01,0,0,0
520 RESTORE 460
540 READ B$
560 READ K1,K2,K3,K4,K5,K6,K7
600 READ C0,C1,C2,C3,C4,C5,C6
620 REM DATA BLOCK
640 LET W1=2*2.54
660 LET M1=.1
680 LET L2=96*2.54
700 LET W2=32*2.54
720 LET M2=1
740 LET S2=1
760 LET D2=40
780 LET E3=.97
800 LET U0=1
820 LET U1=U0
840 LET U2=1
860 LET T0=325
880 FOR T1=T0 TO T0+40 STEP 2
900 LET T2=T0
920 LET R0=.5
940 REM PANEL GEOMETRY
960 LET A1=1
980 GOSUB 2660
1000 LET R=R1
1020 GOSUB 3200
1040 LET V1=V
1060 LET N0=V0/(E3*E3*V)
1080 LET N1=INT((W2-2*M2)/(W1+M1))
1100 LET N2=INT(N0*S2/N1+1)
1120 LET L1=(L2-2*M2)/N2-M1
1140 LET A1=W1*L1
```

```

1160 LET N3=INT(R0*(N1*N2))
1180 LET N4=N1*N2-N3
1200 REM EXECUTE
1220 IF T1#T0 THEN 1260
1240 GOSUB 1460
1260 LET R=1.5*K4/A1
1280 GOSUB 3620
1300 GOSUB 4600
1320 IF T1#T0 THEN 1360
1340 GOSUB 1680
1360 PRINT #1;2*(T1-T0),P,V,100*E
1380 NEXT T1
1400 PRINT #1;"END"
1420 CHAIN JRPL0T
1440 STOP
1460 REM CELL DATA PRINT SUB
1480 GOSUB 2680
1500 LET R=R1
1520 GOSUB 2360
1540 IF T1=T0 THEN 1600
1560 GOSUB 2760
1580 GOSUB 2360
1600 IF T2=T1 THEN 1660
1620 GOSUB 2840
1640 GOSUB 2360
1660 RETURN
1680 REM PRINT PANEL DATA SUB
1700 PRINT "";
1720 PRINT "PANEL DATA, ";B$
1740 :LENGTH=###.##CM WIDTH=###.##CM AREA=##.##M2
1760 :MARGINS: PANEL=##.##CM CELL=##.##CM
1780 :DESIGN VOLTAGE=####VOLTS NO. OF STRINGS=##
1800 :CELLS/STRING=#### CELLS/PANEL=#### CELLS/DIODE=###
1820 :#### ACROSS BY #### DOWN PACKING FACTOR=.###
1840 :REGION-# T=###DEG K INTENSITY=##.###WATTS/CM2 NO.OF CELLS=####
1860 :VOC=####.##VOLTS ISC=####.###AMPS
1880 :VP =####.##VOLTS IP =####.###AMPS POWER=####.##WATTS
1900 :EFFICIENCY=##.##% FILL=.####
1920 :R/CELL=.####OHMS R/INTERCONNECT=.#### R TOTAL=##.##OHMS
1940 :PANEL COST=$####.## $####.##/KW
1960 PRINT USING 1740,L2,W2,L2*W2/10000
1980 PRINT USING 1780,V0,S2
2000 PRINT USING 1760,M2,M1
2020 PRINT USING 1800,N1*N2/S2,N1*N2,D2
2040 PRINT USING 1820,N1,N2,N1*N2*A1/(W2*L2)
2060 PRINT USING 1920,R1,R-R1,(N3+N4)*R/S2
2080 PRINT USING 1840,1,T1,U1*.1,N3
2100 PRINT USING 1840,2,T2,U2*.1,N4
2120 PRINT USING 1860,V3,I3
2140 PRINT USING 1880,V,I,P
2160 PRINT USING 1900,100*E,F
2180 PRINT USING 1940,Z0,Z0*1000/P
2200 PRINT "";
2220 RETURN
2240 REM PRINT PANEL TABLE SUB
2260 PRINT "";
2280 PRINT USING 2300," V0"," VP"," IP","POWER"," EFF","$","$/KW"

```

```

2300 :###.## ###.## ###.## ###.## ###.## ###.## ###.##
2320 PRINT USING 2300,V0,V,I,P,100*E,Z0,Z0*1000/P
2340 RETURN
2360 REM CELL DATA BLOCK
2380 GOSUB 3200
2400 PRINT **;
2420 PRINT "CELL DATA, ";B$
2440 :TEMP=###DEG-K ILLUMINATION=###.###W/CM2
2460 :AREA=###.##CM2 WIDTH=##.##CM LENGTH=###.##CM
2480 :VOC=####VOLTS ISC =##.###AMPS
2500 :VP= .####VOLTS IP =##.###AMPS POWER=###.###WATTS
2520 :EFFICIENCY=##.##% FILL=#### RS=#.###OHMS
2540 PRINT USING 2440,T,.1*U
2560 PRINT USING 2460,A1,W1,L1
2580 PRINT USING 2480,FNV(0),I3
2600 PRINT USING 2500,V,I,P
2620 PRINT USING 2520,100*E,F,R1
2640 RETURN
2660 REM CELL PARAMETER SUB IN=T,U,A1 OUT=FNL(T),R1
2680 LET U=U0
2700 LET T=T0
2720 GOSUB 2920
2740 RETURN
2760 LET U=U1
2780 LET T=T1
2800 GOSUB 2920
2820 RETURN
2840 LET U=U2
2860 LET T=T2
2880 GOSUB 2920
2900 RETURN
2920 DEF FNL(T)=(K1+K2*T)*A1*K5*U
2940 LET E0=K6-(T-300)*2.8*K7
2960 LET I0=A1*K3*T^3*EXP(-E0*300/(.026*T))
2980 LET R1=K4/A1
3000 RETURN
3020 REM CELL IV SUB IN=A1,R,T,U,V OUT=I(V)
3040 DEF FNV(I)=(.026*T/300)*LOG((FNL(T)-I)/I0+1)-I*R
3060 DEF FNI(V)=FNL(T)-I0*EXP((V+I*R)*300/(.026*T))
3080 LET I=0
3100 LET I8=FNI(V)
3120 IF ABS(I8-I)<.00001 THEN 3180
3140 LET I=I8
3160 GOTO 3100
3180 RETURN
3200 REM PMAX SUB IN=IL,I0,R,A1,U,T OUT=I,V,P,E,F
3220 LET V=0
3240 GOSUB 3020
3260 LET I3=I
3280 DEF FNP(I)=(.026*T/300)*(LOG((FNL(T)-I)/I0+1)-FNV(I))-2*I*R
3300 DEF FNQ(I)=I/(FNL(T)-I+I0)
3320 LET I8=FNL(T)/5
3340 LET I9=5*I8
3360 LET I=(I8+I9)/2
3380 IF ABS(FNP(I))<.00001 THEN 3500
3400 IF SGN(FNP(I))=1 THEN 3460
3420 LET I9=I

```



```

3440 GOTO 3360
3460 LET I8=I
3480 GOTO 3360
3500 LET V=FNV(I)
3520 LET P=I*V
3540 LET E=P/(.1*U*A1)
3560 LET F=P/(FNV(0)*I3)
3580 RETURN
3600 LET P9=P9+V9
3620 REM STRING PMAX SUB IN=R,T1,T2,U1,U2 OUT=VP,IP,P,E,F
3640 LET N8=N3
3660 LET N9=N4
3680 GOSUB 2760
3700 LET I3=FNL(T)
3720 LET V3=N3*FNV(0)
3740 LET J8=I0
3760 GOSUB 2840
3780 LET I3=I3 MAX FNL(T)
3800 LET V3=V3+N4*FNV(0)
3820 LET J9=I0
3840 LET I9=I3
3860 LET I8=I9/5
3880 LET I=(I8+I9)/2
3900 LET U=U1
3920 LET T=T1
3940 LET I0=J8
3960 IF FNL(T1)-I>-I0 THEN 4080
3980 LET N8=D2*INT(N3/D2+.999)
4000 LET N9=N1*N2-N8
4020 LET P9=-N8*.6/D2
4040 LET V8=P9
4060 GOTO 4120
4080 LET P9=N8*FNV(I)
4100 LET V8=N8*E3*FNV(I)
4120 LET U=U2
4140 LET T=T2
4160 LET I0=J9
4180 IF FNL(T2)-I>-I0 THEN 4300
4200 LET N9=D2*INT(N4/D2+.999)
4220 LET N8=N1*N2-N9
4240 LET V9=-N9*.6/D2
4260 LET P9=P9+V9
4280 GOTO 4340
4300 LET P9=P9+N4*FNV(I)
4320 LET V9=N4*E3*FNV(I)
4340 IF ABS(P9)<.01 THEN 4460
4360 IF SGN(P9)=1 THEN 4420
4380 LET I9=I
4400 GOTO 3880
4420 LET I8=I
4440 GOTO 3880
4460 LET V=V8+V9
4480 LET P=I*V
4500 LET E=(P/.1)/(L2*W2*(R0*U1+(1-R0)*U2))
4520 LET F=P/(V3*I3)
4540 RETURN
4560 REM PARALLEL STRING PMAX SUB

```

4580 RETURN
4600 REM COST SUB
4620 LET Z0=N1*N2*A1*C0
4640 LET Z0=Z0+W2*L2*C1
4660 LET Z0=Z0+W2*L2*C2
4680 LET Z0=Z0+INT(N1*N2/D2+1)*C3
4700 LET Z0=Z0+N1*N2*C4
4720 LET Z0=Z0+INT(1/.25+1)*N1*N2*C5
4740 LET Z0=Z0+INT(1/.25+1)*2*N1*N2*C6
4760 RETURN
4780 END

LEN
02464 WORDS
DATE
???
GET-4DATE
NO SUCH PROGRAM
GET-\$DATE
RUN
DATE 1751

4/ 5/76

DONE AT 1751
BYE
0203 MINUTES OF TERMINAL TIME
OFF AT 17:51

GET-JRPLLOT
 LIS-P
 JRPLLOT

```

5000 REM*****PLOT ROUTINE
5020 FILES PLOT1
5030 DIM A$(75),B$(75),C$(198),D$(198)
5040 DIM S$(72),T$(72),M$(72)
5060 DIM X(10),U(10),L(10),K(10)
5070 REM      TITLE/COMMENT,SYMBOL STRING
5080 READ #1,1;C$,D$,S$
5100 LET N0=LEN(S$)
5120 PRINT " ";C$;D$;" "
5140 LET T$="`SIXA`Y`"
5200 REM      SCALING
5220 MAT U=ZER
5240 MAT L=CON
5250 MAT L=(1.E+25)*L
5260 MAT K=ZER
5280 FOR I=1 TO N0
5300 GOTO TYP(1) OF 5380,5320,6720
5320 READ #1;M$
5340 IF M$="END" THEN 5480
5360 STOP
5380 READ #1;X(I)
5400 LET U(I)=U(I) MAX X(I)
5420 LET L(I)=L(I) MIN X(I)
5440 NEXT I
5460 GOTO 5280
5480 LET K(I)=(U(I)-L(I))/71
5500 FOR I=2 TO N0
5520 LET K(I)=(U(I)-L(I))/99
5540 NEXT I
5560 REM      PRINT PLOT
5580 FOR J=60 TO 0 STEP -1
5600 READ #1,1;C$,D$,S$
5620 FOR I=0 TO 72
5640 IF I/10+J/6-INT(I/10)-INT(J/6)=0 THEN 5700
5660 LET B$(I+1,I+1)=" "
5680 GOTO 5720
5700 LET B$(I+1,I+1)="+"
5720 NEXT I
5740 IF J>7 THEN 5800
5760 LET B$(1,1)=T$(J+1,J+1)
5780 GOTO 5800
5800 IF J THEN 5860
5820 LET B$(1,10)=" ->U->AXIS"
5840 LET B$(4,4)=S$(1,1)
5860 FOR K=1 TO N0
5880 GOTO TYP(1) OF 5960,5900,6720
5900 READ #1;M$
5920 IF M$="END" THEN 6220
5940 STOP
5960 READ #1;X(K)
5980 IF K>1 THEN 6060
6000 LET X(K)=INT((X(K)-L(K))/K(K)+.5)+1
6020 IF X(K)>72 THEN 6160
6040 GOTO 6160
6060 LET X(K)=INT((X(K)-L(K))/(K(K)/.6)+.5)+1
6080 IF X(K)>60 THEN 6160
6100 IF X(K)#J+1 THEN 6160

```

```

6140 LET B$(X[I],X[I])=S$(K,K)
6160 NEXT K
6180 GOTO 5860
6220 FOR I=72 TO 1 STEP -1
6240 IF B$(I,I)="" THEN 6300
6260 LET B$(I)=""
6280 NEXT I
6300 PRINT B$
6320 NEXT J
6340 REM FOOTING
6360 LET A$="[ ] * * SCALE FACTOR="
6380 FOR K=1 TO NO
6400 LET A$(8,8)=S$(K,K)
6420 LET A$(2,4)="VER"
6440 LET M$=CONV(K[K])
6460 LET A$(24)=MULT(M$,"10",2)
6480 IF K>1 THEN 6520
6500 LET A$(2,4)="HOR"
6520 PRINT A$;
6540 PRINT " ORIGIN (";-L[K];")"
6560 NEXT K
6720 END

```

1.4 CdS Solar Cell Module

1.4.1 Cell Characteristics

Thin film solar cells of the $\text{Cu}_2\text{S}/\text{CdS}$ system are p-n hetero-junction semiconductor devices. They are analogous electrically to other p-n junction solar cells differing only in the magnitude of some of the output parameters. Figure 1.4.1 shows the current voltage characteristic curve of a unit area $\text{Cu}_2\text{S}/\text{CdS}$ thin film solar cell at full sunlight (AM1) illumination at 25°C as projected for the 1985 to 1990 time period.

As the light intensity decreases, the cell output decreases as shown in Figure 1.4.2. The short circuit current varies in direct proportion to the incident light intensity, but the open circuit voltage remains about the same. As the cell temperature changes, the open circuit voltage changes inversely with the temperature as shown in Figure 1.4.3, but the short circuit current remains about the same.

Over wide ranges of sunlight, illumination intensities, and panel operating temperatures, the shape of the current-voltage curve remains the same. The curve translates in the X direction about $-1.5 \text{ mV per } ^\circ\text{C}$ temperature change, and translates in the Y direction in direct proportion to the illumination level. Illumination intensity can change due to the angle of the sun with the normal to the plane of the cells (following the cosine law), or due to partial cloud cover.

At 25°C the open circuit voltage will average 0.53 volts, and the short circuit current will average about 26 mA per cm^2 of cell area at full sunlight intensity. Under these conditions the thin film solar cells are 10.0% efficient. The system performance characteristics

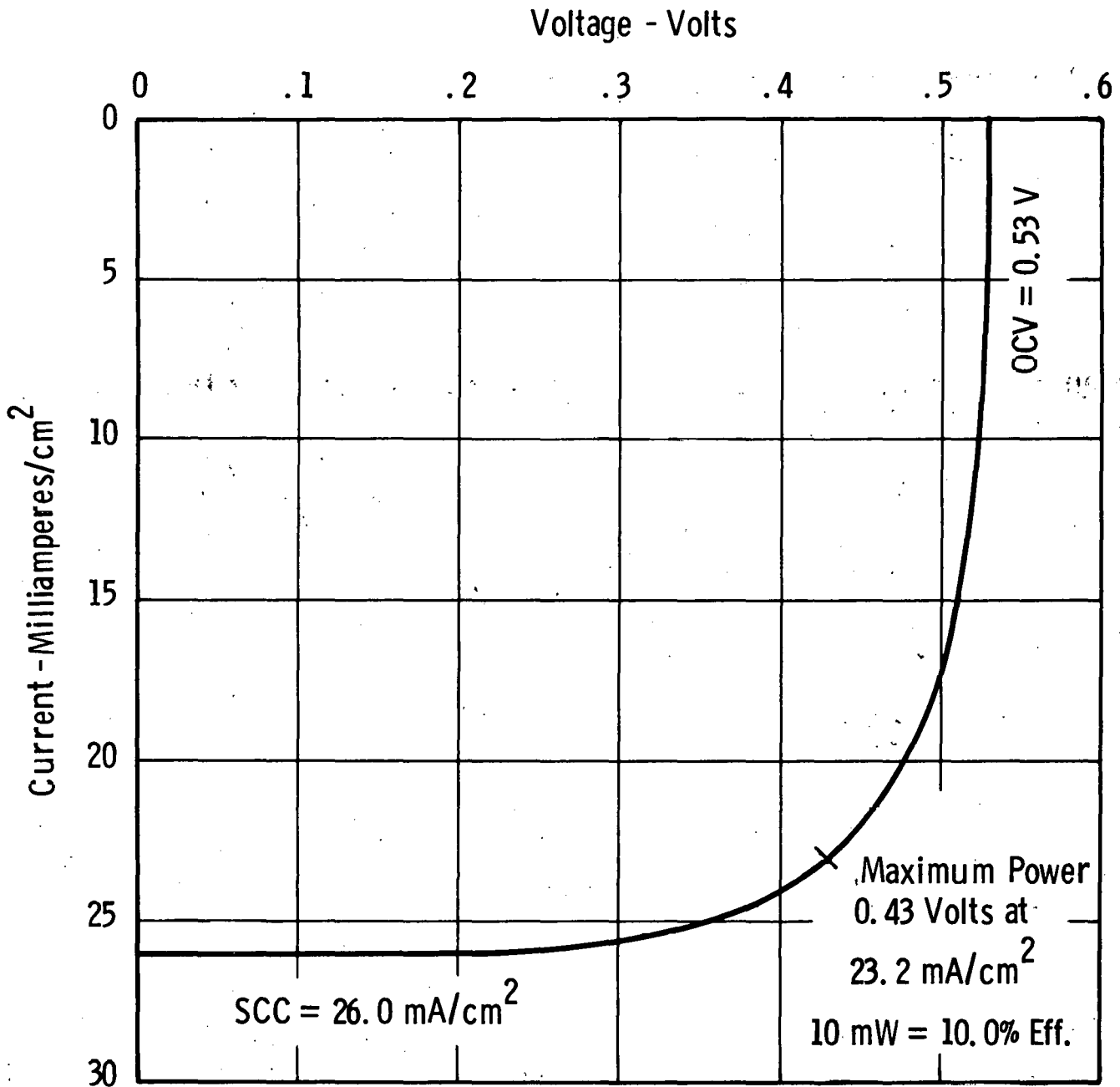


Fig. 1.4.1 - I-V Characteristic curve thin film $\text{Cu}_2\text{S}/\text{CdS}$ Solar Cell
1985 - 1990 at AM 1, 25°C.
(unit area)

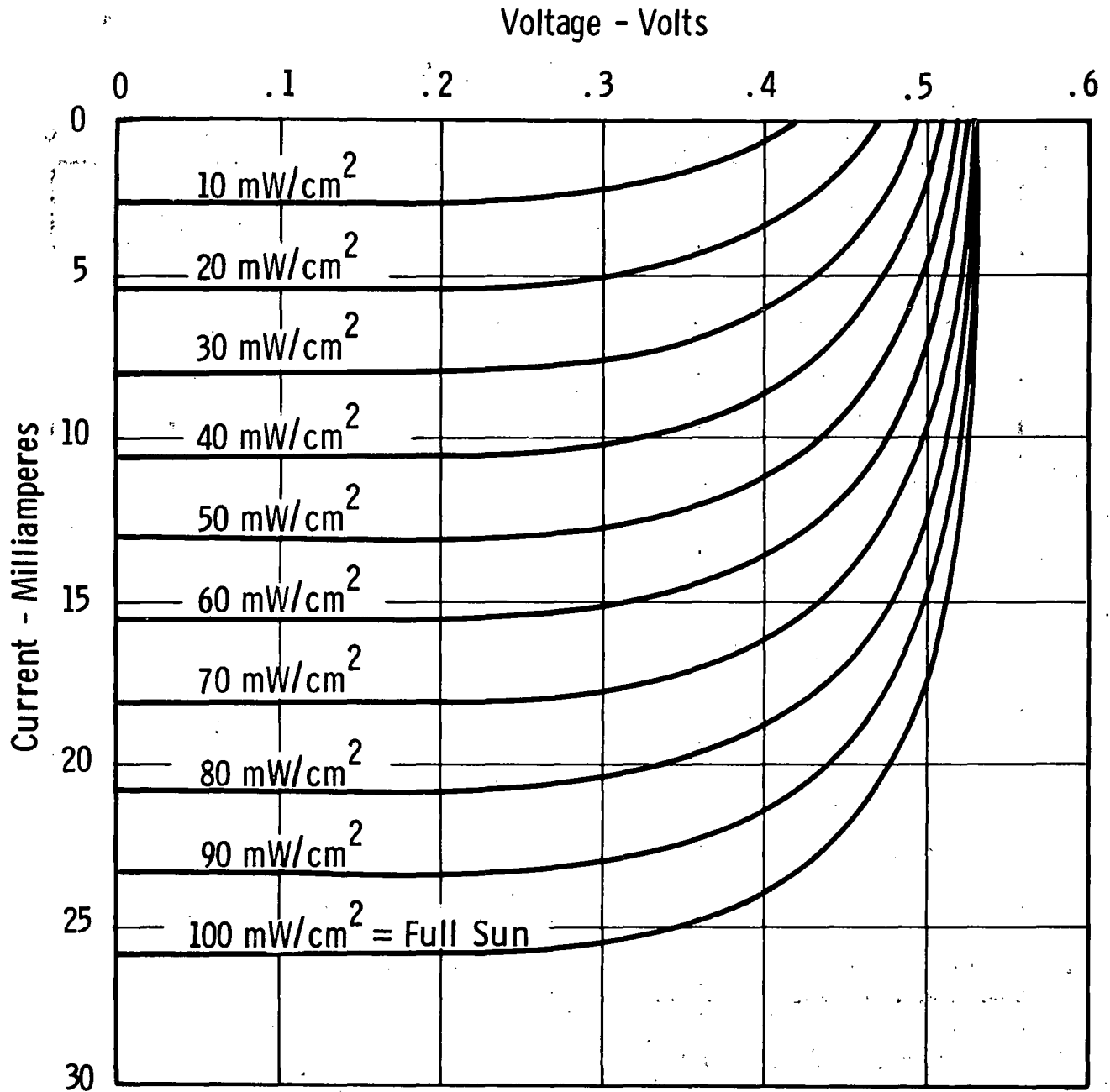


Fig. 1.4.2 - Effect of light intensity on output of $\text{Cu}_2\text{S}/\text{CdS}$ Cell
(unit area at 25°C)

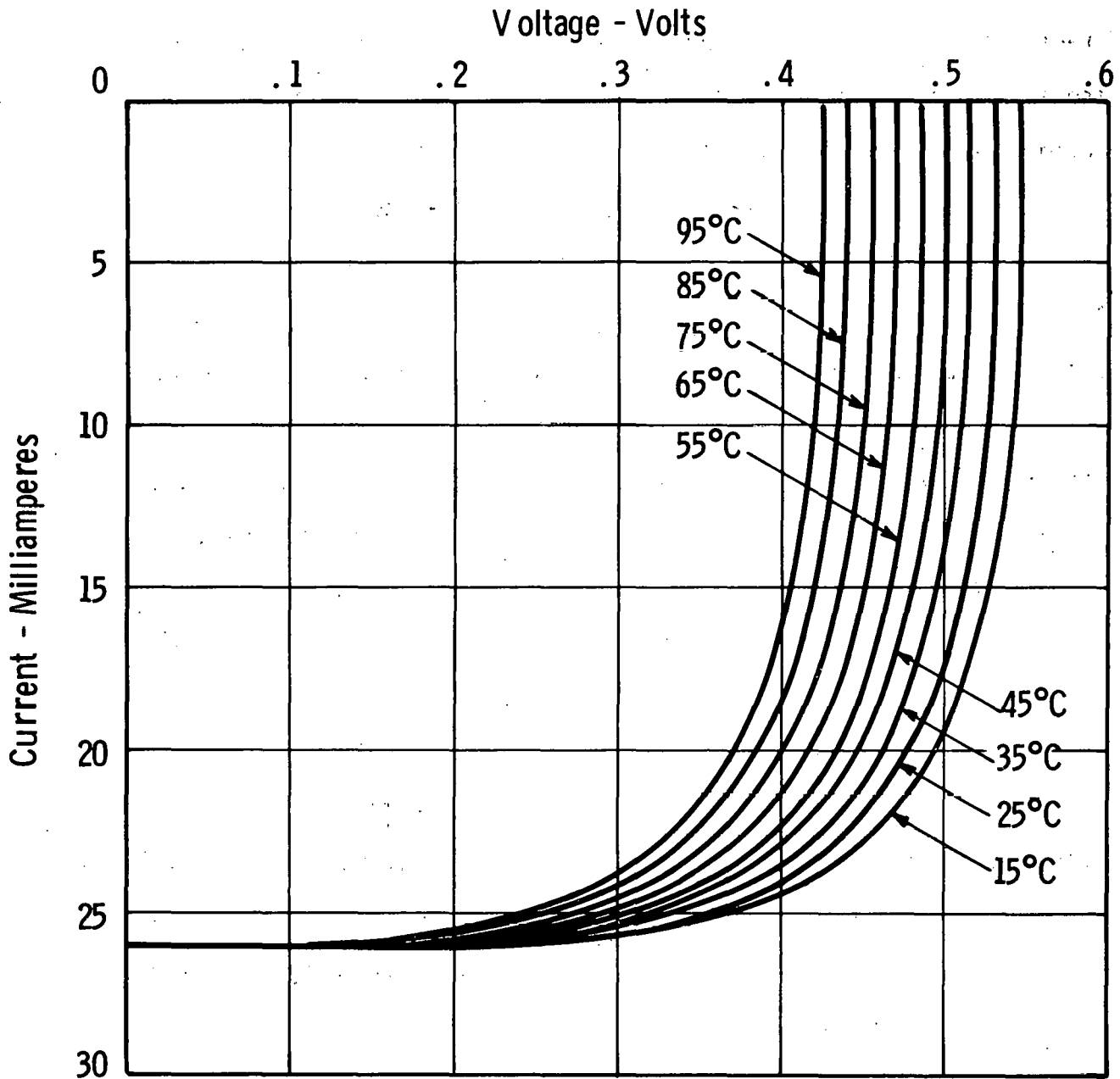


Fig. 1.4.3. - Effect of temperature on output of Cu_2S/CdS Cell
(unit area at AM 1)

predicted for the 1985⁺ time period for thin film arrays are based on these parameters. This is thought to be conservative and the actual parameters achieved at that time are likely to be higher.

Array performance using CdS solar cells was simulated by Professor Martin Wolf using a proprietary computer program. His simulations included as input one year of weather data, and provided as output the annual energy output in kilowatt-hours and peak power output in kilowatts per unit area of cell. Simulations were performed using Phoenix weather and several types of array designs. The simulations of the CdS solar cell arrays are described in Section 2.4 of Volume III(2). The analytical model used is described in the following paragraphs.

Similar to the predictive modeling of the silicon solar cells, the Cu₂S/CdS thin film solar cell modeled is the one expected to be available in mass production in the year 1985. While the modeling of the silicon solar cells was done entirely by the University of Pennsylvania team, the predicted performance data for the Cu₂S/CdS cell were supplied by Fred Shirland of the Westinghouse Research Laboratory.

The silicon solar cell is represented in the program by its commonly used model for the pn-junction device:

$$j = j_0 \left[\exp\left(\frac{q(V - jR_s)}{AkT}\right) - 1 \right] - j_L \frac{A_L}{A_j} \quad [A \text{ cm}^{-2}] \quad (1.4.1)$$

where

- j = terminal current
- V = terminal voltage
- j_0 = diode saturation current density
- j_L = light generated current density
- A = empirical adjustment factor ($A = 1$ for 1985 and 2000 silicon solar cells).
- R_s = effective lumped series resistance based on unit junction area
- A_L = light exposed area
- A_j = junction area
- T = cell temperature
- q, k = physical constants (electronic charge, Boltzman constant)

Terminal voltage, maximum power point, open circuit voltage, power under given load conditions, etc. are all derived from this relationship. The quantities j_L and j_0 are the determining quantities in this relationship.

The applicability of the mathematical model represented by Equation (1.4.1) to the $\text{Cu}_2\text{S}/\text{CdS}$ thin film solar cell has not been determined for the complete range of light intensity and temperature covered in the present simulated output runs. For the purposes of this program, however, the $\text{Cu}_2\text{S}/\text{CdS}$ cell was modelled in conformance with Equation (1.4.1), with an empirical light generated current value of 25 mA/cm^2 for idealized Air Mass 1 conditions. This light generated current was scaled linearly with available light intensity disregarding any effects of changing spectral distribution due to varying atmospheric attenuation.

To closely approximate the current-voltage characteristic at 298^oK, a saturation current value $j_0 = 3 \times 10^{-11} \text{ A cm}^{-2}$ was chosen, together with an A-value (adjustment factor in exponent) of 1.0. These values provide an open circuit voltage of 0.528 V, and a maximum power point of 23.2 mA cm⁻² at 0.43 V, for an output of 10 mW cm⁻² at an irradiance of 100 mW cm⁻².

The temperature dependence has been represented by a decrease of the open circuit voltage by 1.6 mV per degree Celsius. This temperature dependence is simulated through a temperature dependence of the saturation current

$$j_0(T) = j_{00} T^a e^{-\frac{E_{\text{act}}}{kT}} \quad (1.4.2)$$

with $a = 0$ for the Cu₂S/CdS cell.

Using this form together with Equation (1.4.1) yields:

$$\frac{dV_{\text{oc}}}{dT} = \frac{Ak}{q} [\ln j_L - \ln j_{00} T^a - a]; \quad (1.4.3)$$

Equation (1.4.3) provides the j_{00} value ($2.899 \times 10^6 \text{ A cm}^{-2}$), with which the appropriate value for the activation energy $E_{\text{act}} = 1.004 \text{ eV}$ is obtained from Equation (1.4.2) by use of the given value for the saturation current j_0 at 298K.

While the modeling for the Cu₂S/CdS cell for all runs except run K was done on a "predicted performance" basis using light generated current, open circuit voltage, and "fill factor" (for maximum power point), run K contained a model which was more based on "predicted cell characteristics". Thus, the A-factor was set equal to 1, and the

saturation was to be $1 \cdot 10^{-10}$ A cm^{-2} . Since this would have resulted in an open circuit voltage under standard conditions below 0.5 V, the saturation current was decreased to $3 \cdot 10^{-11}$ A cm^{-2} . To compensate for the significantly higher fill factor even with the series resistance value of $1 \ \Omega \ \text{cm}^2$ ($0.35 \ \Omega \ \text{cm}^2$ in the other runs), the light generated current was reduced to $25 \ \text{mA} \ \text{cm}^{-2}$ to maintain an efficiency of approximately 10% under standard conditions. To maintain the temperature dependence of the open circuit voltage at $1.6 \ \text{mV}/^\circ\text{C}$ at the changed saturation current and A-factor values, a j_{00} of $2.899 \cdot 10^6$ A cm^{-2} and an activation energy of 1.004 eV were used.

1.4.2 Module Analysis

A module analysis similar to that conducted for the silicon cell module was not performed for the CdS module. The purpose of performing the analysis on the silicon cell module was to determine optimum cell size and module cost as functions of module voltage. The integrated module concept devised for the CdS solar cell module obviates the need for such an analysis. This concept is described in Section 1.4.4.

1.4.3 Heat Transfer

The thin film solar cell planned for mass production is very thin, thus minimizing material content and cost. It is expected that cells made in the 1985 to 1990 time period will have active Cu_2S and CdS semiconductor layers and positive and negative electrode layers each a few microns or less in thickness. The bulk of the cell will be composed of the insulating substrate and the integral glass cover, and these will be just thick enough to provide physical integrity to the array and protection from the environment.

It is expected that the substrate will be on the order of 10 to 15 microns thick while the encapsulating cover layer will be on the order of 5 to 10 microns thick. Thus, the entire array structure will be 25 to 30 microns thick or just over .001". This will have a profound affect on the heat transfer properties of these arrays.

Thus, the temperatures which the arrays will reach in equilibrium in use will be determined by the structures to which they are attached and by the convective air flow across the surface of the arrays. Temperature gradients in the arrays should be very low and the rate of heat transfer very high.

Design approaches to handle thermal energy transfer are discussed in more detail in the sections concerned with each power system. Residential power systems will usually have the arrays attached like shingles to a wooden roof. In this case, because of the poor thermal conduction properties of the roof, the array temperature rise will be appreciable and heat losses will be principally by convection to the air. For those systems where the solar arrays are bonded to a heat sink, the temperature rise will be minimal and heat losses will be principally by conduction to the heat sink.

1.4.4 Module Design And Application

1.4.4.1 Module Design

The thin film solar cell modules will most advantageously be fabricated as integrated array structures with cells interconnected electrically in series during original manufacture. The conducting base electrode, CdS film, Cu_2S layer, grid pattern, cell interconnects and glass cover layer will all be vacuum deposited in successive steps onto an insulating substrate. This will combine very low original cost with minimal field wiring and deployment costs and yield reliable array constructions that will need little or no maintenance.

A simple pattern with all of the cells connected in a single series string is likely to be suitable for a variety of applications. Figure 1.4.4 shows the pattern contemplated. The arrays will be fabricated in continuous ribbon form with a fixed width, but of endless length. The individual cells will be arranged in rows across the width of the ribbon with successive rows making up the length. It is likely that just a few widths will be made, such as 1 foot, 2 feet, 4 feet, and 8 feet with just a few standardized cell sizes.

It has been discovered that if the individual cell lengths are kept short, about 2 to 3 cm, it becomes feasible to use vacuum deposited base electrodes, grid lines and cell interconnects, and that such vacuum deposited wires are able to carry the generated cell currents over the short distance to the adjacent cell without recourse to busbars or massive

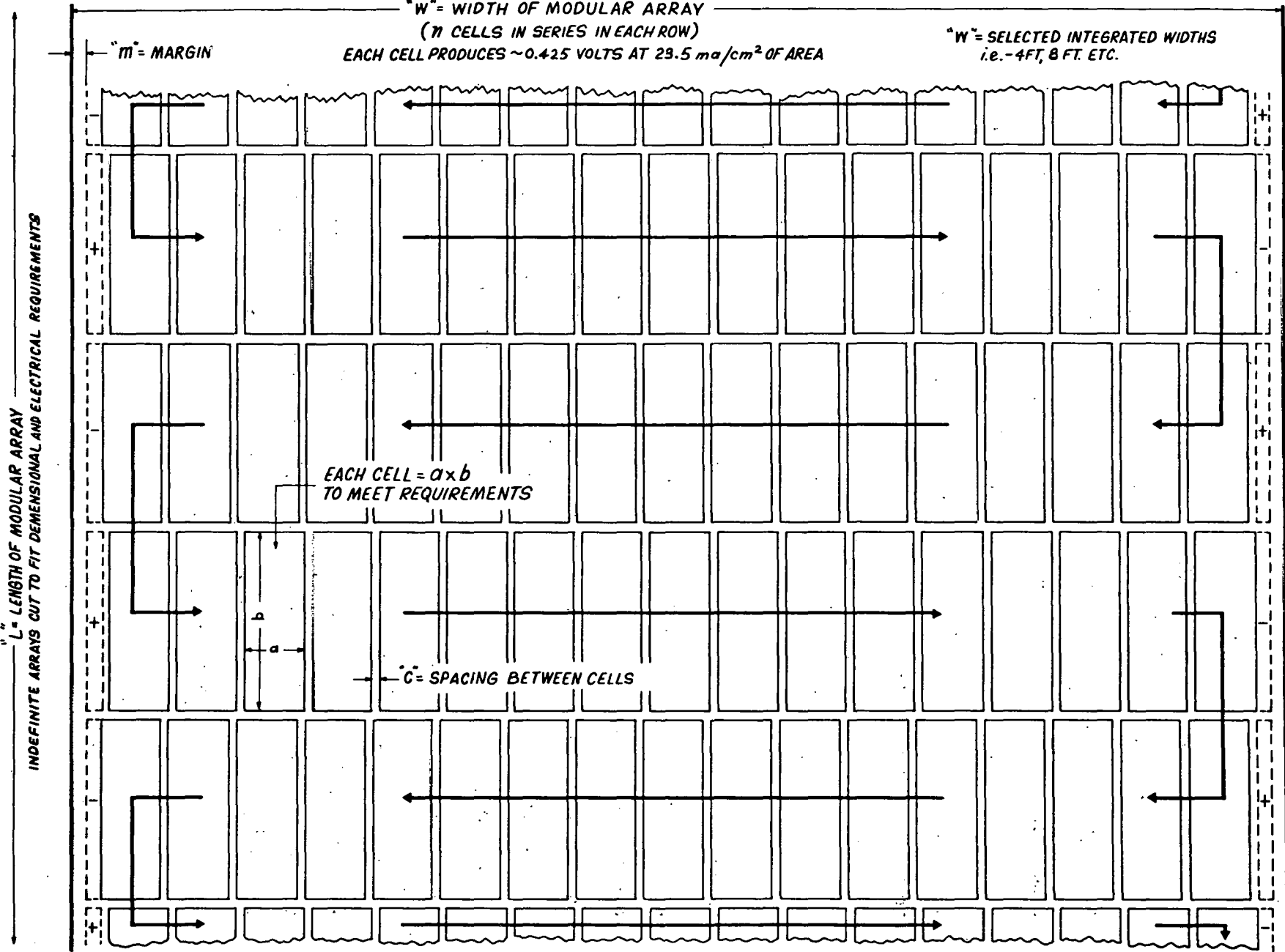


FIG.1.4.4 ARRANGEMENT OF THIN FILM SOLAR CELLS IN SERIES CONNECTED INTEGRATED ARRAY.

electrodes. The total cell area, and thus the desired current rating from a modular array, is obtained then by increasing the width of the individual cells as required. Spacing between cells and between rows of cells can be kept small since the voltage gradients in these devices are very low. However, the total voltage of a modular array can be very high, in the tens of kV's since the high potential difference will appear only over long distances. This design concept is very favorable since cell currents, and hence internal I^2R losses, are kept low.

Packing factors, i.e. active to total array areas, are expected to be 85 to 90% initially, and gradually climb to the 90 to 95% range as closer tolerances are made possible by more sophisticated production technology.

These highly desirable array designs are possible with the Cu_2S/CdS thin film solar cell construction because of the very high yields which are a feature of the simplified design cell with the half-dozen or so production steps. Once a continuous all-vacuum process of this nature is brought on stream, it operates for long periods with virtually no scrap or reject cells. (Overall yields much less than 100% result from start-up operations, or from some parameter of the process going out of control so that the line has to shut down and restart). With the designs planned, the very occasional cell failures will almost invariably be due to short circuits, so that just the single cell will be involved and the series string of cells will be only minimally affected. The chances of an open circuited cell are virtually nil.

Two examples of integrated array module designs are illustrative of the above concepts. The first might be a modular unit for mounting

on the roof of a residence. The second might be a larger modular unit for use at a central power station. The dimensions and electrical parameters selected are illustrative only and not limiting for any particular design unit.

A possibly attractive roof-top modular array might have an array width of 1 foot and an array length of 25 feet. The modules would be mounted in courses, like shingles. Thus the total array width could be wider, say 2 to 3 feet, with the lower edge consisting of active cells and the upper edge without cells so that the courses would overlap on the roof without blocking active cell areas. Such a module might be rated at 250 volts which it could produce with about 580 cells in series ($250 \div 0.43$). The area of each cell could be 34.5 cm^2 and the cells would be arranged in 58 rows of 10 cells each. Individual cell size in this arrangement would be 2.85 cm long by 12.1 cm wide and there would be 0.1 cm spacing between cells and 5 mm margins at the edges. For the 1 foot "line" area, the packing factor of this array would be 86%. The positive and negative terminals would be at opposite ends of the 25 foot lengths, thus facilitating the wiring of a number of such modular units in parallel. One such unit would produce 0.8 amperes at 250 volts, or 200 watts, in full sunlight at 25°C .

An example of a larger modular array design for a central station photovoltaic power system might be rated at 4800 volts and be 4 feet wide by 100 feet long. This panel could have 223 rows of cells with 50 cells in each row and each cell could be 2.3 cm long by 13.4 cm wide for an active cell area of 30.82 cm^2 each. The panel might have 0.1 cm spacing

between cells in each row, as in the smaller array example above, but might have a larger spacing of 0.25 cm between rows because of the number of cells in the rows. With 2.0 cm margins at the edges, the packing factor would be 92.4%. A single module would produce 0.715 amperes at 4800 volts for a power of 3.432 kW in full sun at 25°C.

1.4.4.2 Module Application Considerations

Specific applications for CdS thin film solar array modules in residential, intermediate and central photovoltaic power systems are discussed in more detail in the sections dealing with each system in Volume II. The design of the thin film solar cell modules can be flexible enough to accommodate a wide variety of end uses. The modules can be mounted in many ways. They can be nailed down or cemented down to a rigid surface, they can be stretched on an open frame, they can be built into an inflatable structure and they can be built on rolls and furled and unfurled as desired. The arrays are flexible and should be capable of being bent on a relatively small radius with little or no degradation. In this report just a few of the possibilities for deploying thin film modules are discussed. An attempt is made to capitalize on the unique features of the thin film construction.

Measurements of the lifetime of $\text{Cu}_2\text{S}/\text{CdS}$ thin film solar cells have recently shown that the major intrinsic factor affecting cell life time is the solid state diffusion of copper from the Cu_2S layer into the

CdS layer. This mechanism is temperature and time dependent so that the lifetime will depend on the temperature-time profile. Latest data indicate that with average operating temperatures of 40 to 50°C, useful cell lifetimes on the order of 50 to 70 years are to be expected.

Thus, it is of more concern that extrinsic factors that can affect cell lifetime are understood and provided for. Among possible extrinsic causes of cell degradation are: chemical reaction of the Cu_2S layer with oxygen and/or water vapor from the atmosphere; deterioration of the cover glass layer or the insulating substrate from the action of ultraviolet; corrosion of the leads; physical damage to the cell structure or cell interconnects due to wear, impact of dust particles, flexing in the wind, etc; and loss of light transmission due to dirt, stains or organic matter accumulating on the upper surface of the arrays. Data accumulated so far on thin film arrays in actual outdoor deployment is encouraging in these respects, and the major concern for extrinsic degradation is that of moisture and oxygen reacting with the Cu_2S .

The answer to this problem is the degree of impermeability by the encapsulating glass layer. Data have not yet been obtained on the degree of impermeability afforded by various thicknesses of various dielectric glassy coatings applied by various means. Present concepts are that about 10 microns of vacuum deposited 7059 glass or Si_3N_4 will be adequate to provide hermetic and physical protection of CdS cells for several decades of normal exposure. However, laboratory and accelerated lifetime tests are needed to verify these assumptions.

Similar considerations of course apply to other types of single crystal and thin film solar cells. It is likely that the thin film arrays will be easier to protect from the weather than arrays of single crystal solar cells because of the essentially planar surface over large areas.

Similarly, thin film arrays will also need diode protection for individual strings of series arrays so that an array will not drain the storage system in dark periods or so that faults in one panel will not result in circulating currents in others. Also, the considerations of partial shading of large arrays apply equally to thin film CdS and single crystal silicon cell arrays.

1.4.5 Cost Estimates

A detailed study of the materials needed for a 1985 to 1990 design CdS thin film solar array has been made and was published in the Conference Proceedings of the NSF Symposium on the Materials Aspects of Thin Film Systems for Solar Energy Conversion at Tucson, Arizona in May 1974. This study assumed a 10 micron thick copper substrate, 5 microns of CdS and 5 microns of the glass cover. A production process to fabricate 500 MW of 9% thin film solar cells per year was considered using a continuous all vacuum process. With conservative yields and contingency provisions, cell costs for $\text{Cu}_2\text{S}/\text{CdS}$ cells of \$15 per KW of peak generating capacity were obtained. This was a factory cost figure which included depreciation and engineering, but not profit and sales costs.

The integrated modular arrays as described in the above sections should cost no more than the costs that were predicted for the solar cells alone, since the materials used would be nearly identical and the processes very similar. Since the original study was made, there have been additional inputs. First, the projected efficiency of the cells has been increased from 9% to 10% based on the results of basic investigations at a number of laboratories. Also, sensitivity analyses of the materials and processes predicated for the initial cost study indicate that there is room for considerable lowering of the original cost elements. However, it is doubtful that the lower cost ranges can be achieved until annual production rates are well in excess of 1000 MW of peak generating capacity which would put it beyond the 1985 time period. Thus, cost projections of CdS thin film solar cell modular arrays of \$10 to \$15 per KW of peak capacity are likely to be the best that can be obtained in the next 10 to 15 years.

THIS PAGE
WAS INTENTIONALLY
LEFT BLANK

1.5 Array Structure

1.5.1 RPS Array Structure

1.5.1.1 Silicon Water Cooled Array Structure

The residential water cooled modules, as mentioned in Section 1.3.4 - RPS Design, are based on centerline dimensions of 32" x 96". Because we have identified the residential system as being structurally integrated or nested, this implies that building roof structures with centerline dimensions which coincide with the centerline dimensions of the collector must be constructed. Therefore, the roof framing members of joists will be 32" on center and within the tolerance limits set by Section 1.3.2 - Module Analysis. A Stanlock aluminum extrusion is connected to each joist with 2" pan head wood screws. This provides the vertical structure to receive the Stanlock glazing gasket (see Figure 1.5.1). The horizontal support for the extrusion and glazing is provided by supplementary wood framing 96" on center and fastened at right angles to the main structural joists. The aluminum extrusions then receive a glazing gasket lattice which also conforms to module sizes.

The outside perimeter of the collector array will be waterproofed with 28 gauge aluminum flashing (see Figures 1.5.2 and 1.5.3). The top edge of the collector is flashed continuously from the glazing gasket over the house ridge and attached to the opposing roof pitch (see Figure 1.5.4). The water cooled modules are then placed into the glazing lattice and locked in place with a glazing spline.

Fluid connections from the supply and return headers (see Figure 1.8.43 and 1.8.44) and between each collector module (see

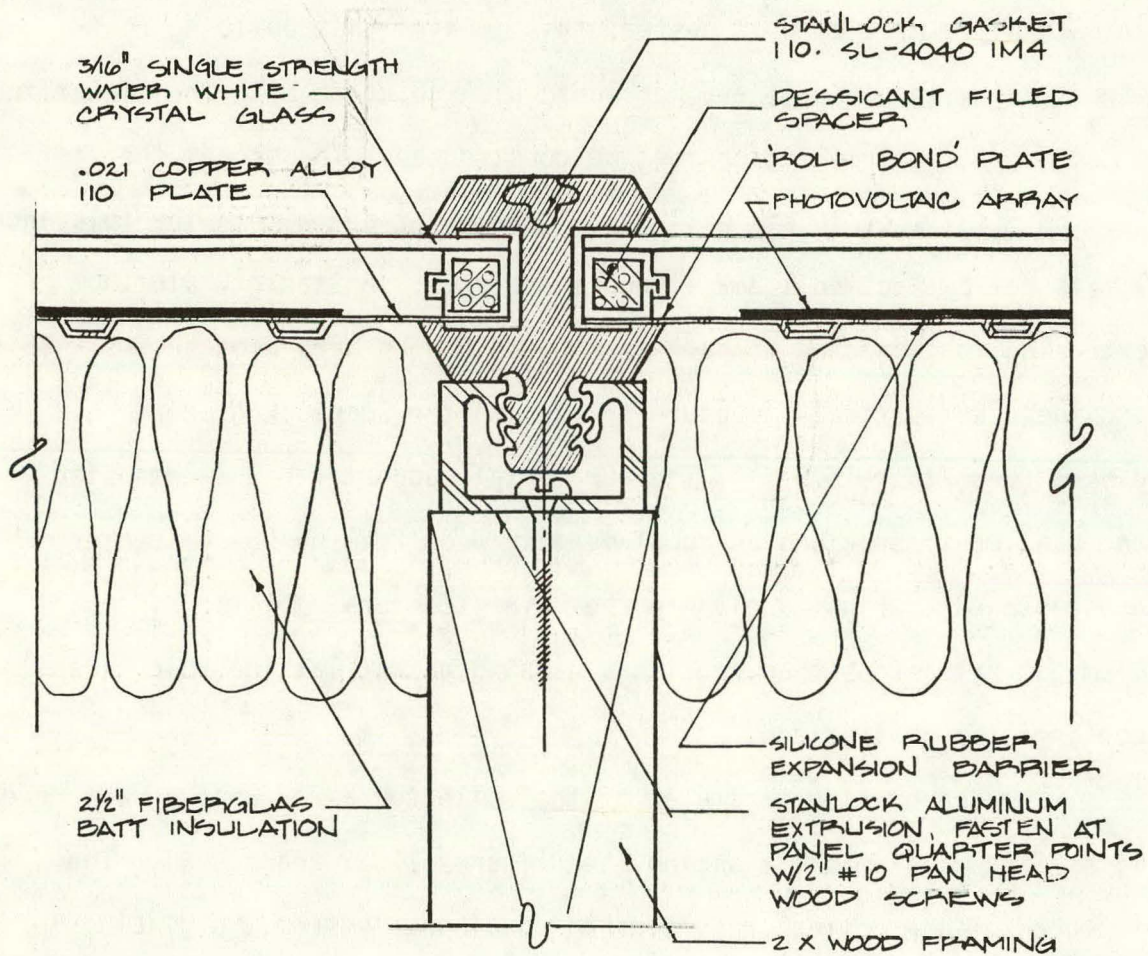


Figure 1.5.1 - RPS proposed collector framing sloped joint detail

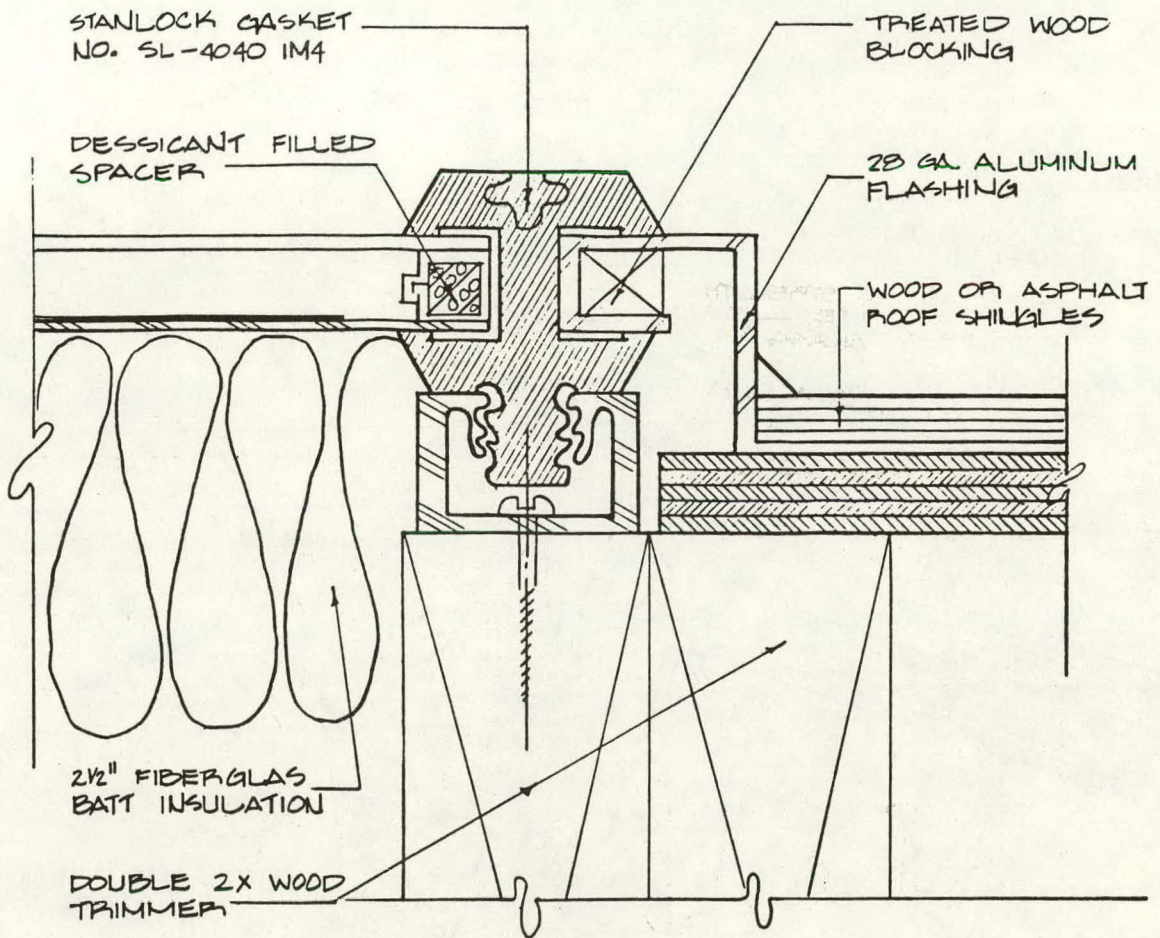


Figure 1.5.2 - RPS proposed collector framing section at sloped roof intersection

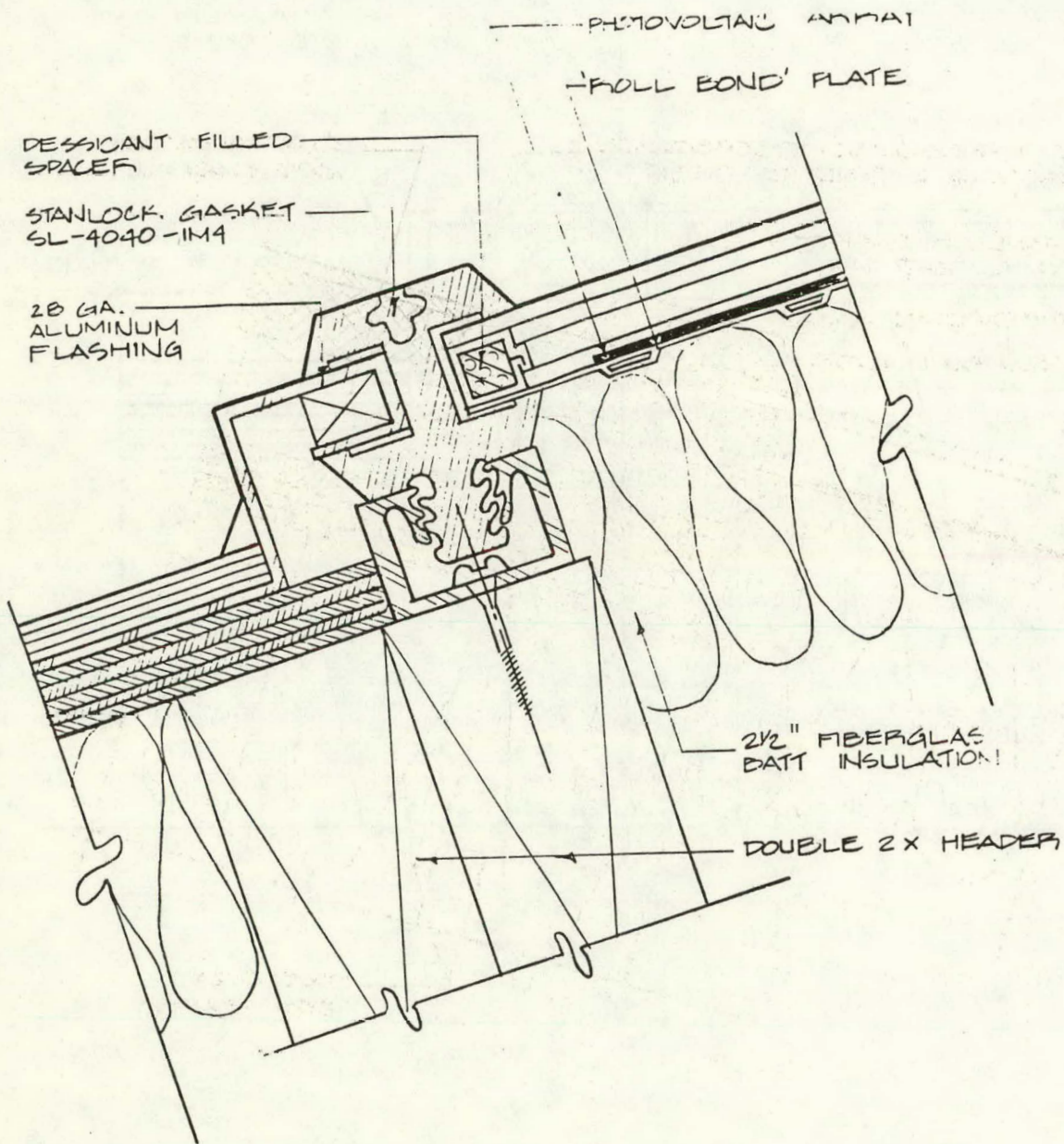


Figure 1.5.3 - RPS proposed collector framing section at bottom edge

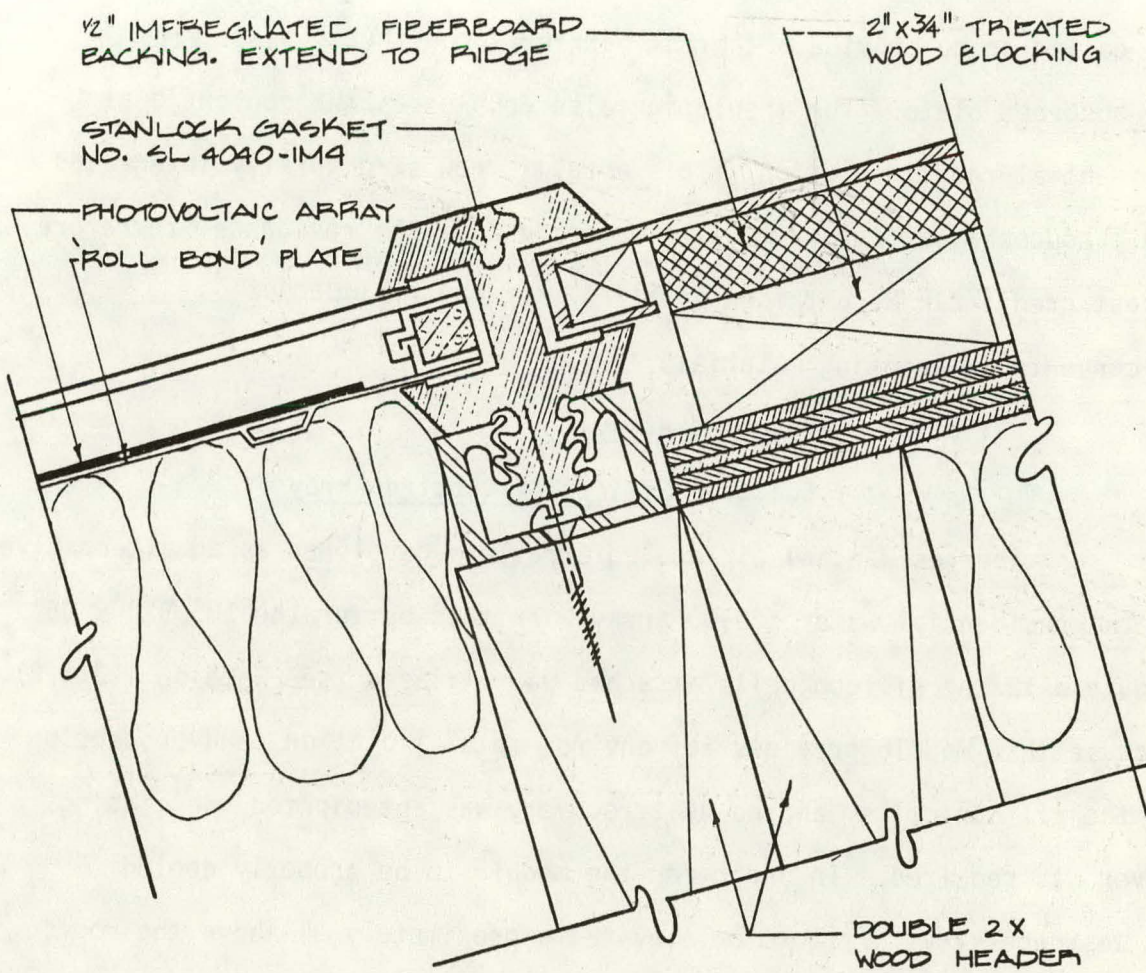


Figure 1.5.4 - RPS proposed collector framing section at top edge

Figure 1.5.5) are made in vertical series with silicon rubber hoses and clamps (see Figure 1.5.6). All of these connections are made without kinks in the hoses which would impede the gravity drain-down system or form air locks. Once all fluid connections are made and the system is tested for water leaks, 2-1/2" of fiberglass insulation is added below the collector to provide a thermal barrier to cut heat losses from the absorber plate. The insulation also doubles as the conventional residential roof insulation. This array is now structurally integrated and produces a waterproof roofing membrane for the residence, therefore, a cost credit can be obtained of \$1/ft² for the replacement of conventional roofing materials.

1.5.1.2 Air Cooled Array

1.5.1.2.1 Silicon Air Cooled Array

The residential air cooled array was developed as an alternative to the residential water cooled array. In this option, the IPS 32" x 96" module with the silicon cells attached was utilized (see Section 1.3.4.2). Because this module provides for environmental isolation and protection of the silicon cells and no heat recovery was anticipated, no glazing cover was required. In order for the module to be properly cooled, it was necessary for it to be elevated approximately 5" above the roof surface. This was achieved by placing the array on elevated plastic (PVC) support towers. Each tower (see Figure 1.5.7) is made up of two PVC components. A threaded PVC flashing collar supporting two modules is attached directly to the roof surface every 64" on center in the horizontal direction (supporting two modules) and every 96" on center in the vertical or pitched direction. A support

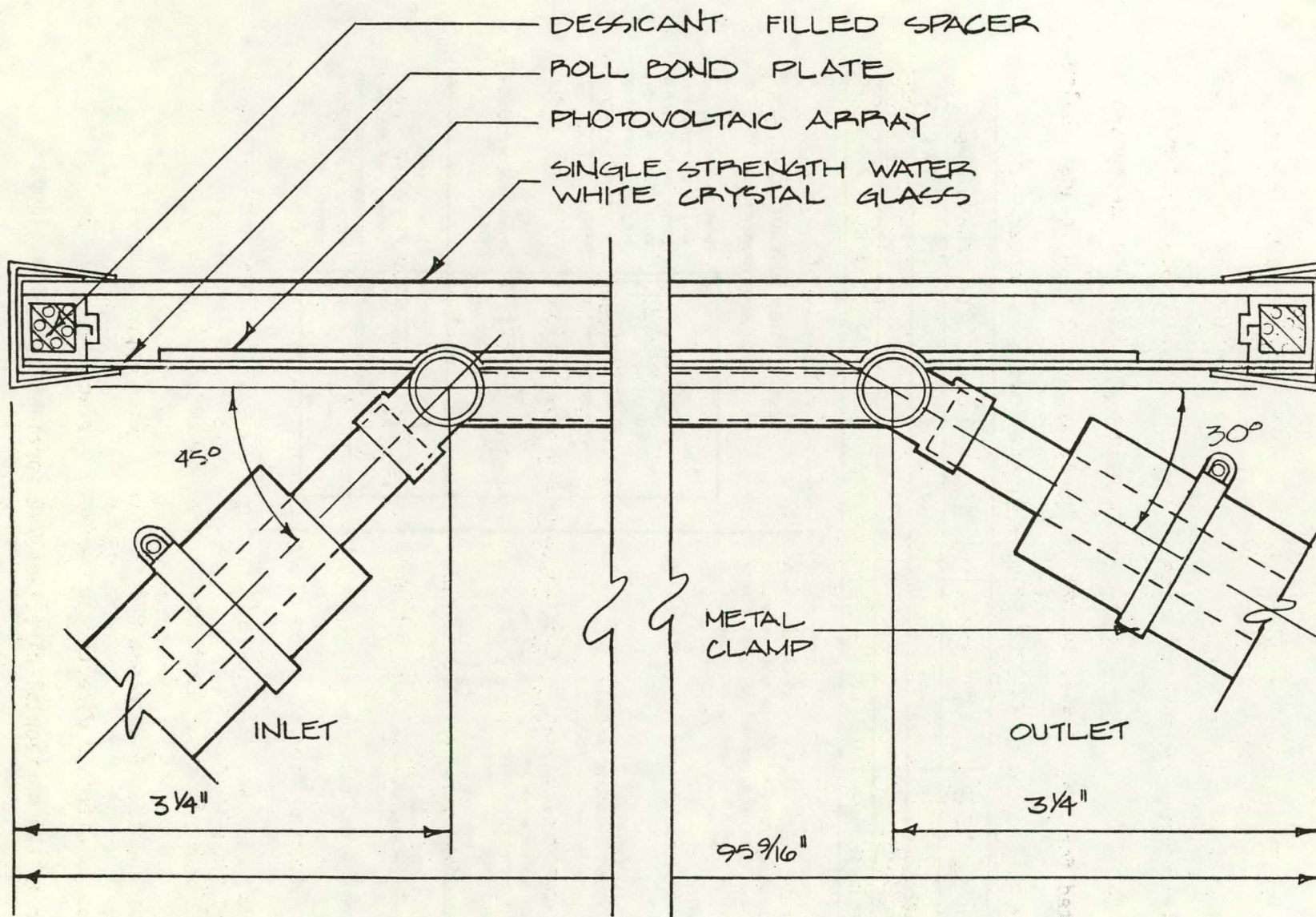


Figure 1.5.5 - Photovoltaic water cooled module piping connections

SPECIFICATIONS
FC252 Silicone Heater Hose

Part Number	Hose I.D. (inches)	Hose O.D. (inches)	Working Pressure (PSI)	Minimum Burst (PSI)
FC252-10	.63	1.02	50	200
FC252-12	.75	1.14	50	200
FC252-16	1.00	1.39	50	200

CONSTRUCTION:

Aeroquip FC252 Silicone Heater Hose is constructed with a specially compounded green silicone rubber tube, one braid of fiber glass reinforcement and green silicone rubber cover.

APPLICATIONS:

Ideal for use in heater hose applications on all diesel and gas engines.

TEMPERATURE RANGE:

-65°F. to +350°F. (-54°C. to +177°C.)

CLAMPS:

Extended tang hose clamps or clamps with a shoe are recommended for securing to formed and beaded male tube ends.

CAUTION: Do not use wire type clamps for securing silicone hose.

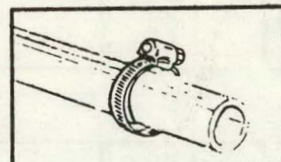


STANDARD PACKAGING:

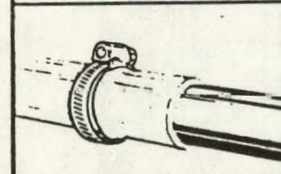
50 feet of hose per dispenser carton.

INSTALLATION INSTRUCTIONS

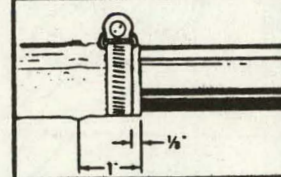
FC252 Silicone Heater Hose



Step 1.
Cut hose square to length required with a knife. Slide extended tang hose clamp over hose cover.



Step 2.
Push hose over beaded tube.



Step 3.
Locate extended tang hose clamp near the end of hose and tighten the clamp.

Figure 1.5.6 - Specifications for hoses and hose clamps

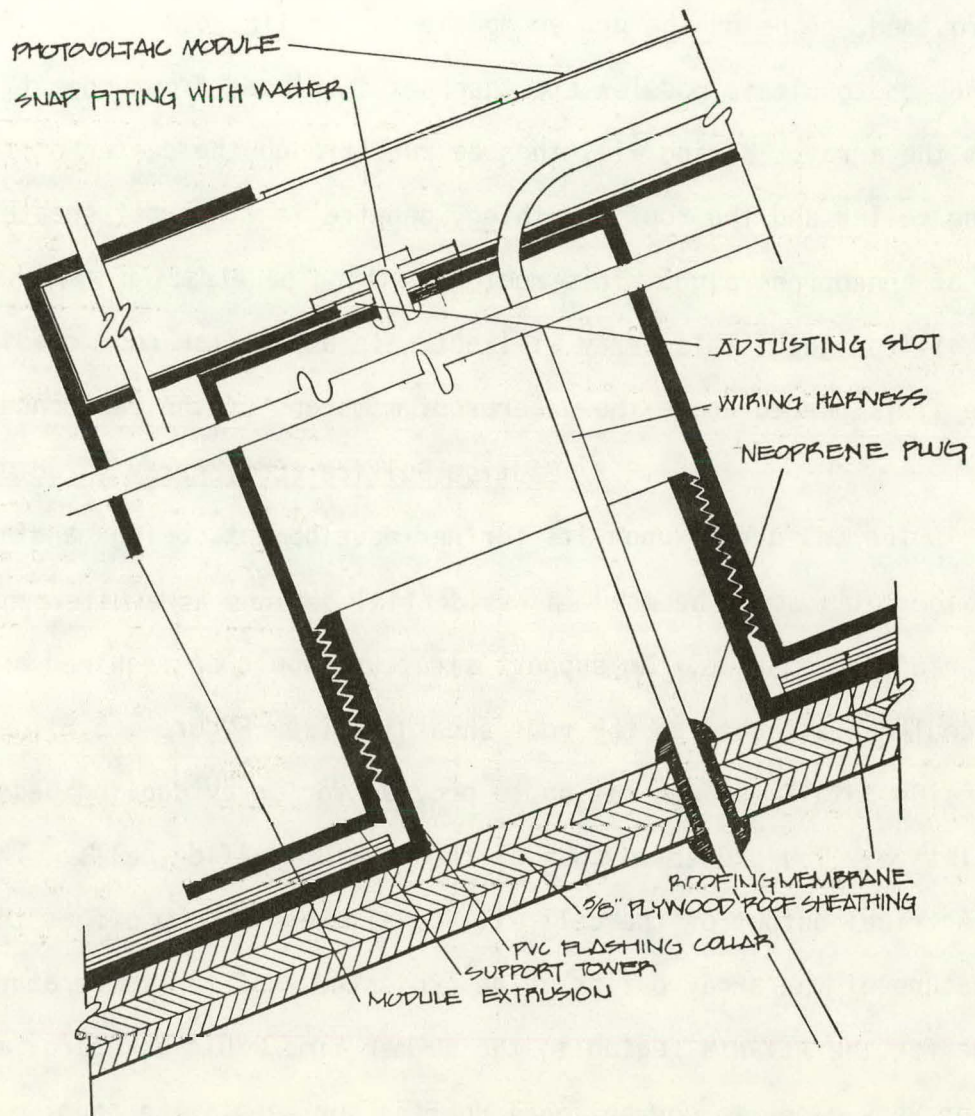


Figure 1.5.7 - Non-thermal residential array edge detail

tower is then threaded onto the flashing collar and leveled with all the other supports thus allowing the array to exist in one plane. Horizontal module extrusions are fastened to the support towers with snap fittings and are adjusted by virtue of the enlarged adjusting hole provided, to be on the proper module center line dimension. The 32" x 96" photovoltaic modules are then set in place, front edge first, to form the array. Wiring will then be run through the center of the flashing collar and the roof sheathing, penetrating the roof sheathing by way of a neoprene plug. This roof sheathing penetration will be sealed with a silicon gel. This array will not gain any dollar roof credit because it is placed above the waterproof membrane of the residence.

1.5.1.2.2 Cadmium Sulfide (CdS) Array Structure

The CdS Array, upon its further development, being manufactured in 4' wide rolls would be used in residential designs as a waterproofed rolled roofing membrane. No support structure would be required and the array could be attached to the roof sheathing (see Figure 1.5.8). This design detail was not set up to provide for array cooling because of the relatively low projected cost of the cadmium sulfide cells. Therefore, the electrical output of the cell will be allowed to drop off as the temperature of the array builds. The projected roof top temperature average for the Atlanta region in the summer time would be approximately 130°F or very close to conventional roofing surfaces. The cadmium sulfide array would appear as illustrated in Figure 1.8.55.

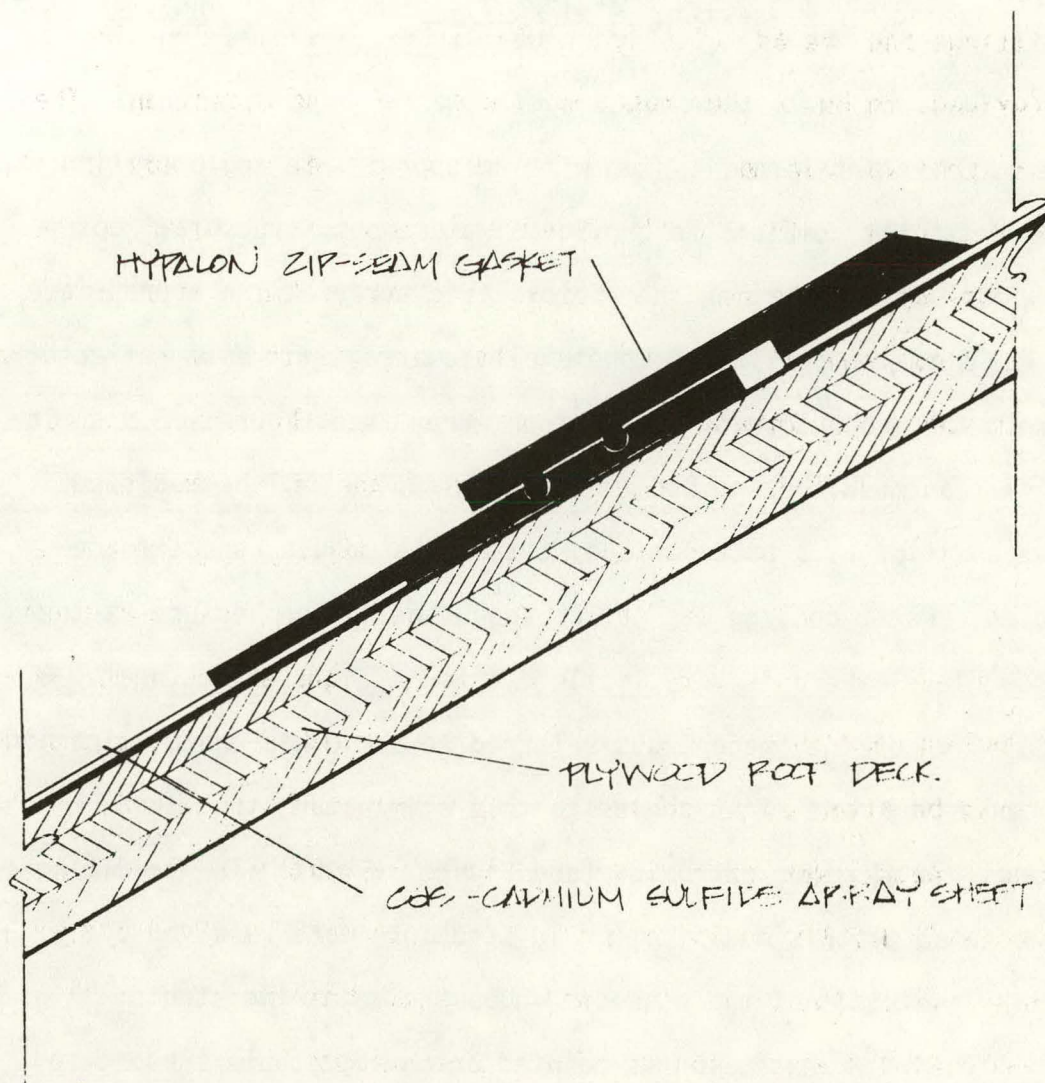


Figure 1.5.8 - Residential cadmium sulfide array connection detail

1.5.2 IPS Array Structure

1.5.2.1 Silicon Array Options

1.5.2.1.1 Total Roof System - Interconnected Triangular Truss (Modified Truss)

This modified space truss system was developed to entirely replace a conventional roof system with an appropriate agglomeration of components that combines to provide a waterproof structural roof system while also supporting the photovoltaic array at the appropriate tilt. The surface opposing the photovoltaic array will be a reflector to augment the production of the silicon array (see Figure 1.5.9). The finned silicon module described in Section 1.3.4.2 will be modified with the addition of a back surface so that the module can be force air cooled. Water cooling was not chosen as an option because at the IPS system level, there is very little use for a 130⁰F reject heat. A remodification of the space truss referred to above was the elimination of the top strut. At right angles to this eliminated strut is a continuous top aluminum extrusion (see Figure 1.5.10). The resulting forces created by this modification in structure were resolved by increasing the sizes of the connector hubs and adjoining struts.

The lower extrusion is mounted on an adjustable support to accommodate slight variations between connector hubs. This extrusion will also incorporate a lined gutter system to carry rain water run-off from the roof system (see Figure 1.5.11). The collector and reflector modules are incorporated into the roofing system by placing them into neoprene glazing gaskets which in turn are incorporated into the top and bottom aluminum extrusions. Air cooling is achieved by passing

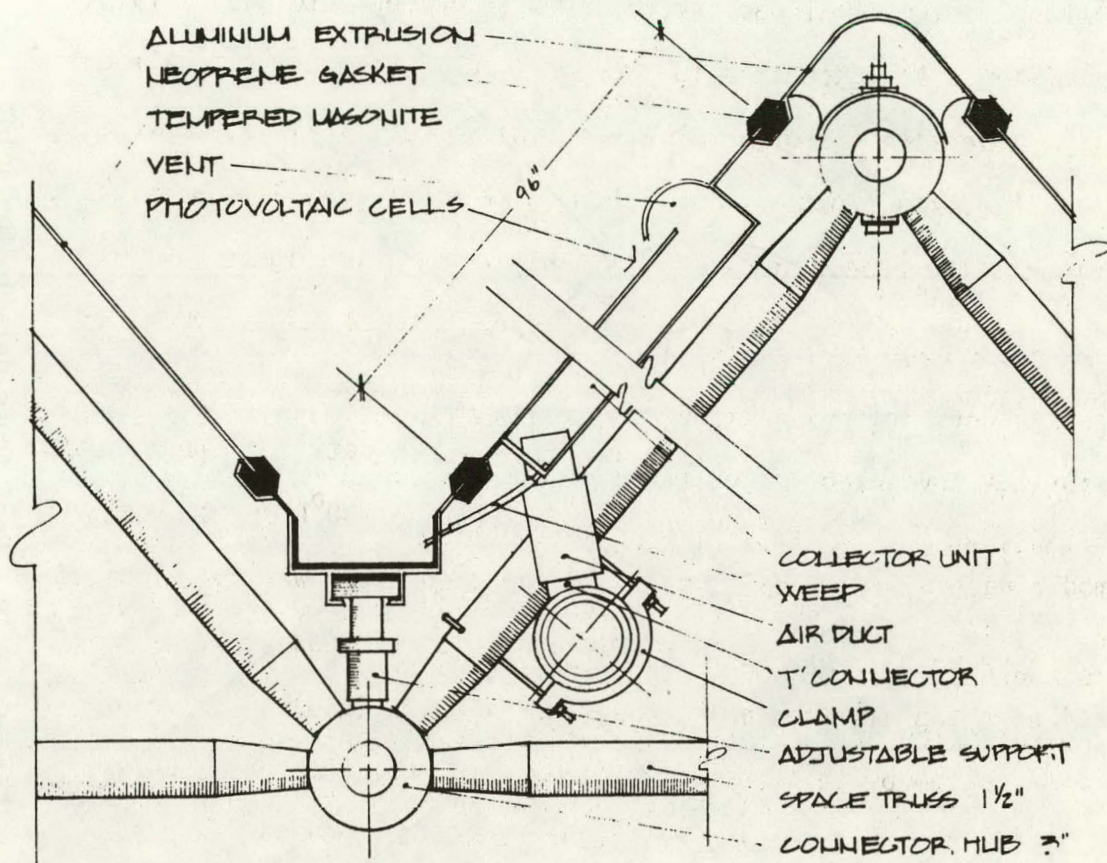


Figure 1.5.9 - IPS flat plate system 1

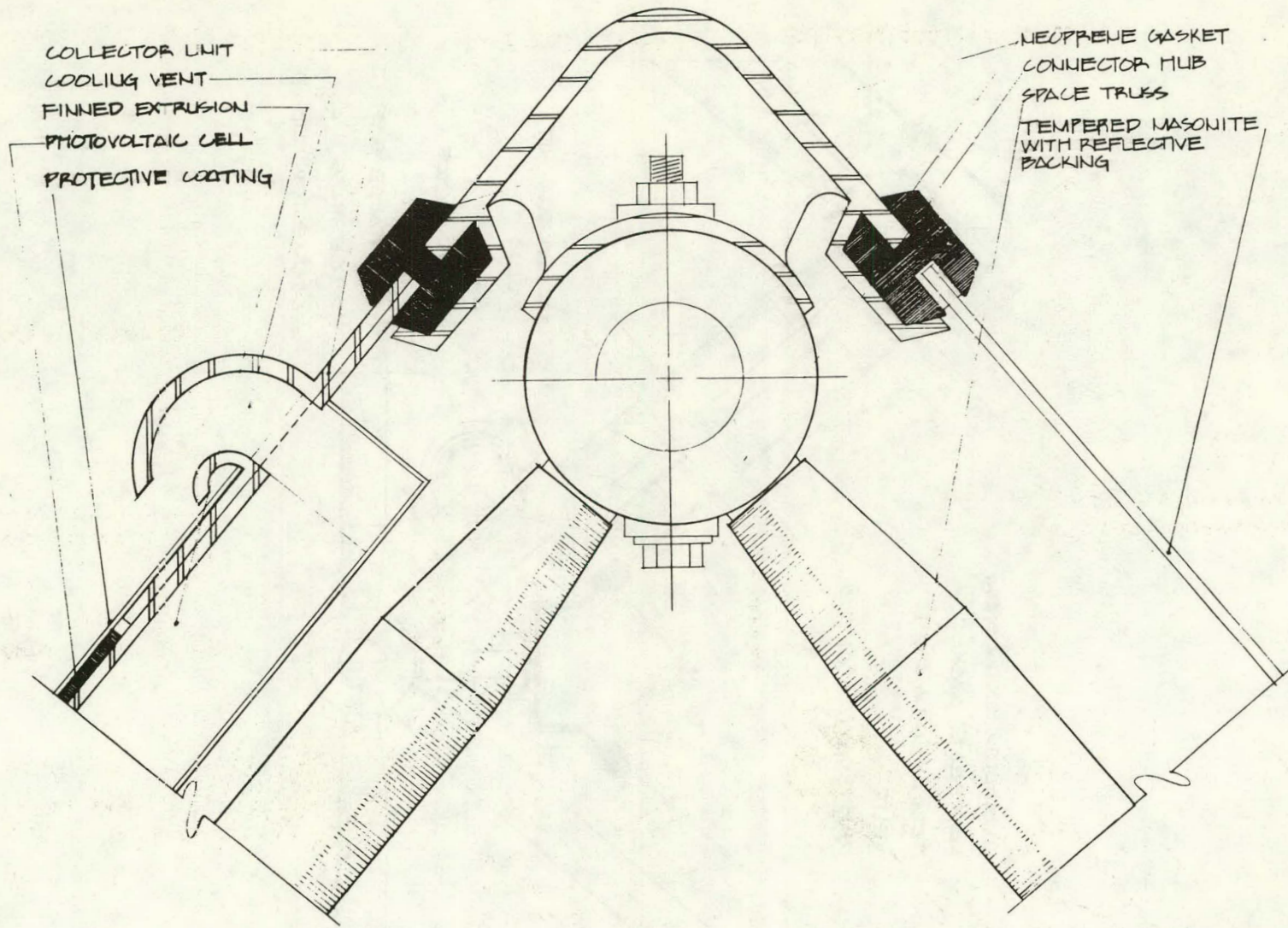


Figure 1.5.10 - Roof truss detail, top joint

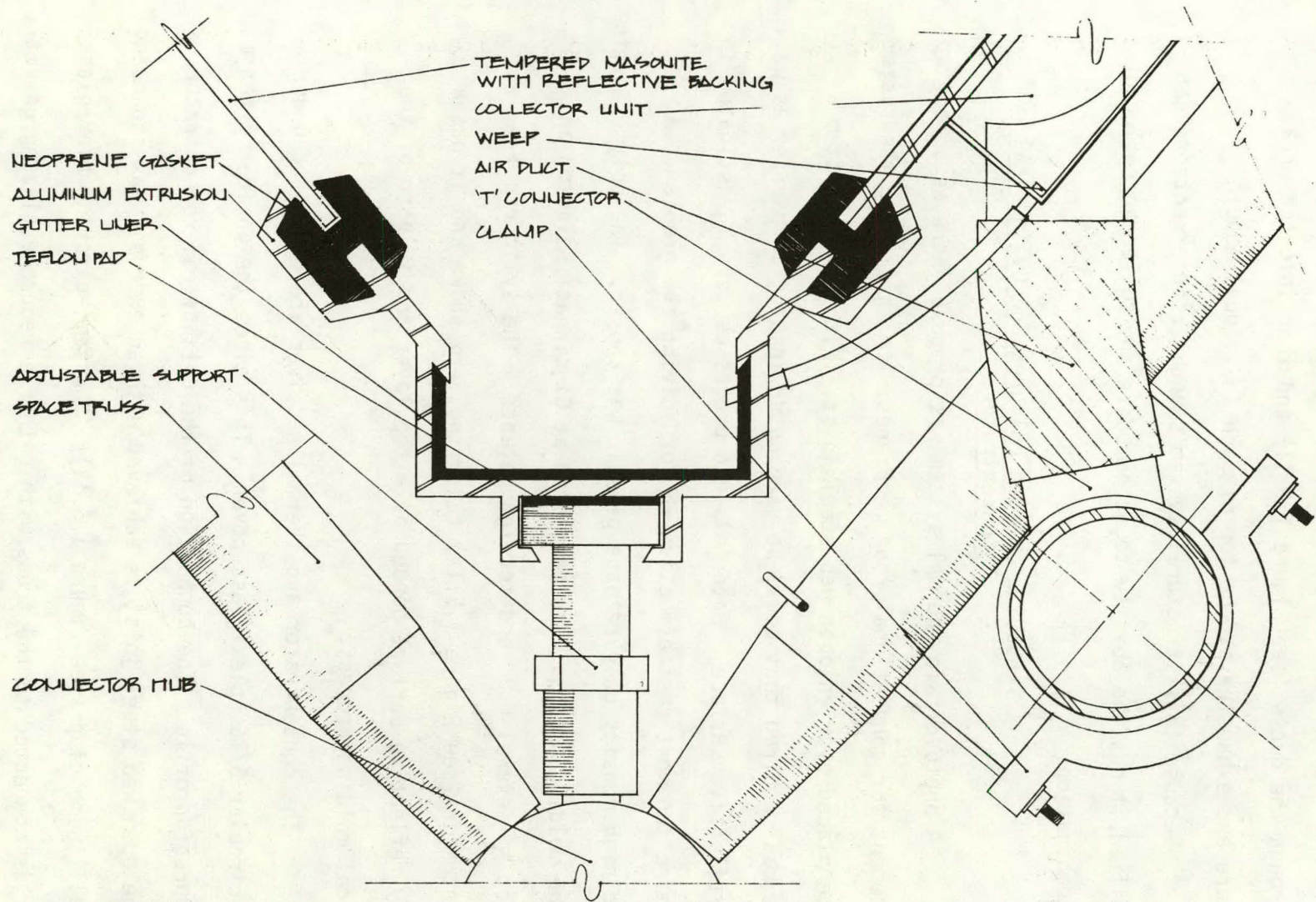


Figure 1.5.11 - Roof truss detail, bottom joint and air ducts

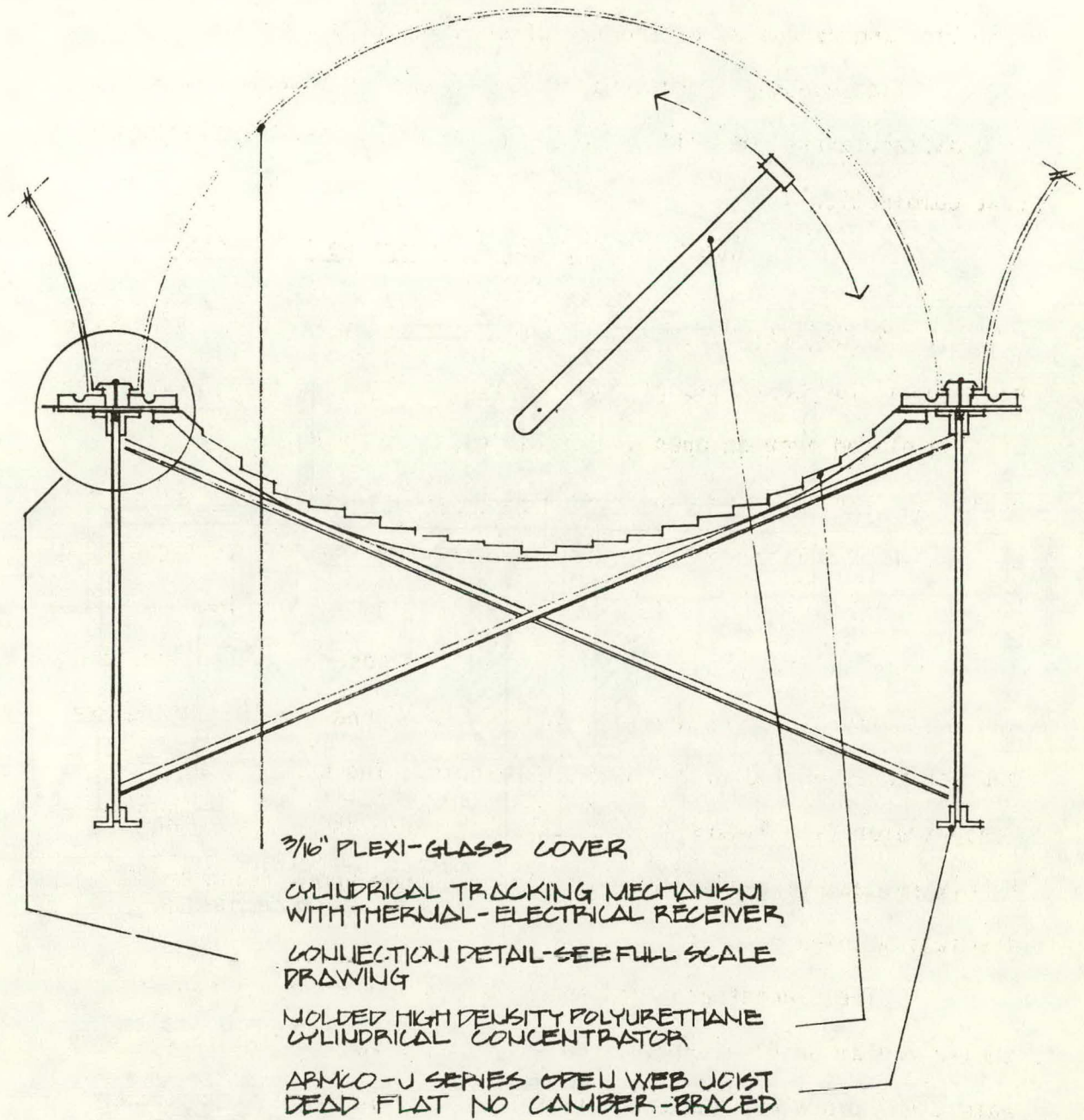
air through the ducts (see Figure 1.5.11) and then into the array structure and exhausted at the top of each individual module.

Because this structural system's angular intersections can be modified, it has the ability to accommodate any collector/reflector tilt combination.

1.5.2.1.2 Molded Polyurethane Cylindrical Concentrator

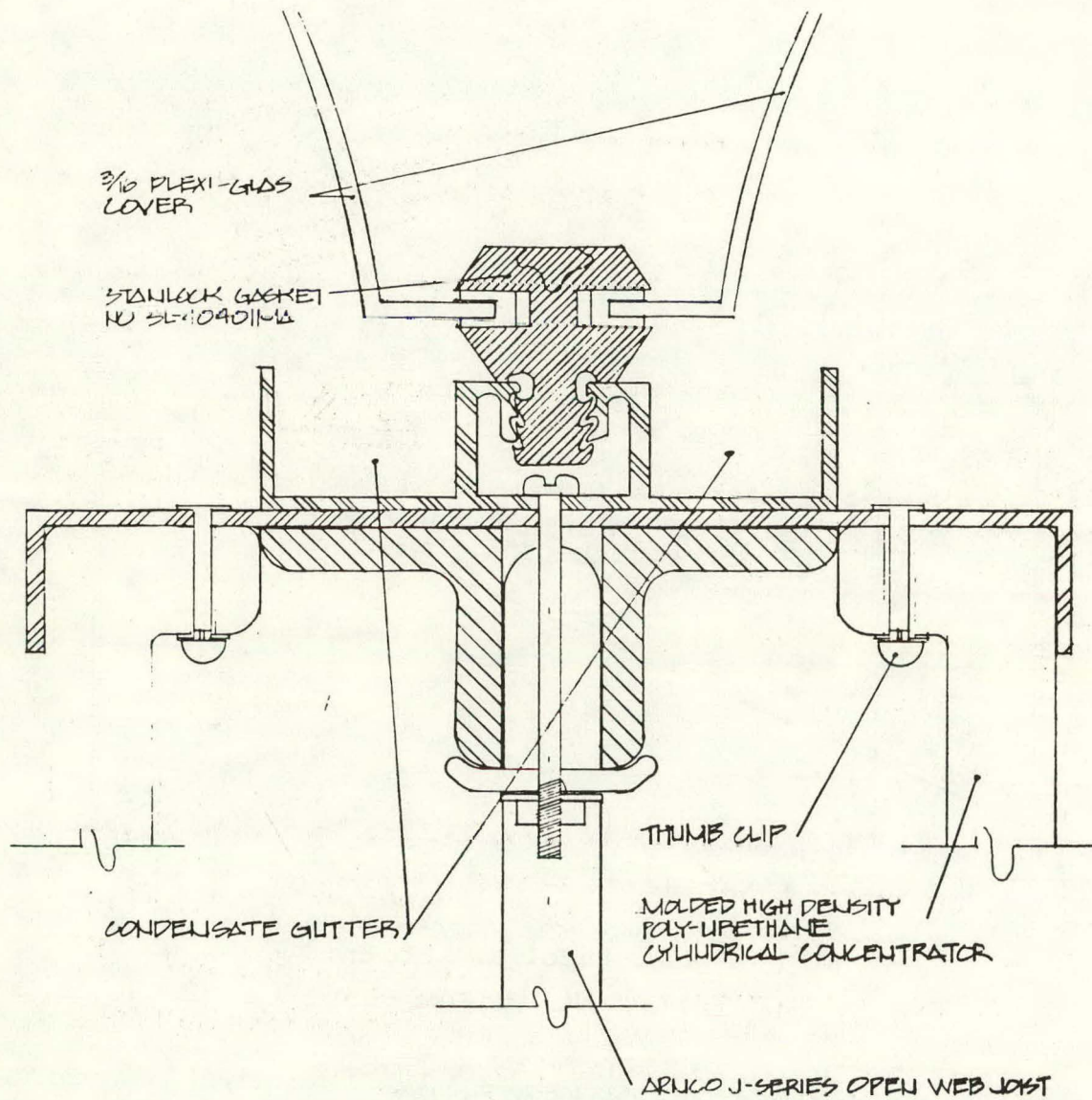
A photovoltaic thermal system was proposed here as a rooftop replacement for conventional roof membranes. In this case, the system will be placed over an open web steel joist. Within this system a device was required that could be used as an insulation barrier as well as a reflective surface. Materials and processes were investigated to determine the most cost effective way of solving the problem. A molded high density polyurethane plastic was chosen. The polymer system and the molding process were developed at Cincinnati Malacron and are subject to several U.S. and foreign patents. The cylindrical concentrator (see Figure 1.5.12) takes the form shown and it has a highly reflective surface bonded as a top layer and is part of the chemical molding process.

The concentrator and thermal receiver are contained under a semi-circular 3/16" plexiglass cover. This gives the entire system a waterproof profile. The connection of the cylindrical concentrator to the open web steel joist is achieved with an extrusion as shown and a small thumb clip (see Figure 1.5.13). The semi-circular plexiglass cover is connected to the truss with either a neoprene glazing gasket (see Figure 1.5.13) or with a more conventional aluminum glazing extrusion (see Figure 1.5.14).



IPS CYLINDRICAL CONCENTRATOR CONNECTION DETAILS 5

Figure 1.5.12



NOTE: POLYURETHANE CONCENTRATOR PROVIDES INSULATION

NOTE: THUMB CLIP PROVIDES FOR EASY REMOVAL OF CONCENTRATOR FOR SERVICING OF RECEIVER

Figure 1.5.13 - IPS cylindrical concentrator connection details - 1

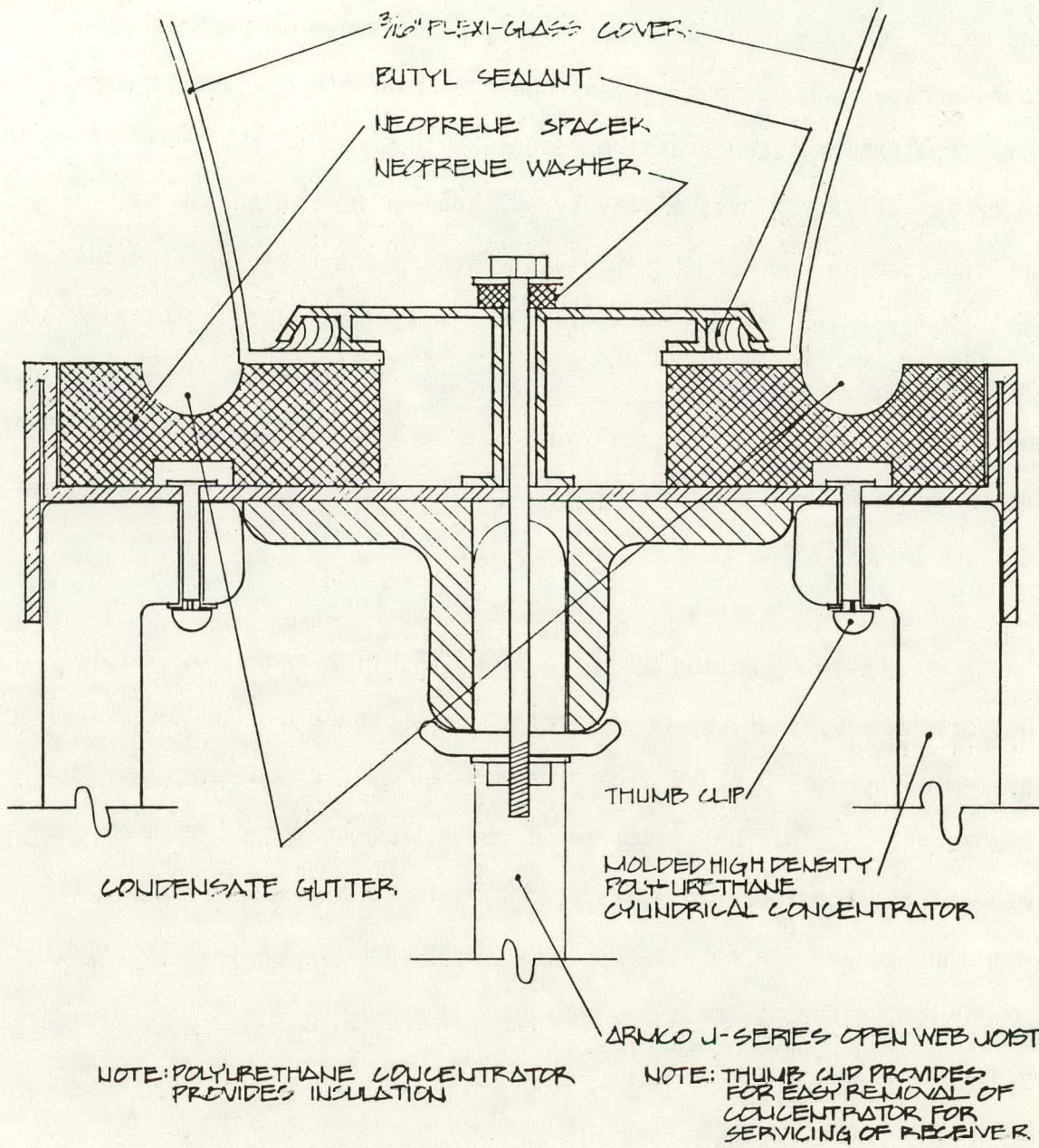


Figure 1.5.14 - IPS cylindrical concentrator connection details - 3

1.5.2.1.3 Non-Waterproof Non-Thermal IPS Photovoltaic Array

A low cost non-thermal silicon array system either as an add on or new component was developed for use above already existing roof surfaces. Long span trusses could be placed above a roof with the dimension between each truss representing the base of the array triangle in cross section. Thus, if the array sides were kept to the same length and the spacing between the joists increased, the angle between them must change. This allows for variation in reflector/collector tilt relationships. The system was also designed to be packaged with the reflector and photovoltaic surfaces protected. To be attached to the trusses, the panel would be unfolded and pinned on the ends and sides thus producing a rigid array system (see Figure 1.5.15).

1.5.2.1.4 Fresnel Type Lens

In this section as in Section 1.5.2.1.2 entitled, "Molded Polyurethane Cylindrical Concentrator", a photovoltaic-thermal building system was proposed to be a rooftop replacement for conventional roof membranes. Again, the system was to be placed on top of a steel open web joist. The tempered glass Fresnel lens is allowed to rest upon continuous neoprene cushions which are captured by curbs on an aluminum extrusion. This assembly is then held in a watertight manner by conventional aluminum glazing extrusions (see Figure 1.5.16). Paper strippable butyl rope sealant is used as a water-proofing barrier. Since the thermal, electrical receiver is below the Fresnel lens and inside the structure, some dust protection is required. Therefore, a metal dust cover, fastened by thumb clips to an aluminum extrusion, was provided.

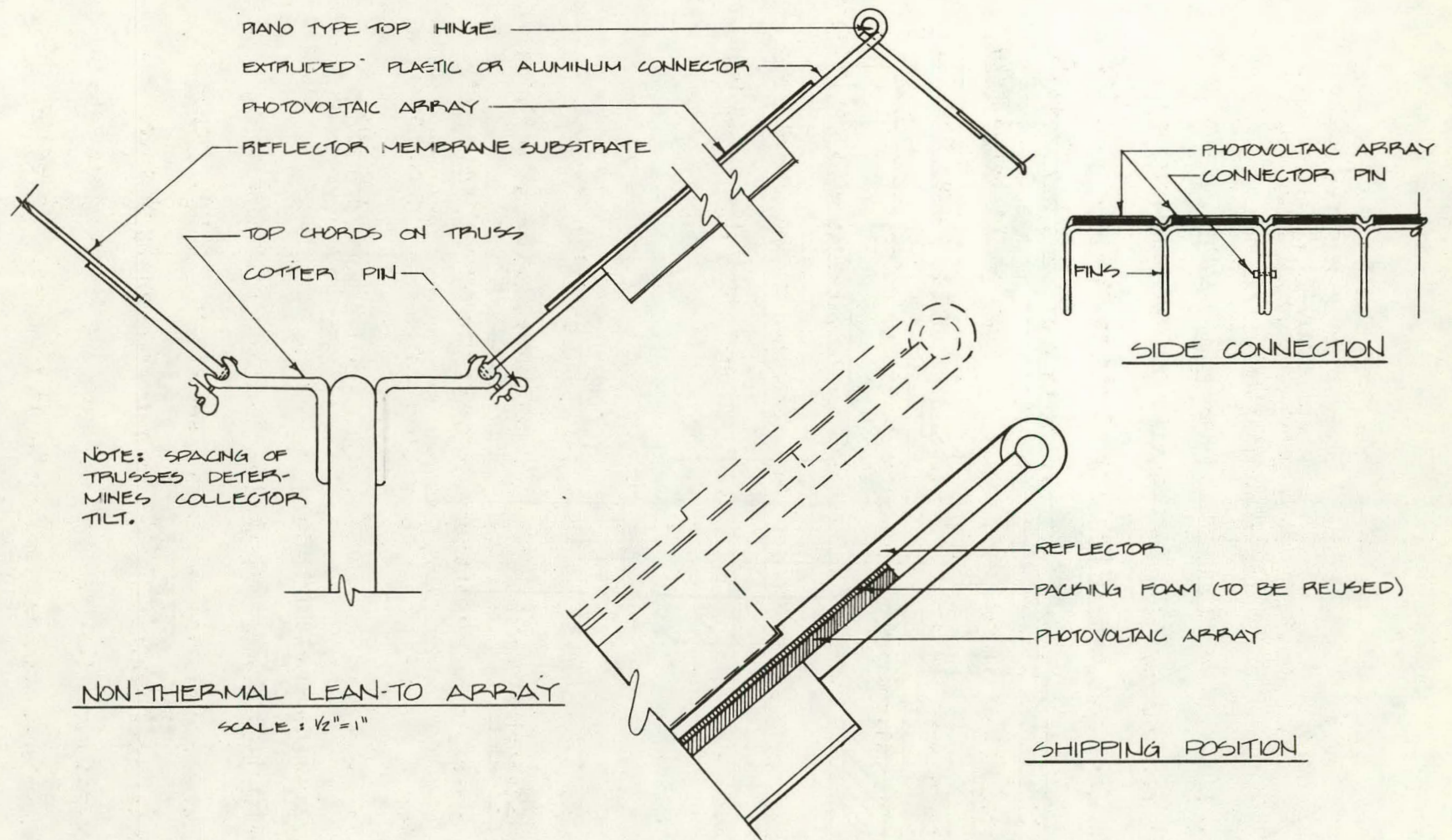
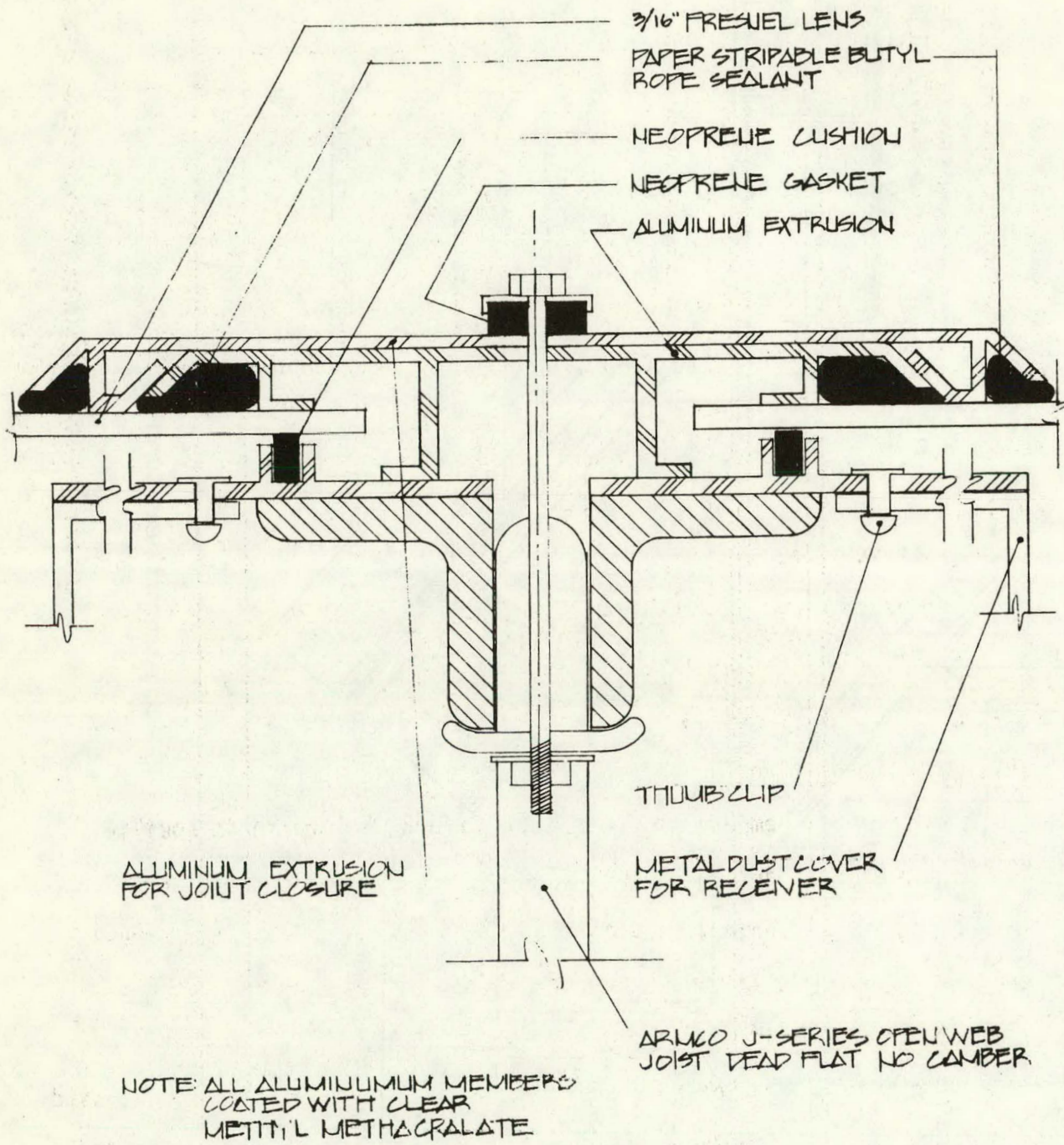


Figure 1.5.15 - Non-thermal lean-to array



IPS FRESNEL LENS

Figure 1.5.16

1.5.2.2 Cadmium Sulfide Array Options

1.5.2.2.1 Flexible - Non-Thermal - IPS Photovoltaic Array

This system was developed to be low cost and easy to install for large on-site electrical production arrays. CdS cell sheets or membrane with added reinforcing, if required, along with a reflective type membrane material were combined to form a skin or tensionable material that, when placed on a semi-rigid frame or when internally tensioned, becomes an array with a triangular cross section. This array would be connected to sand-filled bags to weigh it down to the roof surface. No physical connections would be needed to the actual building roof structure, allowing complete flexibility in array orientation and minimizing leakage problems associated with ordinary physical connections or flat built-up roofs. Each of these arrays would be placed on the roof so as to create a series of parallel triangular arrays thus allowing the back reflective surfaces to augment the CdS array surface directly behind it (see Figure 1.5.17).

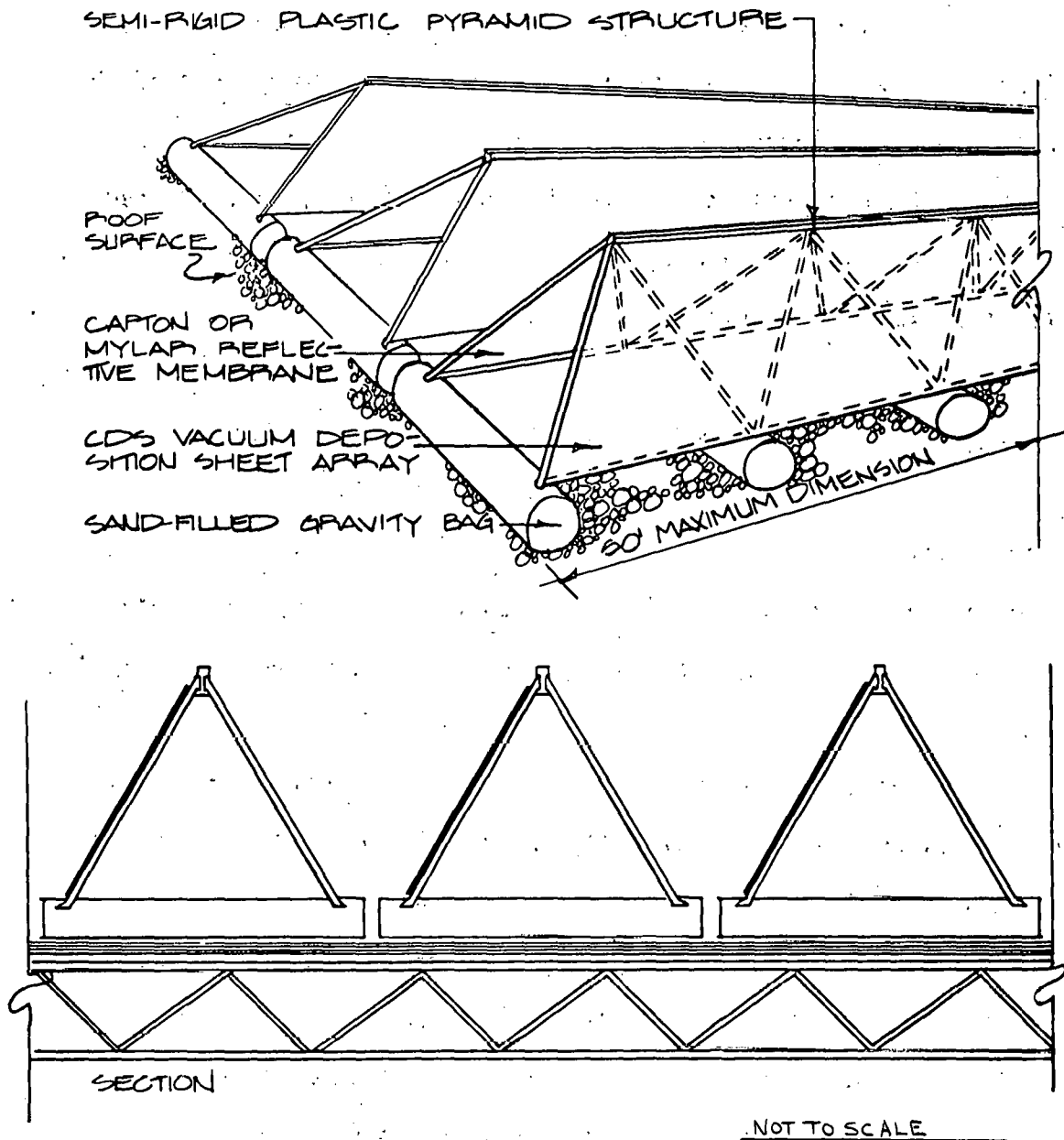


Figure 1.5.17 - Flexible non-thermal IPS photovoltaic array

1.5.3 CPS Array Structure

1.5.3.1 Task Definition

Following development of six types of CPS array systems, a structural analysis was performed on each array. The purpose of the analysis was to insure that all arrays were designed to the same operational parameters thereby permitting direct comparison of each system on the basis of a common factor. That factor was identified as the total weight of the structural steel used in the fabrication of the array.

The array concepts were then modified by performing parametric variations on those concepts which initial calculations showed to be most efficient in the utilization of material. These parametric analyses were carried out by introducing two significant reductions in the wind loads on the array and also by two significant reductions in the area of the array.

The tracking drive mechanisms were not included in the array weights since they are generically quite different, and their costs, which will be developed later, are more labor intensive requiring a different approach during estimating. Parametric variations were not performed on the tracking mechanisms since they did not represent a significant factor in the overall material used in an array system.

1.5.3.2 Analysis Philosophy and Assumptions

In performing the structural analysis of each of the arrays, it was assumed that current fabrication technology and materials would be employed in their construction. The two types of construction

employed were fabrication of the entire array using rolled structural shapes conforming to the current specifications of the American Institute of Steel Construction, Inc., and fabrication of most of the array from bar joists (also known as open web joists) with a few rolled structural shapes being used where necessary. The construction material was assumed to be ASTM A36 Structural Steel. No attempt was made at material reductions by the use of high-strength steels, nor was any consideration given to a change in material to reduce the weathering effects anticipated on the structures. These possible savings in initial cost and maintenance costs were considered to be of a second order nature.

The operational parameters used in the initial analysis of the arrays are as follows:

1. 30 lb/ft^2 wind load (this corresponds to a wind velocity of approximately 108 mi/hr) 0 lb/ft^2 snow load.
2. Maximum bending stress less than 75% of the 36,000 psi in yield stress of ASTM A36 Structural Steel.
3. Nominal array size of 10 m by 10 m to yield a nominal array area of 100 m^2 .
4. 270° horizontal tracking with the 90° sector centered on North being excluded.
5. 70° vertical tracking, i.e., angle of the array collector plane with the horizontal terrestrial plane varies from 0° to 70° .

6. $\pm 2^\circ$ tracking system accuracy. (Due to the level of detail involved in array analysis this parameter was not considered pertinent.)
7. 7° per minute maximum slew rate of array collector plane for stowage during high wind conditions. This parameter permits stowage of the array in a maximum time of 10 minutes.
8. 1° per minute maximum tracking rate of array collector plane. This rate can be achieved by a start/stop motor operation.
9. Ambient temperature will be 45°C (113°F) maximum and -20°C (-4°F) minimum.
10. Design life of 30 years for the CPS.
11. Array assembly will be performed in an assembly shop located at the CPS site and the completed unit will be carried from the shop to the mounting location by a mobile crane.
12. Nominal collector module size is 32 in. by 96 in.

The above parameters were chosen on the basis of general applicability for construction of equipment of this type.

A detailed parametric analysis was conducted to determine the sensitivity of cost ($\$/\text{m}^2$) to differences in such variables as grid size and wind loading criteria. For instance, the structural members of the grid can be made smaller as the grid area is reduced.

Ultimately, the cost of additional support columns and tracking mechanisms will overcome the incremental advantages gained by the smaller grid size. Also, the 30 lb/ft^2 loading criterion is typical of buildings over 50 feet tall built in the Phoenix area (and much of the rest of the country). Where there is no inherent safety hazard (as will be the case for the CPS array), this design specification can be relaxed. The structure can then be made lighter and less expensive. However, this increases the probability of structure failure. An assessment must be made of the possible gains which can be realized with lighter structures against which the risk of losses can be weighed.

The operational parameters used in the parametric variations portion of this analysis are as follows:

1. Initial array loading of 30 lb/ft^2 (108 mi/hr) reduced to 20 lb/ft^2 (88 mi/hr) while keeping all other parameters constant.
2. Initial array loading of 30 lb/ft^2 (109 mi/hr) reduced to 10 lb/ft^2 (60 mi/hr) while keeping all other parameters constant.
3. Initial array area of 100 m^2 reduced to 50 m^2 while keeping all other parameters constant (i.e., 30 lb/ft^2 wind load, etc.).
4. Initial array area of 100 m^2 reduced to 25 m^2 while keeping all other parameters constant (i.e., 30 lb/ft^2 wind load, etc.).

During the structural analysis, the design of the concrete system components was not considered.

1.5.3.3 Array Evaluation Techniques

Two methods were used for the structural analysis of the arrays.

One method used was the classical strength of materials approach in which the geometrical section properties (moment of inertia and section modulus) of each array member were found by imposing the above operational parameters on the appropriate stress analysis relationships. In this method the determination of the minimum section properties also resulted in the determination of the minimum weight of each component analyzed, thereby maximizing the efficiency of material utilization in the structure.

The second method used to analyze the arrays consists of using the design tables contained in the commercial open web joist catalogues to size the array components. This method is similar to the first in that a minimum weight section is determined that is consistent with the operational parameters. A difference in the two exists from the standpoint that the safe design loads for the open web joists taken from the commercial catalogues introduces a safety factor which is slightly higher than is required to meet the operational parameters. This safety factor is not required in the CPS application since the system is not bound by the usual requirements of the codes and specifications written for the construction of buildings, bridges and other similar public structures.

The differences noted above in the analysis of the arrays would indicate that further attempts at refinement of the analysis data should include a review of the two methods used to develop it. In addition, the design of the tracking systems could be optimized since they are a highly labor intensive item as they now exist and therefore more costly per unit weight than the other array components.

1.5.3.4 Description of Arrays Analyzed

A brief description of each of the two-axis trackable arrays appears in Tables 1.5.1 through 1.5.4. Also, orthographic illustrations of each of the concepts are shown in Figures 1.5.18 through 1.5.21.

In addition to the two-axis arrays, three single-axis arrays have been analyzed to the same level of detail as concepts Mark "A" thru "D". Tables 1.5.5 through 1.5.7 and Figures 1.5.22 through 1.5.24 present a brief description of each single-axis trackable array concept.

Finally a non-trackable array was analyzed as above. Table 1.5.8 and Figure 1.5.25 describe the array.

TABLE 1.5.1

MARK "A" ARRAY

(Figure 1.5.18)

- Two axis trackable.
- Bar joist array collector grid.
- Vertical axis tracking driven by double reduction chain drive and 1/4 horsepower gearmotor. Pivot bearings at the edges of grid on the horizontal bisector.
- Horizontal axis tracking driven by spur gear and pinion directly from 1/4 horsepower gearmotor. Pivot bearing at the base of the array support near the foundation.
- Gross weight of array is 31,120 lbs.
- Weight of tracking drive is 23,970 lbs.

CPS ARRAY
MARK "A"

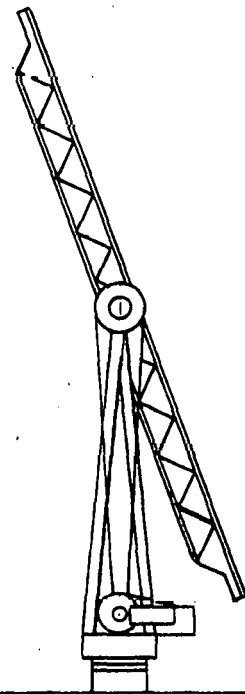
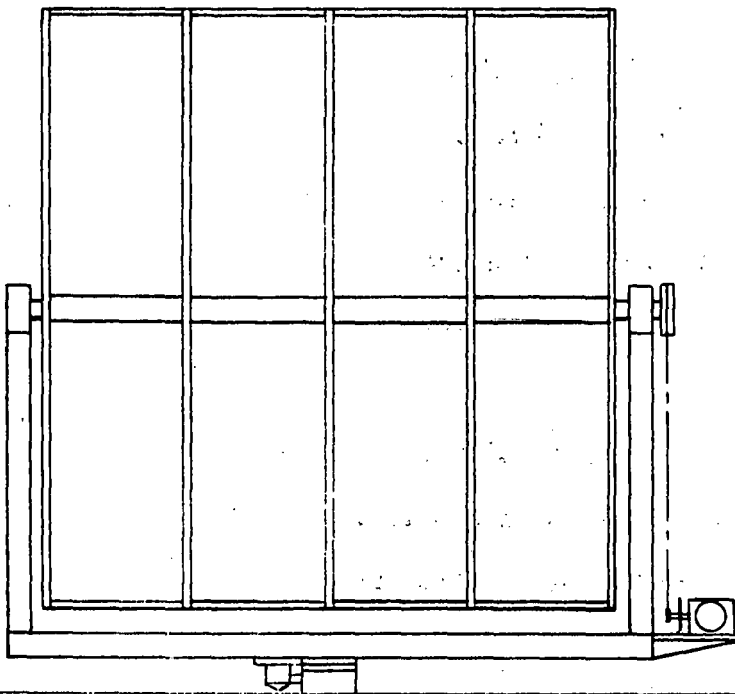
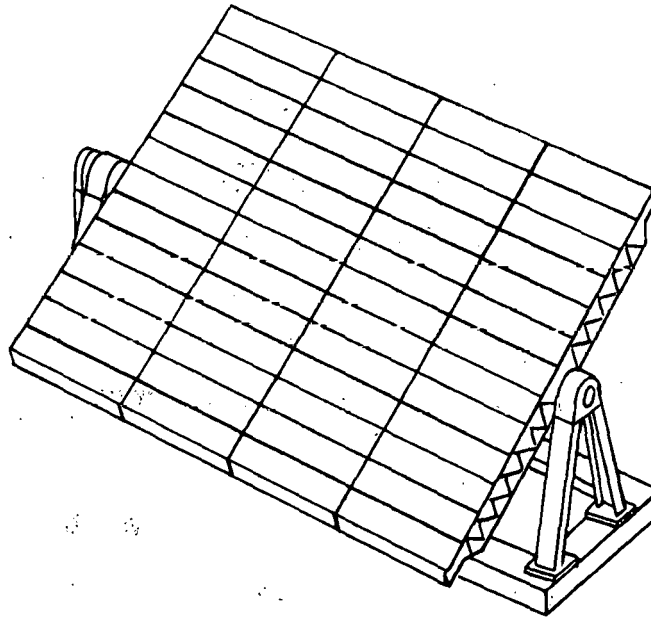


Fig. 1.5.18 - Two axis trackable array

TABLE 1.5.2

MARK "B" ARRAY

(Figure 1.5.19)

- Two axis trackable.
- Rolled structural shape array collector grid.
- Vertical axis tracking driven by single reduction chain drive and 1/4 horsepower gearmotor. Pivot bearings in the center of the array grid.
- Horizontal axis tracking driven by spur gear and pinion directly from 1/4 horsepower gearmotor. Pivot bearing located at the top of the array support column near the vertical pivot.
- Structural steel support column.
- Gross weight of array is 16,270 lbs.
- Weight of tracking drive is 4540 lbs.

CPS ARRAY
MARK "B"

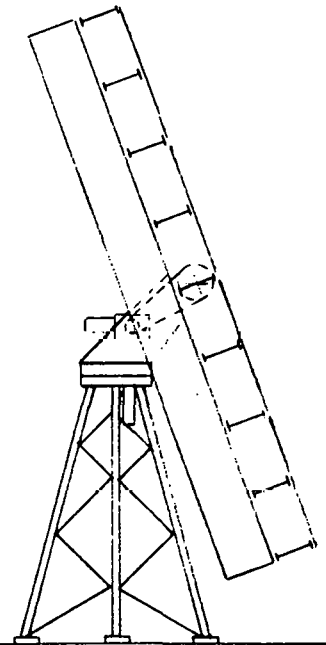
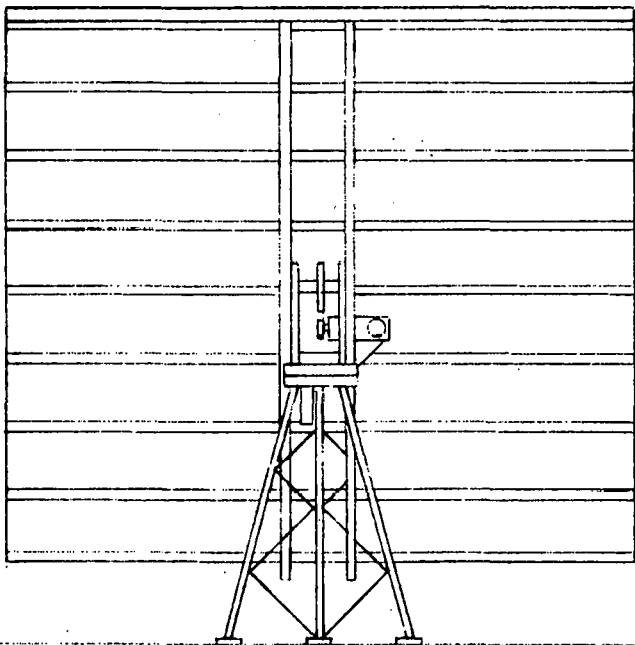
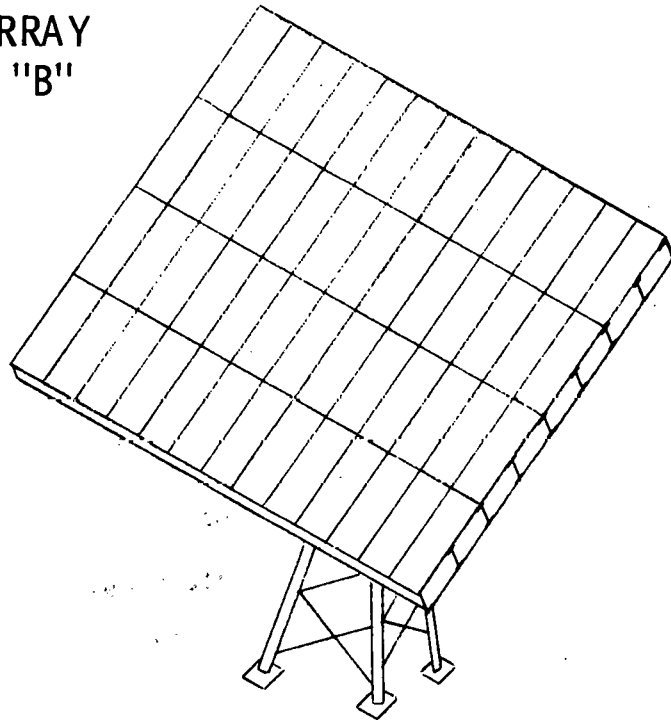


Fig. 1.5.19 – Two axis trackable array

TABLE 1.5.3

MARK "C" ARRAY

(Figure 1.5.20)

- Two axis trackable.
- Bar joist array collector grid with wire rope reinforcing.
- Vertical and horizontal axis tracking achieved by rocking array grid on a two-axis gimbal with an electric winch connected to each corner of the grid. The pivot gimbal is located at the top of the array support column.
- Structural steel support column.
- Gross weight of array is 11,090 lbs.
- Weight of tracking drive is 1800 lbs.

CPS ARRAY
MARK "C"

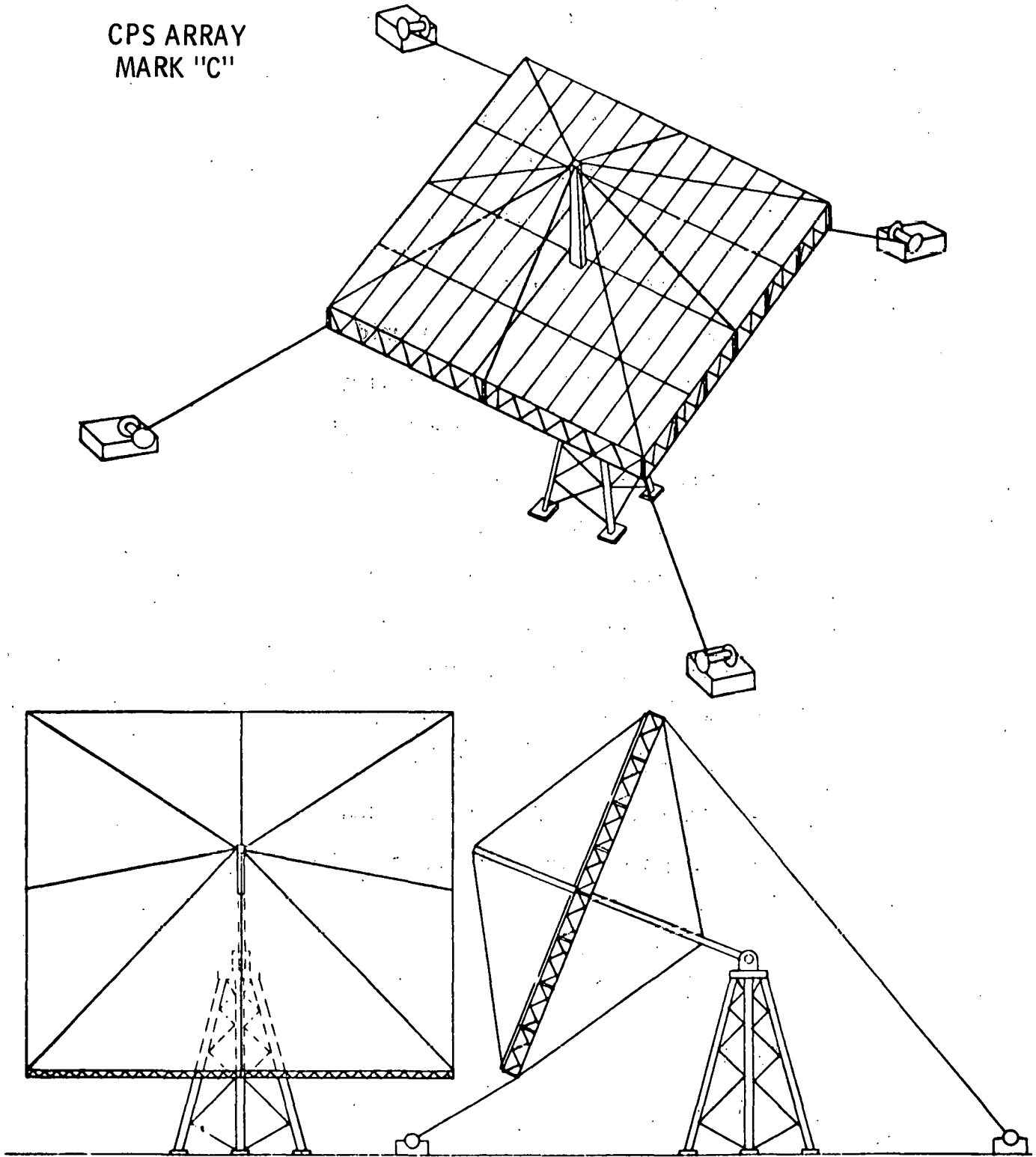


Fig. 1.5.20 - Two axis trackable array

TABLE 1.5.4

MARK "D" ARRAY

(Figure 1.5.21)

- Two-axis trackable.
- Bar joist array collector grid.
- Vertical axis tracking driven by a triple reduction chain drive and gearmotor. Pivot bearing in the center of the grid array.
- Horizontal axis tracking driven by spur gear and pinion directly from gearmotor. Pivot bearing located at the top of the array support column.
- Gross weight of array is 21,140 lbs.
- Weight of tracking drive is 15,280 lbs.

CPS ARRAY
MARK "D"

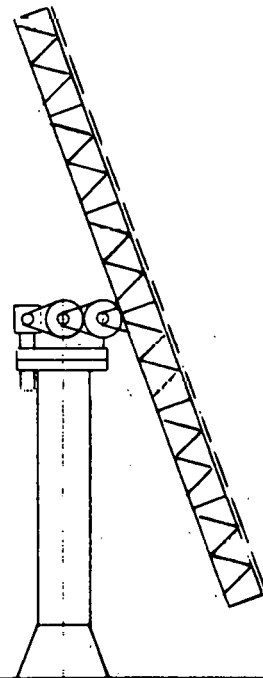
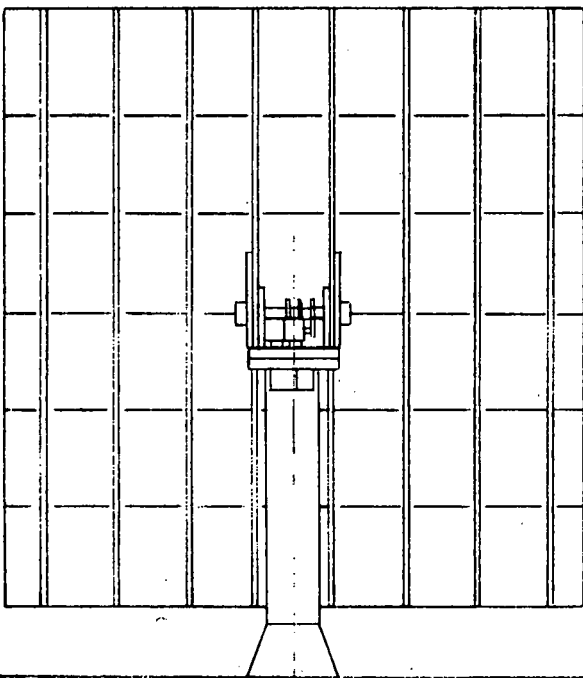
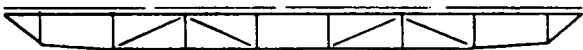
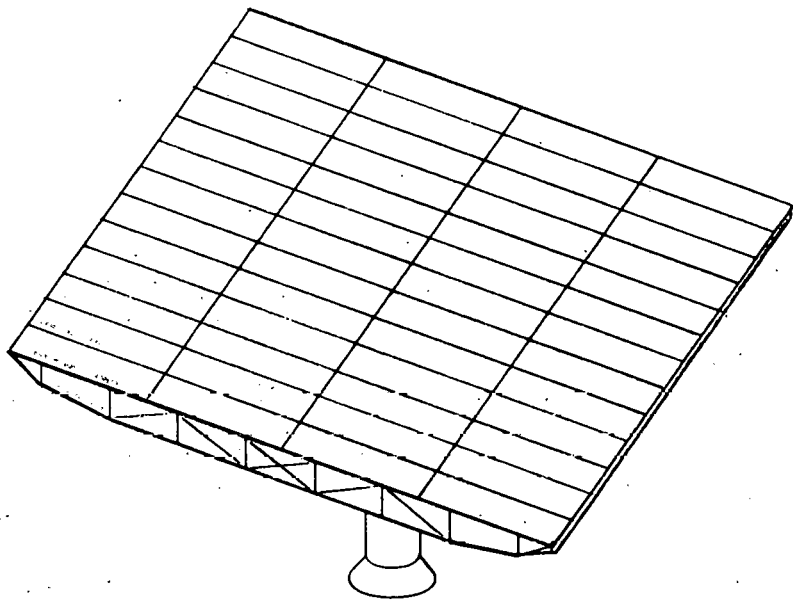


Fig. 1.5.21 - Two axis trackable array

TABLE 1.5.5

MARK "E" ARRAY
(Figure 1.5.22)

- Single-axis trackable.
- Bar joist array collector grid.
- Vertical axis pivot tracking driven by wire rope capstan powered by a 1/4 horsepower motor.
- Structural steel support column.
- Gross weight of array is 10,050 lbs.
- Weight of tracking drive is 2150 lbs.

CPS ARRAY
MARK "E"

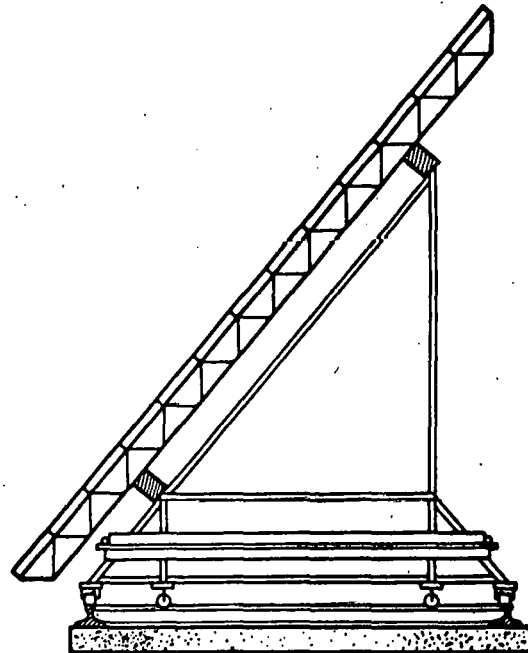
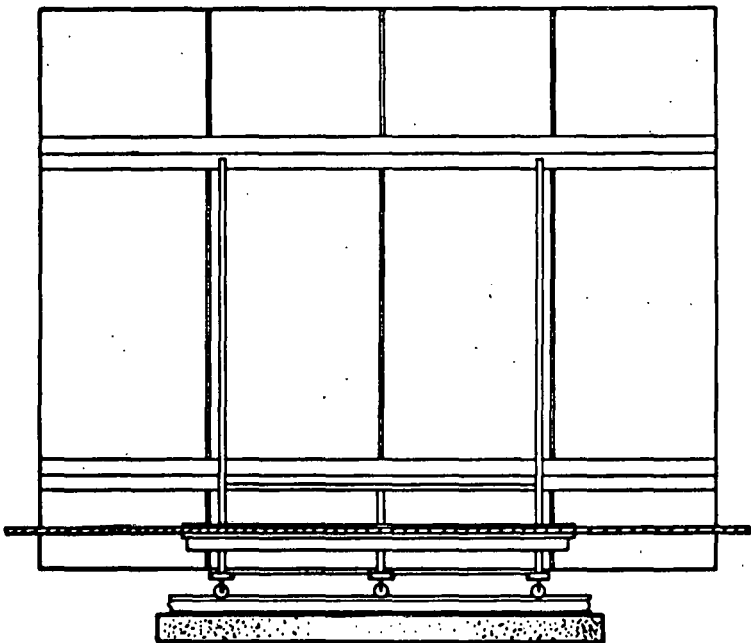
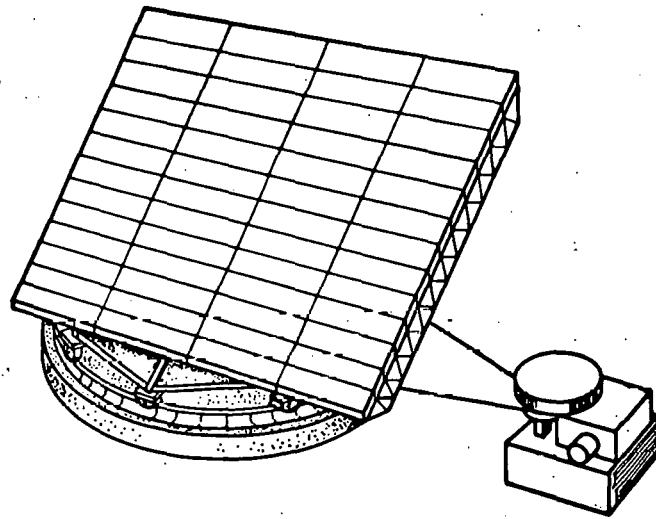


Fig. 1.5.22— Vertical axis tracking array

TABLE 1.5.6

MARK "F" ARRAY
(Figure 1.5.23)

- Single-axis trackable.
- Bar joist array collector grid with wire rope reinforcing.
(Similar to Mark "C").
- Horizontal axis pivot tracking achieved by single reduction chain drive and 1/4 horsepower gearmotor. Pivot bearings at the edges of the grid on the horizontal bisector.
- Concrete support structure.
- Gross weight of array is 9385 lbs.
- Weight of tracking drive is 450 lbs.

CPS ARRAY
MARK "F"

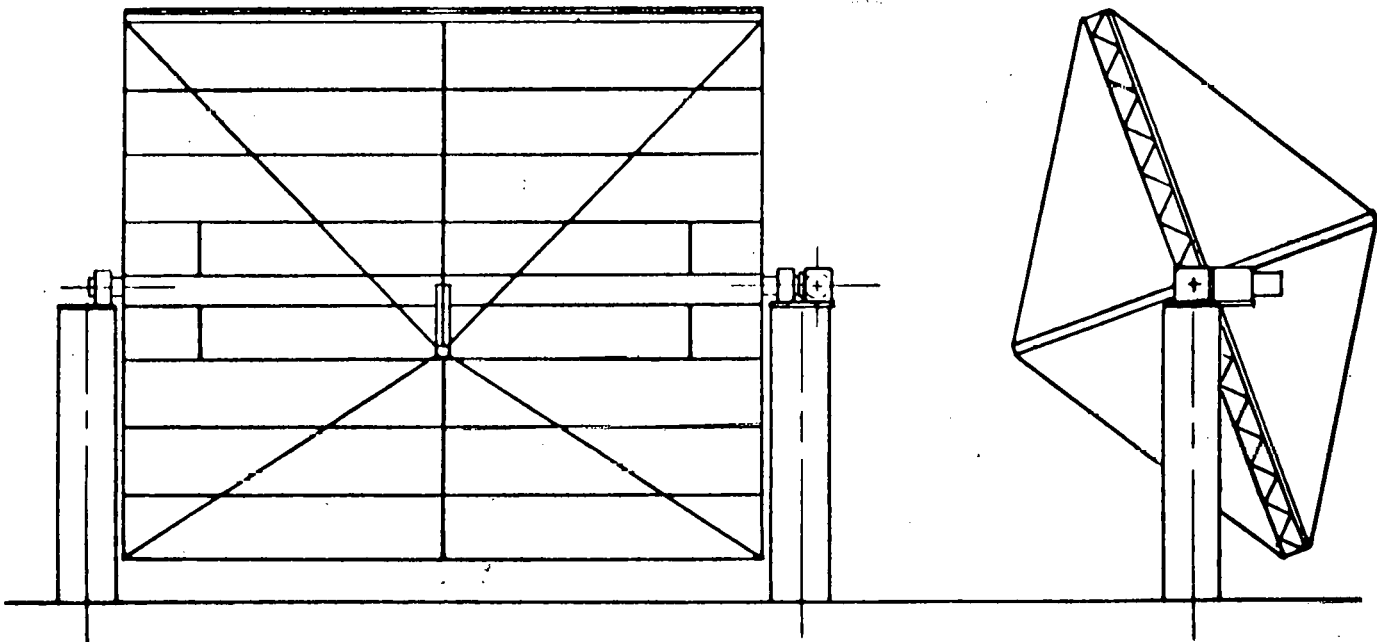
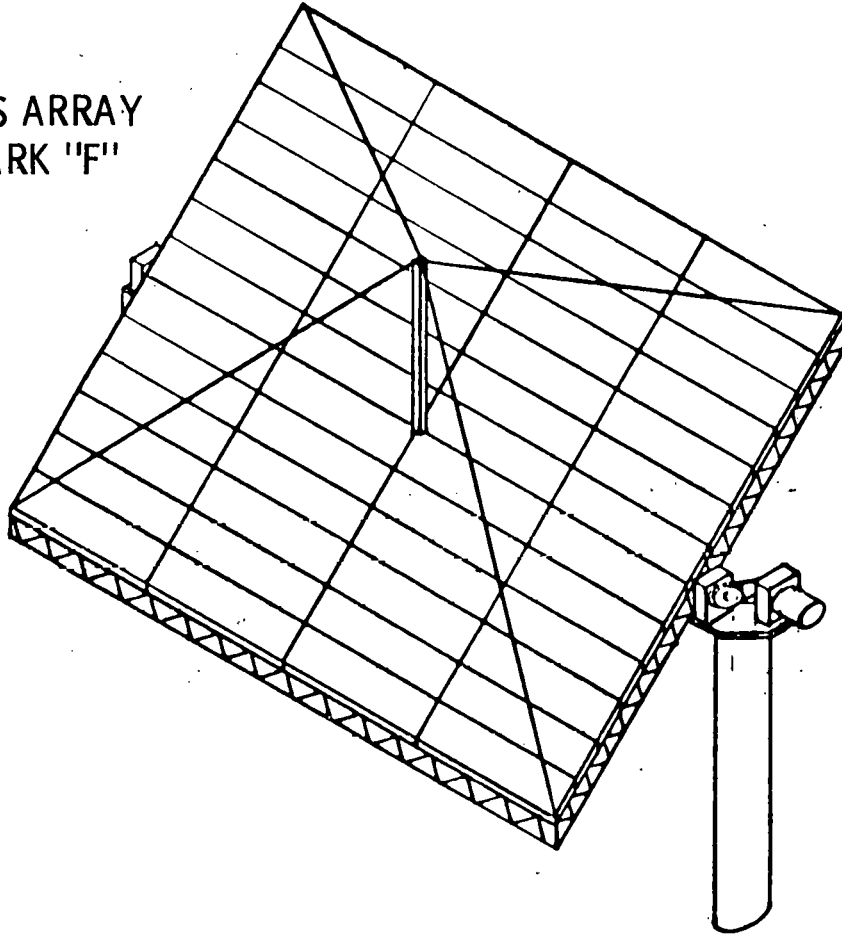


Fig. 1.5.23 - Horizontal axis tracking array

TABLE 1.5.7

MARK "G" ARRAY
(Figure 1.5.24)

- Single-axis trackable.
- Stationary reflector with moveable collector module which tracks the reflected, concentrated image of the sun.
- Water cooled collector module.
- Horizontal axis pivot tracking achieved by a single reduction chain drive and 1/4 horsepower gearmotor per array unit.
- Gross weight of array unit is 4085 lbs. NOTE: This weight is not directly comparable to the others since this concept is a concentrator type and the power output is not equal to a 100 m² flat plate array. Further work will determine the relationship of this concept to the others.

CPS ARRAY
MARK "G"

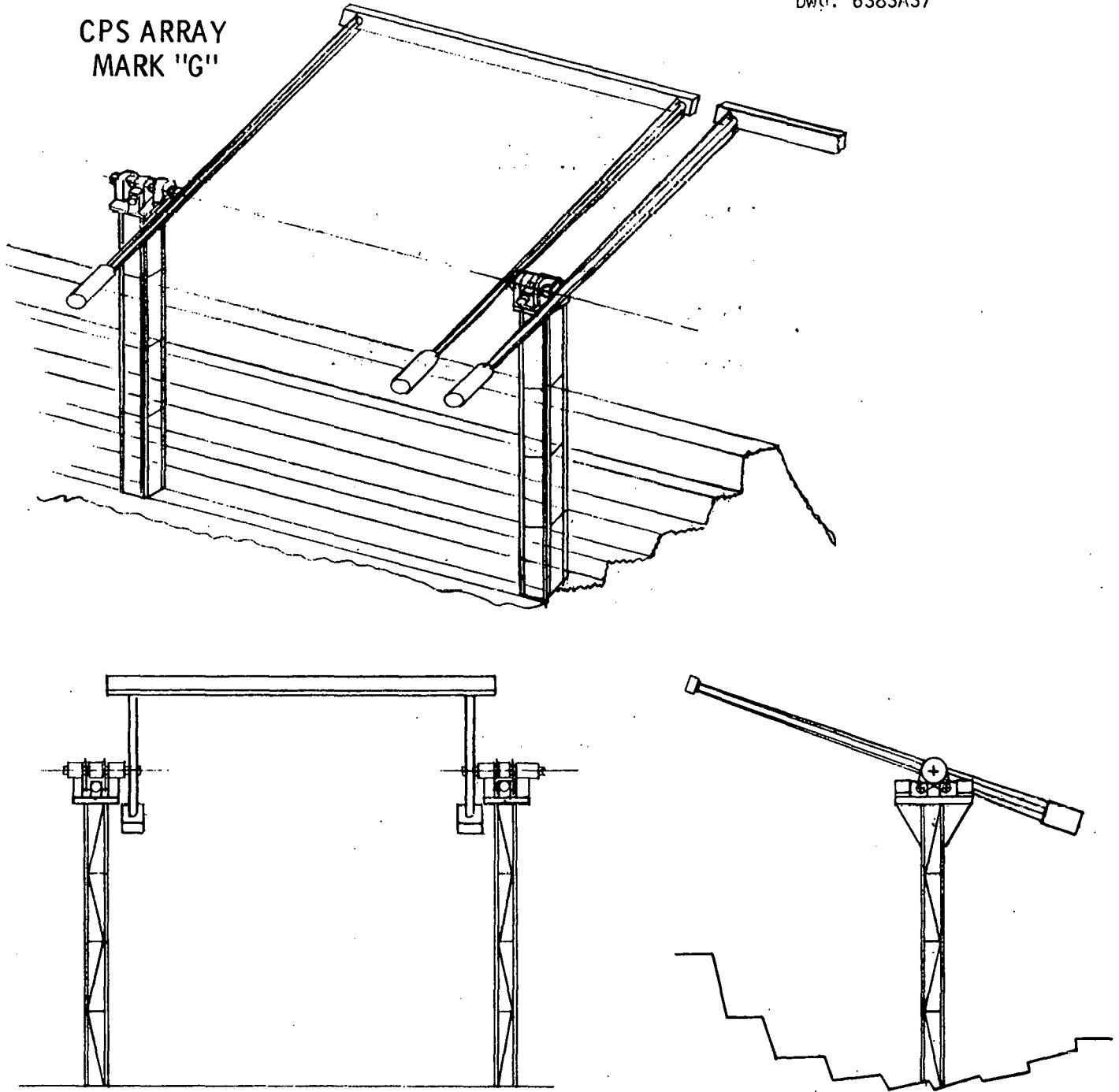


Fig. 1.5.24 - Segmented trough array

TABLE 1.5.8

MARK "H" Array
(Figure 1.5.25)

- Non-trackable.
- Bar joist array collector and reflector grids.
- Gross weight of array is 10,000 lbs.

Dwg. 6383A38

CPS ARRAY
MARK "H"

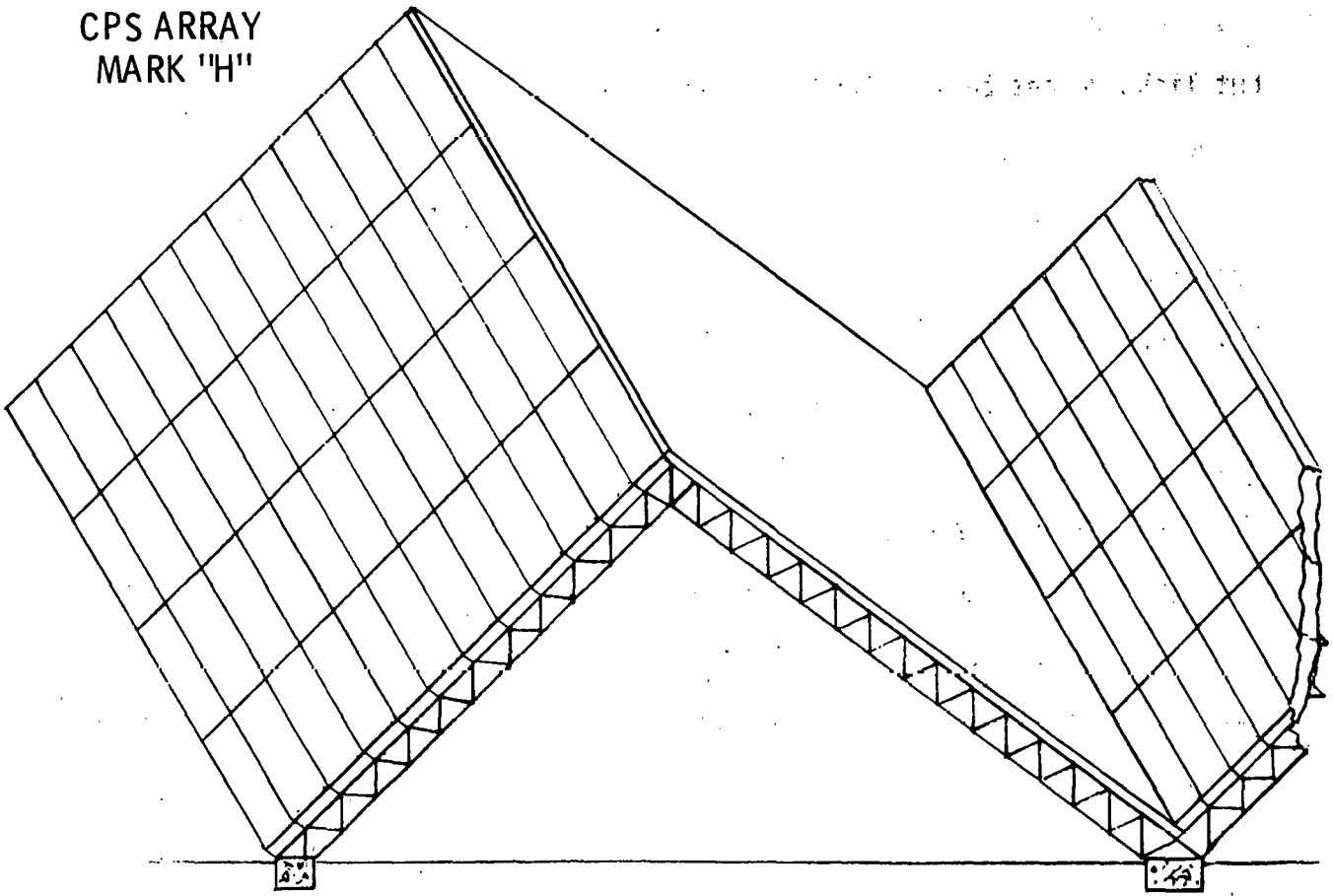


Fig. 1.5.25 - Fixed flat plate array

The array collector grid was studied using three different designs. Marks "A" and "D" were designed using commercially available bar joist girders. These members consist of upper and lower members made of rolled angles placed back to back and joined with a round bar bent in a zig-zag shape. This construction provides a very deep but light weight beam. The bar joist design is illustrated in Figure 1.5.26.

The array collector grid for Mark "B" used standard rolled structural steel shapes. This construction was employed as a baseline case for the cost of the grid.

The array collector grid for Mark "C" incorporated custom designed bar joists and a simple wire rope guy wire reinforcing system. This was done to minimize stress and deflection in the grid members when going to lighter bar joist members.

The support columns for Mark "B" and "C" arrays are standard rolled structural steel shapes which use a conventional lattice trussed construction with four main members.

The support column for Mark "D" used steel reinforced concrete. Making a cost comparison of the two types of construction using data from "Building Construction Cost Data", 1975, Robert Snow Means Company, Inc. we have the following:

(a) Mark "C" Steel Tower - 16 ft. high

Weight = 3430 lbs.

Cost/lb. = \$0.62/lb. (Material & Labor)

Total Cost = \$2126.00

Dwg. 6383A39

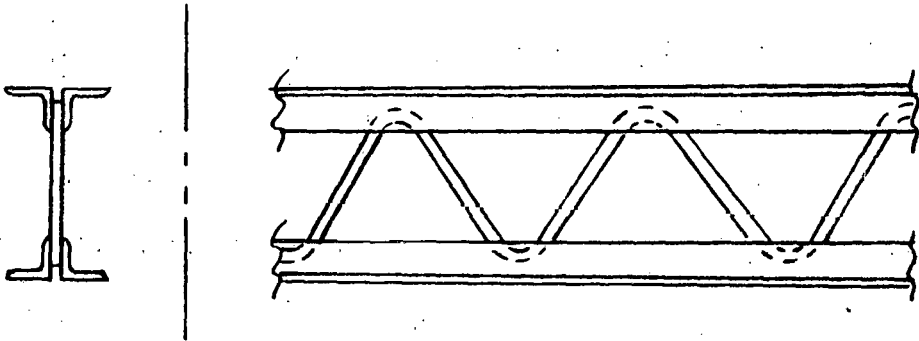


Fig. 1.5.26 - Bar joist - girder details

(b) Mark "D" Concrete Tower - 16 ft. high x 3 ft. dia.

Volume = 4 yd.³

Cost/yd.³ = \$329/yd.³ (Material and Labor)

Total Cost = \$1316.00

The above costs are based on on-site erection/construction costs for power plant type construction. This would indicate that the concrete support tower is the most economical way to proceed under the given conditions. However, considering mass production techniques and their inherent cost savings, the cost of the Mark "C" Steel Tower could approach the cost of material.

(c) Mark "C" Steel Tower - 16 ft. high

Weight = 3430 lbs.

Cost/lbs. = \$0.22/lb. (Material & Labor)

Total Cost = \$754.00

Since the cost of the Mark "D" concrete tower cannot be reduced due to the necessity of maintaining the on-site construction inherent in that design, the true cost of the tower designs now favors the structural steel column design used in Mark "C". The support column is not a major feature of any particular design, however. Therefore, the approach which leads to minimum cost would be used in actual installations.

The array tracking systems were studied using two basic designs. One of these was driven by a commercially available gearmotor with additional external reduction to achieve the low rotational speeds required. This was used on array marks "A", "B",

"D", "F", and "G". The other used a commercially available wire rope winch package. This was used on array marks "C" and "E". The winch-driven tracking array was pivoted at a gimbal arrangement located at the top of the support column. The array concepts which were driven by gearmotors, on the other hand, employed various combinations of pivot bearings and spur gear and pinion arrangements. Because of its simplicity and very lightweight construction, the winching approach has significant advantages over the gearmotor approach.

Discussing the difference in the array designs and the cost benefits of one versus the other, it should be kept in mind that the overall array system cost is the most important criteria in the choice of the preferred array design.

Each of the concepts considered was initially costed using present prices of conventional equipment. For the purpose of selection, however, the different concepts were compared solely on the basis of raw material costs. This assumption reflects the philosophy that the cost of mass produced equipment in high volumes approaches the cost of the raw material used. Since the Mark "C" array is the lightest it has been chosen as representing the most economical two-axis trackable array structure.

1.5.3.5 Discussion of Results

Table 1.5.9 is a matrix of the weights of all arrays analyzed including the parametric variations. These are gross weights which include the weight of the tracking drives, the array grids and the support towers if they are of steel construction.

TABLE 1.5.9

Array Weight Matrix

Array Mark Number	Number of Tracking Axes	Load (lbs/ft ²) Area (m ²) Wind Vel. (mi/hr)	Array Gross Weight and Gross Weight/Unit Area					
			30	20	10	30	30	
A	2		31120 lb					
			311 lb/m ²					
B	2		15310					
			148					
C	2		11090	9495	7420	6790	4310	
			107	92	72	127	167	
D	2		21140					
			211					
E	1		10045	8858	7554	6569	3152	
			100	88	76	131	126	
F	1		9385					
			91					
G	1		NOTE:	THIS DESIGN IS NOT DIRECTLY COMPARABLE				
H	0		1000			3055	1000	
			100			73	48	

Comparing the gross weights of the arrays as shown in Table 1.5.9, it was decided that the minimum weight array for a given loading or size would also be the lowest in cost since the type of construction, level of complexity, and size are similar and the cost of materials is directly proportional to its weight. A plot of the array weight per unit area versus wind load, shown in Figure 1.5.27, indicates that arrays marks "C", "E" and "F" are the most efficient designs for wind loads of 10, 20 and 30 lb/ft². The arrays which are not plotted in Figure 1.5.27 were offscale and therefore less efficient than the others.

Figure 1.5.28 plots array weight per unit area versus array area for a 30 lb/ft² (108 mi/hr) constant wind load. The variation of the parameter, "array area" gives an indication of the most efficient size of array to build. This graph is not conclusive from the standpoint that only three points have been calculated for each of the most efficient trackable arrays, and the shapes of the curves thru these points cannot be rigorously defended. But in the absence of more data the results show that the larger arrays tend to be a more efficient utilization of material.

Table 1.5.10 is a matrix of the weights of the arrays which were selected as the most efficient in their utilization of material due to their low weight to area ratios. The significant difference between this matrix and Table 1.5.9 lies in the fact that the tracking drive weights have been subtracted from the gross weights. This matrix

Curve 685772-A

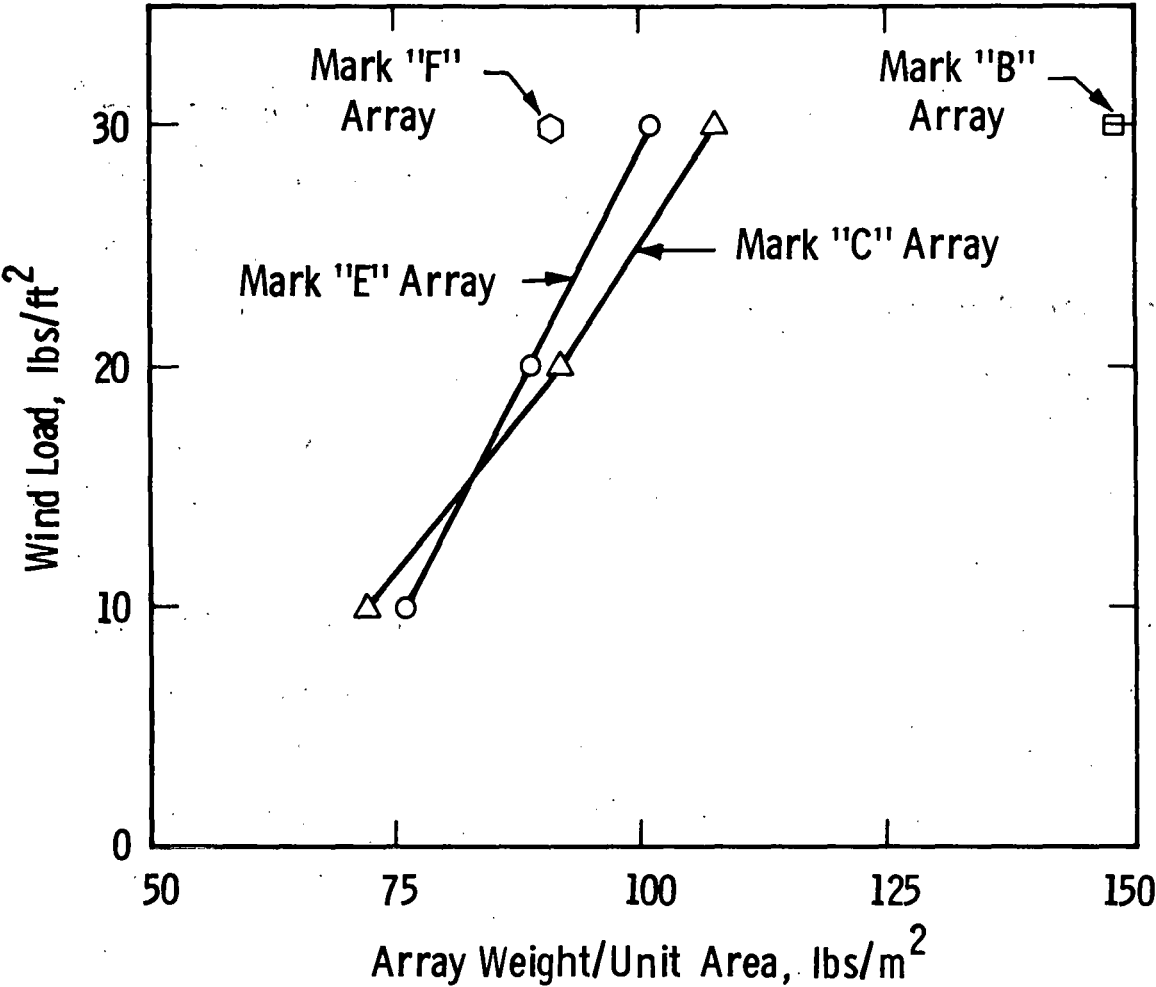


Fig. 1.5.27 - Array design wind loading comparison

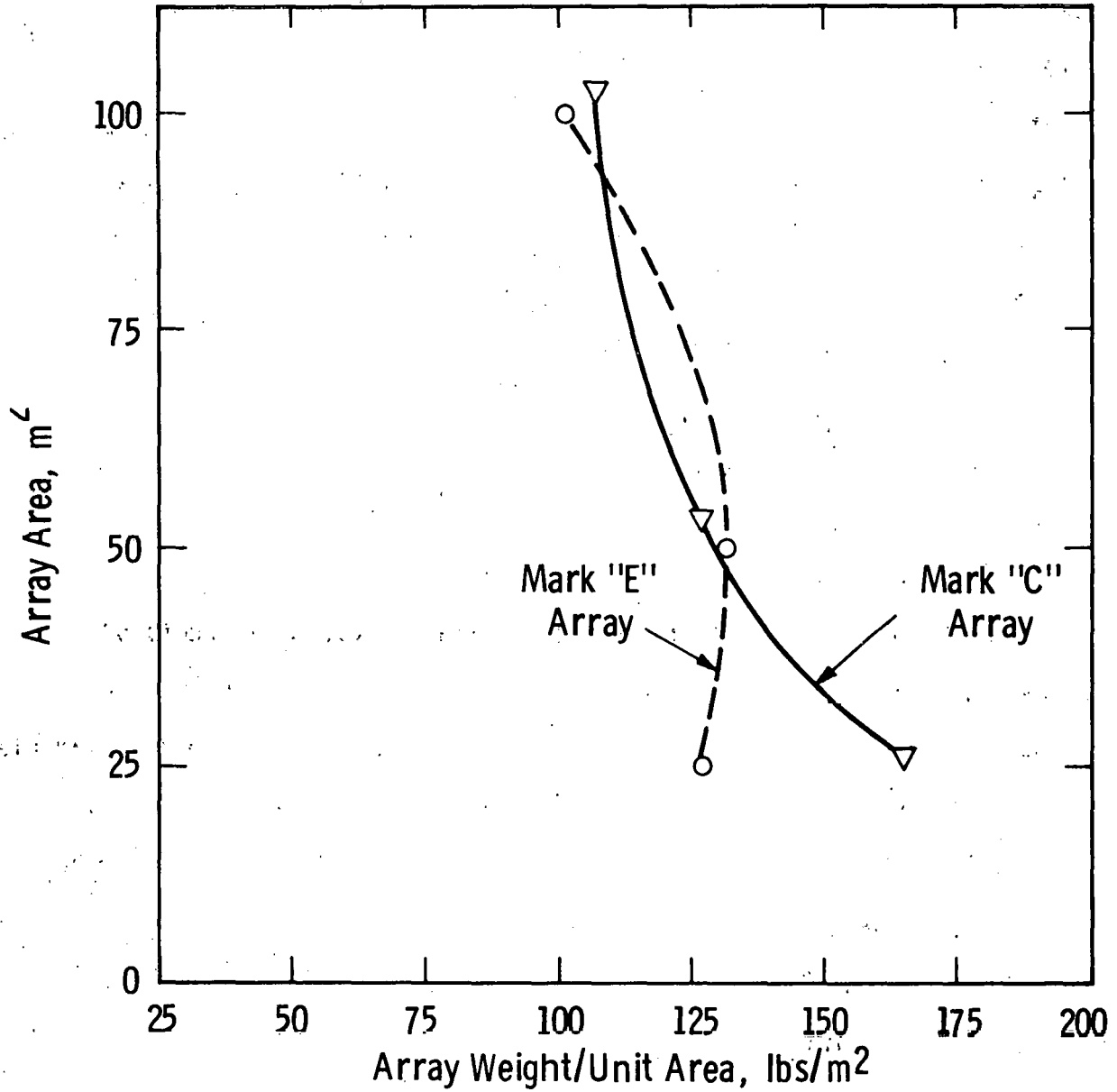


Fig. 1.5.28 — Array area vs. weight per unit area
(Windload is 30 lbs/ft² or 108 mph)

was made to facilitate cost estimating since the structural components and the tracking components have different cost factors.

1.5.3.6. Conclusions

Three types of array construction were analyzed; guyed bar joists, standard rolled structural shapes, and unguyed bar joist. The guyed bar joist construction used the fabrication material most efficiently and should be most cost effective.

Three wind loading parametric variations were analyzed for selected arrays; 30 lb/ft² (108 mi/hr), 20 lb/ft² (88 mi/hr), and 10 lb/ft² (60 mi/hr). The analysis indicated that the configurations that the arrays would take if the reduced safety factors for wind are acceptable.

Three variations of the size (area) of the collection surface of selected arrays were analyzed under a constant 30 lb/ft² (108 mi/hr) wind load; 100 m², 50 m² and 25 m². The analysis indicated that the largest area of the three (100 m²) was most material efficient and therefore should be most cost effective.

Selection of a single preferred array structure for the CPS system will not be as straightforward as choosing a preferred concept for each of the tracking schemes. This is because of the significant differences in performance obtained with each of the tracking modes and the range of values which can be assigned to these differences based on varying assumptions of module cost, net conversion efficiency and energy value. For example, the amounts of energy incident on

two-axis tracked designs will be significantly higher than those of fixed arrays. Likewise, arrays with two-axis tracking are compatible with all of the modules which incorporate concentrators, and may therefore allow the use of a less expensive module. These advantages must be weighed against the added structural cost for each of the different tracking schemes at the system level to determine their relative values.

Areas for further analysis include: tracking system design for high volume production; analysis of cable type tracking system versus direct drive tracking system from standpoints of cost and controllability; additional parametric variations of array area to determine optimum array size; reduction of array material by the use of high-strength steels; development of operating and maintenance costs for all arrays; construction of a 1:10 scale operational prototype of the most cost effective design.

TABLE 1.5.10

Array Weight Matrix
(Without Tracking Drive Weight)

Array Mark Number	Number of Tracking Axes	Load (lb/ft ²) Area (m ²) Wind. Vel. (mi/hr)	Array Gross Weight and Gross Weight/Unit Area				
			30	20	10	30	30
			100	100	100	50	25
			108	88	60	108	108
C	2	9290 lb	7695	5620	4490	2510	
		90 lb/m ²	75	55	84	97	
E	1	9595	8410	7100	6120	2700	
		95	84	71	122	108	
F	1	8935					
		87					

THIS PAGE
WAS INTENTIONALLY
LEFT BLANK

1.6 Battery Energy Storage

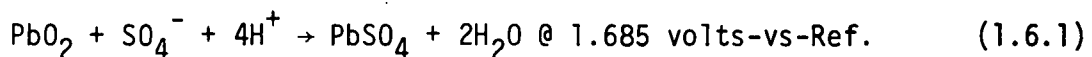
1.6.1 Battery Storage Technology

One of the tasks of this program was to survey the present state of battery technology and, based on the results, project the technology which will be available for the manufacture of batteries to be used in solar photovoltaic power systems installed in the 1985-2000 time period. The results of this work are presented in the following paragraphs.

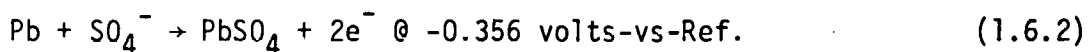
Electrical Storage in Lead Acid Cells

The lead-acid battery has been used as a means of storing electricity for nearly 100 years. The electrodes used consist of a negative electrode which is an electronically conducting sponge lead supported by a lead current collector. The positive electrode is an electronically conducting porous PbO_2 paste which is also supported by a lead current collector. The electrolyte is an ionic conducting solution of sulfuric acid (H_2SO_4) in water. The cell discharges according to a reaction which converts lead and lead oxide (PbO_2) to $PbSO_4$. The individual electrode reactions are:

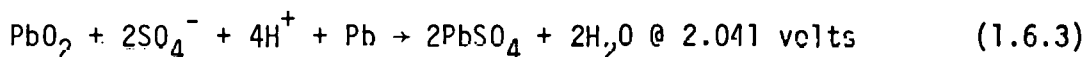
Positive Plate



Negative Plate



Overall Cell Reaction



The electrolyte provides the ionic mass transfer necessary to carry out the overall reaction while electrons pass through the external load. During discharge of the lead-acid cell, the electrolyte concentration

of sulfuric acid decreases as discharge proceeds. On complete discharge, the sponge lead and the porous lead dioxide active materials are exhausted. This situation would occur in a system wherein the electrodes with their individual coulombic capacities are the capacity limiting components. Another mode of capacity limitation is the sulfate ion concentration, which can also limit the coulombic capacity of the system.

Considering the overall reactions which occur in the lead acid cell, the theoretical energy density of the electrochemical couple is about 80 watt-hours per pound. Upon coupling the electrodes in a suitable container with the necessary current collectors and electrolyte, the energy storage density of a lead-acid cell becomes 10-15 watt-hours per pound, depending on the specific design as well as the particular discharge rate.

There are presently three distinct categories of lead-acid batteries. Each of the batteries incorporates special features which are critical to the typical type of service each is used for. The first type of lead-acid battery uses a Standby Design. These cells are used in telephone installations. In use, they furnish the current for transmitting, signaling and switching. Motor Generators (MG's) keep these batteries constantly at full charge. The batteries seldom deliver a deep discharge except on an emergency basis. These batteries, because of their limited use and the special lead alloys used in the positive grid, commonly have lifetimes of 20 years. The alloys used as the positive grid (current collector) are more resistant in the charge mode to corrosion, and are all antimony-free.

The second type of lead-acid cell design is that used in the familiar automotive design, for Starting, Lighting and Ignition (SLI).

These batteries are used to deliver substantial amounts of energy in a short period of time at high power. Their short time discharge at high rates results in a discharge to an intermediate level. The design feature characteristic of these batteries is very thin plates and grid alloys which contain high antimony (~ 5 Wt %) content plus additions of tin and arsenic which may add strength and castability to the grids. In practical use, these batteries commonly suffer severe overcharge which results in substantial overcharge corrosion. As a result of their basic design and use factors, SLI automotive batteries are generally limited to about 4 years service life. In general, because these batteries are manufactured as low-cost, energy storage devices, their materials selection and use, subject to vibration and electrical overcharge, are the life limiting aspects.

The motive power design which presently provides maximum depth-of-discharge in the lead-acid system is provided by heavy duty industrial lead-acid batteries in lift truck applications. In the typical lift truck duty cycle, the batteries survive for approximately 7 years in a work routine which incorporates mechanical shock as well as deep discharge (90% of designed capacity at the 6 hour drain rate). The design aspects which contribute to this stability under these severe use conditions are basically geometrical. The motive power design incorporates a massive positive electrode current collector, about 40% of the electrode. This added positive electrode current collector permits 7 year service life in spite of the use of high antimony grid alloys, (~ 5 Wt.%).

One of the failure mechanisms of the lead-acid battery is associated with the basic volume changes which occur in the chemical

change of metallic lead to lead sulfate and from lead dioxide to lead sulfate and vice versa. The volume changes are accompanied by internal stresses which cannot always be accommodated by strains. The result of this stress relationship is that the active material may flake, shed, or crack away from the grid (current collector). As the process proceeds, the cell tends to lose capacity with an increase in internal resistance. Both of these result in decreased energy density and power carrying capability. The process of degradation is enhanced and increased with the depth-of-discharge since this involves the maximum utilization of an active material within the battery plates. The process of failure is self-perpetuating.

Another significant mechanism in the failure of the lead-acid battery is the corrosion of the positive grid (current collector). The corrosion of the positive current collector is also a function of the depth-of-discharge. The corrosion, which occurs predominantly in the positive grid, results in a decrease in the current collector's cross-section, eventually resulting in disintegration of the structure. The two mechanisms, loss of active material or electrochemical activity for energy storage and positive grid corrosion, are the primary failure mechanisms of lead-acid cells. Both processes are related directly to the specific design and intended application of the battery.

In the case of the SLI, the battery is mass produced by automated techniques and its performance is intended to deliver high power for short periods of time. The typical selling price of the SLI battery is about \$30/kWh. The industrial type lead-acid battery has an oversized positive grid (current collector) and is more of a customized battery from a

manufacturing point of view in that it is not mass produced by automated techniques. In comparison, an industrial type lead-acid battery sells for about \$60/kWh. In use, the industrial type lead-acid will deliver about 90% of its designed capacity at a 6 hour drain rate, but contains approximately 40 Wt % of the positive electrode (as current collector).

Advances in the technology of the lead-acid battery will result when better utilization of the active material is achieved, as well as increased stability of the positive grid (current collector). Studies related to the active material will define and control the morphology of the material such that sulfate ion accessibility will be maximized while maintaining structural integrity between the active material, and the current collector. Studies related to the effect of electrolyte and active material utilization for stationary applications may result in increased life without loss of capacity or increases in the sulfate ion concentration in the electrolyte. This could be accomplished by providing an auxiliary system which would properly maintain the electrolyte concentration to maximize life and performance.

Studies related to the lead alloy used in the positive grid as well as its fabrication and subsequent treatment may result in extended life of the grid. Continuing the advances in the technology related to the active material and the grid network as well as the interrelation between both components and depth-of-discharge could result in enhanced performance and stability of the lead-acid battery for stationary applications for residential and intermediate site energy storage.

Assuming that these technological accomplishments will be forthcoming, we can assume a reasonable life expectancy of the lead-acid

battery of 15 years at 70% depth-of-discharge with an assumed selling price of \$30/kWh. As a minimum condition, we would project that lead-acid cells will be available in 1985 which will last 5 years at 90% of designed capacity at a price of \$20/kWh⁽¹⁾. At the end of our projection, we would predict that lead-acid batteries with 30 years life will be available in the 1985-2000 era which will deliver 60% of design capacity at \$30/kWh. For the 5 and 15 year batteries, we will assume a designed energy density of 12 watt-hours per pound. In the case of the 30 year battery, we will assume a designed capacity of 10 watt-hours per pound. Table 1.6.1 shows the assumptions made related to the designs of the lead-acid system for residential and intermediate site energy storage. Figure 1.6.1 shows the typical, state of the art life of lead-acid cells as a function of depth of discharge⁽²⁾. Figure 1.6.2 shows the relationship between the percent of the 20 hour capacity of a lead-acid battery, and the discharge time in hours⁽³⁾.

¹J. T. Brown, J. H. Cronin, Batteries Systems for Peaking Power Generation, 9th IECEC, San Francisco, Calif., August, 1974.

²Private communication, N. J. Maskalich, W Research Laboratories

³C. J. Mantel, "Batteries and Energy Systems", McGraw-Hill Company, New York, 1970, p. 145.

Curve 689892-A

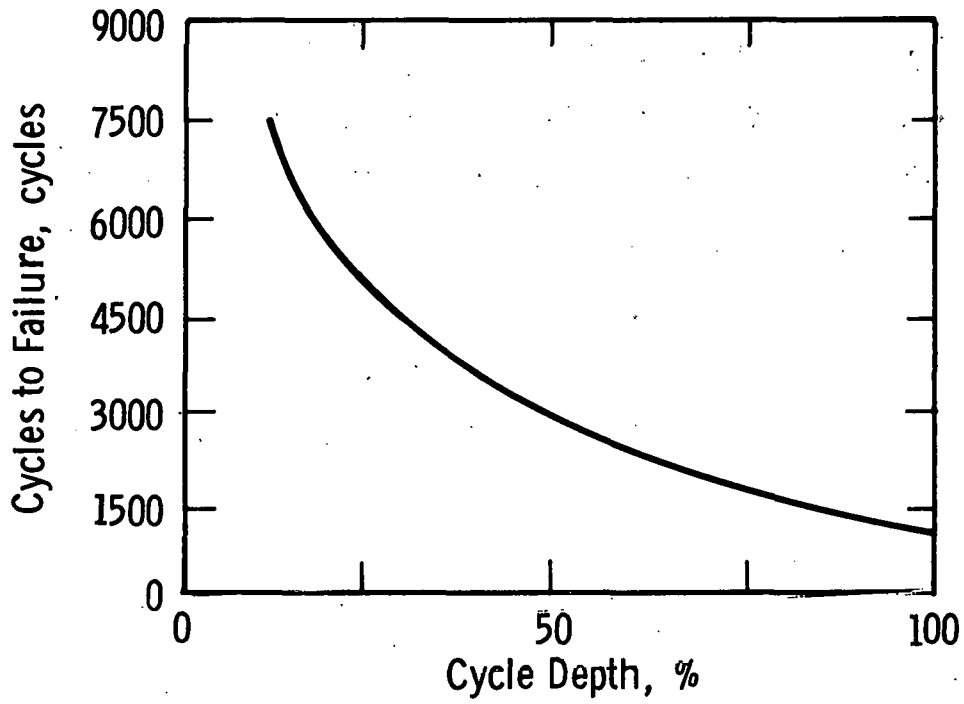


Fig. 1.6.1 – Life of state-of-the-art lead-acid battery

Curve 689891-A

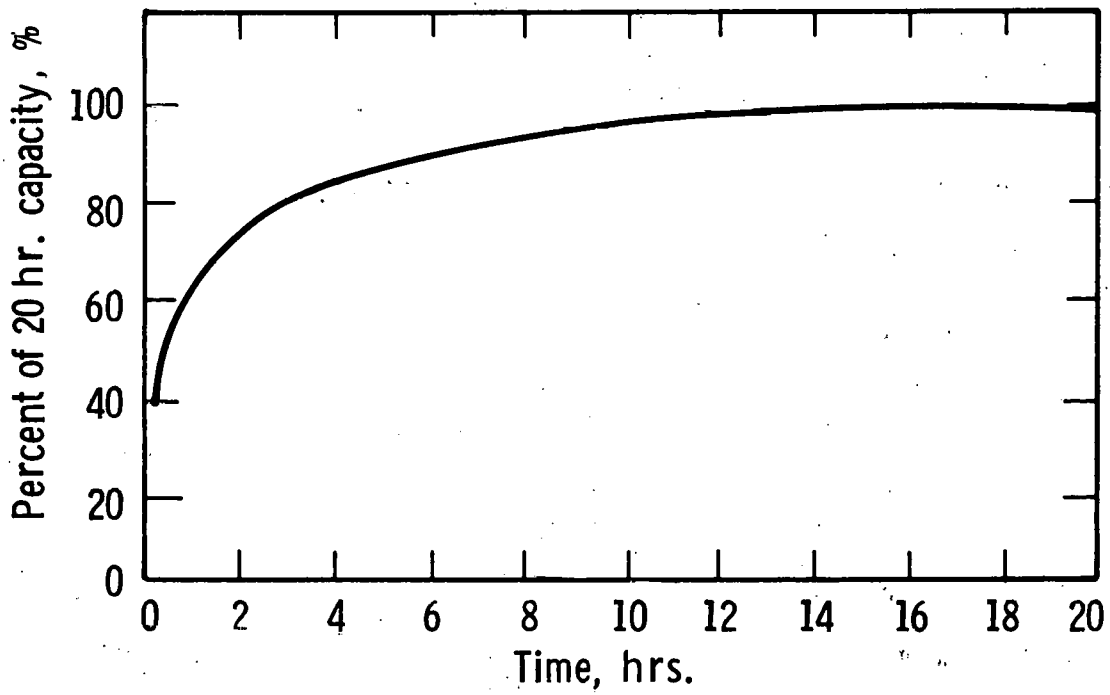


Fig. 1.6.2— Discharge capacity as a function of discharge time for lead acid batteries

Table 1.6.1

Lead-Acid Batteries

	<u>Energy</u> [*] <u>Density</u>	<u>Selling</u> [*] <u>Price</u>	<u>Life</u>	<u>% Discharge</u> <u>Capacity</u>
1985 Minimum	12 Wh/lb	\$20/kWh	5 years	90
1985 Improved	12 Wh/lb	\$30/kWh	15 years	70
1985-2000 Improved	10 Wh/lb	\$30/kWh	30 years	60

*Based on 100% depth-of-discharge

Electricity Storage in Molten Salt Electrolyte Batteries

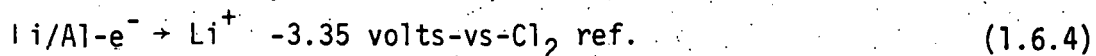
There are presently several molten salt, high temperature batteries under investigation at various research laboratories. These batteries are potentially high energy density systems wherein the electrolyte is typically an ionized melt of alkali metal ions and halogen ions. The most common electrolyte is the eutectic mixture of LiCl-KCl (mp 352°C).

The electrolyte in the molten state has a resistivity of about .1Ω-cm and a decomposition potential of 3.65 volts. At this potential, the decomposition products are metallic lithium and gaseous chlorine. The proposed anodes for use in this electrolyte are either liquid lithium or an alloy of lithium and aluminum. Presently the alloy electrode is preferred as the anode in the molten salt because it overcomes many of the problems inherent with the liquid lithium anode; mainly, severe corrosion, solubility in the electrolyte, and containment problems. The alloy which operates as a solid electrode at a reduced activity

($\sim 10^{-3}$, -0.300 volts) is less corrosive than pure lithium to cell separator materials and easier to handle from a design and engineering point of view. The alloy anode operates by releasing lithium ions to the electrolyte during discharge and accepting lithium during the recharge. The electrodes can operate between about 3 and 20 Wt % lithium in the lithium-aluminum alloy. This electrode has demonstrated cyclic stability during extended cycling for greater than 1000 cycles.

One of the cathodes for use with the lithium-aluminum alloy and most widely studied is a composite of iron sulfide as a current collector. In the discharge mode, lithium reacts with the iron sulfide to form lithium sulfide and iron. The open circuit voltage of the cell is about 2.0 volts with an average discharge voltage of about 1.2-1.5 volts, depending upon the depth of discharge.

Anode Reaction



Cathode Reactions



The theoretical energy density for the LiFeS reaction is about 250 W-hr/lb. Besides the iron sulfide cathodes, a variety of alternate metal sulfides has been considered separately, and in combination with the iron sulfide. The purpose of making the additions to the iron sulfide has been to increase the positive electrode conductivity, thereby enhancing its performance capability. Several critical problems related to the cathode in this system must yet be resolved. The

first is the definition of a suitable, low-cost, electrochemically stable cathode current collector. Work is presently in progress to define a stable current collector. Candidate materials are steel, carbon, graphite and the more expensive but stable materials - molybdenum and tungsten. A more serious problem with this particular cathode is its inability to sustain limited amounts of overcharge. At cell potentials above about 2.2 volts, chlorine from the electrolyte can react with the cathode, iron sulfide, and some of the current collectors (Fe, Ni) to form soluble compounds which result in eventual loss of the cathode. This type of overcharge can easily occur when cells are series connected, and some imbalance in performance exists to permit overcharge to occur. A proposed solution to this problem has been to monitor the charging potential of each cell. When the cell approaches the cathode dissolution potential, the electrical monitoring system would shunt the current through an external load, protecting the cell. This solution could prove to be very complicated and expensive.

The separator material for use in the molten salt cells must be stable in a very hostile environment. It must be stable to both the anode and cathode materials, as well as the electrolyte at temperatures between 350-500°C. The material presently used as the separator material is boron nitride. In a purified state, with the oxide film removed, this material has shown stability in the cell for tests past 1000 hours. At this point in the ongoing research program, the separator can be assumed to be a stable component in systems available during the 1985-2000 period.

In the molten salt cells, the rigorous elimination of moisture must be satisfied. The electrolyte is extremely hygroscopic, with oxygen and water being serious cell contaminants which, if allowed to slowly enter the system, will eventually consume the available lithium causing loss of anode capacity. In a finalized molten salt cell, the system must be hermetically sealed either at the individual cell housings, or in groups of connected cells.

Since the cells will be hermetically sealed, and no losses can occur, the maintenance of molten salt cells and batteries will be minimal. Thermal problems associated with keeping the electrolyte salt molten will not be serious and in most cases additional cooling will probably be necessary to prevent overheating under high drain rates.

The proposed designs for the molten salt Li-Al/FeS battery are for two applications: electric vehicle and cells for off-peak energy storage. Both of the designs differ in their energy and power characteristics. The vehicle design is intended to deliver more power per unit weight with lower energy density than the off-peak design. The battery for the off-peak energy storage has a projected energy density of about 75 watt-hours per pound. The projected materials cost for the off-peak energy cell is \$8.20 per kilowatt-hour⁽⁴⁾. We would assume then a selling price of about \$16 per kilowatt-hour for mass produced cells using readily available components based on technology projections between

⁴P.A. Nelson, et. al., ANL, High-Performance Batteries for Off-Peak Energy Storage and Electric Vehicle Propulsion, Progress Report, January-June, 1974, ANL--8109, Argonne Laboratories, January, 1975.

1985-2000. In this cost analysis, the battery life is assumed to be 5 years, operating at 300 days per year. At this point we will make two further assumptions projected to the era 1985-2000 that molten salt, high energy density cells and batteries will be available with longer lifetimes. The consequence of the longer lifetime will be a decrease in the overall energy density with a modest premium in materials cost to permit the extended life. In order to achieve 15 year life, we predict that the energy density will be reduced to 50 watt-hours per pound with a twenty percent increase in cost of materials, or the materials cost will be \$9.80 per kilowatt-hour with a selling price of \$20 per kilowatt-hour. In both of these design considerations, 80% depth-of-discharge is assumed. In the final design consideration, we assume thirty year life will be accomplished at 40% increase in cost of materials and a 60% depth-of-discharge. This results in a material cost of \$11.50 per kilowatt-hour and a selling price of \$23.00 per kilowatt-hour. These assumptions are made with full recognition that much research, development, and engineering are necessary before serious consideration can be given to the cost and life projections of molten salt batteries. The time scale in which credibility can be established is directly proportional to the amount of sustained effort devoted to solving the problems related to the molten salt battery whether it be the LiAl/FeS or others which use the basic related technology. Table 1.6.2 gives our assumptions based on projections of today's technology as to the practical capability of molten salt batteries in the era 1985-2000.

Table 1.6.2

Molten Salt Batteries (Li-Al/FeS)

	<u>Energy Density</u>	<u>Matls. Cost</u>	<u>Sell. Price</u>	<u>Life</u>	<u>% Disch. Capacity</u>
Design I	75 Wh/#	\$ 8.20/kWh	\$16/kWh	5 yrs.	80
Design II	50 Wh/#	\$ 9.00/kWh	\$20/kWh	15 yrs.	80
Design III	50 Wh/#	\$11.50/kWh	\$23/kWh	30 yrs.	60

Electricity Storage in Solid Electrolyte, Sodium-Sulfur Batteries

Work on the electrochemical couple of sodium and sulfur for secondary batteries started in 1965, and has been ongoing at several research laboratories. The battery mechanism is accomplished in this system by the transport of sodium ions through a solid electrolyte to the sulfur cathode to form a series of sodium polysulfide compounds. The ceramic electrolyte is the key to the use of the two liquid electrodes, sodium and sulfur. The electrolyte is β alumina in which sodium ions are quite mobile and free to selectively move along the conduction planes. The resistivity of the electrolyte varies due to manufacturing procedures and techniques but is generally in the range of 5 to 30 Ω -cm at the cell operating temperature of about 350°C.

The theoretical energy density of the sodium-sulfur couple is about 350 watt-hours per pound, based on a complete sodium-sulfur reaction. The open circuit voltage is about 2.0 volts. In practice, complete reaction of the sodium and sulfur does not occur and some intermediate composition is arrived at. The average voltage during discharge is somewhat less, depending upon the depth-of-discharge.

The sodium-sulfur system suffers from many of the same types of problems related to molten salt batteries. It must be hermetically sealed from the atmosphere, and materials corrosion problems related to the sodium and sulfur containment must be solved. Additional performance problems arise with the sulfur cathode in that it is basically a poor conductor of electricity and suitable current collectors must be interspersed within the sulfur to permit suitable operation compatible with the battery's practical mission. In practice, carbon is used for this purpose. To date, serious problems exist with non-conducting films deposited in the cathode compartment, as well as incomplete reactions resulting in reduced energy density.

The use of sulfur as the active cathode material limits the upper temperature at which the sodium sulfur system may be used. Sulfur vaporizes at about 440°C, limiting the cell and battery to that upper temperature. Means of limiting this cell temperature must be provided during high power drains and rapid recharge cycles.

The basic design of a unit cell using sodium and sulfur falls into one of two classes. The first design uses cylinders of β -alumina with the sodium contained within the tube. Cylinders have been made, and tested with 1 millimeter wall thickness, a 1 centimeter diameter, and a length of 30 centimeters. The cylindrical design approach would simply assemble an array of tubes appropriately sized to provide the necessary capacity for the particular mission. Further series connections would accomplish the voltage level required for the specific application. The problems related to this design are suitable seals for the tubes

and cells for the batteries. Presently, various types of glasses are being used as well as other materials⁽⁵⁾.

The primary failure mechanism of the sodium-sulfur cell with β -alumina is metallic transport of sodium through the ceramic, as a result of fabrication defects or cracks. It is assumed that these life limiting problems will be solved and eventual long-time stability will be achieved.

The second design of the sodium-sulfur couple uses β -alumina in the form of plates or discs⁽⁶⁾. This design approach would lend itself to more flexible series and parallel connections of cells with the eventual possibility of bipolar construction. Once again, the system suffers from the same performance and life limitations as previously discussed in the cylindrical design cells.

The problems related to the demonstration of high quality, high energy density, low-cost sodium-sulfur cells are dependent on a sustained program to achieve its goals. The state of the technology is presently being advanced at about the same rate as the molten salt batteries. Ultimate success of either of the novel high energy batteries is presently very speculative.

The predicted performance for a finally engineered low-cost

⁵W. L. Winterbottom, et. al., Materials Evaluation for the Sodium/Sulfur Cell, Paper No. 29, 1975 Electrochemical Society National Meeting, Dallas, Texas, October, 1975.

⁶L. S. Marcoux, et. al., Performance of Sodium-Sulfur Test Cells Utilizing β -Alumina and Flat Plates, Paper No. 28, 1975 Electrochemical Society National Meeting, Dallas, Texas, October, 1975.

system using the sodium-sulfur couple is quite similar to that of the molten salt cell. From our conceptual point of view related to the photovoltaic power systems, we will use the projected performances in Table 1.6.2 as being synonymous with both the molten salt and sodium-sulfur technology as it might exist between the years 1985-2000.

Electricity Storage in Alternate High Energy Density Batteries

The LiAl-FeS and the sodium-sulfur batteries previously discussed are two of the main candidate systems for new high energy density low-cost battery systems. There are several other systems also under technical investigation which may be viable in the era 1985-2000. Without going into great detail as to their operational mechanisms and technical problems, we will only list the systems with a brief comment relative to each system's ability to fulfill the energy storage requirements for the residential and intermediate site condition.

1. Li-Cl. Molten Salt LiCl-KCl

This secondary couple uses the full potential range of the molten salt, 3.35 volts. The cathode stores both alkali and halide ions. Its projected cost and performance are very similar to the Li/Al-FeS system⁽⁷⁾. It also suffers from the same problems as the FeS systems with the added problem that chlorine gas can be generated during the charge mode, within a sealed cell. This could result in excessive pressure build-up not compatible with the individual cell design.

⁷J. E. Metcalf III, et. al., Characteristics of a Tellurium Lithium/Aluminum Battery, Paper No. 71901, 1971 IECEC Boston, Mass., August, 1971.

2. Sodium-Chloroaluminate

This particular cell uses a low temperature molten salt electrolyte NaAlCl_4 (mp 120°C) in conjunction with a sodium anode and a β -alumina separator restricting the separation of the anode from the molten salt electrolyte, cathode⁽⁸⁾. The cathode is a porous carbon-graphite matrix which utilizes its electrochemical exchange of lithium with the dissolved antimony chloride (SbCl_3) in the electrolyte, cathode compartment. Problems associated with the intercalation of the complex ion AlCl_4^- with the current collector may limit severely the useful life of the cathode. Problems are also encountered in this system because the electrolyte sublimates at about 200°C restricting the upper temperature to a region where the β -alumina is a rather poor conductor of sodium ions. Once again materials compatibility and related design and engineering problems must yet be solved. This system incorporates the problems related to both the molten salt cell and the β -alumina cells. Eventual economic and technical success can only be speculated at this time.

3. Zinc-Chlorine

This low temperature battery (20°C) utilizes the electrochemical reaction of zinc and chlorine to form the basis of a high energy secondary battery wherein the chlorine is stored externally as a solid, chlorine octahydrate. In order for the system to perform properly, it requires

⁸J. Werth, et. al.; The Sodium Chloride Battery, Paper No. 242, 1975
Electrochemical Society, National Meeting, Dallas, Texas, October 1975.

several auxiliary systems for operation. It requires electrolyte circulation, reservoir refrigeration, and possible auxiliary cooling for the battery itself. The cell operates at 2.12 volts with a theoretical energy density of about 380 watt-hours per pound.⁽⁹⁾ The system, for long term operation, requires cathode materials which are stable in the chlorine of the electrolyte environment. To date, low-cost carbon electrodes have displayed limited stability while the more expensive cathodes with various coatings on titanium have been used⁽¹⁰⁾.

This particular system can also be viable in the era 1985-2000 with a projected \$20-\$30/KWh selling price.

1.6.2 Battery Storage for the Residential Power System

The Photovoltaic Power System for the residential site requires electrical storage in the form of secondary electrochemical batteries. The batteries are required to supplement the output of the solar array by providing load maintenance at high power drains for short time periods in addition to providing electrical energy when the solar array output drops off, at night for example. The battery would be expected to supply 5-10 KW for periods of 5 to 10 minutes at any time. The total energy storage capacity of the battery is 15 to 25 KWh depending on the site and the particular mission, especially if air conditioning is required.

⁹A. F. Sammels, Electrolyte Stoichiometric Considerations for Zinc Deposition in the Zinc-Chlorine Battery, Paper No. 236, 1975 Electrochemical Society National Meeting, Dallas, Texas, October 1975.

¹⁰Private communication, P. Symons, ERDA Detroit, Michigan.

The battery system is charged from the array or the supplemental energy supply and delivers energy as required to provide power over and above what the array itself can supply. The combination of the array and battery system provides the energy and power requirements for a residential site free of or in combination with utility line service. For the residential site which can possibly operate without line service, an engine generator or fuel cell can be considered to supplement inadequate array power and insufficient storage from the battery, should the situation ever occur during extended periods of cloud cover or full battery discharge. If line service is available, the residence could maintain power in spite of depletion of the battery and loss of power from the array. In either of these cases, battery system considerations are independent of whether or not line service is available or an engine generator is used to provide auxiliary charging when loss of power from the array occurs and the battery is depleted.

Battery Systems

The technological studies of electrochemical systems concluded that lead-acid and high temperature battery systems would be available in the era 1985-2000. Both of these battery types can be considered for the residential sites with their particular missions and use conditions. The batteries projected for use in 1985 are given in Table 1.6.3.

Table 1.6.3

Lead Acid

Type I	\$20/KWh - 90% DOD* - 5 yr. life
Type II	\$30/KWh - 70% DOD - 15 yr. life
Type III	\$30/KWh - 60% DOD - 30 yr. life

High Temperature

Type I	\$16/KWh - 80% DOD - 5 yr. life
Type II	\$20/KWh - 80% DOD - 14 yr. life
Type III	\$23/KWh - 60% DOD - 30 yr. life

* Depth-of-Discharge

None of the batteries, whether lead-acid or high temperature, is presently available as a high volume, low-cost commercial product. In the era 1985-2000, both systems, because of demand and technological advancement, are expected to fulfill the cost and performance projections given in Table 1.6.3. The basis for these prices and performance characteristics have been previously discussed.

Battery Missions

The use of secondary batteries in the residential site, provides a means of storing and delivering energy to the residence in combination with the solar array. The batteries are expected to deliver high power for short periods of time to supplement the power output from the array. The high power demands are required for the operation of appliances like ranges and driers, and in some instances, air conditioners. The mission profile calls for power levels of 5 to 10 KW for periods of 5 to 10 minutes

throughout the day. The total storage capacity at the battery system will be between 15 and 25 KWh depending on the site location and the requirement of the particular residence with its specific appliance load. The batteries will be electrically charged from the solar array during sunlight hours through the inverter-charger network. The inverter will provide an end-of-charge voltage of 400 volts, with a lower cut-off voltage of 260 volts during discharge. An alternate means of charging the battery would be direct line charging at night, or if no line service were included in the system, an engine generator used when the output of the array was inadequate for charging. In any of these configurations, the battery is insensitive to the charging means.

The battery and its related equipment are designed to be essentially maintenance-free, requiring only periodic visual inspection for proper operation. In operation, the battery and its related systems must also be fail-safe with little or no hazard to other equipment or the surroundings.

The overall life of the energy storage system is expected to be 30 years. The economics, which are considered for the various batteries, will use 30 year life as a common basis for evaluation of the various battery types even if the actual battery life is less.

Lead-Acid Batteries

Lead-acid cells have an average discharge voltage of about 2.0 volts, with an end-of-charge voltage of 2.5 volts. The energy efficiency of the cells is about 80% with approximately 10% coulomb inefficiency. The 10%

coulomb inefficiency appears near the end of charge resulting from the dissociation of water to produce hydrogen gas. During discharge, the state-of-charge of the cell is characterized by the specific gravity of the electrolyte, which participates in the electrode reactions. The preferred temperature for operation of lead-acid cells is about 70°F. At temperatures of 125°F the life of a lead acid cell is reduced by a factor of about 2.

To provide for the safe and reliable operation of the maintenance-free lead-acid battery, several auxiliary systems must be incorporated into the energy storage system as it interfaces with the solar array and the inverter-charging network. The philosophy used in the conceptual design of the residential site was to provide a low cost, maintenance free system, inherently highly reliable and fail-safe with little or no hazard to the residence, associated equipment, and residents. In the event of a failure within the battery system, action taken by the homeowner should be simple and sufficient to keep the overall system in a safe mode of operation for some extended period of time until a service man could provide necessary repairs. To accomplish this, several auxiliary systems must be designed into the battery system. The module of a battery will consist of eight cells and will have an average discharge voltage of 16 volts, with an end of charge voltage of 20 volts. The eight cell module will be the basic battery unit. Each eight cell module will include a voltage sensor to act as a Go-No-GO indicator. Should the voltage of the module ever go below a predetermined lower limit (~ 10 volts), the control sensor at the module would activate a warning

alarm. The alarm can be audible or inaudible, such as a horn or a warning light, on a master control panel or at the battery itself. The alarm of a failure of one module will alert the resident, or the condition. In this situation, the required action would be to short-out (bypass) the appropriate cell, disengage the Go-No-Go alarm, and continue in operation with 5% less capacity until the malfunctioning module could be replaced. This type of failure will occur when one or more of the cells within the module cannot maintain proper voltage characteristics as a result of an internal short or current collector failure.

Electrolyte maintenance will be accomplished by an automated water make-up system which will periodically add predetermined amounts of water to the circulating electrolyte. The necessary water will be drawn from the house supply. The electrolyte circulating system necessary to maintain proper temperature for the cells would circulate the electrolyte through a cooler to insure nearly constant temperature operation around 70°F. Once again an alarm system within the electrolyte maintenance and circulating system will indicate either pump failure or an extreme temperature above a set range. In the residential mission, the batteries are expected to provide high power (5-10 KW) for short periods. The electrolyte circulating system will prevent severe overheating of the cells.

The greatest hazard, with respect to the residential use of lead-acid cells, is evolution of hydrogen at the end of the charging cycle. Approximately 10% of the coulombic input to the cell results in

hydrogen gas. Concentrations of between 4 and 70% hydrogen air, a potentially explosive mixture exists. There are several means of removing and handling the evolved hydrogen gas, the simplest of which would be to locate the battery outdoors and dilute the hydrogen in a flowing air stream. If the battery is situated indoors, a hydrogen removal system within the residence will be required. Several alternate methods may be considered. The recommended procedure is to convert the hydrogen to water via a catalytic converter, and return the water to the electrolyte makeup system. One possibility would be to locate a catalytic converter in the vent cap of each individual cell, making the system safe from the hydrogen problem. The amount of hydrogen which will result from a normal daily cycle can be handled by the converter.

To be successful, this type of recombination system will have to be designed within the overall module assembly to provide the necessary safety factor within the context of the electrolyte circulating and maintenance system so that no possibility of an explosive situation could exist as a result of hydrogen concentration within the system. Another added precaution to insure complete removal of hydrogen would be to circulate the electrolyte through circulating tubes, which contain a porous network with the necessary catalysts (Pt-Rh) dispersed on the network surface to recombine the hydrogen contained in the electrolyte. A more accurate prediction based on this concept would require an experimental evaluation of an actual circulating system as well as an evaluation of cell vent caps which could recombine hydrogen. Further

information with respect to this system life and reliability would also have to be determined to provide a highly reliable and fail safe system.

A state of charge indicator must also be incorporated into the battery system to prevent significant discharge or overcharge. A coulometer, or state of charge indicator, can be included in the system in such a way that it can cause the battery charger during charge and the inverter during discharge to keep battery state-of-charge within predetermined limits.

Size of Lead-Acid Battery

The size of a 20 KWh lead acid battery will be determined by combining the appropriate number of battery modules in series to provide the daily residential mission. A typical cell size will be 2" x 7" x 9" (w x l x h) to provide about 65 amp hours of capacity. A battery module then will consist of 8 cells within one container. The energy contained within a module will then be (65 amp hours x 16 volts), about 1000 watt-hours. If the module has a gravametric energy density of 12 Wh per pound, a module will weight about 90 pounds. The total battery consisting of 20 modules with 8 cells per module will weigh about 1800 pounds. The 20 KWh battery will require about 25 square feet of floor area with a height of about one foot, including the auxiliary equipment. The size of other residential batteries will vary accordingly.

High Temperature Batteries

At this present time, the probability of any one of the candidate high temperature batteries being used in a practical system in 1985

is low. For this reason we have generalized what a typical system might be, in terms of performance, life, and operating characteristics. A high temperature battery will most probably have an end-of-charge-voltage of about 2.0 volts and an average discharge voltage of 1.5 volts. It will have excellent power characteristics and will operate at about 350°C. The cells will be hermetically sealed and will not have gassing problems or hazards. The cells will be about 80% energy efficient, with nearly 100% coulomb efficiency. The cell temperature will be maintained at 350°C by air cooling which is required to prevent overheating. The battery itself will be encapsulated with insulating material to provide an exterior surface temperature of about 30°C. At this time the waste heat from the high temperature battery is not being considered as a useful source of energy. It will amount to about 3-5 KWh of energy @ 350°C per day. Should further studies indicate that the energy in the form of heat can be useful, then a design to utilize it could be incorporated into the residential site.

Central control systems similar to those used on the lead acid system will also be used in the high temperature system, GO-NO-GO and subsystem failure alarms. In the high temperature systems, overcharge - as voltage raises above 2.0 volts - can cause irreversible damage to the cell, and possibly an explosive hazard due to gas pressure build-up. For this reason a somewhat more elaborate control system to prevent overcharge will be incorporated into the high temperature battery. It will sense the terminal voltage of battery modules, and be used as a control signal for the electronic circuitry which controls charging current.

The high temperature battery will require no electrolyte maintenance and the system will be essentially maintenance free except in the case of cell or module failure. Should this occur, corrective action would be required. Because of these maintenance free characteristics and the isolated nature of the cell components from the environment, the high temperature battery could easily be installed within the residence.

The high temperature battery will consist of 20 battery modules with ten cells per module to be charged from the inverter at 400 volts. The average discharge voltage of the battery will be 300 volts, with a lower cutoff at 260 volts. Should the development of a practical high temperature cell have voltage characteristics different from those assumed, alternate configurations compatible with the inverter would be considered.

Size of the High Temperature Battery

A 20 KWh high temperature battery with a gravimetric energy density of about 50 watt-hours per pound will weigh about 500 pounds as a full battery. Each 20 volt module in the battery will weight about 20 pounds. At the present time, there is no well defined size for a high temperature unit cell as a possible module. But, based on today's research projections, the volume of a 20 KWh battery will be about 2.5 cubic feet with a floor area of about 2.5 square feet. Once again these projections are quite speculative and will have to be further verified as progress is made towards the development of a viable high temperature battery. The high temperature battery will require about 10% of the volume of a comparable lead-acid system.

1.6.3 Battery Storage for the Intermediate Power System

Two options are possible choices for the battery mission of the intermediate site. The first one involves the installation of a battery system with a storage capacity of 10 MWh. In this configuration the battery will be discharged 300 times a year at 5 MWh for load leveling, and twenty times a year at 10 MWh for both load leveling and poor weather solar plant assistance. A second and preferred configuration includes the installation of one battery with a capacity of only 5 MWh fulfilling the 300 cycle per year mission, while available utility line service supplies the 20 cycle per year drain to deliver 5 MWh. Battery system life expectancy is 30 years.

The batteries needed for the IPS are presently unavailable. Two types of batteries are considered; an advanced technology lead-acid system and a high temperature system. It is assumed that, in the time period from 1985 to 2000, these batteries could be made available, and furthermore, their costs would be minimized by high volume mass production and cost reduction techniques. This assumption, which for both battery systems is quite speculative, is especially so for the high temperature systems which are presently only in the research phase. The assumption has more credibility for the lead-acid system because of its long commercial history, and because available technical information can be projected to use conditions compatible with the photovoltaic energy storage mission.

The battery system for the intermediate site will have a maximum power level of 1 MW in both the charge and discharge mode. In the discharge mode, the time can vary from one to ten hours. The charge time can be as long as eight hours, once again at a power level not to exceed 1 MW. The requirements imposed by the interface with the power conditioning system include a top-of-charge voltage of 730 volts, which can be lowered, and a low battery cutoff voltage of 430 volts. The preferred voltage range for operation of the batteries from start to end-of-discharge is 565 to 430 volts. If the battery goes below 430 volts, it will be removed from the circuit by the control system. The charging circuit is current and power controlled with a maximum current of 2300 amps and power level of 1 MW.

Further considerations relative to the use of the battery in the IPS are its safety to individuals and equipment, as well as the environmental impact of the battery on the surroundings. The battery must minimize any hazard or potential hazards as well as being fail-safe should any malfunction occur within the battery complex as it interfaces with other systems within the IPS.

The battery system must also be designed to operate unattended and with a minimum of maintenance for extended periods. Within the overall IPS, the battery system will be controlled by a computer or other external management system, whether remote or on-site, which would take action in the event of impending hazard or failure of the battery, a battery module, or battery subsystem necessary for proper and safe operation.

Lead Acid Systems

The lead acid cells have charging voltages of 2.5 volts and average discharge voltages of 2.0 volts with a lower voltage cutoff of 1.8 volts. The lead acid system is assumed to be 80% energy efficient with about 90% coulomb efficiency. The three lead acid cells considered are listed in Table 1.6.4

Table 1.6.4

	<u>Lead Acid Cells</u>			
	<u>Energy Density</u>	<u>Selling Price</u>	<u>Life</u>	<u>Dischg. Cap.</u>
Type I	12 Wh/lb	\$20/KWh	5 years 1500 cycles	90%
Type II	12 Wh/lb	\$30/KWh	15 years 4000 cycles	70%
Type III	10 Wh/lb	\$30/KWh	30 years 9000 cycles	60%

Type I lead acid batteries are considered to be state-of-the-art technology. Although the specific configuration necessary for this particular mission is presently unavailable, the lead acid technology, as it exists today, is compatible with a life of 1500 cycles at about 90% depth of discharge. The projected selling price of \$20 per kilowatt hour is based on several assumptions which tend to minimize this selling price. In a projected Type I battery, 80% of the cell would be lead at an energy density of 12 watt-hours per pound. The present selling price of lead is about \$.20 per pound. We have assumed that future demands and requirements will reduce this cost by encouraging the development of new and improved technologies for the refining and reprocessing of used lead acid batteries.

This will reduce the cost of lead to about \$.14 per pound. At these levels the cost of lead per KWh of energy storage capacity will be about \$11.60. By postulating other cost reductions and mass production techniques, we have projected a \$20 per kilowatt-hour selling price. If a lead acid battery of this type were purchased today at the present level of technology and production, the selling price would most likely be in the range of \$40-\$60 per KWh with a tendency towards the higher value. The salvage value for lead from used lead acid batteries will be assumed to be \$.05 per pound for use in all economic calculations for all the lead-acid batteries considered.

The Type II improved lead acid battery has a projected selling price of \$30 per KWh with a 15 year life including 4000 cycles at 70% depth-of-discharge. The increased selling price is based on the assumption that the increased life will require more material additives and possibly more expensive processing and fabrication than a 1500 cycle battery.

The Type III improved battery is expected to sell for \$30 per KWh with a 30 year life including 9000 cycles at 60% depth-of-discharge. In this instance, the energy density of the system is lowered to 10 Wh per pound. Once again the selling price is based on added costs necessary to extend the cycle life.

Figure 1.6.3 shows the life characteristics of the three types of lead-acid batteries as a function of DOD. Clearly, Types II and III show significant improvements over state-of-the art lead-acid batteries.

Curve 689893-A

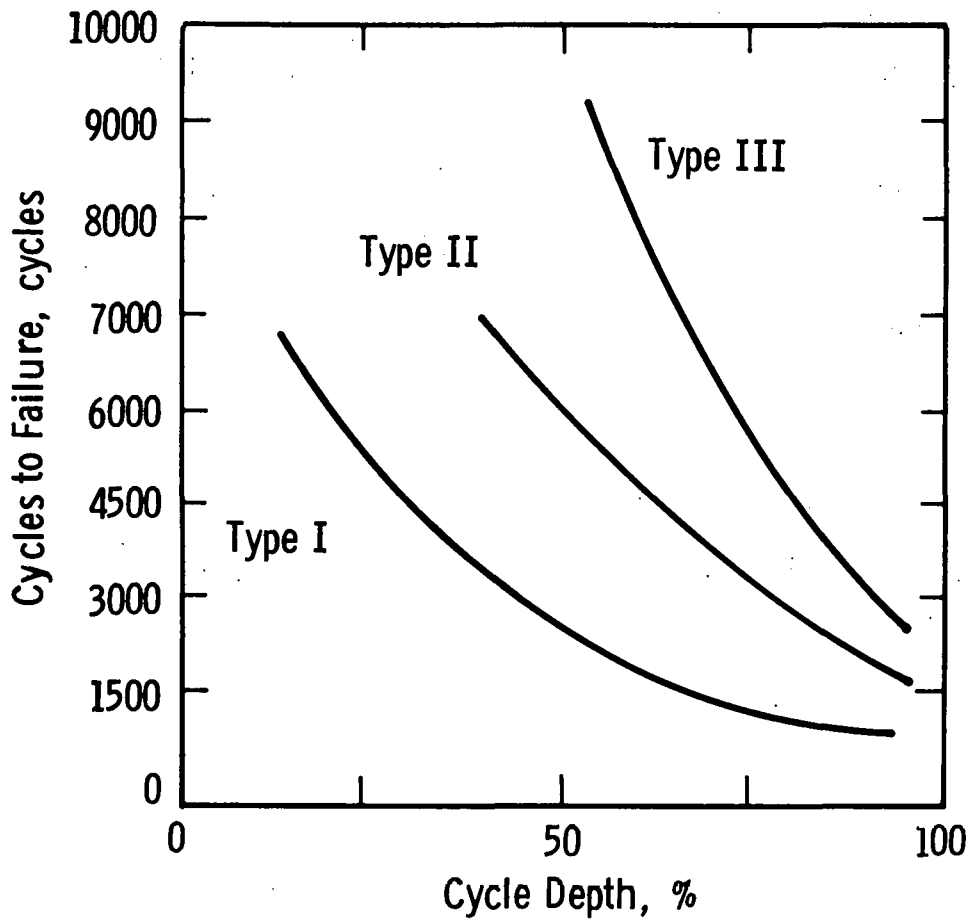


Fig. 1.6.3 – Life characteristics of lead-acid batteries

In the evaluation of the lead-acid system, we have assumed the lifetime to be a direct function of the depth-of-discharge and the number of cycles completed. We have not assumed useful life to be dependent on time in service. As a consequence of this assumption, a Type I lead acid battery which would be cycled 20 times per year would be expected to last 75 years. Based on today's technology, certain standby lead-acid systems have typical lifetimes in excess of 20 years, making a projected 30 year life at 20 cycles per year a reasonable assumption.

The lead-acid battery requires a certain amount of maintenance to insure proper performance and life. The preferred operating temperature is between 70-80°F, with life deteriorating to about 45% at 125°F and less as the temperature increases. This decrease in life at higher temperature will require the use of an auxiliary system for temperature control. Water lost due to dissociation of the electrolyte near the end of charge must be made up by an automated electrolyte maintenance system. Further maintenance in terms of visual inspection and preventive maintenance of interconnections, cell cases, and hardware will be required as a standard operating procedure.

There are several potential safety hazards associated with the lead-acid battery system. Safety hazards with respect to the use and handling of the sulfuric acid electrolyte can be adequately handled. Precautions to prevent accidental short circuiting of modules within the system must be considered. There does not appear to be any special hazard associated with the connection of lead acid cells at

terminal voltages as high as 700 volts, over and above the hazard of the large amount of energy stored and capable of total electrical discharge in a short period of time.

The electrical dissociation of water which occurs towards the end of discharge produces a large quantity of hydrogen gas. At hydrogen concentrations in air of between 4 and 70%, an explosive condition exists. Several procedures can be used to reduce the concentration of hydrogen to less than .1%. It appears that the simplest solution would be to dilute the hydrogen as it evolves from the cells by mixing it with a flowing air stream. A strategically positioned alarm system which will indicate excessive buildup of hydrogen as well as a failure of the air supply stream will be located in the air stream of the hydrogen removal system.

Other alternative means of handling the hydrogen would be storage for chemical reuse, metal hydride formation, catalytic conversion, or flame combustion. In light of the economics and potential hazards involved with these alternate solutions, hydrogen removal by air stream dilution is the preferred choice.

The economics of the lead-acid battery are determined by the depth-of-discharge, and the cycle life. We have assumed three levels of technology with respect to the lead-acid system; the Type I battery being state-of-the-art technology with the Type II and Type III being improved systems presently unavailable. Figure 1.6.3 shows the relationship between life of the three types of batteries depth-of-discharge.

At 100% depth-of-discharge, life expectancy is assumed to be similar for the three battery types. This is based on an actual battery mechanism which predicts certain failure of the electrode structures primarily due to grid failures after about 1000 cycles, with little hope that an advanced technology will increase the life significantly. The advances in the technology of the lead-acid system are expected to increase the life at 60 to 70% depth-of-discharge as indicated in the figure.

High Temperature Batteries

Several high temperature cells were studied and are being considered for use in the IPS. At the present time, no one system can be chosen as the best candidate for use in the 1985-2000 era. As a consequence, we have generalized what may be a feasible system, and have specified probable performance and costs which can be used for comparison with lead-acid batteries. We have not assumed a specific electrochemical couple, instead are considering a generalized, mass produced, high temperature battery using low-cost materials.

The voltage characteristics of the high temperature cell are 2.0 volts at full charge, 1.0 volts at discharge cutoff, and an average voltage during discharge of 1.5 volts. The operating temperature of the cell is 350°C with 80% energy efficiency and 100% coulomb efficiency. The cells will be totally self-contained with no provision for gas evolution. Three conceptual designs for high temperature batteries are considered as listed in Table 1.6.5.

Table 1.6.5

High Temperature Cells

		<u>Selling Price</u>	<u>Life</u>	<u>Depth of Discharge</u>
Design I	75 Wh/lb	\$16/KWh	5 years 1100 cycles	80%
Design II	50 Wh/lb	\$20/KWh	15 years 4500 cycles	80%
Design III	50 Wh/lb	\$23/KWh	30 years 9000 cycles	60%

Design I assumes a 75 Wh/lb battery with a life expectancy of 1500 cycles over a 5-year period at 80% depth-of-discharge. In this design we have predicted a selling price of \$16 per KWh based on the use of various low-cost materials and components which could be used in a high temperature system. These are sodium, lithium, sulfur, and molten salt electrolytes, low-cost separators, and cell containers. The life of a high temperature system is expected to be based on the time in use rather than the number of cycles as in the case for the lead-acid batteries. The expected electrode reactions in the high temperature systems should be more compatible with long cycle life, while the materials problems associated with operation at 350°C is certainly time dependent. As a result of these assumptions, battery designs II and III incorporate somewhat higher cost materials at a lower energy density with an expected increase in life. Presently available information on the performance characteristics of these high temperature systems indicates that several thousand cycles may be feasible if the inherent materials problems can be solved with low-cost materials.

The application of the high temperature battery as a means of energy storage in the IPS differs somewhat from that of the lead-acid battery. The electrical inefficiency of the high temperature system will be about 20%, and the wasted energy will be available as useable heat at 350°C. The temperature will be maintained at 350°C by air cooling. The successful high temperature battery will be a hermetically sealed unit requiring essentially no maintenance except for periodic visual inspection. Since the cells and modules are sealed, there are no problems with gas removal should gassing ever occur. However, an added problem does exist with the high temperature battery because it is sealed. High temperature batteries will not tolerate long periods of sustained overcharge. A control system to maintain cell voltage below a certain maximum charging level will have to be incorporated in the system to prevent overcharge. A lower voltage cutoff control system will also be incorporated into the system similar to that included with lead acid, to prevent deep discharge.

The charge-discharge rates and voltage limits of the charging system for the lead-acid battery are felt to be compatible with both the lead-acid and the high temperature systems. In most cases a high temperature cell can accept and deliver charge more rapidly than the lead acid cell, so that a power conditioning system designed for a lead acid system will easily accommodate a high temperature system as well.

The safety hazards of the high temperature battery system are related principally to the high voltage and the high temperature. The voltage hazards are similar to those experienced in the lead acid

battery system. The thermal hazard will be minimized by designing the case for the high temperature cells to maintain a surface temperature of 30°C. This can easily be accomplished with low cost insulating materials. If a case containing a molten salt cell ruptures, it presents a potential hazard to personnel and equipment. In general, the molten salts would be expected to solidify almost immediately upon case rupture owing to rapid cooling. In order to minimize the hazard of this occurrence, a system sensing cell rupture should be incorporated into the voltage monitoring and control system.

The projections made based on the use of high temperature secondary batteries for energy storage are much more speculative than those made for the lead-acid system. The probability of success of any of the three high temperature designs described is difficult to assess. A considerable amount of research and engineering must be done before a realistic design can be obtained. The reason they were included in this conceptual design was to make possible the evaluation of a technology which may be available in the 1985 to 2000 era offering low-cost energy storage, and to make possible a comparison of its cost with those of the lead-acid systems.

The cost to develop a high temperature battery system to fulfill this mission is expected to be significantly greater than that of extending the life of the lead-acid system. The development of a long-life lead-acid system may cost $\$5 \times 10^6$ whereas the cost to develop a high temperature system may be on the order of $\$10 \times 10^7$ or more if one can ever be developed.

Preliminary Battery Sizing

The preliminary size of a lead-acid battery for the IPS is based on a design wherein the cells will be placed on one level without stacking. Placement, movement and replacement of cells will be accomplished by a movable overhead crane which can be operated by one man. The weight of a battery module will be less than 3000 pounds for the lead acid system. The unit cell size will be (4" x 14" x 40"), (w_xl_xh) with a 1300 amp-hour capacity. Assuming a nominal cell voltage of 2 volts and a battery voltage of 500 volts, we will require a series connection of 250 battery modules. A battery module will consist of 8 cells connected in parallel to give a capacity of about 10,000 ampere-hours per battery module. A 5 MWh installation will be made up of 250 battery modules, with eight cells paralleled per module, making the total battery 2000 cells. A unit cell in this system will have a storage capacity of 2600 watt hours and weighs about 215 pounds. The weight of a 5 MWh battery will be (250 x 1700) or about 430,000 pounds. The floor area required for an eight cell battery module with interspaces for cooling will be about 3 ft². For 250 modules, we will require about 750 square feet of floor space with no provision for aisles or walkways between modules. The cell height will be 40" plus 12" head height, moreover with sufficient space for cell removal and replacement, we will require about a 10 feet ceiling height in the battery placement area. Because of the weight of the lead acid battery, placement on any structure above ground level will be cost prohibitive.

In order to generalize the floor space required for the lead-acid battery, we can say that within limits, 150 square feet will be required per MWh of installed capacity. The number of MWh's of installed capacity will be directly dependent on the type of lead acid battery used. If a Type II lead-acid battery is used and operated at 70% depth-of-discharge to deliver 5 MWh, we will have to install $\frac{5}{.7} = 7.14$ MWh of battery capacity. In order to deliver the proper terminal voltage, more paralleled cells will have to be added to the battery module, or a different cell design will have to be employed for the type of cell used. The use of cells connected in parallel as opposed to one large cell will provide an added degree of protection because should one cell in an 8 cell module fail, the other cells will carry the load for a period of time before shut-down of the battery occurs.

As an example of a battery size for the IPS, consider a Type I battery installed to deliver 5 MWh, 300 cycles per year. The battery installed will be capable of 90% depth-of-discharge. In terms of our previous cell design, this can be accomplished by paralleling 9 unit cells to form a battery module with cell dimensions 4" x 14" x 38". A 5% height decrease will lower the capacity slightly to provide the proper module capacity. A 250 module battery then will have an installed capacity of 5.5 MWh requiring a floor area of about 825 square feet. A variety of lead-acid battery couples can be postulated, with this example requiring minimum space because of the large depth-of-discharge and high energy density.

Economic Comparisons

The initial results of the conceptual system design of the baseline IPS included definition of a battery subsystem comprising a 5 MWh battery to be discharged 300 times per year for load leveling, and a second 5 MWh battery to be discharged 20 times per year to provide power on cloudy days. The three types of lead acid and high-temperature batteries considered, each having a different cost and life, presented a number of options for the construction of a 30 year life battery system.

In order to seek cost/performance optima, four different analyses were performed. These analyses were limited in scope and were not comprehensive, they were performed to provide a means to evaluate various alternatives, and therefore, were not intended to include all cost factors. Included in the analyses were:

1. Computation of net 30 year savings of a 1 MWh load leveling battery operating 300 cycles/year.
2. Comparison of capital cost/kWh of 7 options for construction of a 5 MWh, 300 cycles/year, and 5 MWh, 20 cycles/year battery subsystem.
3. Comparison of the net 30 year cost of a 5 MWh, 300 cycles/year load leveling battery; together with either a 5 MWh, 20 cycles/year battery, or with 5 MWh of energy purchased from the utility 20 times/year.

4. Comparison of capital cost/kWh of 3 options for construction of a 5 MWh, 300 cycles/year battery alone.

The analyses progressed logically from one to another in the following way. The result of Analysis #1 was that a load leveling battery is economically attractive compared with power drawn directly from the utility line as long as the night rate is sufficiently small and the day-to-night rate ratio sufficiently large. This positive result lead to Analysis #2, which sought a cost/performance optimum for a 30 year battery subsystem supplying both the 5 MWh, 300 cycles/year, and 5 MWh, 20 cycles/year loads. Although Analysis #1 verified the economic attractiveness of the 1 MWh, 300 cycles/year load leveling battery, it was not concerned with the economic viability of the 5 MWh, 20 cycle battery. Analysis #3 was then performed to compare a 5 MWh, 20 cycle/year battery with the alternative of drawing the other 5 MWh of energy from the utility line. The result was that power drawn from the utility line presented a less expensive alternative than using a 5 MWh, 20 cycles/year battery. This result lead to Analysis #4, which sought a cost/performance optimum for the 5 MWh, 300 cycles/year battery alone.

Summaries of these analyses are presented in the following sections.

Load Leveling Battery Cost Savings

One strategy used for control of the IPS includes charging the battery during the night when the utilities operate lowest cost base load equipment. Then, late in the day, battery subsystem discharge

is initiated as the solar array output drops off. Power from the solar array is not used to charge the batteries during the day because of the high economic value which can be assigned to solar power generated during sunlight hours.

The cost of electricity delivered from storage is made up of several factors. One of these is related to the 20% inefficiency owing to energy losses in the battery during charge and discharge. Because of this loss, battery storage would not be economical under any normal circumstances if the utilities could generate all needed electrical energy at a constant base load rate. Because this is not the case, and because the cost of electricity to the utility does vary with time of use, batteries may be considered.

In this analysis, the battery was assumed to undergo 300 discharge cycles per year. It was also assumed that the batteries are discharged 60% of their installed capacity, deliver 1 MWh with 80% efficiency and have a 30 year life. The evaluation was based on 1 MWh of battery capacity, but the results can be scaled for any size battery installation by simple multiplication. A comparison was made between electrical power furnished from battery energy storage, and electrical power drawn directly from the utility line at various generation costs based on nighttime power production costs of 10 and 50 mills/kWh. Battery costs from \$20 to \$80/kWh were considered. The costs, though not specific for any battery, are illustrative of the savings provided by using electrochemical energy storage.

The results of the analysis showed that, for the set of assumptions used, the cost of the battery is not a significant factor in the overall cost of storage-supplied electricity, but the ratio of electricity cost during the day to that at night is significant. The results of the analysis show also that electrochemical energy storage can provide a saving to the utility by storing energy generated at low nighttime base rates, and delivering it back into the system during the day as alternative to generating electricity with intermediate or peaking equipment.

Battery Subsystem Capital Cost Comparison

One battery subsystem considered for use with the IPS located in the Phoenix area includes 5 MWh of energy storage discharged 300 days a year for load leveling, and an additional 5 MWh of energy storage discharged 20 days a year due to weather variations. The 20 day mission occurs because of cloud cover where radiation falling on the solar array is insufficient to meet average daily loads. The six battery types considered for this analysis in various modes of operation and in various configurations are listed in Table 1.6.6

Table 1.6.6

Description of Battery Cells Analyzed

	<u>Lead Acid</u>	<u>High Temperature</u>
Type I	\$20/kWh-1500 cycles-90% DOD*	\$16/kWh-1500 cycles-80% DOD
Type II	\$30/kWh-4500 cycles-70% DOD	\$20/kWh-4500 cycles-80% DOD
Type III	\$30/kWh-9000 cycles-60% DOD	\$23/kWh-9000 cycles-60% DOD

* Depth of Discharge

Seven cases for both lead acid and high temperature battery combinations were considered to satisfy the annual load profile. In each case, only the cost of the battery subsystem was determined excluding the O&M cost or the cost of additional auxiliary equipment necessary for safe and proper operation. The purpose of this analysis was to determine which battery or combination of batteries offered the lowest cost over a 30 year period.

The results of the analysis of lead acid batteries show that the life of the battery is not a significant factor in the cost of a subsystem with a 30 year life when the discount rate is high. On the other hand, depth-of-discharge appeared to be a parameter which correlated to some degree with cost/performance optima. Similar analyses were performed using molten salt batteries with similar results.

Cost Comparison of Battery and Utility Options

The analysis just described which sought optima for a battery system which included batteries discharged 300 days per year for load leveling, and 20 days per year to take into account the occurrence of cloudy weather in the Phoenix area. Because the utilization of a 5 MWh battery subsystem discharged only 20 days per year is poor, it seemed appropriate to explore other options available to provide power during the 20 cloudy days.

The photovoltaic power system is designed to provide a portion of the power required by an industrial load together with power supplied by the utility. A second option to provide power for the industrial loads on cloudy days, would be to draw it directly from the

utility line eliminating the need for the 20 cycle per year battery.

An economic comparison of the two options was performed for the supply of power to industrial loads. The total cost of providing this power was calculated for a 30 year plant life.

In the first case, two lead acid batteries were assumed; one with a 5 MWh capacity discharged 300 times per year, and the second with the same capacity, but cycled 20 times per year. The second case varied from the first by eliminating the 20 cycle per year battery and assuming that the power formerly supplied by it is drawn from the utility line. As a point of comparison, a third case was evaluated assuming that no batteries were used and all power was drawn directly from the utility line.

In comparing the results of the three cases, the lowest cost occurs when a 5 MWh battery is used 300 times a year, and direct service from the utility line is used 20 times a year.

A decision based on this analysis would indicate that batteries can economically be used, but the exact choice and the economic impact are clearly related to the cost of electricity to the utility itself. The cost of generating electricity is a function of many variables such as season, time of day, and, in the case of a photovoltaic power system, weather conditions. As the cost differential increases between operating base, intermediate and peaking equipment, the economic advantage more strongly favored electromechanical energy storage. When the differential decreases, the advantage of battery storage is less. In the 1985-2000 era, the ratio of day-to-night costs

of generating electricity may range from 2:1 to as high as 10:1 or higher for peak loads. Therefore, battery storage appears to be economically attractive in this time period.

As the IPS is presently envisioned, it would include a battery with an installed capacity of 5 MWh to be cycled 300 times per year, and it would draw an additional 5 MWh from the utility line 20 times per year. This configuration is preferred based on projections which indicate that the differential between the day and night generation cost of electricity will be equivalent to or greater than present ratios but most probably not large enough to warrant battery storage for the 20 cycle per year mission.

Revised Battery Subsystem Capital Cost Comparison

The conclusion of the preceding analysis was that although batteries can economically be used to supply 5 MWh of load leveling, the additional 5 MWh needed for the industrial loads on the 20 cloudy days can most economically be drawn directly from the utility line.

The 30 year battery system power cost calculation presented earlier included the use of batteries to supply both the 300 cycles/year and 20 cycles/year loads. Because it now appears best to eliminate the 20 cycles/year battery, a revised battery system cost optimization is required.

Costs were determined for battery storage systems which supply 5 MWh 300 times per year for 30 years using three types of lead acid and three types of high temperature batteries. Three cases were analyzed and in each case only capital costs were considered, while

operating and maintenance costs as well as the costs of auxiliaries were excluded.

The preferred economic choices are Type III lead-acid battery and a Type II high temperature battery, both of which have the lowest total costs compatible with the mission. Additional costs related to installation must yet be included for both systems to incorporate them into the IPS.

THIS PAGE
WAS INTENTIONALLY
LEFT BLANK

1.7 Power Conditioning

1.7.1 Residential Power System

1.7.1.1 Power Conditioning Subsystem Requirements

For the residential system to have isolated operating capability, a force-commutated inverter is needed as the major power processing element. In addition, energy storage in the form of a battery will be needed in the system, and therefore, battery charging from the solar array will be required.

It is essential to minimize to the greatest extent possible the use of conventional passive components in the power conversion equipment. The specific cost of small capacitors, inductors, and transformers is high and, to a large extent, irreducible by expansion of production volume because their costs are largely determined by basic raw material requirements. Thus, a transformerless tie to the 230/115 volt distribution in the residence appears to be optimum, although it does seem that a simple center-tapped autotransformer may be the best way to derive 115V from the 230V output.

The residential load, no matter what its total magnitude (i.e., whether heating, air conditioning, or range are included or not), can be regarded as composed of three basic types.

First, there are machines - mainly split phase induction motors in freezers, refrigerators, furnace blowers, washing machines, and dryers. The machines exhibit performance sensitivity largely to the fundamental component of the applied voltage, but in general are so tightly designed from a thermal standpoint, that they cannot tolerate

large amounts of harmonic distortion in the exciting supply unless the harmonics are of such high order that machine impedance limits resulting harmonic currents to negligible amplitude.

Second, there is linear loading which is mostly purely resistive in the form of incandescent lights, and heating elements for dryers, water heaters, irons, toasters, etc. (and, of course, electric heating and range, where present). These artifacts exhibit performance sensitivity to the total rms value of the ac line voltage, and to a first order are not affected by its spectral characteristics.

Third, there are peak sensitive loads, mainly capacitive input filter rectifiers, in TV sets, radio receivers, and other home entertainment products. Such devices are sensitive only to the crest value of an applied voltage, and are largely unaffected by spectral aberrations.

If the output voltage characteristics of any type of simple self-commutated inverter are examined, the fundamental component of the output will be found to vary with variations in dc input, but it can be controlled by appropriate inverter operation (pulse patterning, phase shift between two inverters, etc.). However, neither the total rms value nor the crest value of the total wave is subject to that control. The crest value is never controlled, always reflecting whatever the dc voltage may be. In many instances (a PWM inverter with a "non-commutated" waveform, for example), the rms value is also uncontrolled and simply reflects the dc voltage. Even in those instances where the total rms value does vary with fundamental component control, it never obeys the same law.

Hence, the requirements of the three types of loads which must be satisfied cannot be simultaneously accommodated unless either the dc voltage supplied to the inverter is kept constant, or sufficient filtering is applied at the inverter output to extract the fundamental component of its voltage. If the first path suggested is adopted, an output wave containing appreciable harmonics only of such high order that the machine loads will be run safely must be produced either by filtering or inverter complication, or both.

For the residential system, EMI considerations in the ac distribution are of much more concern than for the larger systems. The character of the distribution buses is almost totally beyond our control, and the potential for interference with home entertainment media and telephone service exists to a very marked degree. Thus, even if the loads could tolerate a relatively crude inverter waveform, it is unlikely that system performance would be satisfactory in regard to EMI. In addition, any inverter with inherently high harmonic content in its output voltage faces difficulties when parallel tie operation is considered, for the resultant harmonic currents would be harmful both to inverter operation and to the utility ac feeder system, with, once again, EMI looming as a further concern.

From these considerations, it appears that the inverter used must deliver a relatively clean sinusoidal waveform to the ac system. Since no voltage wave which is produced by simple switching action from a dc source can be categorized as "relatively clean", filtering is mandated. The size (and hence cost) of the filter needed at a given power level

is a function of both the total harmonic distortion to be removed and the spectral character thereof. The more distortion, the bigger the filter; the higher the frequencies of the distortion components, the smaller the filter. Unfortunately, it is a fundamental fact of inverter technology that increasing the switching rate to create an upward frequency shift in the harmonic spectrum (as in a pulse-width modulated system, for example) necessarily increases the total harmonic distortion. There is, in consequence, no possibility of eventually reducing filter requirements to the "vanishing point".

A corollary consequence of increasing the switching rate to shift the spectrum upward is a decrease in the fundamental, wanted component of the output voltage produced from a given dc input. Hence, the dc source voltage required for transformerless coupling to a fixed ac voltage steadily increases as attempts are made to continue reducing filter size. Obviously, there are constraints, particularly in the residential system where safety is a pronounced consideration, on the dc voltage which can be employed.

The study does, then, consider designs in which attempts are made to optimize the inverter design as regards the compromise between switching rate and filter requirements. However, the optimum is a shifting target, highly dependent on active device performance capabilities and prices, and thus while the basic design concepts examined are likely to remain valid over the long haul, the specific configurations predicated now may not be used at a later date.

So far, we have considered for the most part only the ac interface of the conversion equipment. At the dc interface, we have to contend with the solar photovoltaic array, battery, and inverter interconnection in such a way as to achieve satisfactory system performance.

It was noted previously that battery charging from the array is needed in the residential system. The battery might also be charged from the incoming utility line at times. A force-commutated inverter, being a two quadrant, unidirectional dc voltage, bidirectional dc current device, is eminently capable of performing the charging function without introducing additional elements (provided, of course, it is designed with a sufficient dc voltage range capability to embrace both charge and discharge voltage ranges of the battery). If, however, we insert a dc regulator ahead of the inverter, switching from charge to discharge or vice versa will entail re-configuration of the subsystem because the dc regulator is essentially a single quadrant entity. Because dc regulators, whether linear or switching, are one quadrant, unidirectional voltage and current devices, it is unlikely, in our view, that the chopper regulated dc voltage approach can be economically competitive.

An examination of solar array characteristics reveals that such a source does in fact make a reasonably efficient battery charger without the interposition of power control equipment (other than perhaps a simple disconnect switch) between its terminals and those of the battery. Thus, it appears that a preferred configuration

might well be one where the battery is floated directly across the array, and the inverter has sufficient voltage range to embrace the full charge and discharge variations. During array operation when the battery needs charging and the array can produce more power than is required by the loads, the inverter can be controlled so as to sustain the dc link voltage needed for proper array matching. This type of operation will approximate constant voltage charging from the array.

When charging from the line is underway, some means is needed to prevent delivery of energy to the array. This is easily and cheaply accomplished by inserting a blocking diode in series with the array; however, there is a slight increase in loss during array operation unless a shorting switch is incorporated in shunt with the diode. During battery discharge, the array may continue to supply power, but at a considerable mismatch, if insulated. If not, then it will play no part in the operation since its terminal voltage will be below that of the battery, and the series diode will block. While this configuration is likely to be preferred for residences with Case I loads, i.e., without electric range or air conditioning, it may not be the optimum economic solution for those with greater demands.

1.7.1.2 Subsystem Cost/Performance Analysis

A voltage fed, self-commutated inverter, which is the best choice to meet all requirements of the RPS, can be realized using a variety of power devices. Included as possible candidate devices are conventional thyristors, gate-assisted thyristors, gate-controlled switches, and transistors. Because, in principle, each of the devices

listed could be used to construct a voltage-fed inverter, the choice between devices must be based on differences in device performance and circuit complexity as reflected by cost.

In order to interface with a 220V ac line, a transformerless inverter must operate from a minimum dc voltage of 244V. If the battery is floated across the array and the 244V dc input is assumed to be the battery end-of-discharge voltage, then the top-of-charge voltage to which the switching devices will be subjected will be about 400V.

If the inverter is rated at 5 kW, the average dc current at 244V is 20.5 A. The peak 60 Hz current per device is then 32 A, and the RMS and average current per device are 16 A and 10.2 A, respectively.

In general, safety factors of 2 for blocking voltage and 1.5 for current are used to arrive at device requirements for a given circuit application. In this case, assuming no dc regulator, the rated device maximum voltage should be 800V and peak current 48 A.

Conventional thyristors are readily available at the present time with the required voltage and current ratings. However, their switching speed limitations, creating a need for passive components of substantial rating in the commutating circuit, render them unattractive in the long view.

Improved switching speed results from use of the gate-assisted turn-off thyristor (GATT) structure, which in all other respects, performs in similar fashion to the conventional thyristor. The improved switching speed is obtained at the expense of some additional complexity, and of course cost, in the gate drive circuit. Gate-assisted turn-off

thyristors have been developed and manufactured in both smaller and larger current ratings than the application calls for (though, ironically, not in the rating range needed here) with characteristics offering considerable improvement over conventional thyristors.

The gate-controlled switch (GCS) is a thyristor structure wherein the gate can exert sufficient influence to cause the device to turn off while flowing full rated load current. Although GCS devices in sizes both smaller and larger than that required for the application have appeared on the market from time-to-time, the overall performance of circuits in which they were used always suffered relative to circuits designed to do the same job using thyristors or transistors. Although the GCS cannot be ruled out as a potential candidate device, it appears doubtful at this time that a circuit using it will be the most cost effective of all the alternatives possible for the RPS inverter in the 1985-2000 era.

Of the three candidate latching devices, namely the thyristor, the GATT, and the GCS, the best candidate appears to be the GATT device. However, it requires the use of an auxiliary commutating circuit which contains expensive passive components. On the other hand, the transistor flows a current which is base-controlled, and can be interrupted without the aid of auxiliary commutating components. The transistor inverter is then an appropriate candidate to compare against that using GATT devices.

Although transistors with the required ratings of 800V and 50 A with appropriately fast switching speeds are not presently available, it is safe to assume that such a device will be developed and manufactured

for sale by the time needed, the 1985 to 2000 era. Assuming then that both GATT and transistor devices of requisite performance are available, the choice between the two must be made on the basis of other factors.

Some of the key factors to be considered are as follows:

1. Voltage Safety Factor - General practice for thyristor circuit design is to derate by a factor of two with respect to voltage for circuits where long life and high reliability are required. On this basis, devices which block 800V are required for this circuit. A GATT device which blocks 800V is not difficult to make, but it may be considerably more difficult to make a transistor with such a rating without affecting other parameters. If that is the case, it would appear that the GATT device has an advantage here unless it can be shown that the factor of two voltage safety factor used for thyristors does not apply equally to transistors for a comparable level of reliability.

2. Drive Circuitry vs. Commutation Circuitry Cost - Because the transistor is not a latching type device as is the GATT, it requires continuous base drive when in conduction. Therefore, the cost of base drive circuitry is greater than the corresponding gate drive circuitry of the GATT device. However, because the transistor does not latch, the commutation circuitry necessary for use of the GATT device is not needed for the transistor circuit. When costs of the two are compared, it appears that the transistor has the advantage because the cost of the base drive circuitry is less than that of the commutating circuit.

3. Fault Survival - When a load fault occurs tending to draw excessive output current, or when a logic error occurs owing to noise or some other cause, the active devices must limit the resulting surge current to a survivable level, or else turn on to a surge of current which will blow a fuse before device failure occurs.

In the case of the GATT device, it turns on when a commutation fault occurs and nondestructively flows a fault current until a fuse blows. The transistor would be unable to flow a surge of current large enough to blow a fuse, but it may be able to turn off quickly before the fault current reaches a nondestructive limit. Fault survival in the transistor circuit requires greater study before a judgment can be made.

4. Efficiency - For a given peak current, the losses owing to forward current dissipation should be lower for the transistor than for the GATT device because, everything else being equal, the forward drop of the transistor should be lower than that of the GATT device. More work must be done to determine how much lower the losses are in an equivalent sized transistor to determine the difference in cost credits resulting from it.

5. Cost - The cost of transistor and GATT devices of equivalent performance must be determined. Using flat pack construction with double sided cooling, it is anticipated that the costs of equivalent devices should be roughly equal for equal production volumes. This point must be investigated further.

The results of the discussion of the five factors in relation to GATT and transistor device performance and cost show that the choice between the two is difficult to make. In fact, a firm decision cannot be made until some points are investigated further. However, a choice must be made here because it is impossible to carry along two separate designs within the limits of effort allocated to this task. Upon summarizing all of the discussions regarding both devices, it appears that the GATT device offers a somewhat better and less risky overall compromise of cost and performance at this time. Therefore, the design will proceed based upon the use of the GATT device. This conclusion in no way diminishes the potential of the transistor for use in this application, but is simply an indication of our feeling that more effort is needed on the transistor itself and on associated circuitry before a final choice can be made. In fact, many of the general design considerations, will be applicable to a transistorized circuit as well as one using GATT devices.

In assessing the basic power conditioning scheme selected shown in Fig. 1.7.1 and the alternate shown in Fig. 1.7.2, there are two basic questions. First, what is the optimum compromise between inverter commutation rate (for intrinsic low order harmonic reduction) and output filter? Second, what type of commutation circuit should be used in the inverter?

To a considerable degree, these are not independent choices, since commutation circuit losses and turn-around time have a profound influence on the determination of an upper bound to the switching rate.

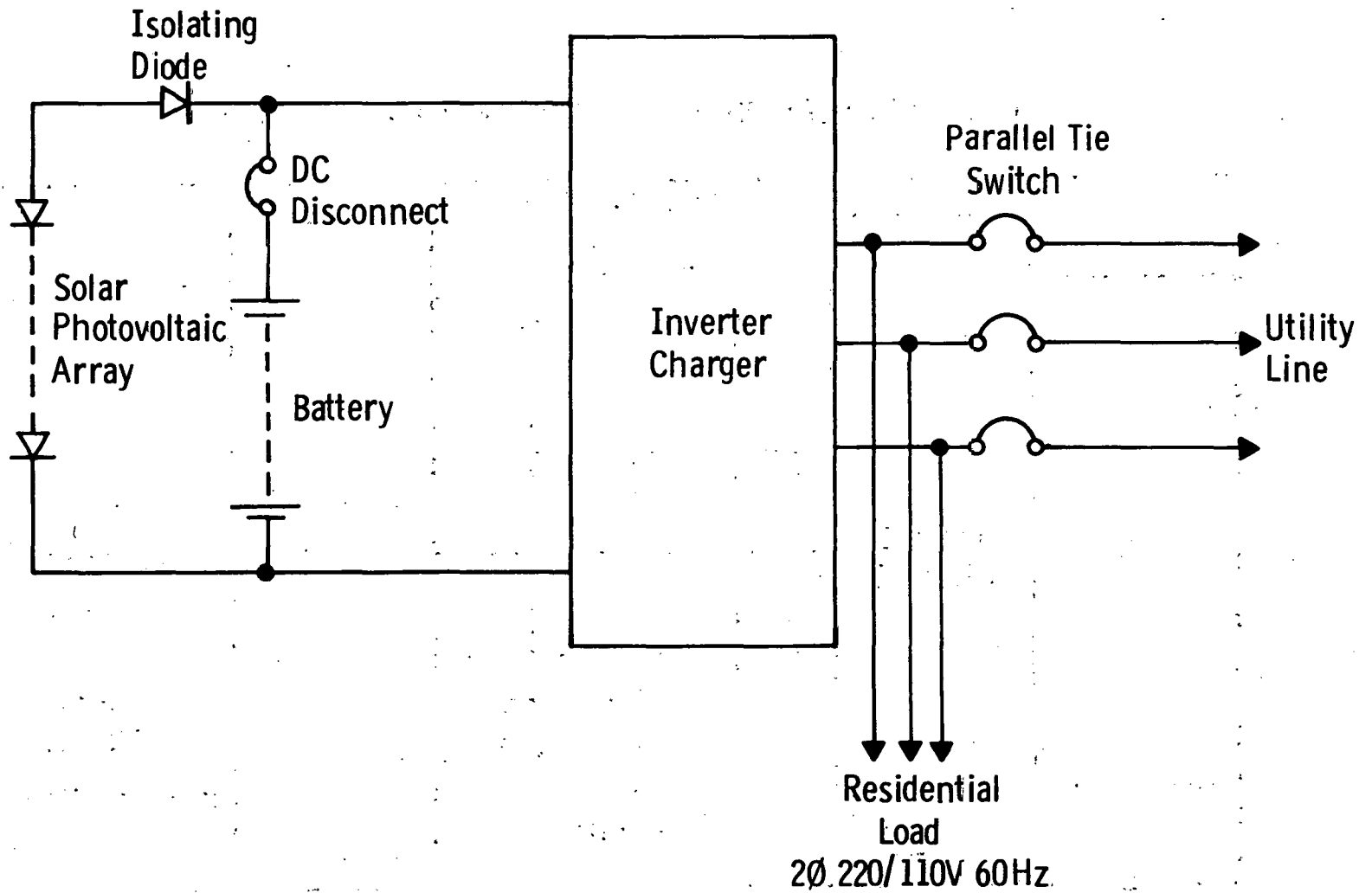


Fig. 1.7.1 – Basic system arrangement for residential application

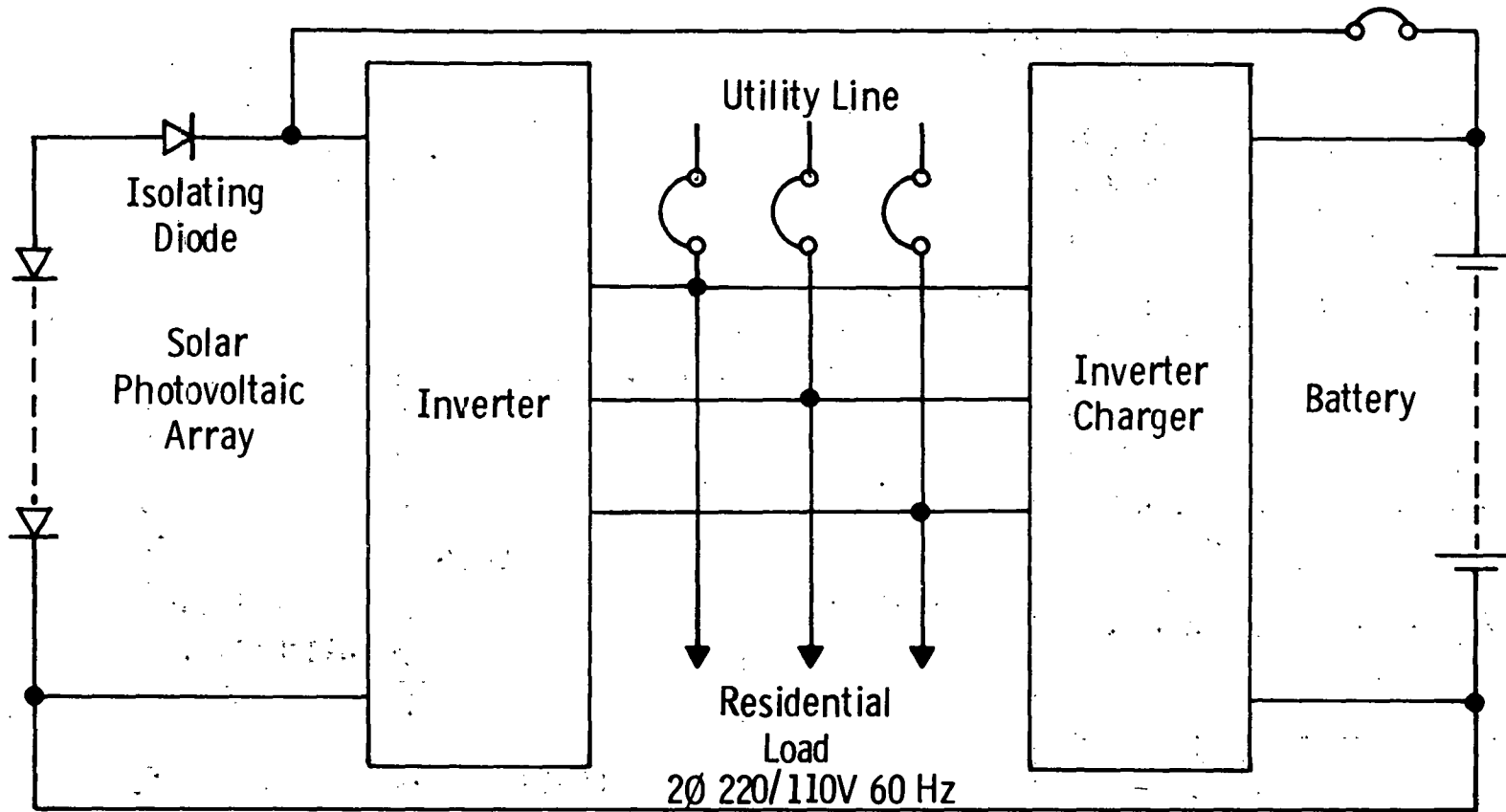


Fig. 1.7.2 – Alternative arrangement for Case II and III loads

However, we can divorce these provided the switching rate resulting from cross-optimization with the output filter is not so high as to cast doubts on its acceptability when practical commutation circuits are employed.

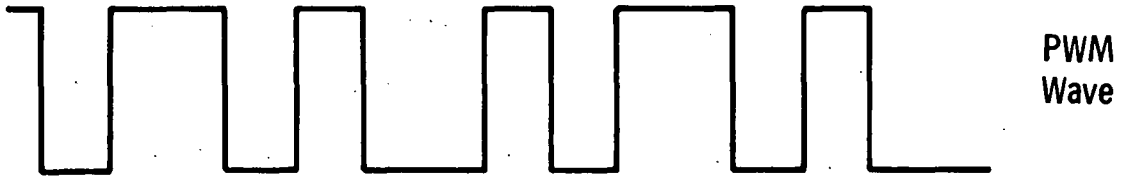
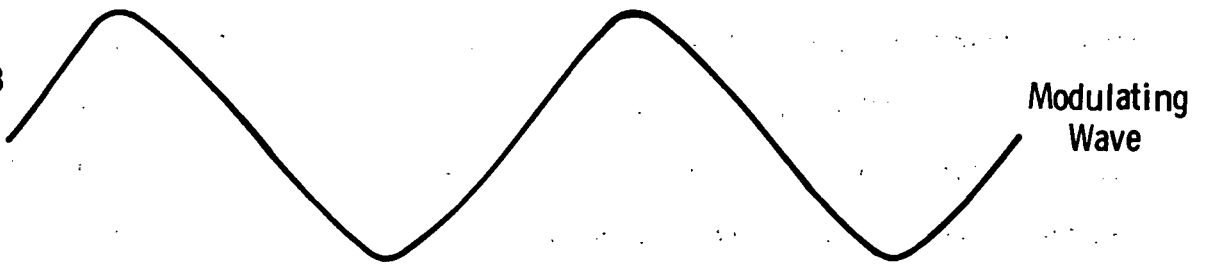
In beginning considerations of the inverter switching rate versus output filter, let us first lay to rest the possibility of full dress pulse width modulation used for both waveform quality improvement and voltage control. Usually, PWM is approached analytically from the standpoint of a high "carrier" switching frequency suitably modulated to produce the "desired" output wave. We believe this approach obscures important fundamental properties of the PWM inverter and prefer the opposite view, that a PWM waveform, as depicted in various stages of sophistication in Fig. 1.7.3, consists of a basic square wave into which a number of "notches", or periods of voltage polarity reversal, have been introduced.

Because the RMS value of a voltage is derived using its square, it is easy to see that the total rms value of the waveforms shown in Fig. 1.7.3, is constant regardless of the number, positioning, or widths of the notches (i.e., in conventional PWM terminology, regardless of the carrier to output frequency ratio and the depth of modulation). This seemingly trivial observation can lead to some interesting conclusions, as will be seen shortly.

It can be readily verified, also, that if the total voltage excursions are $2E$ (i.e., the amplitude of the base square is E) and there are N notches, with angular displacements from a reference angle

Dwg. 6379A57

(I) $\frac{f_c}{f_m} = 3$



(II) $\frac{f_c}{f_m} = 5$

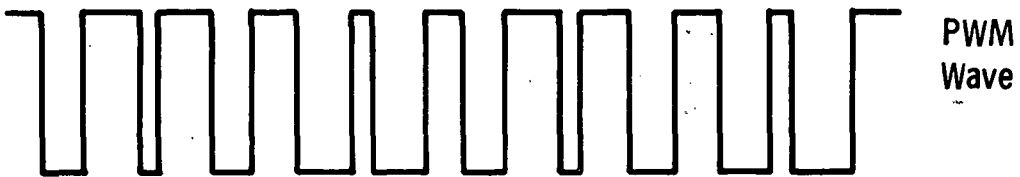
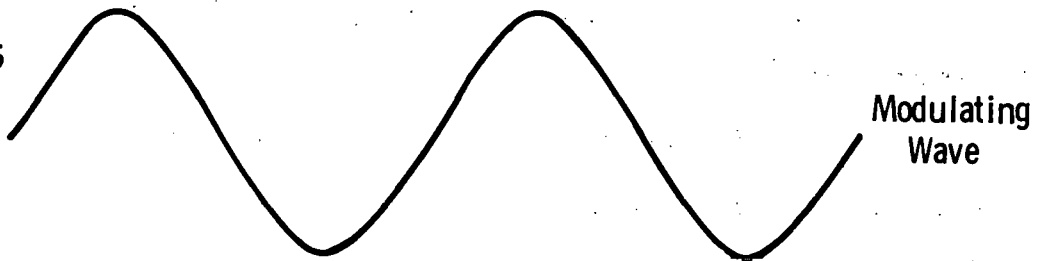


Fig. 1.7.3a — PWM waveforms for $f_c = 3x$ and $5x$ f_m and a modulation index of .75

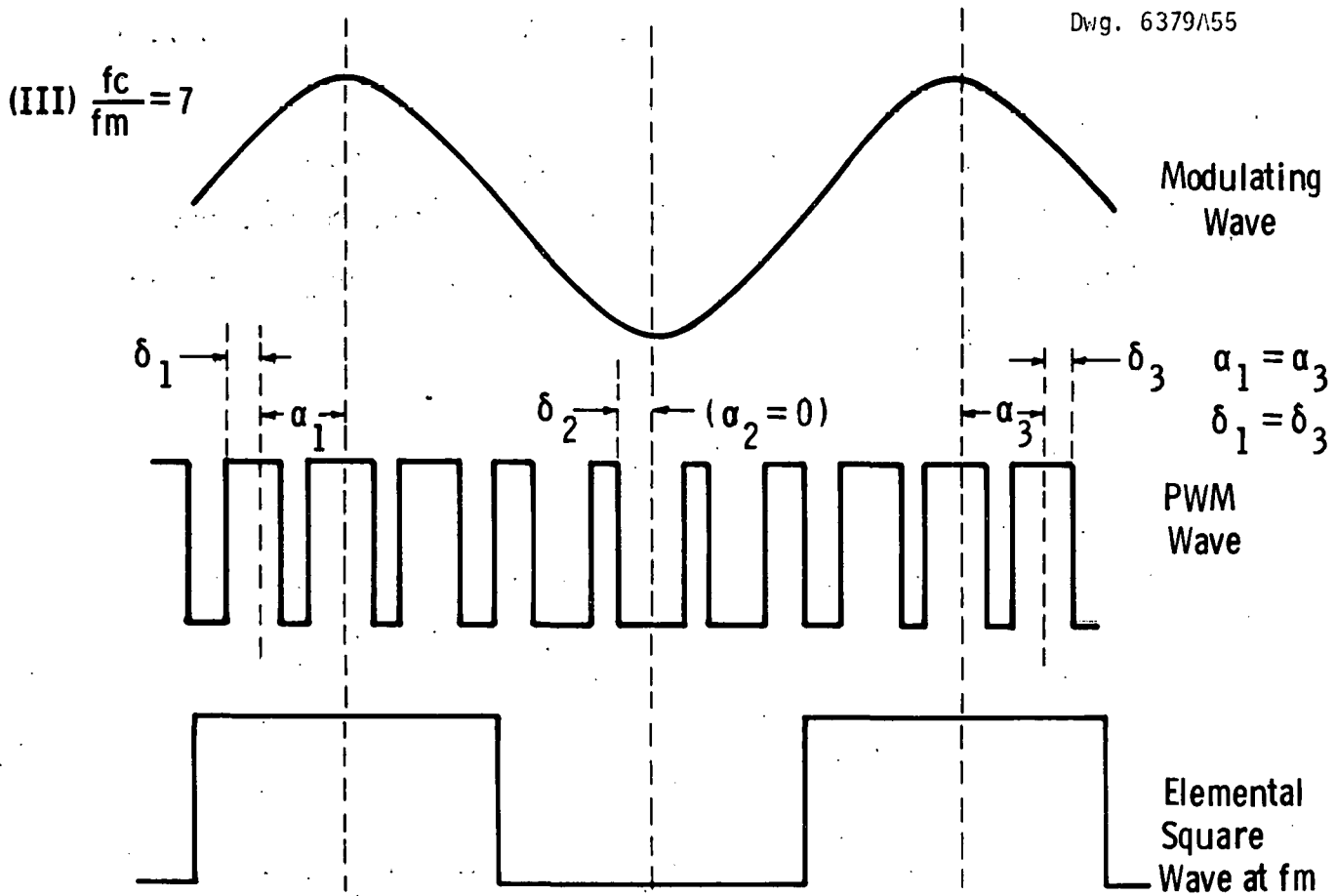


Fig. 1.7.3b — PWM waveform for $f_c = 7 \times f_m$ and a modulation index of .75.

$\pi/2$ radians from the base square wave zero crossing, of $\alpha_1, \alpha_2, \alpha_3 \dots N$ and half duration angles of $\delta_1, \delta_2, \delta_3 \dots N$ radians at the fundamental (output frequency), the amplitude of the fundamental component of the waveform is given by:

$$A_1 = \frac{4E}{\pi} \left(1 - \sum_{i=1}^N 2 \cos \alpha_i \sin \delta_i \right) \quad (1.7.1)$$

Now all α_i 's must lie between 0 and $\pm\pi/2$, and hence all $\cos \alpha_i$'s lie between +1 and 0; similarly, all δ_i 's must lie between 0 and $\pi/2$, and hence all $\sin \delta_i$'s lie between 0 and +1. Therefore, it follows that

$$\sum_{i=1}^N 2 \cos \alpha_i \sin \delta_i$$

must be a positive quantity. The term in the parentheses in Equation (1.7.1) will then be a maximum when the summation is zero. Therefore,

$$\left(1 - \sum_{i=1}^N 2 \cos \alpha_i \sin \delta_i \right) \leq 1$$

and as a result, we can say that, in general, the amplitude of the fundamental component of any notched wave is less than that contained in the original unnotched square wave from which it is desired.

Because the total rms voltage of the wave is constant, if the fundamental is reduced as a result of inserting the notches, then the total rms distortion must rise, or in other words, for any PWM or

pulse patterned waveform, the total rms distortion is worse than that existing for a simple square wave having the same voltage excursions. This is a very fundamental (and absolutely unavoidable) consequence of adopting PWM or pulse-patterning "waveshaping" techniques.

This being so, we are bound, naturally, to inquire as to the motivation for using such schemes. The answer lies, of course, in the upward frequency shift of the distortion spectrum that can be obtained, and the possibility then of reducing output filter size despite the inevitable increase in total rms distortion.

Just as for the fundamental, the amplitude of the Mth order harmonic, $M = 2k+1$, $k = 1, 2, 3, \dots, \infty$, can be written

$$A_M = \frac{4E}{M\pi} \left((-1)^{\frac{M-1}{2}} - \sum_{i=1}^N 2 \cos M \alpha_i \sin M \delta_i \right)$$

Now the restrictions on α_i do not apply to $M\alpha_i$, nor those on δ_i to $M\delta_i$, and in general the only restrictions on

$$\sum_{i=1}^N 2 \cos M \alpha_i \sin M \delta_i$$

become

$$-2N \leq \sum_{i=1}^N 2 \cos M \alpha_i \sin M \delta_i \leq 2N$$

Thus the amplitude of any individual harmonic, with N notches, can range from 0, when the α_i 's and δ_i 's are such that the summation cancels $(-1)^{\frac{M-1}{2}}$, to $(1+2N)$ times its amplitude in the basic

square wave when the α_i 's and δ_i 's are such that the summation equals $+2N$. Viewed as a synchronous PWM system, $2N+1$ is in fact the ratio of carrier to fundamental output frequency, and we have the conclusion that the higher the carrier frequency, the higher can be the amplitude of any individual harmonic of the output frequency.

The accurate mathematical analysis of the spectrum of an asynchronous PWM waveform is somewhat more complex, since the carrier side bands no longer coincide with the harmonics of the output frequency and vice versa. However, an examination of the results^{1,2,3} reveals that the same basic conclusions are valid - total rms distortion is higher and fundamental component lower than those of the elemental square wave, and the maximum attainable amplitude of any unwanted component increases with the carrier-to-output frequency ratio.

In order to achieve the spectral shift required, we need to make A_M for the low order harmonics, or lower frequency unwanted components, zero or very close to it. If we wish to do this over a range of fundamental component amplitudes i.e., with varying α_i 's and δ_i 's, we find that the conditions can only be satisfied if we insert 2 notches for each harmonic to be "neutralized", or increase the carrier frequency by quadruples for each unwanted component frequency we wish to eliminate. If we are prepared to accept a "fixed" amplitude fundamental component as a consequence of attempts to shift the harmonic/unwanted component spectrum, then only one notch per unwanted harmonic or output frequency doubling per unwanted component is required. Of course, the more harmonics/components we eliminate, the

lower will be the fundamental component relative to that in the elemental square wave.

In the synchronous case, elimination of M harmonics for a fixed fundamental component requires selection of α_i 's and δ_i 's to simultaneously satisfy

$$\left[(-1)^{\frac{M-1}{2}} - \sum_{i=1}^N 2 \cos M\alpha_i \sin M\delta_i \right] = 0$$

for the M harmonics to be eliminated, the resultant fundamental being of course,

$$\frac{4E}{\pi} \left[1 - \sum_{i=1}^N 2 \cos \alpha_i \sin \delta_i \right]$$

For simultaneous voltage control, 2N notches are needed and the fundamental equation is embraced in the simultaneous sets. In either event, the resulting sets of simultaneous equations are treacherous indeed. A set may possess multiple solutions, or no real solutions at all, and exact determination of the criteria establishing the α_i - δ_i combinations satisfying any given requirements can only be done through numerical approaches on a digital computer.

However, we can draw some basic conclusions from the rather sketchy results quoted above. If we wish to use PWM for both voltage and harmonic control, then the following series of facts are elicited.

(1) To eliminate the 3rd harmonic only, a carrier frequency of at least 5X, or 300 Hz for 60 Hz output, is required and the 5th harmonic (carrier frequency), 7th, or 9th can assume a magnitude 5

times that it possesses in a simple square wave for some condition of dc voltage in/ac voltage out.

(2) To eliminate the 5th as well, the carrier frequency must go to 9X, or 540 Hz at least, and the 7th thru 13th harmonics can assume 9X their square wave amplitudes.

(3) Eliminating in addition the 7th calls for a carrier of at least 13X, or 780 Hz and the 9th through 17th harmonics can assume amplitudes 13 times their square wave.

It can be seen that this process can be continued by increasing the carrier 4X for each additional harmonic to be removed. Further, as we go through this process, the available fundamental is progressively reduced. In a theoretically perfect system, i.e., one without constraints on notch durations, this would not be true - the fundamental amplitude could be $\pi/4$ that of the fundamental in a basic square wave for all carrier frequencies (i.e., the peak of the modulating fundamental can equal the basic square wave voltage if a modulation index of 1 is attainable). However, if we postulate a minimum notch width at fundamental of $2\delta_1$, then the maximum possible attainable modulation index becomes $M_m = 1 - \frac{4\rho\delta_1}{\pi}$ where ρ is the ratio of carrier to modulating frequency, and this factor is the amount by which the maximum fundamental component is reduced. It should be noted that for relatively low values of ρ , say < 20 , further reduction, due to cancellations from coincident side band components, can occur.

The consequences are pretty clear - as we increase carrier frequency, reducing low order harmonics, the fundamental attainable rapidly decreases. Thus, the dc voltage minimum needed for transformerless intertie to a given ac line voltage rapidly increases, consequently increasing the cost of and losses in the inverter poles. Further, the output filter size (and cost) diminishes rather slowly, since the amplitudes of unwanted components lower in frequency than the carrier can reach values of $3X$ their basic square wave values. It should be apparent that PWM is not a particularly attractive proposition unless the costs and losses of the inverter poles are not significantly affected by either dc voltage level or switching rate. For poles using thyristors, this is distinctly not the case, and PWM must be considered an inappropriate approach.

If we do not attempt control of the fundamental but merely "neutralize" some harmonics using pulse patterning and accept the fundamental component resulting, then the consequences are:

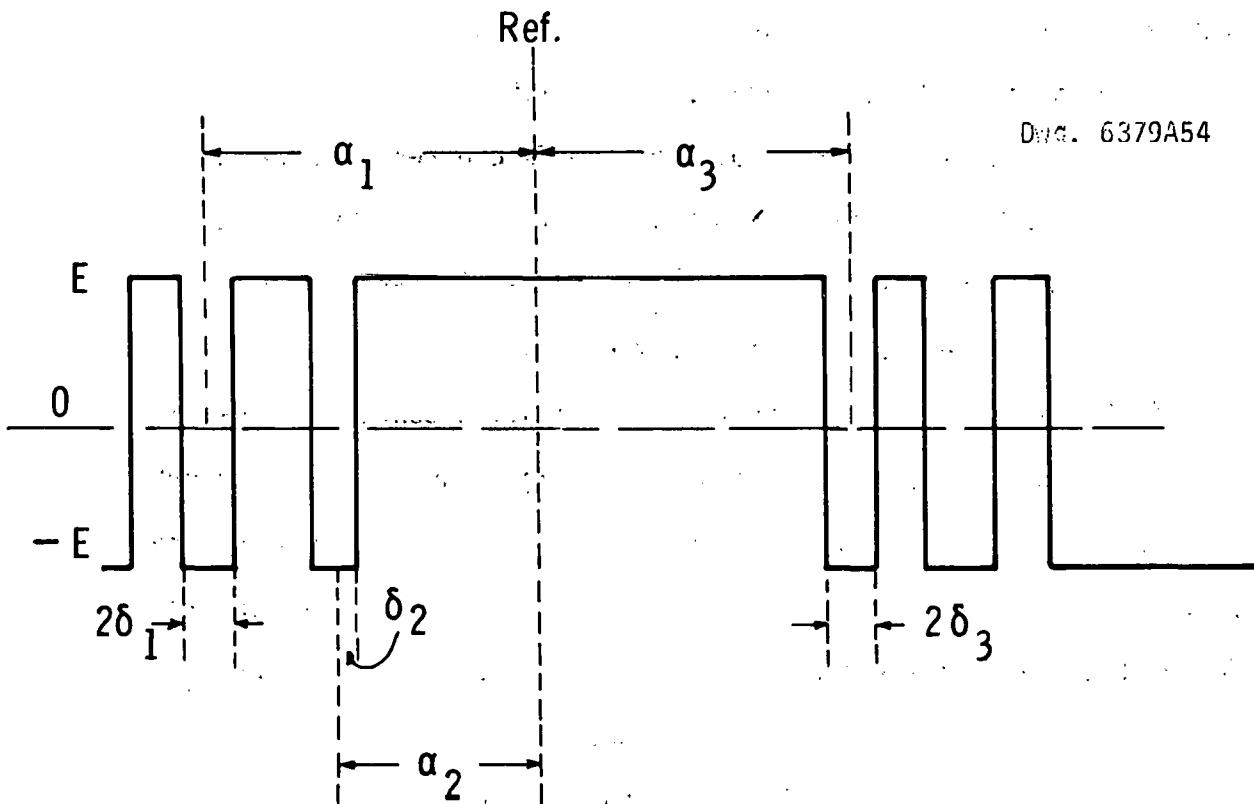
(1) eliminating the third, the "carrier" frequency is $3X$, and the 5th, 7th...can assume $3X$ their basic square wave amplitudes.

(2) eliminating 5th as well, the "carrier" frequency is $5X$, and the 7th, 9th...can assume $5X$ their basic square wave amplitudes.

(3) eliminating 7th as well, the "carrier" frequency is $7X$, and the 9th, 11th...can assume $7X$ their basic square wave amplitudes and so on. The fundamental is reduced from that obtained from a basic square wave by progressively increasing amounts.

Two things are evident from the above. First, in contrast to the results for PWM listed earlier, only components above the "carrier" frequency can possess enhanced magnitude; second, the cost in attainable fundamental is much lower for a given degree of low order harmonic removal, since the required "carrier" frequency is much lower. In view of the character of the inverter poles insofar as costs and losses go, this is a significant benefit. It should still be noted that filter size decreases rather slowly with increasing switching rate (and low order harmonic removal), leading to the suspicion that the optimum compromise between the two may occur at a relatively low switching rate. As previously stated, except for very simple pulse patterns involving low switching rates and neutralization of only one or two harmonics, computer assistance must be called on in determining the proper combinations of α 's and δ 's to effect any given end.

Opting to use this approach, and to use either dc regulation or phase shift between two inverter poles for voltage control, analysis revealed that the optimum balance between output filter size and switching rate (output waveform with no more than 3% of any harmonic deemed adequate) occurred for the latter equal to 5X, i.e., with 3rd and 5th only neutralized. This happens because a simple pulse pattern neutralizing 3rd and 5th harmonics, shown in Fig. 1.7.4, also substantially reduces the 7th and 9th harmonics and leaves the 11th as the dominant, filter determining component. Increasing the switching rate to neutralize the 7th causes the 9th to become dominant and actually increases the filter size required. Increasing switching rate further to eliminate



$$2\delta_1 = 12 \text{ degrees} = 2\delta_3 \quad (\alpha_1 = 90 - \delta_1 = \alpha_3)$$

$$\alpha_2 = 54 \text{ degrees}, \quad \delta_2 = 6.32 \text{ degrees}$$

$$\begin{aligned} \text{Fundamental Amplitude} &= \frac{4E}{\pi} \left\{ 1 - 4 \sin^2 \delta_1 - 2 \cos \alpha_2 \sin \delta_2 \right\} \\ &= \frac{4E}{\pi} \times .827 \end{aligned}$$

Fig. 1.7.4 - Pulse pattern selected

the 9th causes no reduction in filtering from that needed when only the 3rd and 5th are neutralized, and further increases in switching rate add more cost and loss than reductions in filtering can offset.

With the inverter parameters established thus we find a minimum dc voltage of 260V is needed to interface directly with the 220V ac line (assuming a maximum line voltage 5% high), when the slight voltage magnification caused by the output filter is taken into account. Thus the maximum voltage would be about 400V dc, using a lead-acid battery for energy storage. The economic contest between a dc chopper-regulator feeding a "constant voltage" inverter, and inverter poles phase shifted for output voltage regulation was won, albeit rather narrowly the margin being only about 10%, by the phase shifted inverter pole approach despite its requiring a center-tapped auto transformer to produce the 110V split phase output required. The efficiency contest was also won by the phase shifted pole approach, equally narrowly, and both these factors coupled with its better reliability and reduced complexity indicated the choice of the configuration depicted in Fig. 1.7.5 as best for the application.

Once the configuration is accepted, there remains only the determination of inverter pole designs. The wide variety of commutating circuits which might be used fall into two major classes:

(1) auxiliary impulse commutated, requiring the use of switching devices other than the main load bearing thyristors to effect commutation. An example is depicted in Fig. 1.7.6.

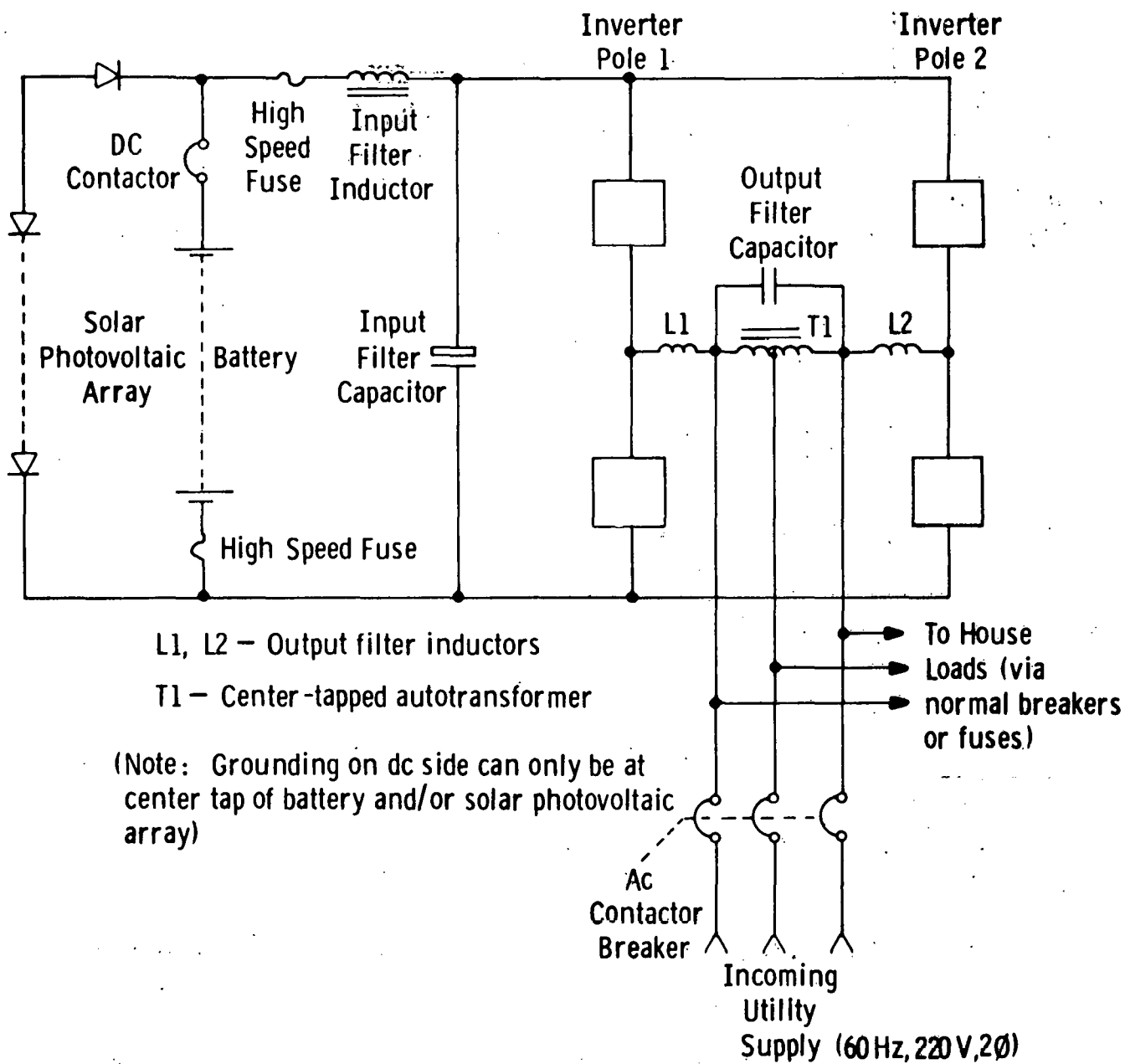


Fig. 1.7.5 – Proposed residential system configuration

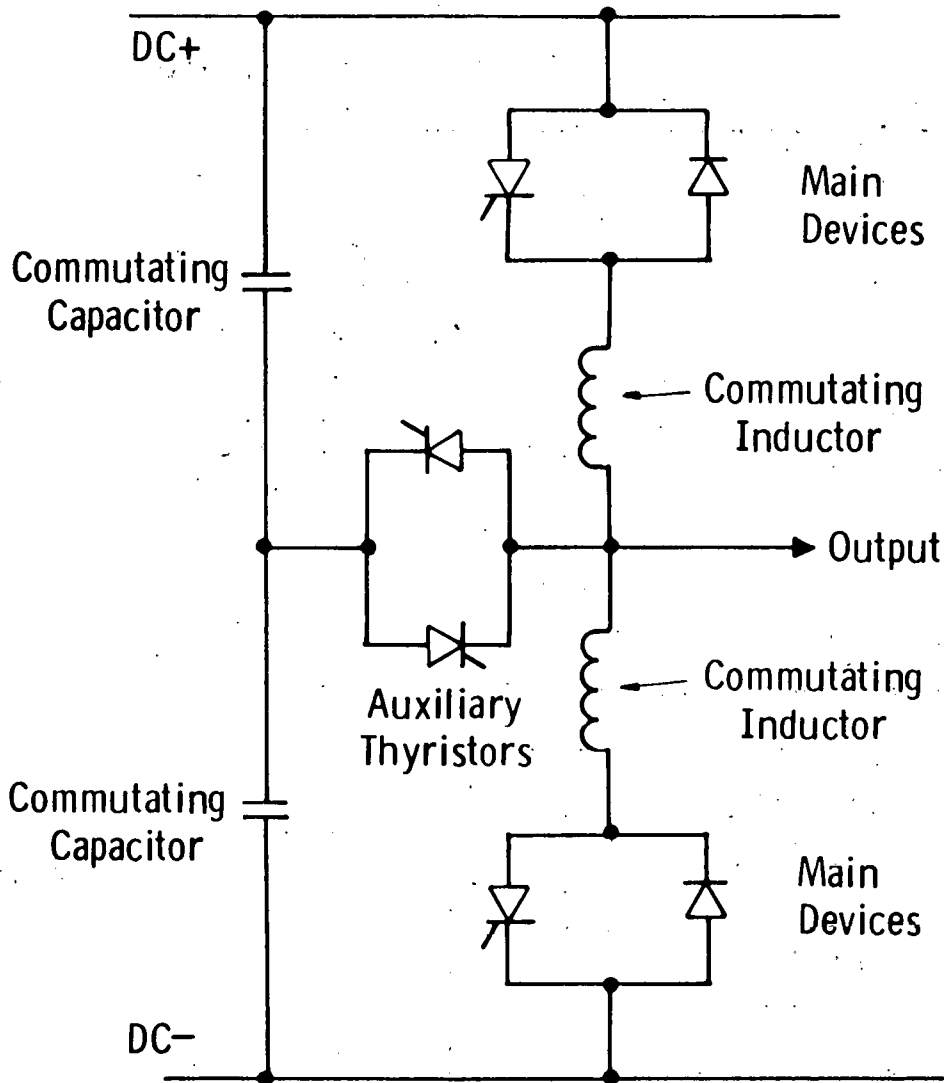


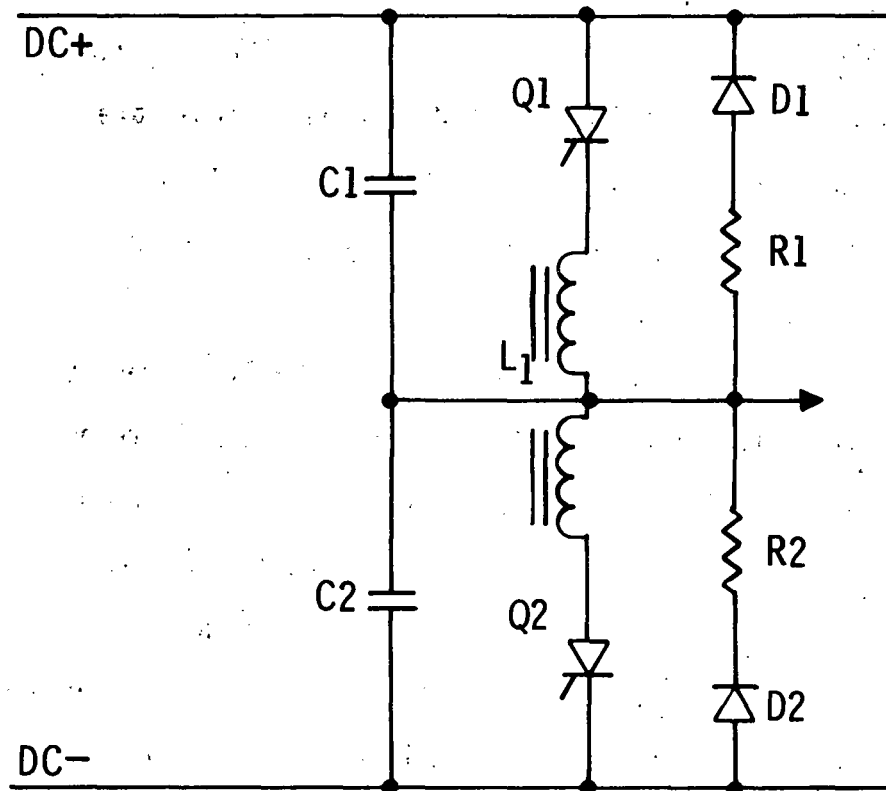
Fig. 1.7.6 – Possible auxiliary impulse commutated inverter pole

(2) auto-commutating poles, in which one load bearing switch is commutated off by switching on another. An example is depicted in Figure 1.7.7.

There exists a third class of inverter poles which may be described as "resonantly commutated" in which the load bearing switches are turned off via a "natural" reversal of current therein. This class is considered both too expensive and too inefficient at 60 Hz or low multiples thereof.

Auxiliary impulse commutated poles suffer, as compared to autocommutating poles, from their complexity, which obviously tends to increase cost and decrease reliability. They benefit, as compared to auto-commutating poles, from smaller passive commutating components, generally lower losses and substantially shorter turn-around times (turn-around time is defined as the minimum permissible interval between successive commutations). The point of cost balance between the two types is a function of switching rate and device recovery time requirements. For the 300 Hz rate here predicated, it occurs for a device with t_q somewhere between 5 and 10 μ S. The auto-commutating pole is never as efficient as an auxiliary impulse commutated pole can be, given the same devices in each.

Thus in designing today, we would inevitably select an auxiliary impulse commutated pole as being both cheaper and more efficient with available thyristor t_q 's of 10-15 μ sec at the 800-1000 volt (voltage safety factor of at least 2) /15.2 amps rms (at 5 kW inverter power) device requirements.



C1, C2 – Commutating capacitors

L1 – Center-tapped commutating inductor

Q1, Q2 – Main thyristors

D1, D2 – Main diodes

R1, R2 – Resistors dissipating trapped energy

Fig. 1.7.7 – Possible auto-commutating inverter pole

Looking into the future, with 5 μ sec devices we probably still choose this configuration because its slight cost disadvantage is counterbalanced by its substantially better efficiency. Only if t_q drops to about 2 μ S (or less), can we develop sufficient cost margin for the auto-commutating pole to consider that its lower efficiency can be tolerated.

Figure 1.7.8 shows anticipated selling prices for 5, 10, 15 and 20 kW inverters using auxiliary impulse commutated poles with devices having t_q 's of 15, 10, 5 and 2 μ sec, with today's manufacturing approach. Figure 1.7.9 shows how volume manufacture would affect these costs, for the 2 μ sec device which we presume will be or can be made available in 1985, and also how an auto-commutated pole will affect pricing. Table 1.7.1 shows the full load efficiencies anticipated.

Table 1.7.1

Calculated Full Load Efficiencies

<u>Power Rating</u>	<u>15 μS Aux-Com.</u>	<u>2 μS Aux-Com.</u>	<u>2 μS Auto-Com.</u>
5 kW	92.6%	93.1%	89.4%
10 kW	92.4%	92.8%	89.2%
15 kW	93.2%	93.5%	89.9%
20 kW	93.5%	93.8%	90.3%

All force-commutated, voltage fed inverters exhibit relatively poor efficiencies at part load because of the "fixed" contribution from the commutation process. The higher the switching rate and the longer

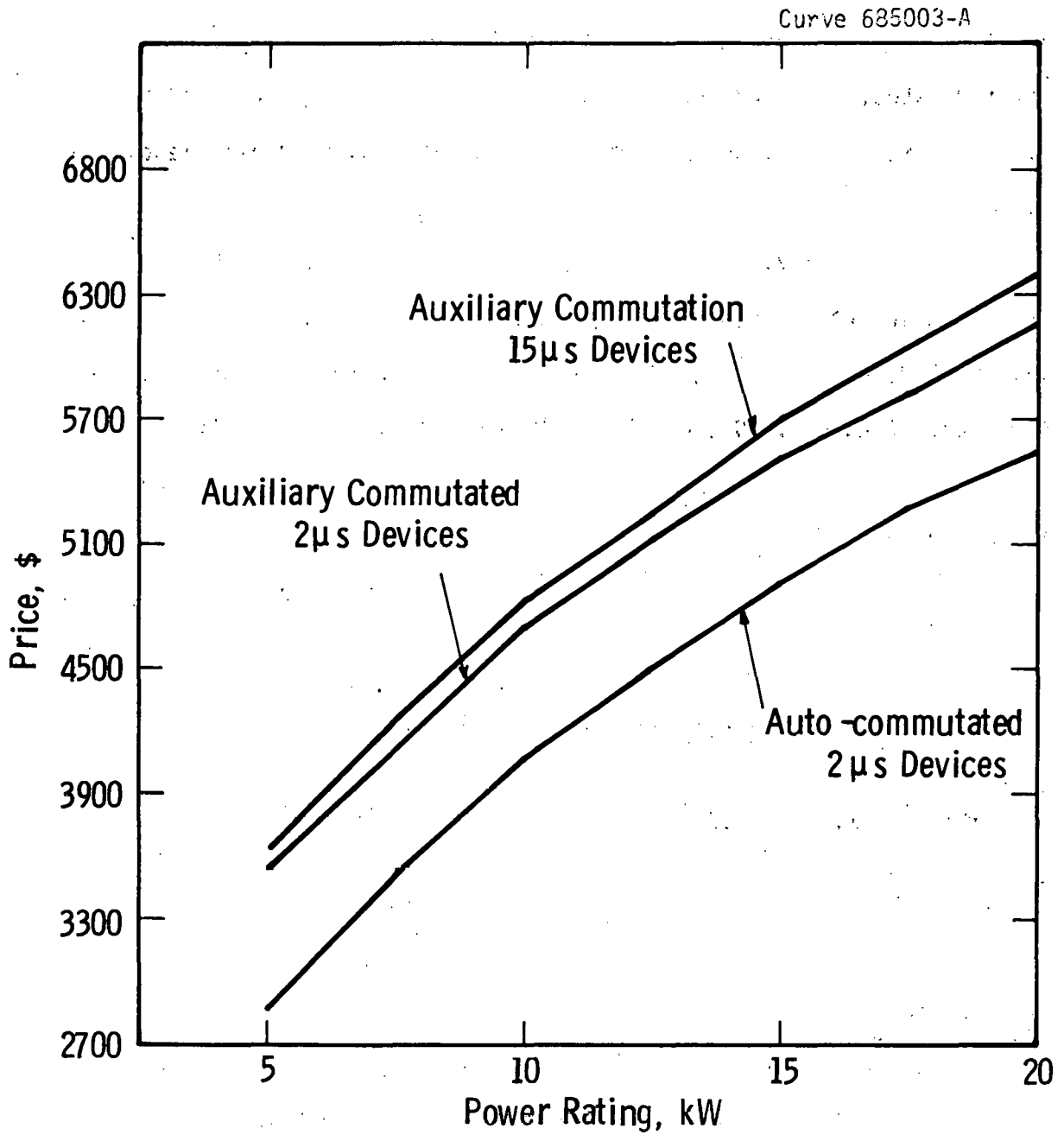


Fig. 1.7.8 — Estimated selling prices; 1975, in modest volume (1000' s)

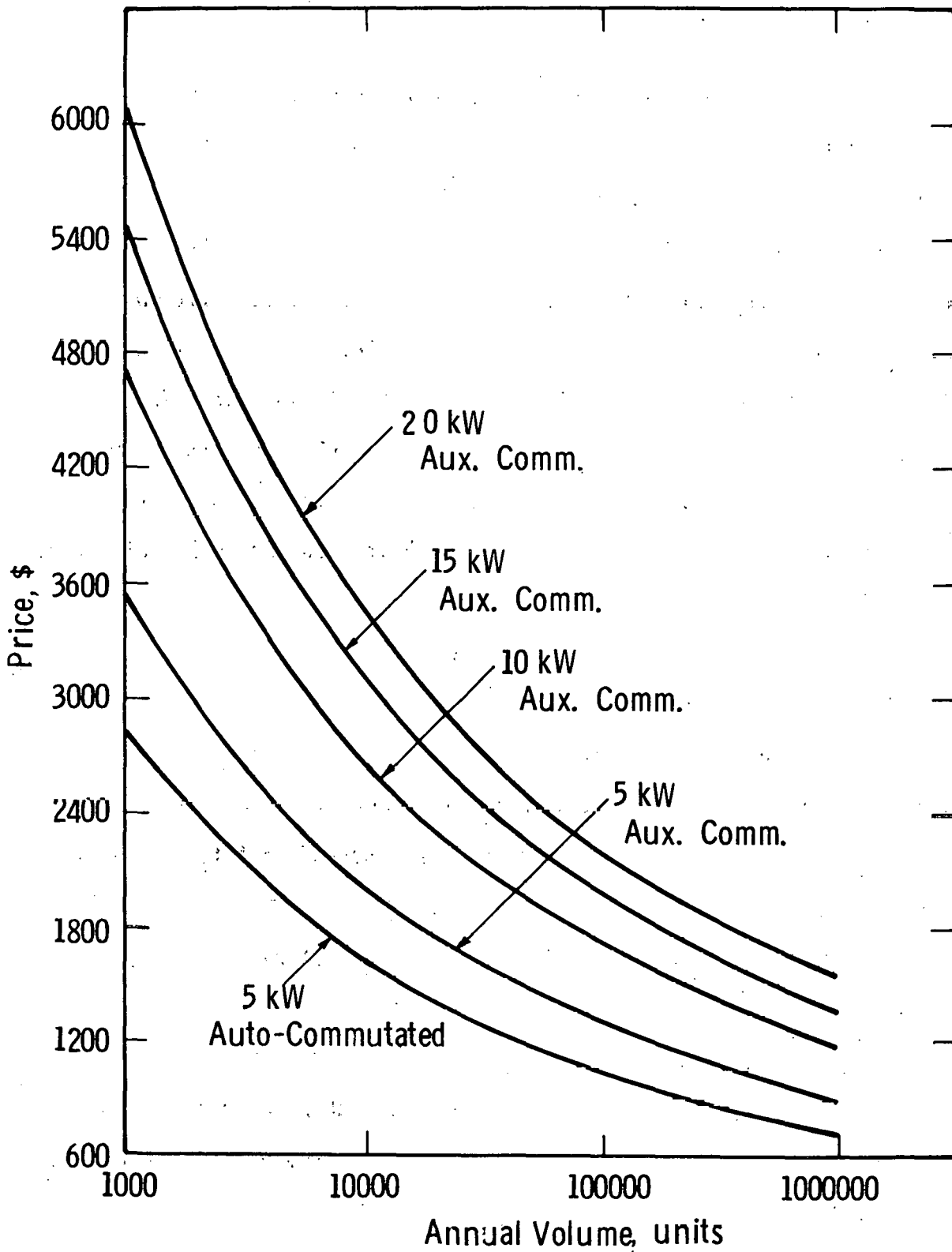


Fig. 1.7.9 - Anticipated selling price versus annual volume

the device t_q , the more pronounced this behavior becomes (and of course, it is worse for the relatively high loss auto-commutating poles than for those auxiliary commutated).

Typically, of the 7% average full load loss of auxiliary commutated poles with 15 μ S devices, some 1% is a fixed commutation loss, 3% active device loss and 3% " I^2r " loss. Thus we can estimate a loss at 50% load of approximately 6-1/2% and at 25% load of 9.75%, figures which are not too discouraging. For the 2 μ S auto-commutating pole, the 10% average loss is 4% commutation, 3% device and 3% " I^2r " and estimates of approximately 12.5% loss at half load and 19.75% at quarter load are obtained - figures which give considerably more cause for concern.

The costs in Figs. 1.7.8 and 1.7.9 indicate that little benefit is obtained from improving device technology unless the significantly higher losses inherent in auto-commutating poles are accepted. In the light of this, it should be observed that t_q is not the only parameter which must improve for these gains to materialize - dV/dt and dI/dt capability must both increase at least as fast as t_q decreases, else it will prove impossible in practice to utilize the increased speed of the device. In the comparison made, we have assumed such simultaneous improvements, coupled with no degradation of forward drop and thermal resistance parameters from those in today's 15 μ sec devices.

There are, as we had anticipated, relatively small increases in absolute cost as one progresses from 5 kW to 20 kW rating, with

20 kW costing less than twice as much as (i.e., exhibiting a specific cost less than 1/2 that of) the 5 kW designs. This fact points up the desirability of establishing large volume manufacture of a single type of inverter for the application, and strongly suggests that the most acceptable solution to the various power needs exhibited in residential systems may well be an adoption of single design satisfying all even though it is over-sized for many.

The estimated sizes and weights for the designs considered are given in Table 1.7.2. We see that as was the case for cost, size and weight are not linear functions of rating. These estimates are based on inverters using 15 μ S (present day) thyristors and would not change significantly with the use of faster devices, including the application of 2 μ S devices in auto-commutating poles. As can be seen, neither the volumes nor the weights should present any significant problems regarding application.

Table 1.7.2

Calculate Weights and Volumes

<u>Rating</u>	<u>Weight, lbs.</u>	<u>Volume, cu. ft.</u>	<u>Probable Cabinet W x D x H, ft.</u>
5 kW	269	8.6	2 x 2 x 2.5
10 kW	368	17.0	3 x 3 x 2
15 kW	438	21.7	3 x 3 x 2.5
20 kW	501	25.9	3 x 3 x 3

Fault clearing normally presents some problems with voltage-fed, self-commutated inverters. The commutation capability designed in must be sufficient to handle load faults, else there will be an unacceptable rate of commutation fault occurrence. Commutation faults, when they occur, must obviously be cleared on the dc side. This calls for forcible interruption of dc fault current with, in general, a very high peak value and a very rapid rate of increase toward that value. Conventional electro-mechanical switchgear of any size is totally unable to meet the demands of this situation. Electronic switching can be employed, but suffers from economic disadvantages -- it is expensive, introduces additional losses and is itself prone to commutation failure, a factor which forces the designer to provide a positive back-up system anyway. Fusing, with high speed current limiting elements, is viable protection provided that the inverter's commutation capability is adequate for riding through or shutting down on, all load faults.

When fusing is selected as the primary protection mechanism, human intervention is required to restore service following a commutation fault. In view of the fact that a properly designed inverter will not experience such faults except as a result of equipment malfunctions or component failures, this is not an unreasonable requirements. The cost of high speed fuses is now somewhat high, and as currently fabricated, they do not lend themselves well to replacement by unskilled personnel. However, adaptation for consumer use, perhaps including the development of suitable safety interlocks, should present no problems.

A summary of the results of the RPS power conditioning system including estimated costs for 5, 10, and 20 kW units at various levels of manufacturing volume is shown in Table 1.7.3. Included also are full load efficiency, weight and size.

Table 1.7.3

RPS Power Conditioning

<u>Power</u>	<u>Price (1975 \$)</u>		<u>Efficiency</u>	<u>Weight</u>	<u>Size</u>
	<u>1000</u>	<u>100,000</u>			
5 kW	\$600/kW	\$180/kW	89 - 92%	269 lb	8.6 Ft ³
10	\$450/kW	\$120/kW	89 - 92%	368 lb	17.0 Ft ³
20	\$300/kW	\$ 75/kW	90 - 93%	501 lb	26.0 Ft ³

References

1. W. R. Bennet, "New Results in the Evaluation of Modulation Products", Bell System Technical Journal, Vol. 12, April, 1933, pp. 228-243.
2. H. S. Black, "Modulation Theory", Chapter 17, pp. 266-276, Van Nostrand Co., 1953.
3. S. R. Bowen and B. M. Bird, "Novel Approach to the Analysis and Synthesis of Modulation Processes in Power Converters", Proc. IEE (London), Vol. 122, No. 5, May, 1975.

1.7.2 Intermediate Power System

1.7.2.1 General Considerations

The lowest cost power conversion equipment for any particular installation is achieved by a custom design made specifically for that location. However, this is not an attractive overall approach, largely because of the number of installations predicated, and because we seek a "modular" power conversion technique. In view of the span of installed power contemplated, from 100 kW to 10 MW, a single product line does not appear feasible to cover all usage, although a common technology would undoubtedly be employed. Hence the sample design for a 1 MW installation does not represent what would be done for lower power applications, from 100 kW to 500 kW, which would use smaller modules; nor does it embrace the higher power installations, say for 4 MW to 10 MW, which would use higher power modules.

At the interface with the utility, parallel tie operation will be the dominant mode even for those installations where isolated operating capability is deemed desirable, or even mandatory. Thus similar constraints on operating power factor and harmonic injection pertain here as they do to the central station. In fact, the generally more uncontrolled geometry of the ac distribution and the close proximity of sensitive loads at an intermediate size installation make elimination of potential EMI causing components more pressing in this case. Also, we face utility voltage variations and transients of the same order as those seen by the central station.

The harmonic injection requirements, therefore, call for 12-pulse inverter operation (i.e., fabrication of an output wave which before filtering contains no harmonics of order less than 11). The significance of conventional passive component costs in the total price of power conversion equipment makes it imperative that we minimize such costs at the ac interface. If possible, we would prefer to operate transformerless into the local 440/480, 3 phase, 60 Hz network, but cannot do so without extensive inverter complications if 12 pulse operation is needed. However, a phase shifting autotransformer can be used to minimize interface costs and deliver the proper sets of line voltages for a 12-pulse inverter. The phase shift required is ± 15 degrees electrical, so that the inverter line voltages become nominally 540 volts when connecting to 440 volt distribution.

The inverters to be used for the basic conversion required could, in principle, be any of a number of types. However, considerations of cost, losses (particularly at part load), and conventionality lead us to conclude that a current-fed, line-commutated approach is the lowest cost where isolated operation is not planned.* Should isolated operating capability be required, the premium paid for this when using a current-fed inverter is substantial, and a voltage-fed, self-commutated inverter becomes the preferred approach.

* A complete discussion of inverter types and tradeoffs is presented in Section 1.7.3.

For the power range involved in the IPS, to employ a refrigerated liquid cooling system for the inverter is not economic. For most of the range, 100 kW to 4 MW, forced air cooling of the active power semiconductors should be employed. From 4 MW to 10 MW, assuming individual module sizes of 1-1/2 to 2 MW, liquid cooling with direct heat exchange to ambient air is the cheapest approach, but the cost margin over forced air is not great and we could consider air cooled design throughout.

At the dc interface, the presence of both the battery and solar array must be considered. The battery will in general only be charged from the utility line (i.e., when array power is available, it will all be delivered to the line because the cost of power from conventional sources is greater during the day than at night). When there is a need to use the battery in its discharge mode, maintaining proper array matching is not important. This permits the use of very simple power conversion configurations in which the inverter is also used as the battery charger. The battery, when connected for either charge or discharge, is placed in direct parallel connection with the array as shown in Fig. 1.7.10. A protective diode, which may be internal to the array, is used to prevent delivery of charging energy to the array.

When using a current-fed inverter, which is a two quadrant device with unidirectional current and bidirectional voltage capabilities, dc reversing switchgear is required to allow both charge and discharge of the battery. This can be either electro-mechanical or solid-state. The latter holds a decided speed advantage and is marginally lower in cost

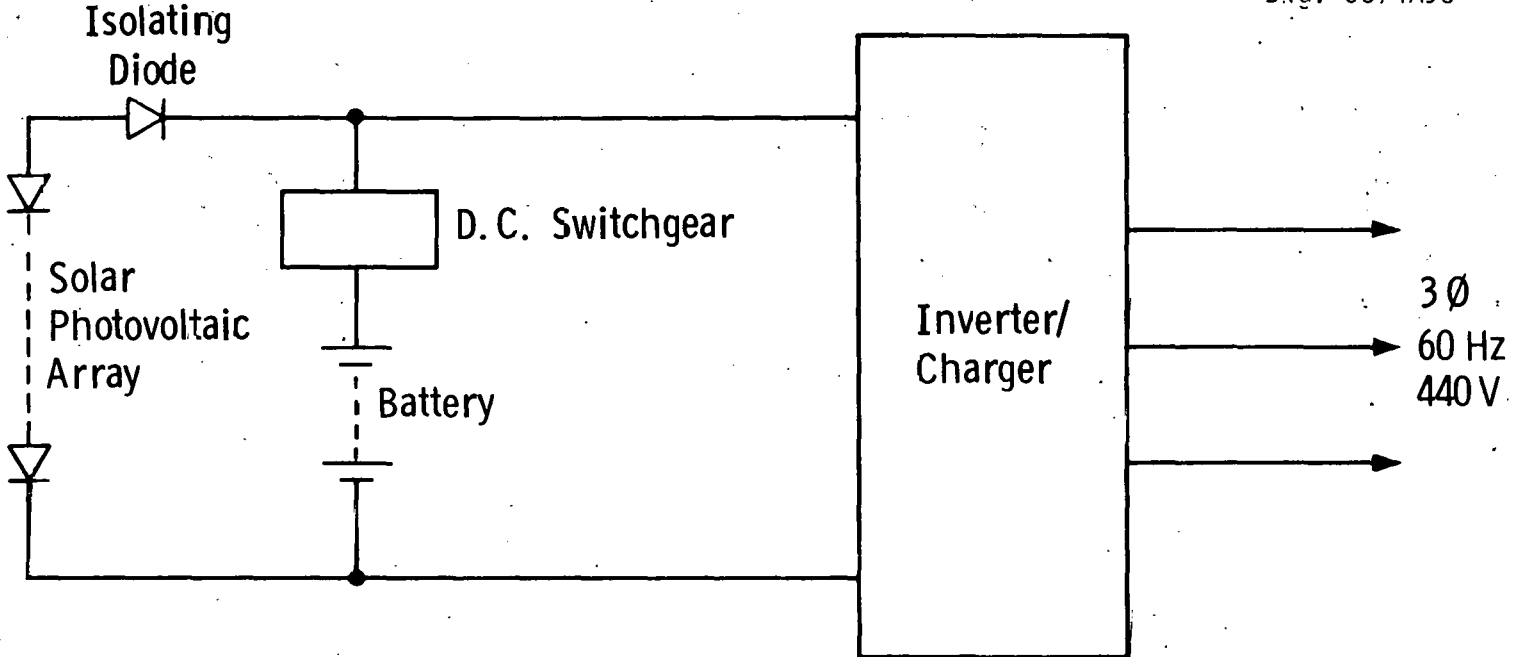


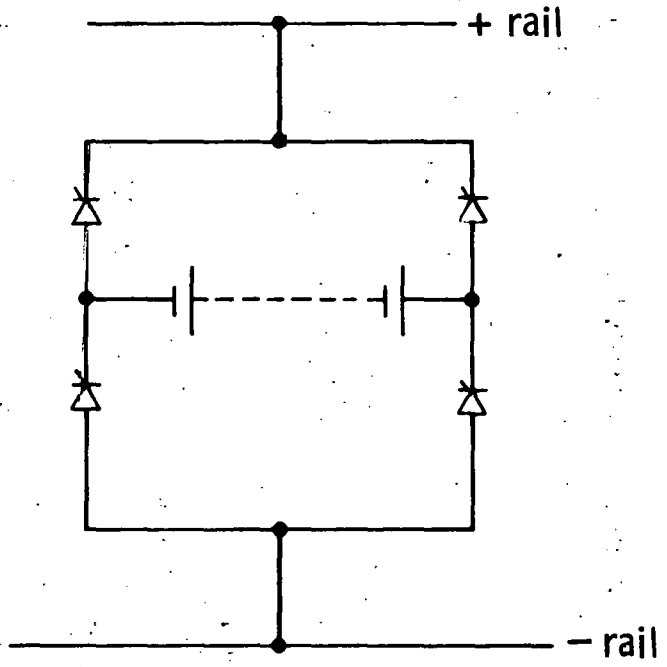
Fig. 1.7.10 – Basic power conversion arrangement, intermediate system

if a simple thyristor bridge configuration, depicted in Fig. 1.7.11(a) is used. Bearing in mind that a high speed dc interrupter is needed to clear inverter commutation faults, and that this device can be used to quench the battery current at any time, the solid-state interrupter arrangement is both viable and preferred.

Where a voltage-fed, self-commutated inverter is employed, no dc reversing switchgear is needed, only a simple battery isolating switch. This is because a voltage-fed inverter is a two-quadrant device having unidirectional voltage and bidirectional current capability. This isolating switch can again be either electro-mechanical or solid-state, the latter via an inverse parallel connected thyristor pair as depicted in Fig. 1.7.11(b). This is more expensive than the electro-mechanical single pole, single throw contactor by a factor approaching 2, and since operating speed would appear not to be a major consideration, we would in this instance favor the more conventional electro-mechanical approach.

As mentioned, there is a need for the high speed dc interrupting capability to contend with commutation faults when a current-fed inverter is used. With the introduction of the battery, the need is even more definite, for the low source impedance exhibited by lead acid cells makes it impossible to attempt "ride through" of a commutation fault without the use of prohibitively large and expensive dc reactor. Even the considerably higher impedances anticipated for high temperature couples do not significantly improve the situation -- they do not approach the current limiting inherent in the solar photovoltaic array.

a) Reversing and Disconnect Combined



b) Disconnect Only

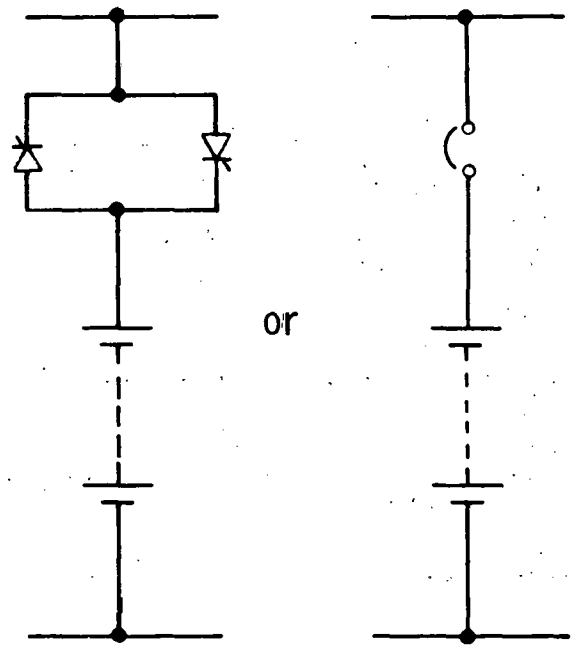


Fig. 1.7.11 – DC reversing and disconnect switchgear

For a voltage fed-inverter, high speed dc interruption can only be effected by interposing additional devices in the dc current path. Fortunately, in a properly designed and controlled system, commutation failures should be infrequent, being related to equipment malfunctions and/or component failures rather than to utility voltage transients. Therefore, high speed fusing will be considered as a viable means of protection for voltage-fed inverters.

The possibility of EMI emanating from the solar arrays in the intermediate size installations is a concern as it is for the central station case. Both current-fed and voltage-fed inverters are prolific generators of ripple currents at their dc terminals; however, the latter are the worst offenders. Avoiding the delivery of these harmonics to the array panels, which can prove to be very effective antennae, may present a formidable task. Passive filtering may prove overly costly -- it is difficult to determine whether this is indeed so until a more precise characterization of solar array and dc bus work ac impedances is available -- and active filtering, while deemed possible, presents significant technical difficulties and would require a substantial development effort for successful implementation.

On the ac side, we are concerned with EMI because we view the low voltage ac distribution to which we tie as being not physically entirely under our control. Furthermore, harmonic sensitive loads will be directly connected to this distribution network. Here, active filtering does not offer a readily feasible technical solution, and passive filtering seems to be the only approach available. Fortunately,

no part of the ac network is required to carry unfiltered inverter current, a fact which does help the situation.

There is considerable uncertainty regarding the best long-term power conversion technology for the IPS. In particular, fast switching device improvements which can reasonably be predicted (switching speed and/or blocking voltage upgraded by factors of 1.5 to 2) will make the voltage-fed, self-commutated approach economically superior to the simple current-fed technology, and will improve its efficiency sufficiently to offset its inevitably worse part load efficiency. Further, it is likely that other applications in this power range will cause development of both complementary current-fed inverters and HF base power conversion equipment which may prove superior to either inverter approach so far discussed. Also, the impact of semiconductor device improvements on equipment cost is likely to be more marked at these intermediate system power levels than in the central station, since the active circuitry represents a higher fraction of total cost. Note that in neither case, central station nor intermediate, are reductions in semiconductor prices considered likely to affect future power conversion costs significantly. This is because inverter cost, defined as the cost of active circuitry, is a much more pronounced function of both device performance and the required number of devices than it is of the price of individual devices.

So far, we have discussed only the simplest basic power conversion approaches for the IPS. With the restrictions on operation previously established, i.e., charging the battery only from the utility and allowing solar array mismatch when the battery is discharged, they

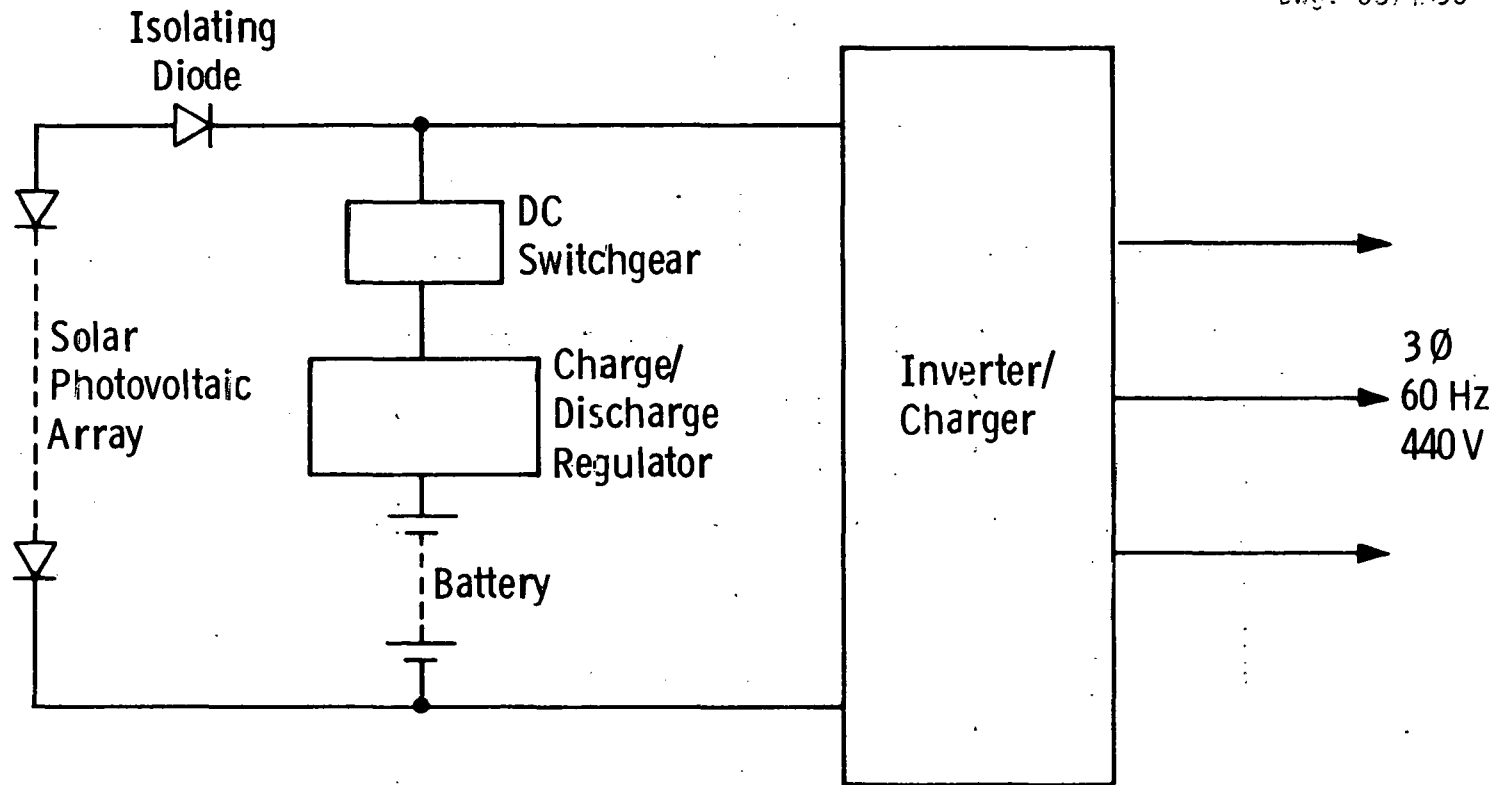
are the preferred approaches. Should it be necessary or desirable to remove either or both of these restrictions, then it is necessary to make the power conversion equipment more complex and more expensive.

Both restrictions can be removed by inserting a charge/discharge regulator between the battery and the inverter-solar array interface as shown in Fig. 1.7.12. This regulator could take the form of a dc chopper, but if it does, there are two detrimental factors. First, reversing switchgear is required at the battery regardless of the type of inverter used. Second, the cost premium is approximately one-half of the inverter cost.

A lower cost approach is to make the charge/discharge regulator a line commutated converter/inverter. The cost premium is still substantial, however, (about 2/3 that for the chopper) and reversing switchgear is still required. This approach does not mate as well with a voltage-fed inverter, either, and is perhaps only marginally preferable where that is the power conversion approach used.

For both of these regulator configurations, the total power deliverable to the load when both battery and array are used as sources is inverter limited. Thus the only benefits gained for the very high cost premiums are to charge the battery with array power when desired and to minimize the use of battery energy when array power is available.

It appears that more system benefits result, despite further increased costs, by adopting the type of scheme shown in Fig. 1.7.13. Here the inverter is essentially duplicated, and battery charging from the array is indirect. However, such a scheme, costing 75-80% more than



346

Fig. 1.7.12 – Showing introduction of charge/discharge regulator

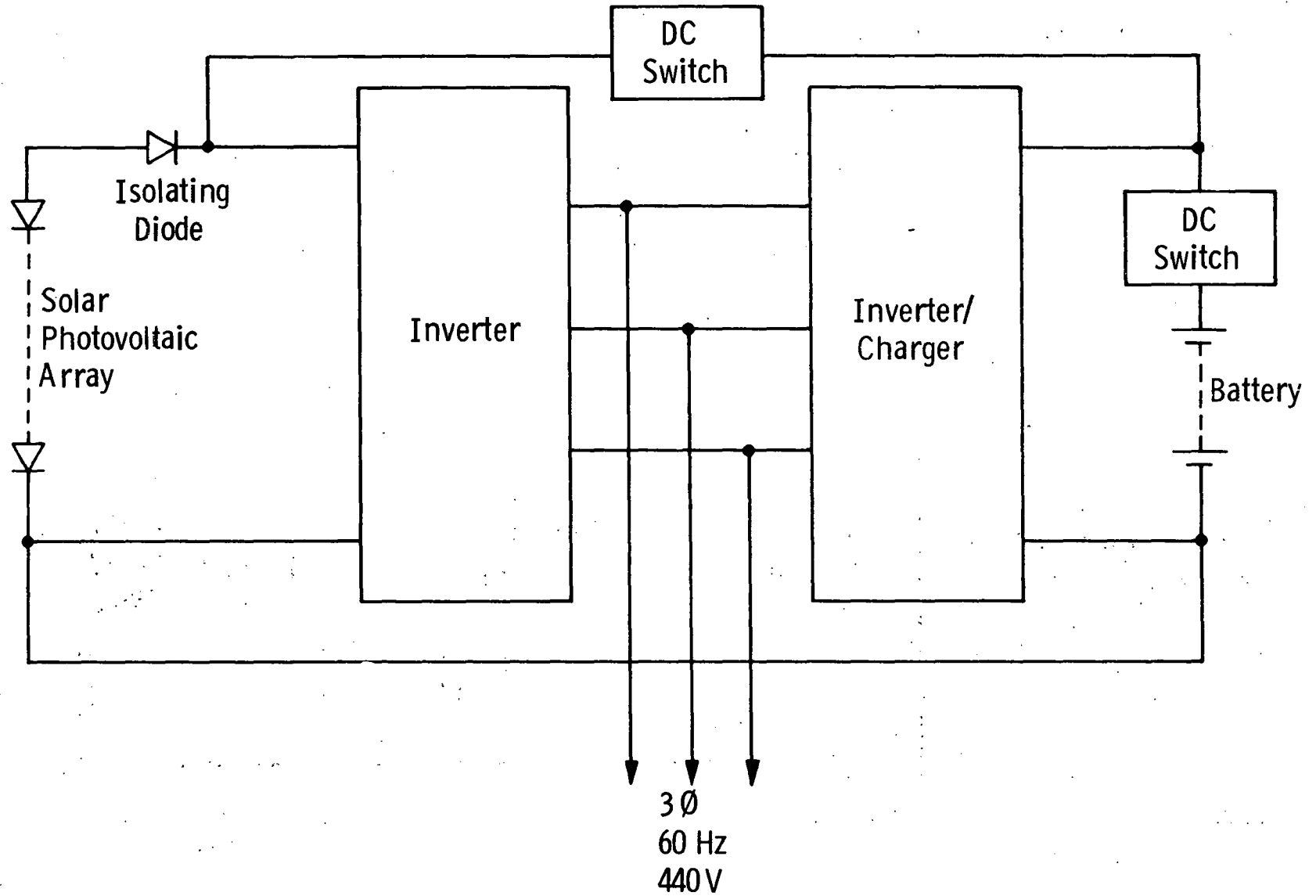


Fig. 1.7.13 – Double inverter/charger arrangement

the simplest inverter only scheme, permits both battery and array to jointly deliver maximum power to the loads when needed. Thus, at a relatively small cost premium over the arrangement shown in Fig. 1.7.12, substantial emergency operating benefits are obtained. In particular, the mixing of a voltage-fed inverter and a current-fed inverter/charger, using the former to support the reactive VA demands of the latter, affords considerable economies by eliminating major passive components at the ac interface while preserving full isolated operating capability. The permanent connection of the battery in this case may also significantly enhance its life, since charging would probably be at a slower rate and operation would be continuous (i.e., the battery would permanently float on the system).

Finally, the power factor correction needed for the simple current-fed approach must be considered. In the central station, conventional electro-mechanical switchgear was chosen to achieve the variation needed as inverter operating conditions change. At distribution voltages, the cost of solid state switchgear is several times (perhaps 4 to 5) that of vacuum or oil breakers. In the IPS, the output connects into 440/480 volt lines, and the switchgear required, being low-voltage high-current equipment, is only slightly cheaper than solid-state equivalents. The performance benefits obtained with solid-state switchgear, coupled with the strong possibility it will ultimately prove the lowest cost approach to capacitor switching at these low voltages, lead to the conclusion that while conventional switchgear is the best choice for the present, static switches are probably the best for future designs.

1.7.2.2 Sample Designs for a 1 MW Installation

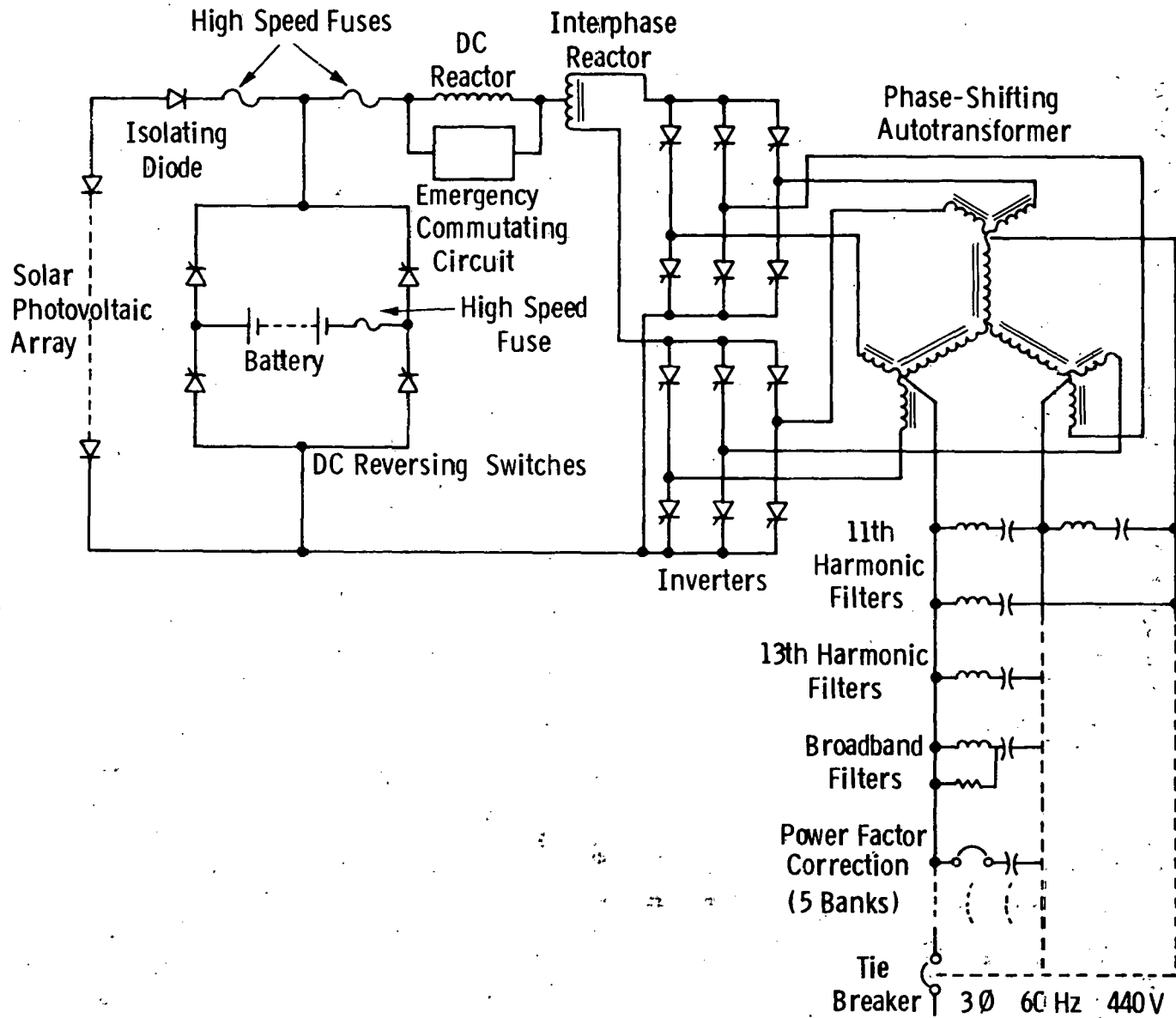
Current-Fed, Line-Commutated Inverter

An elementary schematic for this equipment is shown in Fig. 1.7.14. Two 500 KW modules are chosen for the 1 MW IPS, anticipating the use of these modules in other installations from 1 MW to about 4 MW in power rating. Each module is completely independent including its autotransformer. Power factor correction and harmonic filtering are applied to the total installation.

The battery and/or the solar arrays may feed both modules together or independently, as desired. It is slightly preferable to split the battery, from the conversion equipment's viewpoint, and avoid parallel connection of the reversing switches.

In each of the two 500 KW modules, the autotransformer produces two 3-phase voltage sets, mutually displaced by 30 electrical degrees, from the 440 volt bus. In so doing, the nominal line voltage applied to the inverter is increased to 540 volts by the "forked-Y" arrangement shown. Alternative autotransformer arrangements are the extended delta and closed polygon which give inverter nominal line voltages of 850V and 456V respectively; the former is not favored because of the large voltage transformation, the latter because it is a very unusual configuration in power transformers due to the very large difference between current levels in the main and branch windings.

A nominal inverter line voltage of 540V leads to a maximum dc voltage, in inverter operation, of 562.5V. This then is the peak loaded operating array voltage, and the corresponding minimum array operating voltage is 432.7V, using the ratio of 1.3 previously established.



350

Fig. 1.7.14 - Elementary schematic of current-fed power conversion arrangement

These values are obtained using a minimum extinction angle of 15 electrical degrees at 0.8 X nominal line voltage in the inverter design.

For 1 MW to be delivered at minimum voltage, the dc current required is 2311 amps, i.e., 1155 amps per 500 kW module or 578 amps per bridge. The 193 amps average required per device is easily attained using T7 (33 mm) devices with forced air cooling. By using voltraps of appropriate rating at the 440 volt intertie, the inverter device blocking voltage requirements can be held at 1600 volts, again readily obtainable.

On this basis, using a rectification end-stop of 10 electrical degrees, the equipment is capable of delivering charge to the battery up to 731 volts dc from an ac line at 95% of the 440 volt nominal, more than adequate for a stack of lead acid cells with discharge cut-off rated to the 433 volt minimum array voltage and still satisfactory if molten salt cells are projected.

The worst case operating power factor is about 0.5, so the required phase-shifting autotransformer rating is about 250 kVA (equivalent double wound transformer) per 500 kW module, and 1.7 per unit, or 1700 kVA per MW, of power factor correction is needed. Harmonic filters for the 11th, 13th and higher order components will supply about .58 pu or 580 kVA per MW with remainder furnished by 5 switched capacitor banks. Comparison of solid-state and electro-mechanical switchgear for these at present indicates the latter to be slightly lower in cost, and for the long term the static approach is preferred.

The high speed dc interrupter is a scaled model of that proposed for use with the central station inverters. However, the use of an electro-mechanical breaker as back-up would be prohibitively expensive for the intermediate system. Since the location is not remote from maintenance personnel, fusing is chosen as the back-up. Furthermore, fuses can readily be obtained with the requisite capabilities, whereas for the central station inverters, such devices do not exist.

The overall full load efficiency of this current-fed inverter approach, one-way, is calculated to lie in the range 94-95%; at part load, down to 20-25% of rating, it will maintain close to this level of one-way efficiency, but below about 20% load, the fixed loss contributions of device "threshold" voltages, snubber networks, control and gate drive power and magnetization losses in magnetic components cause a steady degradation in efficiency.

The total cost, in 1975 \$, of this approach designed strictly for parallel tie operation, is estimated at about \$128 per kW; the breakdown for the several major elements is as follows:

*Inverters	\$25.5/kW
dc Interrupter (Including dc reactor)	\$42.1/kW
dc switches	\$14.4/kW
Power factor correction and filters	\$26.4/kW
Transformers	\$16.4/kW
Breakers	\$ 3.1/kW

*Devices with heat sinks, snubbers, controls, etc.

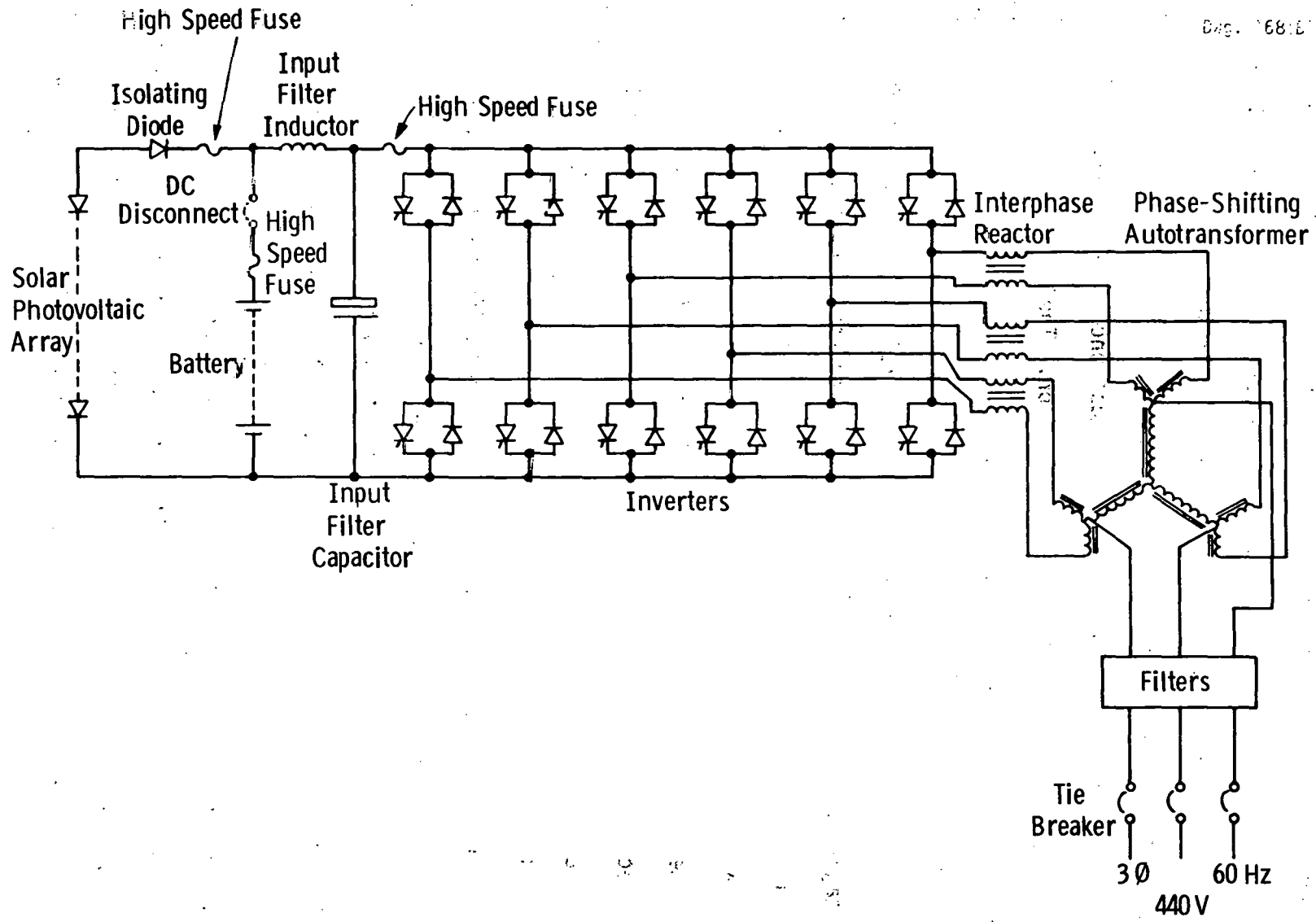
It is perhaps not generally recognized that a current-fed line commutated inverter is capable of isolated operation with appropriate additions to the output network and provision of means for starting. The design for parallel tie can be adopted for isolated operation into loads of no worse than 0.8 power factor by adding the capacitive VA required to compensate the load and by replacing the capacitor switching by a continuously variable (thyristor controlled) shunt reactor. Starting is achieved by adding temporary series capacitor commutation, which is switched out as the load/output network combination develops sufficient voltage for successful "line" commutation to occur.

The additional cost involved amounts to some \$31 per kW. With isolated operational capability then, the simple current-fed line commutated inverter cost estimate is increased to \$159/kW.

Voltage-Fed, Self-Commutated Inverter

This alternative, for which the schematic is shown in Fig. 1.7.15, calls for considerably more complexity in the inverter, but dispenses with the power factor correction and repetitive dc interrupting capability requirements imposed by current-fed technology.

There are three means of voltage control available for use with self-commutated inverters; the first, phase displacement of two inverters with phasor summation by series connection of transformer windings, mandates the use of double wound transformers and is, therefore, because of the cost of those items, dismissed for this application. The second, a method of control of the conduction angles of the main load bearing thyristors in the inverter, proved the most economic and was selected as



354

Fig. 1.7.15 – Elementary schematic of voltage-fed power conversion arrangement

the preferred technique. The third, pulse width modulation (of which the second method described may be considered the crudest example) permits a completely transformerless interface to the 440 volt ac line but nonetheless proved overly costly.

With conduction angle control, we must once more use phase shifting autotransformers for 12 pulse operation. Their rating is now only that required for power throughput, or some 125 kVA (equivalent double wound transformer) per 500 kW module.

The dc-ac voltage relationships are considerably different for the voltage-fed inverter than they are for the current-fed circuit. Connecting to the same nominal 540 volt lines produced by the phase shifting autotransformers from a 440 volt supply, requires a minimum array/battery voltage of 846.5 volts. Thus the peak full load array voltage becomes 1100 volts, and the peak battery charging voltage (using the same relationship as for the current-fed line-commutated scheme) is 1430 volts.

Thus, the dc current per 500 kW module is 590 amperes, 295 amperes per inverter bridge. The 98 ampere average current per device is easily handled by T6 (25 mm) devices using forced air cooling; at this size, devices with 25 μ s guaranteed recovery time can be obtained, but the present restriction of blocking voltage to 1200 volts calls for 3 devices in series for each switching position when commutation over-voltage and adequate safety margins are considered. While it is anticipated that the switch blocking requirement of about 3000 volts can ultimately be met by two series devices, it would be even more desirable if a single

fast switching silicon device with this capability would become available in the future.

The commutation circuit could take any one of a number of well-known forms. There is little variation between them in terms of overall economics, and we have chosen for the arrangement shown in Fig. 1.7.16 which is familiar to us and known to be competitive, both in price and performance, with its possible rivals.

The interphase reactors are a relatively minor item in the current-fed scheme previously described, but assume major significance in the voltage-fed design. They must supply, in addition to their harmonic supporting capability, the necessary line tie reactance. This impedance is needed for two purposes; first to ease the control of real and reactive current flow between the inverters and line by adjustment of inverter voltage phase and magnitude respectively, and second to provide the series arm of the harmonic voltage attenuating filters required with this type of inverter.

The final major system component in this scheme is the input filter capacitor. Voltage-fed inverters, particularly with conduction angle voltage control, impose very heavy ripple current demands on their dc sources. The demands in this instance are well beyond the capabilities of either the solar array or the battery to sustain without excessive joule heating. Further, if the source impedance to the ripple current is not low enough, serious disturbances of inverter operation (to the point of possible malfunction) can occur. Hence, the input capacitor bank is provided within the inverter to create an adequately low ac

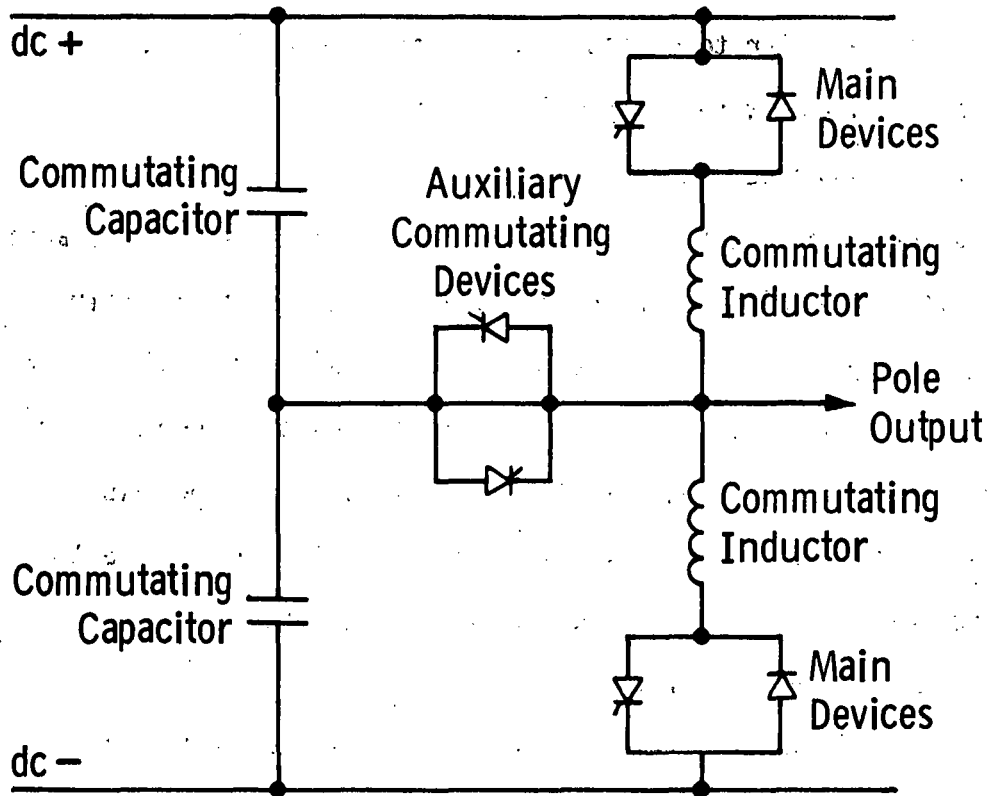


Fig. 1.7.16 — Possible voltage-fed inverter commutating circuit

impedance at the dc terminals and to divert ripple current from the dc source. It should be observed that economics forces the use of electrolytic capacitors in this position, and thus there is no effective filtering provided by the input capacitor bank for those ripple components of sufficiently high frequency to pose an EMI threat - these frequencies are well above the self-resonant frequency of large electrolytic capacitors.

The calculated full load efficiency for this system is about the same as for the current-fed approach, i.e., 94-95%. However, "fixed" losses are substantially higher in this instance because of the perpetual contribution of commutation circuit losses, and part load losses are much worse than for the current-fed scheme. Figure 1.7.17 shows typical efficiency versus load curves for both current and voltage-fed schemes.

The total cost for this scheme designed for parallel tie operation is estimated at \$137/kW (in 1975 \$). The self-commutated inverter has, of course, the inherent ability to operate in the isolated mode, but slight commutating circuit design changes are necessary for successful accommodation of load switching transients in the event of a "black start," and the premium for isolated operation is about \$5/kW.

The cost of the approach is proportioned to the major system components as follows:

"Inverters"	\$106.8
Interphase Reactors	11.4
Transformers	12.2
Output Filters	3.9
Breakers	3.1

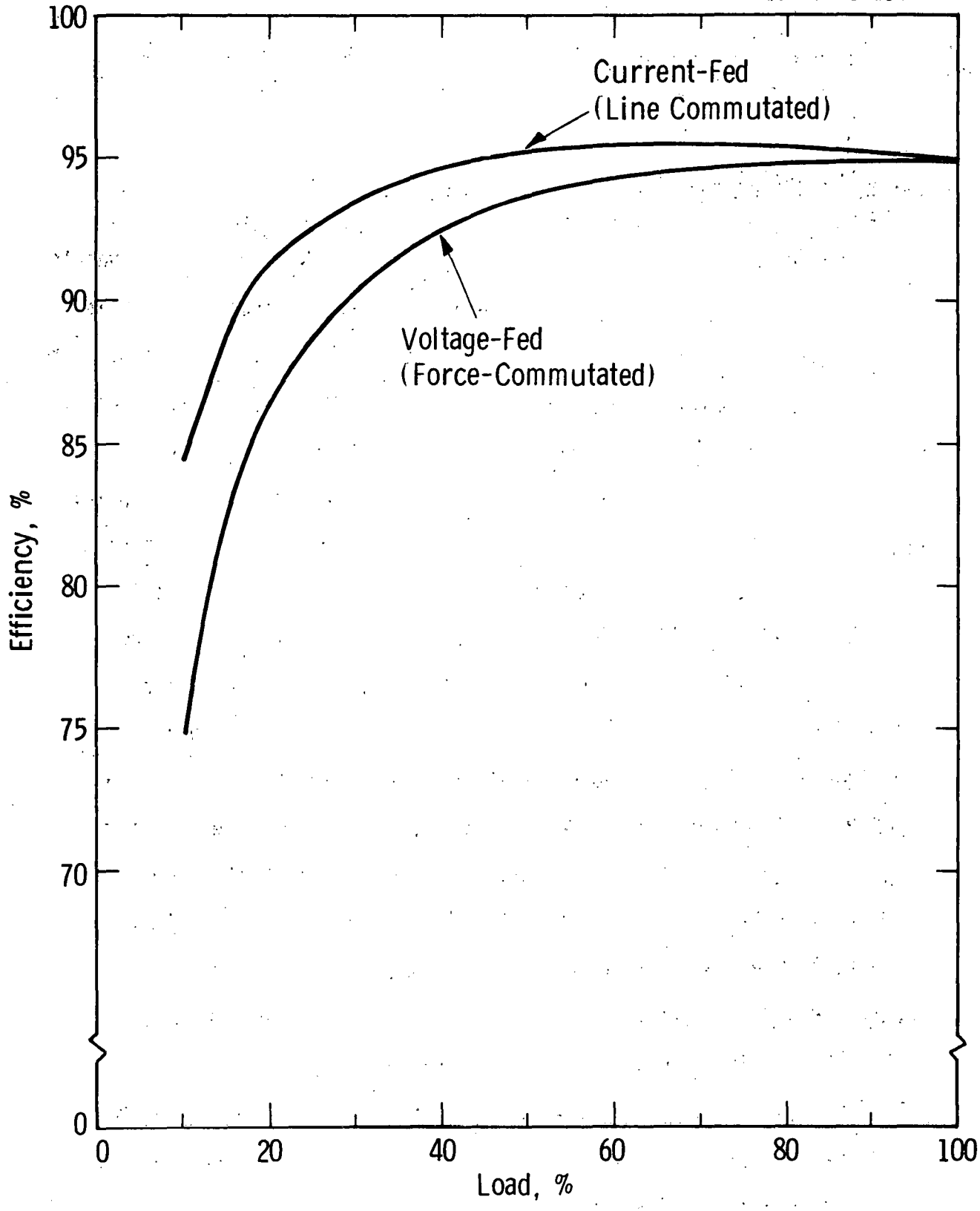


Fig. 1.7.17 - Calculated efficiency versus load for current-fed and voltage-fed inverters

The inverter costs break down into:

Main Devices with Heat Sinks, etc.	\$54.9
Auxiliary Commutating Devices	15.8
Commutating Circuit Passive Components	18.8
Input Filter Capacitors	9.8
dc Switch (for battery connection)	7.5

Voltage-Fed, Self-Commutated Inverter with Auxiliary Rectifier for Battery Charging

An elementary schematic for this arrangement is shown in Fig. 1.7.18. Because the inverter now sees only the array dc voltage variation, voltage requirements and costs are reduced. However, the added cost of the rectifier plus the increment in transformer costs more than offsets these reductions, and the total cost for parallel tie operation is estimated, in 1975 \$, at \$143/kW. The changes are:

- Inverters from \$106.8 to \$83/kW
- Rectifier and dc switchgear adds \$21.8/kW
- Transformers increase from \$12.2 to \$20.9/kW
- Interphase reactors decrease from \$11.4 to \$9.5/kW
- Filters increase from \$3.9 to \$4.6/kW
- Net increase \$5.5/kW

Double Inverter Scheme

This scheme is shown in block diagram form in Fig. 1.7.13. The voltage-fed inverter is run from the solar array only, and thus benefits from reduced voltage requirements. However, its volt-ampere rating is increased so that it can sustain the demands of the current-

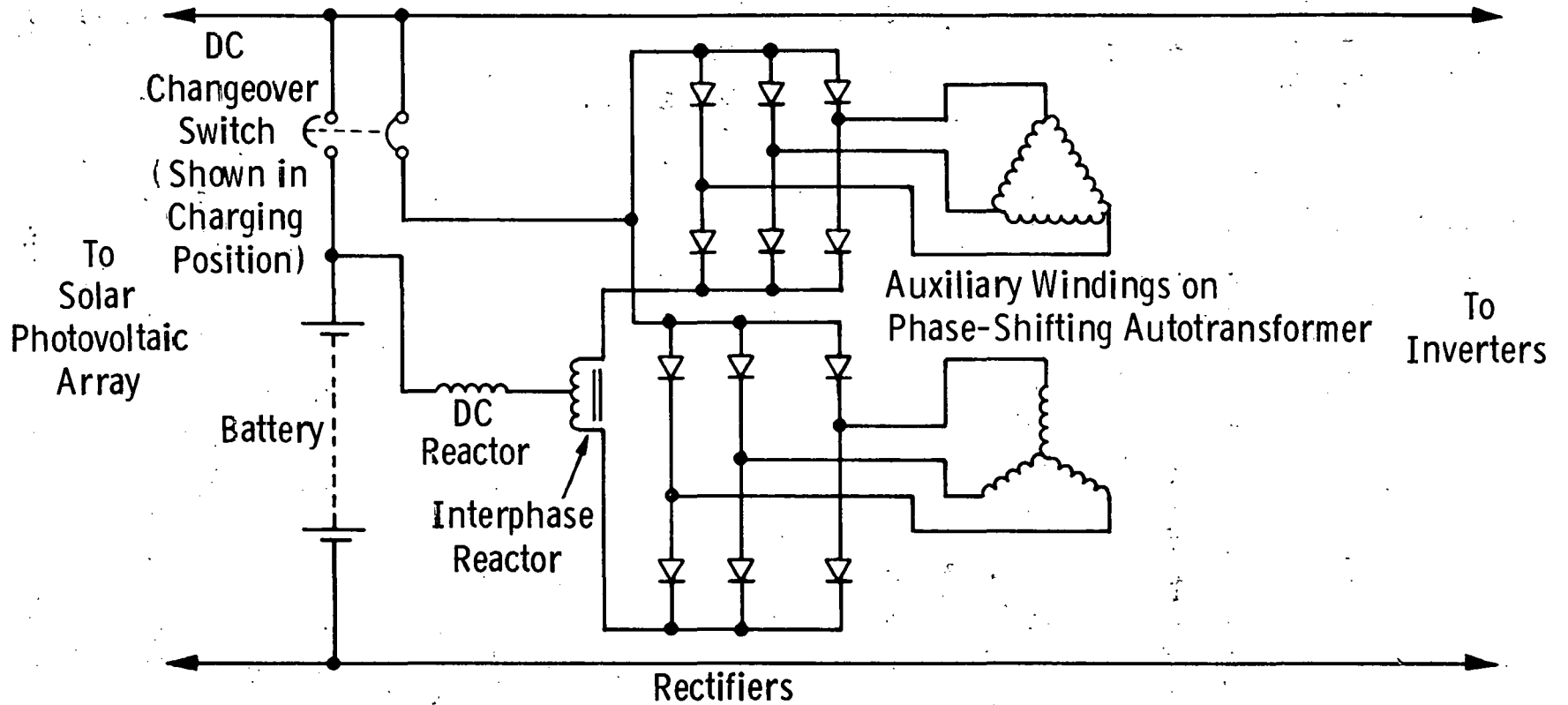


Fig. 1.7.18 - Showing addition of charging rectifier to inverter system

fed converter/inverter used to charge and discharge the battery. When array power is not available, the voltage-fed unit is connected to the battery (discharge mode only) in order to support the current-fed unit. Total cost is estimated as \$213/kW on the 1 MW base, but note that the system is capable of delivering 2 MW when both battery and array power are available and is capable of isolated operation. Hence, the premium of \$70-80/kW for such an arrangement over the simple power conversion schemes is paid primarily for enhanced emergency operating capability. There may be circumstances where this cost can be justified.

The cost breakdown for this scheme is:

Voltage-fed self-commutated inverter	\$83.5
Current-fed line-commutated inverters (including dc interrupter and switchgear)	83.3
Transformers	23.7
Interphase reactors	9.5
Breakers	3.9
Filters	9.1

A summary of the costs of the four inverter approaches discussed is shown in Table 1.7.4.

Table 1.7.4 -- IPS POWER CONDITIONING SUMMARY

500 kW Modules

Cost includes Inverter, dc Interrupter, dc Switch, PF Correction
Cap. and Filters, Transformers, ac Breakers

	(1975 \$)
1. Current-Fed, LC Inverter	\$128/kW
2. Voltage-Fed, SC Inverter	137
3. Voltage-Fed, SC Inverter with Aux. Batt. Chg.	143
4. Double Inverter (Twice Capacity)	213
Full Load Efficiency	95%

1.7.3 Central Power System

The CPS comprises a number of inverter substation modules with dedicated array areas surrounding each inverter substation unit. The outputs of these units (17.6 MW per unit) are transmitted through a subtransmission network to a single CPS transmission substation. At this substation, the outputs of all inverter modules are combined and the voltage transformed to the required transmission level to interface with the electric utility transmission network. The plant central or supervisory control facility may or may not be co-located with the plant transmission substation.

For baseline design purposes, we have assumed that a number of individual array units will be paralleled onto a common busbar to feed a single 4.4 MW inverter module. Assuming the availability of a 3 kV, 50 mm thyristor, the maximum array voltage should be in the neighborhood of 1 kV if individual semiconductor devices are not connected in series. We have chosen 750 V as the minimum dc collection bus voltage to feed each inverter module. An adequate number of arrays must be paralleled onto each bus to provide the total input current to an inverter bridge. At 750 V, the dc collection bus current will be 8800 A. It is likely that arrays will be served by a tree-like bus branching arrangement, so the maximum current will only be seen at the final summing point prior to entering the inverter unit.

1.7.3.1 Inverter Tradeoffs

It is impossible to consider the requirements, trade-offs and optimal configurations for power conversion without considering the overall system arrangement. The active portion of the power conversion

equipment (or inverter) is but a small part, both physically and in economic terms, of the installation needed to interface solar photovoltaic arrays and utility networks, regardless of which of the many available circuit technologies is adopted. The economics and performance of the power conversion process are vitally affected by the "conventional" components which must be used both at the array-inverter and inverter-utility interfaces. These elements depend on the total system configuration and geometry as well as the inverter characteristics, and hence any attempt to define an inverter apart from these is misleading at best.

As mentioned, there are many possibilities insofar as inverter technology is concerned. From the viewpoint of equipment performance and economics, the best realization of any of them for a central station of any size in the 50-1000 MW range considered is a single installation of 2 "inverters" working from balanced dc buses as a pair of 6 pulse groups, which is the classic HVDC configuration delivering 12 pulse output waves to the utility via a pair of transformers or transformer banks. (Dependent on the size, single phase transformer banks may be preferred to three phase transformers). The operating dc voltage of inverters so designed for minimum inverter cost per kW would range from about 11.4 kV at 40 MW to some 228 kV at 1000 MW. These numbers do not, apparently, fit well with realistic solar photovoltaic array concepts. Also, such designs are normally customized to each installation, which is a disadvantage if a large number are to be built.

Array and dc bus considerations will effectively limit the

source voltage to about 1 to 1.5 kV. Under these circumstances, the optimum inverter size is about 4-1/2 to 9 MW, depending on the technology used and assuming that the direct parallel connection of semiconductor devices is avoided. From the conversion equipment view, then, a central station becomes a collection of such 12-pulse inverters each fed by its own photovoltaic arrays and all feeding a common ac collection point.

A dc voltage of 1 to 1.5 kV will produce an inverter line voltage of from 900 to 1350 volts. At power levels from 50-1000 MW, the intertie to the utility will be at intermediate or prime transmission levels; from 50 to about 150 MW, we would normally expect to tie to lower transmission voltages in the 69 to 161 kV range, from 150-300 MW to intermediate transmission in the 115-345 kV range and from 300 to 1000 MW to prime transmission in the 230 to 500 kV (or above) range. In any event, such tie voltages prohibit the use of a single transformation between inverters and the utility -- transformers of the required ratio with the required characteristics simply cannot be fabricated.

The result indicates the use of transformers with individual inverters or small groups thereof, avoiding any attempt at direct parallel connection of inverter bridges (which is the same as direct parallel connection of devices). Further, it allows the ac voltage at which final collection will occur, i.e., the voltage of the intermediate ac network between inverters and utility tie point, to be elevated to a convenient level in the normal distribution range, say 6.9, 13.8 or 34.5 kV. This permits the use of a standard station transformer as the final interface, and allows good utilization of conventional switchgear and other components (including feeders) in this network. Finally, the

station transformer used as a final interface can be equipped with a load tap changer. Such a step, grossly uneconomic if applied to individual inverter transformers in the 5-20 MVA size range, can become cost effective on a large conventional transformer, the cost of tap changing equipment being offset by reduced costs in the inverters themselves, their associated transformers, and other conventional components.

Now that the overall conversion concept has taken shape, we can address the specific requirements of the application as they pertain to the 100 MW baseline central station. Most considerations will apply equally to stations of any size in the 50-1000 MW range, but exceptions will be noted as they arise.

Since no on-site storage is included, reversibility of power flow through the conversion equipment is not a consideration in selecting the technology to be employed. We do not believe that the capability to operate isolated, i.e., without the support of conventional generation (which would usually be geographically remote) is an important consideration either. Hence any technology which permits controlled unidirectional power flow while connected to a load consisting essentially of a balanced set of three phase sinusoidal voltages is satisfactory. The conclusion can hardly be said to limit the field of potential candidate inverter schemes -- we can readily list several, given below:⁽¹⁾

(1) The conventional current-fed line-commutated inverter, as used for HVDC terminals but with firing delay angle control to accommodate array load matching and utility voltage variations.

(2) A variant of (1) using two inverters, one with fixed

extinction angle and the other used, as source and line voltage in combination demand, at delay angles anywhere from rectification end stop to inversion end stop. This is termed a "buck-boost" inverter scheme.

(3) Another variant of (1) using two inverters of equal rating; one of which is force-commutated and run at an advance angle equal to the delay angle of the load-commutated half at all times. Termed "complementary inverters", this arrangement has the distinction of running at unity power factor under all combinations of source voltage, line voltage and power throughput.

(4) A variant of (1) in which a dc chopper is used between the source and the inverter, the latter being run at constant extinction angle and the former's voltage control capability being used to effect source-line matching.

(5) Voltage-fed, force- (or self, dependent on one's preference in terminology) commutated inverters using either phase angle or conduction angle control of the dc source-ac line voltage ratio to match existing conditions at any time.

(6) The HF base -- a relatively little known concept in power conversion technology which involves using a current-fed inverter as in (1) which feeds a high frequency passive resonant load; this in turn is the source for a naturally commutated cycloconverter which interfaces with the utility.

An analysis of the economics of these diverse technologies reveals that whereas the "inverters" differ substantially in cost, the total power conversion equipment does not. The estimated costs differ

by less than the anticipated errors in these estimates. Thus we must use criteria other than cost in making our selection, and the most obviously significant of these are efficiency (full and part load since the inverters are anticipated to spend a good part of their existence delivering less than peak capacity), and projected reliability. Shown in Figure 1.7.19, are the variations in inverter losses with load for several of the candidate inverter circuit configurations.

Efficiency, particularly part load efficiency, can be used to eliminate the HF base, voltage-fed, force-commutated inverters, and dc-chopper current-fed inverter approaches. The projected reliability of the approaches of (5) and (6) is low, further pointing toward their elimination from consideration.

The buck-boost system of (2) cannot be eliminated for these reasons, nor does conventionality rule it out. However, it is more complex and fragmented than (1) and (3) without offering any benefits in price or performance in return for these complications, now or in the foreseeable future. As a result, it will be eliminated from consideration.

The simple current-fed inverter of (1) and the complementary scheme of (3) are so close that a decision is impossible. However, practical realizations of (3) at high power levels do not yet exist, while for (1) they do. Therefore, at least for the time frame through 1985, we select the simple current-fed load (or line, or naturally commutated inverters. Beyond this time frame, the decision becomes much more difficult. Not only is it likely that (3) will by then be

Curve 685407-A

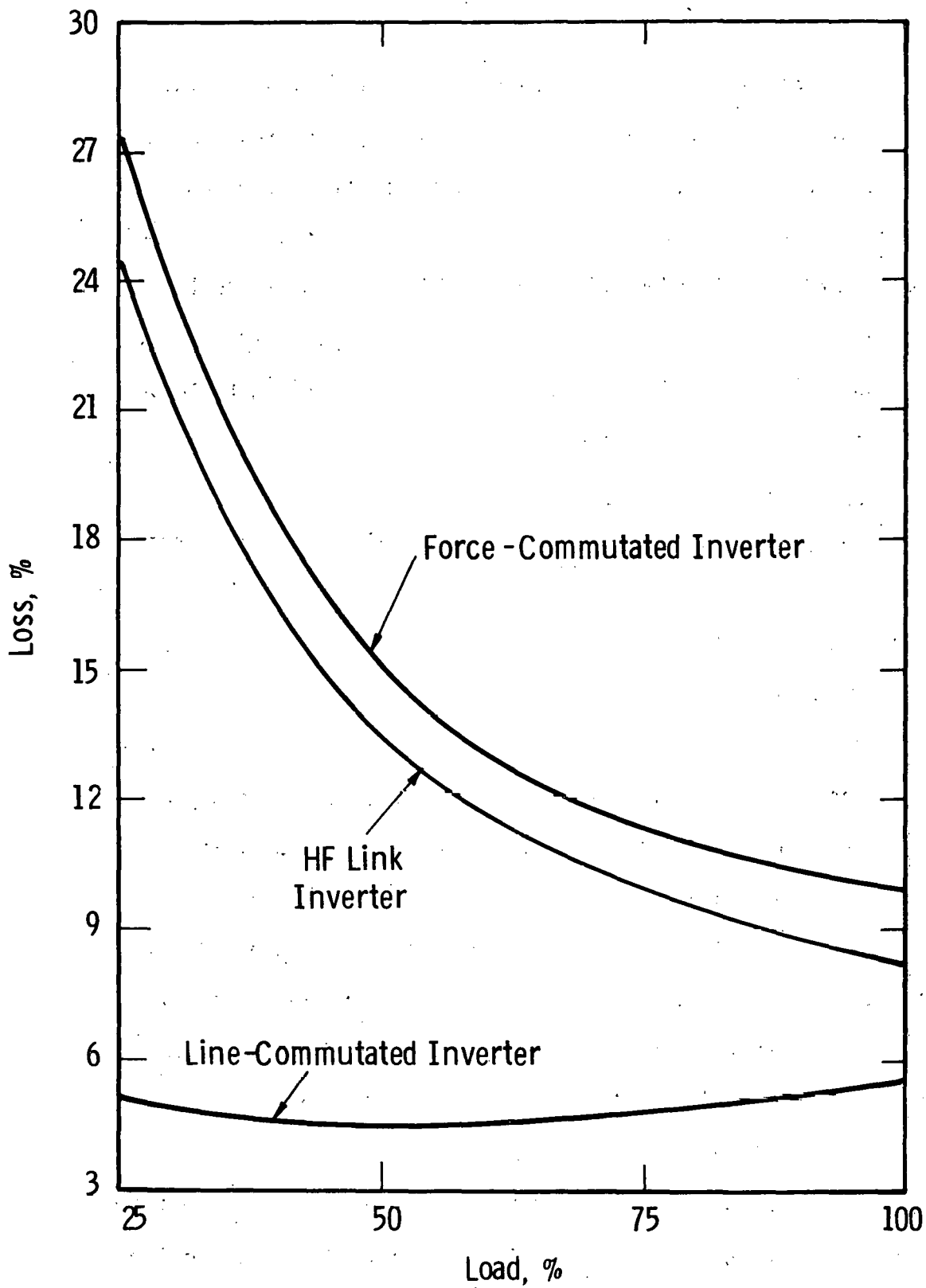


Fig. 1.7.19 – Comparative part load inverter losses

an existing competitive technology, improvements in fast switching device technology and developments and in related peripheral components may well make voltage-fed, force-commutated and HF base techniques equally attractive candidates. We must, therefore, conclude that while we can make a clear cut and readily justifiable decision as to the best approach for the short term, we cannot do so for the long term view. It is not possible, by projecting device developments along reasonable paths, to eliminate the long term uncertainty.

1.7.3.2 Design Considerations

Having selected (1) as our present candidate, we may proceed to examine the interface parameters and design criteria which determine the inverter specifications, and also the specifications for associated major passive components.

The range of dc voltage anticipated, under normal operating conditions, is about 1.3:1 at the array terminals. Thus, if a peak array voltage of 1 kV is chosen, the minimum will be ~ 750 volts. Allowing for $\pm 10\%$ normal line voltage variation and maintaining inverter operation down to -20% of normal line voltage before commutation failure occurs, the nominal inverter bridge output voltage becomes 940 volts ac and the worst case operating power factor is 0.6 (i.e., at worst, 1.33 per unit compensating reactive volt-amperes will be required by the inverter).

Using liquid cooled 2" thyristors, the dc current rating for a 6 pulse Graetz bridge is 2200 amperes. Thus a pair of such bridges, run in parallel on the dc side and displaced in phase by $\pi/6$ radians

(30°) on the ac side to provide 12 pulse operation, will handle 4400 amperes and have a power rating of 3.3 MW at 750 volts dc.

The most economic arrangement for the power conversion equipment is obtained when two of these 12 pulse inverters feed a common transformer having 4 low voltage windings (2 wye and 2 delta) as shown in Figure 1.7.20. It is not practical, because of physical limitations in the transformers, to have more than 4 low voltage windings brought out for connection.

A nominal ac output voltage of 940 volts requires the use of thyristors with forward/reverse voltage blocking ratings of 2900 volts when the effects of arrester-limited transients on the transmission and local distribution networks are considered. Such devices are not currently available in quantity from major US manufacturers, and are not available with the requisite current ratings from foreign sources. However, we would anticipate that such devices will be available before 1985. For the present, costing is done for a range of array peak dc voltages from 775 V, requiring one 2200 V device and with power rating 2.55 MW per 12 pulse bridge pair at minimum array voltage, to 1800 volts, requiring 3 series connected 1800 volt devices and with power rating 6 MW per 12 pulse bridge pair.

The basic interface between array and inverter consists simply of a reactor. From an operational view, the sole function of this component is to support the ripple voltage at the inverter dc terminals while maintaining the peak ripple current within reasonable bounds.

However, there are other constraints which cause the reactor to be nearly an order of magnitude larger than would be dictated by

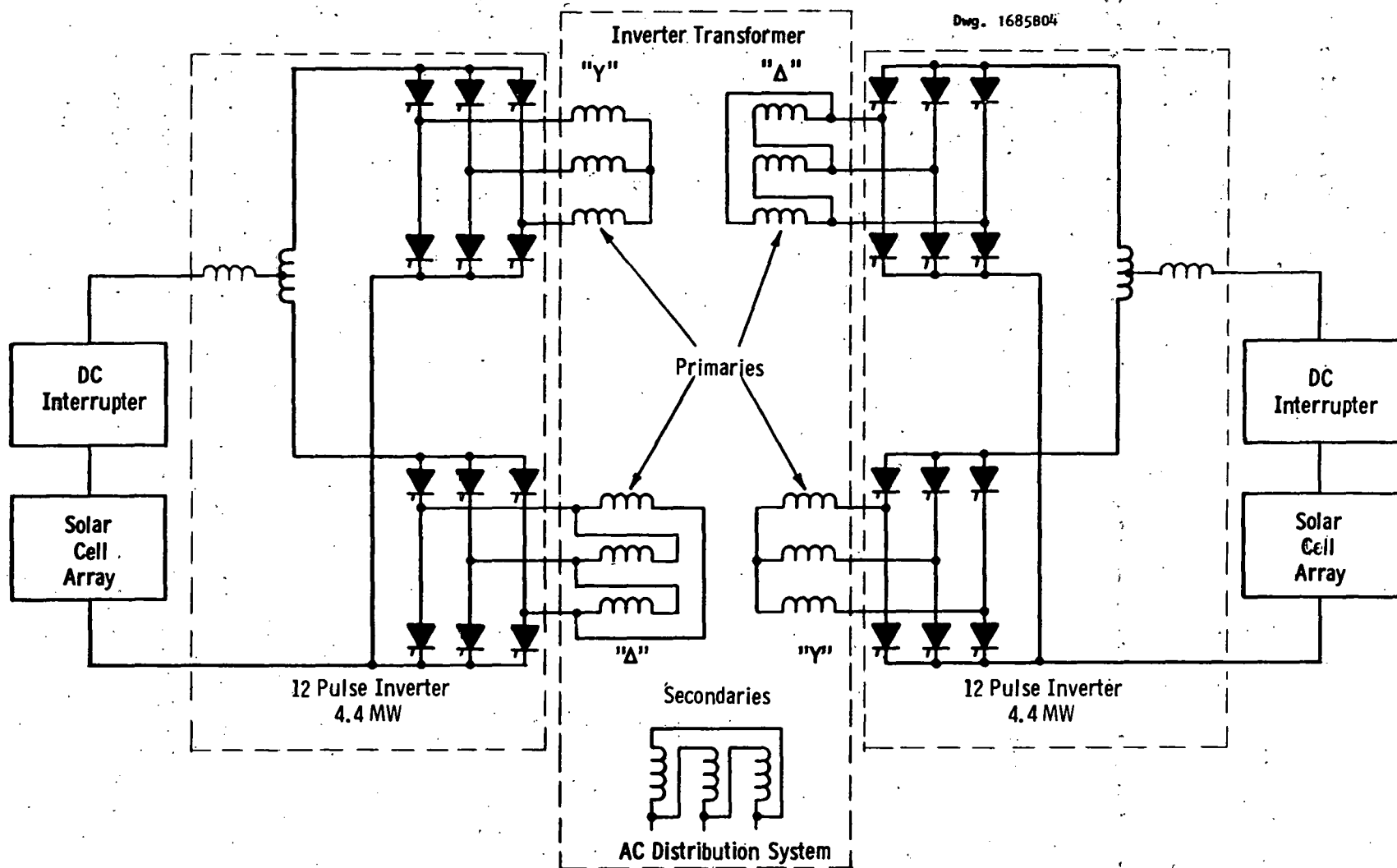


Fig. 1.7.20 - Nominal 8 MW line - commutated inverter submodule (two submodules per 17.6 MW module)

ripple considerations. We anticipate that inverter commutation faults will be a relatively frequent possibility despite the design margins used. The obvious first protection tactic, in view of the limited short circuit current of the array (which is estimated to be less than 1.5 times normal operating maximum) is to attempt a "ride-through". This is done by suspending normal gate firing of the thyristors, thus causing a double commutation fault and locking on to one converter line voltage for one cycle, the inverter swinging into the rectification region of operation for a full half cycle. The fault current, of course, increases by an amount corresponding to the volt-seconds impressed on the dc filter reactor. As the inverter re-enters the inversion region, the commutation which failed is reattempted. Should commutation now succeed, normal operation can be restored very quickly and the maximum time of outage is about 1 cycle. Should it fail once more, we must conclude that a serious problem exists and shut the inverter down by means of a high speed solid state dc interrupter taking the form of a ringing bypass valve connected in parallel with the dc reactor. Although an electro-mechanical breaker could perform the function, the life of such a component is short, and maintenance costs would be inordinately high.

Thus, the reactor's sizing is determined by the permissible rise of fault current when ride-through is attempted and/or the ringing bypass valve interrupter's requirements, rather than by ripple considerations.

Of course, we cannot rely on the solid-state interrupter alone to effect fault clearing under any and all circumstances. It may fail

itself, and so must be backed either by a fuse or an electromechanical breaker.

We observe that the increase in fault current during an attempted commutation failure ride through may carry the dc loop current beyond the short circuit capacity of the solar array. In that event, the array can be protected by connection of an inverse shunt diode, of suitable voltage and current rating, at the dc input terminals of the inverter equipment (i.e., effectively in parallel with the array dc terminals).

The only other component in the dc interface is an interphase transformer between the dc terminals of the two 6 pulse bridges forming a 12 pulse system. This element supports the difference in ripple voltage between the two inverters (i.e., it supports the 6 pulse constituents of the dc voltage ripple). We do not use series connection of the bridges, which would not require such a component, because to do so would halve the power rating per bridge at a given dc source voltage. Such a move, therefore, halves the ratings of the associated transformer and dc reactor, with a resulting pronounced increase in their specific cost.

Between inverters and inverter transformer, we would use simple disconnects (motor driven, so that remote operation is possible) to isolate faulted units; thus any single fault would only reduce to 50% the capacity of any sub-system comprising 2 - 12 pulse inverters feeding a single transformer.

The high side voltage of the inverter transformer could be chosen anywhere in the distribution voltage range. 13.8 kV is the most

logical choice, since it permits a number of economic goals to be readily realized, at least up to power levels of ~ 300 MW for the total installation. Above this, or more accurately when finally interfacing with transmission voltages above 230 kV, we would normally choose 34.5 kV as being best suited.

All harmonic filtering and power factor correction is applied at the intermediate voltage. A voltage of 13.8 kV permits most economical use of the capacitor banks, switchgear and reactors needed (the filtering being via conventional shunt-connected tuned traps); 34.5 kV is slightly more expensive for these items, but at higher transmission voltage levels we need to adopt 34.5 kV to make a reasonable central substation transformer design available. From the viewpoint of electromagnetic interference potential of the intermediate ac collection, it is obviously preferable that filtering and power factor correction be distributed, i.e., that each of the two $\times 12$ pulse inverter sub-systems have local filtering and power factor correction. This is, however, uneconomic, and we are constrained to locate all filters and power factor correction banks at the central collection point. EMI can be minimized by using suitably shielded and transposed feeders in the ac collection network. If it proves necessary to distribute the filters and/or power factor correction for any particular installation, the cost penalty will be severe.

The final transformation is entirely conventional, as are the high side line tie breaker and arresters. Arresters will also be used at each inverter transformer high voltage tie point.

The cost of such equipment, fulfilling all required conversion and protection functions and including telemetered status and control functions to a remote dispatch center, is estimated in 1975 dollars at ~ \$82/kW for 775 volt peak arrays to ~ \$70/kW for 1800 volt peak arrays at the 100 MW level. Costs would reduce slightly at higher powers, up to about ~ \$2/kW less at 1000 MW (because of steadily reducing central transformer specified cost). It should be noted that these are costs per peak kW; the conversion equipment price is peak power sensitive, provided peak power is to be sustained for periods greater than 1-2 hours.

Peak load efficiency of the power conversion process is calculated to range from 93% to 93.5% over the array peak voltage span considered. These figures include allowances for the intermediate ac feeder network and the central transformer, but do not include dc bus losses. At reduced load, efficiency actually will remain at about 93% until in the vicinity of 50% load. This behavior results from the largely resistive nature of system losses, with greater heating and higher component resistance at high current levels.

The foregoing exposition of interface parameters and system design is based on a system not involving load tap changing on any transformer. If a standard $\pm 10\%$ voltage regulating tap changer were used on the central transformer, we would get improvement of the worst case operating power factor to .72, reducing the power factor correcting VARs required to 0.96 per unit, and reducing inverter device voltage requirements and inverter transformer size by about 20%. These factors would obviously reduce costs in these areas, but such reductions are at

least partially offset by an increase in the cost of the central transformer and the cost of the tap changing equipment added thereto.

If a wider range, $\pm 23\%$, voltage regulating transformer is applied, then the worst case operating power factor increases to ~ 0.87 . Substantial further savings are possible in inverters, inverter transformers and power factor correction but, of course, the premium for the central transformer and its tap changing equipment increases markedly. The results of the economic evaluation are listed in Table 1.7.5 for the three alternative system configurations. It can be seen that there is only a marginal advantage to a $\pm 10\%$ or $\pm 23\%$ tap-changing transformer.

There is one potential major drawback to the use of load tap changing gear which must not be overlooked when assaying the economic benefits attributed thereto. Large tap changing switches for transmission voltage applications have a life, typically, of between 10^5 and 3×10^5 operations. This is perfectly adequate for normal applications predicated a 20-30 year life, and would be satisfactory in our application should the standard $\pm 10\%$ regulating device be employed solely to compensate for transmission voltage fluctuations. However, should the extended range regulator prove attractive, or indeed should the use of either transformer be proposed for part of the solar array load matching duty, then the increased frequency of operation would shorten the life and increase the maintenance requirements on the equipment.

1.7.3.3 dc Buswork Considerations

One of the considerations which must be dealt with in the design of the solar plant is the means whereby the power generated by

TABLE 1.7.5

Comparison of Costs for Three Alternative
CPS Power Conditioning Systems

Substation Transformer	\$ 606,480	\$ 906,480	\$ 1,056,480
Inverter Transformers	2,557,860	2,277,860	1,999,860
Filters & Power Factor Capacitors	1,796,090	1,742,090	1,669,090
Other	<u>5,899,120</u>	<u>5,899,120</u>	<u>5,899,120</u>
TOTAL	\$10,859,550	\$10,825,550	\$10,624,550
\$/kW _{OUT}	108.6	108.3	106.2

the individual arrays is collected and delivered to the inverter.

The optimum 12-pulse inverter size is 4.4 MW. For example, if land usage of 30% and conversion efficiency of 10% are assumed, the approximate land area required for a 4.4 MW array field is $1.47 \times 10^5 \text{ m}^2$ or a square 383m on a side. It is visualized that the inverter module would be located at one corner, so that a 17.6 MW inverter module station composed of 4 12-pulse inverters would be located at the center of a 766m x 766m array field.

The collection arrangement visualized is one in which the 4.4 MW array field is divided into 4 equal areas. The arrays along a diagonal within each area would have their leads buried together in a shallow trench. At the end of the diagonal closest to the inverter, the leads would be fed into a pad- or post-mounted box containing breakers and protective devices. At this "summing point", they would be connected to a heavier "spine" conductor which would feed directly into the inverter. The size of the spine conductor is assumed to be selected so that the current density is the same as in the lead wires. With this busing arrangement, the average distance over which the power from a 10 kW array flows is approximately 322 m, with the maximum distance being 542 m.

The losses encountered with 9 AWG conductors (or their equivalent in the case of spine conductors) would be approximately 55 kW or 1.4% of the 4.4 MW array field output. With 8 AWG wires, the losses would be 40 kW or 1% of the 4.4 MW array field output. The voltage drop from the most distant array to the inverter would be 46 volts for the 9

AWG conductor and 36 volts for 8 AWG. This may have some array design implications in that special voltage compensating array panels may be required for the most distant arrays in order that all of the arrays contribute an equal amount of power.

The amount of trenching required would be approximately 7,740 m/4.4 MW of array field. At an installation cost of \$2/foot, the cost of trenching translates to \$13/kW. The cost of the conductors will be about \$12/kW (9 AWG), while the dc circuit breakers, isolating diodes, etc., will add another \$3/kW. The total cost of the dc collection system will then be approximately \$28/kW for the CPS.

Harmonic Radiation

From preliminary calculations, it appears that the electromagnetic interference problem will not be too severe on the ac side of the inverter, because of the balanced nature of the three phase ac system. If the problem should be significant, however, it can be minimized through the use of shielded ac overhead cable or by putting the conductors underground.

The electromagnetic interference problem is much more pronounced on the dc side where even small harmonic ripple voltages can be radiated rather efficiently by the arrays serving as antennas. In an effort to avoid expensive filtering of the dc side, it may be necessary to have ungrounded arrays with balanced leads to cancel higher order harmonics which would interfere at communications and navigation frequencies. Such an approach would eliminate the possibility of using the return conductor as a part of the array field grounding mat and might ultimately

result in higher costs than would be incurred by placing filters on the dc collection bus.

Power Conditioning Subsystem Cost Example

The power conditioning subsystem is one of two major subsystems comprising the 100 MW baseline CPS. The other, of course, is the array subsystem. A sample component cost summary for the power conditioning subsystem is included here for purposes of illustration of typical costs of the components and how they compare with the total subsystem cost. We have defined the power conditioning subsystem as including all components between the array output terminals and the ac transmission line leaving the CPS.

The costs shown in Table 1.7.6 are in 1975 dollars and are based on the design parameters assumed for the baseline 100 MW CPS. Although the nominal station output is 100 MW_e, the maximum inverter output is about 106 MW. The maximum output can only be realized when the array dc bus voltage is at design maximum, however, so a realistic derating factor is used to arrive at the 100 MW_e electrical output rating.

It is interesting to note that of the total \$109 per kW cost, the inverter element (minus transformer) accounts for less than \$30 per kW, or about 27% as shown in Table 1.7.7. The remainder of the power conditioning costs are divided among a number of elements. As can be seen from Table 1.7.6, the most significant of these are inverter transformers, dc power collection, and power factor correction.

TABLE 1.7.6

100 MW_e CPS. POWER CONDITIONING SUBSYSTEM COMPONENT
CAPITAL COSTS (1975 DOLLARS)

Inverters (24 required @ \$123,380 each)	\$2,961,120
Transformers (12 @ \$213,155 each)	2,557,860
Harmonic Filters at Substation (13.8 kV assumed)	699,580
Power Factor Correction Capacitors and Switchgear (Substation)	1,126,510
Substation Transmission Transformer	606,480
OH ac Inverter Station Feeder Conductors	25,000
ac Spine Conductor	35,000
Inverter Station Line Breakers (6 @ \$3,000 each)	18,000
High Side PCB at Substation	40,000
dc Collection Cable Trenching (\$2 per foot)	1,290,000
dc Collection Conductors (9 AWG)	1,200,000
Miscellaneous dc Hardware (Isolation Diodes, Switches, Circuit Breakers)	300,000
	<hr/>
	\$10,859,550

TABLE 1.7.7

CPS POWER CONDITIONING

	<u>(1975 \$)</u>
Inverters	\$ 29.60/kW
Remaining Equipment	<u>78.90/kW</u>
TOTAL	\$108.50
FL Efficiency	93%

REFERENCES

1. "AC/DC Power Conditioning and Control for Advanced Conversion and Storage Technology", EPRI 390-1-1, Key Phase Report 1, Westinghouse Electric Corp., August 1975.

THIS PAGE
WAS INTENTIONALLY
LEFT BLANK

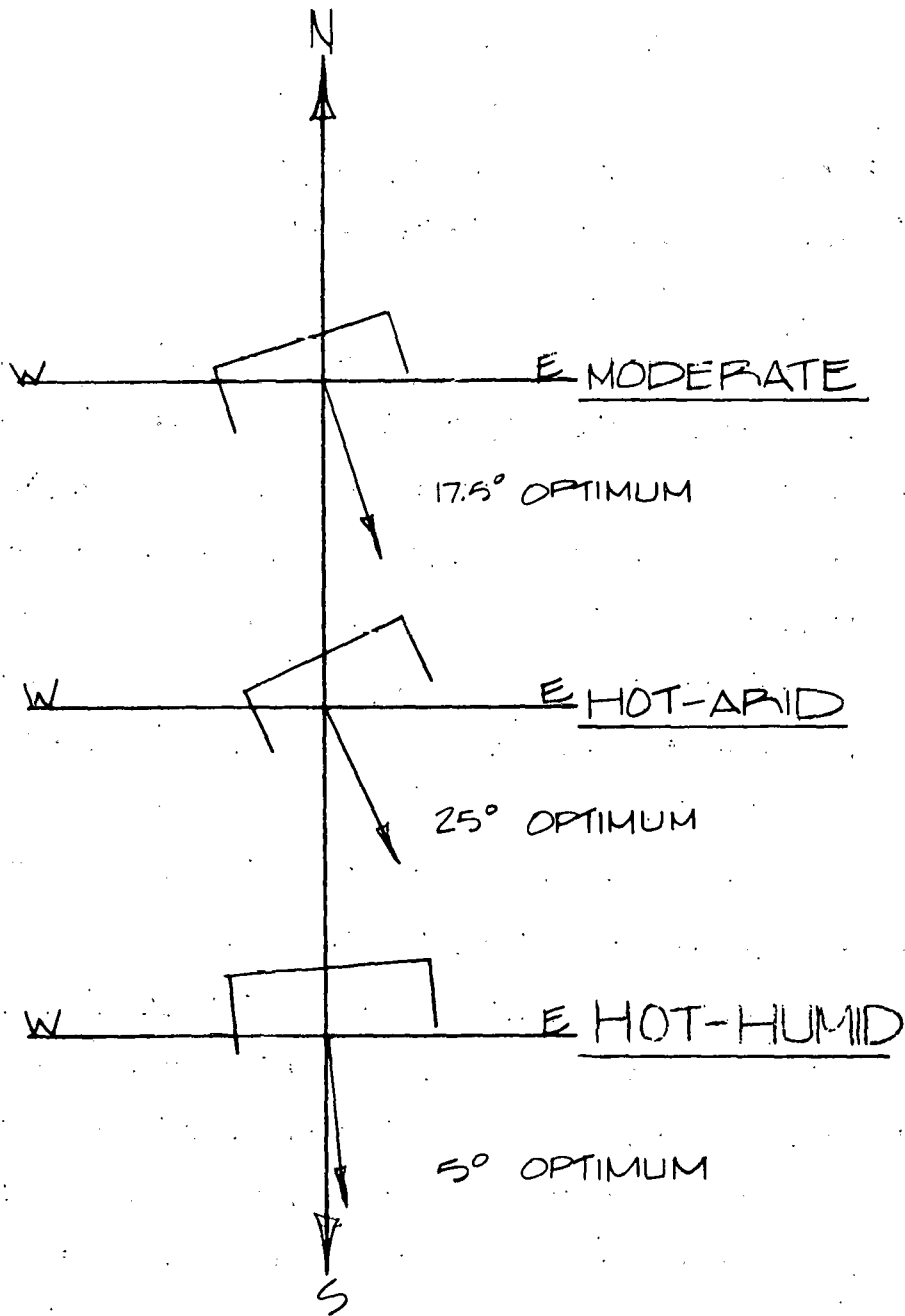
1.8 RPS Architectural Designs

1.8.1 General Architectural Considerations

1.8.1.1 Climatic Considerations

Because the largest element of residential energy consumption is space heating and air conditioning, a building which is to receive a photovoltaic system should be designed to be compatible with its local climatic situation to minimize energy consumption. A first step in the mating of climate and building is perhaps best approached by establishing regional climate zones and generating a form for the buildings, which by taking advantage of natural conditions, saves energy in space heating. For this study, three general climate zones were established - Hot, Humid (Atlanta, Georgia; Mobile, Alabama), Hot, Dry (Santa Maria, California; Phoenix Arizona), Moderate (Madison Wisconsin; Wilmington, Delaware; Cleveland, Ohio).

These zones relate favorably to the climate zones established by Victor Olgyay in his book Design With Climate. In each of these zones, Olgyay relates average daily temperature and humidity ranges to human comfort. When temperature or humidity conditions are such that human comfort cannot be maintained, then he determines what percentage of available wind during cooling periods and solar flux during heating periods are needed to return the space back within the comfort zone established. These relationships then generate orientation requirements for buildings in the specific regional areas. This combined effort generates a building which carefully uses wind and solar forces to minimize energy consumption (see Figure 1.8.1).



ORIENTATIONS FOR 3 CLIMATE ZONES

CREDIT: VICTOR OLGAY
DESIGN WITH CLIMATE

Figure 1.8.1

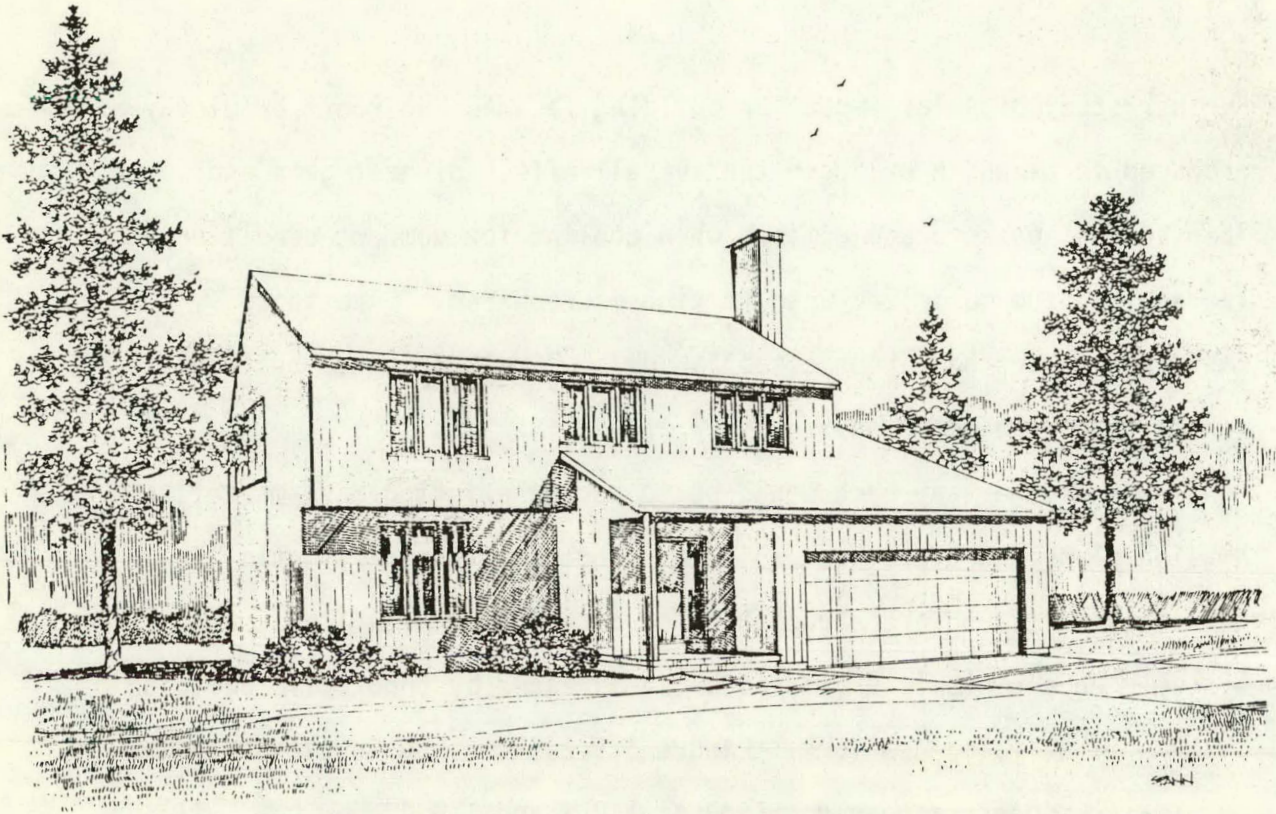
Further study of solar impact on building facades and roofs by Olgyay produced forms which balanced the overall effect of heat gain and loss so that gains are minimized when cooling for comfort conditioning is required and maximized when heating is required. Once these basic parameters have been established, a climate oriented building schematic can be designed.

Another approach would be to review existing mass-marketing housing plans and pick those which meet both the basic climatic characteristics and are acceptable for interfacing with a photovoltaic system. An example is a pre-fab house marketed by Innovative Building Systems of Buffalo, New York. Figure 1.8.2 shows how in elevation the original residence appeared. Figures 1.8.3 and 1.8.4 show how, without any structural modifications, small size arrays could be accommodated assuming the residence would have the proper orientation. Figures 1.8.5 through 1.8.7 show how a large roof surface could be provided and how the plan and sections might appear.

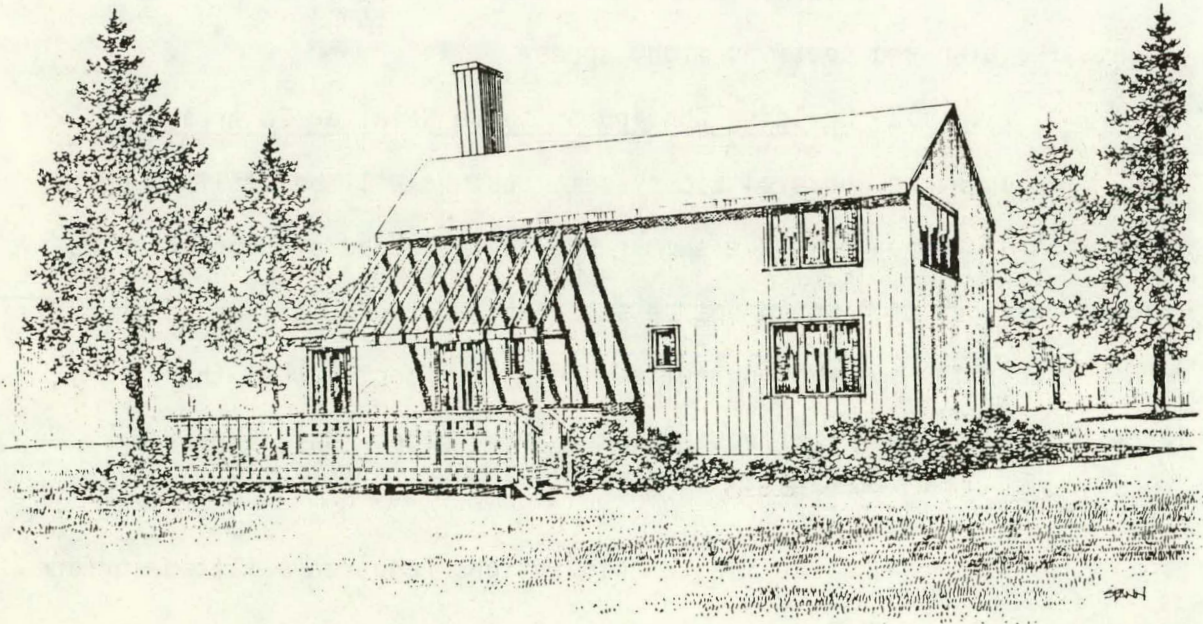
1.8.1.2 Building Configuration In Relation To Array Tilt

Since the photovoltaic system output will be utilized year round with an increase in the summer due to the added air conditioning load, a vertical tilt would not be acceptable because this would severely reduce either the system output during summer months when the largest demand occurs, or require large array sizes thus increasing initial costs.

Therefore, if initial considerations required a tilted surface and a large market application is desired, it is appropriate to assume

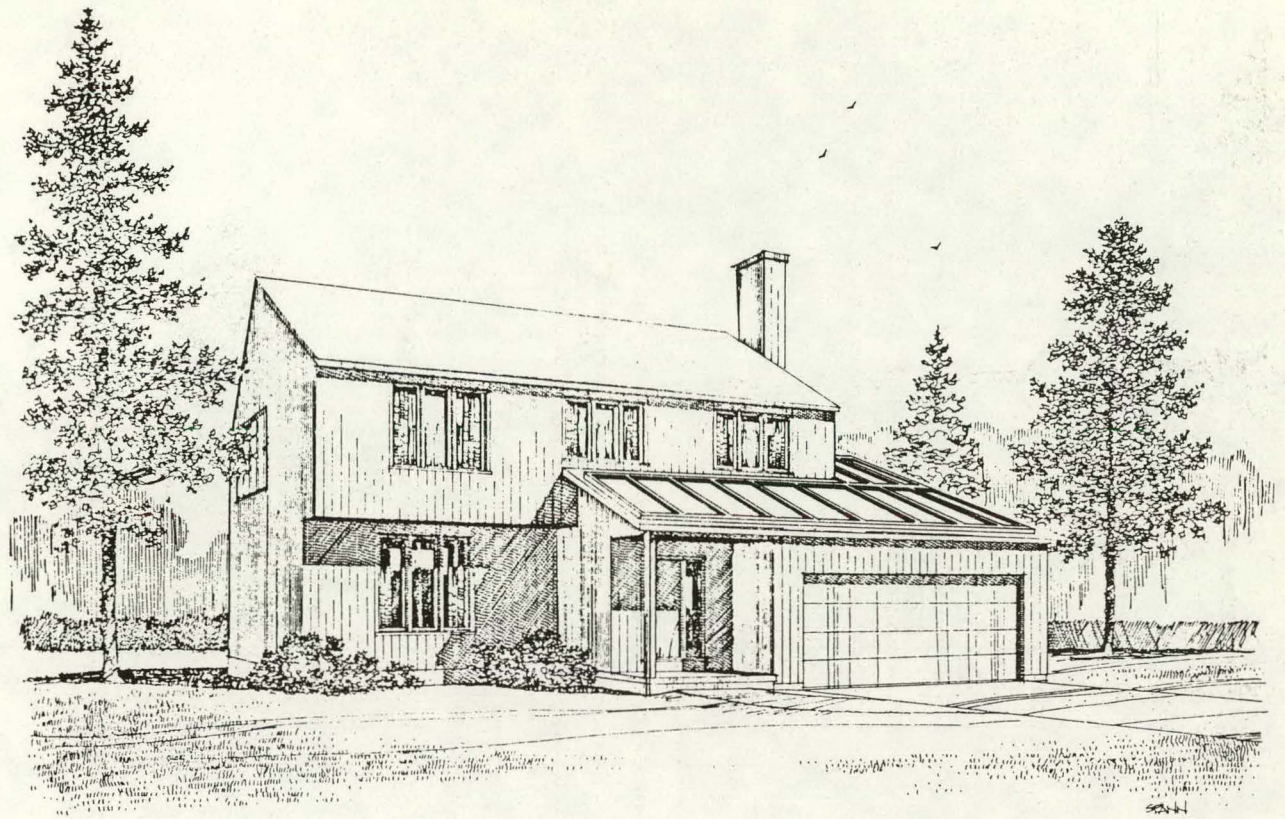


North View

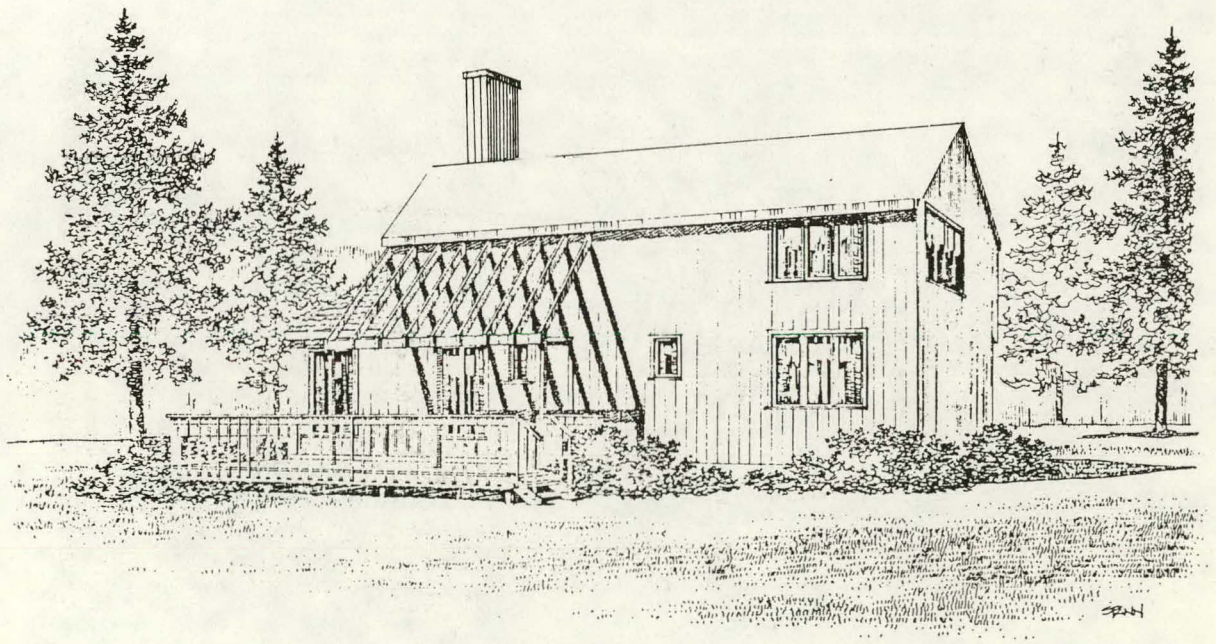


South View

Figure 1.8.2

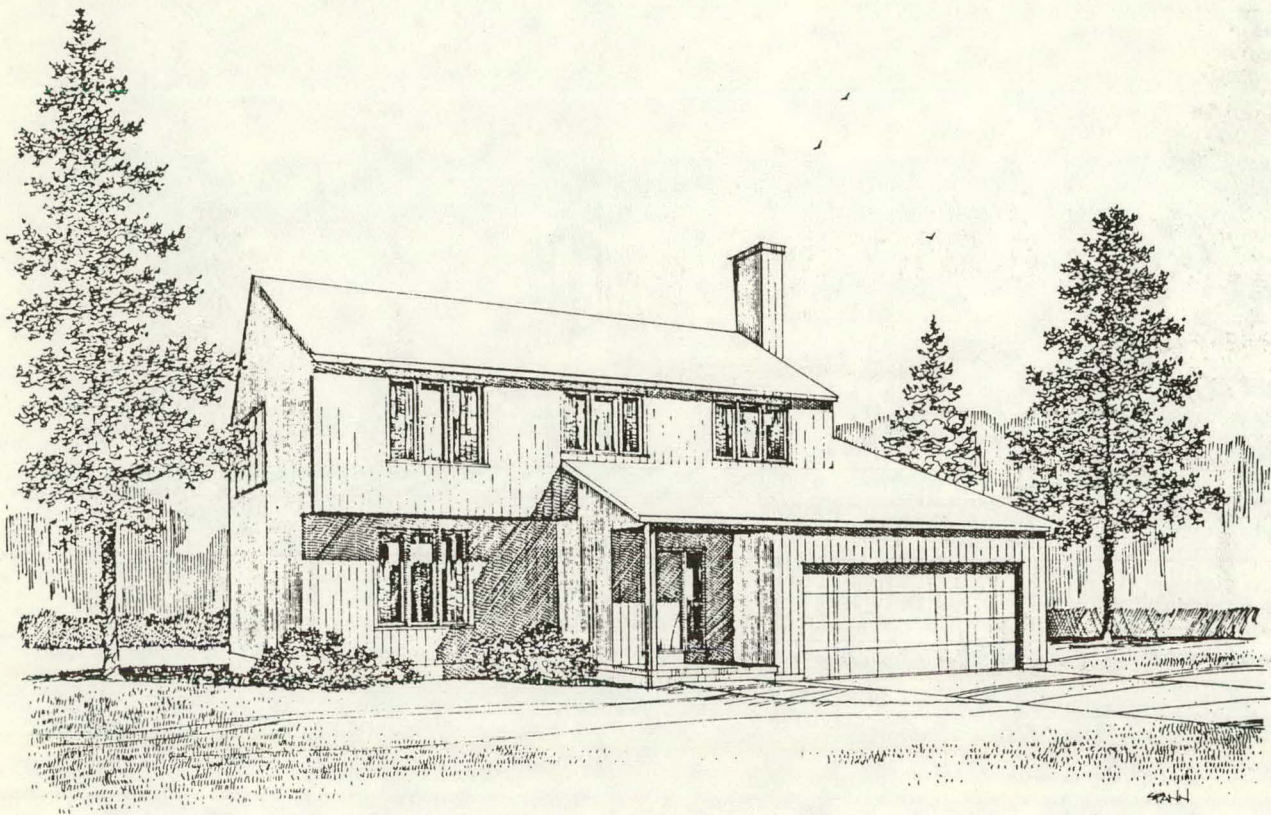


South View

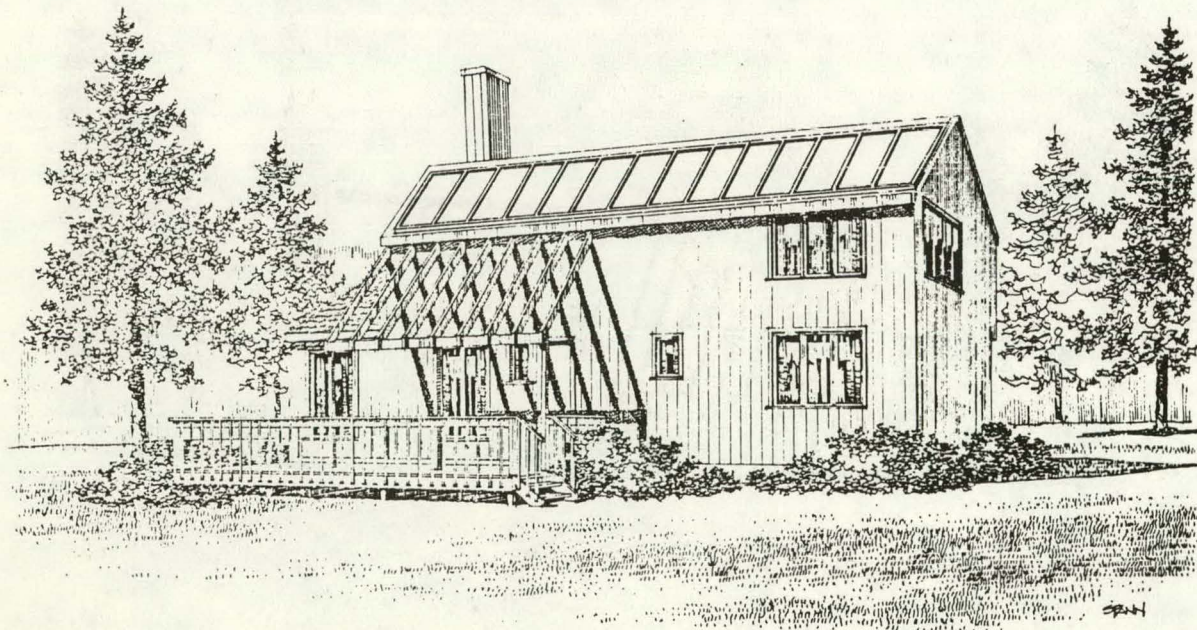


North View

Figure 1.8.3

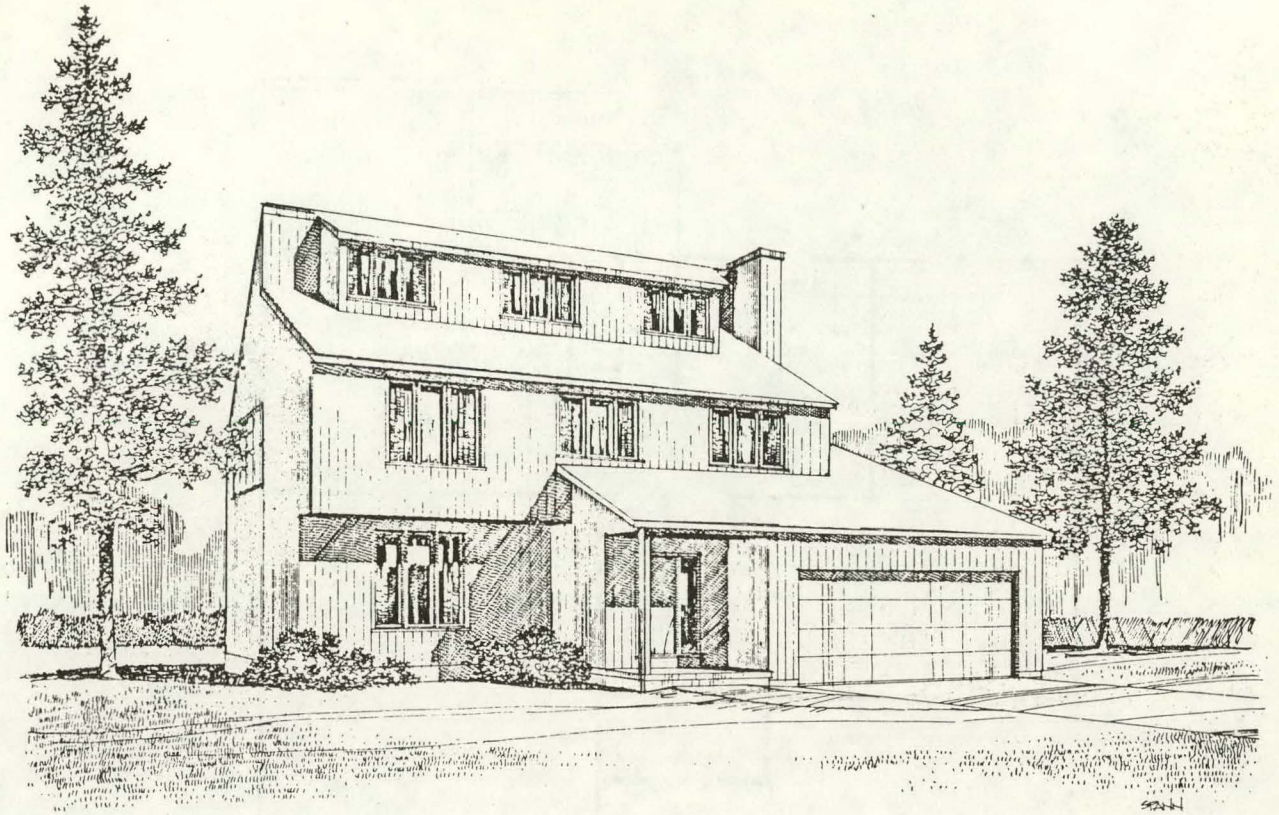


North View

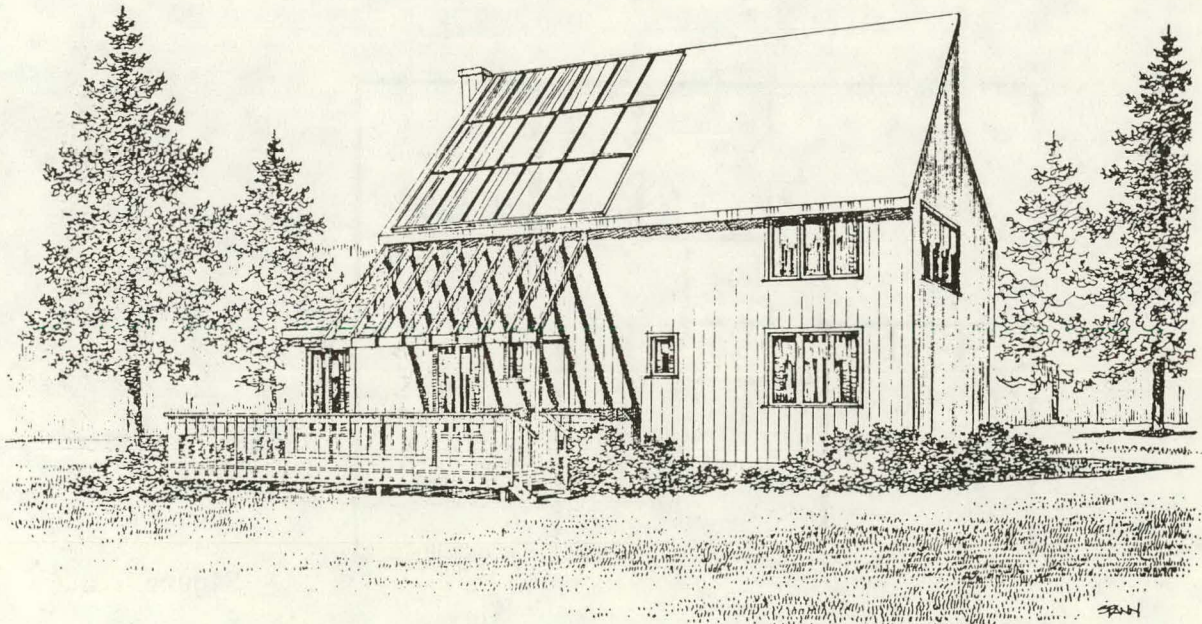


South View

Figure 1.8.4



North View



South View

Figure 1.8.5

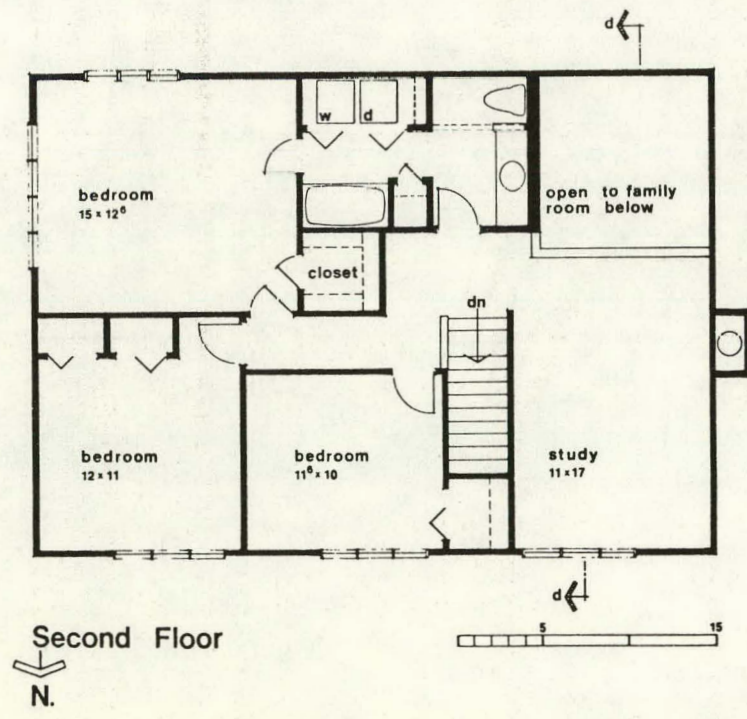
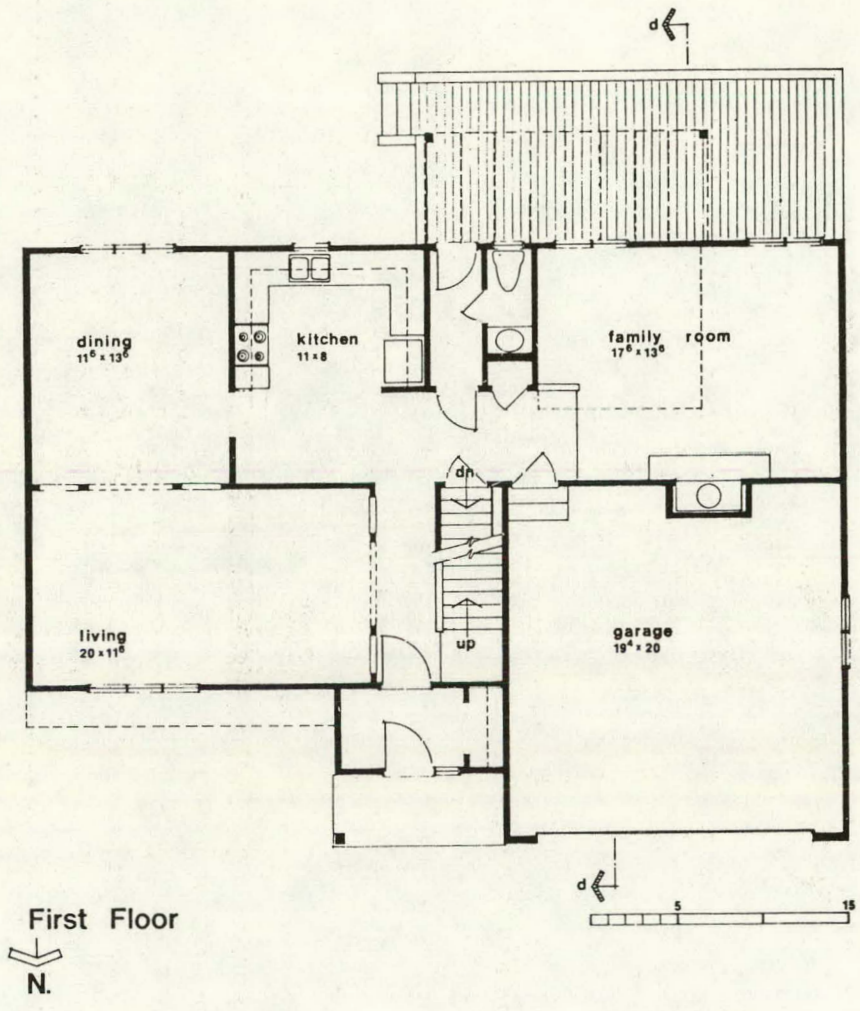


Figure 1.8.6

395

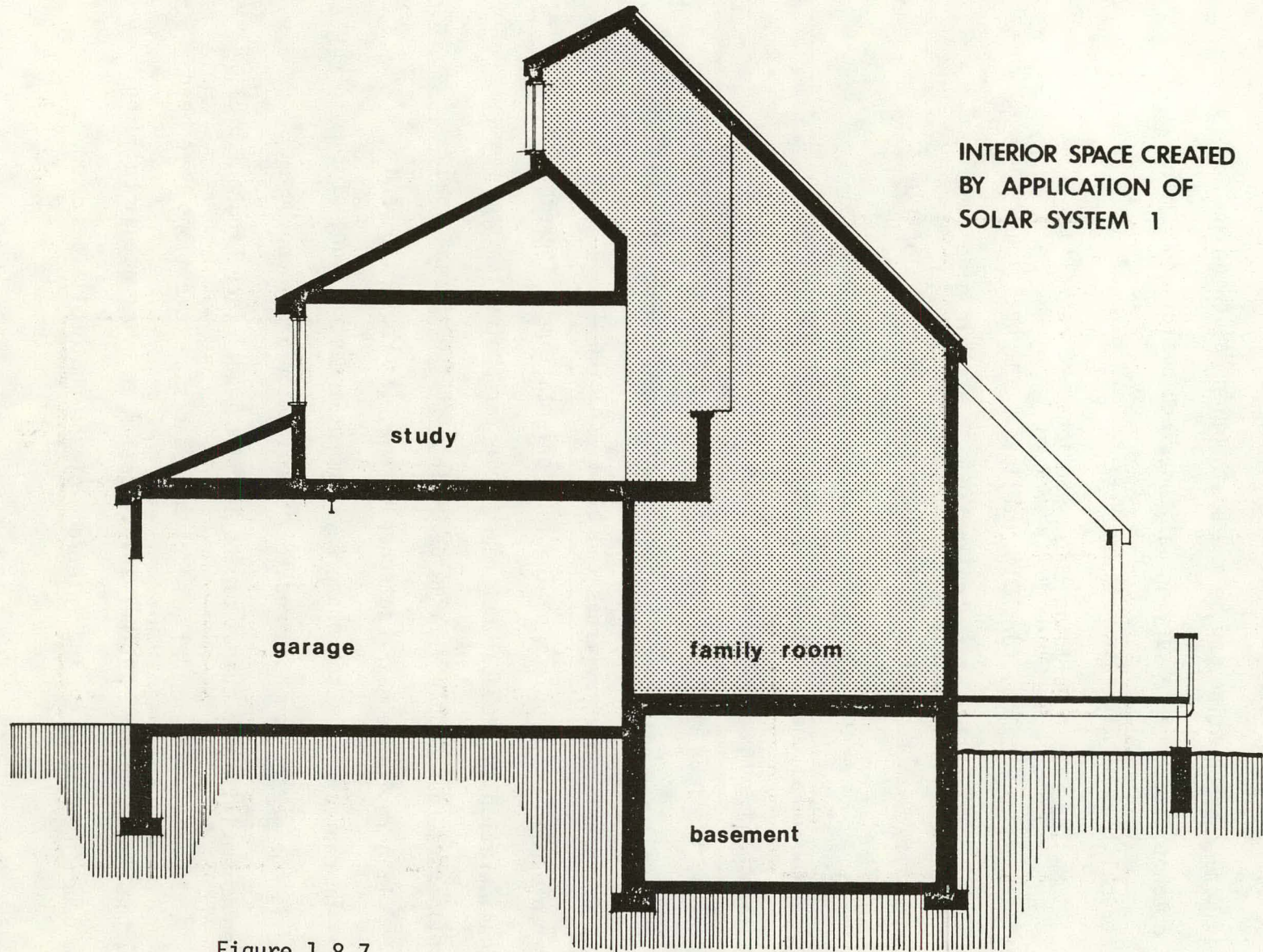
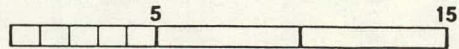


Figure 1.8.7

Section d - d



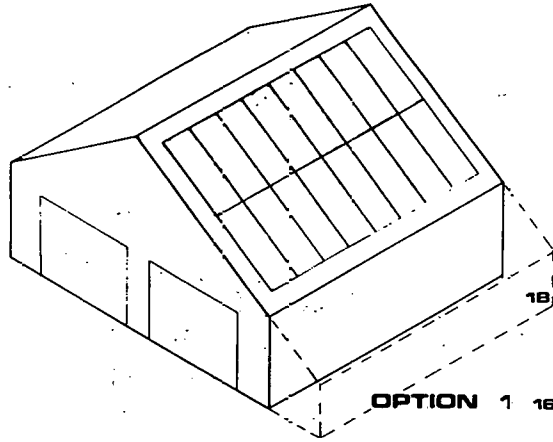
a roof mounted array, as stated previously in the RPS Design Section 1.3.4, of some configuration may be the best option allowing variations in roof pitch to accommodate varying latitudes and building thermal and electrical load situations.

Some acceptable building cross-sections are as follows. A double-pitched roof allows for 180° rotation of the building with respect to the orientation of the collector. This would give some plan flexibility with respect to environmental restrictions of the site.

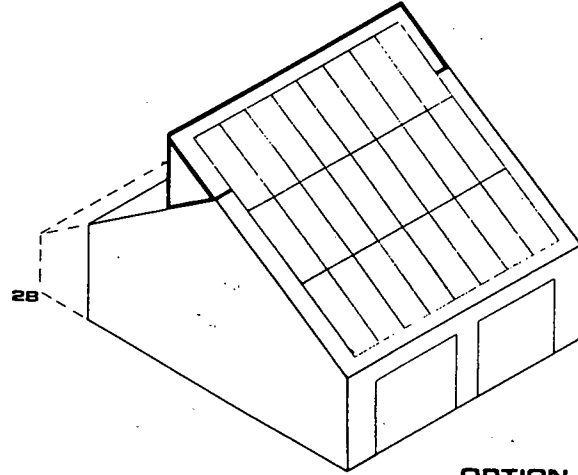
A double-pitched roof with a wing addition allows for 90° incremental changes in the orientation. The collector could be placed on any one of the four roof pitches allowing for better accommodation of environmental and site restrictions. One restriction of this method, however, is that large array areas cannot be achieved without considerable roof areas on one of the four orientations. Therefore, this consideration is probably not reasonable for photovoltaic systems with collectors that supply a large percentage of the thermal load.

If a residence has a detached garage, its roof pitch and orientation can vary to accommodate environmental restrictions of the side while the garage can accommodate the collector array and be oriented to maximize the output of the thermal load. (see Figure 1.8.8)

If at this point, all the climate and site conditions have been met by the chosen design, further investigation into the actual building can be done in relation to the interface of the photovoltaic system.

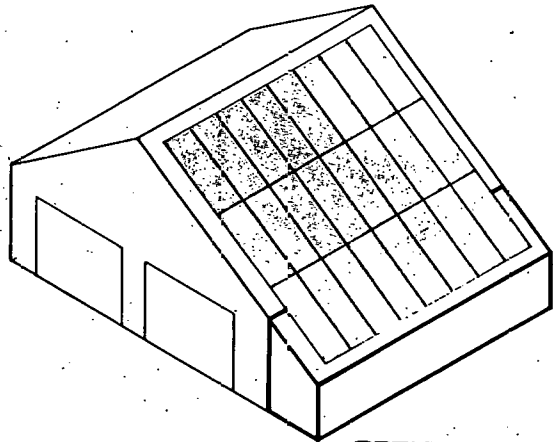


OPTION 1 16 COLLECTORS

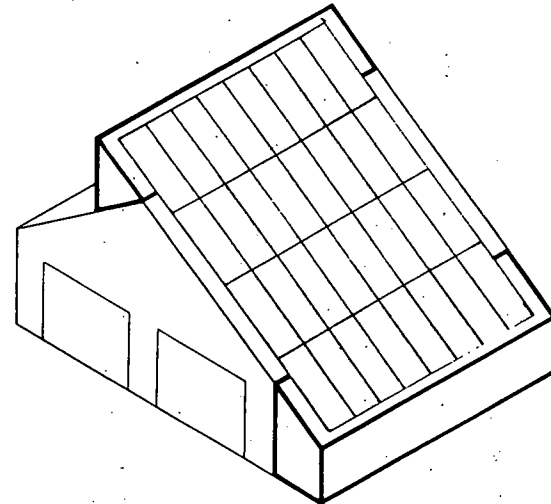


OPTION 2 24 COLLECTORS

**GARAGE RETROFIT
SYSTEM OPTIONS**



OPTION 3 24 COLLECTORS



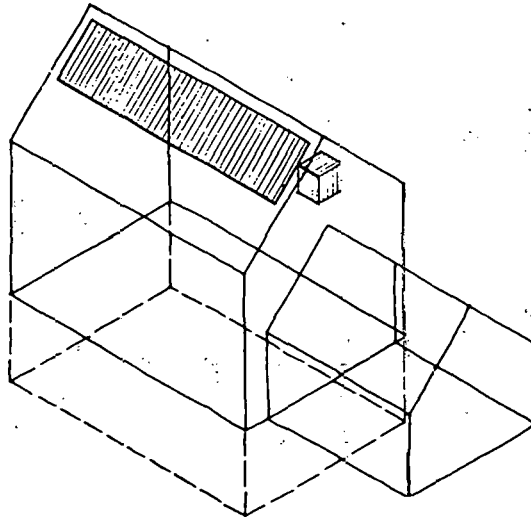
OPTION 4 32 COLLECTORS

Figure 1.8.8 - Detached garage retrofit options

1.8.1.3 General System Placement

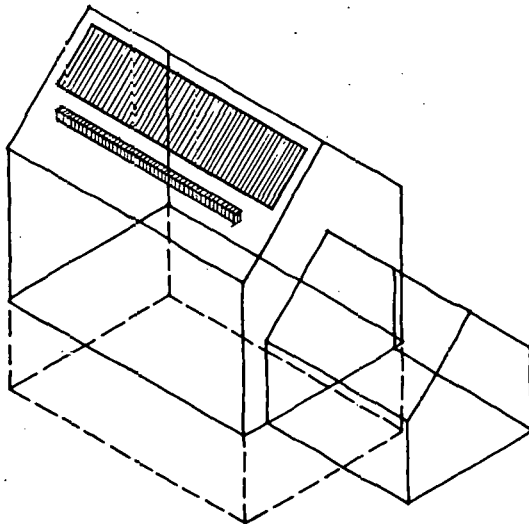
This section will deal in general with six particular options of arranging the photovoltaic array, the electrical power conditioning system, and the thermal storage system.

Option 1, as illustrated in Figure 1.8.9, is a residence with a roof mounted collector and both thermal and electrical systems in the attic. Because of the relationship of the collector array to the thermal storage and other accompanying systems, a possibility exists to design a thermosiphon system to transfer the heat from the collector to the storage tank. The storage tank, however, would be expensive in relation to a ground or basement positioned tank. The positioning of the storage tank in the attic space poses three specific problems. The first is that the weight of the storage tank and the water contained in it will add additional structural costs to the support system. Potential leakage problems in the storage tanks are critical because leakage would be to a finished ceiling of an interior space, thereby, causing costly structural damage. Any heat loss which would also occur from the storage tank would be to an unheated space. The advantages set forth by this particular option for the electrical system are that the gases expelled during a charging mode could be easily vented; that the electrical system is in close proximity to the collector; and that the batteries are not occupying useable floor space and also are not occupying area in a heated space. Again, as with the thermal system, the major disadvantage with placing the electrical system in the attic space is that loads on the ceiling structural system would



ROOF MOUNTED COLLECTOR
THERMAL STORAGE IN ATTIC

- POSSIBILITY TO DESIGN A THERMAL SIPHON SYSTEM TO TRANSFER HEAT FROM COLLECTOR TO STORAGE TANK
- STORAGE TANK WOULD BE EXPENSIVE IN RELATION TO A GROUND OR BASEMENT MOUNTED UNIT
- EARTHQUAKE PROBLEMS IN AFFECTED AREAS
- ADDITIONAL STRUCTURAL COST TO SUPPORT ADDED WEIGHT OF STORAGE TANK
- ACCESS PROBLEMS
- POTENTIAL LEAKAGE PROBLEMS - DAMAGE TO INTERIOR STRUCTURE OR FINISHES
- GOOD RELATION OF COLLECTOR DISTRIBUTION SYSTEM TO SPACE HEAT DISTRIBUTION SYSTEM
- HEAT LOSS FROM STORAGE TANK IS TO AN UNHEATED SPACE



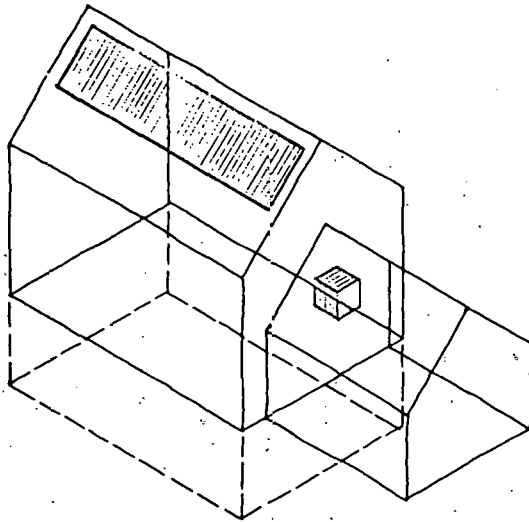
ROOF MOUNTED COLLECTOR
ELECTRICAL SYSTEM IN ATTIC SPACE

- GASES EXPELLED DURING CHARGING MODE CAN BE EASILY VENTED
- ELECTRICAL SYSTEM IS APPROXIMATE TO COLLECTOR
- LOADS ON CEILING REQUIRE ADDITIONAL STRUCTURAL MATERIAL
- ACCESS TO STORAGE SYSTEM IS A PROBLEM
- LEAKAGE BECAUSE OF OVERCHARGE OR DAMAGE IS A PROBLEM
- EXPLOSIONS COULD OCCUR IF GASES ARE NOT PROPERLY VENTED
- NOT OCCUPYING USABLE FLOOR SPACE IN A HEATED SPACE
- FREEZING DURING DEEP CYCLING MIGHT BE A PROBLEM

Figure 1.8.9 - General system placement, option 1

require additional materials. Further problems are access, battery fluid leakage, and potential freezing during deep cycling.

Option 2 is a roof mounted collector with thermal and electrical storage in the garage truss space (see Figure 1.8.10). In this option, the possibility also exists to design a thermosyphon system to transfer heat from the collector to the storage tank, if the collector system is mounted close to the thermal storage on the garage roof. As opposed to the last option, access to the thermal system is much more acceptable, and leakage of water from the tank is minimized because it is in an unfinished space. The disadvantages are as follows: the thermal storage tank would be again more expensive than a ground or basement positioned unit; additional structural cost is required to support the added weight of the storage tank, and heat loss from the storage tank is again, as in the last option, to an unheated space. The advantages for the electrical system in this option are that the gases can be expelled very easily during a charging mode, there is good access for servicing or replacement of any of the components of the system, and that the system is not occupying usable floor space in a conditioned or heated area. The disadvantages of this option are that long wiring runs are required from the collector to the electrical system, again additional loads on the structural materials require a greater cost investment, leakage of any of the fluid from the battery system during an overcharge mode or due to damage is still a problem, and explosions could occur if gases from the battery charging mode are not properly vented.



ROOF MOUNTED COLLECTOR
THERMAL STORAGE IN GARAGE TRUSS SPACE

POSSIBILITY TO DESIGN A THERMAL SIPHON SYSTEM TO TRANSFER HEAT FROM COLLECTOR TO STORAGE TANK PROVIDED COLLECTOR IS MOUNTED ON GARAGE ROOF

STORAGE TANK WOULD BE EXPENSIVE IN RELATION TO A GROUND OR BASEMENT MOUNTED UNIT

EARTHQUAKE PROBLEMS IN AFFECTED AREAS

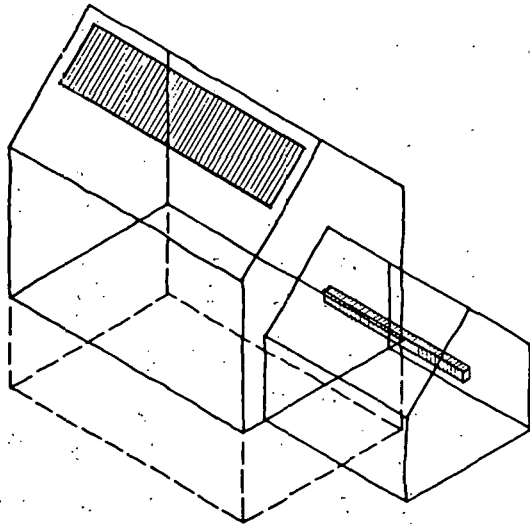
ADDITIONAL STRUCTURAL COST TO SUPPORT ADDED WEIGHT OF STORAGE TANK

ACCESS IS ACCEPTABLE

LEAKAGE PROBLEM IS MINIMIZED

ACCEPTABLE RELATION OF COLLECTOR DISTRIBUTION SYSTEM TO SPACE HEAT DISTRIBUTION SYSTEM

HEAT LOSS FROM STORAGE TANK IS TO AN UNHEATED SPACE



ROOF MOUNTED COLLECTOR
ELECTRICAL SYSTEM IN GARAGE TRUSS SPACE

GASES EXPELLED DURING CHARGING MODE CAN BE VENTED

LONG WIRING RUNS FROM COLLECTOR TO ELECTRICAL SYSTEM

LOADS ON TRUSS REQUIRE ADDITIONAL STRUCTURE MATERIAL

GOOD ACCESS FOR SERVICING OR REPLACEMENT

LEAKAGE BECAUSE OF OVERCHARGE OR DAMAGE IS A PROBLEM

EXPLOSIONS COULD OCCUR IF GASES ARE NOT PROPERLY VENTED

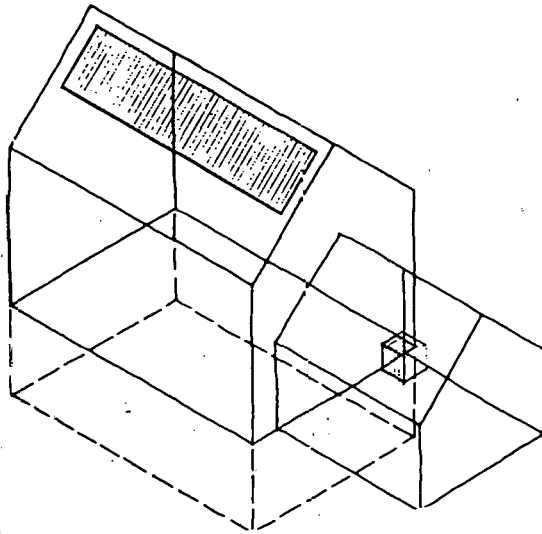
NOT OCCUPYING USABLE FLOOR SPACE IN A HEATED SPACE

FREEZING DURING DEEP CYCLING MIGHT BE A PROBLEM

Figure 1.8.10 - General system placement, option 2

Option 3 is a collector system mounted on the roof, but the thermal and electrical systems are in place on the garage floor (see Figure 1.8.11). The advantages of this placement for the thermal system are that the cost of the building structure and storage tank are reduced in relation to the attic and garage truss system, access is much improved, and potential leakage problems could now be easily handled. The large disadvantage is that the heat loss from the storage tank is still to an unheated space. The advantages for the electrical conditioning system in this option are that the gases created during the charging mode could be easily vented, structural problems and additional structural costs due to the weight of the electrical system are reduced, access is good for servicing or replacement of the components, and any leakage problems which might occur could be easily handled. The disadvantages of the system are that long wiring runs from the collector to the electrical system are required, explosions still could occur if the gases are not properly vented, the system now occupies usable floor space in the garage, freezing still could occur during deep charging or deep cycling, and that potential damage by vehicles might be a problem.

Option 4 is a roof mounted collector with thermal and electrical systems in the basement of the residence (see Figure 1.8.12). The advantages of this arrangement with the thermal system are that the costs of the building structure and storage tank are again reduced in relation to the attic and garage truss system, potential leakage of the thermal storage tank could be easily handled, relation of the



ROOF MOUNTED COLLECTOR
THERMAL STORAGE ON GARAGE FLOOR

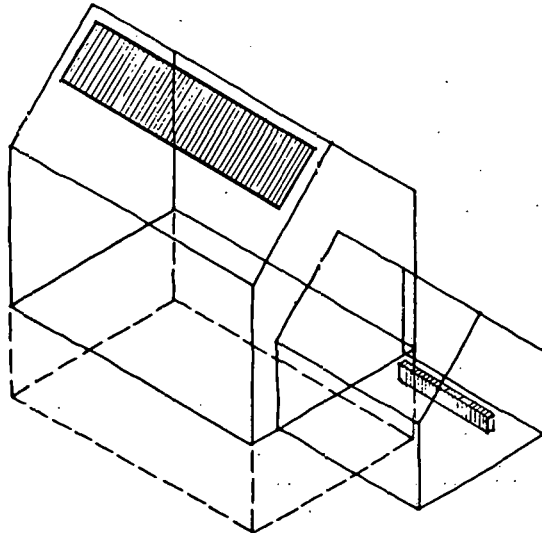
COSTS OF STRUCTURE AND STORAGE TANK ARE REDUCED IN RELATION TO ATTIC AND GARAGE TRUSS SYSTEMS

ACCESS IS GOOD

POTENTIAL LEAKAGE PROBLEMS COULD BE HANDLED EASILY

RELATION OF STORAGE SYSTEM TO COLLECTOR AND SPACE HEAT SYSTEMS BECOMES A PROBLEM

HEAT LOSS FROM STORAGE TANK IS TO AN UNHEATED SPACE



ROOF MOUNTED COLLECTOR
ELECTRICAL SYSTEM IN GARAGE FLOOR

GASES EXPELLED DURING CHARGING MODE CAN BE EASILY VENTED

LONG WIRING RUNS FROM COLLECTOR TO ELECTRICAL SYSTEM

NO STRUCTURAL PROBLEMS

GOOD ACCESS FOR SERVICING OR REPLACEMENT

NO LEAKAGE PROBLEMS

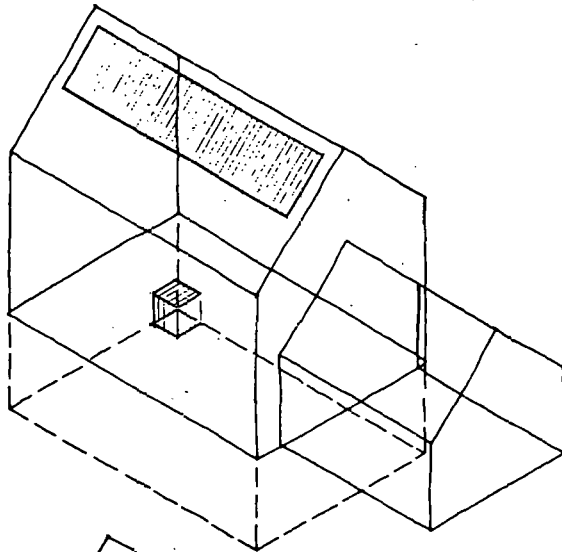
EXPLOSIONS COULD OCCUR IF GASES ARE NOT PROPERLY VENTED

OCCUPIES USABLE FLOOR SPACE IN GARAGE

FREEZING DURING DEEP CYCLING MIGHT BE A PROBLEM

DAMAGE BY VEHICLES COULD BE A PROBLEM

Figure 1.8.11 - General system placement, option 3



ROOF MOUNTED COLLECTOR
THERMAL STORAGE IN BASEMENT

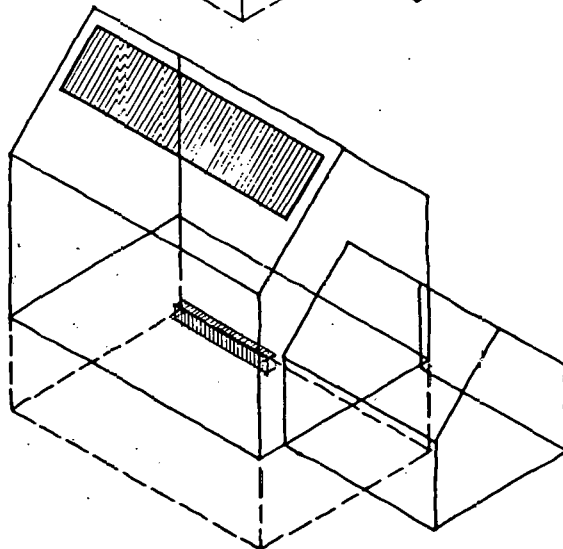
COSTS OF STRUCTURE AND STORAGE TANK ARE REDUCED IN
RELATION TO ATTIC AND GARAGE TRUSS SYSTEMS

ACCESS IS A PROBLEM.

POTENTIAL LEAKAGE PROBLEMS COULD BE HANDLED EASILY.

RELATION OF STORAGE SYSTEM TO COLLECTOR AND SPACE HEAT-
ING SYSTEMS IS GOOD

HEAT LOSS FROM STORAGE TANK IS TO A POTENTIALLY HEATED
SPACE



ROOF MOUNTED COLLECTOR
ELECTRICAL SYSTEM IN BASEMENT

GASES EXPELLED DURING CHARGING MODE MUST BE MECHANI-
CALLY VENTED

WIRING RUNS FROM COLLECTOR TO ELECTRICAL SYSTEM ARE
REDUCED

NO STRUCTURAL PROBLEMS

ACCESS COULD BE A PROBLEM

NO LEAKAGE PROBLEMS

EXPLOSIONS COULD OCCUR IF GASES ARE NOT PROPERLY VENTED

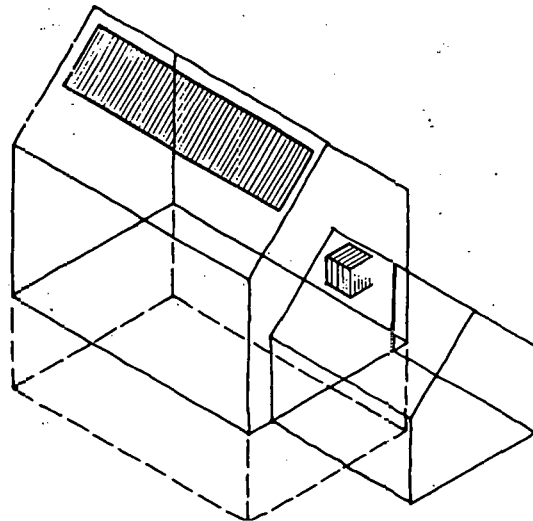
OCCUPIES USABLE FLOOR AREA IN A HEATED INTERIOR SPACE

Figure 1.8.12 - General system placement, option 4

storage system to the collector in space heating system is good, and heat loss from the storage tank is to a potentially heated space. The only problem that exists is access or maintenance of the storage system. The only advantage that the electrical system incurs by this placement is the decrease in building structure costs that occurred in previous options. The disadvantages are as follows: the gases expelled during the charging mode of the batteries must be mechanically vented, access to the system for replacement or repairs could be a problem, explosions could occur if the batteries are not properly vented, and the entire system occupies usable floor area in a heated interior space.

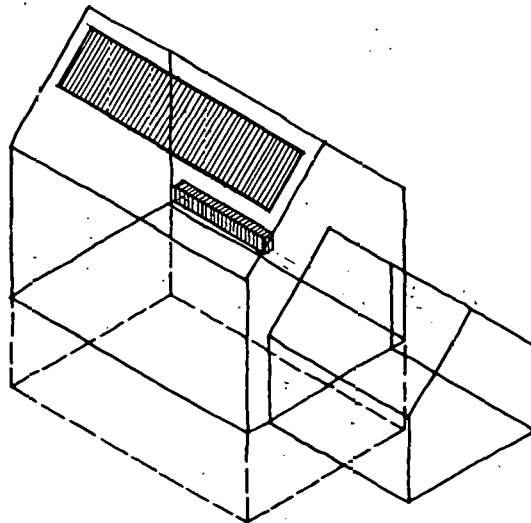
Option 5 is a roof mounted collector with the thermal system and electrical system on ground level outside the structure (see Figure 1.8.13). The major advantages for the thermal system are that access to all of the thermal system components is excellent, and all leakage problems from the storage tank are completely eliminated. The major drawback for this particular option is that additional structural costs are required for the exterior support pad and exterior enclosures.

The relation of the storage system and mechanical components to the collector and interior space heat system does become a problem, nor does heat loss from the storage tank to outside air. Other problems such as vandalism, severe architectural design restrictions and doubtful client acceptability occur in this option. The advantages for the electrical system in this option are as follows: gases that are expelled by the batteries during the charging mode can



**ROOF MOUNTED COLLECTOR
THERMAL STORAGE ON-GROUND LEVEL**

- ADDITIONAL COSTS FOR EXTERIOR SUPPORT PAD AND ENCLOSURE
- ACCESS IS GOOD
- LEAKAGE PROBLEMS ELIMINATED
- RELATION OF STORAGE SYSTEM TO COLLECTOR AND SPACE HEAT SYSTEMS BECOMES A PROBLEM
- HEAT LOSS FROM STORAGE TANK IS TO OUTSIDE AIR
- VANDALISM COULD BE A PROBLEM
- SEVERE ARCHITECTURAL DESIGN RESTRICTION
- DOUBTFUL CLIENT ACCEPTABILITY



**ROOF MOUNTED COLLECTOR
ELECTRICAL SYSTEM OUTSIDE STRUCTURE ABOVE GRADE**

- GASES EXPELLED DURING CHARGING MODE CAN BE EASILY VENTED
- LONG WIRING RUNS FROM COLLECTOR TO ELECTRICAL SYSTEM
- ADDITIONAL CONSTRUCTION COSTS FOR CONCRETE PLATFORM AND ENCLOSURE
- GOOD ACCESS FOR SERVICING OR REPLACEMENT
- NO LEAKAGE PROBLEMS
- EXPLOSIONS ARE LESS OF A PROBLEM OUTSIDE THE BUILDING STRUCTURE
- FREEZING DURING DEEP CYCLING MIGHT BE A PROBLEM
- VANDALISM COULD BE A PROBLEM
- AESTHETIC DESIGN RESTRICTIONS
- OCCUPANT ACCEPTABILITY OF OUTSIDE STRUCTURE COULD BE A PROBLEM

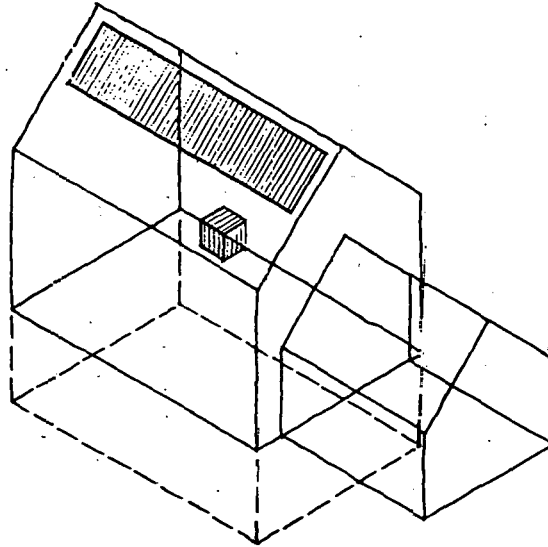
Figure 1.8.13 - General system placement, option 5

be easily vented, access for all the electrical system components is excellent, any leakage problem which might occur due to fracturing of battery cases is eliminated, and explosions are less of a problem due to the ease of the venting in the placement of the components outside the structure. The primary disadvantage with the electrical system like the thermal system is the additional construction costs required for a concrete platform and structural enclosure. Additional disadvantages are as follows: long wiring runs from the collector to the electrical system are required because of the electrical system placement, freezing of the batteries during deep winter time cycling could become a problem.

Option 6 is a roof mounted collector with the thermal system and the electrical system below grade (see Figure 1.8.14). The advantages and disadvantages of both the thermal and electrical systems are similar to Option 5 with the exception that excavation costs replace the additional costs for the exterior support and pad enclosure. The problems with vandalism, severe architectural design restrictions, and client acceptability are eliminated because there is no visual contact with the elements.

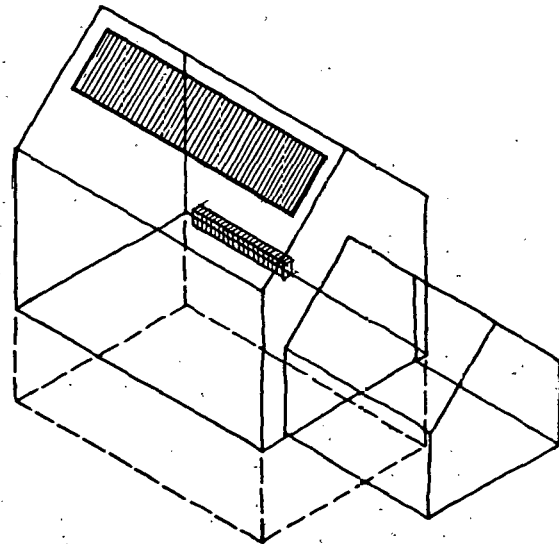
1.8.2 General System Descriptions

In this particular category, both the direct solar heating system and the solar-assisted heat pump system will be discussed. Under each of these systems, variations will be described and all of the pertaining operational modes will be discussed.



ROOF MOUNTED COLLECTOR
THERMAL STORAGE BELOW GRADE

- ADDITIONAL COSTS FOR EXCAVATION
- LEAKAGE PROBLEM ELIMINATED
- RELATION OF STORAGE SYSTEM TO COLLECTOR AND SPACE HEAT SYSTEMS BECOMES A PROBLEM
- HEAT LOSS FROM STORAGE TANK IS TO OUTSIDE AIR
- ACCESS IS GOOD



ROOF MOUNTED COLLECTOR
ELECTRICAL SYSTEM OUTSIDE STRUCTURE BELOW GRADE

- GASES EXPELLED DURING CHARGING MODE CAN BE EASILY VENTED
- LONG WIRING RUNS FROM COLLECTOR TO ELECTRICAL SYSTEM
- ADDITIONAL CONSTRUCTION COST FOR EXCAVATION
- ACCESS PROBLEMS FOR REPLACEMENT
- NO LEAKAGE PROBLEMS
- EXPLOSIONS ARE LESS OF A PROBLEM OUTSIDE THE BUILDING STRUCTURE
- FREEZING DURING DEEP CYCLING MIGHT BE A PROBLEM

Figure 1.8.14 - General system placement, option 6

1.8.2.1 Direct Solar Heating Systems

This section will deal with those photovoltaic systems in which the photovoltaic array cooling fluid is used only in a direct solar heating mode. The decision to use the reject heat directly was based on the fact that small array sizes; 30 square meters; could satisfy a large percentage of the yearly residential heating load.

1.8.2.1.1 Hybrid Silicon Water-Cooled and Air-Cooled Array with a Fossil Fuel Backup

This system, used in both Phoenix and Santa Maria with only minor variations, consists of a water-cooled silicon array coupled with a direct solar heating system modified somewhat to adapt it to a temperature limit of the photovoltaic array and an air-cooled silicon array. The thermal system provides, in each region, nearly 100% of the total heating requirement of the schematic residence with an accompanying fossil fuel backup system providing the remainder (see Figure 1.8.15). The thermal storage tank (see Figure 1.8.16) will either be a 60-mil butyl rubber or a 20-mil reinforced elasticized polyolefin sheeting formed as a bladder container. In each of the two residential applications, the bladder will be placed in an excavated trench within the perimeter foundations of the residence, and lined with styrofoam insulation. The bladder will then be filled with water while in this hole, capped and therefore maintain its shape. Then a concrete slab will be poured in such a way as to cover the top of the bladder and so formed as to provide a grade beam around the tank opening. In most cases the accompanying mechanical components:

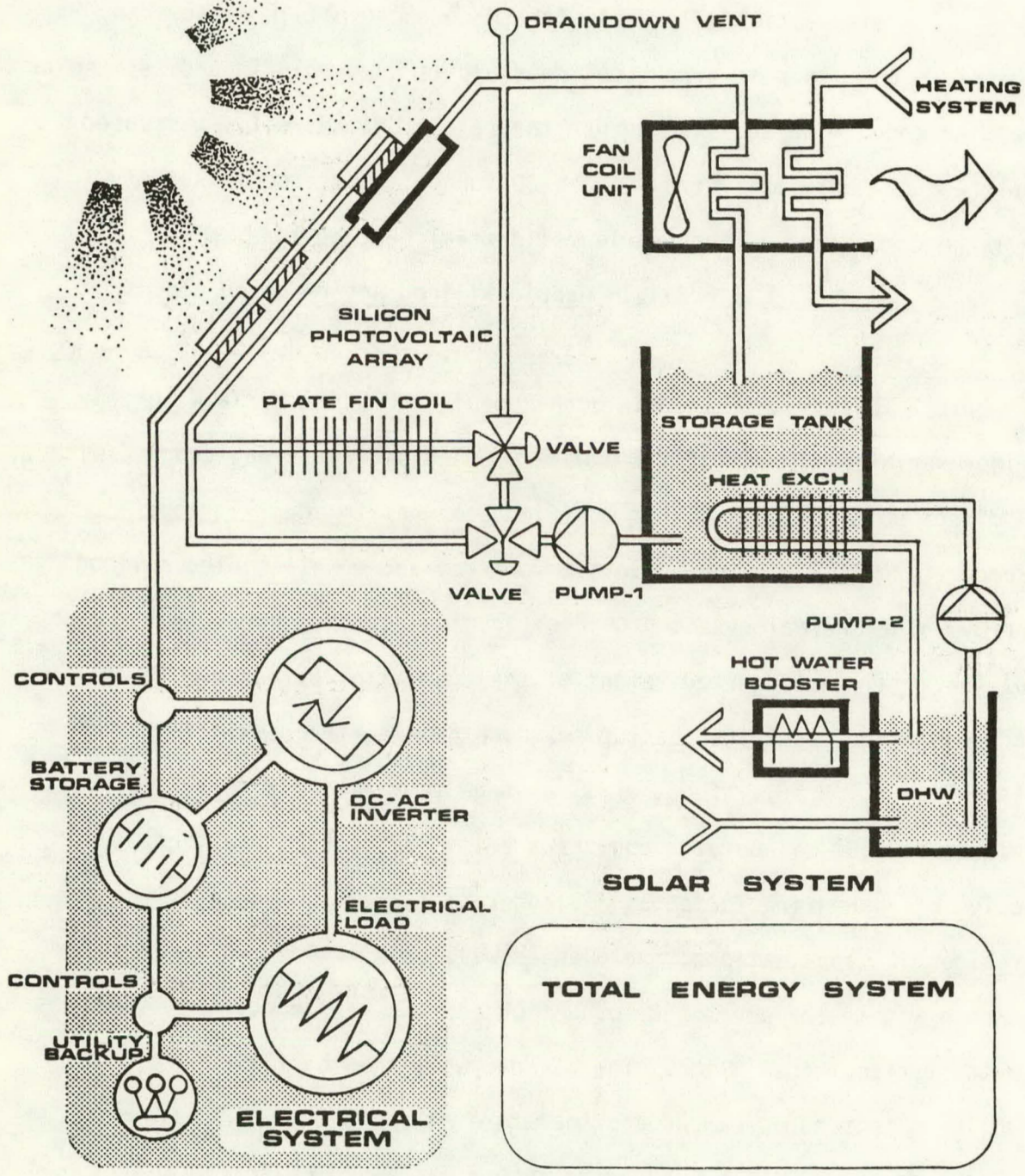


Figure 1.8.15 - Total Energy System, general schematic

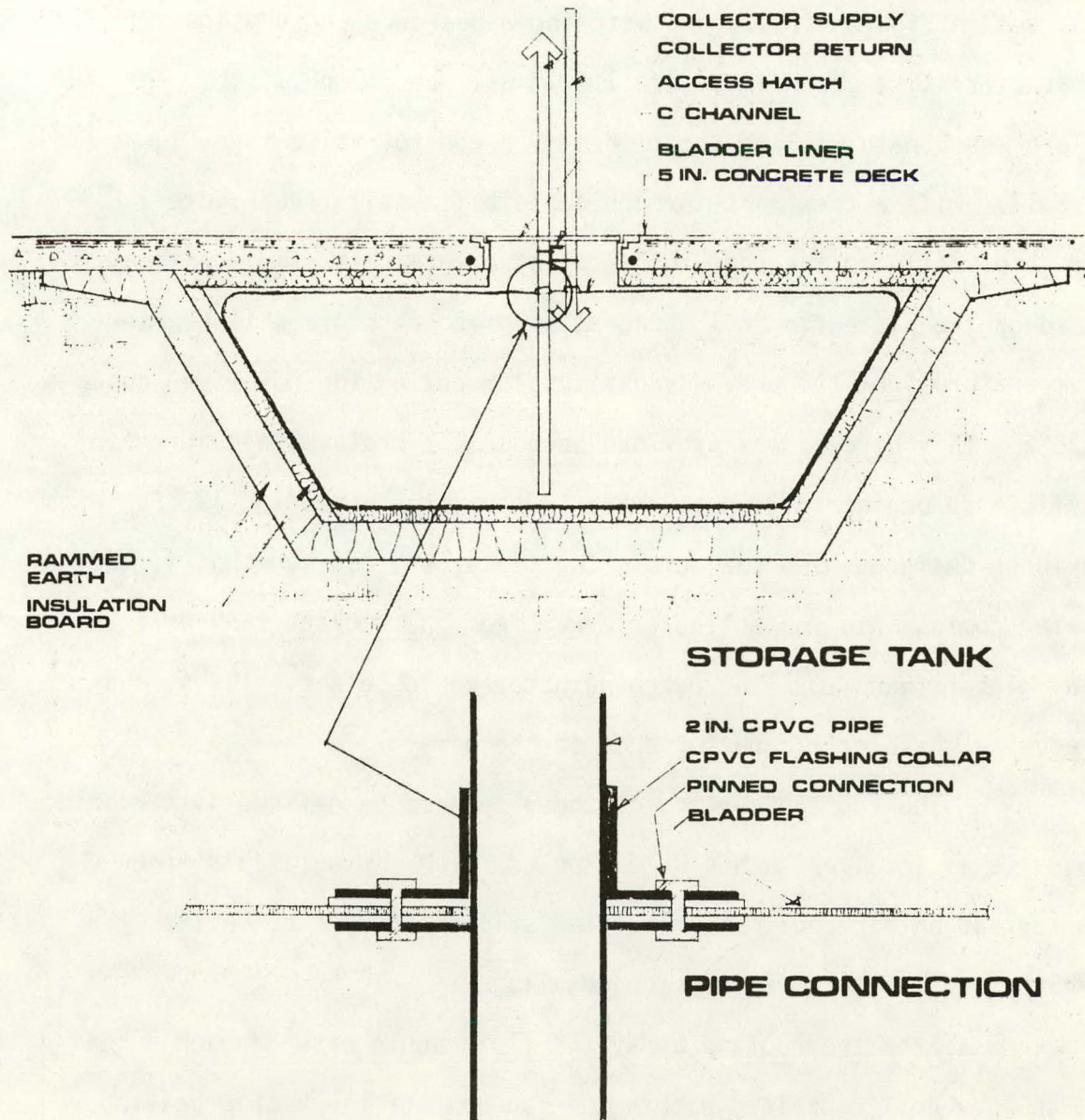


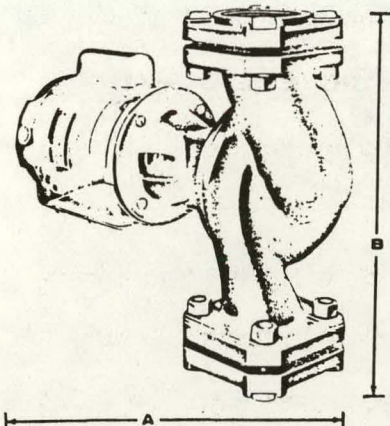
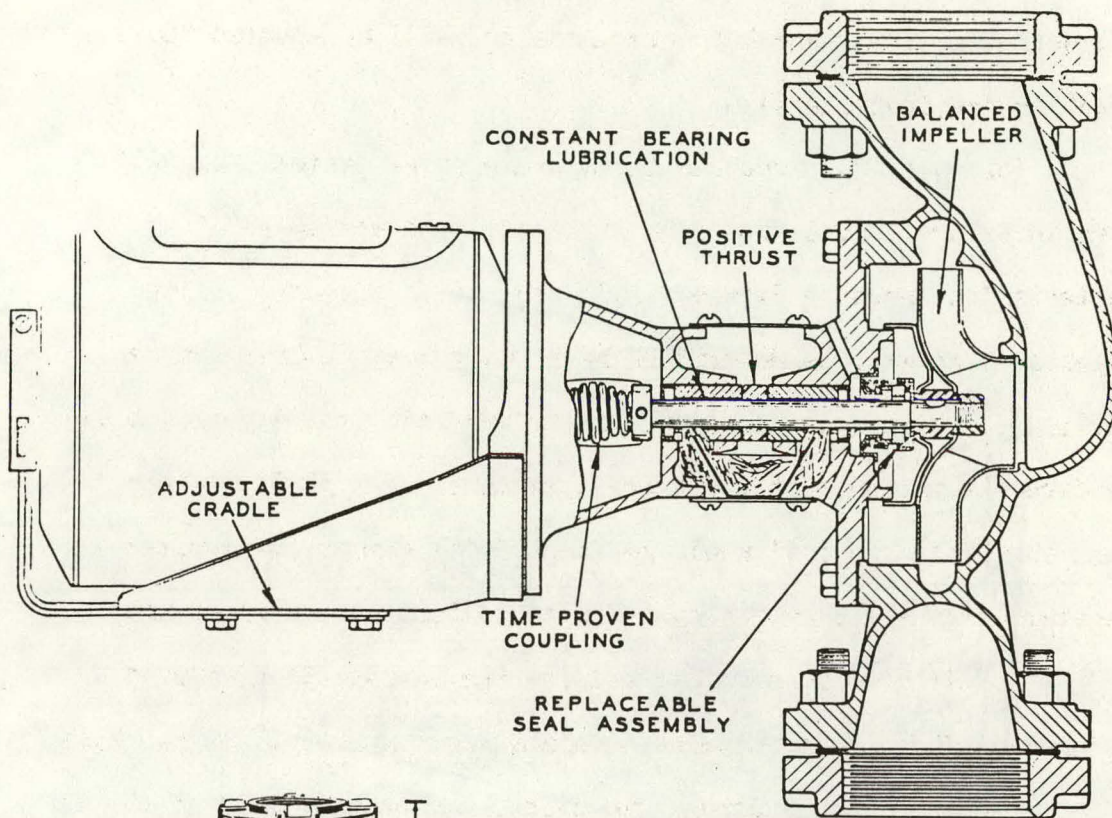
Figure 1.8.16 - Thermal storage tank and pipe connection

pumps, hot water tank, and hot water booster, will be mounted above the tank on the concrete slab.

For water to circulate through the solar system, Pump #1 as seen in Figure 1.8.15, and with the appearance and physical characteristics shown in Figure 1.8.17, will be in operation. The fluid whose path will be determined by a control valve (see Figure 1.8.18), will either pass through a plate fin coil (see Figure 1.8.19) or go directly to the roof top array structure. The fluid pathway through the plate fin coil would be used if the storage tank water temperature from the previous day's solar collection had risen above 120°F. This circuit was provided because the photovoltaic array's efficiency begins to drop at array temperatures exceeding 130°F. With a 10° Δ designed to occur across the plate, one can see that if the water coming into the collector array from the storage tank were any higher than 120°F the outgoing water could be above 130°F, thus reducing the electric performance of the array.

The rooftop portion of these systems is defined as a hybrid because it involves both a water-cooled, fully integrated silicon array and an air-cooled, roof mounted silicon array (see Section 1.5.1 - RPS Array Structure , for design details).

From the rooftop array, the fluid would pass through a heat exchanger coil contained within the fan unit of the backup heating system. If the residence were in a heating mode, the fan would be operational and heat would be transferred from the water to the return air side of the auxiliary heating system air ductwork to satisfy the residential heating load.



Specifications

Motors— $\frac{1}{2}$ and $\frac{3}{4}$ H.P.*
 1750 RPM, 115/230 volt, 60 cycle, 1 phase.
 $\frac{1}{2}$, $\frac{1}{2}$ or $\frac{3}{4}$ 1750 RPM, 208 volt or 230/460
 volt, 60 cycle, 3 phase
 $\frac{1}{2}$ H.P.*
 1750 RPM, 115 volt, or 230 volt, 60 cycle,
 1 phase

*Special characteristic motors also available

Impeller Shaft—Stainless Steel

Size—3"

Maximum suggested operating temperature—250° F.

Maximum suggested operating pressure—125 psi.

Mechanical Water Seal

Closed Impeller

	RC-0	RC-1	RC-2	RCB-0	RCB-1	RCB-2
Motor	$\frac{1}{2}$ H.P.	$\frac{1}{2}$ H.P.	$\frac{3}{4}$ H.P.	$\frac{1}{2}$ H.P.	$\frac{1}{2}$ HP	$\frac{3}{4}$ H.P.
Construction	Bronze Fitted**		All-Iron	All-Bronze	All-Bronze	All-Bronze

**Must specify

Replacement Bracket No.	RC-0	RC-1	RC-2	B-8	B-6	B-7
Replacement Seal Kit No.	RC	RC	RC	RC	RC	RC

CIRCULATOR	SIZE	SHIPPING WEIGHT	DIMENSIONS	
			A	B
RC-0	3"	66 lbs.	21 $\frac{3}{4}$ "	14 $\frac{1}{2}$ "
RC-1	3"	74 lbs.	23"	14 $\frac{1}{2}$ "
RC-2	3"	80 lbs.	24 $\frac{1}{2}$ "	14 $\frac{1}{2}$ "
RCB-0	3"	66 lbs.	21 $\frac{3}{4}$ "	14 $\frac{1}{2}$ "
RCB-1	3"	74 lbs.	23"	14 $\frac{1}{2}$ "
RCB-2	3"	80 lbs.	24 $\frac{1}{2}$ "	14 $\frac{1}{2}$ "

Figure 1.8.17 - Water pump specifications

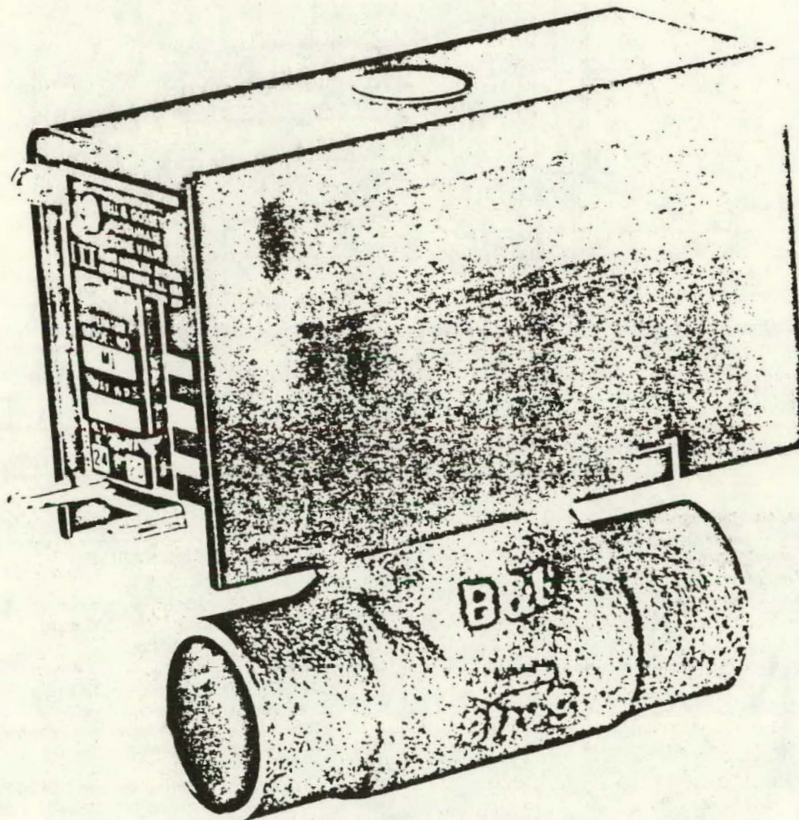


Figure 1.8.18 - Residential control valve

TURBU-FLO' PLATE FIN SURFACE
Corrugated for greater air wash, more effective heat transfer. Standard material is aluminum. Copper can be substituted, if specified.

PERMANENT TUBE/FIN BOND
Fins are mechanically bonded to tubes to form a vibration-free, permanently-joined unit.

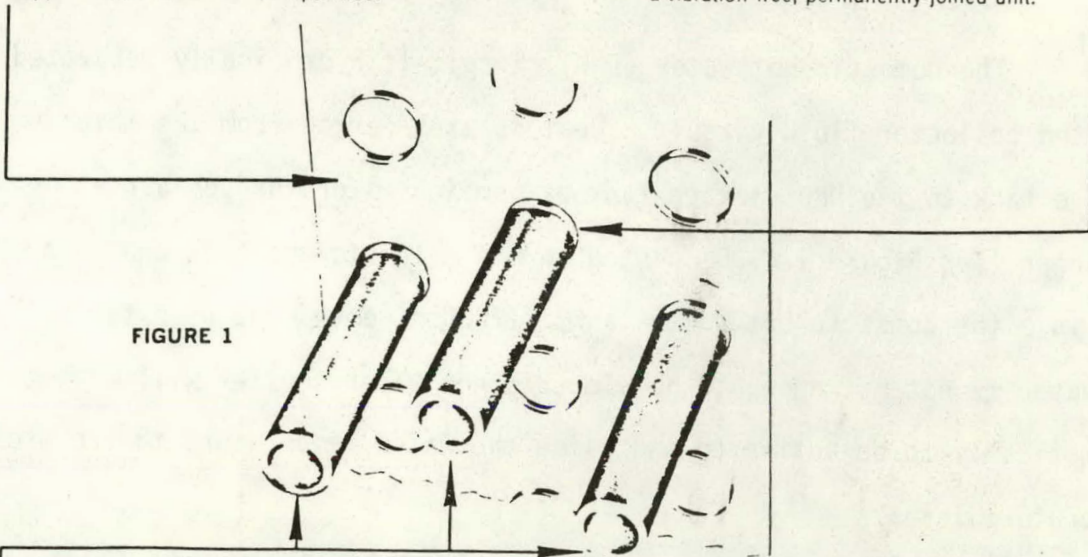


FIGURE 1

STAGGERED TUBE DESIGN

Creates an extra measure of heat transfer. $\frac{3}{8}$ " OD seamless copper tubing spaced 1.50" vertically and 1.299" horizontally on row centers.

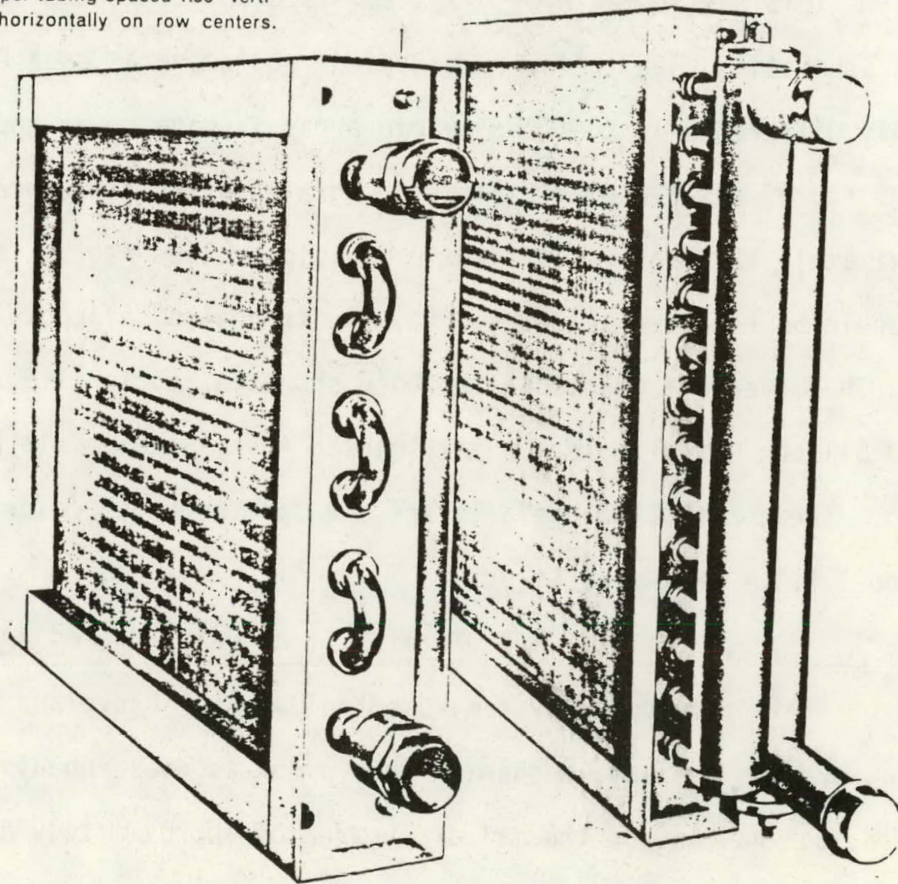


Figure 1.8.19 - Plate fin coil

The domestic hot water (DHW) circuit is hydronically separated from the collector fluid circuit. Heat is transferred from the main storage tank to the DHW storage tank by pumping water through a heat exchanger (see Figure 1.8.20) nested in the main storage tank and then back into the domestic hot water tank. If, upon demand, the domestic hot water is not hot enough, the electric hot water booster will automatically be activated and raise the water temperature to the preset temperature level.

1.8.2.1.2 Hybrid Silicon Water-Cooled Array and Roof Membrane Cadmium Sulfide Array

This particular hybrid system, used only in the Atlanta Design Schematic, uses the same mechanical equipment as does Phoenix. The only difference is that the hybrid array is made up of approximately 450 sq. ft. of water-cooled silicon integrated array structure and approximately 1200 sq. ft. of cadmium sulfide rolled roofing array. This could be replaced by 700 sq. ft. of air-cooled silicon at higher cost. The modes are identical to those shown in Section 1.8.2.1.1 - Hybrid Silicon Water-Cooled and Air-cooled Array with Fossil Fuel Backup. The construction details are the same as those described in Section 1.5.1 - RPS Array Structure.

1.8.2.1.3 Total Silicon Water-Cooled Array

This particular system, used only in the Cleveland design schematic, uses the same mechanical equipment as does Phoenix and Atlanta, but has only a thermal array area of approximately 330 sq. ft. which is being used in a direct heating mode. It supplies the nominal 115 volt load and has a fossil-fuel backup.

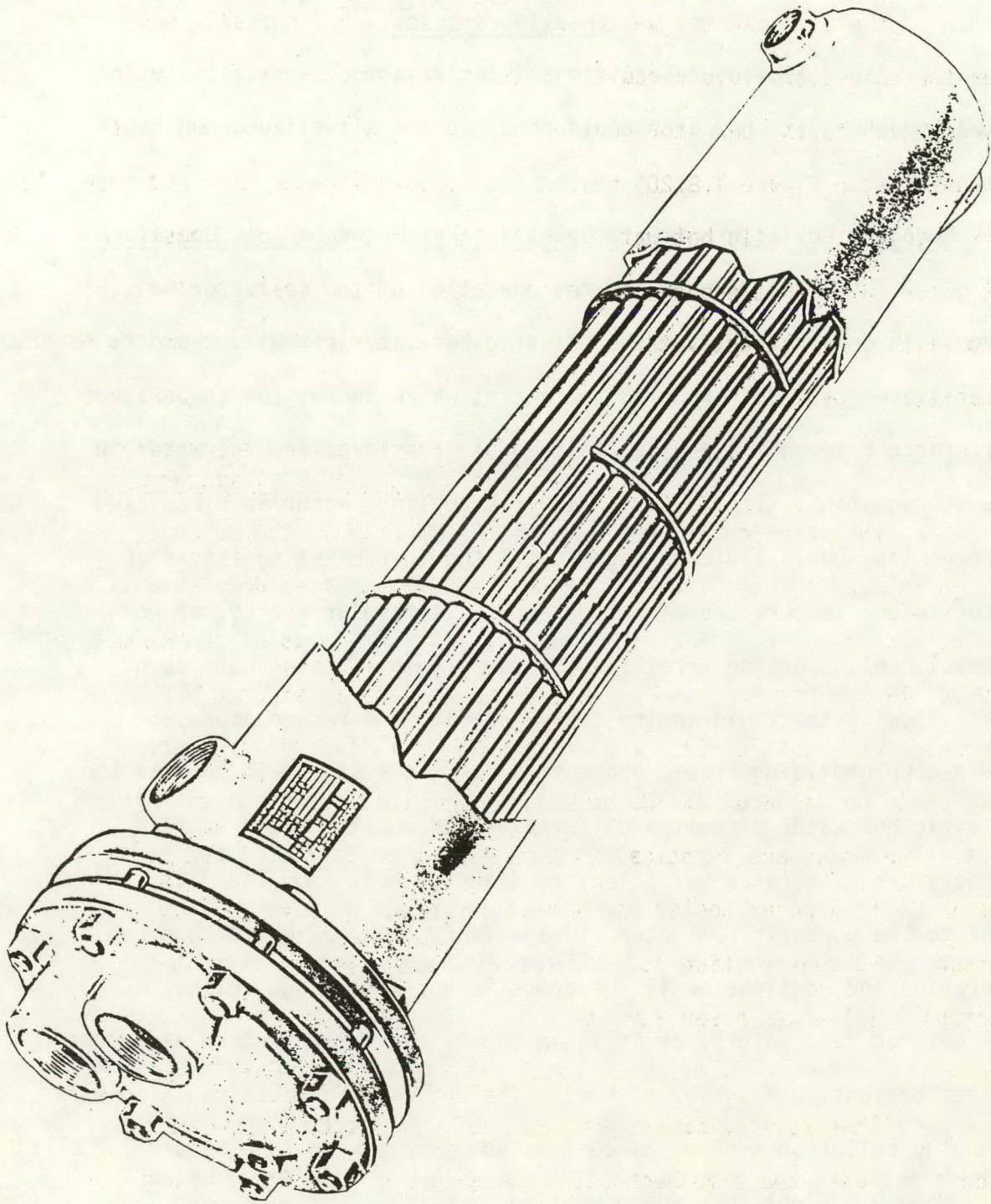


Figure 1.8.20 - Residential heat exchanger

1.8.2.1.4 Mode Descriptions of the Direct Solar Heating Systems

The following descriptions illustrate more specifically the actual mode conditions which would occur in the all-silicon non-heat-pump system.

Mode 1 - Collector Circuit Operation-Hot Water Circuit Operation

This mode illustrates the operation of the collector cooling circuit in conjunction with the domestic hot water circuit. Pump #1 is activated by a differential thermostat which senses the temperature difference between the photovoltaic module substrate and the water in the storage tank. If the array requires cooling, water is circulated through the module fluid passages until the thermostat registers an insufficient temperature difference to collect solar energy, or no thermal cooling of the array is required. Pump #1 then shuts down thus allowing the fluid in the array, supply, and return pipes to drain down providing freeze protection for the system. To operate the domestic hot water circuit, a differential thermostat would sense a temperature difference sufficient to transfer heat from the main storage tank to the domestic hot water storage tank. Pump #2 would then begin operation and continue until the domestic hot water tank reaches the desired temperature, or until an insufficient temperature difference exists preventing transfer of heat. The hot water circuit can also work when the collector cooling circuit is not functioning (see Figure 1.8.21).

Mode 2 - Night-Time Space Heating

In this mode, the residential space heating thermostat senses a night-time heating requirement. If the storage tank water temperature

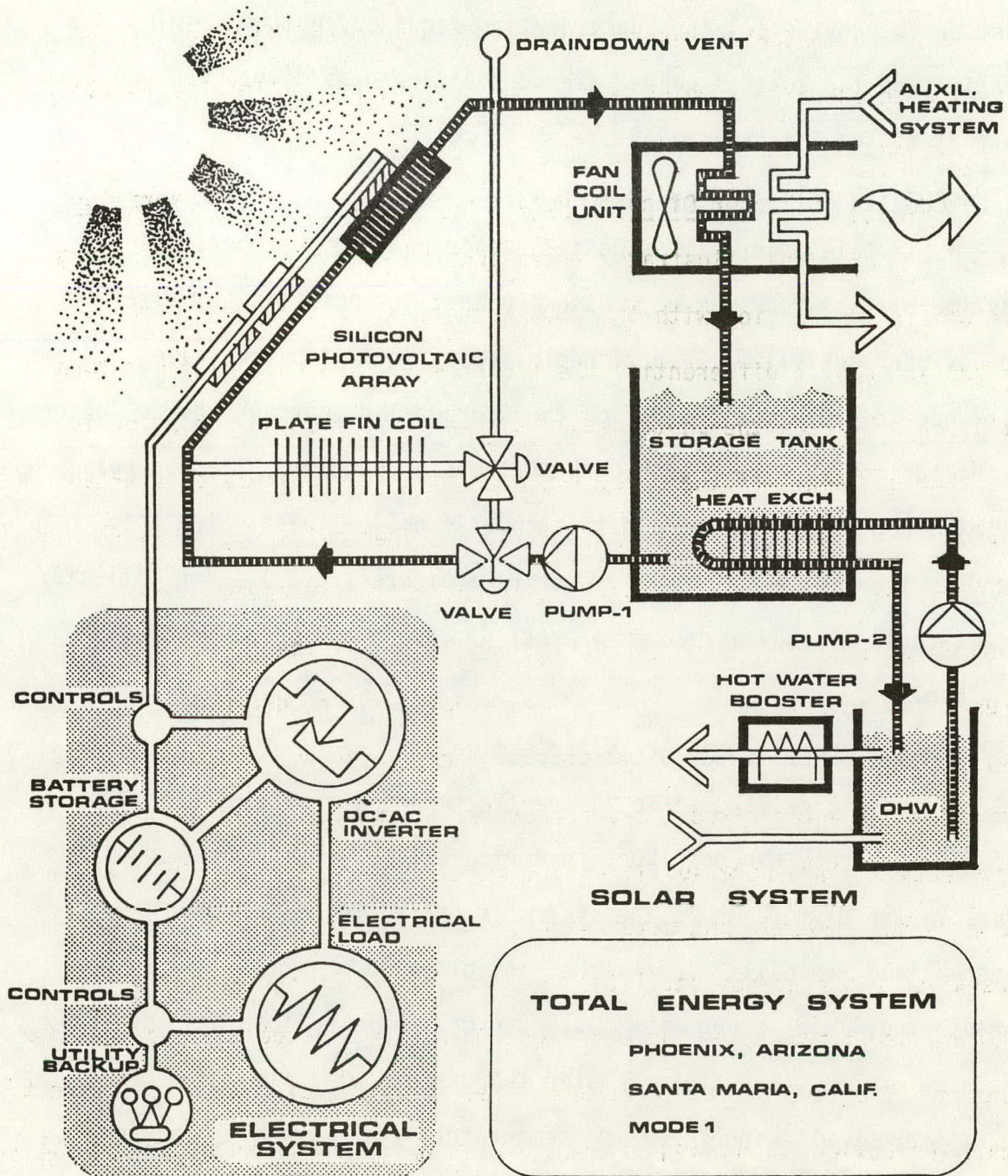


Figure 1.8.21 - Total Energy System for Santa Maria, California - Mode 1

is sufficiently warm to effect a heat boost to the auxiliary heating system or to provide all the space heating required, Pump #1 begins operation and the control valves are so positioned as to produce the flow illustrated (see Figure 1.8.22).

Mode 3 - Day-Time Space Heating

In this mode the residential space heating thermostat senses a daytime heating requirement. Assuming that the domestic hot water load has been satisfied, Pump #1 begins operation, with the valves positioned to route the fluid from the storage tank through the collector and the fan coil unit and then back to the storage tank. The fan coil unit also begins operation to extract heat from the solar water coil placed in the residential supply duct (see Figure 1.8.23). The collector circuit could already have been operating to keep the photovoltaic array cool.

Mode 4 - Photovoltaic Array Protection

This mode is used to assure that the photovoltaic cell temperature rarely exceeds 130⁰F (see Figure 1.8.24). If this condition occurs in the daytime while the system is collecting heat, the differential thermostat signals the control valve to switch and to re-route the fluid through the plate fin coil before it enters the array. This assures that the entering water temperature will always be below 120⁰F, thereby allowing for a 10⁰ temperature rise across the plate without affecting the photovoltaic array's electrical performance. The tank temperature can also be reduced at night by using the same circuit and re-radiating heat to the night sky.

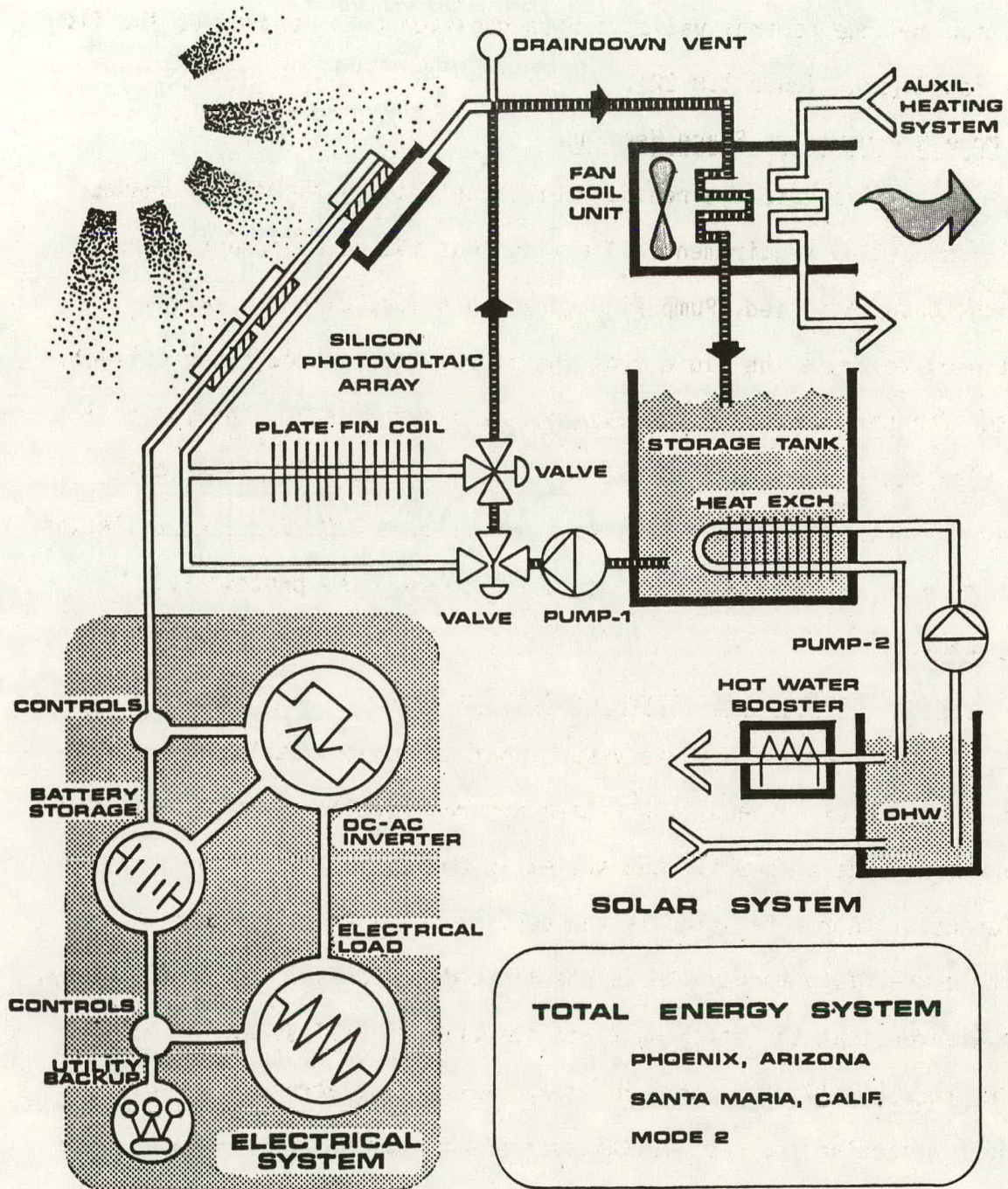


Figure 1.8.22 - Total Energy System for Santa Maria, California - Mode 2

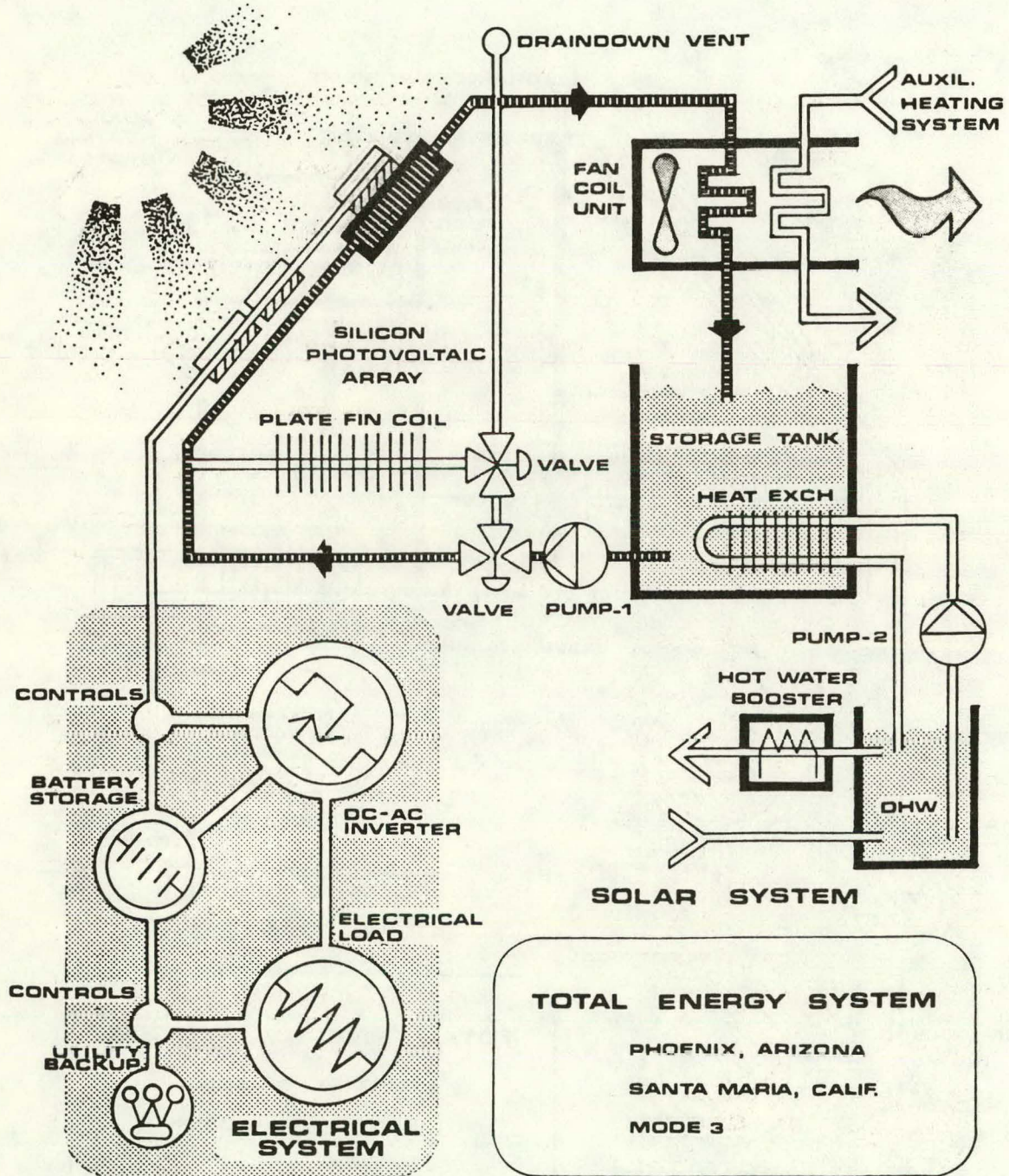


Figure 1.8.23 - Total Energy System for Santa Maria, California - Mode 3

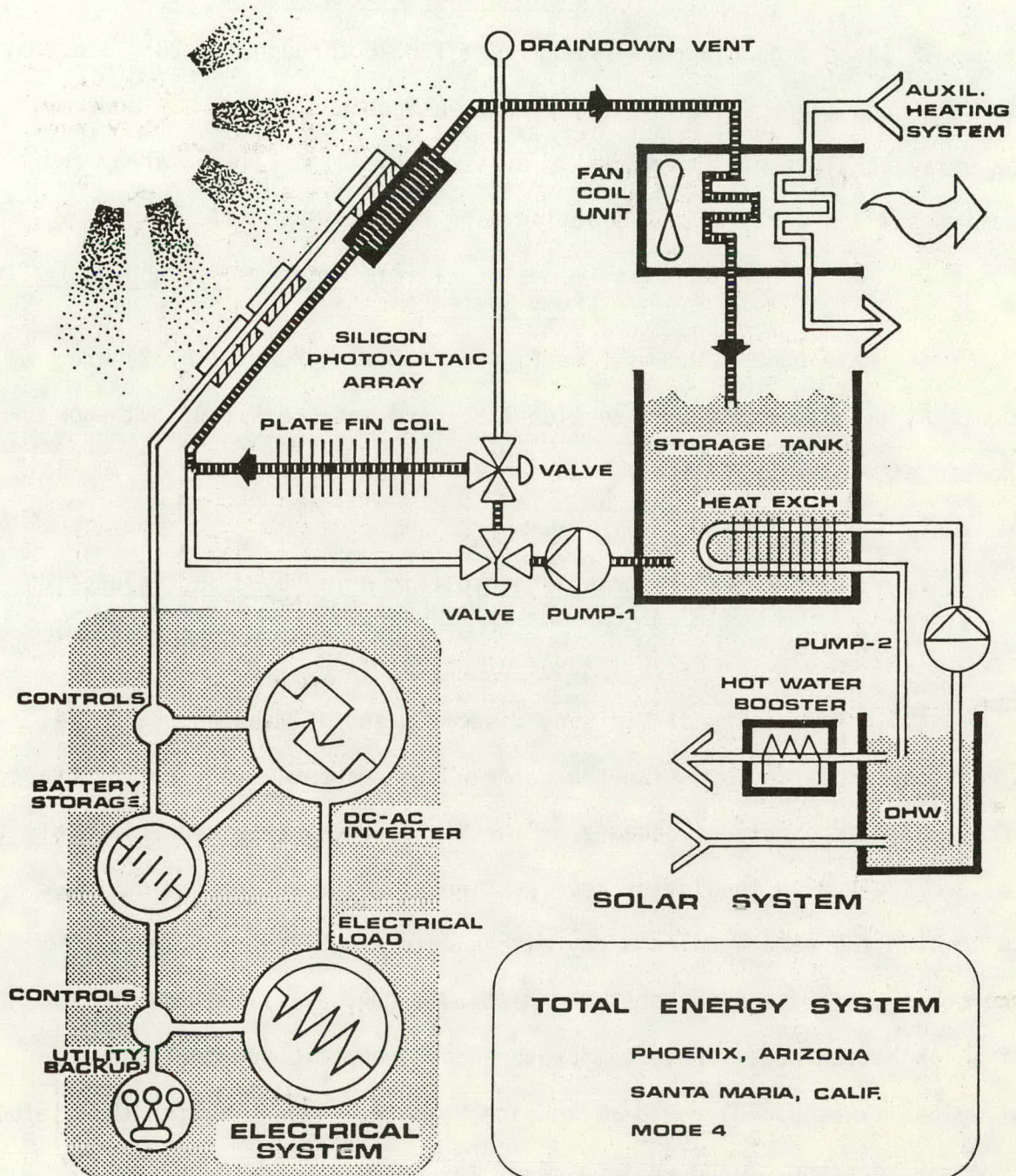


Figure 1.8.24 - Total Energy System for Santa Maria, California - Mode 4

1.8.2.1.5 Modes of the Non-Heat Pump Hybrid Silicon and Cadmium Sulfide Array Systems

These mode diagrams (see Figure 1.8.25 through 1.8.28) illustrate the same conditions as the mode diagrams in Section 1.8.2.1.4. However, the array consists of a combination of a water-cooled silicon array and a cadmium sulfide array which is acting as a roofing material.

1.8.2.1.6 Modes of Silicon Water-Cooled Non-Heat-Pump System

These mode diagrams (see Figures 1.8.29 through 1.8.32) are identical to the diagrams in Section 1.8.2.1.4 and 1.8.2.1.5, but show the use of a non-hybrid all-silicon water-cooled array. This system is used only in the Cleveland, Ohio example.

1.8.2.2 Water Cooled Photovoltaic Array Used in Conjunction with a Solar-Assisted Heat Pump

1.8.2.2.1 General Description

In the cities of Madison, Wisconsin and Wilmington, Delaware, direct space heating by using the water which has cooled the photovoltaic array was less practical because of the high requirements and relatively low average yearly insolation levels. Therefore, a system was designed to combine the water-cooled array with a water-to-air heat pump with the solar system used to boost the heat pump COP. This allowed the use of solar heated water whose temperature has dropped below the point at which it was useful for direct space heating, thereby making the useful temperature range of the waste heat of the array larger, producing significant economic benefits over a simple direct space heating system.

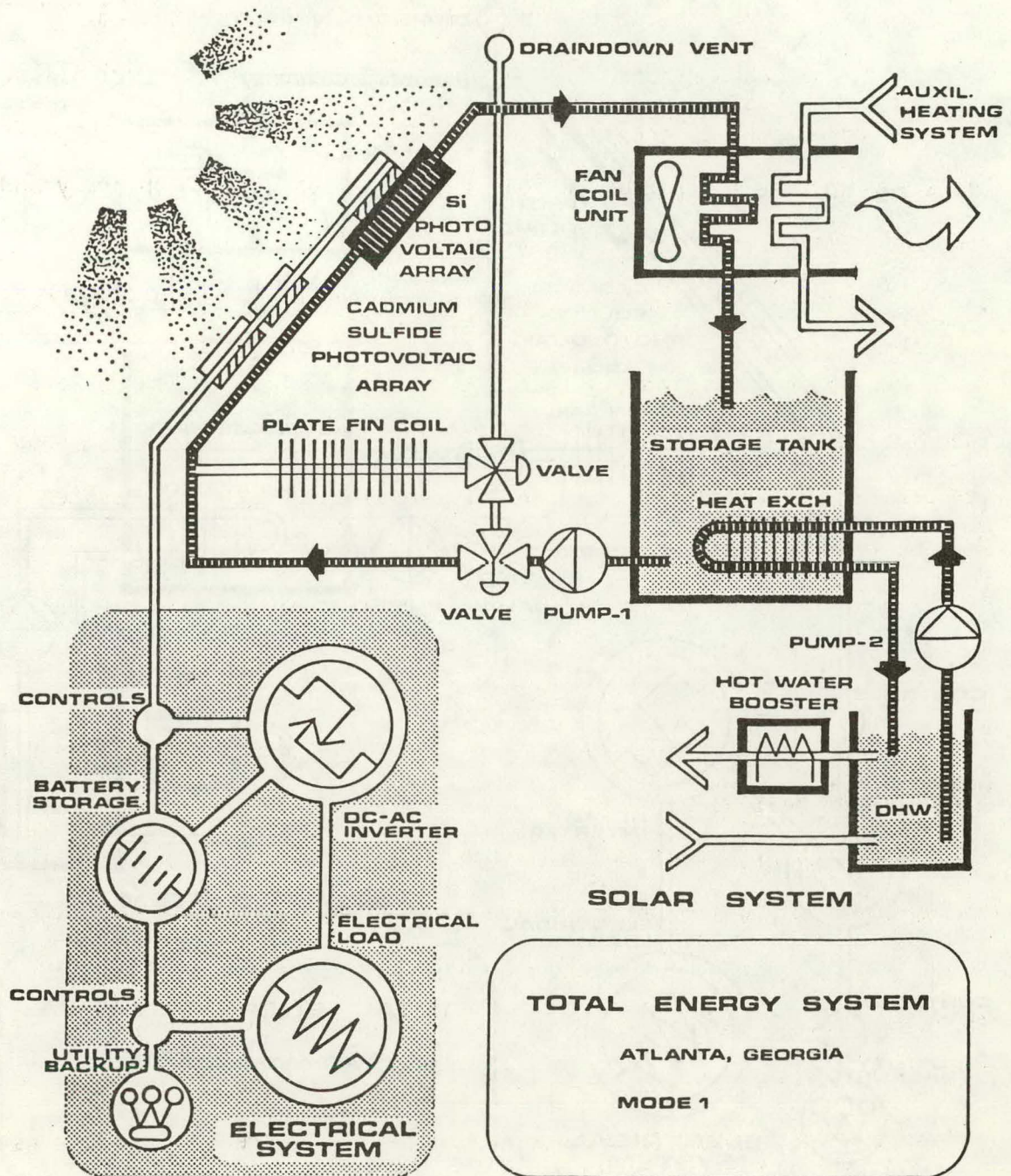


Figure 1.8.25 - Total Energy System for Atlanta, Georgia - Mode 1

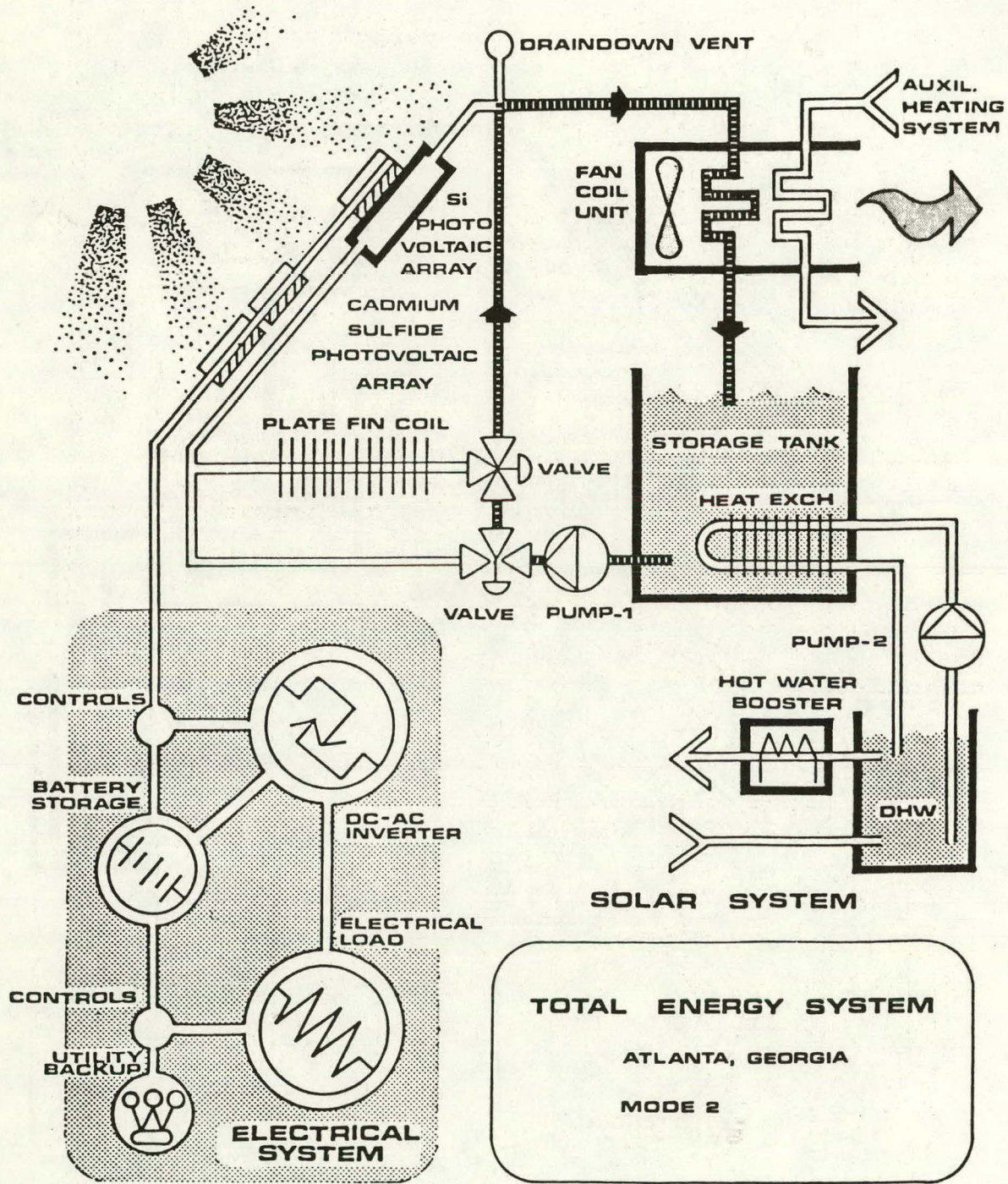


Figure 1.8.26 - Total Energy System for Atlanta, Georgia - Mode 2

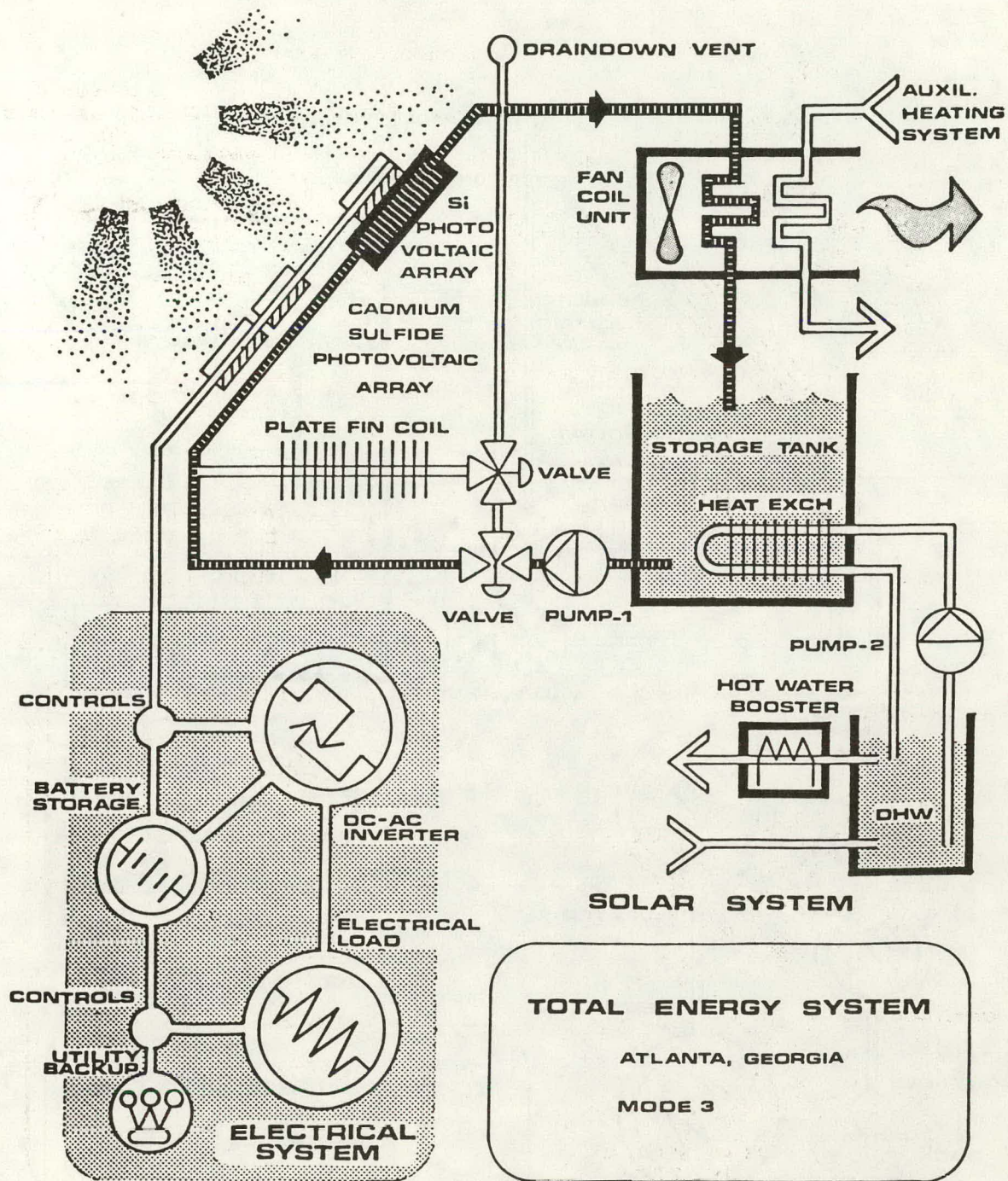


Figure 1.8.27 - Total Energy System for Atlanta, Georgia - Mode 3

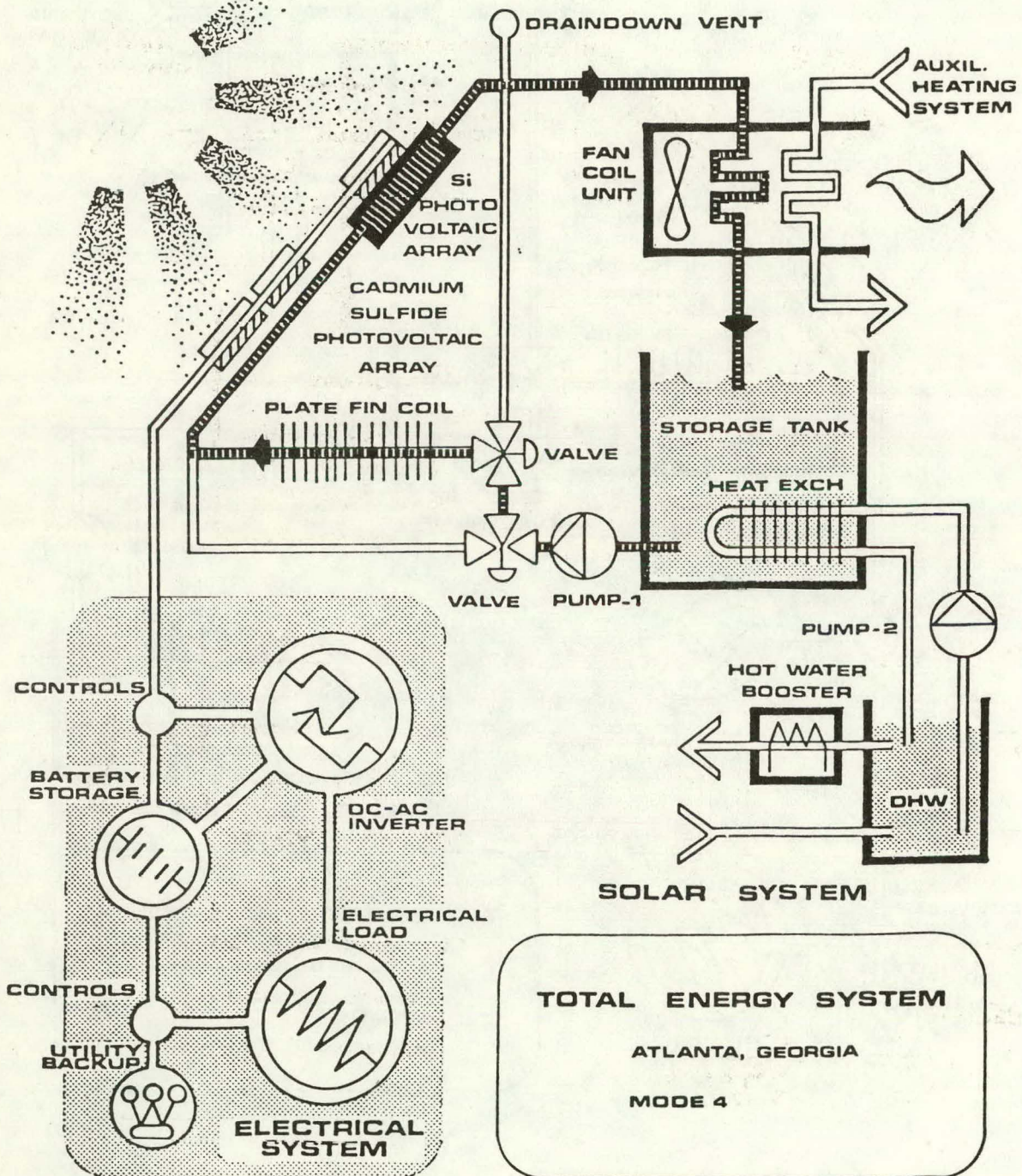


Figure 1.8.28 - Total Energy System for Atlanta, Georgia - Mode 4

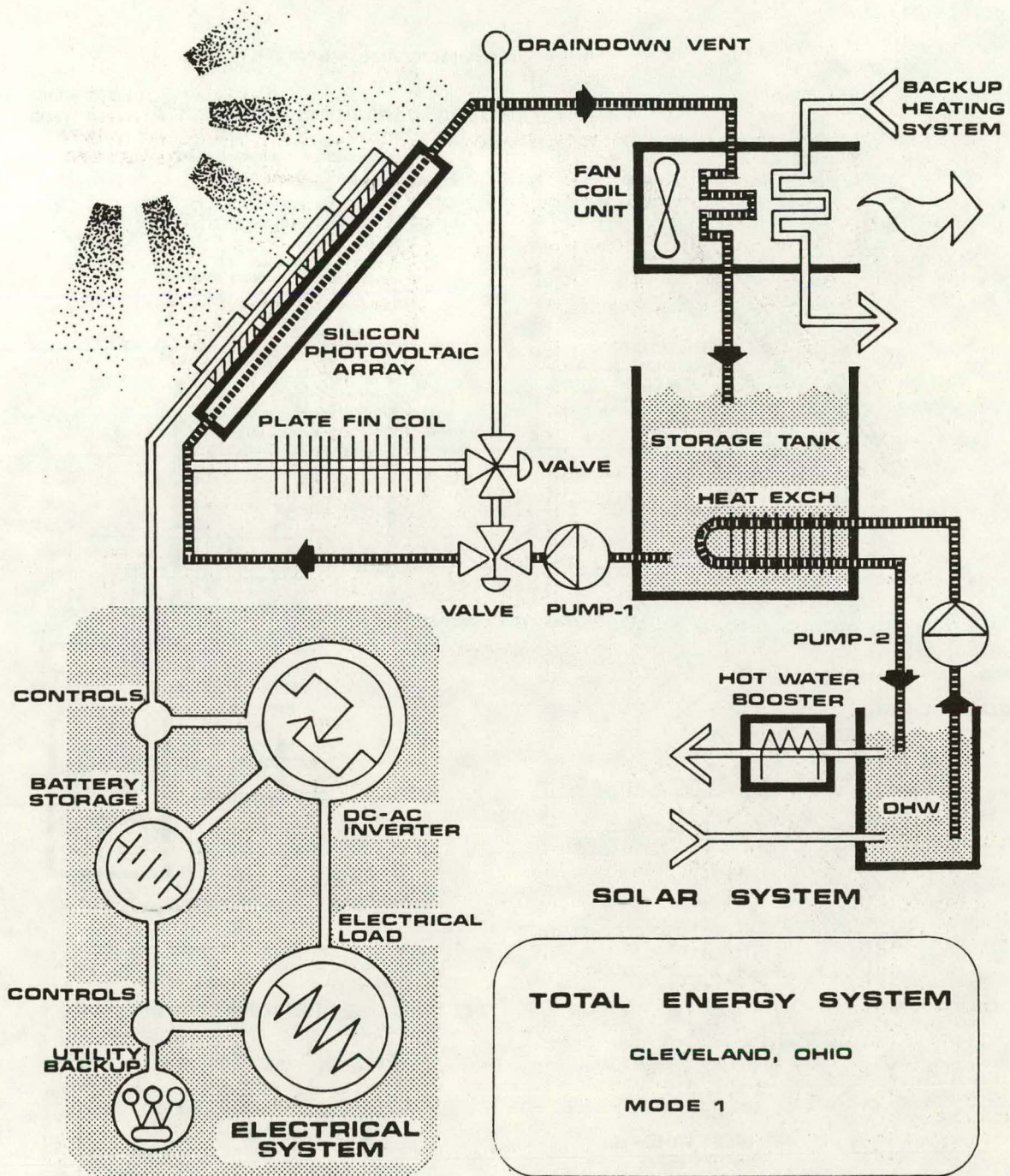


Figure 1.8.29 - Total Energy System for Cleveland, Ohio - Mode 1

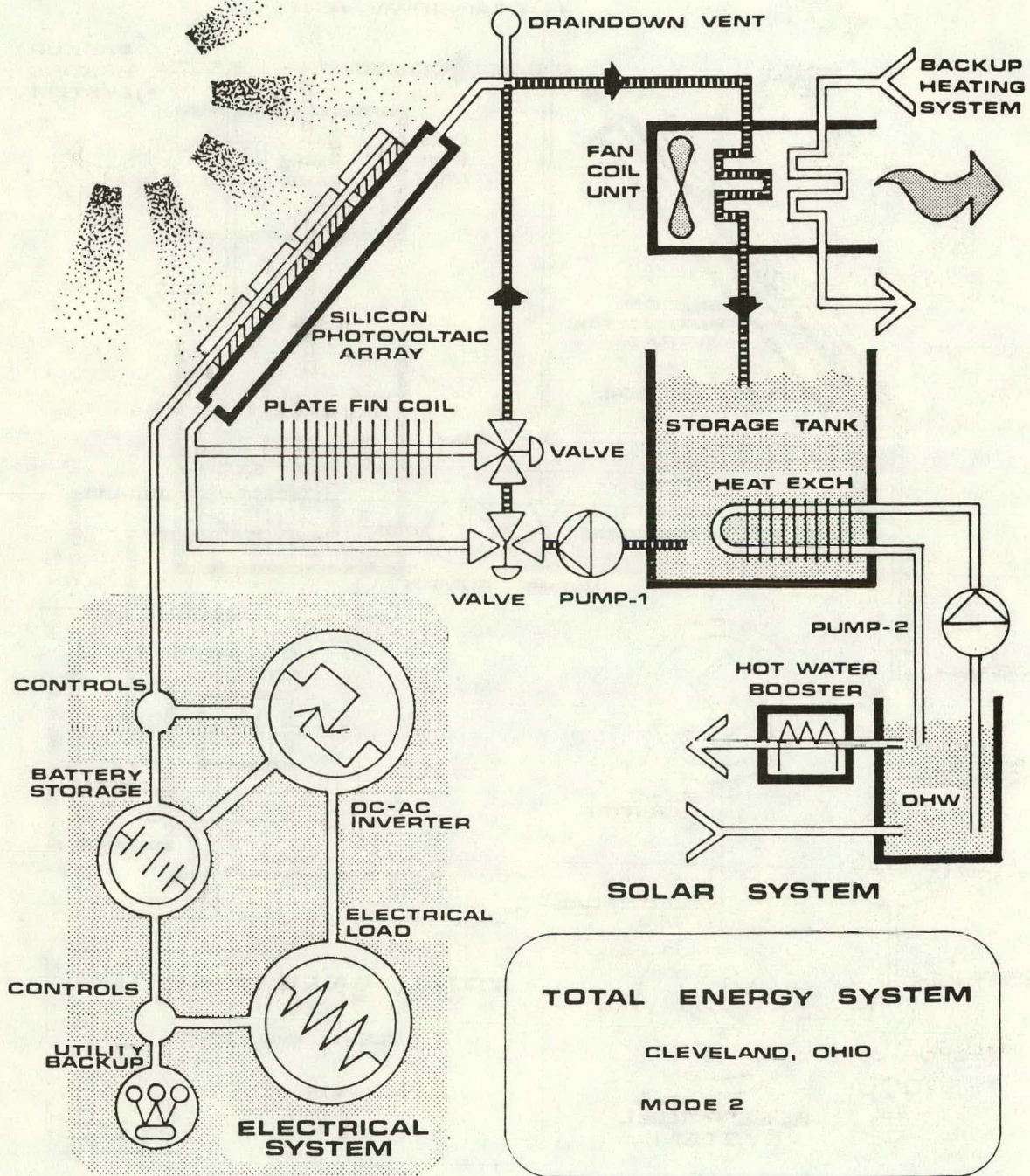


Figure 1.8.30 - Total Energy System for Cleveland, Ohio - Mode 2

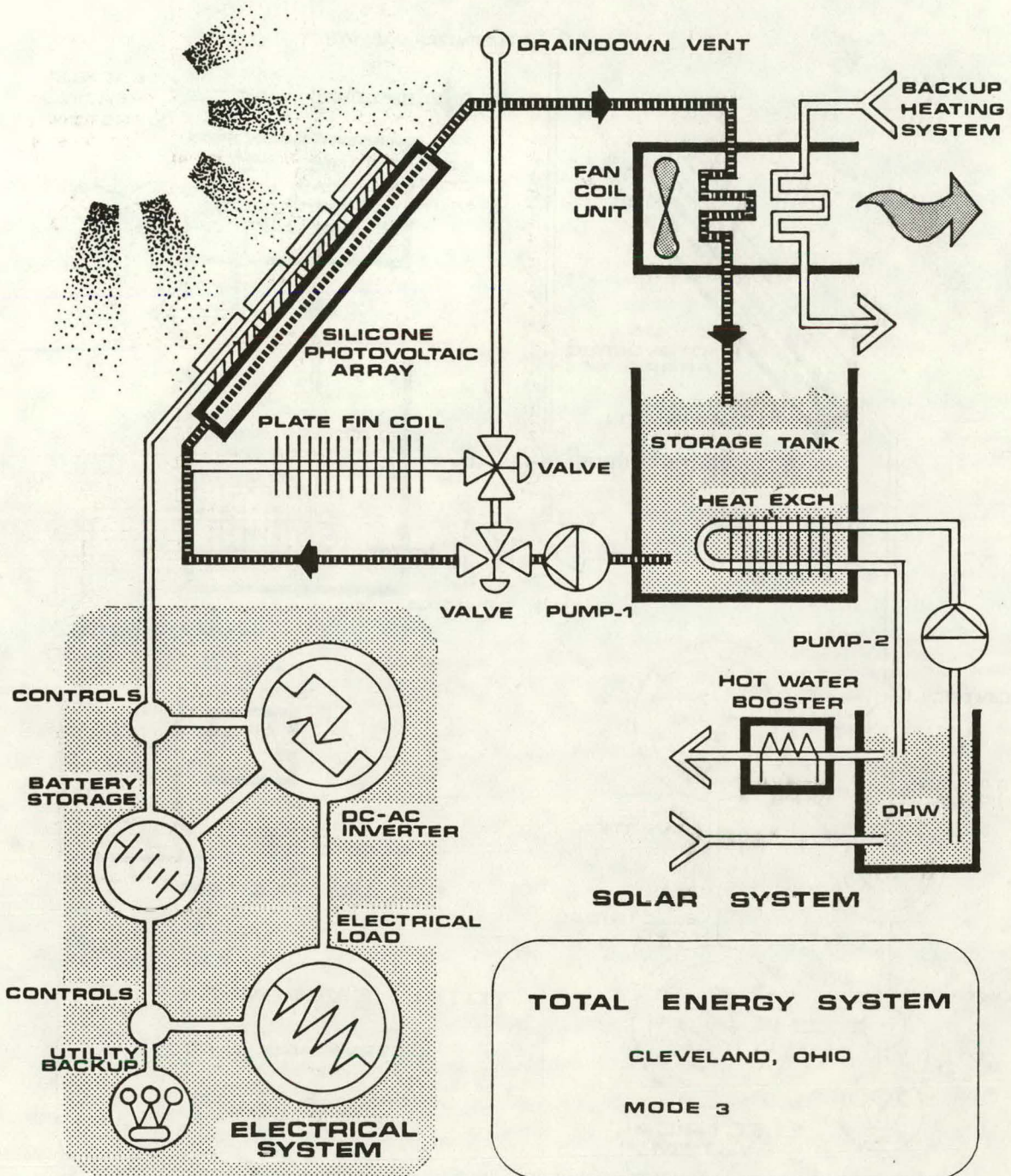


Figure 1.8.31 - Total Energy System for Cleveland, Ohio - Mode 3

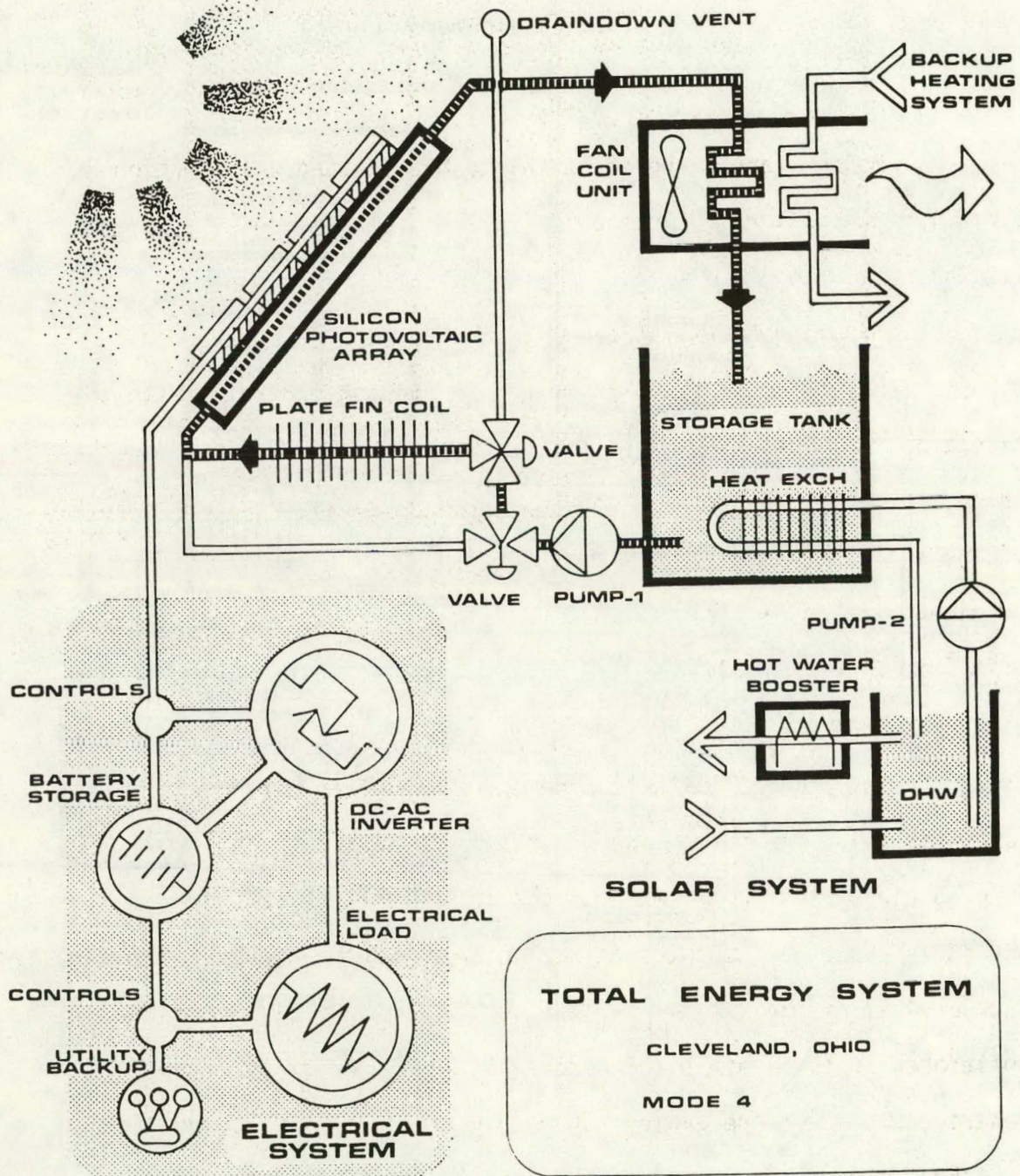


Figure 1.8.32 - Total Energy System for Cleveland, Ohio - Mode 4

1.8.2.2.2 Water-Cooled Photovoltaic Array Used
In Conjunction with the Solar Heat Pump
Mode Definition

Mode 1 - Collector Circuit Operation - Hot Water Circuit Operation

Mode 2 - Night-Time Space Heating

Modes 1 and 2 are identical to Modes 1 and 2 in Section 1.8.2.1.4 and will not be discussed further (see Figures 1.8.33 and 1.8.34).

Mode 3 - Day-Time Space Heating

Mode 3 corresponds to Mode 3 in Section 1.8.2.1.4 with the exception that Pump #3 circulates the hot water from the storage tank through a solar water coil placed in the air handling or indoor unit of the split heat arrangement. The backup heating system is provided with an electrical resistance coil mounted in the indoor unit (see Figure 1.3.35).

Mode 4 - Solar-Assisted Heat Pump

This mode illustrates the operation of an air-to-air heat pump with solar input from the water storage tank. In this mode, Pump #3 circulates the water from the solar storage tank through the solar water coil located in the ductwork of the evaporator or outdoor unit of the air-to-air heat pump. The operable damper is positioned in this unit to re-circulate the stream of air from the centrifugal fan of the evaporator refrigerant coil. No outdoor air is taken in during this mode. The heat is transferred to the

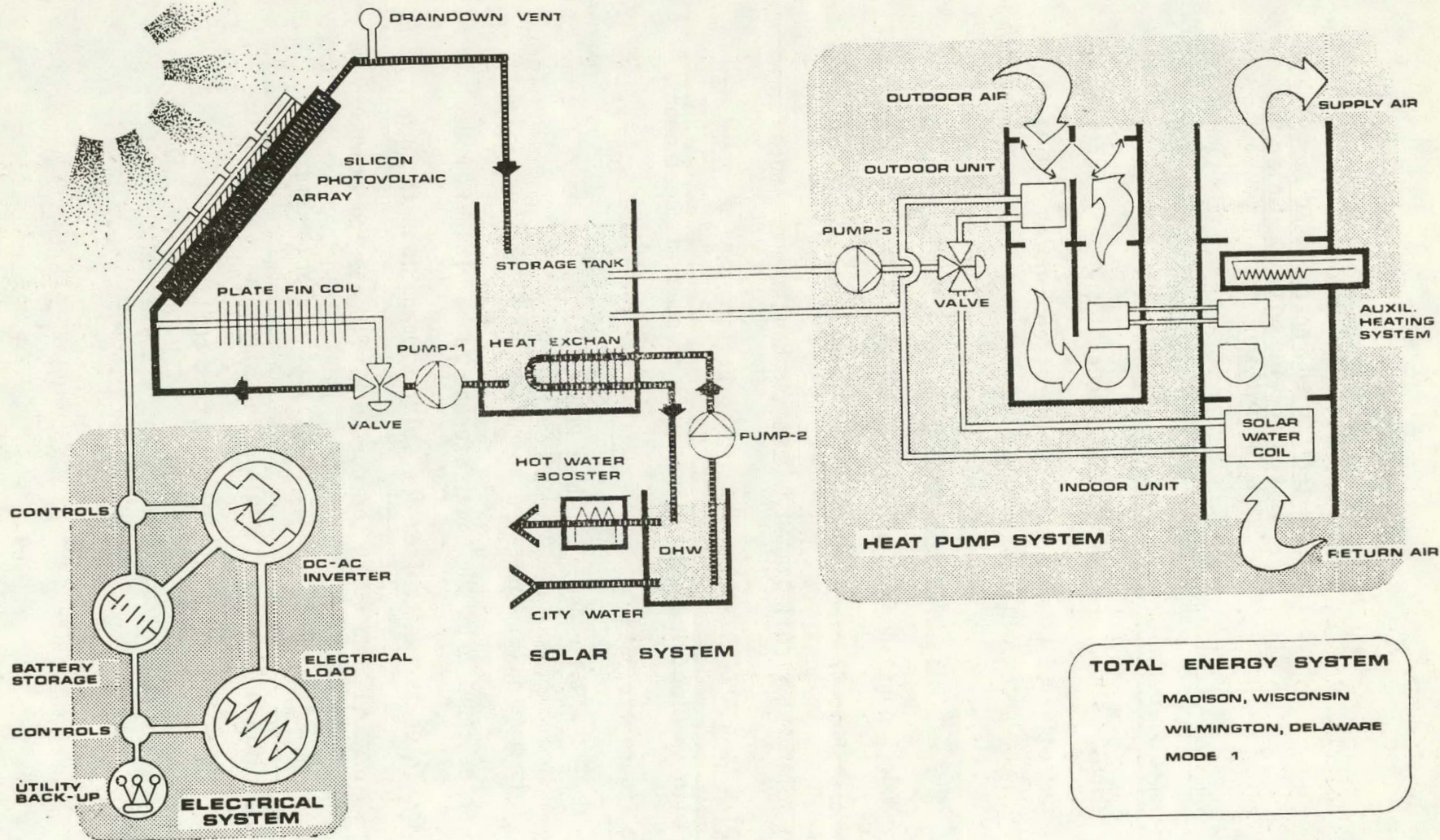


Figure 1.8.33 - Total Energy System for Madison, Wisconsin - Mode 1

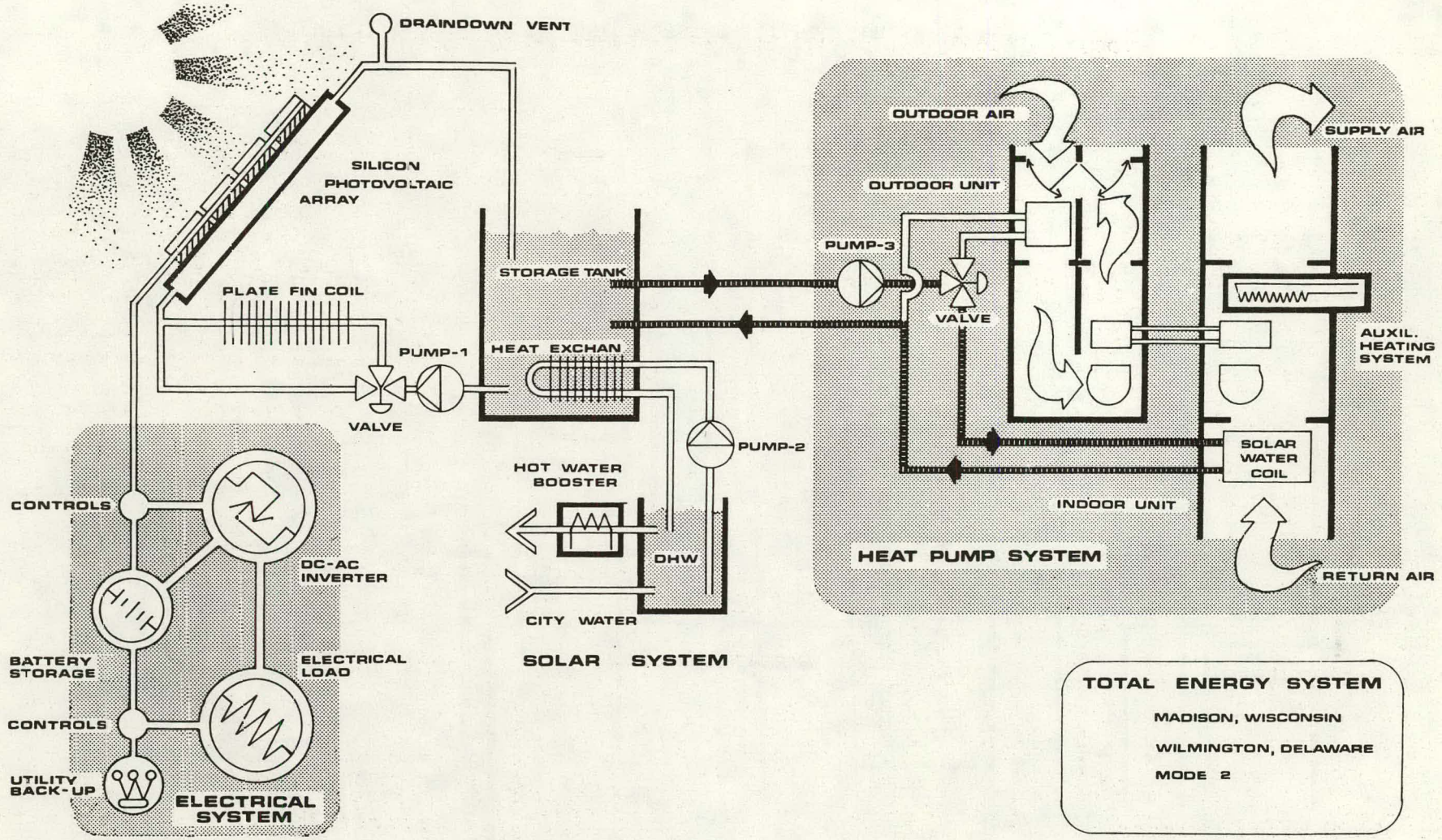


Figure 1.8.34 - Total Energy System for Madison, Wisconsin - Mode 2

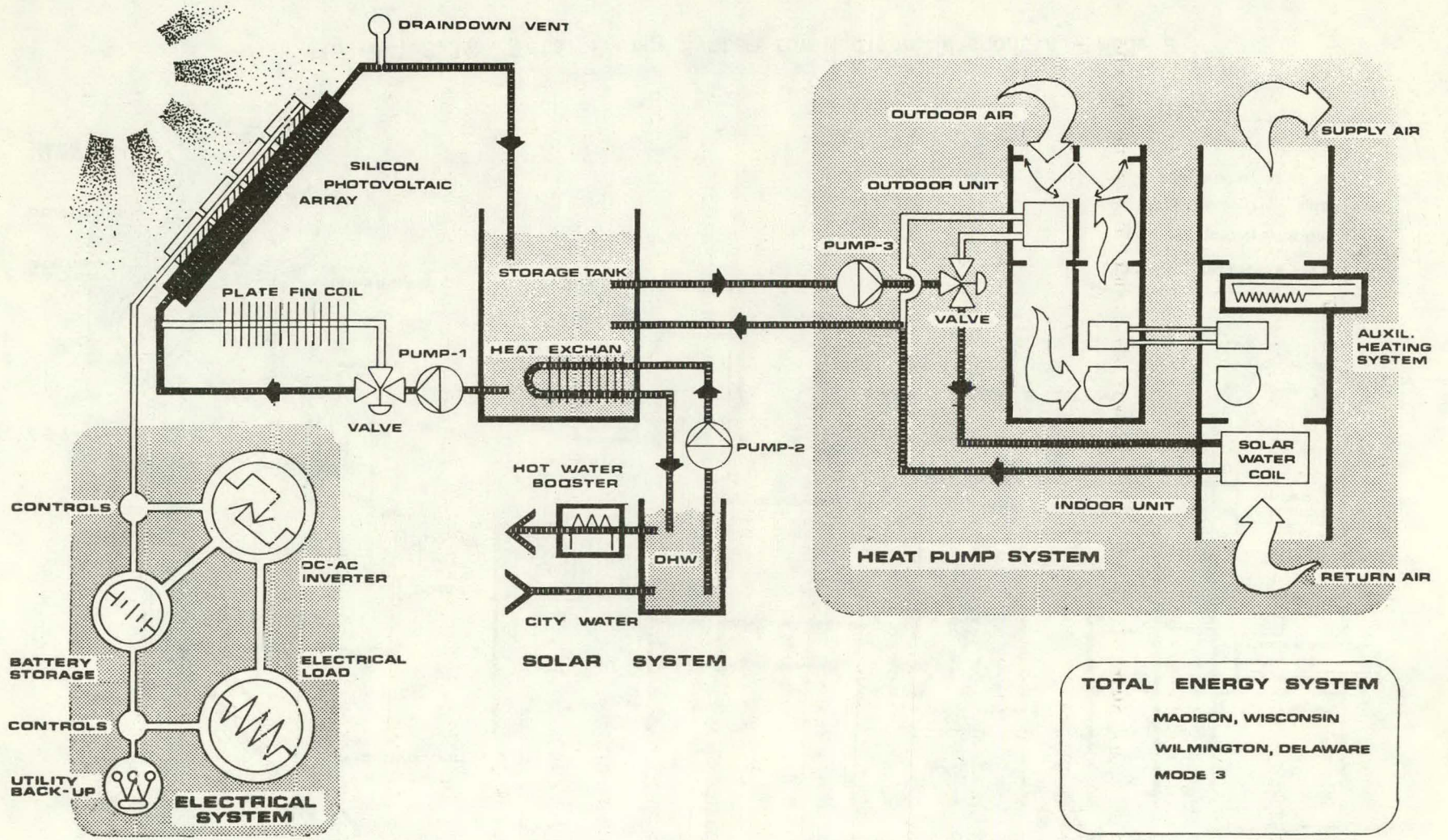


Figure 1.8.35 - Total Energy System for Madison, Wisconsin - Mode 3

condenser refrigerant coil in the other section of the heat pump where the centrifugal fan circulates the house supply air through the coil. In this mode the automatic control valve is positioned to return water from the solar coil to the water storage tank. An outdoor air sensor operates and air solenoid valve (not shown) to permit draining of the solar water coil when freezing is a possibility (see Figure 1.8.36).

Mode 5 - Conventional Heat Pump Operation

This mode indicates the operation of the air-to-air heat pump in a conventional mode using outside air as the heat source. The operable damper moves to admit outdoor air which is circulated by the centrifugal fan in the evaporator section of the heat pump through the evaporator refrigerant coil and exhausted to the outside. The heat is transferred to the condenser refrigerant coil in the other section of the heat pump where the centrifugal fan circulates the house supply air through the coil. There is no solar input in this mode of operation (see Figure 1.8.37).

Mode 6 - Photovoltaic Array Protection

This mode illustrates the photovoltaic array protection which corresponds directly to Mode 4 in Section 1.8.2.1.4 and need not be discussed again (see Figure 1.8.38).

1.8.3 Madison Residential Schematic

1.8.3.1 Form In Relation to Climate

As mentioned in Section 1.8.1.1 - General Climatic Considerations, Madison, Cleveland, and Wilmington all fall into the general category of moderate climate zone. This doesn't mean, however, that

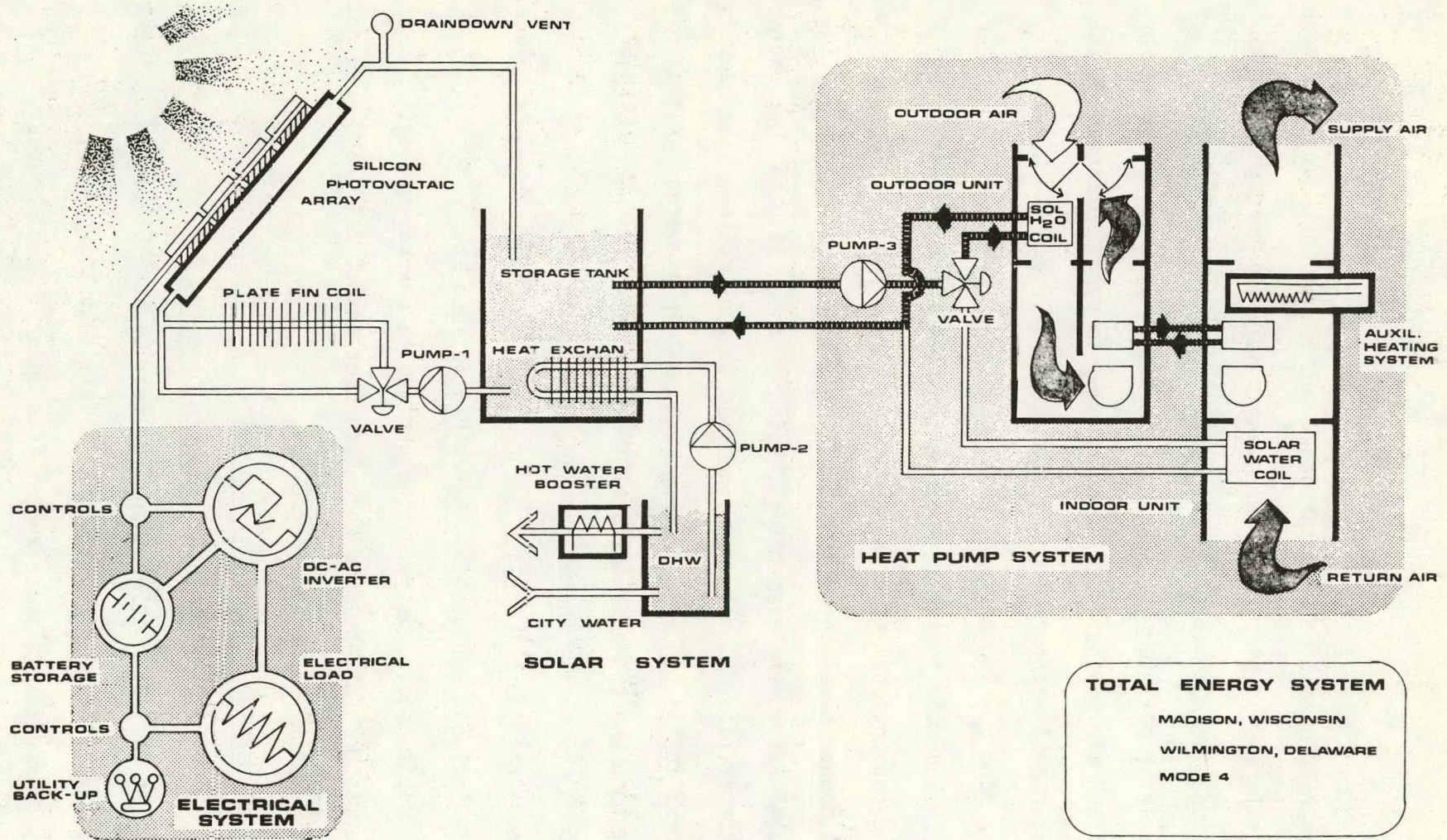


Figure 1.8.36 - Total Energy System for Madison, Wisconsin - Mode 4

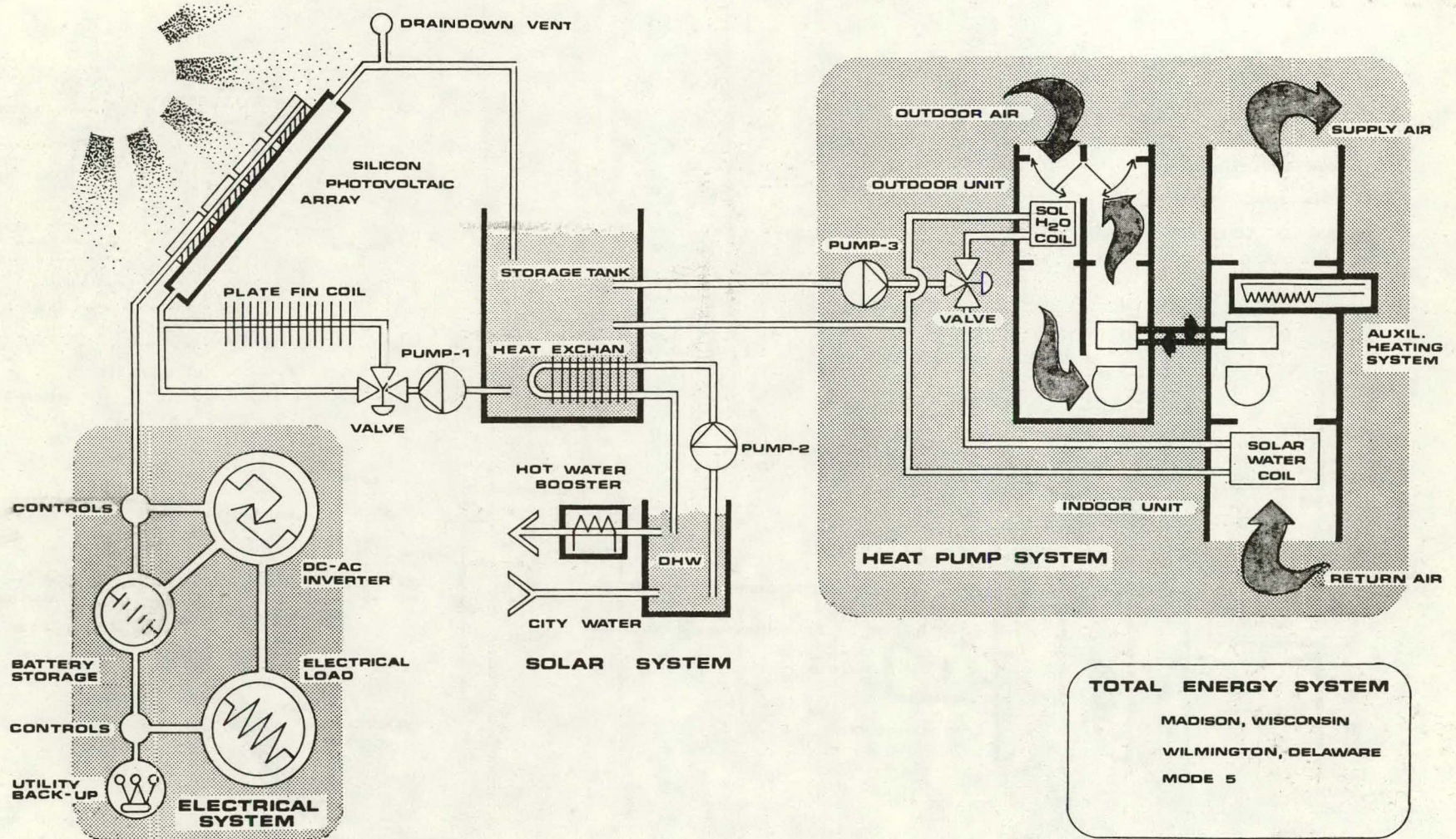


Figure 1.8.37 - Total Energy System for Madison, Wisconsin - Mode 5

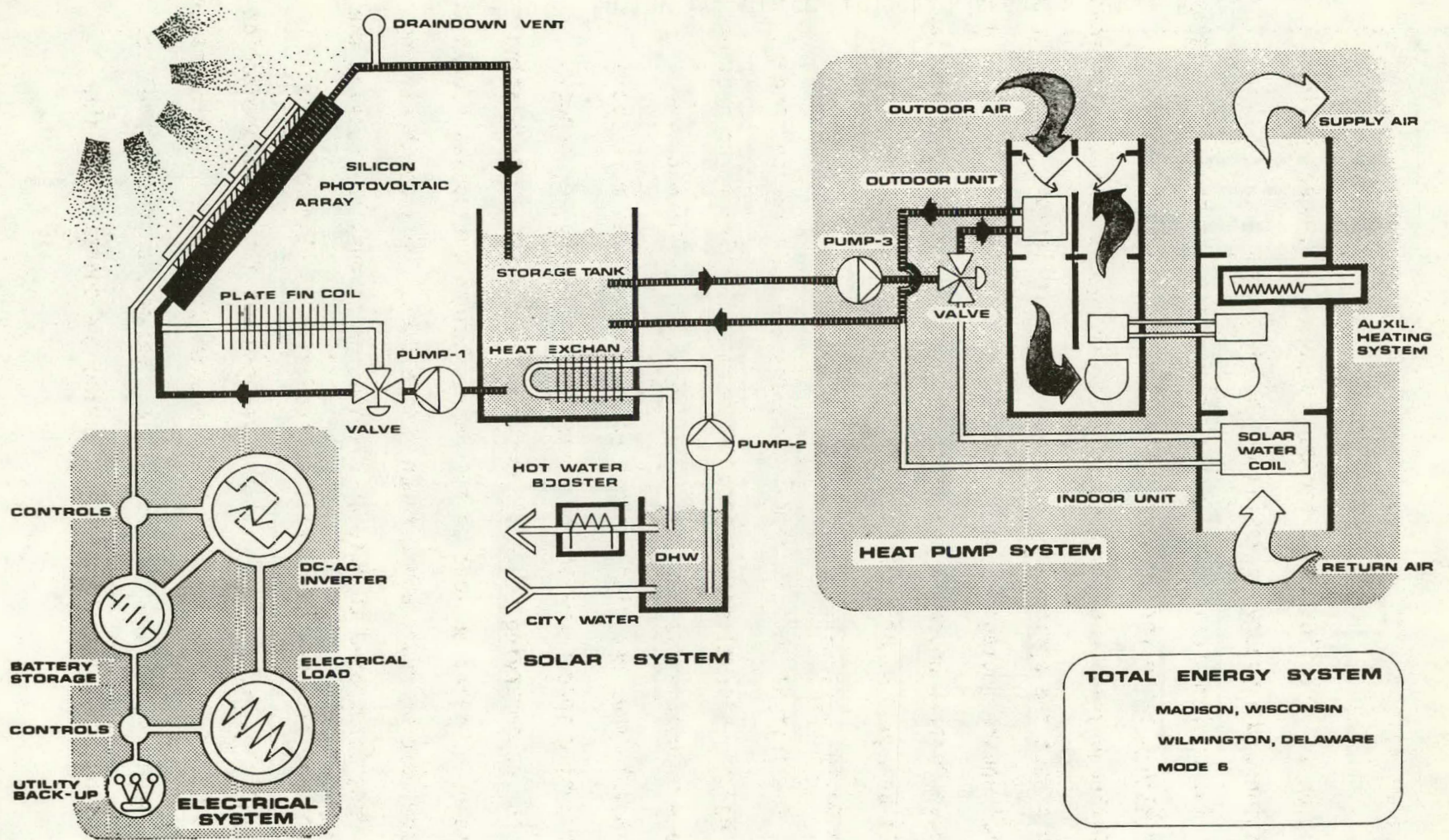


Figure 1.8.38 - Total Energy System for Madison, Wisconsin - Mode 6

each location is identical, but for our purposes of general design considerations, the schematic design can be the same.

The optimum residential orientation suggested by Victor Olgyay in Design with Climate for a moderate climate zone is 17.5° east of south. Although this is not due south, its divergence is not significant enough to affect the performance of photovoltaic collector. The residential square footage is about 1600 ft^2 , approximately equal to a Westinghouse Phase 0 house in the same region. The heating and cooling loads will be equal to or less than the Phase 0 house because of the following design considerations.

The initial design schematic study gave rise to the concept of dividing the internal spaces into two definite divisions or sections. The private or night-time spaces are to the north and bermed (see Figure 1.8.42), thus reducing heating requirements. The more social spaces or public spaces are on the southern side of the residence, and with the accompanying south windows, receive passive solar heating during the underheated periods of the year. Beyond the social spaces - living room, dining room, and kitchen - is a deck. Outside the living room the deck is exposed to outdoor climate variations, but outside the dining room and kitchen the deck is covered with a cylindrical acrylic glazing cover to create both a green-house for plant production and an additional barrier against heat loss in the winter. The entrance to the residence is on the leeward side and below the ground level to protect against cold air infiltration during the operation of the

entrance door in cold weather (see Figure 1.8.40). Further protection against heat loss is achieved by reducing exposed window surface on the north facade.

1.8.3.2 RPS - Madison System Integration

This schematic residence, because it was proposed for various regions, was designed to accommodate a variety of array sizes depending on what part of the residential load could be economically satisfied. The particular region illustrated is Madison (see Figure 1.8.39). Because it was decided that placing the collector system on the roof as an integral building component would produce the best economic profile, the roof must then have the proper pitch to accommodate the entire collector array. It was determined that a pitch of $+10^{\circ}$ from the latitude would be acceptable. Therefore, a 45° pitch for Madison, Cleveland and Wilmington was chosen because of its relation to current building practices, and ease of construction. The accompanying mechanical systems were placed in the basement of this residence for two reasons. First, the garage in the scheme is completely detached, thereby making all interconnections between garage mechanical systems and the residential rooftop array extremely expensive. Second, the basement area on the east side of the residence is above grade (see Figure 1.8.41) allowing for the air intake of the heat pump and the exhaust fan from the fin plate coil to have access to outside air. The storage tank is located as shown in the Madison section (see Figure 1.8.42) and is a 60-mil butyl rubber or a 20-mil reinforced elasticized polyolefin sheeting formed as a bladder. The concrete floor is then poured on top of

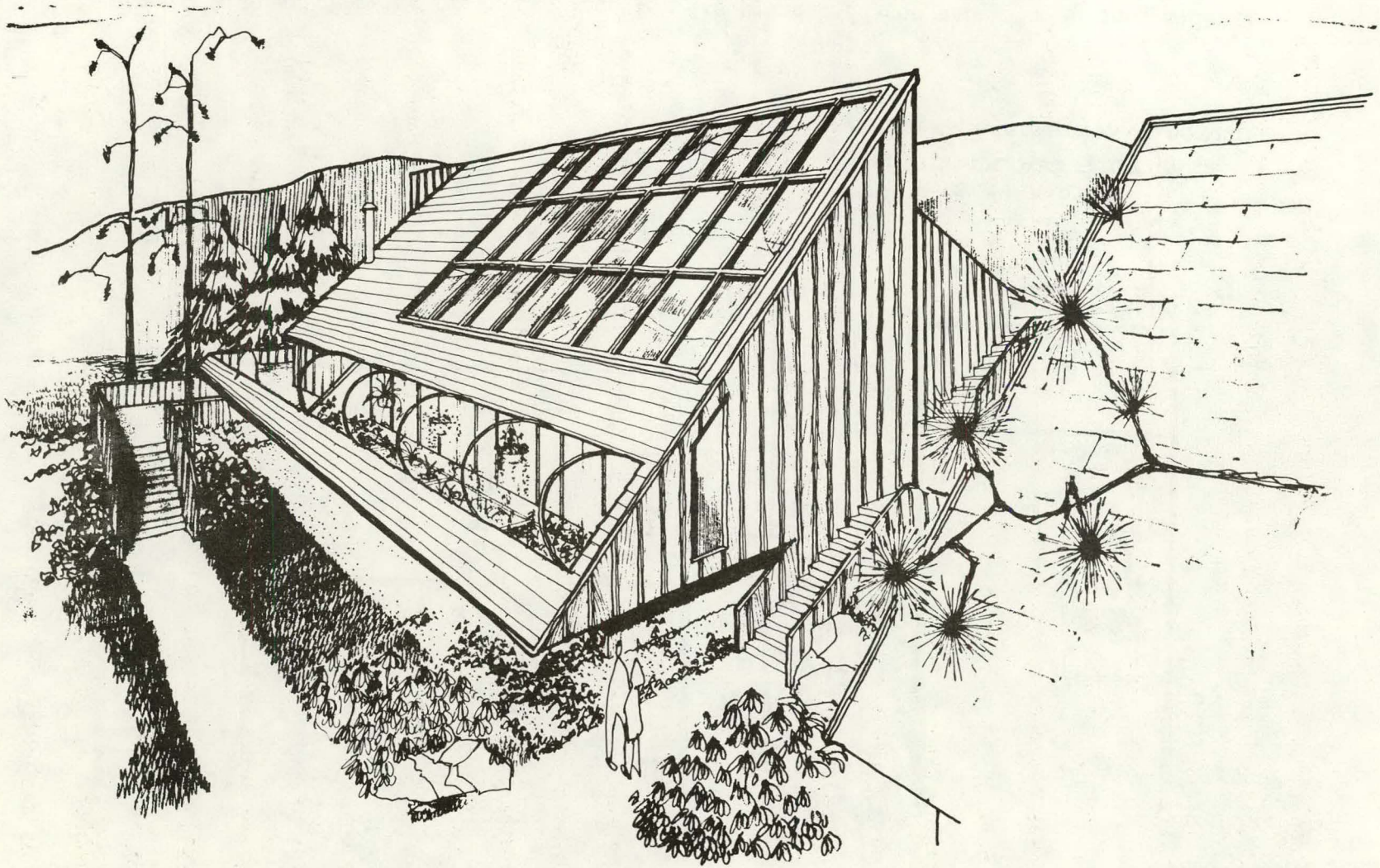


Figure 1.8.39 - Artists sketch of a residence suitable for the region represented by Cleveland, Madison and Wilmington

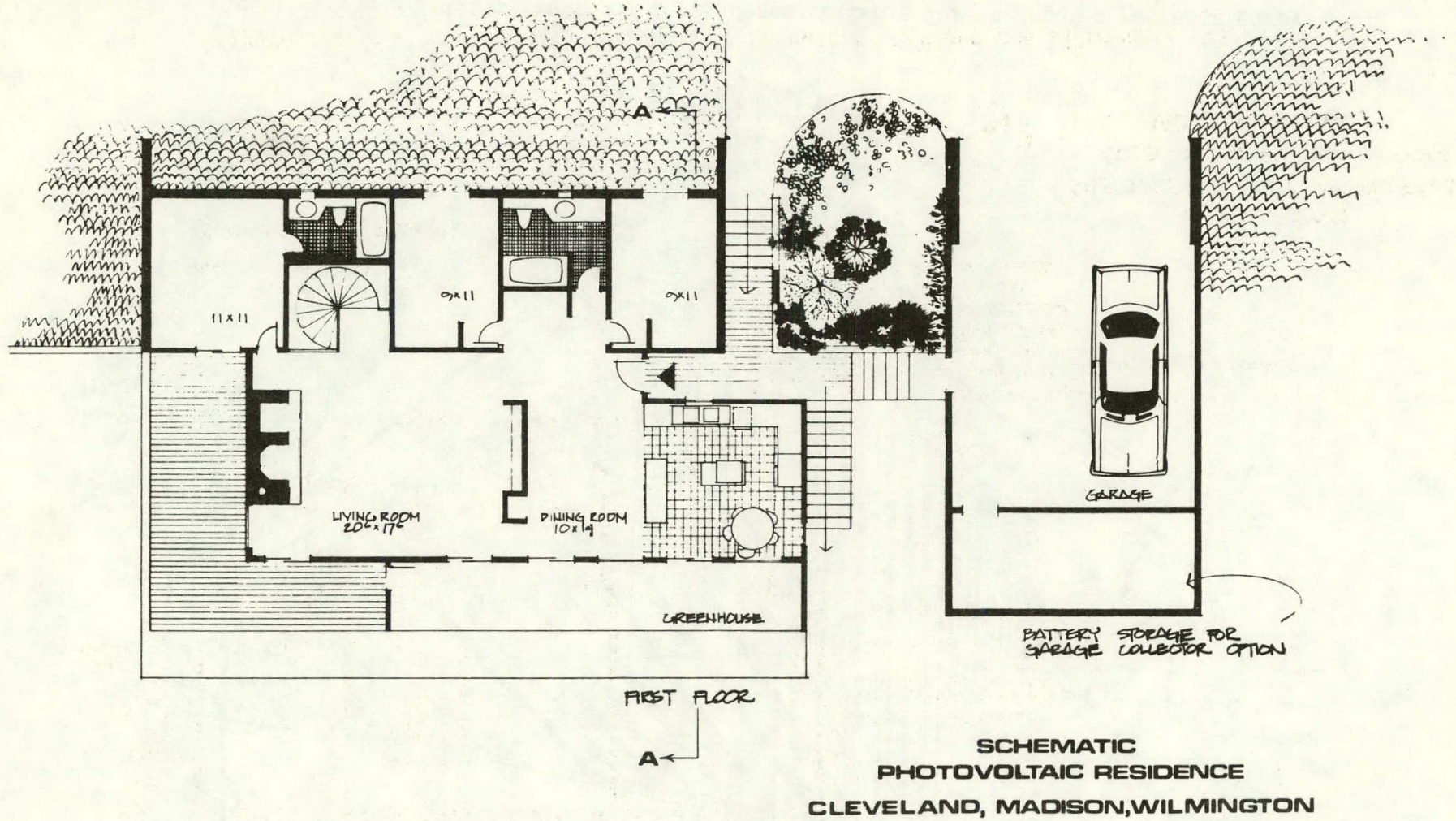


Figure 1.8.40 - Schematic of first floor for Cleveland, Madison and Wilmington residence

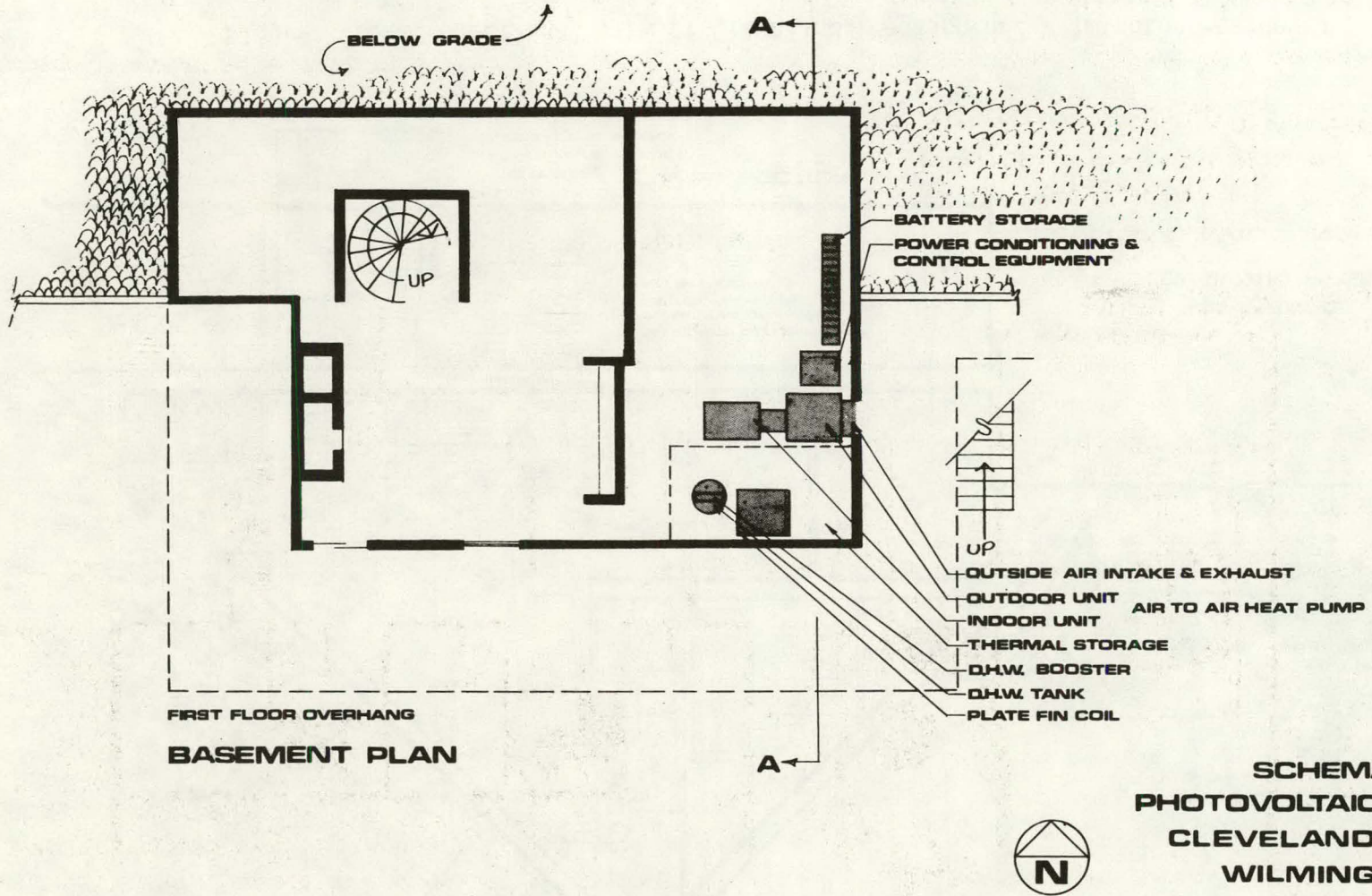


Figure 1.8.41 - Schematic of basement of Cleveland, Madison and Wilmington residence

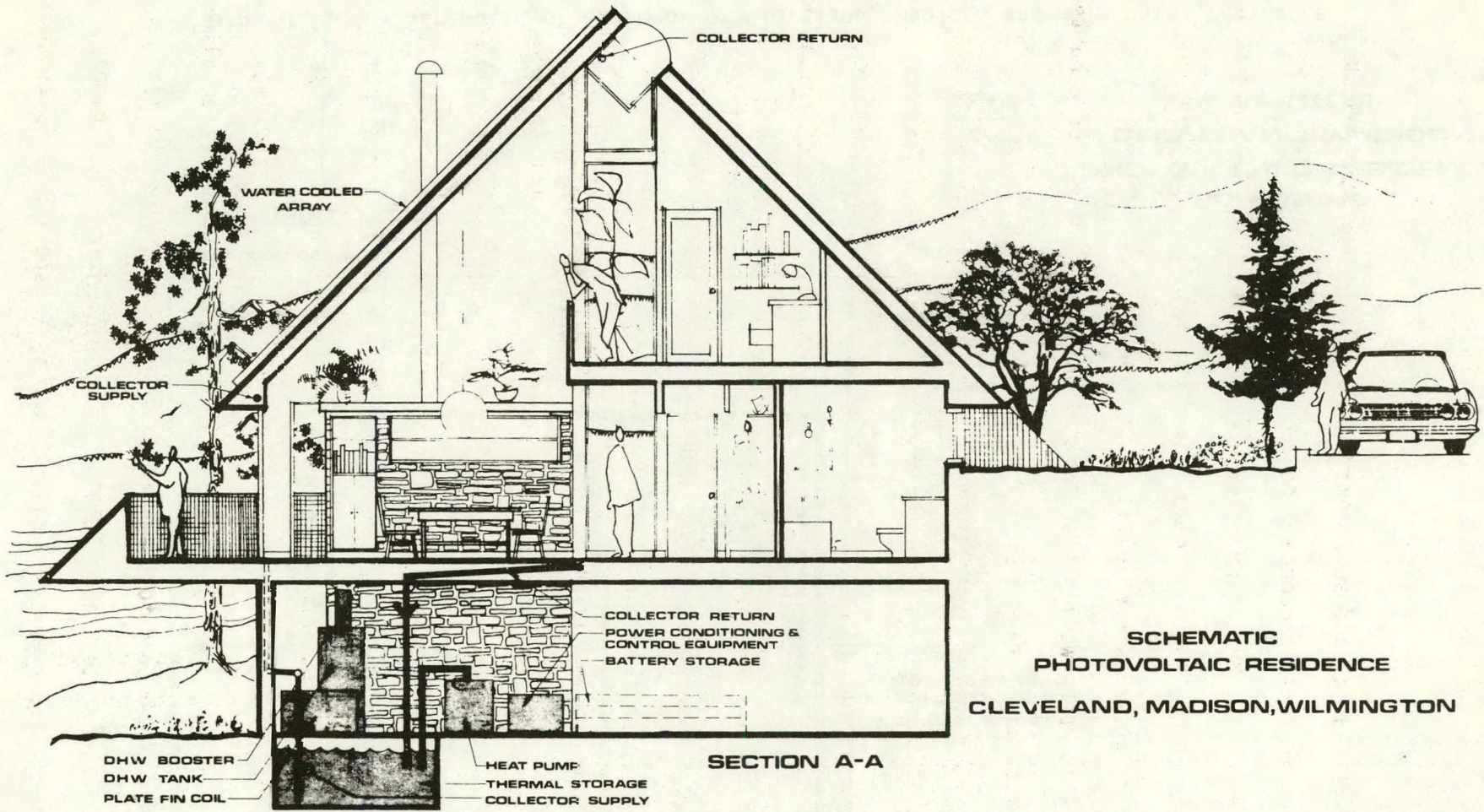


Figure 1.8.42 - Sectional view of Cleveland, Madison and Wilmington residence

this water-filled bag and so formed to provide a grade beam around the tank opening. All accompanying mechanical components -- pumps, hot water tank, and hot water booster -- are mounted above the tank on the concrete slab. The heat pump, power conditioning equipment and controls and batteries are adjoining the tank in the same room.

This space will not be heated, thereby allowing for a battery venting system to operate when the batteries are in a charging mode. Therefore, additional insulation will be required to isolate this particular mechanical system room from the rest of the residence, so as not to increase the residence's overall heating requirement.

The array piping and manifolding system will be discussed and illustrated in the Madison, Wilmington and Cleveland schematic only. Each of the remaining residential schematics uses primarily the same system with only minor changes in piping lengths.

The supply manifold, illustrated by Figure 1.8.43 shows an insulated 2" collector supply pipe connected to the fitting at the bottom of each collector module with a high temperature silicone hose and clamps. Care must be taken to assure that the hose connection point at the collector module is higher than the supply manifold. It is also important that the hose is not kinked or bent because collector draindown, which prevents the collector from freezing, will be impaired. The supply manifold must also be pitched to allow for drainage. The manifold is placed in the eave space and is accessible along its entire length through interior access panels. The two inch return manifold illustrated by Figure 1.8.44 is connected

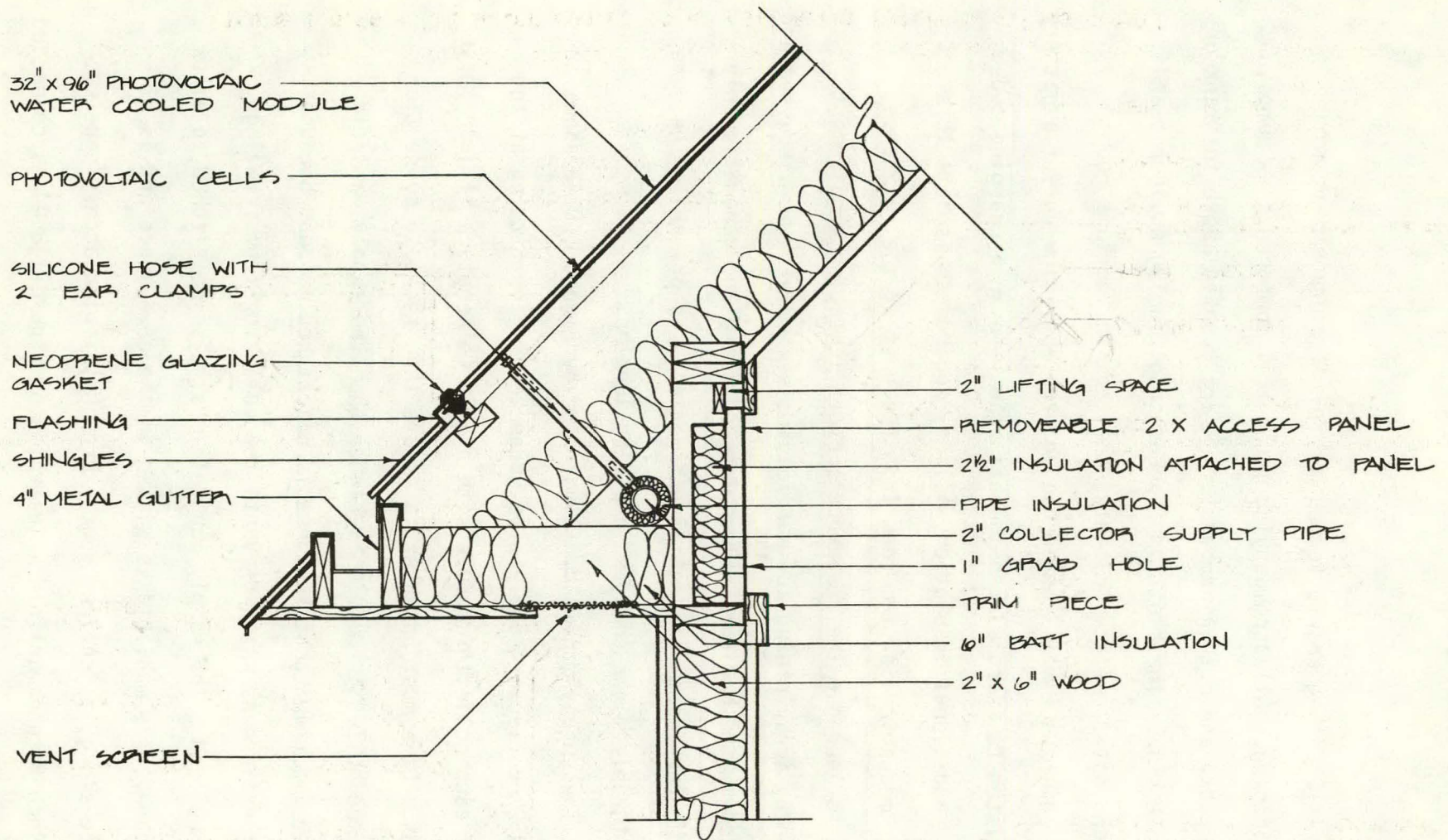


Figure 1.8.43 - RPS water cooled solar cell array feed manifold detail

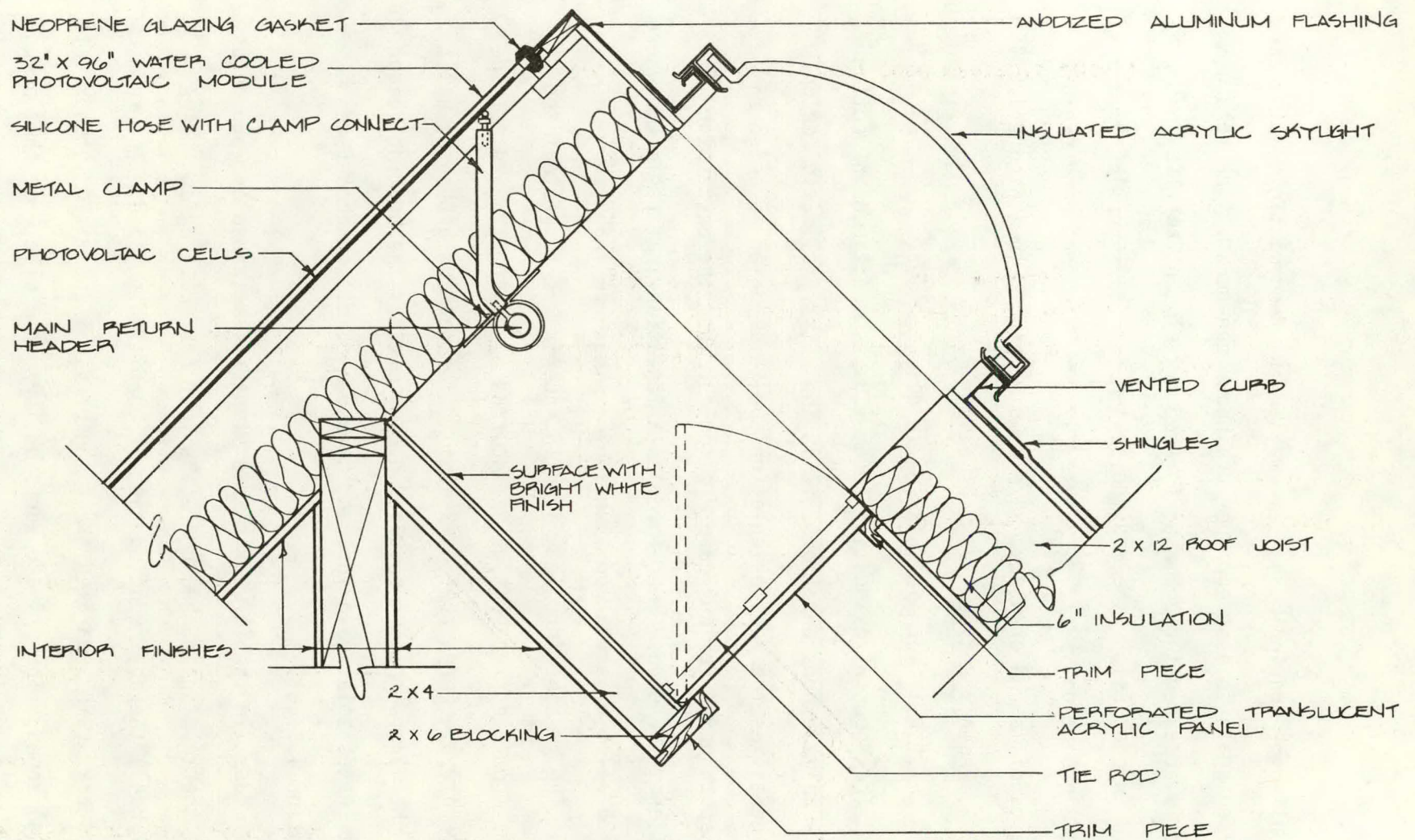


Figure 1.8.44 - RPS water cooled solar cell array return manifold detail

to the collector module in the same way as the feed manifold, with care being taken again to assure proper draindown can occur. The return manifold is accessed through a perforated translucent acrylic panel.

In conclusion, the Madison system relates to Option 4 discussed in Section 1.8.1.3 - General System Placement, and exhibits the same benefits and drawbacks already discussed. (see Figure 1.8.45)

1.8.4 Phoenix Residential Schematic

1.8.4.1 Form in Relation to Climate

The Phoenix residential schematic, as mentioned in Section 1.8.1.1 - Climate Considerations, is in the hot-dry climatic region. Olgyay identifies the best orientation for this region as being 25° east of south which for our case is too far from the best solar orientation to be used. Therefore, an orientation that falls somewhere between 25° east of south and true south is more desirable.

The greatest problem faced in Phoenix was to protect the residents from excessive heat gains incurred by solar flux and outside air temperature. Large roof overhangs in conjunction with wing walls provide the window shading required during most of the heating season. This eliminates solar gain through the south glass surfaces (see illustration 1.8.46).

Mass, in the form of simple stonebeds retained by wood curbs, provides thermal lag in the roof - the most critical region - (see Figure 1.8.47) thereby reducing the air conditioning load. The room locations are again separated as in the previous schematic into private and social zones. The private zones on the north side - or that area

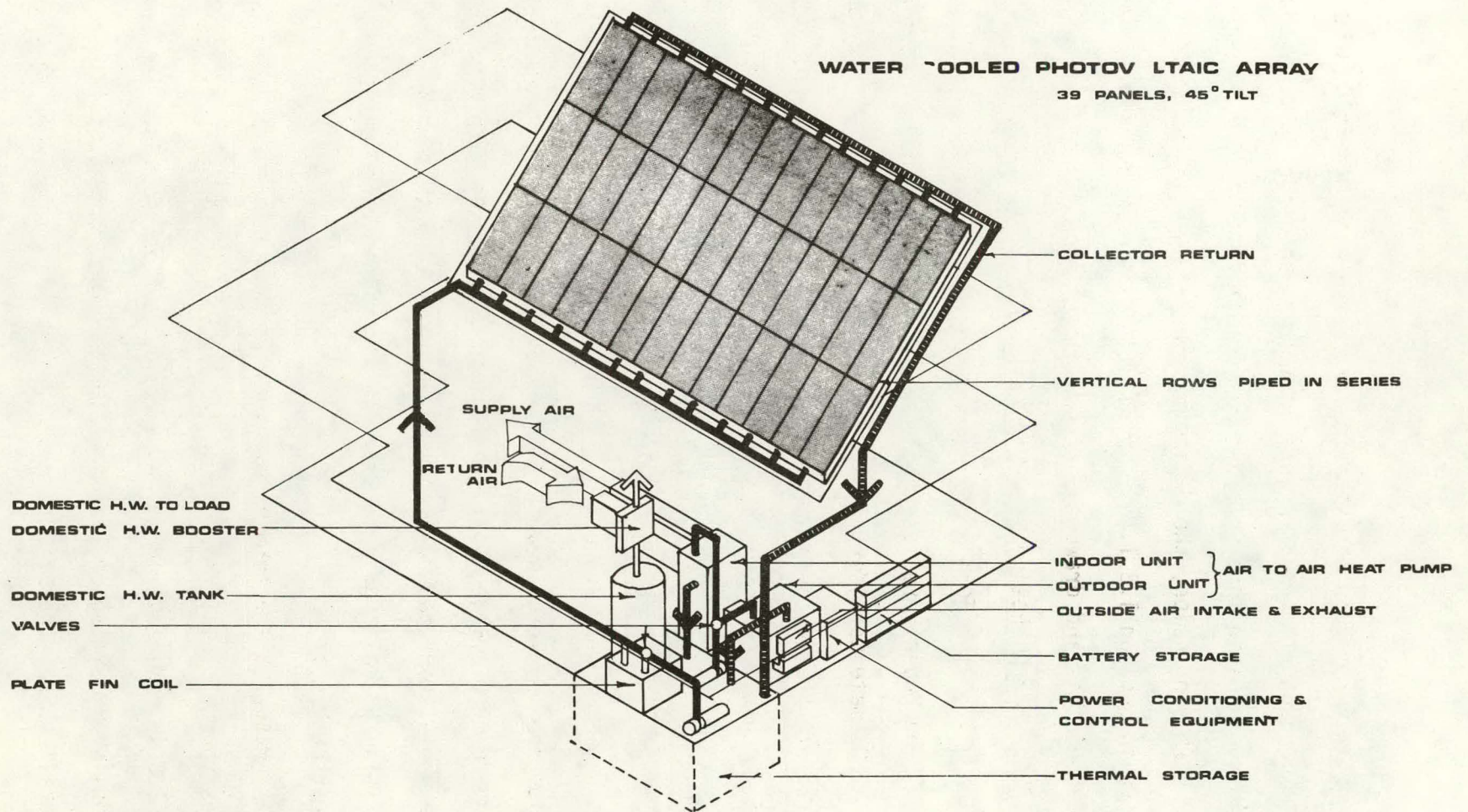
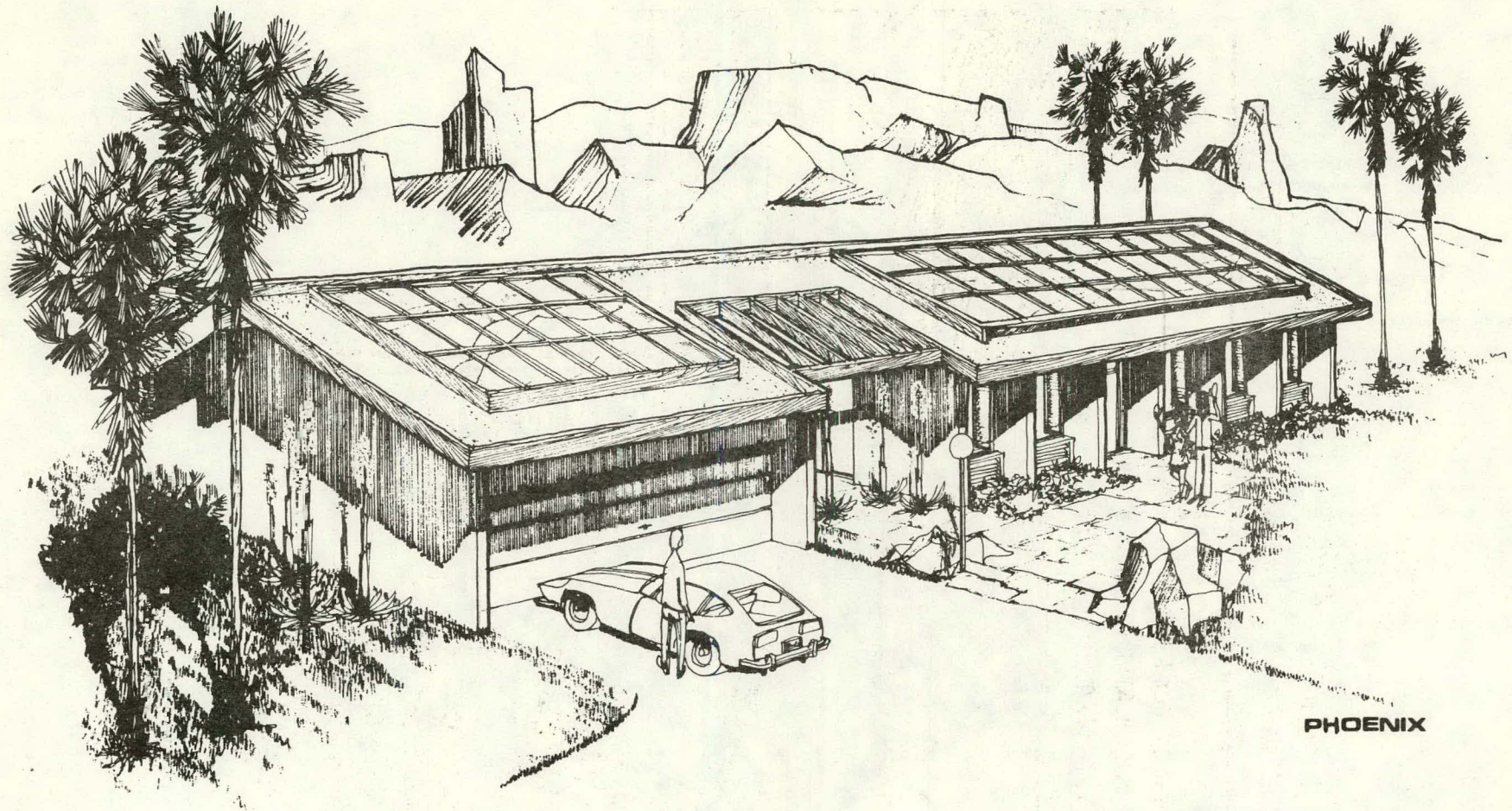


Figure 1.8.45 - Isometric view of RPS for Cleveland, Madison and Wilmington residence



PHOENIX

Figure 1.8.46 - Artists concept sketch of a residence suitable for construction in the Phoenix area

BUILT-UP GRAVEL ROOF ON SLOPED WOOD ROOF

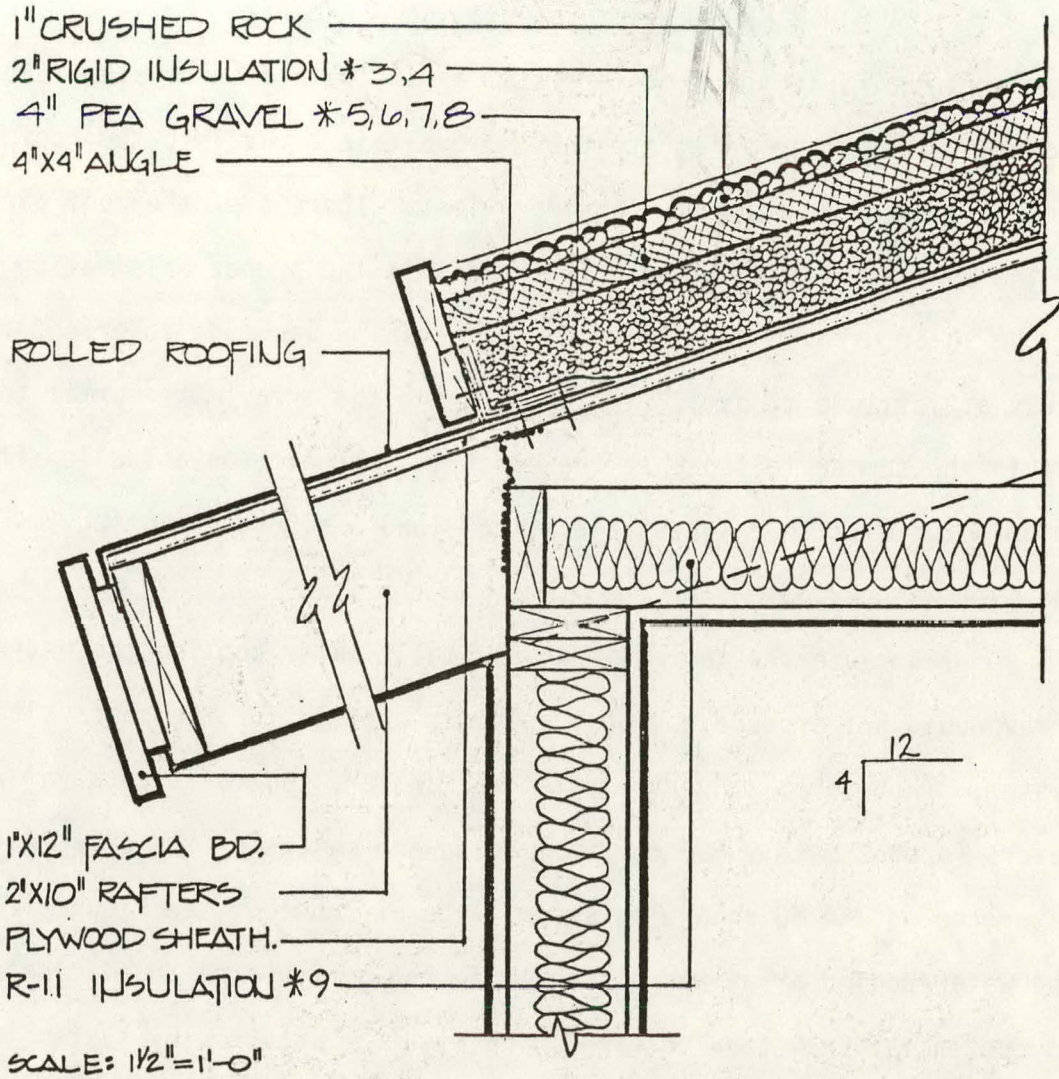


Figure 1.8.47

of the house not normally requiring heat during the day - and the social or public zones of the house on the south side do benefit from passive solar heating - sunlight passing through the south windows during the heating season.

1.8.4.2 RPS System Integration - Phoenix

Again, in the Phoenix system as in the Madison system, the decision was made to integrate the photovoltaic array into the roof structure based on economic considerations. Therefore, the roof pitch of the Phoenix residence must also relate to the proper orientation of the solar array. In this case, the decision was made to orient the array at latitude minus 12° to 21° to bring the array more normal to the sun in the summer to increase the electrical production and allow it to coincide with the highest electrical load - air conditioning - during the overheat period.

Because the thermal load is small, water cooling the entire array would not produce the best economic profile for the photovoltaic system. Therefore, a hybrid system was chosen. Out of a total of 70 square meters (approximately 800 sq. ft.), 30 square meters of the array will be water cooled and 40 square meters will be air cooled (see Figure 1.8.50). The water-cooled array was placed above the garage area to eliminate any potential structural damage which might be incurred by system leakage, and because the piping runs could be reduced significantly by placing the accompanying equipment, thermal storage, pumps, domestic hot water tank and booster, and plate fin coil in the garage area (see Figure 1.8.48 and Figure 1.8.49). Since 100% of the heating load

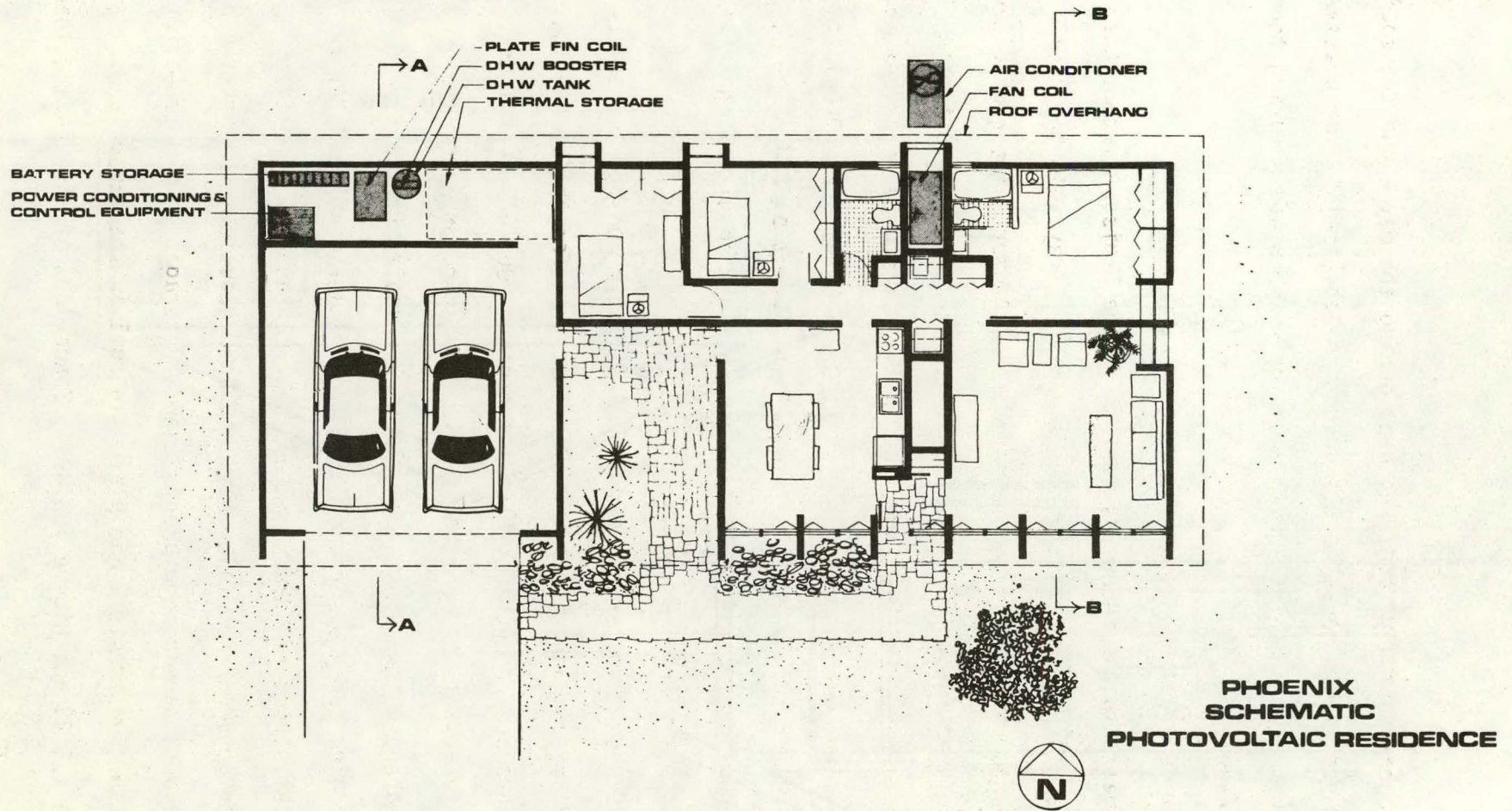


Figure 1.3.48 - Schematic of first-floor of Phoenix residence

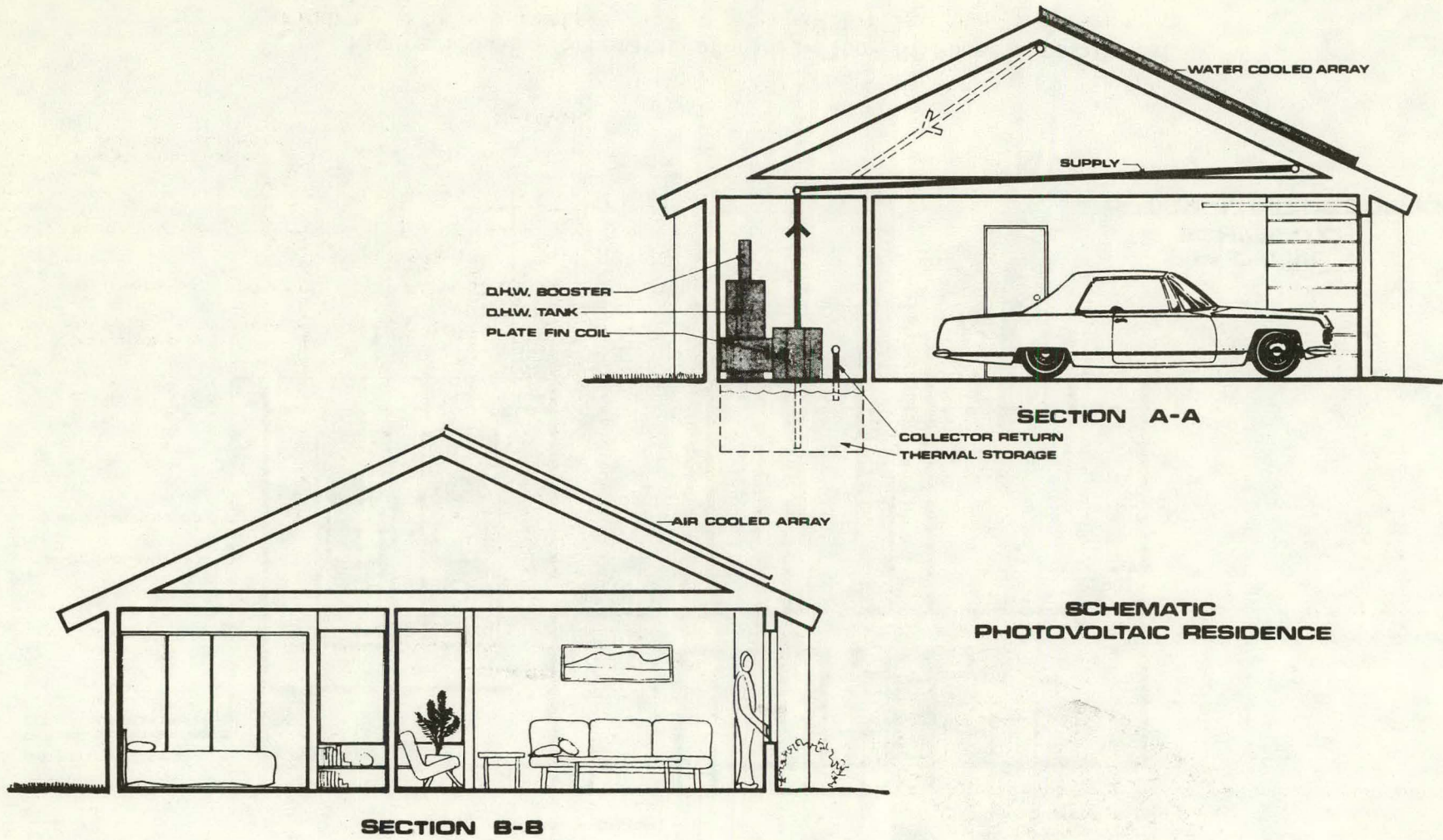


Figure 1.8.49 - Cross-sectional views of the Phoenix residence

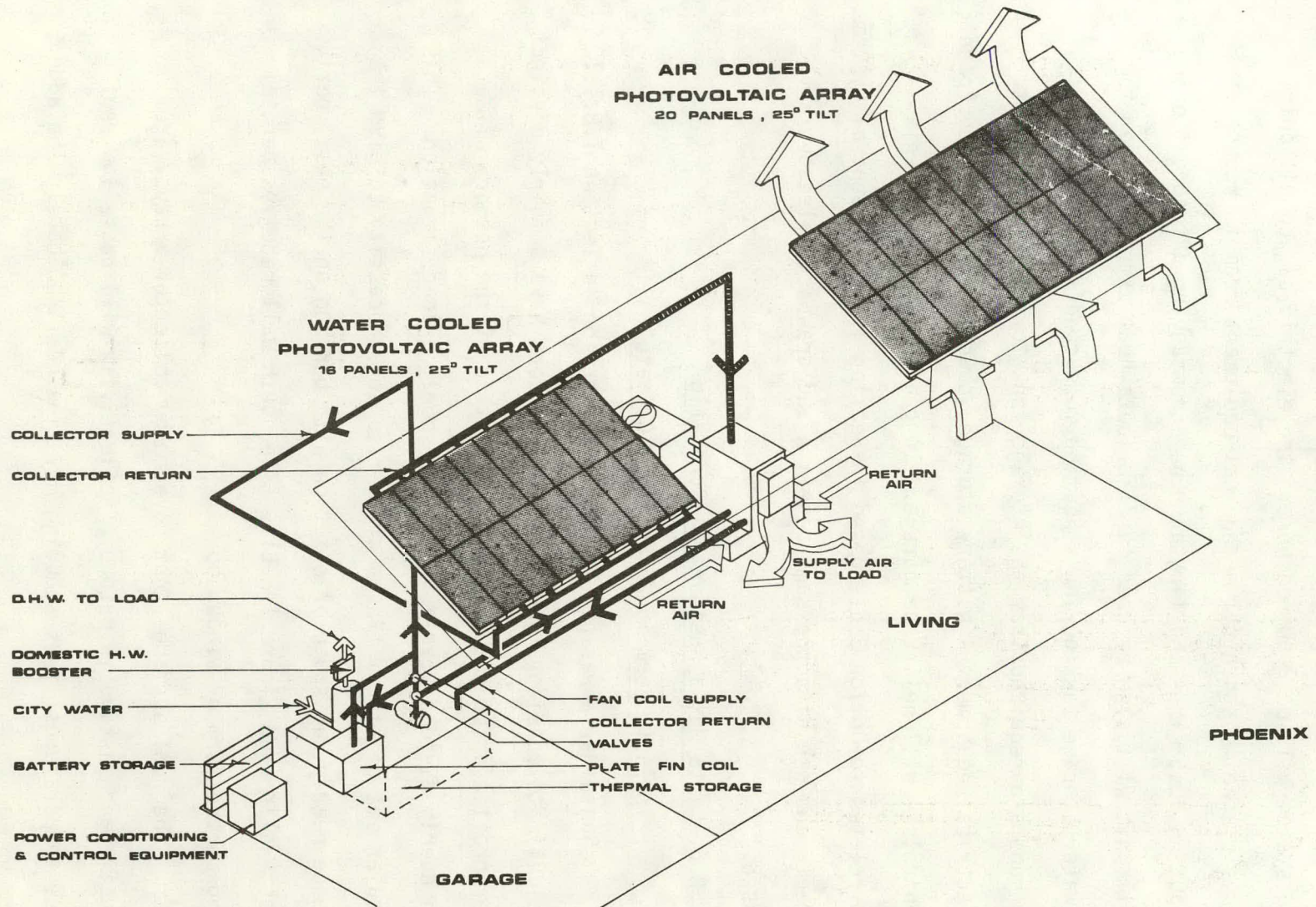


Figure 1.8.50 - Isometric view of the RPS for the Phoenix residence

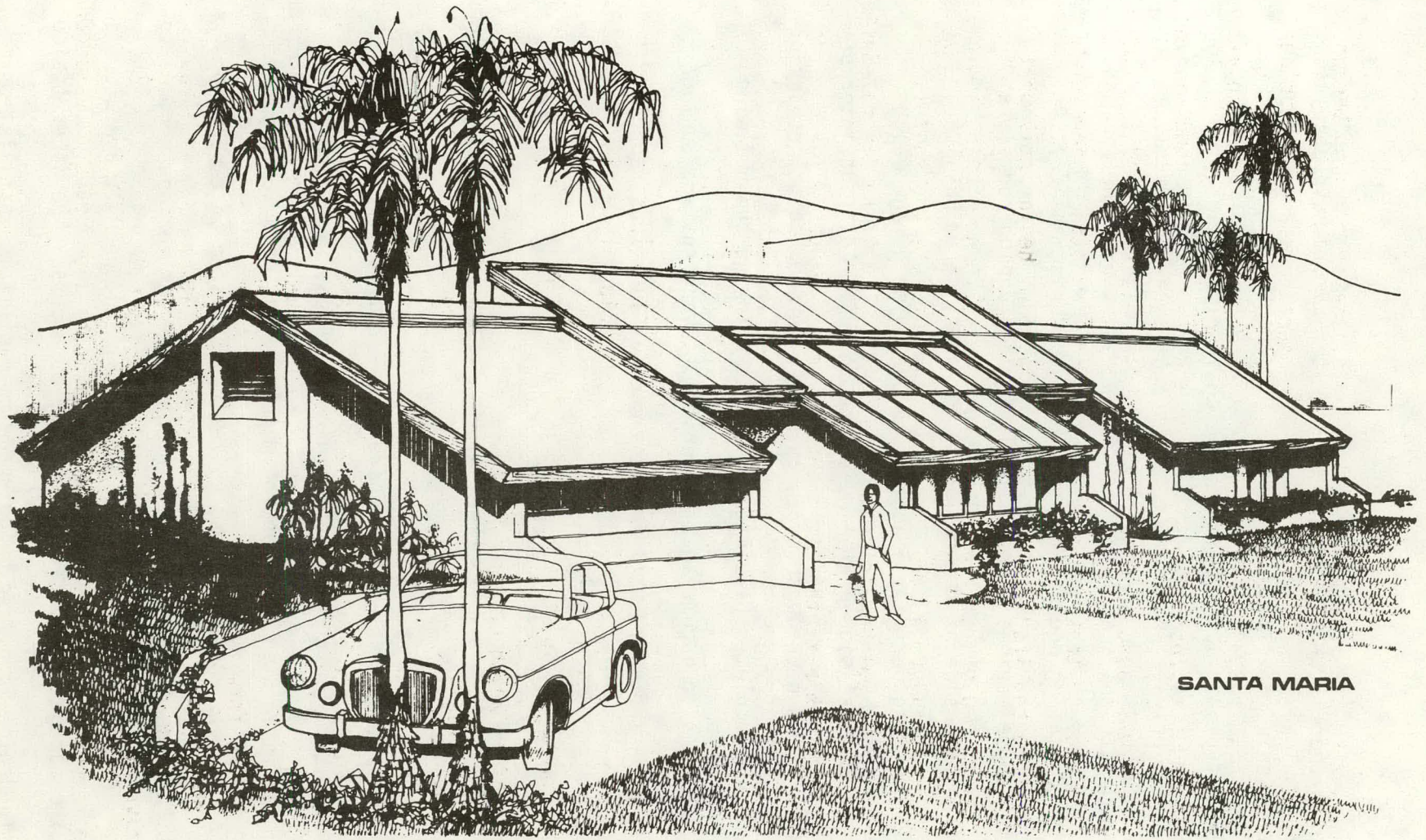
can be satisfied with the water-cooled photovoltaic array, no backup heating system will be required here. The electric air conditioning system is placed in a central mechanical equipment room to reduce air distribution duct sizes and length. The accompanying air conditioning fan coil unit will also be used to distribute heat extracted from the solar water storage tank during a heating mode condition, therefore piping runs are required from the storage tank to the fan coil unit. All electrical equipment - battery storage, power conditioning equipment, and controls - will be in the garage. In conclusion, the Phoenix system relates to Option 3 discussed in Section 1.8.1.3 - General System Placement, and exhibits the same benefits and drawbacks already discussed.

1.8.5 Santa Maria Residential Schematic

1.8.5.1 Form in Relation to Climate

Santa Maria was placed in the dry region in Section 1.8.1.1 - General Climate Considerations, however, it does have a fairly distinct weather profile which combines characteristics of the hot dry climate and an evenly divided yearly heating and cooling load situation. This particular set of circumstances gives rise to a necessity to give the residence nearly due south orientation with berming on the east, north and west walls (see Figure 1.8.51). The south wall receives partial berming in the form of window boxes.

The roof surfaces, not covered by collector arrays, are reflective and massive in nature. Reflectivity will cause low roof surface temperatures, thus reducing day time heating loads. The added



SANTA MARIA

Figure 1.8.51 - Artist's concept sketch of a residence suitable for construction in the Santa Maria area

mass creates a thermal time lag which reduces the daytime air conditioning load and the evening heating load.

Room types or activity zones are again divided into two categories. The private and service type spaces such as bedrooms, bathrooms, and kitchens are placed upon the north side of the residence to reduce their heating and cooling requirements during the daytime period. And, social spaces such as the living and dining rooms are placed on the south side of the residence to benefit from passive daytime solar heating during the heating season. The garage was positioned on the west side of the residence to buffer all the interior spaces from the heat gain contributed by late afternoon solar insolation. The south facade undulates (see Figure 1.8.52) allowing the building elements themselves to become shading devices. Overhangs are further provided to shade the south wall from the mid-day sun, thus reducing the daytime air conditioning loads.

1.8.5.2 Santa Maria System Integration

In Santa Maria, like Phoenix, the heating load of the residence requires far less solar thermal array area than the electrical load requires photovoltaic array area. Therefore, a hybrid system of a water-cooled integrated array - approximately 210 sq. ft. - and an air-cooled non-integrated array approximately 357 sq. ft. was used (see Figure 1.8.54). Both of these systems were placed on a roof, pitched at latitude (34°) and placed in such a way as to appear visually integrated. The mechanical systems, electrical and thermal, are all placed in the garage area to allow for ease of access. The water-cooled collector feed pipe is placed below grade to facilitate installation

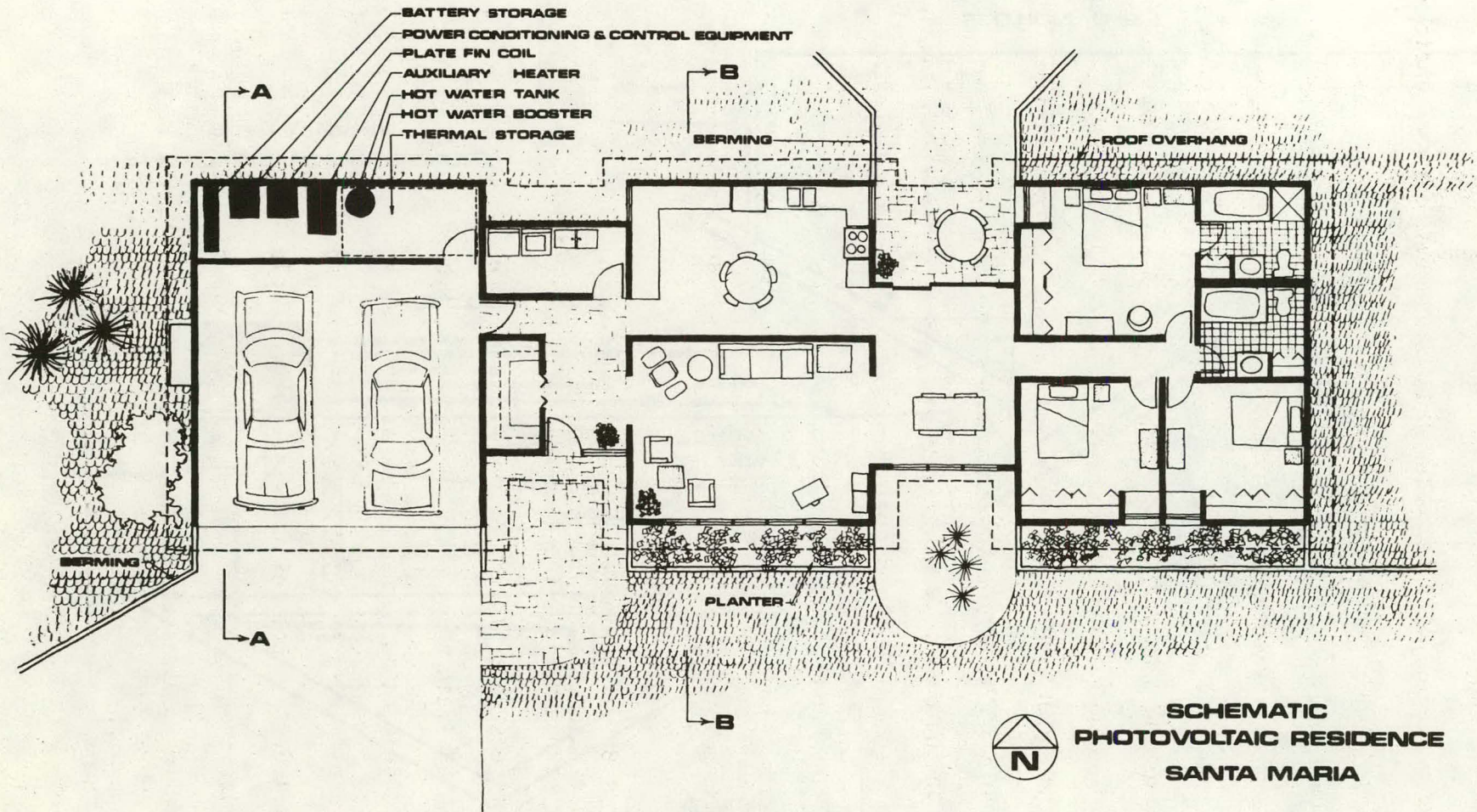


Figure 1.8.52 - Schematic of first floor of Santa Maria residence

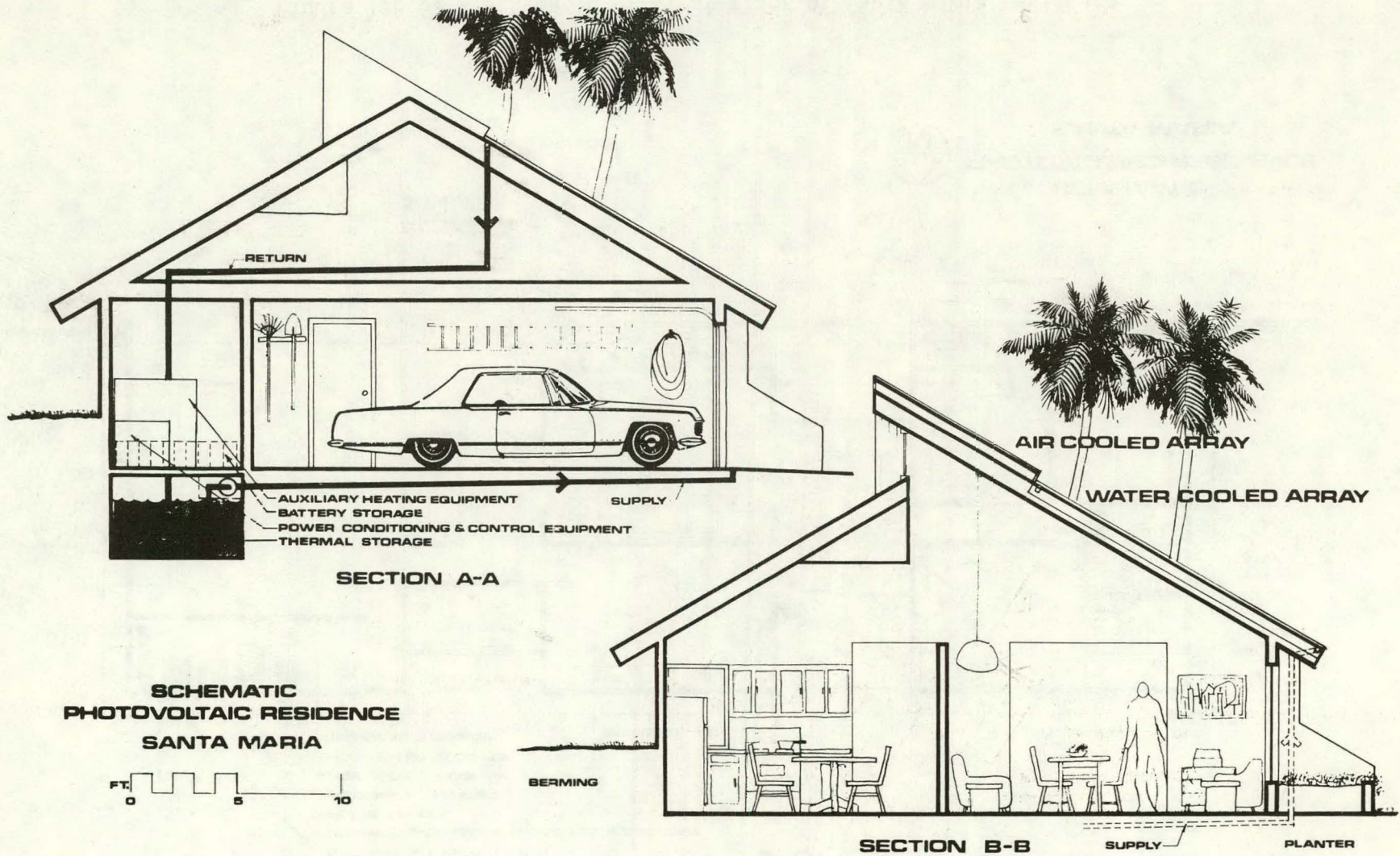


Figure 1.8.53 - Cross-sectional views of the Santa Maria residence

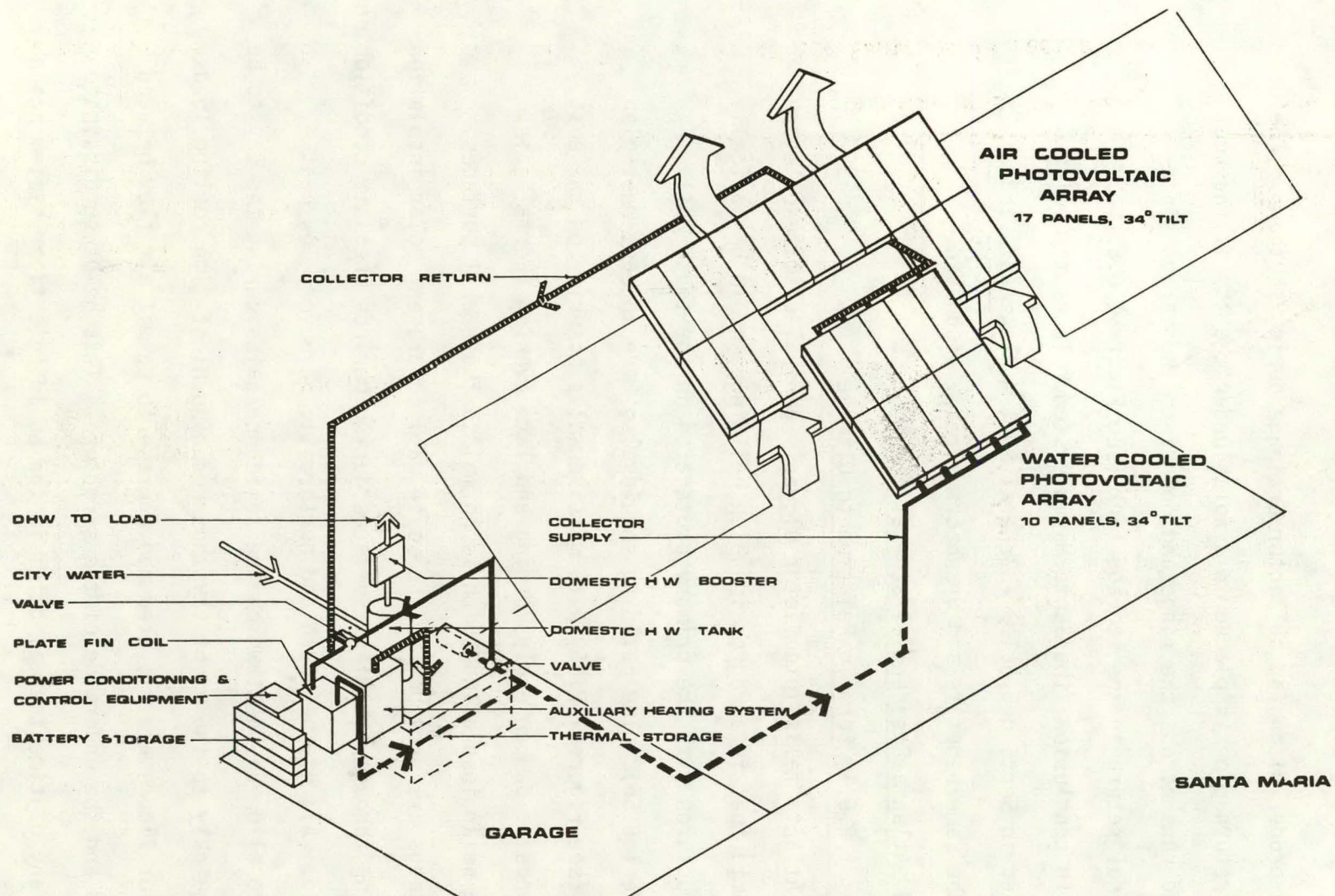


Figure 1.8.54 - Isometric view of the RPS for the Santa Maria residence

and assure proper pitch for collector drainage during shutdown. The collector return pipe is placed in a notch under the top of the roof rafters and runs across the ridge and down into the garage space for its final return in the storage tank (see Figure 1.8.53).

In conclusion, the Santa Maria system relates to Option 3 as discussed in Section 1.8.1.3 - General System Placements, and exhibits the same benefits and drawbacks already discussed.

1.8.6 Atlanta Residential Schematic

1.8.6.1 Form in Relation to Climate

Atlanta falls into Victor Olgyag's general climate category of hot, humid, that is, a region in which buildings should be basically shaded structures with the primary protection on the south wall (see Figure 1.8.55). The building should also have an east-west plan elongation (see Figure 1.8.56) with massive walls occurring on the east and west ends to dampen early morning and late evening thermal gains due to the solar insolation which is normal to these wall surfaces. Deep overhangs are provided on the south wall to prevent solar insolation from passing through the glass surfaces during periods when air conditioning is required. All of the south and north walls have very low heat capacity to allow any heat which the residence gains during the day to be radiated quickly to the night sky thus reducing night-time cooling loads. The interior floors are elevated above grade to permit air flow between the ground and the underside of the structure. This helps to dissipate or dampen any daytime thermal gains in the building's floor system again reducing cooling loads. The interior plan is primarily open across the

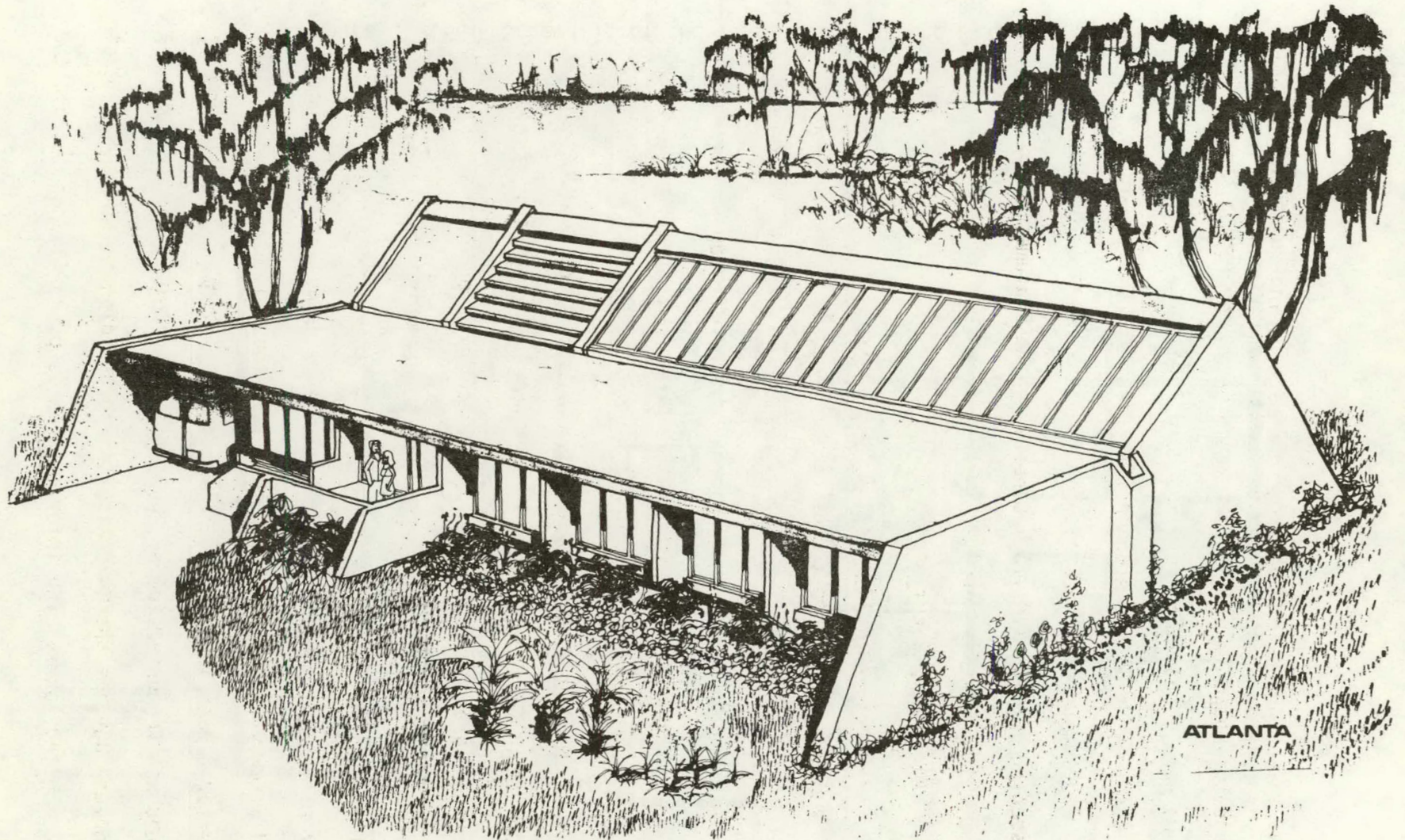


Figure 1.8.55 - Artist's sketch of a residence suitable for the region represented by Atlanta

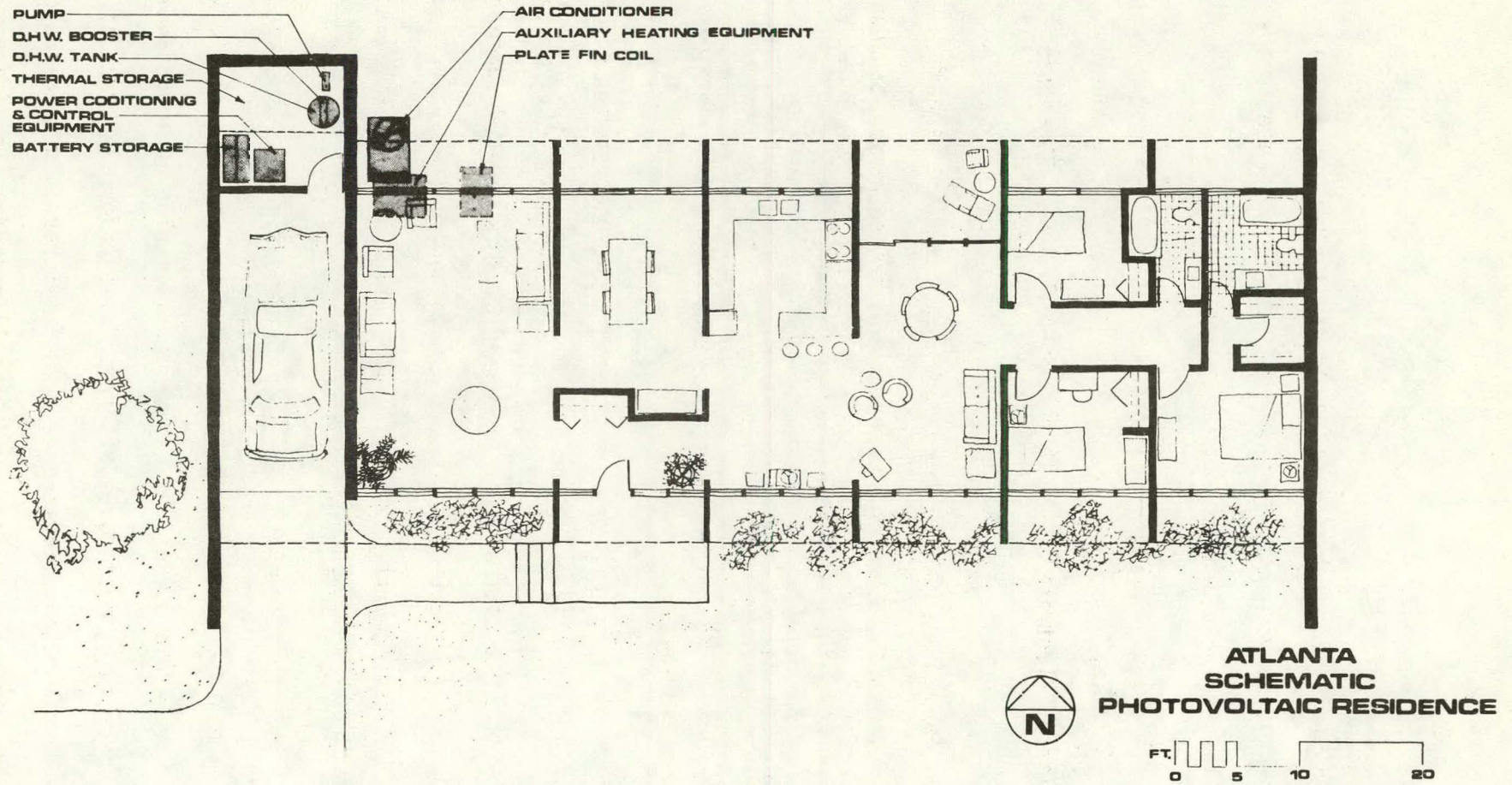


Figure 1.8.56 - Schematic of the first floor of the Atlanta residence

east-west axis (see Figure 1.8.56) allowing for natural ventilation to assist in cooling when outside conditions are approximate to the interior desired temperature and humidity range.

1.8.6.2 Atlanta System Integration

In Atlanta, like Phoenix and Santa Maria, the residence has a much larger electrical load than a thermal load. Therefore, a hybrid array is again used. This time approximately 450 sq. ft. of thermal array tilted at latitude is electrically coupled with a cadmium sulfide (CdS) sheet array which covers the remainder of what is nearly a flat roof (see Figure 1.8.55).

This residence demonstrates how this juxtaposition of two arrays, very dissimilar in construction requirements and in purpose, can work together. The best tilt for averaging electrical and thermal production on a yearly basis is close to latitude. Therefore, the water-cooled silicon array is mounted on a roof area pitched at latitude (33°) in the rear of the structure. The underside of this trussed space then provides for central location of some of the mechanical equipment required for heating and air conditioning (see Figure 1.8.57). The cadmium sulfide array, being only an electrical production array, is then oriented to intercept the most solar insolation during the time when the residence has the greatest electrical load. This greatest electrical load in Atlanta occurs during the summer air conditioning season when the sun reaches its highest daily altitude. The cadmium sulfide is therefore almost horizontal acting as a roof membrane and a reflector to augment the water-cooled array while still providing significant electrical power to satisfy the air conditioning load.

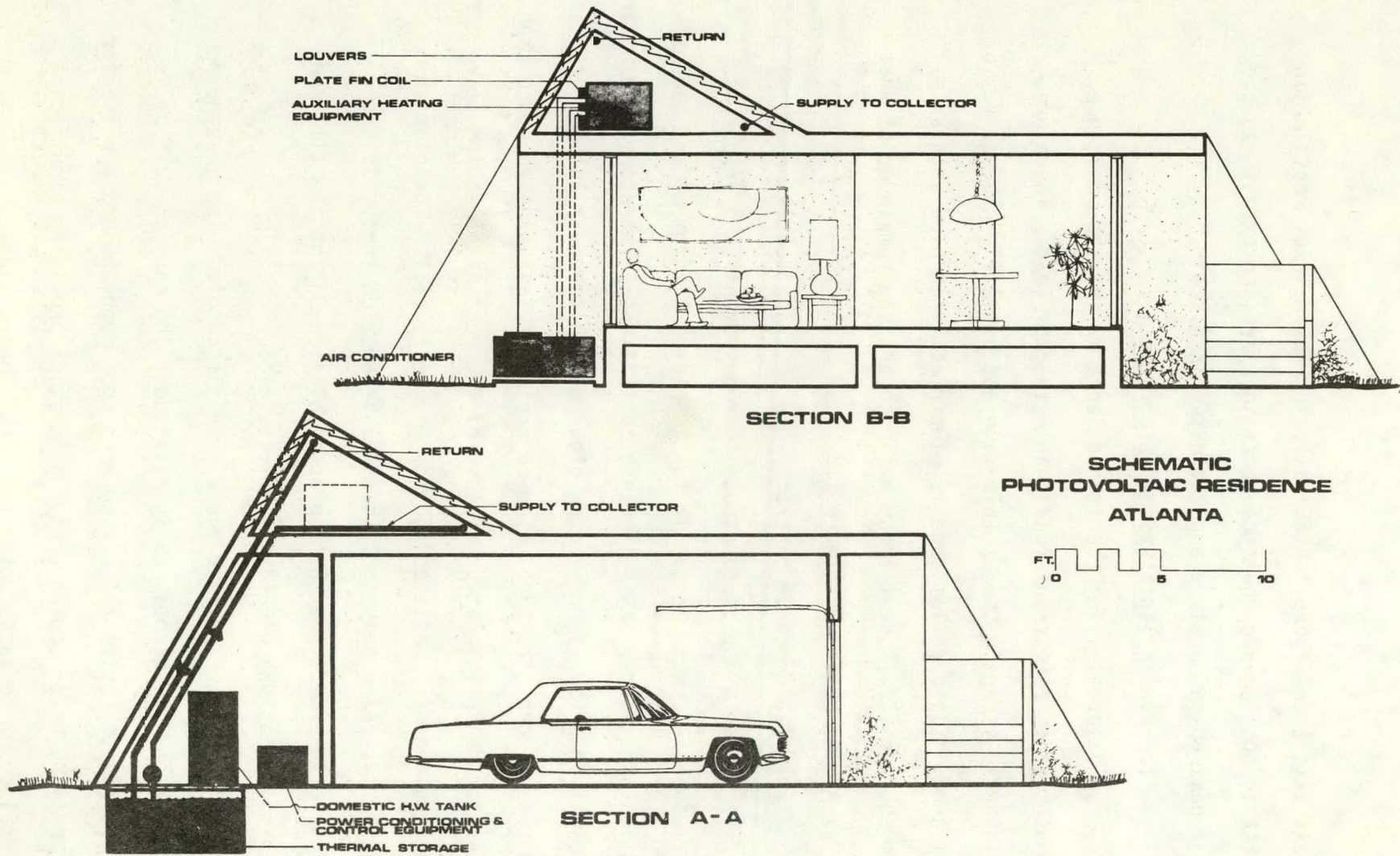


Figure 1.8.57 - Cross-sectional views of the Atlanta residence

The thermal storage tank and electrical power conditioning equipment controls are placed on grade in a mechanical area as opposed to truss space because of weight and ventilation problems (see Figure 1.8.58).

In conclusion, Atlanta is a combination of Options 3 and 4 as mentioned in Section 1.8.1.3 - General System Placement, and exhibits all of the benefits and drawbacks that are pertinent from each option.

1.8.7 Garage Retro-Fit System

1.8.7.1 General System Description

The use of the garage allows for integration of a solar system into either new or existing homes which lack proper orientation or do not adapt easily to solar installations. In such cases, the garage retro-fit system would be able to assume the proper location and orientation and would be adaptable to a variety of situations. The system can vary in size to meet a specified load demand, it can be a totally self-contained system, or it can be a supplement to an existing system whether solar or conventional. The garage lends itself well to installation of the solar system and all the variety of array options since it is a relatively open structure and does not produce the problems of installation and operation common to a residence. Advantages of the garage retro-fit system include easy venting of gases expelled during the battery charging mode, minimal structural problems, good access for servicing and replacement of the thermal and electrical components, elimination of damage caused by leakage problems occurring in residential construction, and an increase of usable floor space in some instances. Disadvantages include heat loss

470

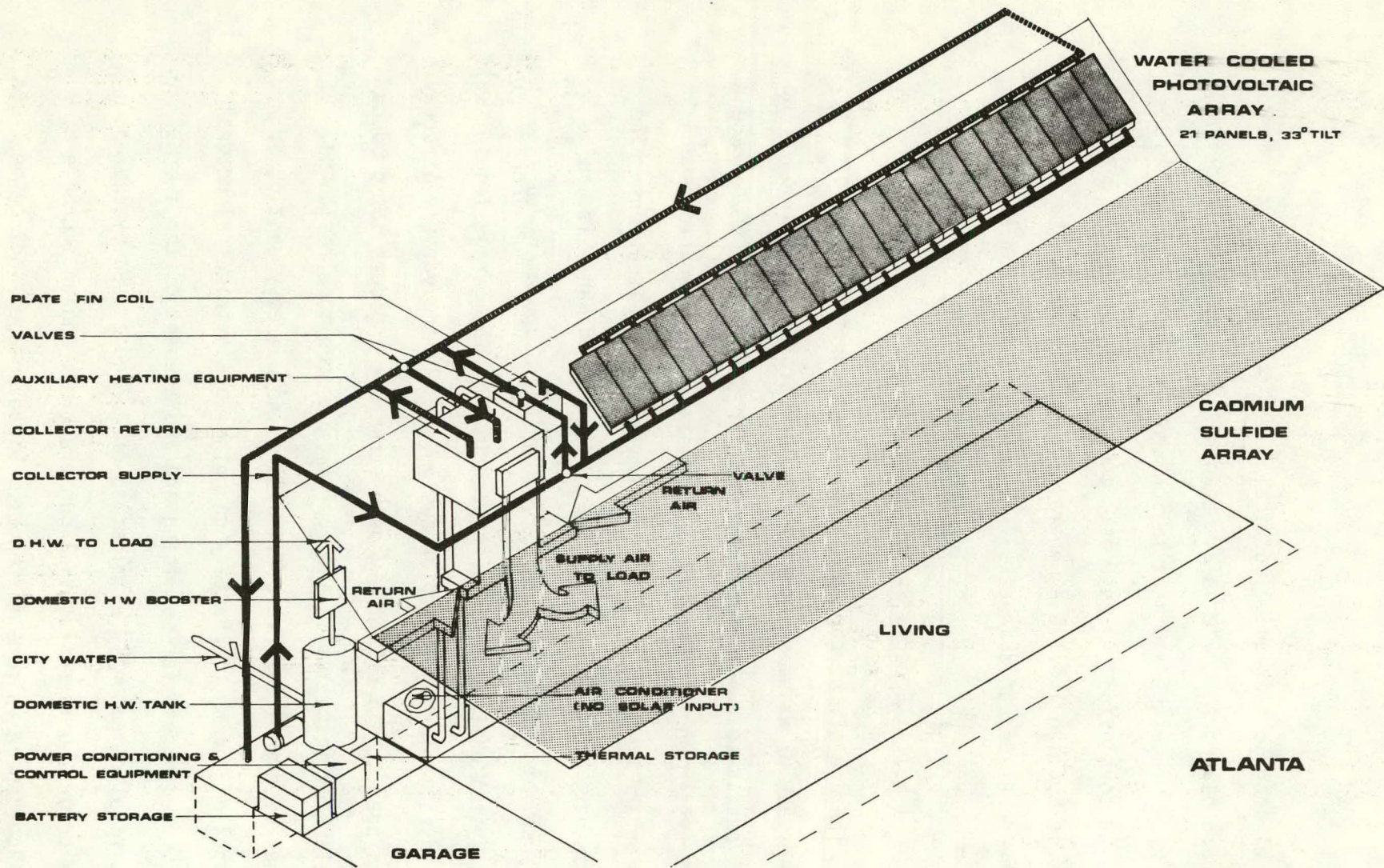


Figure 1.8.58 - Isometric view of the RPS for the Atlanta residence

from the storage tank to an unheated space, possible freezing during deep cycling of the batteries, long pipe runs to the heating equipment in the residence, and the threat of vandalism when the collector array is near the ground on the side addition (see Figure 1.8.59).

1.8.7.2 Garage Options

Options include a garage with no addition to its roof area, an extension to the roof, a side addition, and a combination of roof extension and side addition.

Option 1 (see Figure 1.8.59) is a retro-fit system requiring a minimum of construction. It will contain 16 collector panels without relying on additions or extensions of the roof area. Thermal and electrical storage will be contained within the existing garage thus reducing the usable floor space. With this option, vehicular access is possible on all four sides of the garage. However, an addition (Option 1B) can be constructed if space within the garage is limited. Due to the small array size, the system can handle only small load demands and would, if compared to larger array systems, be an inefficient use of the thermal and electrical storage, and other required equipment in the system.

Option 2 is a retro-fit system containing 24 collector panels, an increase of 50 percent over Option 1, by addition of a roof extension. Thermal and electrical storage will be contained within the existing garage, reducing usable floor space. However, a side addition (Option 2B) could house the thermal and electrical storage, but would limit vehicular access to only three sides. This is a more efficient use

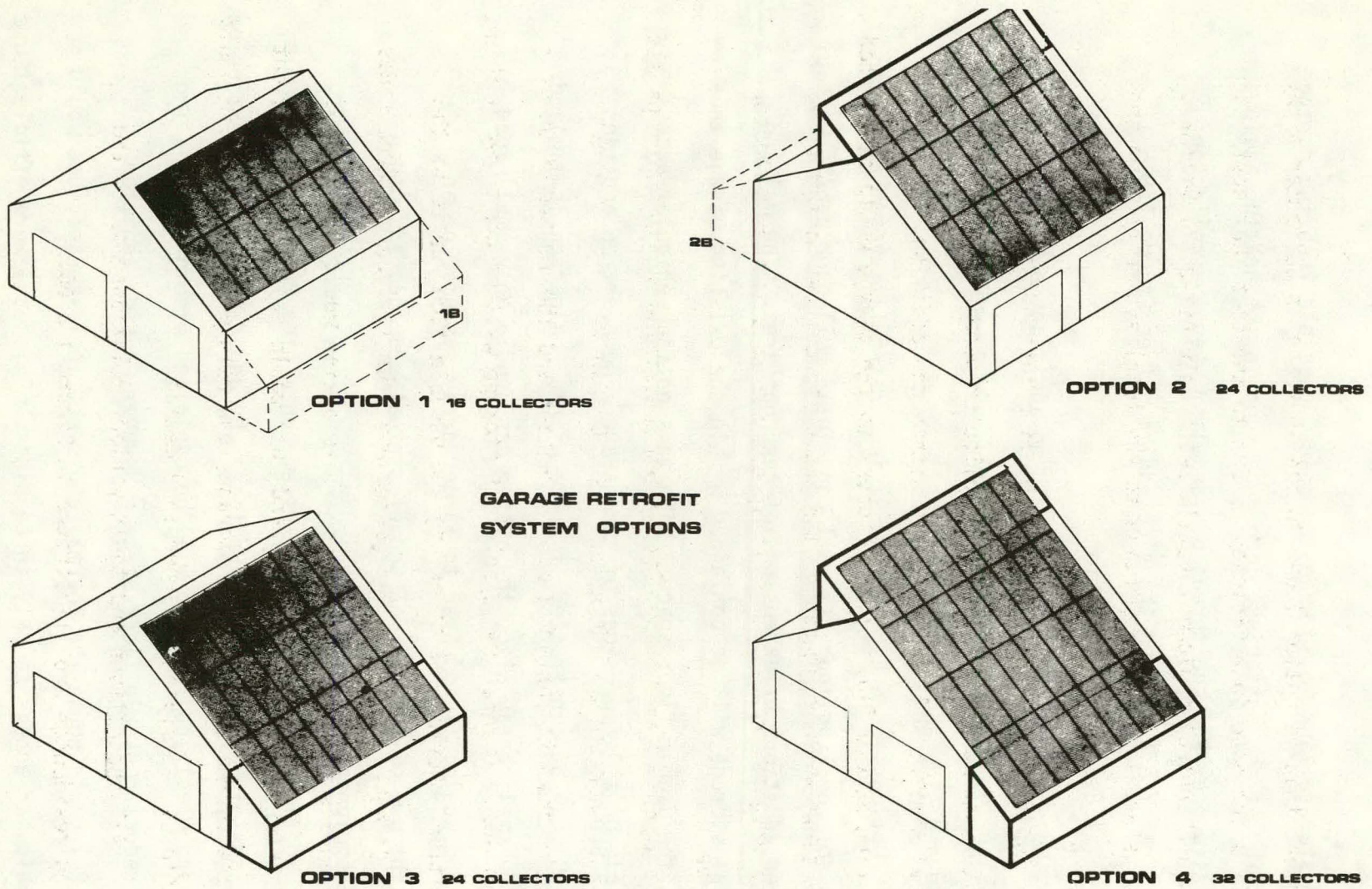


Figure 1.8.59 - Garage retrofit options for the RPS

of equipment than in Option 1 due to the increase in collector array area. This increase in efficiency is due to the fact that costs such as pumps and control equipment remain relatively fixed. Therefore, their costs are lower in proportion to the total system cost on the larger array.

Option 3, by the installation of a side addition, is a retro-fit system also containing 24 collector panels. Thermal and electrical storage will be contained within the addition, thereby not reducing usable floor space. Access to the garage would be limited to three sides with no access on the south facade. As in Option 2, this is a more efficient use of equipment due to a larger collector array area.

Option 4 is a retro-fit system containing 32 collector panels which is an increase of 100 percent over Option 1. This increase is achieved by the addition of a roof extension and the installation of a side addition. Thermal and electrical storage will be contained within the addition, thereby not affecting the useable floor space of the existing garage. Access to the garage would be limited to three sides with no access on the south facade. This option would contain the largest array of the four options and thus would be the most efficient use of the thermal, electrical storage, and related equipment, and would be capable of satisfying a larger load demand.

All the options and their various relationships to the adjoining residences are illustrated in Figure 1.8.60.

**GARAGE RETROFIT
OPTIONS**

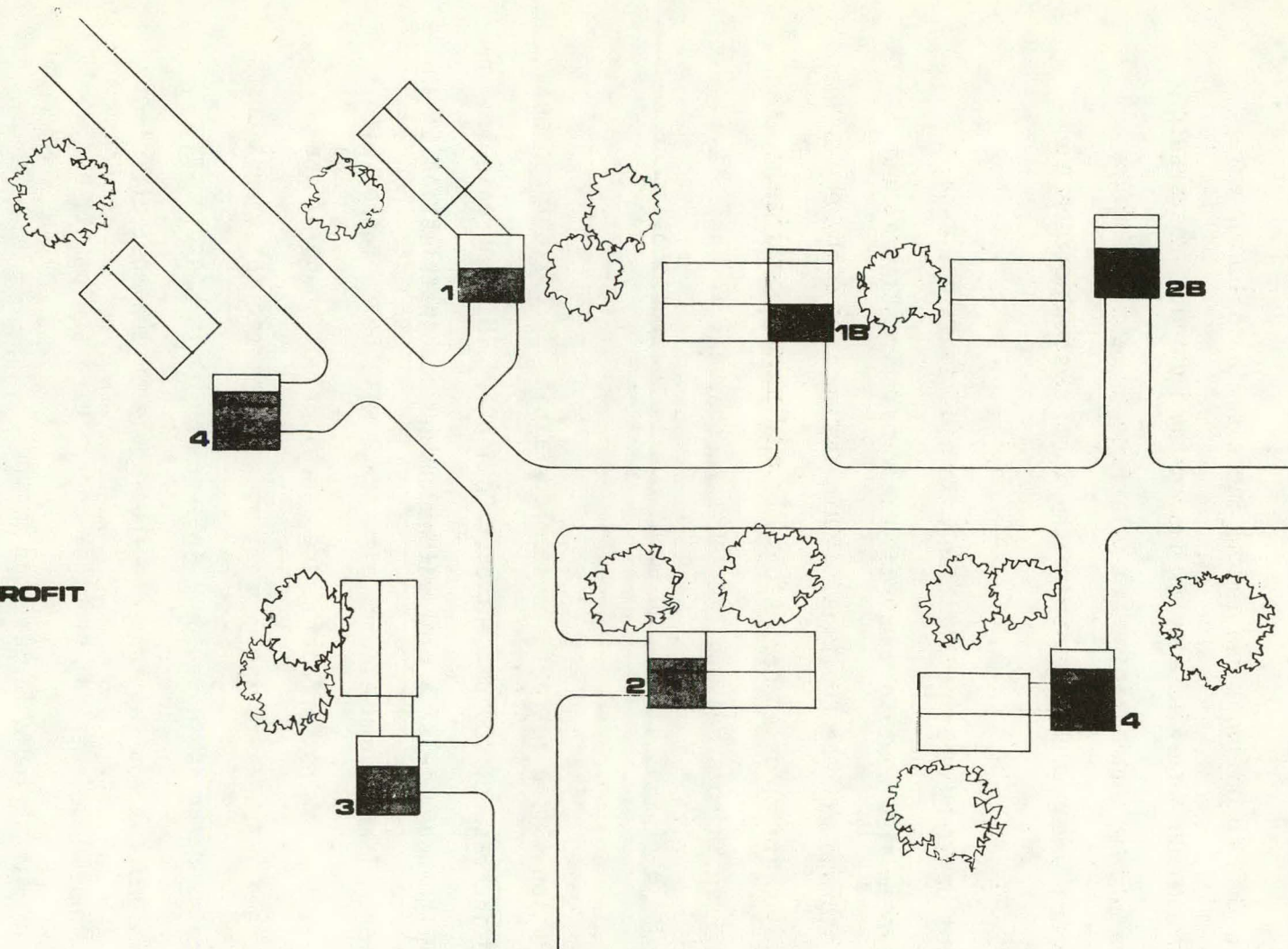


Figure 1.8.60 - Garage retrofit location options for the RPS

1.8.7.3 Garage Mechanical System

The garage mechanical system package and particular component functioning would be identical to that described in Section 1.8.2 and would have rooftop array integration details identical to those described in Section 1.5.1 - RPS Array Structure.

The system isometric shown in Figure 1.8.61 is a two pump solar assisted heat pump array identical to the system illustrated in Section 1.8.2.2 However, a direct solar heating system, identical to the one illustrated in Section 1.8.2.1, could also be utilized.

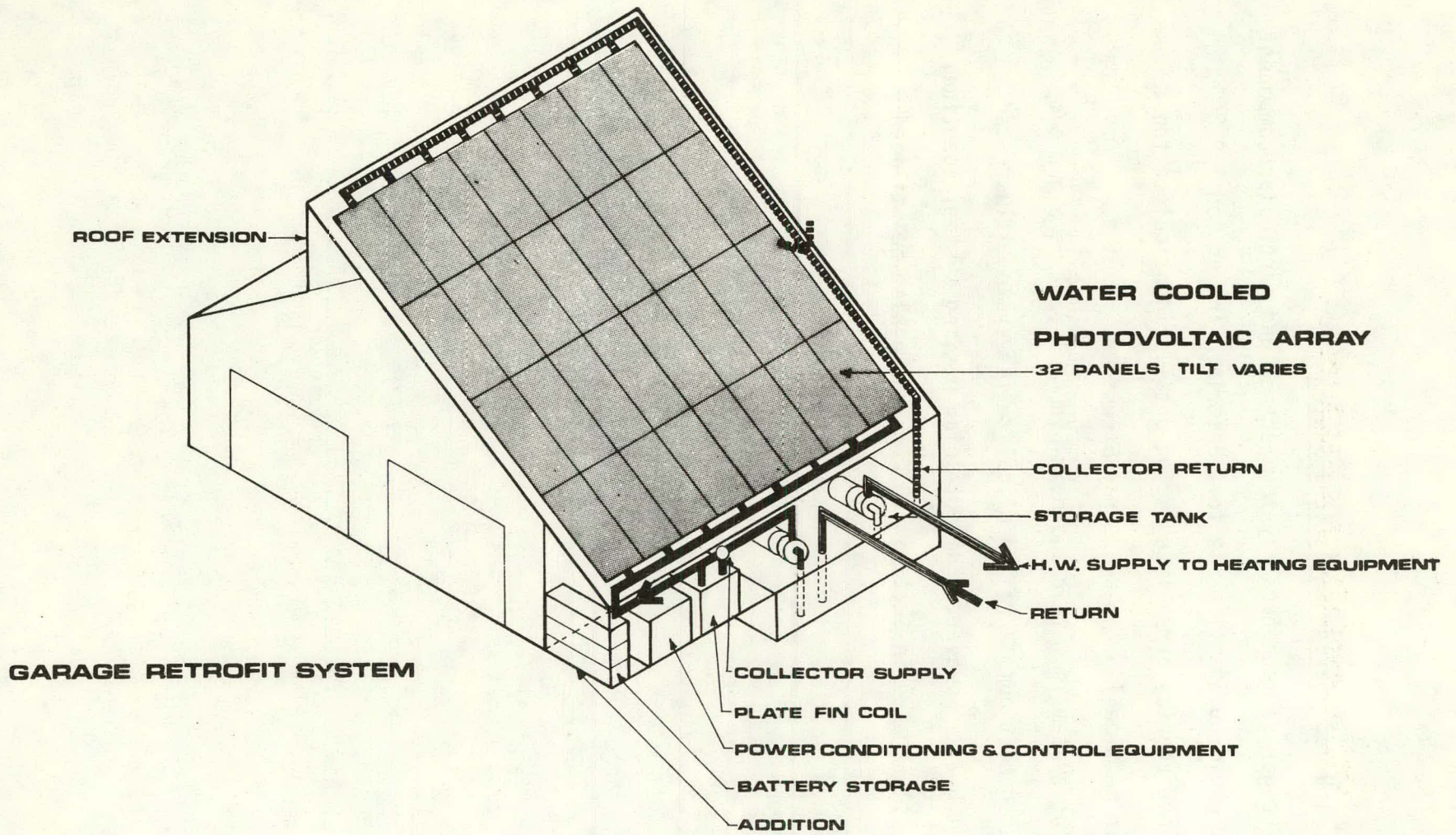


Figure 1.8.61 - Isometric View of garage retrofit RPS

1.8.8 RPS Equipment Lists and Cost Summaries

TABLE 1.8.1

Pricing Data For RPS Systems

ATLANTA - WATER COOLED ARRAY - 333 SQ. FT.

VARIABLE COSTS

* Non Mature Market Components

Item	Unit	Quantity	Price/Unit	1985 Regional Cost [†]	1990 Cost	2000 Cost
Glazing Gasket	/ft.	220	\$ 1.30	\$ 212	\$ 159	\$ 106
Glazing Gasket	/unit	4	1.55	5	4	3
Glazing Gasket	/unit	30	3.25	72	54	36
Glazing Extrusion	/ft.	220	.50	81	61	41
Collector Module Less Photovoltaic	/sq. ft.	333	8.00	1971	1478	986

* Note: Labor Costs for installation of gaskets are included in module installation costs. Extrusion price includes labor.

Subtotal Costs	<u>\$2341</u>	<u>\$1756</u>	<u>\$1172</u>
Subtotal Costs (-Roof Credit)	\$2008	\$1423	\$ 839

* Mature Market Components

Item	Unit	Quantity	Price/Unit	1985 Regional Cost	1990 Cost	2000 Cost
Module Assembly	/module	16	\$ 12.00	\$ 142	\$ 142	\$ 142
Aluminum Flashing	/sq. ft.	200	1.40	260	260	260
2½" fiberglass Insul.	/sq. ft.	333	.23	69	69	69
Hoses & Clamps	/conn.	32	2.26	75	75	75
2" CPVC Plastic	/ft.	116	4.76	547	547	547
Subtotal Costs				<u>\$1093</u>	<u>\$1093</u>	<u>\$1093</u>
TOTAL WATER COOLED SYSTEM VARIABLE COSTS				<u>\$3101</u>	<u>\$2516</u>	<u>\$1932</u>

[†] Includes unit price multiplier for the region.

TABLE 1.8.2

Pricing Data For RPS Systems

ATLANTA - WATER COOLED ARRAY - 333 SQ. FT.

FIXED COSTS

* Non Mature Market Components

Item	Unit	Quantity	Price/Unit	1985 Regional Cost †	1990 Cost	2000 Cost
½ hp, 2½" inlet single phase	/unit	2	\$387.51	\$ 760	\$ 570	\$ 380
Plate Fin Coil	/unit	1	300.00	294	265	265
Modulating Valve	/unit	1	339.74	333	250	167
Control Valve	/unit	2	154.87	304	228	152
Controls	/unit	1	300.00	294	147	74
Butyl Rubber Storage Tank	/sq. ft.	334	.60	200	150	150
Subtotal Costs				\$2185	\$1610	\$1185

* Mature Market Components

Item	Unit	Quantity	Price/Unit	1985 Regional Cost	1990 Cost	2000 Cost
Expansion Valve	/unit	1	\$ 43.53	\$ 43	\$ 43	\$ 43
Shut Off Valve	/unit	1	40.00	39	39	39
Subtotal Costs				\$ 82	\$ 82	\$ 82
Total Water Cooled System Fixed Costs				\$2267	\$1692	\$1270
Total Water Cooled System Variable Costs,				3101	2516	1932
TOTAL WATER COOLED SYSTEM COST				<u>\$5368</u>	<u>\$4208</u>	<u>\$3202</u>

† Includes unit price multiplier for the region.

TABLE 1.8.3

Pricing Data For RPS Systems

CLEVELAND - WATER COOLED ARRAY - 376 SQ. FT.

VARIABLE COSTS

* Non Mature Market Components

Item	Unit	Quantity	Price/Unit	1985 Regional Cost [†]	1990 Cost	2000 Cost
Glazing Gasket	/ft.	232	\$ 1.30	\$ 292	\$ 219	\$ 146
Glazing Gasket	/unit	8	3.50	27	20	14
Glazing Gasket	/unit	4	1.55	6	5	3
Glazing Gasket	/unit	18	3.25	57	43	29
Glazing Extrusion	/ft.	232	.50	112	84	56
Collector Module Less Photovoltaic	/sq. ft.	376	8.00	2909	2182	1455

*Note: Labor Costs for installation of gaskets are included in module installation costs. Extrusion price includes labor.

Subtotal Costs	<u>\$3403</u>	<u>\$2553</u>	<u>\$1703</u>
Subtotal Costs (-Roof Credit)	\$3027	\$2177	\$1327

* Mature Market Components

Item	Unit	Quantity	Price/Unit	1985 Regional Cost	1990 Cost	2000 Cost
Module Assembly	/module	18	\$ 12.00	\$ 209	\$ 209	\$ 209
Aluminum Flashing	/sq. ft.	160	1.40	224	224	224
2½" fiberglass Insul.	/sq. ft.	375	.23	86	86	86
Hoses & Clamps	/conn.	27	2.26	59	59	59
2" CPVC Plastic	/ft.	147	4.76	<u>672</u>	<u>672</u>	<u>672</u>
Subtotal Costs				\$1250	\$1250	\$1250

TOTAL WATER COOLED SYSTEM VARIABLE COSTS \$4277 \$3427 \$2577

[†] Includes unit price multiplier for the region.

TABLE 1.8.4

Pricing Data For RPS Systems

CLEVELAND - WATER COOLED ARRAY - 376 SQ. FT.

FIXED COSTS

* Non Mature Market Components

Item	Unit	Quantity	Price/Unit	1985 Regional Cost [†]	1990 Cost	2000 Cost
¼ hp, 2½" inlet single phase	/unit	2	\$387.51	\$ 764	\$ 573	\$ 382
Plate Fin Coil	/unit	1	300.00	296	266	266
Modulating Valve	/unit	1	339.74	335	251	168
Control Valve	/unit	2	154.87	305	229	153
Controls	/unit	1	300.00	296	148	74
Butyl Rubber Storage Tank	/sq. ft.	334	.60	200	150	150
Subtotal Costs				\$2196	\$1617	\$1193

* Mature Market Components

Item	Unit	Quantity	Price/Unit	1985 Regional Cost	1990 Cost	2000 Cost
Expansion Valve	/unit	1	\$ 43.53	\$ 43	\$ 43	\$ 43
Shut Off Valve	/unit	1	40.00	40	40	40
Subtotal Costs				\$ 83	\$ 83	\$ 83

Total Water Cooled System Fixed Costs	\$2279	\$1700	\$1276
Total Water Cooled System Variable Costs	<u>4277</u>	<u>3427</u>	<u>2577</u>
TOTAL WATER COOLED SYSTEM COST	<u><u>\$6556</u></u>	<u><u>\$5127</u></u>	<u><u>\$3853</u></u>

[†] Includes unit price multiplier for the region.

TABLE 1.8.5

Pricing Data For RPS Systems

MADISON - WATER COOLED ARRAY - 807 SQ. FT.

VARIABLE COSTS

* Non Mature Market Components

Item	Unit	Quantity	Price/Unit	1985 Regional Cost †	1990 Cost	2000 Cost
Glazing Gasket	/ft.	472	\$ 1.30	\$ 518	\$ 389	\$ 259
Glazing Gasket	/unit	24	3.50	71	53	36
Glazing Gasket	/unit	4	1.55	5	4	3
Glazing Gasket	/unit	28	3.25	77	58	39
Glazing Extrusion	/ft.	472	.50	199	149	100
Collector Module Less Photovoltaic	/sq. ft.	807	8.00	5458	4094	2729

* Note: Labor Costs for installation of gaskets are included in module installation costs. Extrusion price includes labor.

Subtotal Costs	<u>\$6328</u>	<u>\$4747</u>	<u>\$3166</u>
Subtotal Costs (-Roof Credit)	\$5521	\$3940	\$2359

* Mature Market Components

Item	Unit	Quantity	Price/Unit	1985 Regional Cost	1990 Cost	2000 Cost
Module Assembly	/module	38	\$ 12.00	\$ 385	\$ 385	\$ 385
Aluminum Flashing	/sq. ft.	232	1.40	298	298	298
2½" fiberglass Insul.	/sq. ft.	800	.23	169	169	169
Hoses & Clamps	/conn.	52	2.26	113	113	113
2" CPVC Plastic	/ft.	167	4.76	<u>767</u>	<u>767</u>	<u>767</u>
Subtotal Costs				\$1732	\$1732	\$1732
TOTAL WATER COOLED SYSTEM VARIABLE COSTS				<u>\$7253</u>	<u>\$5672</u>	<u>\$4091</u>

† Includes unit price multiplier for the region.

TABLE 1.8.6

Pricing Data For RPS Systems

MADISON - WATER COOLED ARRAY - 807 SQ. FT.

FIXED COSTS

* Non Mature Market Components

Item	Unit	Quantity	Price/Unit	1985 Regional Cost †	1990 Cost	2000 Cost
¼ hp, 2½" inlet single phase	/unit	3	\$387.51	\$1125	\$ 844	\$ 563
Plate Fin Coil	/unit	1	300.00	290	261	261
Modulating Valve	/unit	1	339.74	329	247	165
Control Valve	/unit	2	150.00	300	225	150
Controls	/unit	1	200.00	290	145	73
Butyl Rubber Storage Tank	/sq. ft.	334	.60	<u>200</u>	<u>150</u>	<u>150</u>
Subtotal Costs				\$2534	\$1872	\$1362

* Mature Market Components

Item	Unit	Quantity	Price/Unit	1985 Regional Cost	1990 Cost	2000 Cost
Expansion Valve	/unit	1	\$ 43.53	\$ 42	\$ 42	\$ 42
Shut Off Valve	/unit	1	40.00	<u>39</u>	<u>39</u>	<u>39</u>
Subtotal Costs				\$ 81	\$ 81	\$ 81
Total Water Cooled System Fixed Costs				\$2615	\$1953	\$1443
Total Water Cooled System Variable Costs				<u>7253</u>	<u>5672</u>	<u>4091</u>
TOTAL WATER COOLED SYSTEM COST				<u>\$9868</u>	<u>\$7625</u>	<u>\$5534</u>

† Includes unit price multiplier for the region.

TABLE 1.8.7

Pricing Data For RPS Systems

PHOENIX - WATER COOLED ARRAY - 322 SQ. FT.

VARIABLE COSTS

* Non Mature Market Components

Item	Unit	Quantity	Price/Unit	1985 Regional Cost †	1990 Cost	2000 Cost
Glazing Gasket	/ft.	210	\$ 1.30	\$ 235	\$ 176	\$ 118
Glazing Gasket	/unit	7	3.50	21	16	11
Glazing Gasket	/unit	4	1.55	5	4	3
Glazing Gasket	/unit	16	3.25	45	34	23
Glazing Extrusion	/ft.	210	.50	90	68	45
Collector Module Less Photovoltaics	/sq. ft.	322	8.00	2219	1664	1109
				Subtotal Costs	<u>\$2615</u>	<u>\$1962</u>
				Subtotal Costs (-Roof Credit)	<u>\$2293</u>	<u>\$ 987</u>

*Note: Labor Costs for installation of gaskets are included in module installation costs. Extrusion price includes labor.

* Mature Market Components

Item	Unit	Quantity	Price/Unit	1985 Regional Cost	1990 Cost	2000 Cost
Module Assembly	/module	16	\$ 12.00	\$ 165	\$ 165	\$ 165
Aluminum Flashing	/sq. ft.	162	1.40	210	210	210
2½" fiberglass Insul.	/sq. ft.	323	.23	69	69	69
Hoses & Clamps	/conn.	24	2.26	68	68	68
2" CPVC Plastic	/ft.	174	4.76	<u>1037</u>	<u>1037</u>	<u>1037</u>
				Subtotal Costs	<u>\$1549</u>	<u>\$1549</u>
TOTAL WATER COOLED SYSTEM VARIABLE COSTS				<u>\$3842</u>	<u>\$3189</u>	<u>\$2536</u>

† Includes unit price multiplier for the region.

TABLE 1.8.8

Pricing Data For RPS Systems

PHOENIX - WATER COOLED ARRAY - 322 SQ. FT.

FIXED COSTS

* Non Mature Market Components

Item	Unit	Quantity	Price/Unit	1985 Regional Cost [†]	1990 Cost	2000 Cost
¼ hp, 2½" inlet single phase	/unit	2	\$387.51	\$ 759	\$ 569	\$ 380
Plate Fin Coil	/unit	1	300.00	294	265	265
Heat Exchanger & Hot Water Booster	/unit	1	339.74	333	250	167
Control Valve	/unit	2	154.87	303	227	152
Controls	/unit	1	300.00	294	147	74
Butyl Rubber Storage Tank	/sq. ft.	334	.60	200	150	150
Subtotal Costs				\$2183	\$1608	\$1188

* Mature Market Components

Item	Unit	Quantity	Price/Unit	1985 Regional Cost	1990 Cost	2000 Cost
Expansion Valve	/unit	1	\$ 43.53	\$ 43	\$ 43	\$ 43
Shut Off Valve	/unit	1	40.00	39	39	39
Subtotal Costs				\$ 82	\$ 82	\$ 82

Total Water Cooled System Fixed Costs	\$2265	\$1690	\$1270
Total Water Cooled System Variable Costs	3842	3189	2536
TOTAL WATER COOLED SYSTEM COST	\$6107	\$4879	\$3806

[†] Includes unit price multiplier for the region.

TABLE 1.8.9

Pricing Data For RPS Systems

PHOENIX - AIR COOLED ARRAY - 430 SQ. FT.

VARIABLE COSTS

* Mature Market Components

Item	Unit	Quantity	Price/Unit	1985 Regional Cost [†]	1990 Cost	2000 Cost
3" PVL Flashing Collar	/unit	33	\$ 3.00	\$ 92		\$ 92
Support Tower	/unit	33	3.00	92		92
Clip & Spacer	/unit	33	.30	9		9
Module Extrusion	/ft.	79.8	2.50	<u>185</u>		<u>185</u>
Subtotal Costs				\$ 378		\$ 378

* Non Mature Market Components

Item	Unit	Quantity	Price/Unit	1985 Regional Cost	1990 Cost	2000 Cost
Alum. Roll Form	/sq. ft.	430.6	\$ 1.55	\$ 571		\$ 202
TOTAL AIR COOLED SYSTEM VARIABLE COSTS				<u>\$ 949</u>		<u>\$ 580</u>

TOTAL COST - PHOENIX RPS SYSTEM

Water Cooled System Cost - 322 Sq. Ft.	\$6107	\$4879	\$3806
Air Cooled System Cost - 430 Sq. Ft.	<u>949</u>	<u>4879</u>	<u>580</u>
	<u>\$7056</u>	<u>\$4879</u>	<u>\$4386</u>

[†] Includes unit price multiplier for the region.

TABLE 1.8.10

Pricing Data For RPS Systems

WILMINGTON - WATER COOLED ARRAY - 807 SQ. FT.

VARIABLE COSTS

* Non Mature Market Components

Item	Unit	Quantity	Price/Unit	1985 Regional Cost [†]	1990 Cost	2000 Cost
Glazing Gasket	/ft.	472	\$ 1.30	\$ 572	\$ 429	\$ 286
Glazing Gasket	/unit	24	3.50	78	59	39
Glazing Gasket	/unit	4	1.55	6	5	3
Glazing Gasket	/unit	28	3.25	85	64	43
Glazing Extrusion	/ft.	472	.50	220	165	110
Collector Module Less Photovoltaic	/sq. ft.	807	8.00	6020	4515	3010

*Note: Labor costs for installation of gaskets are included in module installation costs. Extrusion price includes labor.

Subtotal Costs	<u>\$6981</u>	<u>\$5237</u>	<u>\$3491</u>
Subtotal Costs (-Roof Credit)	\$6174	\$4430	\$2684

* Mature Market Components

Item	Unit	Quantity	Price/Unit	1985 Regional Cost	1990 Cost	2000 Cost
Module Assembly	/module	38	\$ 12.00	\$ 425	\$ 425	\$ 425
Aluminum Flashing	/sq. ft.	232	1.40	312	312	312
2½" fiberglass Insul.	/sq. ft.	800	.23	177	177	177
Hoses & Clamps	/conn.	52	2.26	112	112	112
2" CPVC Plastic	/ft.	167	4.76	<u>759</u>	<u>759</u>	<u>759</u>
Subtotal Costs				\$1785	\$1785	\$1785

TOTAL WATER COOLED SYSTEM VARIABLE COSTS \$7959 \$6215 \$4469

[†] Includes unit price multiplier for the region.

TABLE 1.8.11

Pricing Data For RPS Systems

WILMINGTON - WATER COOLED ARRAY - 807 SQ. FT.

FIXED COSTS

* Non Mature Market Components

Item	Unit	Quantity	Price/Unit	1985 Regional Cost [†]	1990 Cost	2000 Cost
¼ hp, 2½" inlet single phase	/unit	3	\$387.51	\$1104	\$ 829	\$ 552
Plate Fin Coil	/unit	1	300.00	285	257	257
Modulating Valve	/unit	1	339.74	323	242	162
Control Valve	/unit	2	154.87	294	221	147
Controls	/unit	1	300.00	285	143	71
Butyl Rubber Storage Tank	/sq. ft.	334	.60	<u>200</u>	<u>150</u>	<u>150</u>
			Subtotal Costs	\$2491	\$1842	\$1339

* Mature Market Components

Item	Unit	Quantity	Price/Unit	1985 Regional Cost	1990 Cost	2000 Cost
Expansion Valve	/unit	1	\$ 43.53	\$ 41	\$ 41	\$ 41
Shut Off Valve	/unit	1	40.00	<u>38</u>	<u>38</u>	<u>38</u>
			Subtotal Costs	\$ 79	\$ 79	\$ 79
Total Water Cooled System Fixed Costs				\$2570	\$1921	\$1418
Total Water Cooled System Variable Costs				<u>7959</u>	<u>6215</u>	<u>4469</u>
TOTAL WATER COOLED SYSTEM COST				<u>\$10529</u>	<u>\$8136</u>	<u>\$5887</u>

[†] Includes unit price multiplier for the region.

TABLE 1.8.12

Pricing Data For RPS Systems

SANTA MARIA - WATER COOLED ARRAY - 215 SQ. FT.

VARIABLE COSTS

* Non Mature Market Components

Item	Unit	Quantity	Price/Unit	1985 Regional Cost [†]	1990 Cost	2000 Cost
Glazing Gasket	/ft.	144	\$ 1.30	\$ 146	\$ 110	\$ 73
Glazing Gasket	/unit	5	3.50	14	10	7
Glazing Gasket	/unit	4	1.55	5	4	3
Glazing Gasket	/unit	12	3.25	31	23	15
Glazing Extrusion	/ft.	144	.50	57	42	28
Collector Module Less Photovoltaic	/sq. ft.	215	8.00	1350	1013	675

*Note: Labor Costs for installation of gaskets are included in module installation costs. Extrusion price included labor.

Subtotal Costs	<u>\$1603</u>	<u>\$1202</u>	<u>\$ 801</u>
Subtotal Costs (-Roof Credit)	\$1388	\$ 987	\$ 586

* Mature Market Components

Item	Unit	Quantity	Price/Unit	1985 Regional Cost	1990 Cost	2000 Cost
Module Assembly	/module	12	\$ 12.00	\$ 113	\$ 113	\$ 113
Aluminum Flashing	/sq. ft.	128	1.40	173	173	173
2½" fiberglass Insul.	/sq. ft.	215	.23	48	48	48
Hoses & Clamps	/conn.	18	2.26	40	40	40
2" CPVC Plastic	/ft.	128	4.76	606	606	606
Subtotal Costs				\$ 980	\$ 980	\$ 980
TOTAL WATER COOLED SYSTEM VARIABLE COSTS				<u>\$2368</u>	<u>\$1967</u>	<u>\$1566</u>

[†] Includes unit price multiplier for the region.

TABLE 1.8.13

Pricing Data For RPS Systems

SANTA MARIA - WATER COOLED ARRAY - 215 SQ. FT.

FIXED COSTS

* Non Mature Market Components

Item	Unit	Quantity	Price/Unit	1985 Regional Cost †	1990 Cost	2000 Cost
¼ hp, 2½" inlet single phase	/unit	2	\$387.51	\$ 777	\$ 582	\$ 388
Plate Fin Coil	/unit	1	300.00	301	271	271
Modulating Valve	/unit	1	339.74	340	255	170
Control Valve	/unit	2	154.87	310	233	155
Controls	/unit	1	300.00	300	150	75
Butyl Rubber Storage Tank	/sq. ft.	334	.60	200	150	150
Subtotal Costs				\$2228	\$1641	\$1209

* Mature Market Components

Item	Unit	Quantity	Price/Unit	1985 Regional Cost	1990 Cost	2000 Cost
Expansion Valve	/unit	1	\$ 43.53	\$ 44	\$ 44	\$ 44
Shut Off Valve	/unit	1	40.00	40	40	40
Subtotal Costs				\$ 84	\$ 84	\$ 84

Total Water Cooled System Fixed Costs	\$2312	\$1725	\$1293
Total Water Cooled System Variable Costs	2368	1967	1566
TOTAL WATER COOLED SYSTEM COST	\$4680	\$3692	\$2859

† Includes unit price multiplier for the region.

TABLE 1.8.14

Pricing Data For RPS Systems

SANTA MARIA - AIR COOLED ARRAY - 405 SQ. FT.

VARIABLE COSTS

* Mature Market Components

Item	Unit	Quantity	Price/Unit	1985 Regional Cost	1990 Cost	2000 Cost
3" PVL Flashing Collar	/unit	36	\$ 3.00	\$ 108	\$ 108	\$ 108
Support Tower	/unit	36	3.00	108	108	108
Clip & Spacer	/unit	16	.30	5	5	5
Module Extrusion	/ft.	80	2.50	193	193	193
Subtotal Costs				\$ 414	\$ 414	\$ 414

* Non Mature Market Components

Item	Unit	Quantity	Price/Unit	1985 Regional Cost	1990 Cost	2000 Cost
Alum. Roll Form	/sq. ft.	405	\$ 1.55	\$ 628	\$ 345	\$ 345
TOTAL AIR COOLED SYSTEM VARIABLE COSTS				<u>\$1042</u>	<u>\$ 759</u>	<u>\$ 759</u>

TOTAL COST - SANTA MARIA RPS SYSTEM

Water Cooled System Cost - 215 Sq. Ft.	\$4680	\$3692	\$2859
Air Cooled System Cost - 405 Sq. Ft.	1042	759	759
	<u>\$5722</u>	<u>\$4451</u>	<u>\$3618</u>

THIS PAGE
WAS INTENTIONALLY
LEFT BLANK

1.9 IPS Structural Design

For all of the intermediate power systems considered, the solar cell arrays were assumed to be mounted on the roofs of an existing structures. Furthermore, except for moveable collectors needed for certain types of arrays, tracking was not considered. Because the supports of the fixed arrays considered were discussed together with the arrays, and because no other structure is needed, there is no need for a discussion of IPS structural design.

THIS PAGE
WAS INTENTIONALLY
LEFT BLANK

1.10 CPS Site Survey

A survey was made by Ford, Bacon, and Davis Utah of sites in the vicinity of Phoenix Arizona which might be potentially suitable for CPS plant location. The results of this survey are presented in this section.

Ford, Bacon & Davis Utah Inc.

ENGINEERS — CONSTRUCTORS

A SUBSIDIARY OF

Ford, Bacon & Davis
Incorporated

CENTRAL POWER PLANT

SITING STUDY

March 1976

ENGINEERING SUPPORT SERVICES
FOR
CONCEPTUAL DESIGN AND SYSTEM ANALYSIS
OF
PHOTOVOLTAIC POWER SYSTEMS

Ford, Bacon and Davis Utah Contract UC-160

Westinghouse Subcontract 34-JP-26539-A

LOCATION OF THE SOLAR ARRAY

GENERAL CRITERIA FOR SELECTION OF A SOLAR ARRAY SITE

Factors that will influence the selection of a site for a solar array include the solar properties of the area, the availability of support facilities, and the compatibility of the solar array with the natural ecosystem.

Some of these criteria have been generalized and applied by other researchers to the southwestern United States (see Figure 1 and 2). Using these criteria and others applicable to this project, areas within 100 miles of Phoenix were examined as potential solar array sites. These criteria are listed in Table 1.

Although many areas within a 100-mile radius of Phoenix have excellent site characteristics, three in particular combine advantageous characteristics in a manner that makes them more suitable as locations of a solar facility (see Figure 3.) These three sites listed in preferential order are: The Vulture Mountain site, The Rainbow Valley site, and The Maricopa Mountain site. Each is described in this section of the report. Cost estimates in other sections of the report are based on the Vulture Mountain location.

VULTURE MOUNTAIN SITE

The proposed Vulture Mountain site is located 50 miles northwest of Phoenix on the southern slope of the east-west trending Vulture Mountains. It lies in sections 8 and 9 of T5N R6W of the Gila Bend Salt River Coordinate System (see Figure V-1).

The comparative advantages of the Vulture Mountain site to the other potential sites include its southern exposure, remote location from resource development and population centers, its proximity to power transmission lines and to an existing road network, and its distance from croplands and other major sources of dust and sand. Its comparative disadvantages include the questionable availability of water and the site's distance from Phoenix.

SOLAR PROPERTIES OF THE SITE

The site faces south with no apparent shading from mountains, man-made structures, or clouds. Although insolation studies have not been performed at the site, it lies in a favorable locale that receives greater than 3,800 and less than 4,000 annual mean total hours of sunshine (Langleys) and greater than 500 (Langleys) of annual daily mean solar radiation (see Appendix Figures 2 and 3). It is located near radiation instruments of Desert Sunshine Exposure Testing. Normal annual precipitation averages 8-12 inches, 60 percent of which falls in the winter. Evaporation and evapotranspiration are very high (annual pan evaporation exceeds 110 inches)

and temperatures are high (July maximum temperatures average 105 degrees Fahrenheit, July minimum temperatures average 75 degrees Fahrenheit).

SUPPORT FACILITIES FOR THE SITE

The Vulture Mountain site is located 50 miles northwest of Phoenix, 15 miles southwest of Wickenburg, 15 miles west-southwest from Morristown and 15 miles northwest of Tonopah. Two transmission systems traverse the immediate area: the Parker Dam - Phoenix 161 KV power transmission line lies three miles from the site, and the Mead Liberty 345 KV power transmission line lies tangent to the northeast corner of the site. The proposed Liberty - Parker Dam 230 KV power line also would use the Parker Dam - Phoenix corridor.

Access to the site would be from Wickenburg, Morristown or from Interstate I-10 (when road construction is completed). Access roads to the Parker Dam - Phoenix utility corridor would provide alternate access to the north (highways 60 & 70 at Aguila). An unimproved road borders the site on the south and connects with an all weather road $3\frac{1}{2}$ miles to the west. No new construction roads would be necessitated, nevertheless the site is isolated from populated areas. The land is federally controlled and administered by the Bureau of Land Management. The sections surrounding the tract are BLM land except for section 16 to the south which is a state section (see Figure V-2).

Water availability may be a problem, but according to a recent publication by the Arizona Water Commission, the area is one of "possible potential for groundwater development" (see Appendix Figure 4). A more reliable source could be the proposed Granite Reef Aqueduct which will be located 12 miles south of the site (see Figure V-3).

The site area and its environs are of doubtful agricultural, residential, or natural resource potential although there has been some mining 5 miles northeast of the site and a dry wildcat well drilled 4 miles west of the site.

COMPATIBILITY WITH THE LOCAL ENVIRONS

The site appears to be stable with virtually no seismic activity, subsidence caused by water withdrawal or mining activities, sifting sand dunes or evidence of landslides. Severe wind erosion or gullying from water erosion is not evident from aerial photographs and the land has not been disturbed except for the transmission line and dirt road (see Figure V-4). Major dust producers such as cropland lie over 15 miles to the northwest (see Figure V-4). A buffer of at least 1 mile could easily be established to isolate the site from further (but unlikely) development. The slope is gentle (<200 ft/mile) and stabilized by vegetation. Disruption of the soil structure, loss of vegetation, and the impermeable nature of the photo-electric structures on or above the surface of the land will alter the erosional characteristics of the area. Necessarily, extreme precautions taken during construction could reduce future problems of wind blown particles, increased soil erosion and encourage stabilization.

RAINBOW VALLEY

The Rainbow Valley site is located southwest of Phoenix on the southwestern slope of the Sierra Estrella in T3S R1E Sections 4, 5, 8 and 9 (see Figure R-1). Its unique characteristic is that it is located near a proposed pumped storage power plant, the Salt River Montezuma Plant and could be operated in conjunction with it.

Compared to the other two sites it is closer to Phoenix, its potential for water availability is high and it could feed directly into a power generating site. Its disadvantages include its southwestern exposure, possible mountain shadows very late in the day, the chance of residential development, potential windblown sand and dust, and potential land subsidence due to groundwater withdrawal.

SOLAR PROPERTIES

The Rainbow Valley site is on a southwestern exposure in an area of high insolation that receives greater than 3,800 but less than 4,000 annual mean total hours of sunshine (Langleys) and greater than 500 (Langleys) of annual daily mean solar radiation (see Appendix Figures 2 and 3). It is located within 15 miles of a radiation instrument station in Phoenix. Normal annual precipitation averages 8 inches, 55-60 percent of which falls in the winter. Evaporation and evapotranspiration are very high (annual pan evaporation exceeds 105 inches) and temperatures are high (July maximum temperatures average above 105 degrees Fahrenheit, July minimum temperatures average above 75 degrees Fahrenheit).

The site has an uninterrupted view to 10 degrees above the local horizon, but because it faces west-southwest, it may lose some sunlight hours from shadows off the Sierra Estrella. The array could be located farther west to minimize such shadows, but the farther west the structure is located, the farther its distance from the power plant, and the increased potential of conflicting land uses.

SUPPORT FACILITIES

The Rainbow Valley site is located 20 miles southwest of Phoenix, 12 miles north of Mobile, and 4 miles due west of Montezuma Peak.

There is no major transmission line in the immediate vicinity although there is a proposed 345 KV transmission corridor through the valley and a proposed power project at the southeastern foot of the Sierra Estrella. This hydroelectric plant, the Salt River Montezuma Project, is licensed, has begun construction and is scheduled for completion in 1982. The plant's two pumped storage reservoirs will be located approximately 6 miles east-southeast of the site, the power plant itself would be located underground (see Figure R-2).

The Phoenix area has experienced a continued high rate of growth some of which has expanded to neighboring valleys. The Rainbow Valley site may be protected from this growth by its location behind the Sierra Estrella from Phoenix. The distance from the site to Phoenix as the crow flies is 20 miles, but by car the distance would be at least 30 miles. Land use planners do not expect residential or subdivision growth along the Sierra Estrella foothills, although there is such growth expected further

east in Rainbow Valley. Cropland lies 5 miles to the west of the site in Rainbow Valley, and the nearest town is Mobile, 8 miles to the south. Mining activity has been limited to quarry prospects in the Sierra Estrella. The site is located on Federal land administered by the BLM (see Figure R-3). Two quarter-sections of private land lie within 1 mile of the site to the east.

Accessibility to water might be dependent upon an arrangement with the Salt River Project and their well field or from potential groundwater aquifers in the Sierra Estrella foothill deposits.

Access to the site could be provided by existing unimproved roads (see Figure R-1) that join Mobile with ranching properties, the quarry prospects in the mountains and eventually connect to Liberty to the northwest. One of these roads crosses the potential tract and another runs tangent to it at the southeastern corner.

There has been considerable groundwater withdrawal in the Phoenix area and in Rainbow Valley. Although the foothills of the Sierra Estrella have not yet been affected, they will likely be subject to subsidence should extensive groundwater withdrawal continue in Rainbow Valley. In other respects the site is apparently stable with little chance of seismic, landslide or sand dune activity.

Photographs of the area show no evidence of excessive wind or water erosion and roads in the area are limited, although they will increase in density with future development (see Figure R-4). Cropland is relatively limited and distant (over 6 miles northwest) from the site (see Figure R-5). The Sierra Estrella might provide some protection from winds from the north, northeast, east, and southeast.

Extreme care during construction would have to be taken to disturb the site as little as possible, in order to avoid later wind and water erosion. The slope of the site is gentle (see Figure R-6), but the impermeable nature of the sheet array structures will tend to promote erosion. Pit structures would tend to retard erosion, but act as sediment basins.

MARICOPA MOUNTAIN SITE

The Maricopa Mountain site is located southeast of Phoenix in sections 31 and 32 of T5S R3W on the southern slope of the Maricopa Mountains (see Figure M-1). Compared to the other two sites, it has the best solar characteristics. It also is in an area that is unlikely to be developed but is accessible to population centers. Disadvantages are: it is not near to major transmission lines, it might be visible from a highway, water availability may be limited, and the site could be subject to high winds and consequent pitting and dust deposition.

SOLAR PROPERTIES

The site has a western exposure, even though it borders the southern section of the Maricopa Mountains. There is an uninterrupted view to the south down to an angle of 10 degrees above the horizon; and also there is no shading from mountains or man-made structures. The insolation potential is high. The Maricopa Valley site lies in an area of well above 3,800

annual mean total hours of sunshine (Langley's) and greater than 500 (Langley's) of annual daily mean solar radiation (see Appendix Figures 2 and 3). It is not located near solar radiation instrumentation, although data can be extrapolated from that gathered from the Phoenix and Yuma areas. Normal annual precipitation averages less than 8 inches, 55-60 percent of which falls in the winter. Evaporation and evapotranspiration are very high (annual pan evaporation averages 110 inches) and temperatures are high (July maximum temperatures average above 105 degrees Fahrenheit, July minimum temperatures average 75 degrees Fahrenheit).

SUPPORT FACILITIES

The Maricopa Mountain site is located 45 miles southwest of Phoenix, 8 miles northeast of Gila Bend, and 5 miles southeast of Cotton Center.

The Gila Bend 60 KV power transmission line runs north-south approximately 3 miles west of the site, but there are no large transmission lines in the immediate vicinity of the site. Arizona State Highway 80 runs north - south, less than two miles from the site, but there is no easy access from the site to it. Access to the site is afforded by unimproved roads that serve local ranches and the Gila Southern Pacific Company's tracks which originate in Gila Bend or Estrella. The road that would most likely service the site terminates at the site (see Figure M-1). There is a corral and wind mill one mile south of the site, but otherwise it is desolate country. (The site may be visible from highway 80 - depending on the array's conformation).

The BLM administers this Federal land and all the sections surrounding it, except the state section to the southwest (see Figure M-2).

There is extensive agricultural land cultivated in the Gila River Valley north of Gila Bend (see Figure M-3). These lands lie $2\frac{1}{2}$ miles west of the site and could serve as a source of windblown sand and soil that could coat or damage the solar array during westerly, northwesterly, or southwesterly wind storms. A buffer of at least one mile of undisturbed land could be established around the site, but this might not be sufficient for severe storms.

The Painted Rock Dam, 25 miles downstream from the solar site, was constructed by the Corps of Engineers as a flood control project on the Gila River. The reservoir area is rarely inundated and is extensively farmed. Groundwater for development in the immediate vicinity only has potential in wells deeper than 500 feet (see Appendix Figure 4).

Land uses in the immediate area are for ranching with little prospect for expanded agricultural use, residential, subdivision, or mining development. The site was selected because of the convenience of an existing road to the area and to minimize distance from a transmission line. However, the site could be relocated to the east in order to achieve greater isolation and protection from wind problems.

COMPATIBILITY WITH THE LOCAL ENVIRONS

The area is not seismically active, nor is groundwater withdrawal a problem. There is no potential for landslides and the subsurface appears stable.

As discussed previously, wind blown sand and dust from croplands to the west could be a problem even if a one mile buffer of undisturbed land were established. There is no evidence of sand dunes or excessive wind or water erosion on photographs (see Figure M-4). The slope is gentle (50 ft/mile) with some steeper areas such as near a "bump" north of the site (see Figure M-1). Revegetation and rehabilitation of the natural site conditions would be extremely difficult, but could be facilitated by careful planning and extreme care during construction. Without such care, wind and water erosion will be a problem.

TABLE I

SOLAR ARRAY SITE CRITERIA

SOLAR PROPERTIES

OBJECTIVES

- a) Maximize direct sunlight.
- b) Maximize period of time exposed to sunlight.
- c) Minimize shadows from mountains, clouds or structures.

SITING CRITERIA

- a) Areas west and south of Phoenix.
- b) Southern exposures preferable with an uninterrupted view to the south down to an angle of 10 degrees above the local horizon.
- c) Absence of shading.

SUPPORT FACILITIES

OBJECTIVES

- a) Supplement the Phoenix electric system.
- b) Reduce costs of construction (travel, cost of land).
- c) Minimize disruption of the countryside and minimize visibility from population centers.
- d) Sufficient water availability for cooling purposes.
- e) Limited alternative land uses for site.

SITING CRITERIA

- a) Location within 100 miles of Phoenix.
- b) Location within 10 miles of a power transmission line.
- c) Location not visible from major highways, but located within 5 miles of a road.
- d) Location on Federal land (preferably land administered by the BLM).
- e) Accessibility to a water supply of 10 million gallons/year.
- f) Agricultural areas, residential areas, and subdivisions unacceptable.
- g) Major resource areas unacceptable (agricultural, forest, or mining).
- h) Areas underlying aviation flight paths unacceptable.

COMPATIBILITY WITH THE LOCAL ENVIRONS

OBJECTIVES

- a) Once installed the solar array alignment should not shift.
- b) Pitting of the cells by wind blown sand or coating by dust should be minimized.

- c) Disruption of the local environment should be minimal and the array should not adversely affect the environment near the site over the long term.

Factors to be considered include:

- destruction of vegetation
- loss of soil structure
- increased wind and water erosion

SITING CRITERIA

- a) Seismically active areas, areas prone to subsidence, landslide areas, and unstable subsurfaces are unacceptable.
- b) Areas prone to wind storms should be avoided and areas known to produce dust (roads, cropland) should be remote. A buffer of 1 mile of undisturbed land should be able to be established around the array.
- c) Avoid slopes greater than 15 degrees.
- d) Avoid areas of endangered plant or animal species.

LIST OF FIGURES

- Figure 1 Solar array siting exclusion criteria - Arizona.
Source: Solar Thermal Conversion Mission Analysis.
The Aerospace Corporation, 1975.
- Figure 2 Solar array location summary - Arizona.
Source: Solar Thermal Conversion Mission
Analysis, The Aerospace Corporation, 1975.
- Figure 3 Location map of the three potential solar array sites.
Source: Arizona State Highway Map 1975.
- Figure V-1 Vulture Mountain solar site location map.
Source: General Highway Map, Maricopa County
sheet #4, Arizona Department of Transportation.
- Figure V-2 Vulture Mountain solar site land ownership map.
Source: General Highway Map, Maricopa County,
sheet #4, Arizona State Land Department.
- Figure V-3 General location map, Central Arizona Project.
Source: U.S. Department of the Interior, Bureau
of Reclamation, Map #344-314-944, August 1968.
- Figure V-4 Aerial photograph of the Vulture Mountain solar site.
Scale 1:24,000, ARIS photo date August, 1972;
Vulture Mountains SW Arizona 1776; Arizona
Resources Information System.
- Figure V-5 Vulture Mountain solar site cropland map.
Source: Cropland Atlas of Arizona, Arizona Crop
and Livestock Reporting Service, 1974.
- Figure R-1 Rainbow Valley solar site location map.
Source: General Highway Maps, Pinal County sheet
#1, Maricopa County sheets #6 and #8, Arizona
Department of Transportation.
- Figure R-2 Montezuma hydroelectric pumped storage project
location map.
Courtesy: Salt River Project
- Figure R-3 Rainbow Valley solar site land ownership map.
Source: General Highway Maps, Pinal County sheet
#1, Maricopa County sheets #6 and #8, Arizona State
Land Department.
- Figure R-4 Aerial photograph of the Rainbow Valley solar site.
Scale 1:24,000 ARIS photo date November, 1972:
Mobile NE Ariz. 2281; Arizona Resources Information
System.

List of Figures (cont'd)

- Figure R-5 Rainbow Valley solar site cropland map.
Source: Cropland Atlas of Arizona, Arizona
Crop and Livestock Reporting Service, 1974.
- Figure R-6 Rainbow Valley solar site slope map.
Source: Slope Map, Mobile NE quadrangle;
7.5 Minute Series (topographic); U.S.
Geological Survey; 1975; for the Tucson-
Phoenix Urban Area Study Project.
- Figure M-1 Maricopa Mountain solar site location map.
Source: General Highway Map, Maricopa
County, sheet #8, Arizona Department of
Transportation.
- Figure M-2 Maricopa Mountain solar site land ownership map.
Source: General Highway Map, Maricopa County,
sheet #8, Arizona State Land Department
- Figure M-4 Aerial photograph of the Maricopa Mountain
solar site. Scale 1:24,000 ARIS photo date
November, 1972; Cotton Center SE Ariz 2082;
Arizona Resources Information System.
- Appendix -
Figure 1 Annual mean total hours of sunshine (Langleys).
Source: Solar Energy, Arizona Resources
Information System Cooperative Publication #5.
- Appendix -
Figure 2 Annual daily mean of solar radiation (Langleys).
Source: Solar Energy, Arizona Resources
Information System Cooperative Publication #5.
- Appendix -
Figure 3 Suitability of groundwater for development of
municipal and industrial water supplies-Southwest
Arizona
Source: Phase 1-Arizona State Water Plan,
Inventory of resource and uses, 1975, Arizona
Water Commission.
- Appendix -
Figure 4 Subdivisions in Southwestern Arizona (indicative
of areas of future residential growth).
Source: Remote Subdivisions Recorded 1879 -
1973; Office of Economic Planning and Development;
State of Arizona, 1974.
- Appendix -
Figure 5 Public Land Ownership in Arizona, 1971.
Source: Department of Economic Planning and
Development, State of Arizona.

List of Figures (cont'd)

Appendix -
Figure 6

Public Land Ownership in Arizona, 1971.
Source: Department of Economic Planning and
Development, State of Arizona.

FIGURE# 1

Terrain

- 20% GRADE



Terrain

- SURFACE EROSION



Soil

- EXPANSIVE SOILS
- SAND DUNES
- DRY LAKE BEDS
- LAVA FLOWS
- LAKES, RIVERS, MARSHES



Surface Vegetation

- MAJOR RESOURCE



Surface Vegetation

- SIGNIFICANT IMPACT



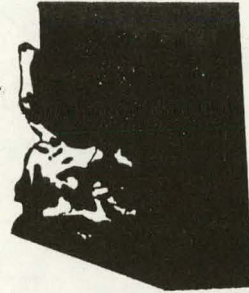
SOLAR ARRAY SITING EXCLUSION CRITERIA — ARIZONA —

(ADAPTED FROM AEROSPACE CORPORATION, 1975)

FIGURE #2

Siting Area Location Summary

- MOST STRINGENT CRITERIA



Siting Area Location Summary

- LEAST STRINGENT CRITERIA



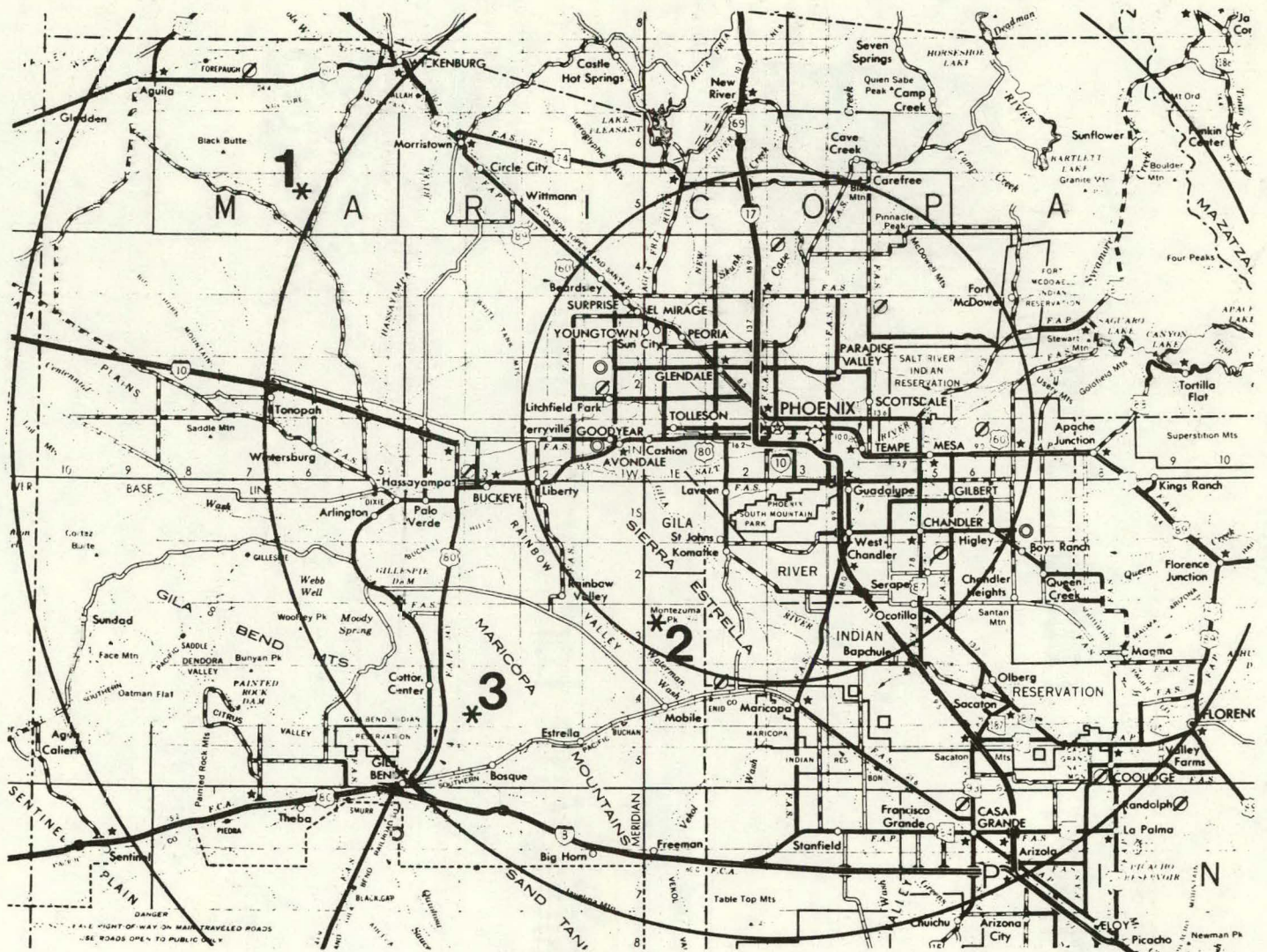
SOLAR ARRAY SITING AREA LOCATION SUMMARY — ARIZONA —

(ADAPTED FROM AEROSPACE CORPORATION, 1975)

SOUTH WESTERN ARIZONA, POTENTIAL SOLAR ARRAY SITES,

SHOWING DISTANCES FROM PHOENIX

1. VULTURE MOUNTAIN SOLAR SITE
2. RAINBOW VALLEY SOLAR SITE
3. MARICOPA MOUNTAIN SOLAR SITE



ADAPTED FROM 1975 ARIZONA HIGHWAY MAP

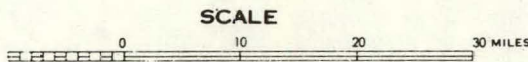


FIGURE 3
510

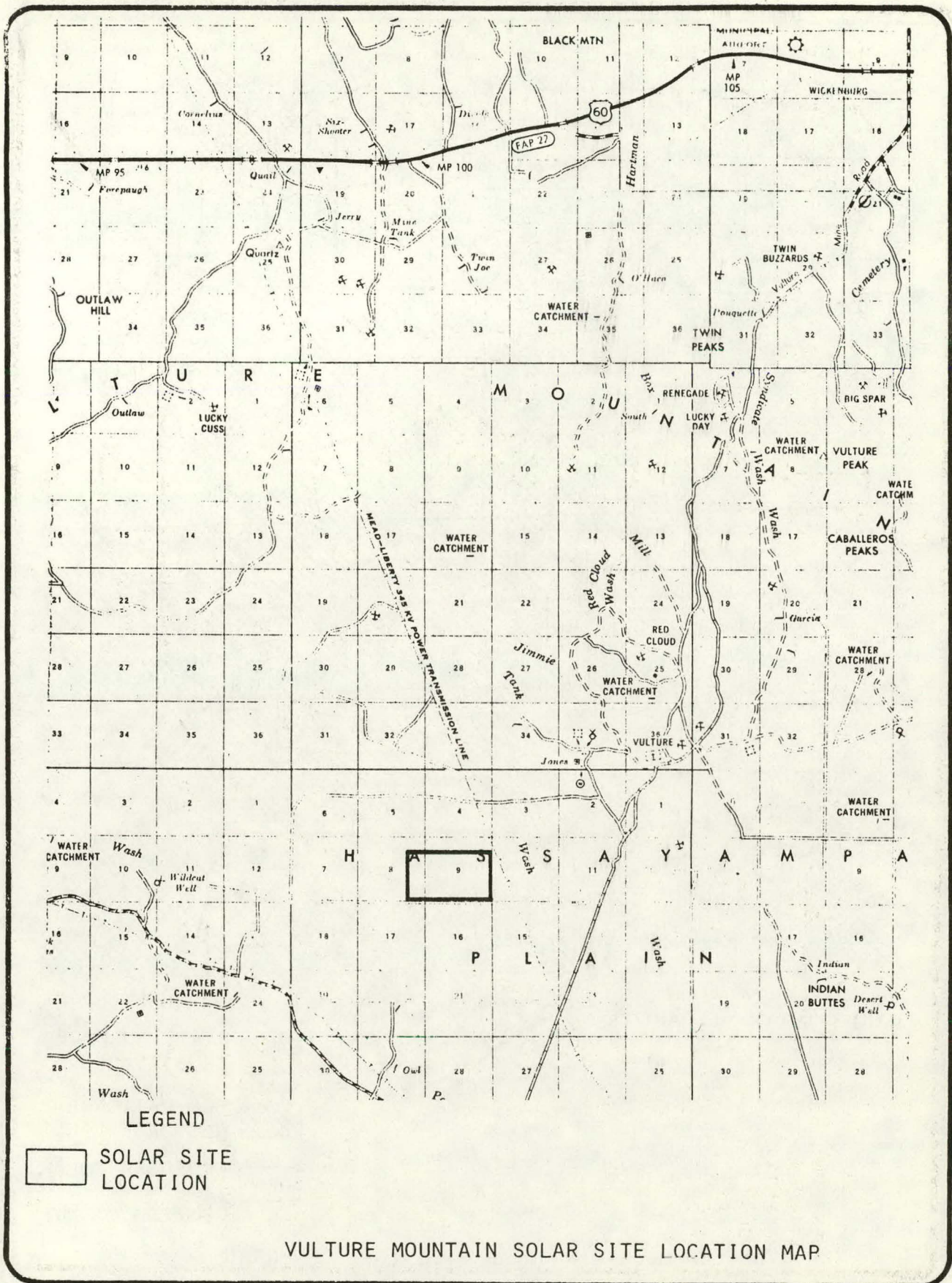
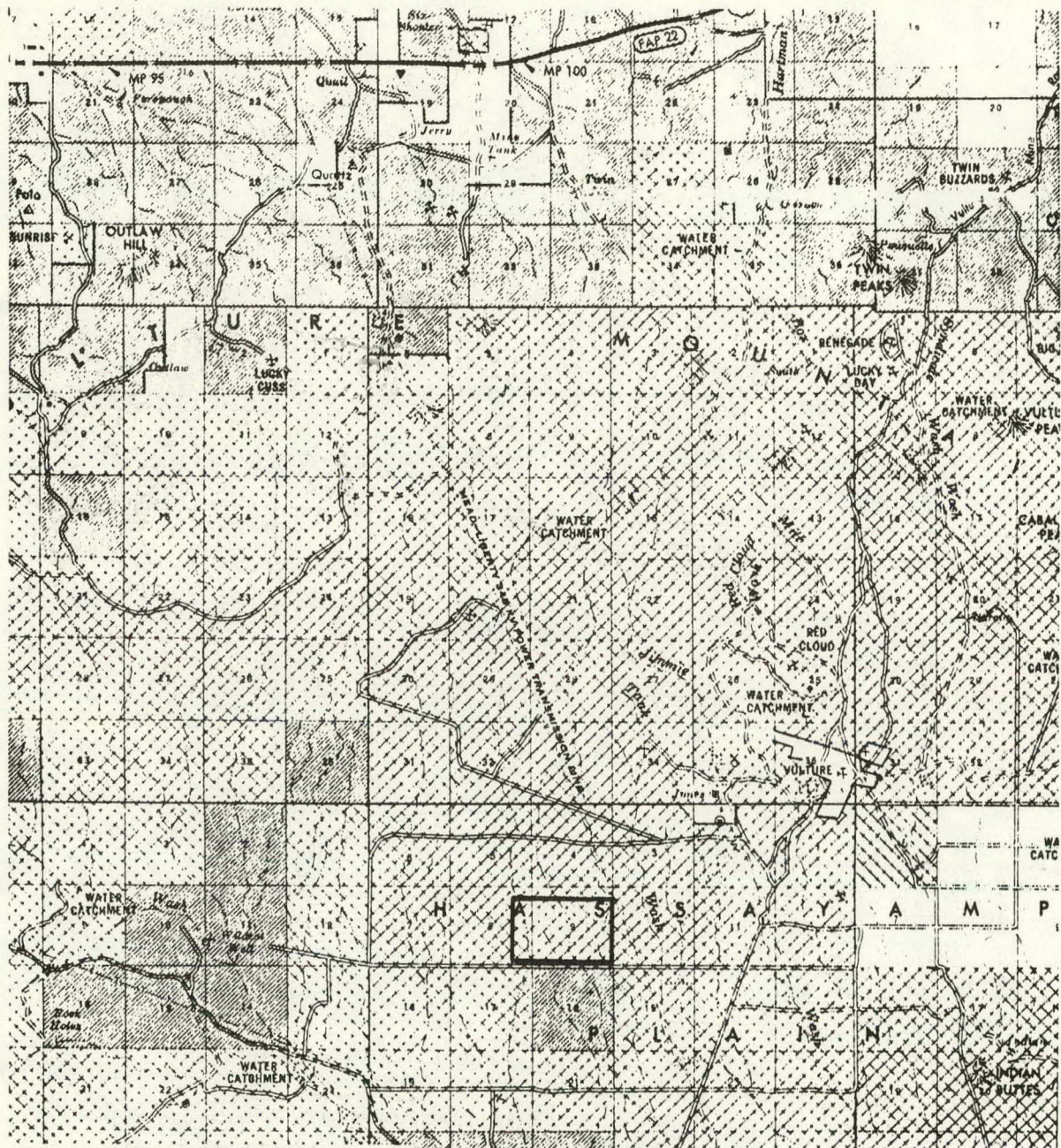


FIGURE V-1



GENERAL HIGHWAY MAP
MARICOPA COUNTY, ARIZONA

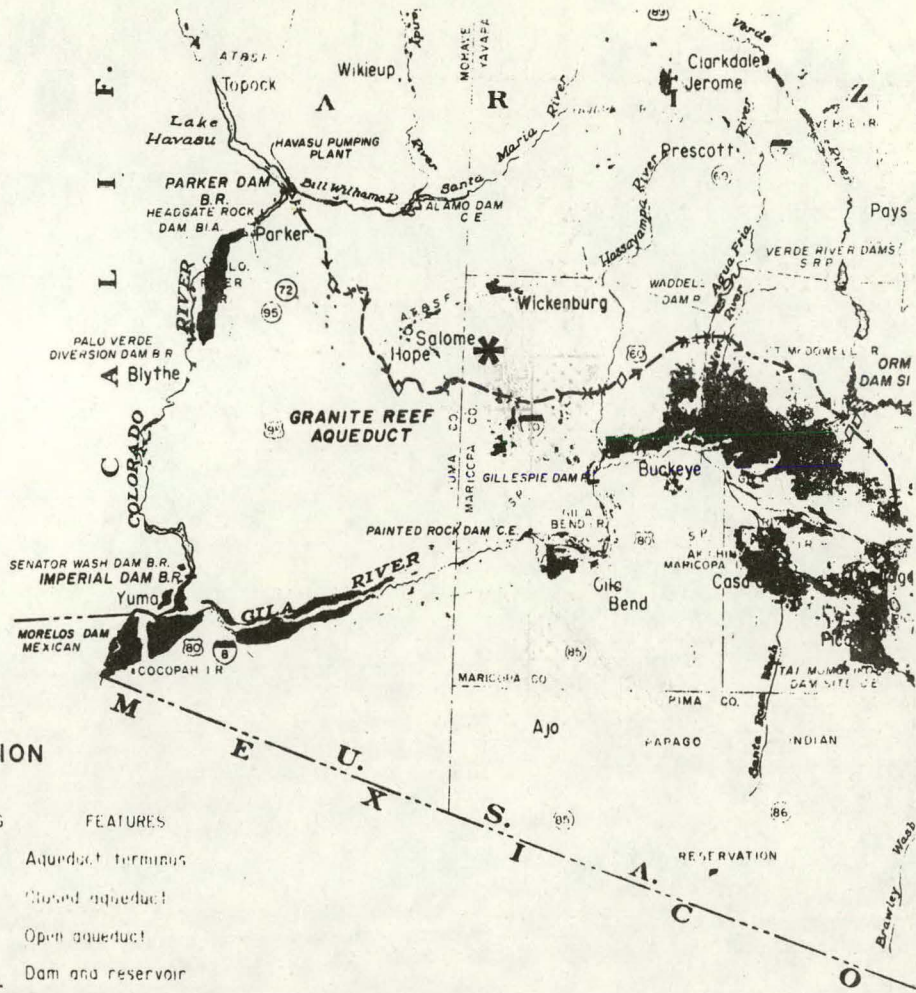
ARIZONA DEPARTMENT OF TRANSPORTATION
 DIVISION OF HIGHWAYS
 PHOTOGRAMMETRY AND MAPPING
 IN COOPERATION WITH THE
 U.S. DEPARTMENT OF TRANSPORTATION
 FEDERAL HIGHWAY ADMINISTRATION



LEGEND

-  STATE SURFACE TRUST LANDS
-  BLM-NATIONAL RESOURCE LANDS
-  PROPOSED SOLAR SITE (MARICOPA COUNTY)

VULTURE MOUNTAIN SOLAR SITE LAND OWNERSHIP



EXPLANATION

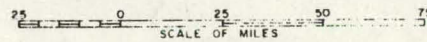
UNDER		FEATURES
AUTHORIZED	CONSTRUCTION EXISTING	
— —		Aqueduct terminus
— —		Closed aqueduct
— —		Open aqueduct
		Dam and reservoir
		Generating station
		Pumping plant
		Siphon
		Tunnel
		Indian reservation
		Water use areas

ABBREVIATIONS

- B. I. A. Bureau of Indian Affairs
- B. R. Bureau of Reclamation
- C. E. Corps of Engineers
- P. Private
- C. R. P. Salt River Project

UNITED STATES
DEPARTMENT OF THE INTERIOR
BUREAU OF RECLAMATION
CENTRAL ARIZONA PROJECT - ARIZONA-NEW MEXICO

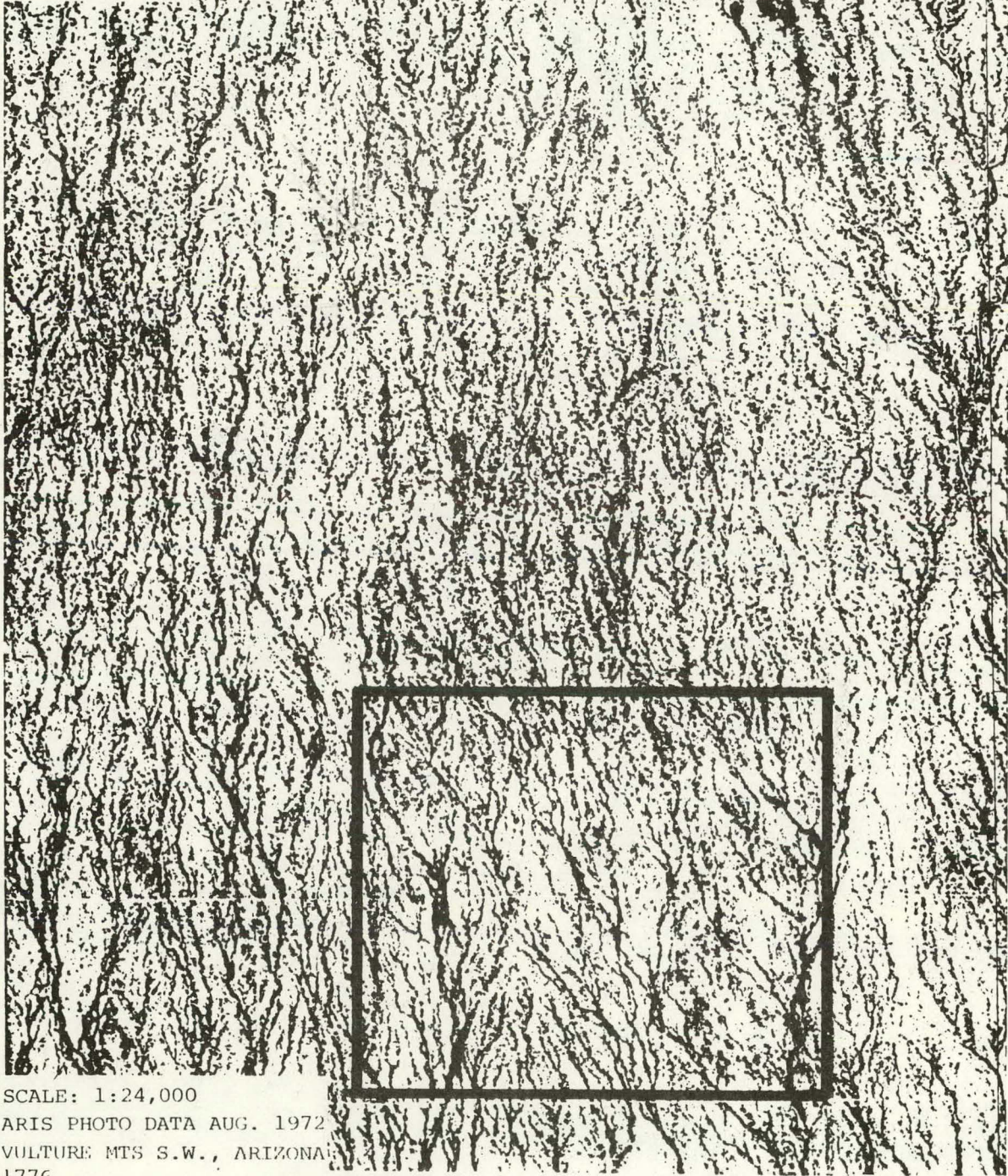
GENERAL LOCATION MAP



MAP NO. 344-314-944
AUGUST 1968

* VULTURE MOUNTAIN SOLAR SITE

VULTURE MOUNTAIN SOLAR SITE

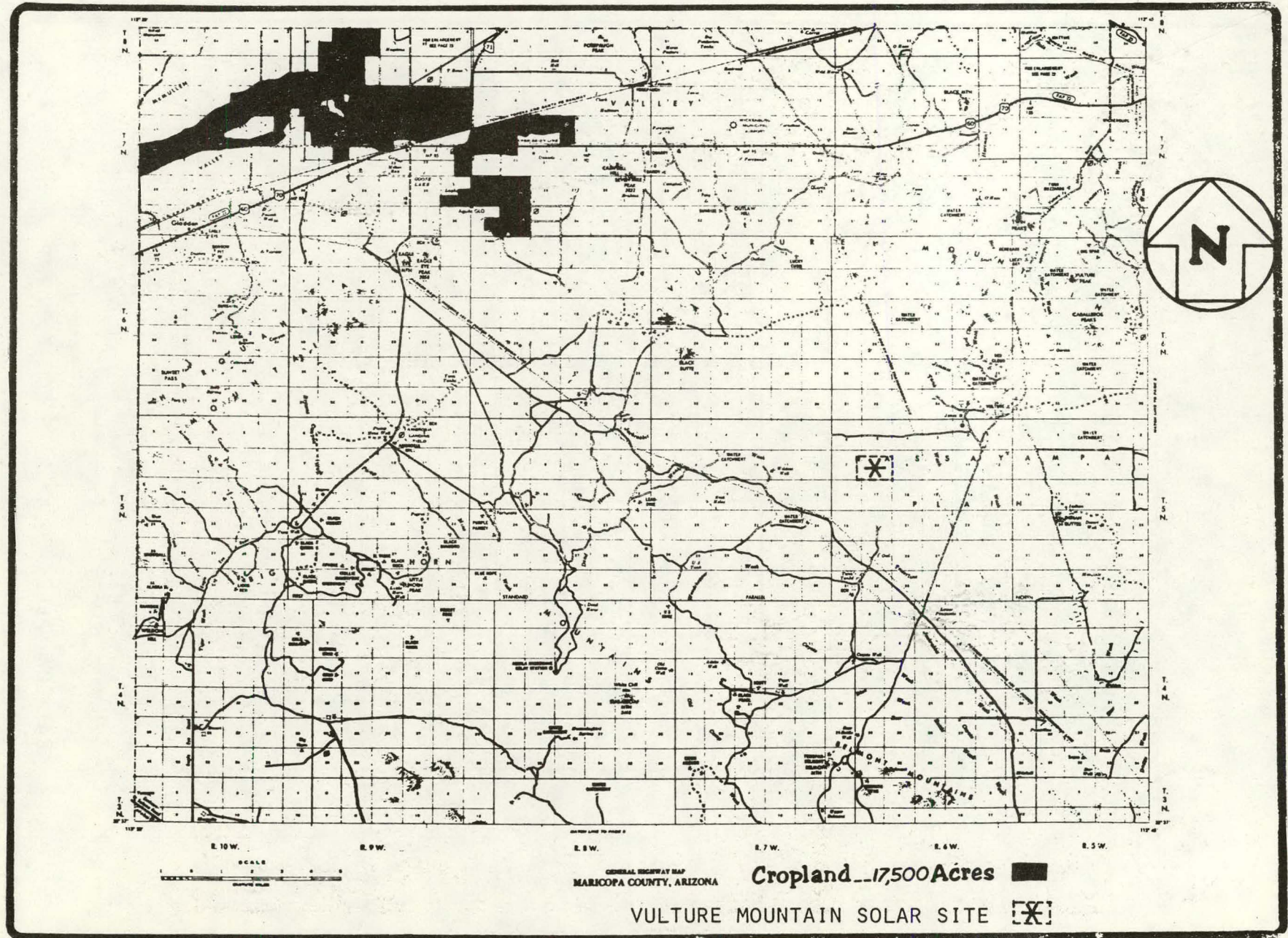


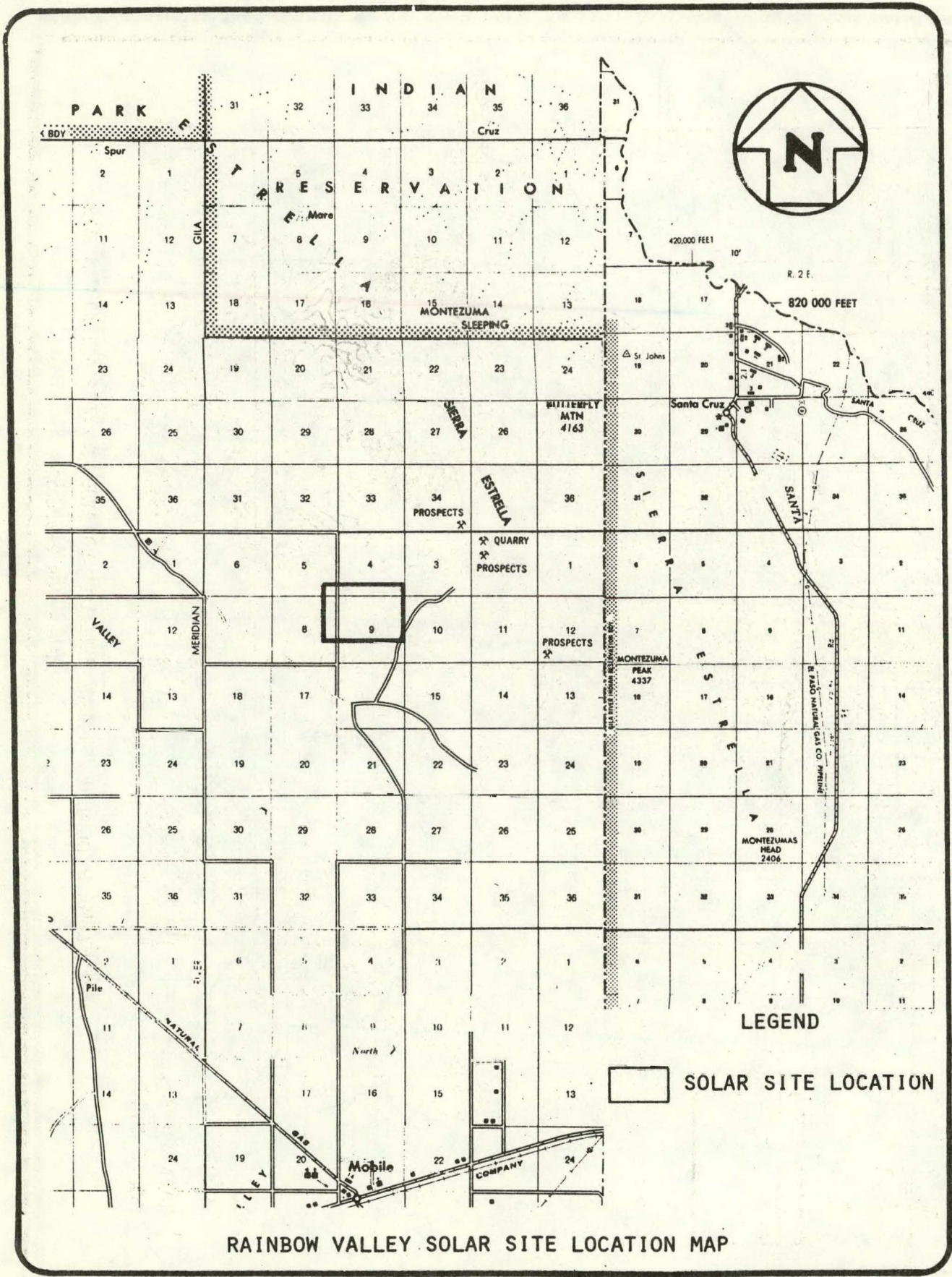
SCALE: 1:24,000
ARIS PHOTO DATA AUG. 1972
VULTURE MTS S.W., ARIZONA
1776

VULTURE MOUNTAIN SOLAR SITE

FIGURE V-4

515
FIGURE V-5

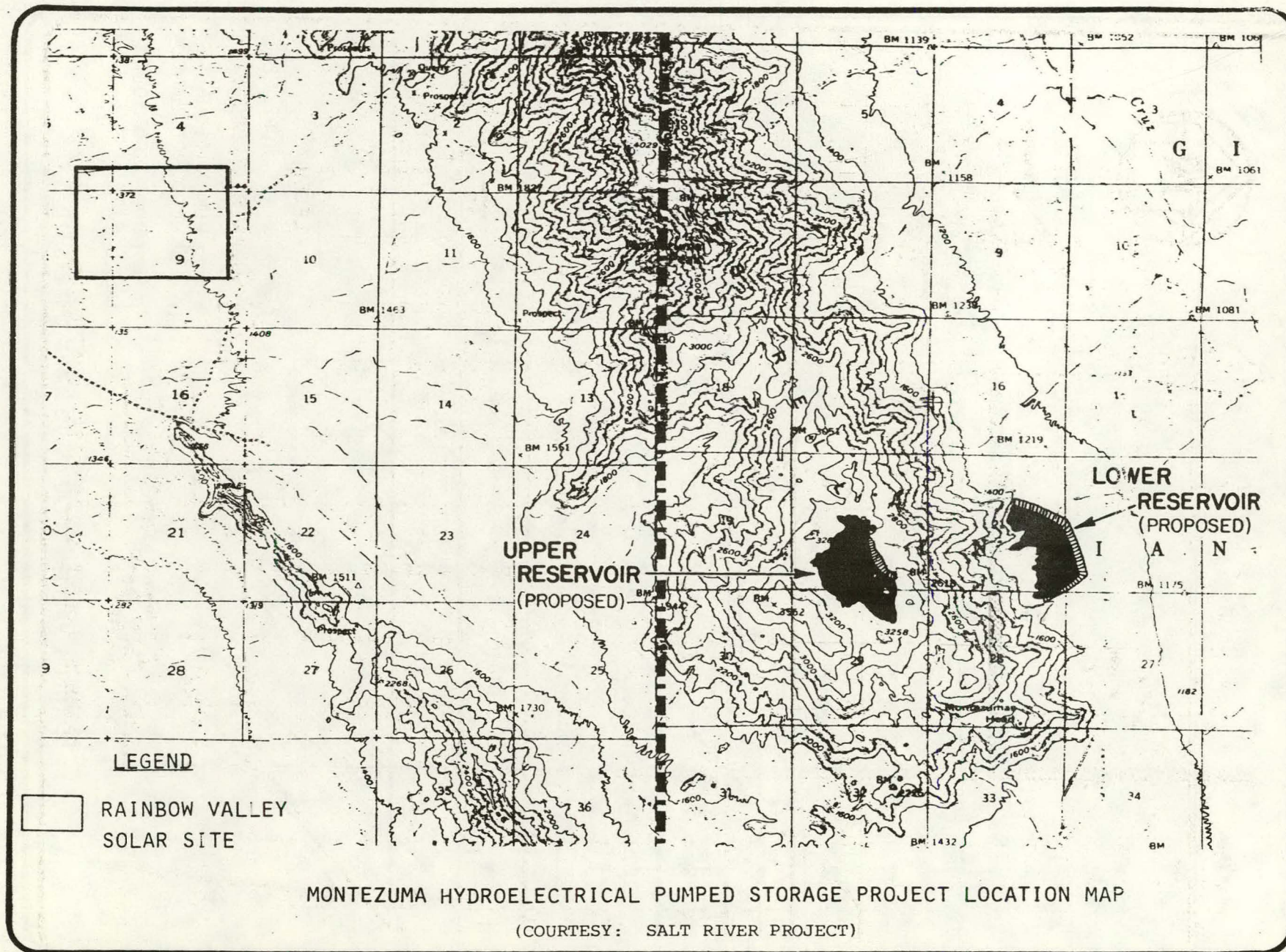




RAINBOW VALLEY SOLAR SITE LOCATION MAP

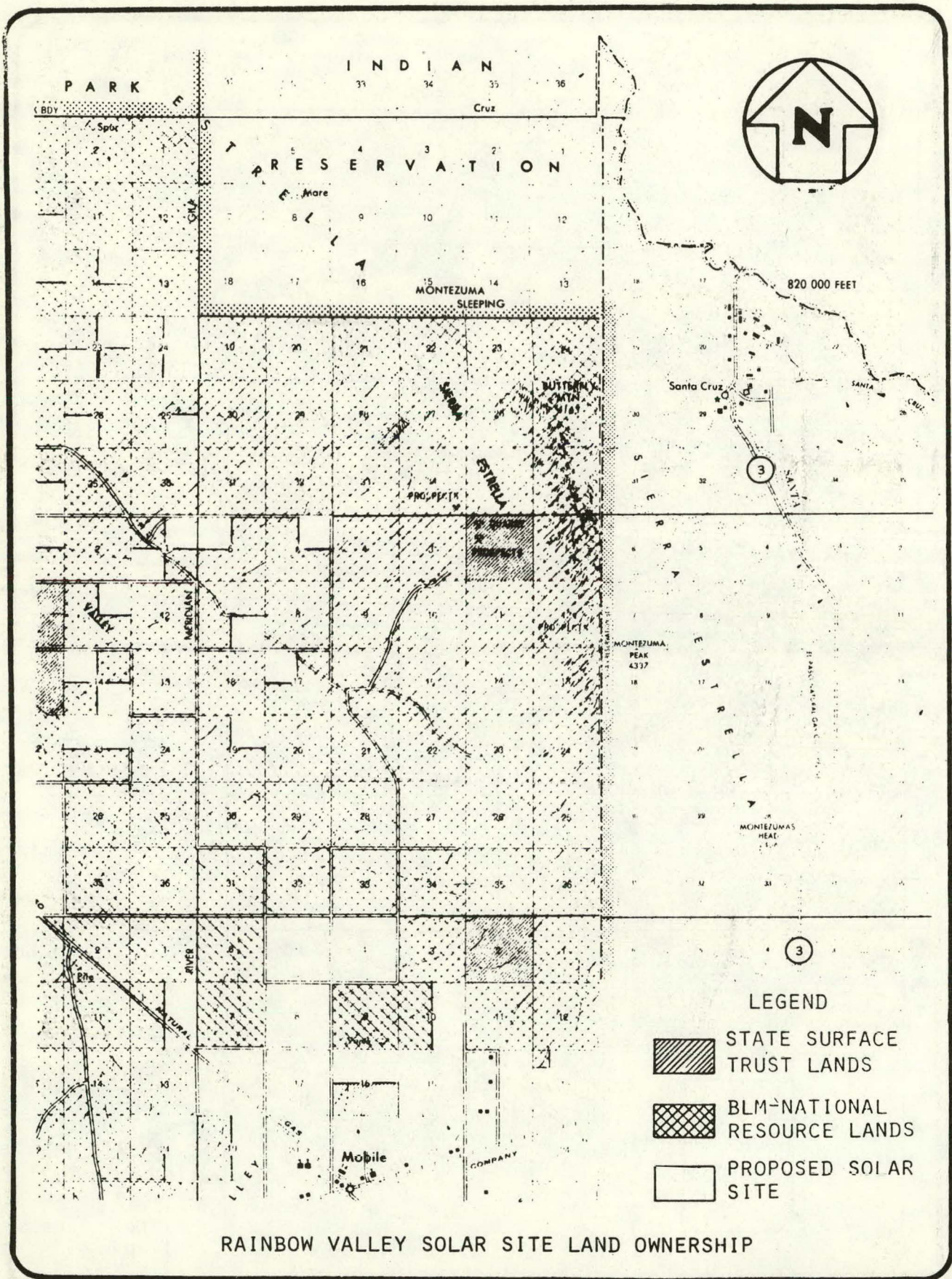
FIGURE R-1

FIGURE R-2
517



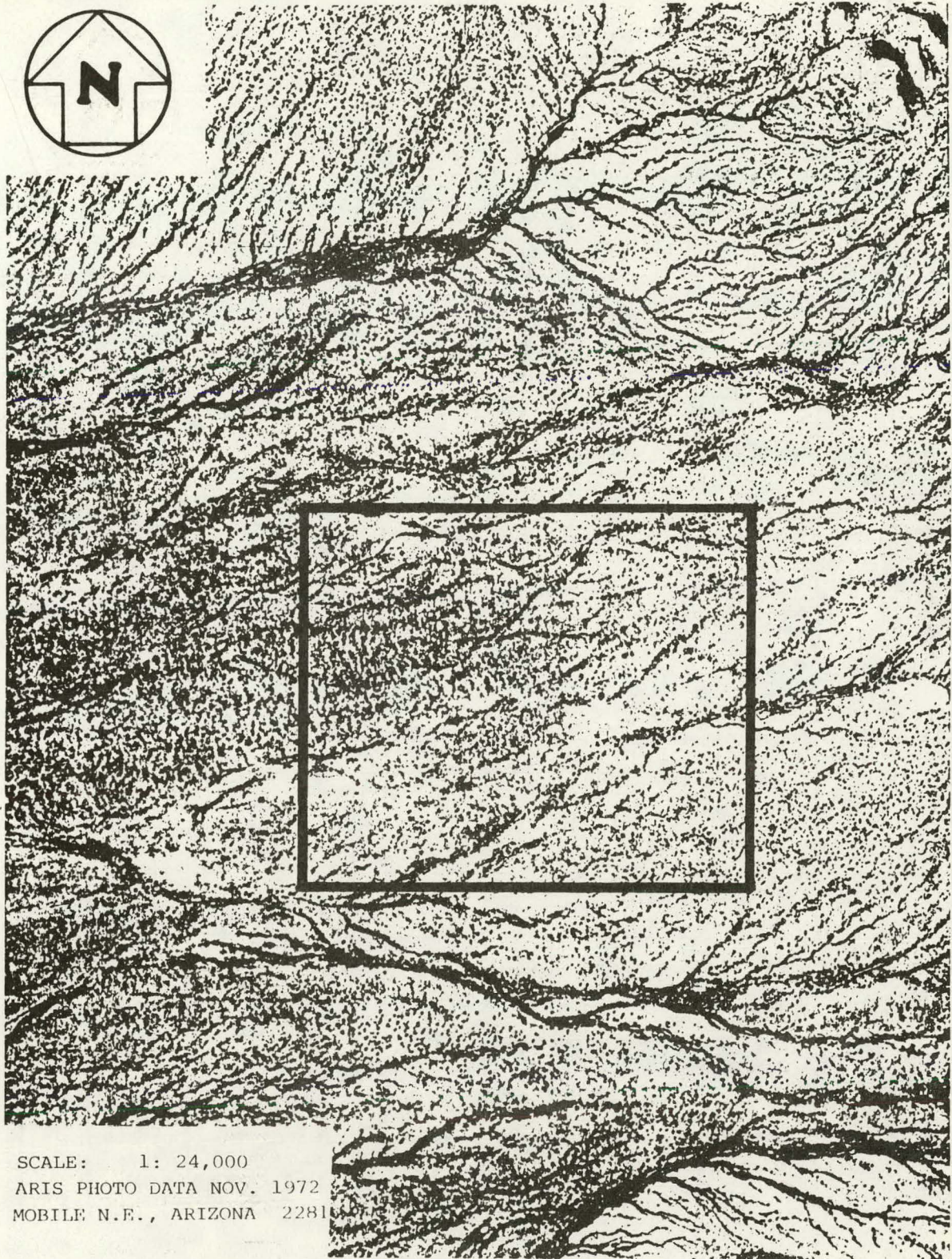
MONTEZUMA HYDROELECTRICAL PUMPED STORAGE PROJECT LOCATION MAP

(COURTESY: SALT RIVER PROJECT)



RAINBOW VALLEY SOLAR SITE LAND OWNERSHIP

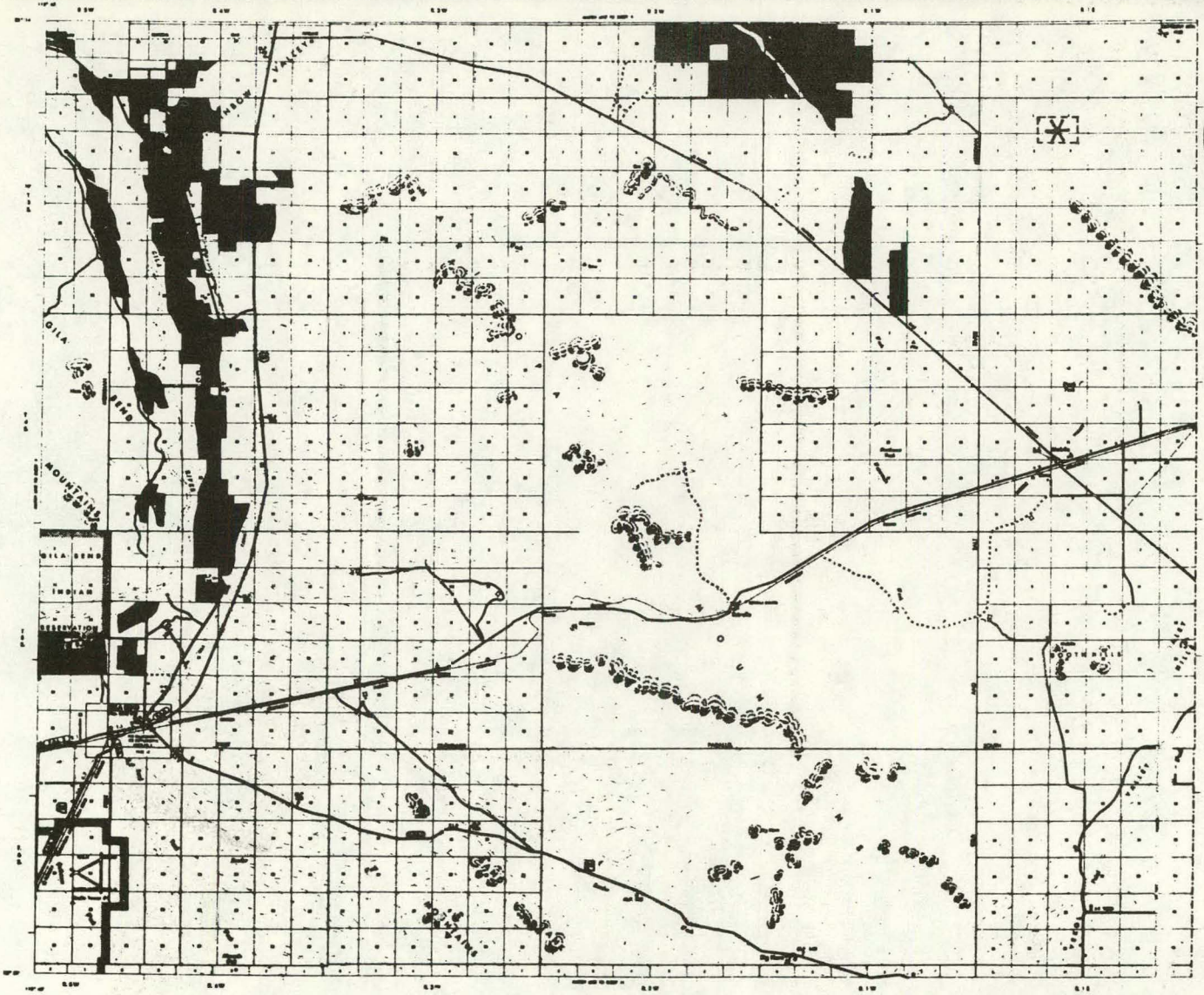
FIGURE R-3



SCALE: 1: 24,000
ARIS PHOTO DATA NOV. 1972
MOBILE N.E., ARIZONA 2281

RAINBOW VALLEY SOLAR SITE

FIGURE R-4



Cropland 25,000 Acres

GENERAL REFERENCE MAP
MARICOPA COUNTY, ARIZONA

RAINBOW VALLEY SOLAR SITE *



FIGURE R-5
520

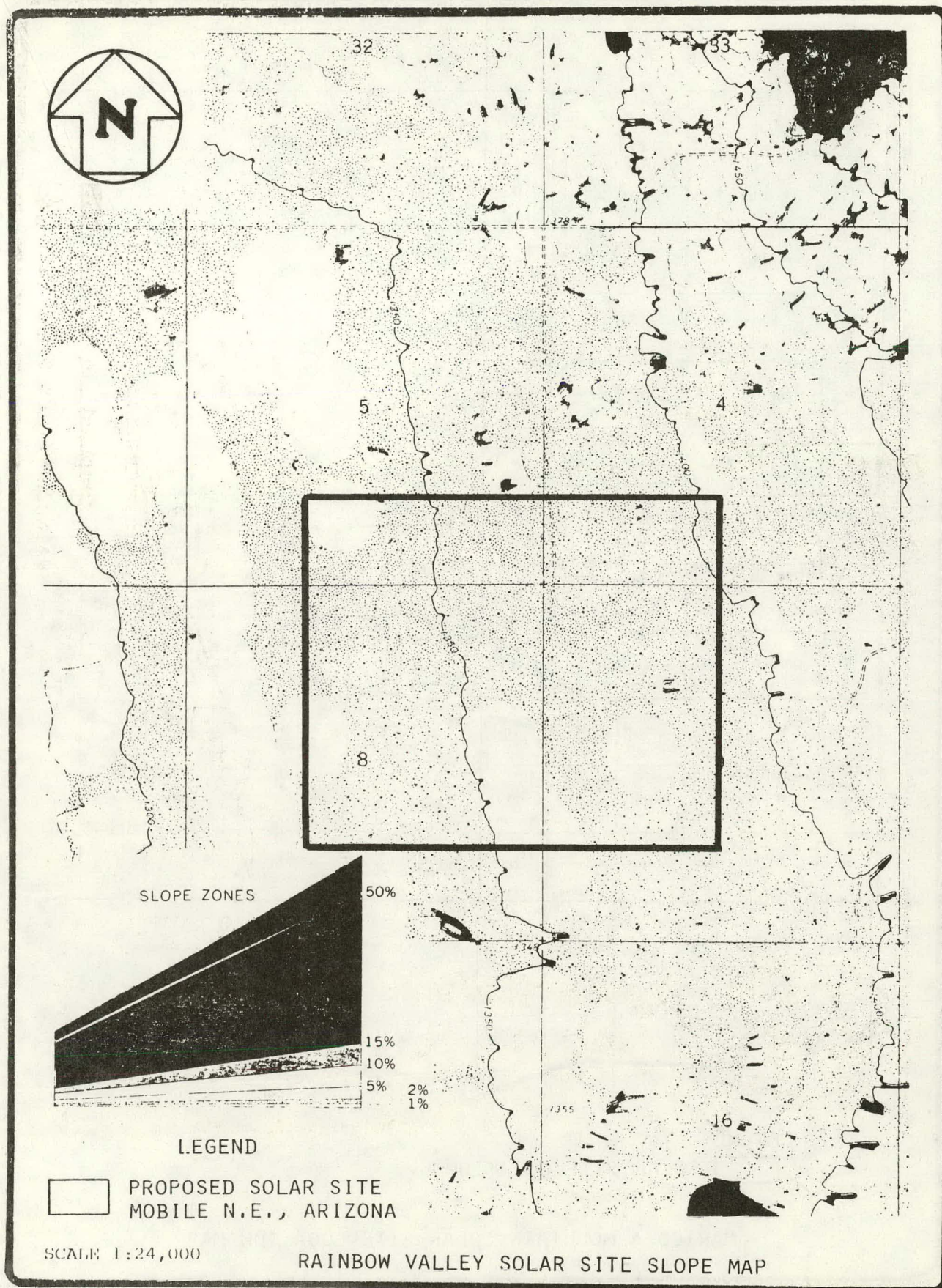
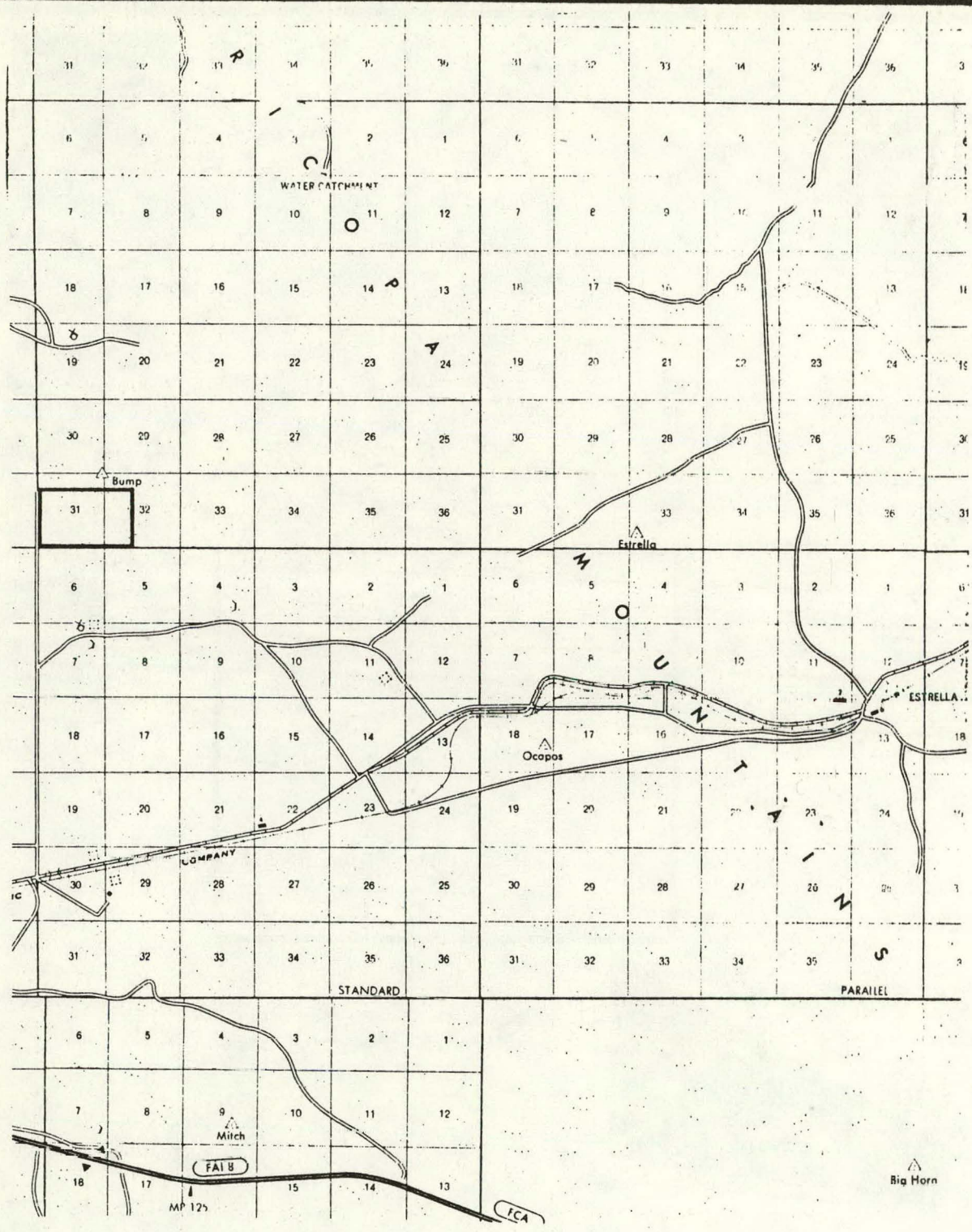


FIGURE R-6



LEGEND
 SOLAR SITE LOCATION

MARICOPA MOUNTAIN SOLAR SITE LOCATION MAP

FIGURE M-1
 522

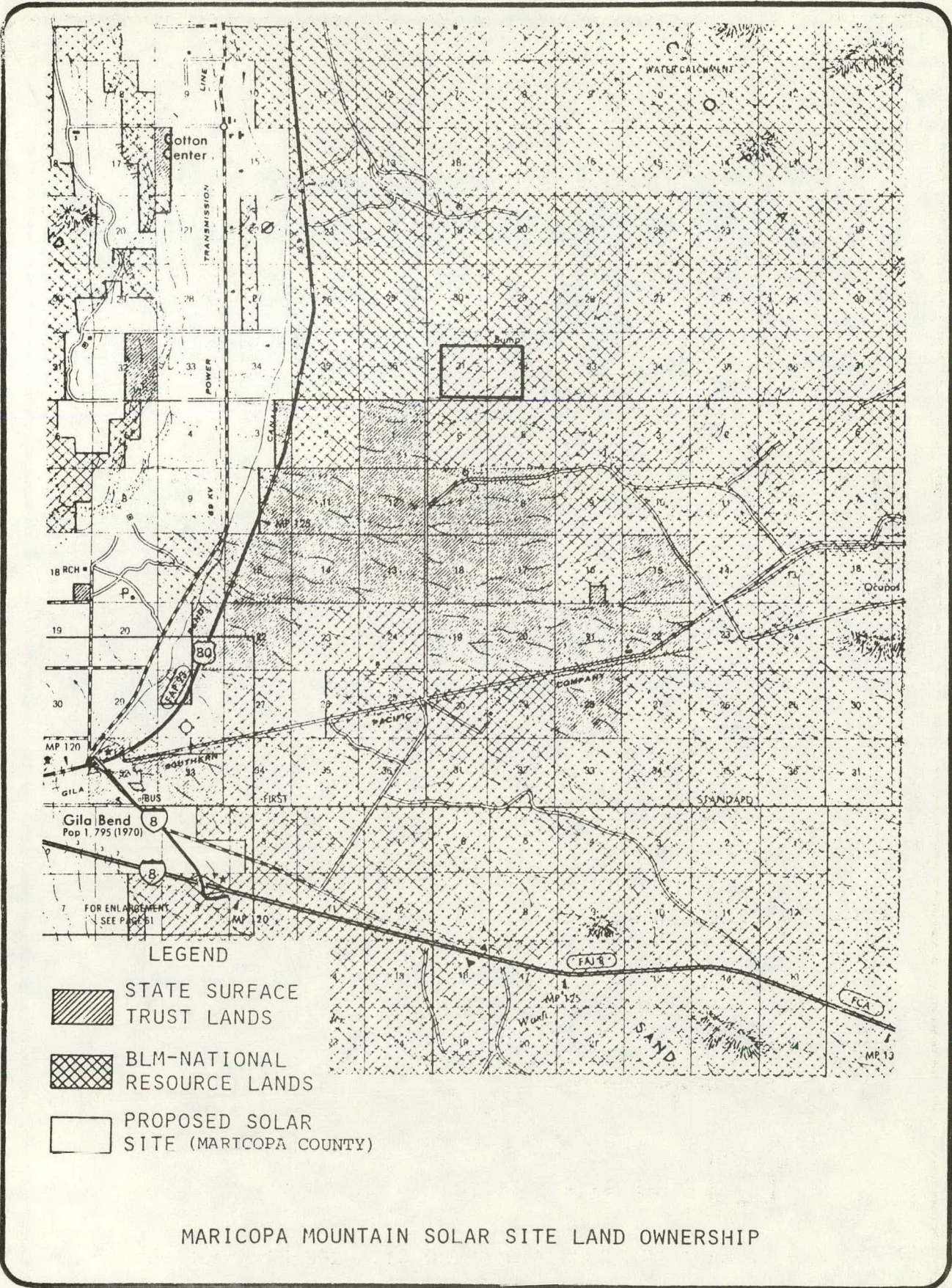
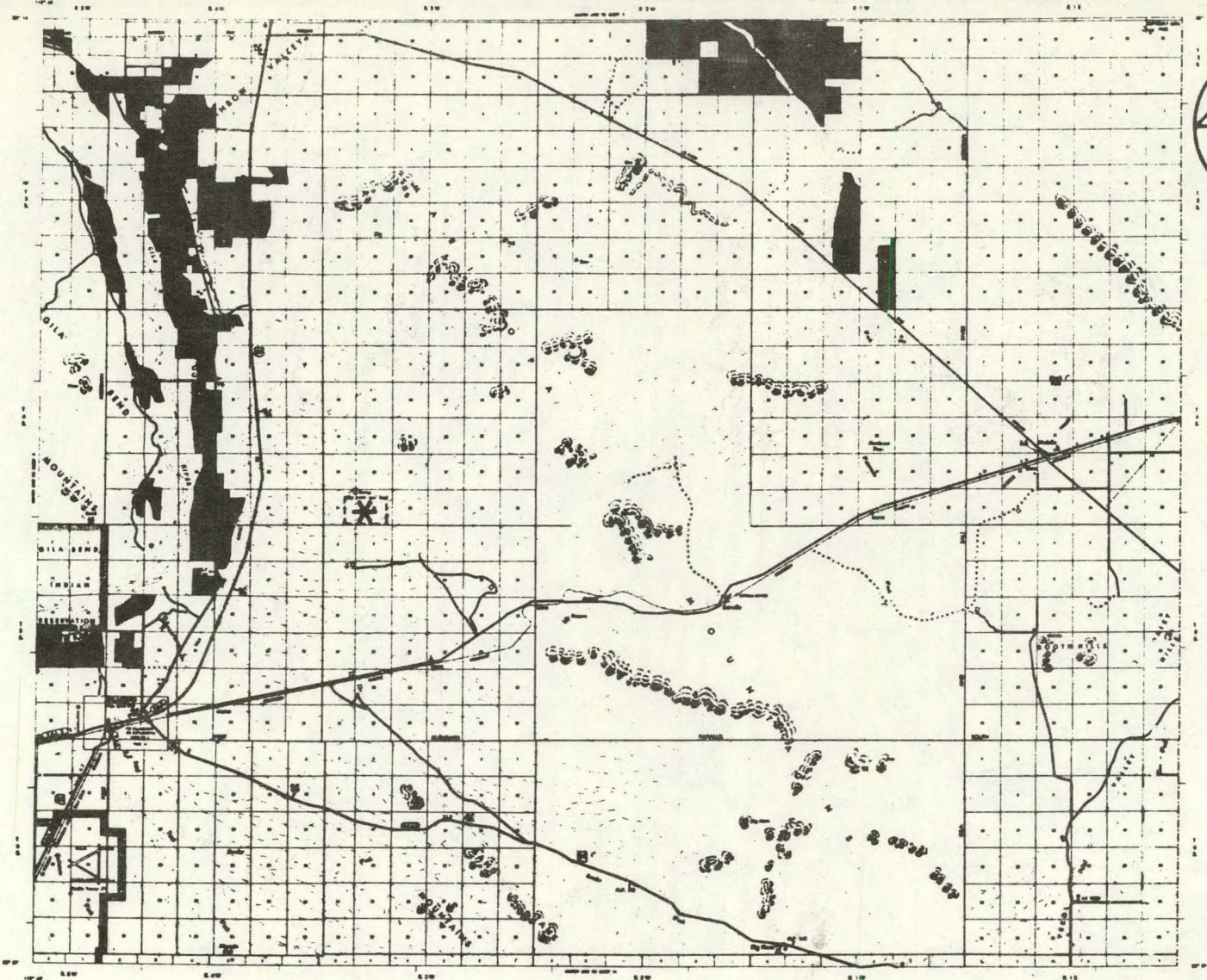



FIGURE M-2



Cropland...25,000 Acres 


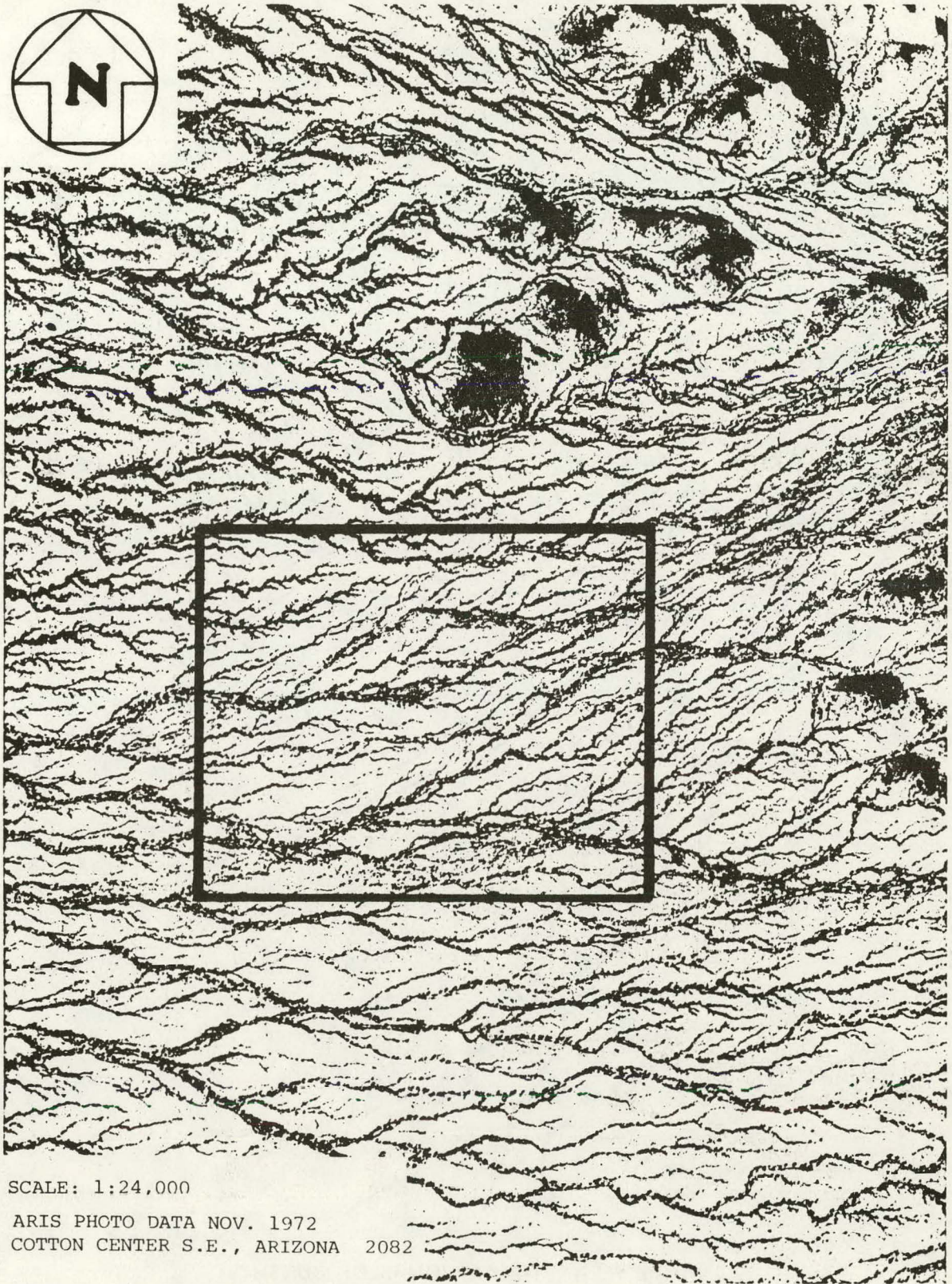
MARICOPA MOUNTAIN SOLAR SITE 

FIGURE M-3



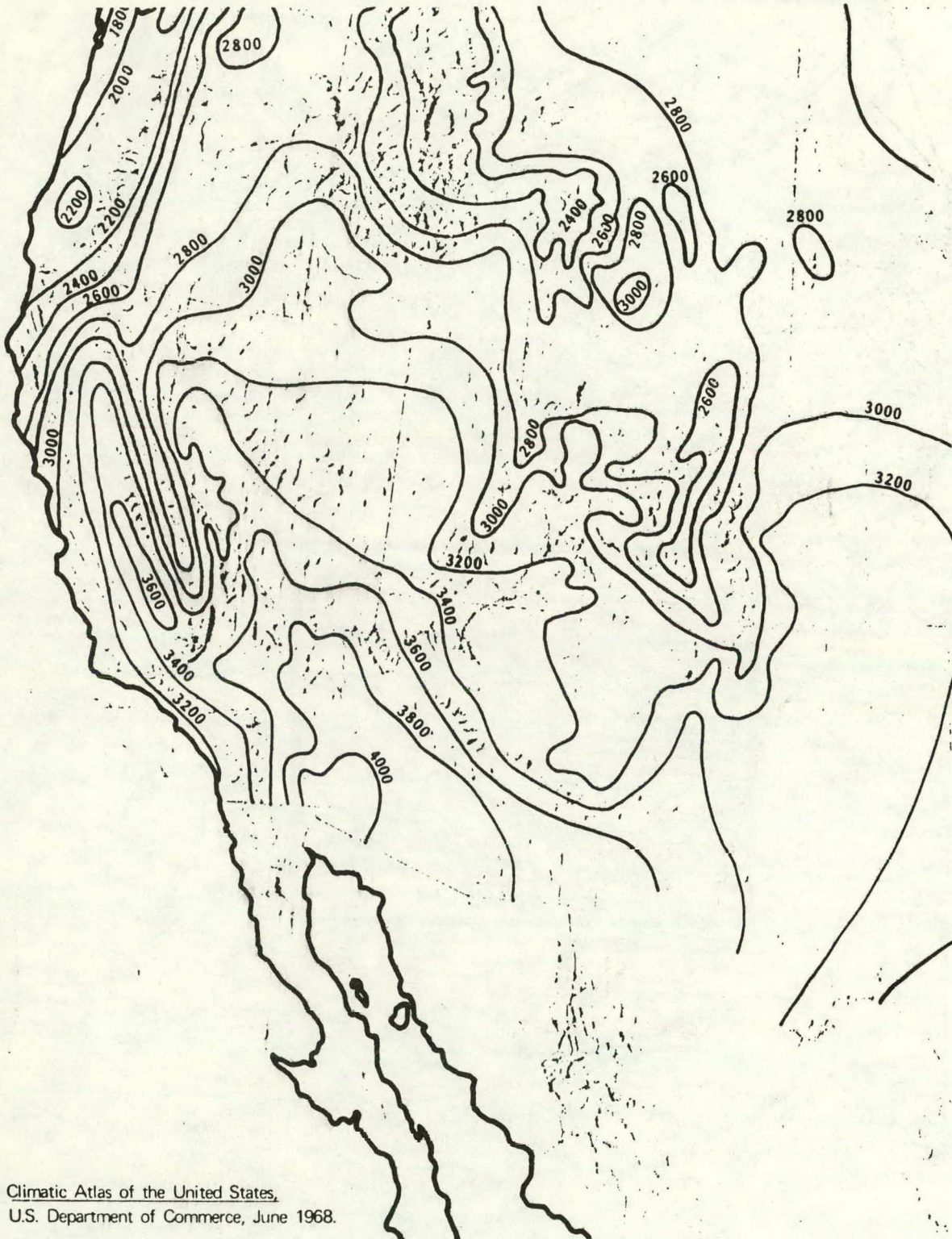
SCALE: 1:24,000

ARIS PHOTO DATA NOV. 1972
COTTON CENTER S.E., ARIZONA 2082

MARICOPA MOUNTAIN SOLAR SITE

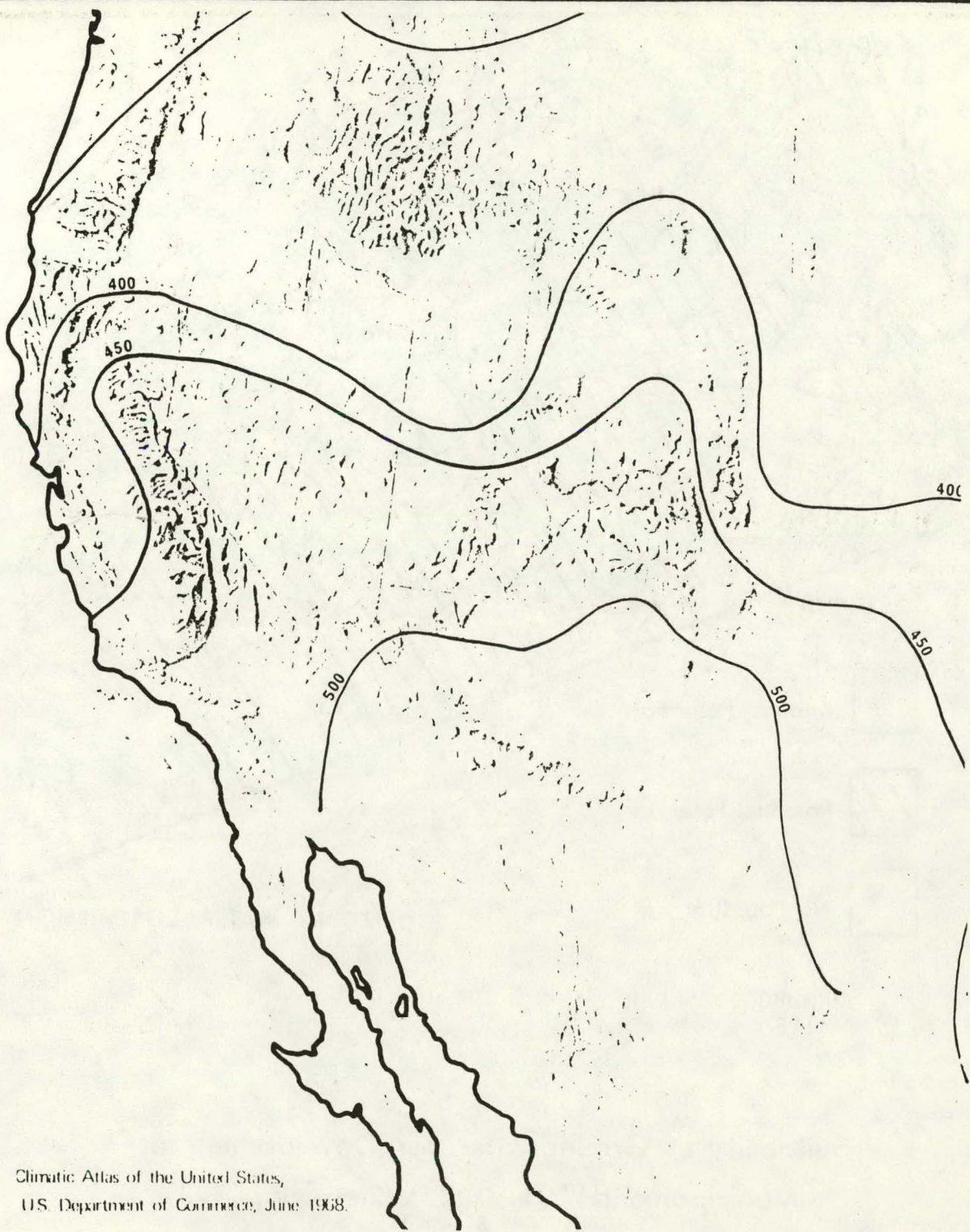
FIGURE M-4

525



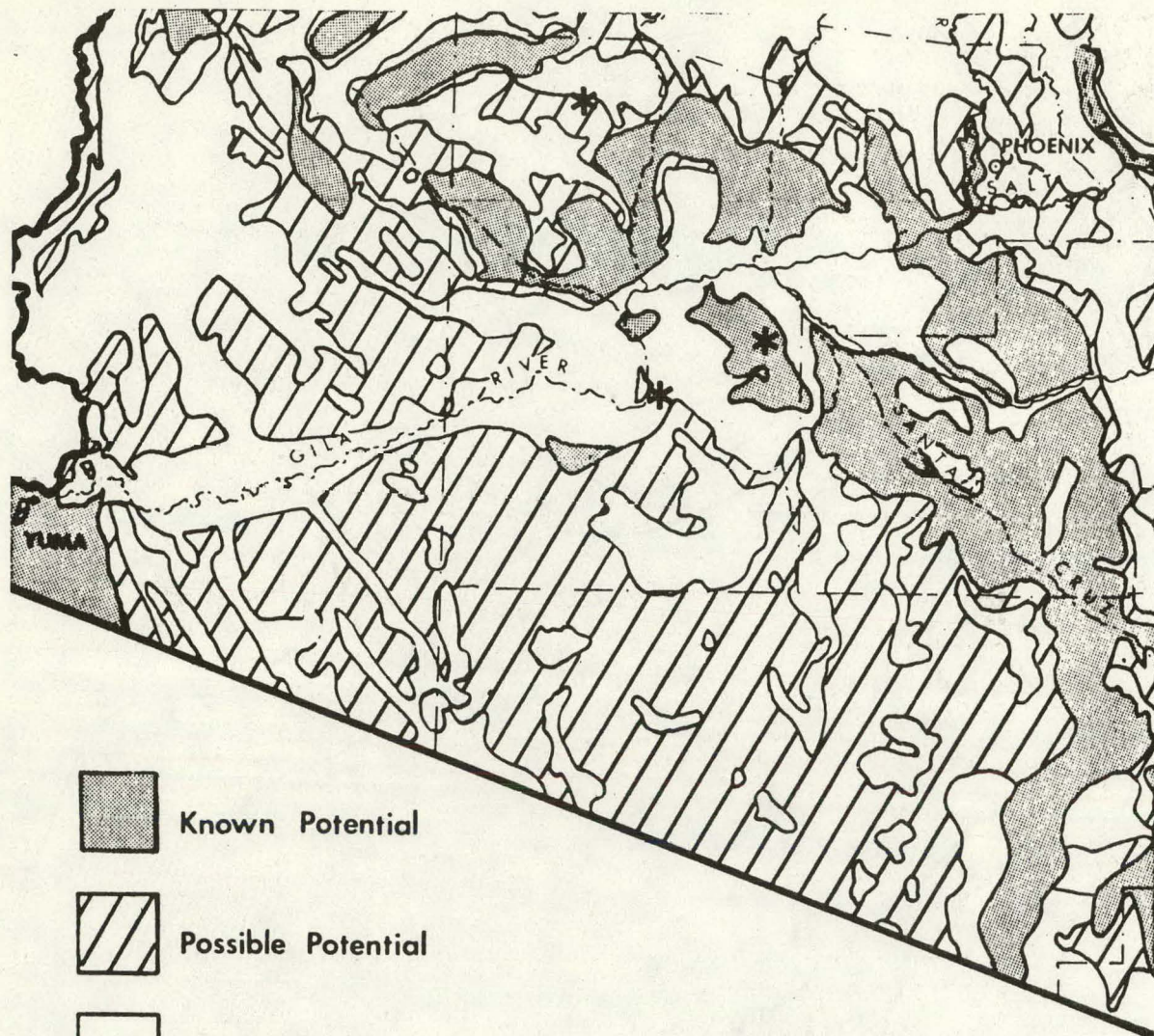
Climatic Atlas of the United States,
 U.S. Department of Commerce, June 1968.



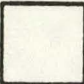
ANNUAL MEAN TOTAL HOURS OF SUNSHINE



Climatic Atlas of the United States,
U.S. Department of Commerce, June 1938.

ANNUAL DAILY MEAN OF SOLAR RADIATION



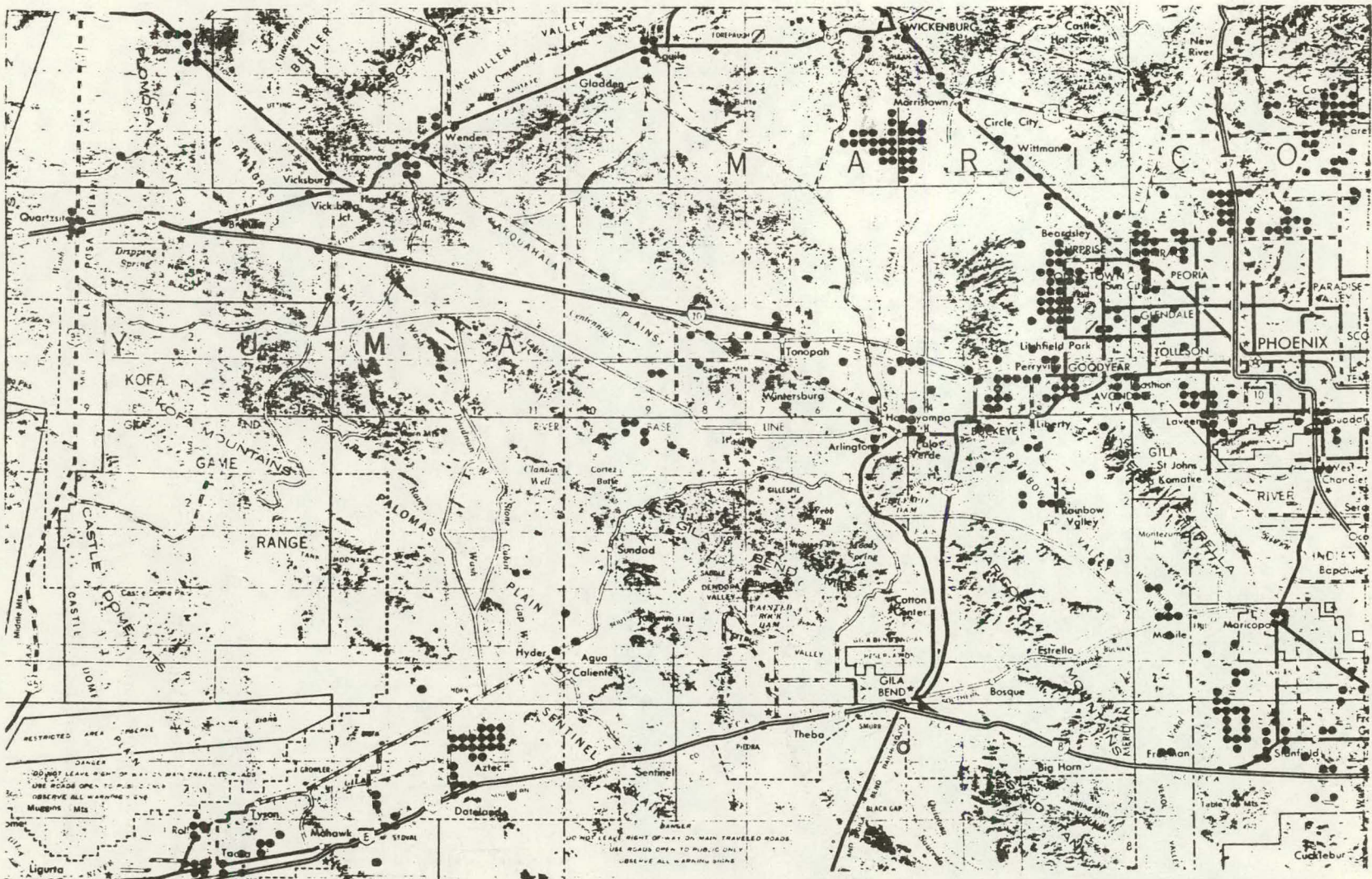
-  Known Potential
-  Possible Potential
-  No Potential

ARIZONA WATER COMMISSION

* PROPOSED SOLAR SITE

Suitability of Groundwater for Development of Municipal and Industrial Water Supplies (SOUTHWESTERN ARIZONA)

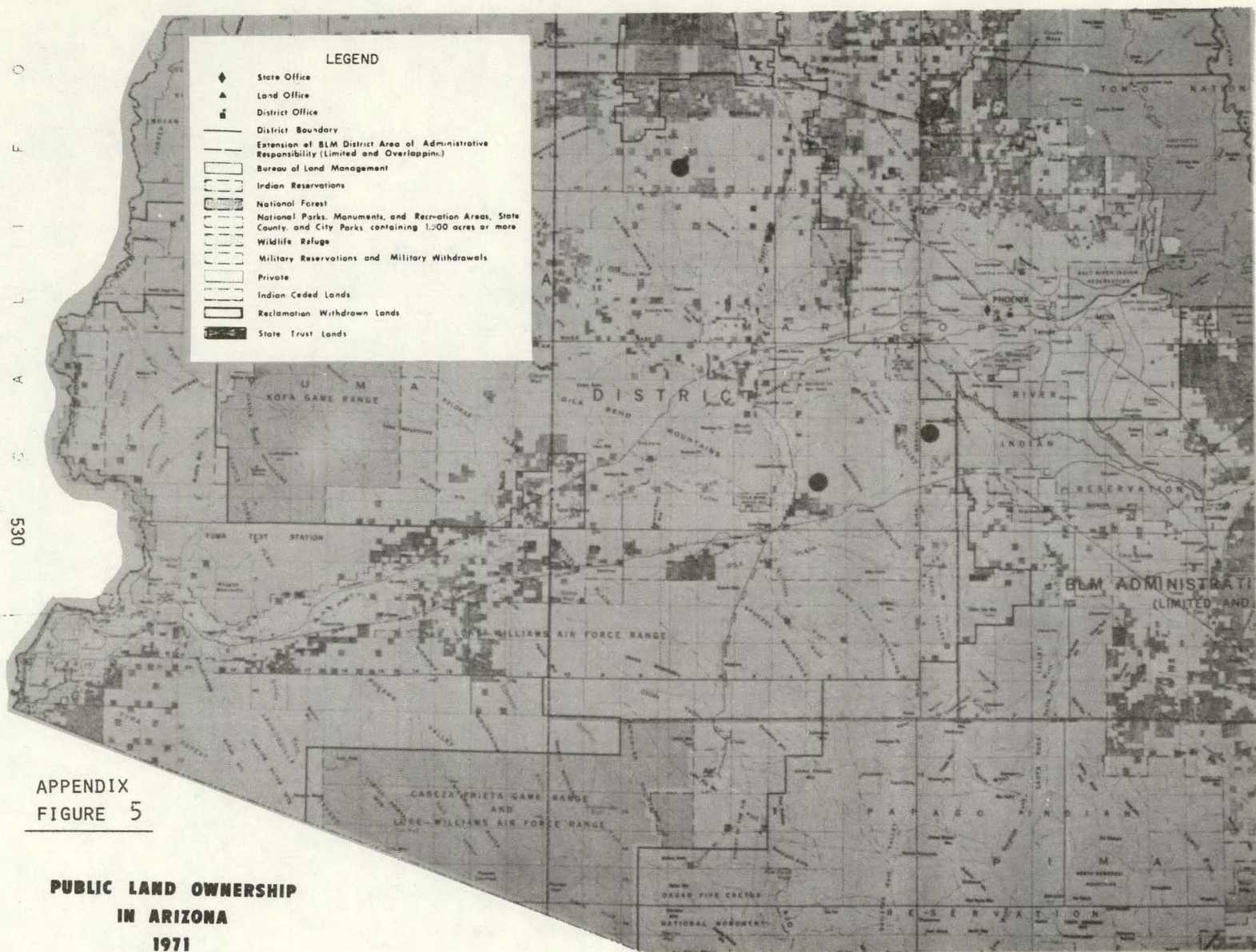
In Areas Of Known Potential For Development The Depth To Water Is Less Than 1,000 Feet, The Water Contains Less Than 1,000 mg/l Of Dissolved Solids, And Most Wells Are Capable Of Yielding 200 gpm.



EACH DOT REPRESENTS A SUBDIVISION OF LAND IN WHICH ONE OR MORE SURVEYS HAVE BEEN RECORDED PRIOR TO 1974.

SOURCE: REMOTE SUBDIVISIONS RECORDED 1879-1973,
OFFICE OF ECONOMIC PLANNING AND DEVELOPMENT,
STATE OF ARIZONA, 1974

SUBDIVISIONS IN SOUTHERN ARIZONA
(INDICATIVE OF AREAS FUTURE RESIDENTIAL GROWTH)



1.11 CPS Facilities

A conceptual design was made by Ford, Bacon, and Davis Utah of the facilities necessary for a 100 MW CPS installation. The results of this work are presented in this section.

Ford, Bacon & Davis Utah Inc.

ENGINEERS — CONSTRUCTORS

A SUBSIDIARY OF

Ford, Bacon & Davis
Incorporated

CENTRAL POWER PLANT

COST STUDY

APRIL 1976

ENGINEERING SUPPORT SERVICES

FOR

CONCEPTUAL DESIGN & SYSTEMS ANALYSIS

OF

PHOTOVOLTAIC POWER SYSTEMS

FORD, BACON & DAVIS UTAH CONTRACT UC-160

WESTINGHOUSE SUBCONTRACT 34-JP-26539-A

- 1.0 PURPOSE
- 2.0 SUMMARY
- 3.0 SYSTEMS CRITERIA
- 4.0 STATION DESCRIPTION
- 5.0 COOLING SYSTEMS CONSIDERED
 - 5.1 Backflow Through Arrays
 - 5.2 Forced Draft Air-Fin Heat Exchanger, Nighttime Only
 - 5.3 Forced Draft Air-Fin Heat Exchanger, Daytime Only
 - 5.4 Forced Draft Air-Fin Heat Exchanger, Day and Night Operation
- 6.0 COST ESTIMATES DESCRIPTION
 - 6.1 Site Preparation
 - 6.2 Foundations
 - 6.3 Buildings and Structures
 - 6.4 Cooling System Piping
 - 6.5 Cooling Water Pump House
 - 6.6 Storage Tanks
 - 6.7 Air-Fin Heat Exchangers
 - 6.8 Heat Exchanger Pump House
 - 6.9 Electrical Power Collection Network
 - 6.10 Electrical Power Distribution

1.0 PURPOSE

The purpose of this portion of the study is to determine the costs for selected portions of a 100 megawatt photovoltaic central power station as follows:

- A. Site preparation and foundations
- B. Array erection
- C. Array power collection and supply network
- D. Array cooling system
- E. Support buildings

Array installation costs included in the report are for field erection only. Costs of fabricating and assembling the arrays at a field fabrication shop are not included.

Four potential photovoltaic collection arrays were examined; a two axis tracking array, a fixed array, a one axis tracking trough array, and a cadmium sulfide mylar film array.

2.0 SUMMARY AND CONCLUSION

Installed costs for the following portions of a 100 megawatt photovoltaic central power station have been estimated:

- A. Site preparations and foundations
- B. Array installation
- C. Array power collection and supply network
- D. Array cooling system
- E. Support buildings

Costs of the above facilities were estimated for a two axis tracking silicon array system, a fixed axis silicon array system, a one axis tracking (trough) silicon array system and a cadmium sulfide, mylar film array system. Cost summaries are presented in Table 2-1. This table also presents the effect of various cooling methods on the installed cost of the above listed facilities.

The cost summary indicates that the most economical method for cooling the arrays is an air-fin heat exchanger designed to operate on a continuous basis. Storage tanks for both hot and cold water are required for this cooling system, since enough water must be stored at the end of the production day to allow the air cooled heat-exchanger to operate during the night. The use of a cooling system sized for a 40° F. rise in cooling water temperature across the arrays costs approximately 17% less than a system sized for a 20° F. rise in cooling water temperature. In addition, the parasitic power load for the 40° F. system is approximately 60% less than for the 20° F. system. Total cooling water storage capacity, and peak and average parasitic power loads for the different cooling systems are presented in Table 2-2.

TABLE 2-1

PHOTOVOLTAIC POWER SYSTEM
SYSTEM COST ESTIMATES SUMMARY

(All Costs in 1976 Thousands of Dollars)

METHOD OF COOLING	TWO AXIS TRACKING ARRAY		FIXED AXIS ARRAY		TROUGH ARRAY	
	COOLING WATER TEMP. CHANGE		COOLING WATER TEMP. CHANGE		COOLING WATER TEMP. CHANGE	
	20 ⁰ F ΔT	40 ⁰ F ΔT	20 ⁰ F ΔT	40 ⁰ F ΔT	20 ⁰ F ΔT	40 ⁰ F ΔT
Natural Radiation & Convective Night-Time Cooling From Arrays	Not Practical	\$87,722	Not Practical	\$76,808	Not Practical	Not Practical
Forced Air Cooling Night Time Only	\$134,460	\$105,781	\$115,531	\$90,998	\$118,267	\$99,610
Forced Air Cooling Day-Time Only (No Storage)	\$116,718	Not Practical	\$108,940	Not Practical	\$115,723	Not Practical
Combination Forced Air Cooling Day & Night Operation (Some Storage Req'd)	\$117,167	\$95,141	\$105,996	\$84,732	\$112,778	\$93,342
Passive Cooling		21,130		17,493		Not Practical

Cadmium Sulfide

Flexible Mylar Film

\$18,089

TABLE 2-2

WATER STORAGE & PARASITIC POWER REQUIREMENTS

METHOD OF COOLING	SYSTEM REQUIREMENTS		TYPE OF ARRAY SYSTEM					
			TRACKING ARRAY		FIXED ARRAY		TROUGH ARRAY	
			COOLING WATER TEMP. CHANGE		COOLING WATER TEMP. CHANGE		COOLING WATER TEMP. CHANGE	
		20°F ΔT	40°F ΔT	20°F ΔT	40°F ΔT	20°F ΔT	40°F ΔT	
Forced-Air Cooling Night-Time Only	Storage Req'd (GAL)		129,000,000	64,500,000	90,300,000	45,150,000	90,300,000	45,150,000
	Parasitic Power Load	Peak (HP)	34,400	24,800	25,300	17,400	25,300	17,400
		Avg. (HP)	20,683	11,400	14,500	8,000	14,500	8,000
Forced-Air Cooling Day-Time Only	Storage Req'd (GAL)		18,800,000	NP	18,800,000	NP	18,800,000	NP
	Parasitic Power Load	Peak (HP)	71,800		71,800		71,800	
		Avg. (HP)	50,600	NP	35,400	NP	35,400	NP
Forced-Air Cooling Day & Night Time Combination	Storage Req'd (GAL)		71,000,000	35,500,000	71,000,000	35,500,000	71,000,000	35,500,000
	Parasitic Power Load	Peak (HP)	52,200	24,100	36,600	19,000	36,600	19,000
		Avg. (HP)	41,200	12,000	29,000	8,400	29,000	8,400
Natural Radiation & Convective Night-Time Cooling	Storage Req'd (GAL)		NP	64,500,000	NP	45,150,000	NP	45,150,000
	Parasitic Power Load	Peak (HP)		11,400		8,000		8,000
		Avg. (HP)	NP	10,354	NP	7,250	NP	7,250

NP - Not Practical

3.0 DESIGN CRITERIA

The study was made on the basis of the following power plant criteria.

1. The plant shall produce 100 megawatts of peak power.
2. Four array systems were considered
 - a) Tracking array (two axis) - arrays are 10 meters X 10 meters
 - b) Fixed array - arrays are 10 meters X 10 meters
 - c) Trough array (or axis trackers) - troughs are 9.1 meters wide with a radius of 6.1 meters, and a length of 7.6 meters.
 - d) Cadmium Sulfide - thin flexible mylar sheet 1.2 to 2.4 meters wide, and of any convenient length.
3. Annual average solar energy input to the tracking array is 10 KW-HR/m²/day. The peak summer input is 11.9 KW-HR/m²/day.
4. Solar energy input to the fixed array, the trough array and the cadmium sulfide collector is 70% of the two axis tracking array.
5. For the tracking and fixed arrays, 1/3 of the available land area is covered by arrays, while for the trough system, 1/2 of the land area is covered by trough arrays.
6. Of the solar energy striking the arrays, 15% is converted to electricity, 5% is reflected and 80% is assumed to be absorbed and must be removed as waste heat.
7. Maximum desired temperature for cooling water is 130°F.
8. Two cooling water system temperature differentials across the arrays were considered: 20°F ΔT, and 40°F ΔT.

4.0 STATION DESCRIPTION

Power stations with four types of arrays were examined: two axis tracking array, fixed array, trough array, and cadmium sulfide flexible film.

4.1 Tracking Array

The tracking array power station is an assembly of 6600 ten meter by ten meter square arrays. The arrays are grouped together in six identical sections with each section containing 1100 individual array units and one inverter located in the center of each section. The site for the total systems including support facilities is 1470 meters wide by 1925 meters long for a total area of 2.8 square kilometers. To minimize shadowing problems, the system is oriented with the longer dimension in the east-west direction. See Figure 4-1.

Access roads are provided to all array locations. Roads in the north-south direction are major access roads ten meters wide and spaced 210 meters apart beginning at the western boundary of the arrays. East-west access roads seven meters wide are also provided. These roads are spaced 35 meters apart beginning at the northern array boundary. The center of the sections are void of arrays and are used for the inverter building and equipment parking. The roads provide direct equipment access to all arrays for ease of installation and maintenance.

Drainage ditches are provided around the plant site to prevent off-site surface water from entering the site boundaries. Within the site, drainage ditches are provided along all roadways to collect and direct surface water off the site in a controlled manner.

Electrical lines and cooling water lines are routed east-west through each subsection above ground between the two rows of arrays. At the north-south roads the lines are buried and routed north or south as necessary to their respective distribution or collection centers. The north-south lines are buried to allow unrestricted equipment access to all arrays with no overhead or above ground obstructions.

Cooling water storage tanks, air-fin heat exchangers, pump houses, and other necessary equipment are located to the north of the array sections. This location will prevent any decrease in array output from shadows caused by these structures.

Minimal lighting is provided near all buildings, pumps and heat exchanger systems. A 2.4 meter high security fence with a limited number of access gates is also provided. Power supply lines are supplied to each array for the 2 one-HP motors needed to provide two axis tracking capability.

4.2 Fixed Array

The fixed array power station is an assembly of 6600 ten meter by ten meter square arrays. The station is layed out in the same manner as the two axis tracking array power station, and is the same physical size. See Figure 4-1.

The fixed arrays will not follow the track of the sun during the day and as a result will produce approximately 70% of the power produced by the tracking arrays. No power is supplied to the arrays since tracking capability is not included.

4.3 Trough Array

The trough array power station is an assembly of 9486 trough arrays 7.6 meters long. The trough for each array is 9.1 meters wide, 8.8 meters long and 1.5 meters deep. Seventeen array units are connected together to form a continuous trough 151 meters long. The site is divided into six identical sections, each section measures 455 meters north to south and 473 meters east to west and contains 1581 array units. An inverter building is located at the center of each section. The overall site including support facilities is 1365 meters by 1158 meters for a total area of 1.6 square kilometers. See Figure 4-2.

Access roads are provided to all array locations. The main access roads run north to south and are 6.1 meters wide and spaced 158 meters apart, centerline to centerline. East-west roads are 4.6 meters wide and are spaced 27.4 meters apart. The roads provide direct access to each array unit for ease of installation and maintenance.

Drainage ditches are provided around the exterior of the plant site to prevent offsite surface water from entering the site boundaries. Within the site, drainage ditches are provided along all roadways to collect and direct surface water off the site in a controlled manner. Troughs are sloped slightly to the east or west (depending on site contour) to provide trough drainage. Culverts are installed beneath the lower end of all troughs to provide trough drainage. The culverts will discharge offsite in natural drainage channels.

Electrical lines and cooling water lines are routed throughout the site in the same manner as used for the tracking and fixed arrays. All north-south lines will be buried to provide unobstructed access by maintenance equipment to all array units.

Array cooling is provided by pumping cooling water throughout the station. The trough arrays are mounted on a rectangular tube through which the cooling water flows. The tube has a cross-section 7.6 centimeters by 15.2 centimeters and is 7.6 meters long. All 17 array units in each trough of a subsection are cooled in series.

As with the other array systems all water storage tanks, pump houses, cooling towers etc. are located on the north side of the power station to eliminate shadows on the arrays.

Lighting is provided for the inverters. Also, an electrical distribution system is included to provide power for 2 one Hp motors needed to move each of the array units. A security fence 2.4 meters high surrounds the site area.

4.4 Cadmium Sulfide Collectors-Mylar Film

The potential methods evaluated for structurally supporting the cadmium sulfide on mylar film arrays are summarized below:

1. The mylar film could be supported by a wire mesh backing, which would be attached to metal or wood posts. This method was discarded because it lacked the structural strength required to withstand the expected wind loads.
2. The mylar film could be laid on an earth windrow, and secured to wood tie down rails along both edges of the windrow. This method is low in cost and structurally sound.
3. The mylar film could be attached to a light plywood or metal backing, which would be supported on a concrete or steel structure. This approach would require a continuous "A" frame support, with both sides covered to provide the required wind load support. This method was discarded because of high costs.
4. A continuous concrete support system would provide the necessary wind load strength. This method was discarded because of high costs.

Of the support systems evaluated, placing the cadmium sulfide array on an earth windrow offered the lowest cost, while meeting wind load requirements. Therefore, cost estimates are based on this approach.

The cadmium sulfide power station is made up of 2064 groups of arrays supported on windrows of soil compacted to provide a smooth support surface. The windrows are 3 meters wide at the base, 1 meter high, and run east-west to provide a southern exposure surface. The array is supported on the south surface which slopes at 34° to the horizon.

The rows of array are grouped together into six identical sections 853 meters wide by 629 meters long. An inverter building is located at the center of each section. The six sections are positioned together to form a plant array area including support facilities, 1707 meters long in the north-south direction by 1887 meters wide in the east-west direction for a total area of 3.2 square kilometers. See Figure 4-3.

Each section is further divided into three smaller subsections by 6.1 meters wide north-south access roads. The east and west subsections of each section are 234 meters wide while the center subsection is 162 meters wide. Secondary access roads 3.7 meters wide are also provided in the east-west direction after every two windrows. The two windrows are spaced 2.4 meters apart.

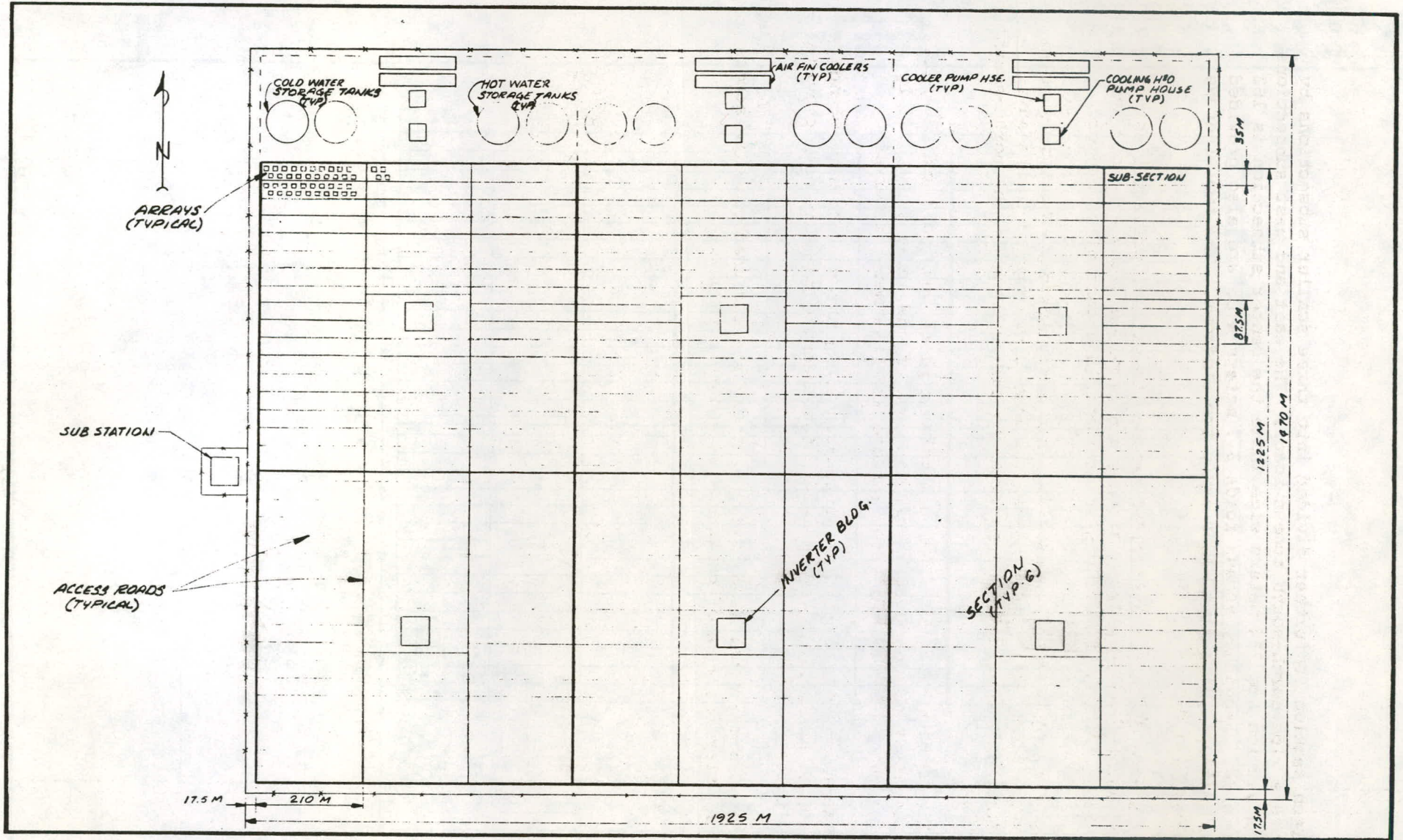
Drainage ditches are provided around the site to prevent offsite surface water from entering. Ditches are provided along all roadways and between the rows to allow site drainage in a controlled manner.

No cooling system is needed for this array system. Electrical power collection lines are routed between the rows above ground in the east-west direction and are buried parallel to the roadways in the north-south direction.

The cadmium sulfide arrays are held in place upon wood and concrete foundations by redwood slates over the edge of the array sheet, and by slats placed on top of the array surface at three meter intervals.

The electrical substation is located along the western site boundary at the site centerline. A 2.4 meter high security fence is also provided around the site.

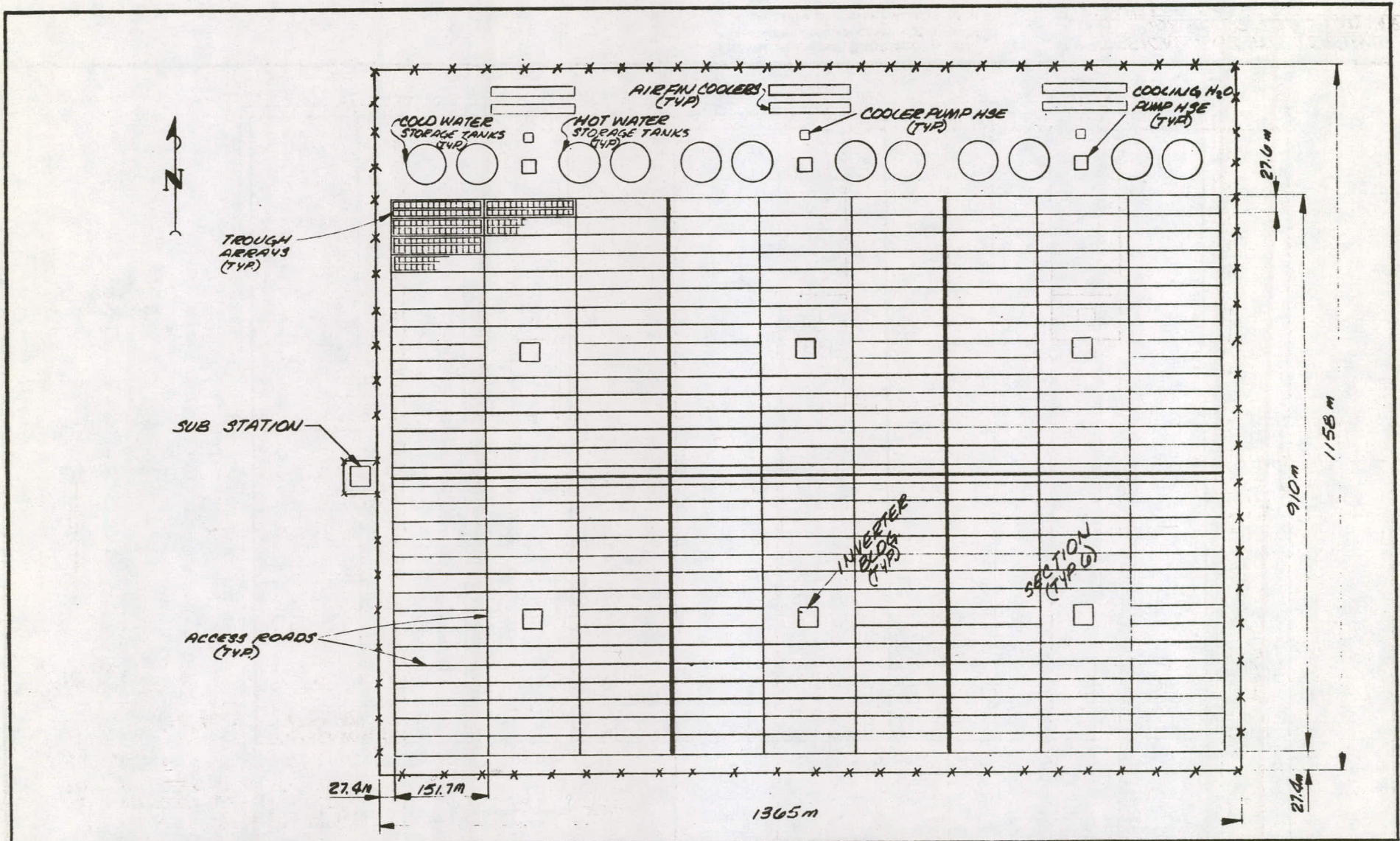
As with the other array systems, roads are included to allow access to each array for ease of construction and maintenance.



Ford, Bacon & Davis Utah Inc.
 ENGINEERS - CONSTRUCTORS
 SALT LAKE CITY, UTAH

TYPICAL LAYOUT - 2 AXIS TRACKING
ARRAY - NIGHT TIME COOLING WITH
AIR FIN COOLERS

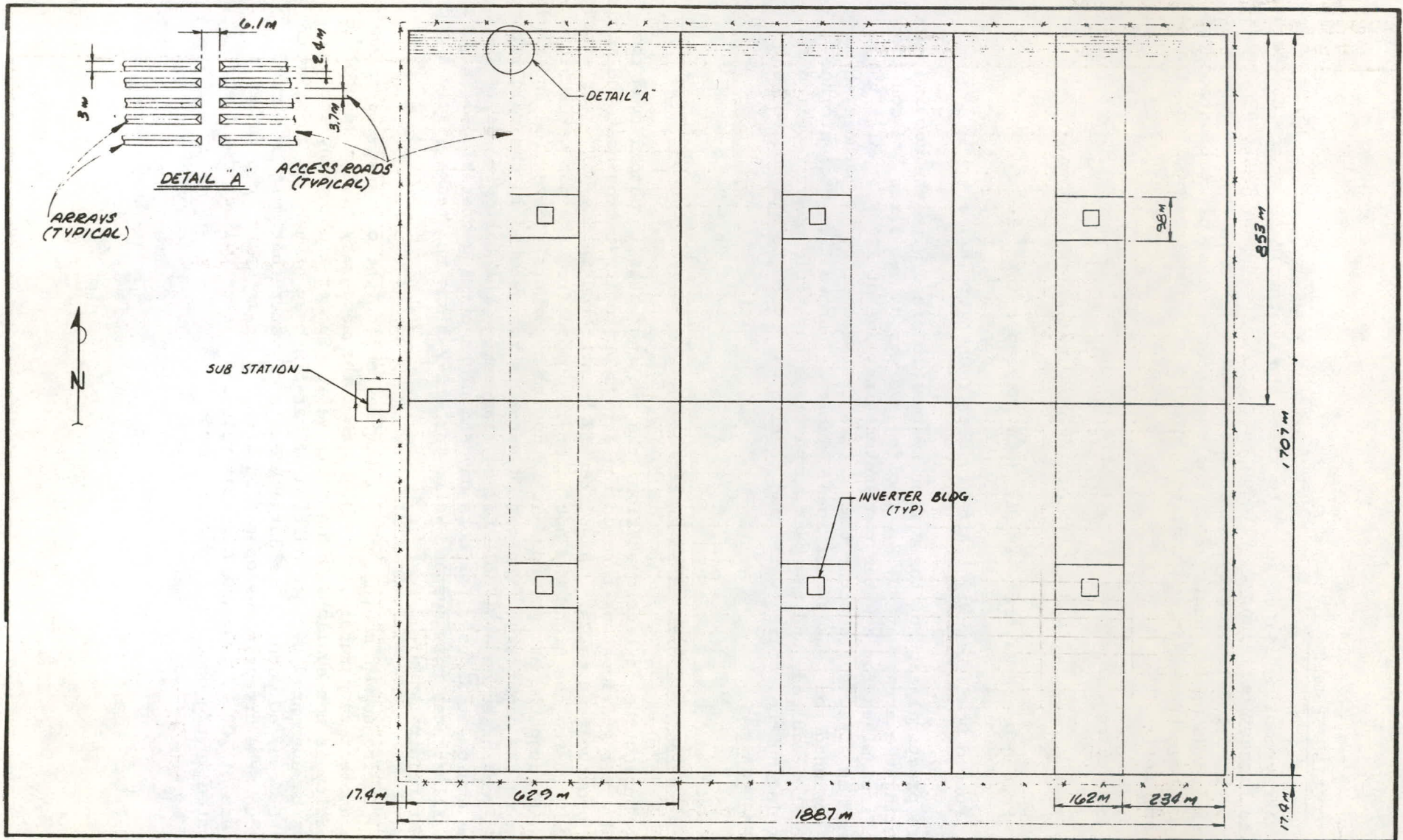
FIGURE NO. 4-1



Jed. Bacon & Davis Hish Inc.
ENGINEERS - CONSTRUCTORS
SALT LAKE CITY, UTAH

TYPICAL LAYOUT - TROUGH
ARRAY - NIGHT TIME COOLING
WITH AIR FIN COOLERS

FIGURE No. 4-2



545

Ford, Bacon & Davis Utah, Inc.
 ENGINEERS - CONSTRUCTORS
 SALT LAKE CITY, UTAH

TYPICAL LAYOUT - CADMIUM
 SULFIDE COLLECTOR'S - MYLAR
 FILM

FIGURE NO. 4-3

5.0 COOLING SYSTEMS

Array cooling is necessary to allow the photovoltaic system to operate at its highest efficiency. Fifteen percent of the energy striking the arrays is converted to electricity, 5% is reflected and 80% is absorbed and must be removed as excess heat. Four cooling water systems or combinations of systems have been examined that will provide the required cooling. These systems are:

Nighttime back flow through arrays

Forced Draft Nighttime Air-Fin Heat Exchanger (HX)

Forced Draft Daytime Air-Fin Heat Exchanger (HX)

Forced Draft Day-Night Air-Fin Heat Exchanger (HX)

Where practical each of these four systems is sized with the cooling water entering the arrays at 90° F. Cooling systems of two sizes are considered; the first sized for a water temperature increase of 20° F., while the second is sized for a water temperature increase of 40° F. The systems are designed for peak summer load. Table 1-2 shows the water storage capacity required, and the peak and average parasitic power required for circulating the cooling water and forcing air over the air cooled heat exchangers.

5.1 Nighttime Backflow Through Arrays

During the daytime operation, the cooling water is pumped from the cold water storage tank through the arrays where it absorbs heat and cools the photovoltaic cells. This water is then stored in the hot water storage tank. During the night the hot water is pumped from the hot water storage tank through the arrays where it is cooled by natural convection and radiation to the night sky. The cooled water is then stored in the cold water storage tank to be available for cooling during the following day. The same equipment is used for both day and night pumping operations. Figure 5-1 illustrates this system, while Table 2-2 lists the tankage volume and power requirements.

During summer months, the nighttime cooling period is so short and the ambient temperature is so high, that the necessary nighttime cooling capacity is not available from the arrays. Summer night array cooling must be augmented by the addition of air-fin heat exchangers to maintain 90° F. cooling water. The large amounts of water that must be pumped through the arrays makes operation with a daytime water temperature increase of 20° F. impractical. Controls and electrical equipment are located in the cooling water pump house.

5.2 Forced Draft Air-Fin Heat Exchanger - Night Operations

For this system, the arrays are cooled during the daylight hours by cool water pumped from the cold water storage tanks through the arrays and back to the hot water storage tanks. This hot water is then cooled during the night by pumping it from the hot water storage tanks through an air-fin heat exchanger and back to the cold water storage tanks. The air-fin heat exchanger is supplied with pumps to move the water from the hot water storage tanks through the heat exchanger back to the cold water storage tanks. Heat exchangers of different sizes can be provided to allow the cooling water temperature to increase 20° or 40° F. as it passes through the array cooling system. Figure 5-2 illustrates this system, while Table 2-2 lists the tankage and power requirements.

Three heat exchangers are required, each servicing two array sections. A pump house is furnished for each air-fin heat exchanger. Pumps, valves, electrical equipment, and controls are located in this building.

5.3 Forced Draft Air-Fin Heat Exchanger - Day Operations

Cooling water is pumped from the storage tank through the arrays, to the air-fin heat exchanger, and back to the storage tank.

The heat exchangers are sized to remove peak heat input during a summer day when air temperatures are at maximum levels. This requires a large amount of air to be moved since the higher daytime air temperatures provides little heat transfer potential at the desired cooling water operating temperatures. Therefore, the day operation heat exchanger has a much larger surface area and requires many more cooling fans than does the night heat exchanger. However, only one small storage tank is necessary rather than the two or four large tanks that are required with the night heat exchanger system. For these reasons, the minimum summer daytime temperature of the water leaving the air-fin heat exchanger will be about 115° F. Therefore, for a 20° F. increase across the arrays, the system must operate between 115° F. and 135° F.

Operation of this system in months when the air temperature does not reach high levels will allow array cooling water temperatures to be lowered.

Three heat exchanger systems are required. Each system is furnished with one single tank and a pump house where pumps, valves, electrical equipment and controls are housed. Each heat exchanger cools two array sections. Refer to Figure 5-3.

5.4 Forced Draft Air-Fin Heat Exchanger - Day-Night Operation

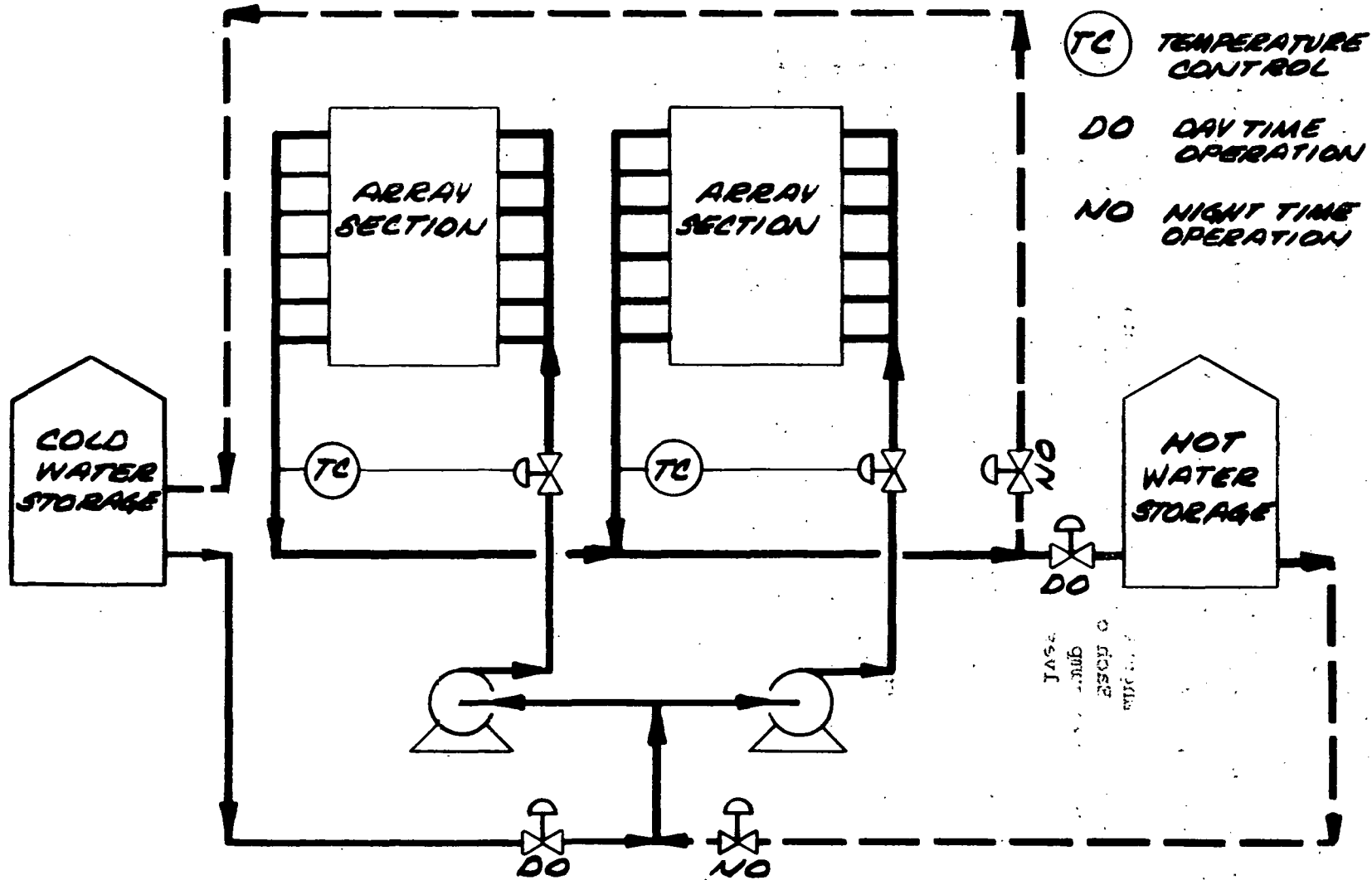
The arrays are cooled by water that is pumped from a cold water storage tank through the arrays where it absorbs the excess heat and cools the photovoltaic cells. The heated water then leaves the arrays and is

stored in the hot water storage tanks. The hot water is pumped from the hot water storage tanks through the air-fin heat exchanger, where it is cooled to the original cooling water temperature, then pumped to the cold water storage tank. Cooling water is pumped through the arrays only during the daylight hours, while the heated water is pumped through the air-fin exchanger on a continuous operation, except for a few hours a day in hot summer months when the air reaches its maximum temperature. Figure 5-4 illustrates this cooling system, while tankage and power requirements are shown in Table 2-2.

Three heat exchangers with the associated pump houses and storage tanks are provided. Each of these cooling systems is used to cool two array sections. Two pump houses are provided with each system to house the required pumps, valves, electrical equipment and controls.

These systems can be sized to allow cooling with either a 20° F. or 40° F. increase in the cooling water temperature as it passes through the arrays.

This system, although not eliminating the storage tanks, offer savings in overall equipment size. The air-fin heat exchanger can be smaller than the night only heat exchanger since it will operate over a longer period of time. The heat exchanger is much smaller than the day heat exchanger since average ambient air temperatures are much lower than the daytime maximums. Storage tanks are also smaller than those required for night only operations.



**COOLING SYSTEM SCHEMATIC
NIGHT TIME COOLING USING ARRAYS**

Ford, Bacon & Davis Utah Inc.
ENGINEERS - CONSTRUCTORS
SALT LAKE CITY, UTAH

FIGURE 5-1

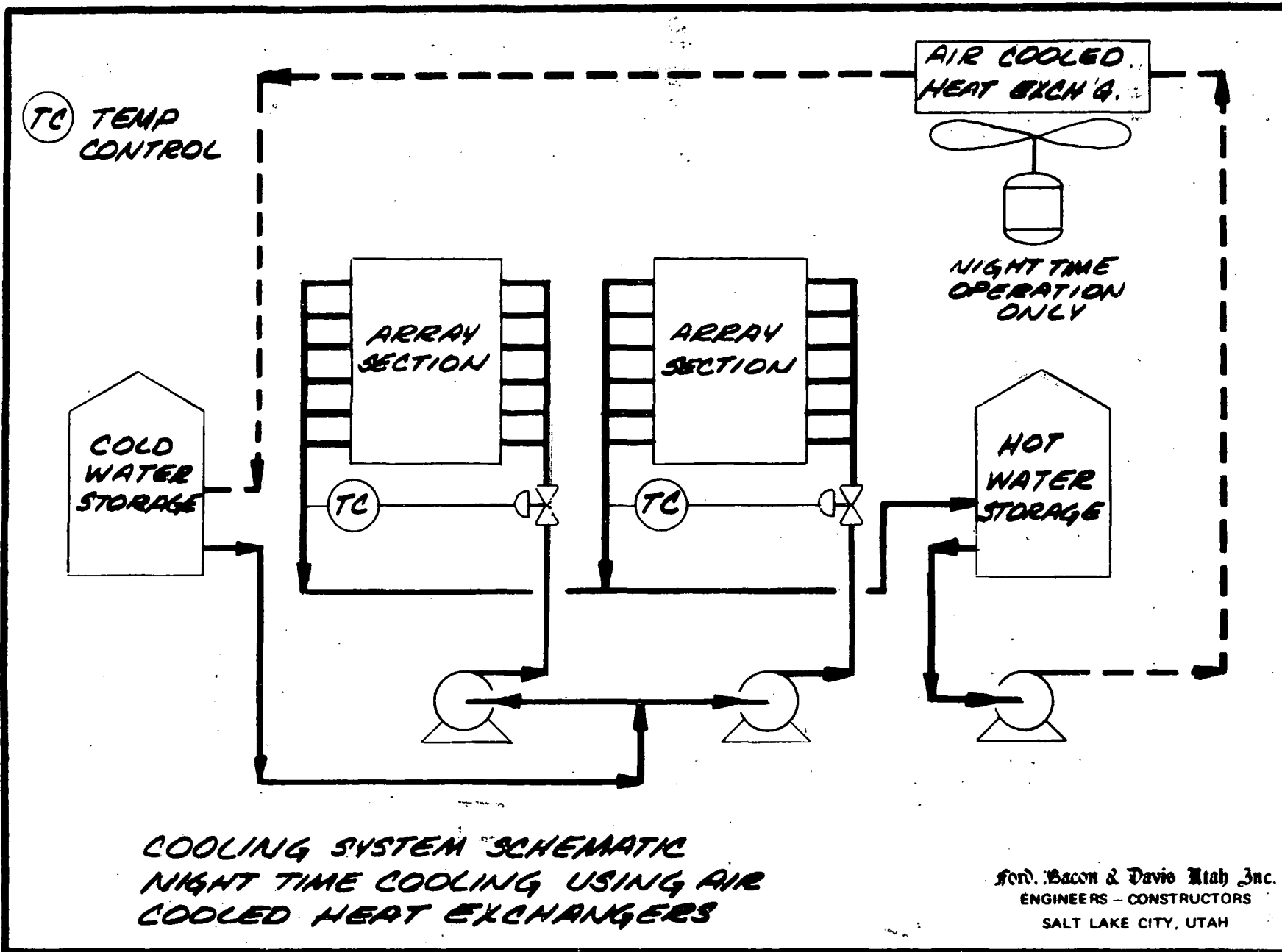
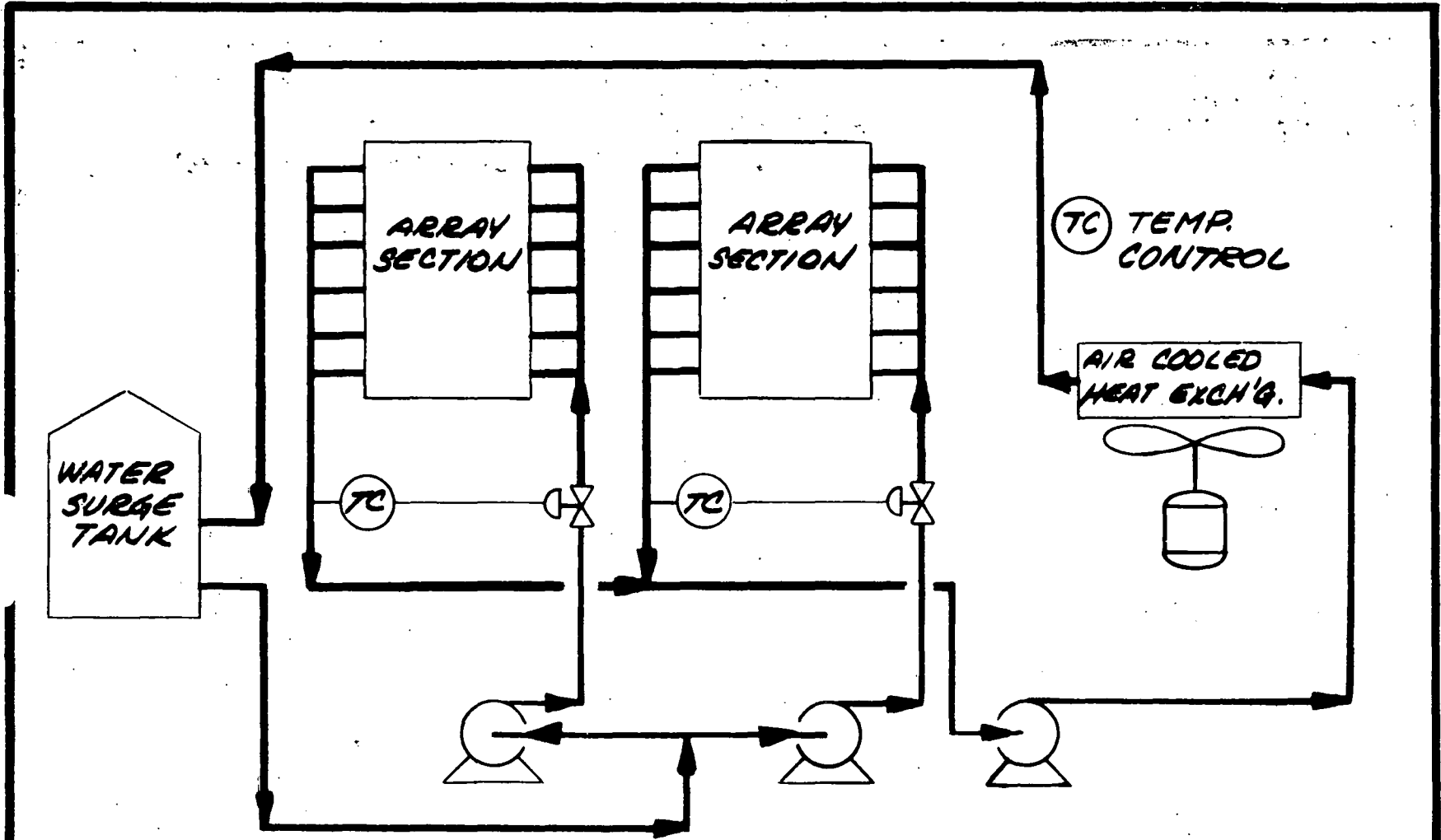


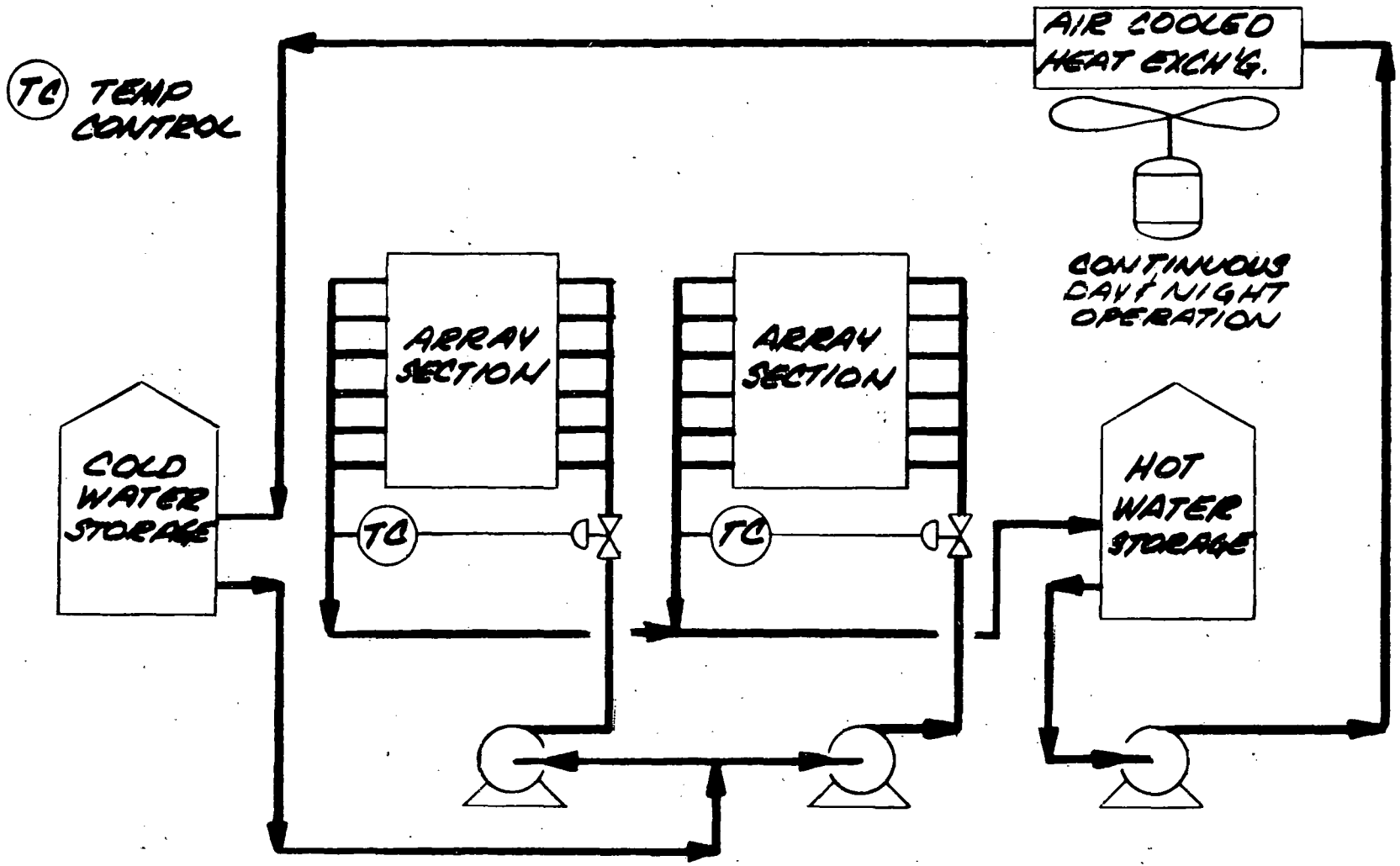
FIGURE 5-2



**COOLING SYSTEM SCHEMATIC
DAYTIME COOLING USING AIR
COOLED HEAT EXCHANGERS**

**Ford, Bacon & Davis Utah Inc.
ENGINEERS - CONSTRUCTORS
SALT LAKE CITY, UTAH**

FIGURE 5-3



**COOLING SYSTEM SCHEMATIC
DAY AND NIGHT TIME COOLING USING
AIR COOLED HEAT EXCHANGERS**

**For. Bacon & Davis Utah Inc.
ENGINEERS - CONSTRUCTORS
SALT LAKE CITY, UTAH**

FIGURE 5-4

6.0 COST ESTIMATES

The following costs have been estimated for each of the array systems considered:

- A. Site preparation and foundations
- B. Array erection
- C. Array power collection and supply network
- D. Array cooling system
- E. Support buildings.

Tables 6-1 through 6-6 summarize the estimated costs of the above for each of the array systems. The costs for each of the potential cooling systems are also included in these Tables.

Costs have been included for the erection of the arrays. The cost for installation of the reflective surface needed for the trough system has not been included. Also, no costs have been included for installation of a transmission line or access roads since these both exist for the recommended Vulture Mountain Site. Items included in the estimates are as follows:

6.1 Site Preparation

Site preparation includes the cost to level the site, prepare and construct access roads and drainage ditches, prepare parking and equipment storage areas, and all other earth moving work. Also, included is the construction of a drainage ditch around the periphery of the site, and the construction of a 2.4 meter high chain link security fence on the site boundary.

6.2 Foundations

This cost includes forming and pouring foundations for all equipment and buildings except those needed for heat exchanger installation. All building foundations and floors are included as well as array support foundations, and foundations for the water storage tanks. The cost for trough construction is also included for the trough array system.

6.3 Buildings

The cost of materials and construction of the cooling water pump houses, and the central electrical control station and inverter buildings are included under this heading. The heat exchanger pump house building is included with the heat exchanger cost. Prefabricated metal buildings are used.

TABLE 6-1

PHOTOVOLTAIC POWER SYSTEM
TWO AXIS TRACKING ARRAY

(All Figures in 1976 Thousands of Dollars)

COOLING SYSTEM DESCRIPTION	NATURAL RADIATION FROM ARRAY		AIR FIN COOLERS NIGHT OPERATION		AIR FIN COOLERS DAY OPERATION		AIR FIN COOLERS NIGHT & DAY OPERATION	
	20	40	20	40	20	40	20	40
COOLING WATER ΔT °F								
Estimate Item								
Site Preparation	NP	800	800	800	800	NP	800	800
Foundations	NP	4,458	4,458	4,458	4,458	NP	4,458	4,458
Buildings and Structures	NP	500	500	500	500	NP	500	500
Cooling Water Piping System	NP	12,470	20,295	12,470	20,295	NP	20,295	12,470
Cooling Water Pump Hse. Equip.	NP	1,940	5,497	1,940	5,497	NP	5,497	1,940
Storage Tanks	NP	7,998	15,996	7,998	789	NP	8,351	4,380
Air-Fin Heat Exchanger	NP		14,366	11,978	16,754	NP	9,399	7,836
HX Pump House & Equipment	NP		5,202	3,202	3,236	NP	3,403	2,095
Electrical Collection System	NP	Incl.	Incl.	Incl.	Incl.	NP	Incl.	Incl.
Electrical Dis- tribution System	NP	9,917	9,917	9,786	9,917	NP	9,917	9,786
Array Installation	NP	9,404	9,404	9,404	9,404	NP	9,404	9,404
Sub Total		47,487	86,453	62,536	71,650		72,024	53,669
20% Contingency		9,497	17,287	12,507	14,330		14,405	10,734
TOTAL		56,984	103,722	75,043	85,980		86,429	64,403

NP - Not Practical

TABLE 6-2

PHOTOVOLTAIC POWER SYSTEM
FIXED ARRAY

(All Figures in 1976 Thousands of Dollars)

COOLING SYSTEM DESCRIPTION	NATURAL RADIATION FROM ARRAY		AIR FIN COOLERS NIGHT OPERATION		AIR FIN COOLERS DAY OPERATION		AIR FIN COOLERS NIGHT & DAY OPERATION	
	20	40	20	40	20	40	20	40
COOLING WATER ΔT OF								
Estimate Item								
Site Preparation	Not Practical	800	800	800	800	Not Practical	800	800
Foundations	Not Practical	4,458	4,458	4,458	4,458	Not Practical	4,458	4,458
Buildings and Structures	Not Practical	500	500	500	500	Not Practical	500	500
Cooling Water Piping System	Not Practical	12,470	20,295	12,470	20,295	Not Practical	20,295	12,470
Cooling Water Pump Hse. Equip.	Not Practical	1,940	5,497	1,940	5,497	Not Practical	5,497	1,940
Storage Tanks	Not Practical	5,513	11,026	5,513	789	Not Practical	8,351	4,380
Air-Fin Heat Exchanger	Not Practical		11,191	9,331	16,754	Not Practical	7,322	6,104
EX Pump House & Equipment	Not Practical		4,053	2,494	3,235	Not Practical	2,651	1,632
Electrical Collection System	Not Practical	Incl.	Incl.	Incl.	Incl.	Not Practical	Incl.	Incl.
Electrical Dis- tribution System	Not Practical	5,188	5,318	5,188	5,318	Not Practical	5,318	5,188
Array Installation	Not Practical	7,523	7,523	7,523	7,523	Not Practical	7,523	7,523
Sub Total		38,392	70,661	50,217	65,169		62,715	44,995
20% Contingency		7,678	14,132	10,043	13,034		12,543	8,999
TOTAL		46,070	84,793	60,260	78,203		75,258	53,994

TABLE 6-3

PHOTOVOLTAIC POWER SYSTEM
TROUGH ARRAY

(All Figures in 1976 Thousands of Dollars)

COOLING SYSTEM DESCRIPTION	NATURAL RADIATION FROM ARRAY		AIR FIN COOLERS NIGHT OPERATION		AIR FIN COOLERS DAY OPERATION		AIR FIN COOLERS NIGHT & DAY OPERATION	
	20	40	20	40	20	40	20	40
Estimate Item								
Site Preparation	NP	NP	1,661	1,661	1,661	NP	1,661	1,661
Foundations	NP	NP	25,042	25,042	25,042	NP	25,042	25,042
Buildings and Structures	NP	NP	8,784	8,784	8,784	NP	8,784	8,784
Cooling Water Piping System	NP	NP	20,627	11,923	20,627	NP	20,627	11,923
Cooling Water Pump Hse. Equip.	NP	NP	2,587	1,433	2,587	NP	2,587	1,433
Storage Tanks	NP	NP	7,654	5,514	789	NP	8,351	4,380
Air-Fin Heat Exchanger	NP	NP	11,191	9,331	16,754	NP	7,322	6,104
HX Pump House & Equipment	NP	NP	4,053	2,494	3,235	NP	2,651	1,632
Electrical Collection System	NP	NP	Incl.	Incl.	Incl.	NP	Incl.	Incl.
Electrical Dis- tribution System	NP	NP	9,917	9,786	9,917	NP	9,917	9,786
Array Installation	NP	NP	7,040	7,040	7,040	NP	7,040	7,040
Sub Total			98,556	83,008	96,436		93,982	77,785
20% Contingency			19,711	16,602	19,287		18,796	15,557
TOTAL			\$118,267	\$99,610	\$115,723		\$112,778	\$93,342

NP - Not Practical

TABLE 6-4

PHOTOVOLTAIC POWER SYSTEM
 CADMIUM SULFIDE MYLAR FILM ARRAY
 (All Figures in 1976 Thousands of Dollars)

Estimate Item

Site Preparation	\$1,467
Foundations	376
Buildings and Structures	1,603
Cooling Water Piping System	N.R.
Cooling Water Pump House Equip.	N.R.
Storage Tanks	N.R.
Air-Fin Heat Exchanger	N.R.
HX Pump House & Equipment	N.R.
Electrical Collection System	INCL.
Electrical Distribution System	3,378
Array Installation	8,250
Sub Total	<u>\$15,074</u>
20% Contingency	<u>3,015</u>
TOTAL	<u>\$18,089</u>

N.R. - Not Required

TABLE 6-5

PHOTOVOLTAIC POWER SYSTEM WITHOUT LIQUID COOLING
TWO-AXIS TRACKING ARRAY

(All Figures in 1976 Thousands of Dollars)

<u>Estimate Item</u>	
Site Preparation	\$ 670
Foundations	\$ 4,458
Buildings	\$ 500
Electrical Distribution System	\$ 2,450
Array Installation	<u>\$ 9,404</u>
Sub-Total	\$17,480
20% Contingency	<u>\$ 3,436</u>
Total	\$20,976

TABLE 6-6

PHOTOVOLTAIC POWER SYSTEM WITHOUT LIQUID COOLING
FIXED - ARRAY

(All Figures in 1976 Thousands of Dollars)

<u>Estimate Item</u>	
Site Preparation	\$ 670
Foundations	\$ 4,458
Buildings	\$ 500
Electrical Distribution System	\$ 1,297
Array Installation	<u>\$ 7,523</u>
Sub-Total	\$14,448
20% Contingency	<u>\$ 2,890</u>
Total	\$17,338

6.4 Cooling System Piping

The cooling water piping includes the costs for materials and construction of all cooling water piping, pipe fittings, array isolation valves, flexible hose, etc. Also included are all pipe supports in the array areas.

6.5 Cooling Water Pump House Equipment

These costs include pumps, piping, shut-off valves, and the flow control valves installed in the pumphouse.

6.6 Storage Tanks

All water cooling systems require either hot and cold water storage tanks or a single tank. The cost of construction of these tanks is included under this heading.

6.7 Air-Fin Heat Exchangers

All costs associated with the heat exchangers are included under this heading. Items considered are the heat exchangers, all structural supports and foundations, fans and fan drivers, and piping headers, which are part of the heat exchanger. The cost of shipment, assembly and construction as well as material costs are also included.

6.8 Heat Exchanger Pump House and Equipment

Costs included are:

1. All piping between the water storage tank and the heat exchanger.
2. All pumps and shut-off valves located inside the pump house.
3. Pump house construction and materials, including foundations.

6.9 Electrical Power Collection Network

All arrays require a network of conductors to route the power generated in the photovoltaic cells to the inverters. The cost of the collection network is included under this heading.

Costs for equipment needed in the inverter building, the inverter to the main substation network, or control center are not included in this estimate.

6.10 Electrical Power Distribution Network

Power is needed throughout the facility to provide operating capability. This power is used by the cooling water pumps, the heat exchanger fans, and the motors used to position the tracking arrays. Minimal lighting systems also must be provided with power. Equipment and construction costs for these facilities are included under this heading.

6.11 Array Installation

The array sections are assumed to be assembled on site in an assembly shop. The assembled arrays will then be moved by truck and crane to their final location and installed on the support structures. The cost for material and shop assembly of the arrays is not included in this study. The costs for installing the arrays, including transportation from the assembly shop to the final location are included. Tables 6-1 through 6-4 list the estimated costs of each of the systems studied.

★U.S. GOVERNMENT PRINTING OFFICE:1978 -740 -306/ 9445 REGION NO. 4